



HAL
open science

The physical vulnerability of urban areas facing the threat of inundation from lahars and flash floods: application to the case study of Arequipa, Peru

Kim Martelli

► **To cite this version:**

Kim Martelli. The physical vulnerability of urban areas facing the threat of inundation from lahars and flash floods: application to the case study of Arequipa, Peru. Earth Sciences. Université Blaise Pascal - Clermont-Ferrand II, 2011. English. NNT : 2011CLF22157 . tel-00881754

HAL Id: tel-00881754

<https://theses.hal.science/tel-00881754>

Submitted on 8 Nov 2013

HAL is a multi-disciplinary open access archive for the deposit and dissemination of scientific research documents, whether they are published or not. The documents may come from teaching and research institutions in France or abroad, or from public or private research centers.

L'archive ouverte pluridisciplinaire **HAL**, est destinée au dépôt et à la diffusion de documents scientifiques de niveau recherche, publiés ou non, émanant des établissements d'enseignement et de recherche français ou étrangers, des laboratoires publics ou privés.

N° d'Ordre : D.U. 2157

UNIVERSITE BLAISE PASCAL
U.F.R. Sciences et Technologies

ECOLE DOCTORALE DES SCIENCES FONDAMENTALES
N° 684

THESE

présentée pour obtenir le grade de
DOCTEUR D'UNIVERSITE
Spécialité : Volcanologie

Par **MARTELLI Kim**

Titulaire du Master 2 Recherche :
« Earth Science in volcanology »

**THE PHYSICAL VULNERABILITY OF URBAN AREAS FACING
THE THREAT OF INUNDATION FROM LAHARS AND FLASH
FLOODS: APPLICATION TO THE CASE STUDY OF
AREQUIPA, PERU**

Soutenue publiquement le 15 septembre 2011, devant la commission d'examen :

M. Michael SHERIDAN	Professeur, University at Buffalo	Rapporteur
M. Cees Van WESTEN	Professeur, University of Twente	Rapporteur
M. Benjamin Van WYK de VRIES	Professeur, LMV, Université Blaise Pascal	Examineur/Président
M. Denis FABRE	Conservatoire National des Arts et Métiers, Paris	Examineur
M. Bernard MASSINON	Ingénieur CEA, Fondation MAIF	Invité
M. Jean-Claude THOURET	Professeur, LMV, Université Blaise Pascal	Directeur de thèse

Résumé

Les écoulements volcaniques (lahars, écoulements hyperconcentrés) et les crues soudaines représentent des phénomènes destructeurs et dangereux. Malgré leur pouvoir destructeur (e.g. Armero, Colombie, 1985), il existe très peu d'études centrées sur les effets des lahars en zone urbaine, alors qu'ils représentent une menace réelle pour de nombreuses villes, comme Arequipa, au Pérou. Arequipa est une ville de presque 1 million d'habitants située à 17 km au sud-est du volcan El Misti. La dernière éruption majeure du Misti remonte à 550 ans (1460 après J.C.) et de plus petites éruptions ont parsemé le 18 et le 19^{ème} siècle. Des lahars dont les volumes sont compris entre $0,01 \times 10^6$ et 11×10^6 m³ se sont formés et des inondations ont balayé les vallées tous les 5 à 10 ans. Suite à l'augmentation de la population d'Arequipa, la zone urbanisée s'étend maintenant sur les flancs du volcan, jusqu'à 9 km du sommet. En réponse à cette croissance rapide et apparemment incontrôlée, il est essentiel d'évaluer l'utilisation des sols, les bâtiments et les infrastructures en fonction de leur vulnérabilité.

Des scénarios d'aléas ont été développés à partir d'anciennes et d'actuelles études géologiques, de cartes traditionnelles et des modèles numériques (tels que Titan2D) des dépôts volcaniques et fluviaux, d'études de terrain sur l'utilisation des sols, le type de bâtiments et d'infrastructures, d'analyses statistiques (y compris des analyses multi variantes) et enfin des caractéristiques géotechniques des matériaux utilisés pour les constructions. Trois scénarios de référence ont été utilisés allant d'un scénario de crue (récurrence de 5 à 10 ans) à une éruption (sub) Plinienne (VEI >3, récurrence de 5000 à 20 000 ans). Les zones inondables ont été délimitées en utilisant des résultats de code de simulation couplés à des cartographies géologiques et à des analyses de magnitude/fréquence. L'amélioration d'un MNT, construit à partir d'études DGPS et de données ASTER (10 m de résolution), a permis de modéliser les écoulements à partir de Titan2D. Les résultats du modèle montrent une extension des écoulements plus longue que celles proposées dans les études précédentes (e.g Vargas et al, 2010)

L'étude de terrain a permis de classifier l'utilisation des sols selon 19 catégories et les principaux bâtiments et infrastructures selon 10 catégories. Par exemple, les bâtiments ont été classés et ordonnés selon des critères de nature du matériau principal les constituant, nombre d'étages, etc. De la même manière, la classification de l'utilisation des sols et du type d'infrastructures ont été classés en fonction de différents éléments comme le taux d'occupation, l'importance des évacuations d'urgence etc. Les effets mécaniques des écoulements sur les immeubles et les infrastructures ont été recherchés dans le but d'élaborer des fonctions de vulnérabilité. Cette étude a révélé que les bâtiments et l'utilisation des sols du Quebrada Huarangal sont particulièrement vulnérables et exposés au risque même lors d'un écoulement de faible magnitude. Ceci est essentiellement dû à la très faible

qualité des constructions dans les zones à hauts risques du Quebrada Huarangal. Au contraire, le risque présent dans la vallée du Rio Chili est une zone à faible risque. Le niveau de risque inhérent au système d'énergie hydroélectrique et aux réserves d'eau potable reste inquiétant pour la ville, notamment durant une crise volcanique.

Cette étude a mis en évidence les capacités d'intégration des données SIG générant de l'information sur le risque via la combinaison de scénarios d'aléas et d'éléments de vulnérabilité. Ces méthodes semblent être prometteuses pour l'étude et la prévention des risques volcaniques. De plus, une base de données mise à jour pourrait aider à gérer de manière efficace un possible crise volcanique en temps réel, et ce qui est plus important encore, assister les tâches de réduction des risques.

Mots-clés : Misti, aléa, risque, vulnérabilité, lahar, système d'information géographique, Titan2D, environnement urbain, Arequipa, Pérou.

Abstract

Volcanic mass flows (lahars, hyperconcentrated flows) and flash floods represent destructive and dangerous phenomena. Given evidence concerning the destructive nature of lahars (e.g. Armero, Colombia, 1985) there appears to be a lack of studies into the effect of lahars in dense urban environments; a very real threat for many cities worldwide including the Arequipa, Peru. Arequipa, with nearly 1 million inhabitants, is located 17 km SW of El Misti Volcano. El Misti's last major eruption occurred 550 years ago (1460AD), with smaller eruptions occurring in the 18 and 19th Centuries. Lahars with volumes ranging from $0.01 \times 10^6 \text{ m}^3$ to $11 \times 10^6 \text{ m}^3$ have occurred, and flash floods have swept down valleys every 5 to 10 years. Population growth has resulted in urban sprawl to within 9 km of El Misti's summit. It is this rapid and seemingly uncontrolled expansion which warrants the assessment of building, land use and infrastructure within a vulnerability framework.

Hazard scenarios were developed from former and current geological studies; conventional and computer-aided (e.g. Titan2D numerical modelling) mapping of volcanoclastic and fluvial deposits; field surveys of land use, buildings and infrastructure; statistical analysis (including multivariate analysis); and geotechnical characteristics of building materials. Three reference scenarios were used from a flash flood scenario (recurrence interval of 5 to 10 years) to a (sub)Plinian eruption (VEI >3, recurrence interval of 5000 to 20,000 years). Inundation zones were defined using simulation code results coupled with geological mapping and magnitude/frequency analysis. The results of Titan2D modelling feature a longer flow runout than in previous studies (e.g. Vargas et al., 2010) due to the creation of an enhanced 10 m DEM, constructed from DGPS surveys and ASTER data.

Land-use, building and infrastructure surveys identified nineteen different land-use patterns, ten main building types and many key infrastructures. Building types were classified and ranked according to a number of components, such as the dominant building material, number of floors etc. Similarly land use and infrastructure were ranked according to a number of different elements such as occupancy rate, emergency importance etc. The mechanical effects of the flows on buildings and infrastructure were then investigated to elaborate vulnerability functions. The vulnerability and risk assessment have indicated that building, land use and infrastructure on the Quebrada Huarangal fan are particularly vulnerable and at risk even during the smallest magnitude flow. This is primarily due to very poor quality construction in high hazard areas on the Quebrada Huarangal fan. In contrast the risk posed in the Río Chili Valley is in general much less. The level of risk posed to the hydroelectric power scheme and the potable water supply is concern for the city, especially during a volcanic crisis.

Data integration abilities of GIS in generating risk information by combining hazard scenarios with vulnerability elements have been highlighted in this research and offer promising prospects in the field of volcanic risk assessment and management. In addition, an updated database could help to

efficiently handle possible volcanic crisis in real-time, and more importantly assist the risk reduction tasks.

Keywords: El Misti Volcano, hazards, risks, physical vulnerability, lahars, GIS, Titan2D, urban environment, Arequipa, Peru.

Acknowledgements

Firstly, I would like to thank Professor Jean-Claude Thouret for making this PhD project possible, and giving me the opportunity to live in France, work in the USA and undertake fieldwork in Peru. It has definitely been a world-wide adventure!

This project would not have been possible without the financial support of the Foundation MAIF. Additional financial support was also received from the Laboratoire Magmas et Volcans (LMV), the ANR project “laharisk”, l’Ambassade de France en Nouvelle-Zélande, CROUS Clermont-Ferrand, IRD and the Franco-Peruvian network (R. Porrás Barrenechea).

I would like to thank my colleagues at LMV, including Ben Van Wyk de Vries, Tim Druitt, Hérve Martin, Jean-Françoise Lenot, Jean-Claude Besson, Charley Merciecca and Phillipe Labazay. Thank you also to all the support and technical staff.

I am grateful for all the help I received in Peru, notably from Peruvian students Edwin Suaña and Edgar Romero Valero, Nikki Watson, Aude de la Rupelle, Jean-Claude and Lilane Thouret, INGEMMET (Geological, Mining, and Metallurgical Institute), Arequipa Civil Defense, and IRD.

Equally I would like to thank to all those who helped me with Titan2D at the University at Buffalo (USA) including: Mike Sheridan, Keith Dalby, Dinesh Kumar, and Scott Gallas. Thank you also to Jon Procter (Massey University, NZ) for additional support with Titan2D.

Thank you to Ruben Vargas for many useful discussions about El Misti, Arequipa, Titan2D, hazards, vulnerability and risk. I really appreciated your help.

I am grateful to the members of my thesis committee, Michael F. Sheridan (University at Buffalo, NY), Cees van Westen (ITC, University of Twente, Netherlands), Denis Fabre (CNAM, Paris), Bernard MASSINON (Fondation MAIF), Ben Van Wyk de Vries (LMV, Clermont-Ferrand) and Jean-Claude Thouret (LMV, Clermont-Ferrand) for their useful comments and discussions about this research project.

Thank you very much to Vince Neall (Massey University, NZ) for the support, advice and kind words of encouragement you have given me since my first year of university.

Je remercie mes amis/amies à LMV. There are too many of you to thank individually – but you know who you are. Thank you so very much for everything!! You all have made this journey worthwhile. I feel so fortunate to have met you and to have made such wonderful friends. Merci encore! (said with a strong kiwi accent).

To my family and friends located throughout the World: thank you for listening to, and encouraging, me no matter what the outcome could have been. You are truly brilliant people!

None of this would have been possible without the support of my Mum and Dad. You have always been there for me and encouraged me when things seemed too much to bear. Your continual encouragement, love and support have meant more to me than you will ever know – I am, and will be, forever grateful.

Last but by no means least; I would like to thank Phil, for everything. Words cannot describe how much I have appreciated all that you have done for me. I am so lucky.

***“Civilization exists by geological consent,
subject to change without notice.”*** – Will Durant

TABLE OF CONTENTS

Résumé	i
Abstract.....	iii
Acknowledgements.....	v
Table of Contents	vii
<u>PART ONE: Setting and methods</u>	1
INTRODUCTION.....	3
Scope: Large cities exposed to volcanic eruptions.....	3
Assessing the volcanic hazard, vulnerability and risk of communities.....	9
Thesis aims and objectives.....	17
Case study: Arequipa in south Peru – a large city in the shadow of the active El Misti volcano	20
<i>Proposed Eruption Scenarios for El Misti</i>	26
<i>Study areas in Arequipa</i>	32
Thesis outline	34
CHAPTER ONE: Methods and rationale.....	35
1.0 Introduction	35
1.1 Selection of valleys to study in Arequipa.....	37
1.1.1 <i>Río Chili canyon</i>	37
1.1.2 <i>Quebrada Huarangal volcanoclastic fan</i>	41
1.2 Fieldwork conducted in Arequipa	42
1.2.1 <i>DGPS surveying</i>	43
1.2.2 <i>Surveying the building stock, land use and infrastructure</i>	47
1.2.3 <i>Lahar and flood deposits</i>	50
1.3 Laboratory experiments.....	51
1.3.1 <i>Unconfined Compressive Strength</i>	52
1.3.2 <i>Density and porosity</i>	53
1.3.3 <i>Ultrasonic Pulse Velocity (UPV)</i>	57
1.3.4 <i>Radio-carbon dating</i>	59
1.4 Geographical Information Systems.....	59
1.4.1 <i>Data acquisition and availability</i>	60
1.4.2 <i>Creating an enhanced DEM for Arequipa</i>	61
1.4.3 <i>Creation and management of GIS data</i>	67
1.4.4 <i>Displaying and analysing data</i>	69
1.5 Computer modelling of mass flows	70
1.5.1 <i>Introduction to Titan2D</i>	72
1.5.2 <i>Methods for Titan2D two phase modelling at El Misti</i>	74
1.6 Hazard analysis	78
1.6.1 <i>Determining the magnitude, frequency and extent</i>	78
1.7 Vulnerability analysis.....	79
1.7.1 <i>Buildings</i>	79
1.7.2 <i>Land use</i>	79
1.7.3 <i>Infrastructure</i>	80
1.8 Risk analysis.....	81
1.9 Conclusion.....	81

<u>PART TWO: Lahars and flash floods in an urban environment</u>	83
CHAPTER TWO: Mass flow hazards from El Misti Volcano	85
2.0 Introduction	85
2.1 The mass-flow hazard at El Misti volcano.....	85
2.2 Field studies of lahar and flood deposits	90
2.2.1 <i>Sections A and B: Charcani Quinto</i>	93
2.2.2 <i>Sections C: Rio Chili Canyon Entrance</i>	95
2.2.3 <i>Sections D: Chilina</i>	95
2.2.4 <i>Section E: Chilina</i>	97
2.2.5 <i>Section F: Tennis court lahar</i>	97
2.2.6 <i>Section G: Downstream Rio Chili</i>	99
2.2.7 <i>Section H: Uchumayo</i>	99
2.3 Flash flood occurrence in Arequipa based on historical events	101
2.3.1 <i>8-9 February 1989</i>	103
2.3.2 <i>25 February 1997</i>	106
2.3.3 <i>February 2011</i>	108
2.4 Dam-break floods in Arequipa?	113
2.5 Flow magnitude and frequency of lahars, dam-break and flash floods.....	114
2.5.1 <i>Lahars</i>	114
2.5.2 <i>Floods</i>	114
2.5.3 <i>Dam-break floods</i>	116
2.6 Extent of lahars and flash floods	117
2.7 Hazard scenario evaluation	121
2.7.1 <i>Determination of scenarios for lahars, dam-break and flash floods</i> .	121
2.7.2 <i>Hazard zone maps</i>	123
2.8 Discussion and conclusion	126
CHAPTER THREE: Modelling lahars using Titan2D	129
3.0 Introduction	129
3.1 New Titan2D simulations at El Misti Volcano, Arequipa	131
3.1.1 <i>The effect of input parameters</i>	131
3.2 Titan2D outputs and flow behaviour.....	152
3.3 Lahar inundation zones	155
3.4.1 <i>Rio Chili Valley</i>	158
3.4.2 <i>Quebrada Huarangal Fan</i>	159
3.4 Discussion	160
3.4 Concluding remarks	162
<u>PART THREE: Vulnerability and risk assessment within an urban setting</u>	163
CHAPTER FOUR: Elements at risk: land use, building stock and infrastructure	165
4.0 Introduction	165
4.1 Arequipa: A rapidly expanding city	167
4.2 Land-use classification.....	169
4.2.1 <i>Introduction</i>	169
4.2.2 <i>Land-use classification in Arequipa</i>	171
4.2.3 <i>Susceptibility of land use in Arequipa</i>	177
4.3 Building stock classification	182
4.3.1 <i>Introduction</i>	182

4.3.2	<i>Construction types and building materials used in Arequipa</i>	182
4.3.3	<i>Physical properties of building materials</i>	193
4.3.4	<i>Classification of building types in Arequipa</i>	202
4.3.5	<i>Susceptibility of building types in Arequipa</i>	210
4.4	Susceptibility of building types and land use in Arequipa.....	217
4.5	Infrastructure classification	222
4.5.1	<i>Introduction</i>	222
4.5.2	<i>Infrastructure present in Arequipa</i>	223
4.5.3	<i>Susceptibility of infrastructure in Arequipa</i>	245
4.6	Summary of the susceptibility of land use, buildings and infrastructure in Arequipa	251
 CHAPTER FIVE: The risk facing the city of Arequipa		253
5.0	The effects of lahars and flash floods on buildings and infrastructure	253
5.2	Arequipa case study: risk assessment.....	257
5.2.1	<i>Building Risk</i>	257
5.2.2	<i>Land use risk</i>	262
5.2.3	<i>Combined building and land use risk</i>	264
5.2.4	<i>Infrastructure risk</i>	273
5.3	Discussion of risk for future volcanic and hydrologic crises in Arequipa	284
 CONCLUSIONS AND RECOMMENDATIONS		285
Conclusions		285
Recommendations to reduce the risk in Arequipa		291
Recommendations for further research		293
 REFERENCES		295
 APPENDICES		313
Appendix A		315
Appendix B		327
Appendix C		337

**PART ONE:
SETTING AND METHODS**

INTRODUCTION

Scope: Large cities exposed to volcanic eruptions

Natural hazards such as earthquakes, floods and volcanic eruptions are threatening events which are capable of producing damage to people (death or injury), and the physical (e.g., building and infrastructure destruction), social and economic environments in which they take place. This not only happens at the moment of occurrence (i.e. the aftermath) but on a long-term basis due to their associated consequences (e.g. lahars that occur months, even years, after an eruption).

Urbanisation has led to an ever-increasing global exposure to a multiplicity of natural hazards as an estimated 50% of the world's population lives in urban areas (Chester et al., 2001). More people are being placed at risk as cities become overcrowded, forcing populations to live on the outskirts where land may be hazardous or unsuited for residential development, such as along drainage channels in cities. Furthermore, urbanisation in developing countries is increasing considerably - 17 out of 20 of the world's largest cities are now located in the developing world (Small and Naunmann, 2001). Alarmingly, volcanically active areas in developing countries are home to some of the densest populations including Yogyakarta (Indonesia), Quito (Ecuador), Mexico City (Mexico) and Guatemala City (Guatemala) (Chester et al., 2001).

It has been estimated that 500 million people worldwide (~9% of the world's population) live in volcanic zones that are at risk from future eruptions (e.g., Tilling, 2005). In addition, over 200 million people now live in large cities (with greater than 1 million inhabitants) near volcanoes; cities such as Tokyo, Mexico, Naples and Arequipa are all located within the shadow of an active volcano (Tilling, 2005; Chester et al., 2001). During the 20th Century alone over 90,000 people were killed and over 5 million affected by volcanic phenomena (Table 1) (Witham, 2005). The volcanic disaster death toll is dominated by the disasters at Mt Pelée, Martinique (1902) and Nevado del Ruiz, Columbia (1985), which together account for 50% of deaths.

Human consequence	Number of events	Number of people
Killed	260	91 724
Injured	133	16 013
Homeless	81	291 457
Evacuated/affected	248	5 281 906
Any incident	491	5 595 500

Table 1: Best estimates of human impacts in 20th Century volcanic events from Witham (2005). The database has been compiled from a wide range of sources – CRED-EMDAT database, *Volcanoes of the World* (Simkin and Siebert, 1994), the *Global Volcanism Network Bulletin* (the Smithsonian Institute), and the *Catalogue of Active Volcanoes*, in addition to many peer-reviewed articles and press reports – and has considered all volcano-related incidents.

Witham's (2005) database for volcanic disasters not only takes into consideration deaths but also those people injured, made homeless, evacuated and affected. Nevado del Ruiz also accounts for approximately 28% of the total number of injuries resulting from lahars generated by a small eruption (0.02 km³) that melted part of the snow and ice on the volcano. Lahars killed approximately 22,000 people and caused widespread devastation (Voight, 1990). The catastrophe is the worst volcanic disaster since the 1902 eruption of Mt. Pelée, which resulted in the deaths of around 29,000 people when pyroclastic density currents destroyed the town of St. Pierre (Blong, 1984).

The immediate effects of the 1991 Pinatubo (Philippines) eruption and the subsequent and protracted impacts on the region from lahars more than ten years after the eruption rank highly in the homeless and evacuated or affected fields (accounting for 26% of people made homeless and 33% of those evacuated or affected in the 20th Century; Witham, 2005). Merapi, Indonesia, also ranks in the top ten volcanoes for deaths, injuries and homelessness; and of the 1.1 million people living on the flanks of the active Merapi volcano, 440,000 are living in areas prone to pyroclastic flows, surges, and lahars (Thouret et al., 2000). As summarised above, the volcanic disaster databases have all revealed that pyroclastic flows were the main cause of death, followed by lahars, which were also the principal cause of injuries.

Lahar (also called volcanic debris flow or mudflow) is an Indonesian term for mixtures of water-saturated rock debris that flow downslope. Naturally occurring high-discharge flows of water and sediment in open channels vary over a wide and continuous spectrum of sediment

concentration and particle-size distribution. However, to classify a lahar rheologically is difficult because a lahar event can comprise of one or more flow phases, including a debris-flow phase, a transitional or hyperconcentrated-flow phase, and a streamflow phase (Vallance, 2000) (Table 2). Therefore, the term lahar is applied to high-sediment-fraction volcanic debris flows, low-sediment fraction hyperconcentrated flows, and gradational flows in between, but does not include unsaturated parts of debris avalanches or sediment water floods (Pierson, 2005).

Phase	Description
Debris flow	Solid and liquid fractions are approximately equal volumetrically. The two fractions in vertical section move downstream approximately in unison.
Streamflow	Fine-grained sediment moves in suspension with the fluid (suspended load) and coarse-grained sediment moves along the bed at discrete intervals (bedload).
Transitional flow (hyperconcentrated flow)	Intermediate between that of debris flow and streamflow. This transitional phase carried high sediment loads, and coarse-grained solid tend to separate vertically from the liquid-and-fines-solids mixture.

Table 2: Definitions of the main flow phases. Note that transitions are gradational and dependent on other factors such as sediment-size distribution and energy of the flow (from Pierson, 2005).

Lahars may be syneruptive (primary), posteruptive (secondary) or unrelated to eruptions, and can be initiated by: (a) rapid melting of snow and ice, (b) an avalanche, induced by an eruption, depositing material into a stream or lake, (c) a lava or pyroclastic flow moving into a stream or lake, (d) a volcanic earthquake inducing slope failure and initiating mass movement, (e) heavy rains on a volcano, (f) sub-glacial eruptions, and (g) breaching of a crater lake (Vallance, 2000). Water that is generated from pyroclastic flows and surges, eruptions through crater lakes, subglacial eruptions or lahars owing to intense rainfall can incorporate easily erodible volcanoclastic sediment on the volcano and may form lahars. Edifice collapses may also form lahars if there is enough water present (e.g. hydrothermal fluids in porous material) in the rock to liquefy the material as it collapses (Pierson, 2005). This can occur during a shallow magma intrusion (for larger lahars), magmatic or phreatic volcanism, and volcanic or tectonic earthquakes.

Hyperconcentrated streamflows are usually formed by the downstream transformation of the flow through loss of sediment, and also from dilution by the streamflow (Cronin et al. 1997; Vallance, 2005). Additional dilution downstream may result in transformation of hyperconcentrated flows into normal streamflows, or floods (Pierson and Scott, 1985; Scott, 1988). Water floods normally transport mostly fine sediment and in relatively small quantities – containing generally less than 4% by volume (vol.%) or 10% by weight (wt.%) suspended sediment (Pierson, 2005). In contrast, high-discharge debris flows (and/or mudflows) may transport more sediment than water with sediment concentrations in excess of 60 vol.% (80 wt.%) (Pierson and Costa, 1987; Costa, 1988). A hyperconcentrated flow is often applied to intermediate flows. In all cases the sediment concentration plays a critical role in the flow behaviour and mechanics (Iverson, 1997; Pierson, 2005).

Rock debris in a lahar can range in size from clay particles (>0.003 mm) to blocks several tens of metres in maximum dimension. Volcanic debris flows and hyperconcentrated flows contain a high concentration of rock debris which gives the flow an internal strength capable of carrying large boulders as well as other objects such as cars, parts of buildings, and water tanks. Such flows also exert high impact forces against objects in their paths (Figure 1). As flows dilute and become hyperconcentrated they lack internal strength which causes the mixture of rock debris and water to take on different flow properties.

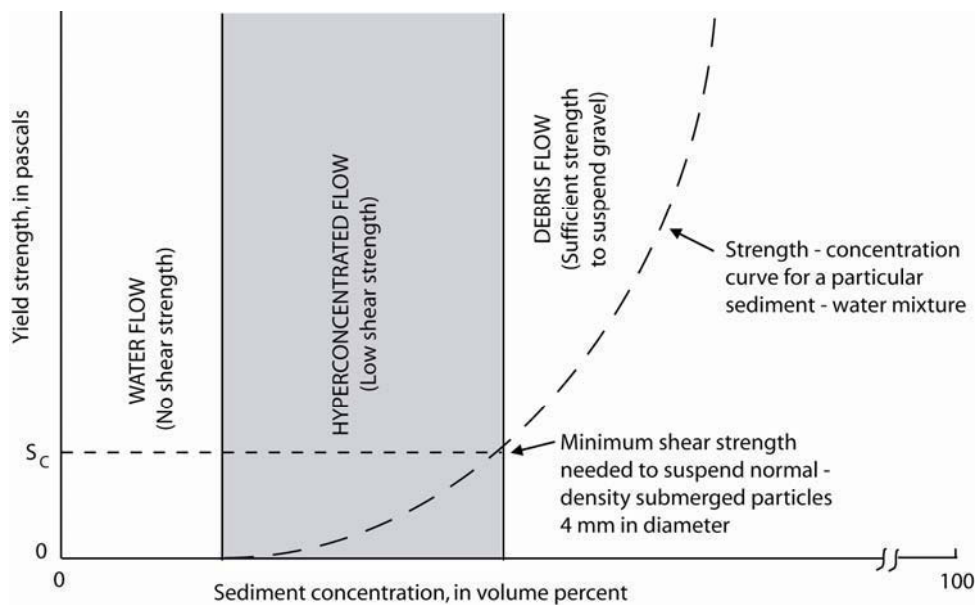


Figure 1: Yield strength of sediment-water mixtures as a function of suspended sediment concentration. Definitions based on an idealised yield-strength curve of poorly-sorted sediment-water mixture (from Pierson, 2005)

Lahars, when moving, resemble masses of wet concrete and tend to flow downslope along channels or stream valleys delivering large amounts of sediment to the rivers and streams that drain the volcano. Small lahars, commonly less than $\sim 10^6 \text{m}^3$, tend to coalesce quickly forming bouldery fronts (through size-segregation processes), coming to halt only once they reach a low-gradient (Pierson, 2005). In the case of large lahars that travel tens of kilometres, downstream dilution and erosion processes become more important than size segregation.

Lahars are also erosive, with erosion more predominant in the upper reaches where the gradient is steeper and there is less cohesive volcanoclastic sediment. Hyperconcentrated flow phases tend to be more erosive than the more sediment-rich debris flow phase (Vallance, 2000). Erosion occurs due to the undercutting of steep slopes, stream banks and terrace scarps, in addition to bed scouring. Boulders greater than 10 m in dimension and trees can become incorporated in the flow. Rapid river bed aggradation can also occur in the hyperconcentrated-flow phase, particularly where channel gradients shallow and/or channels widen. Over time, and/or with repeated events, incremental infilling of channels can lead to the lateral migration of channels, reduction of flood-conveyance capacity, and the burial of low-lying areas/structures. Lahars have been capable of filling valleys to heights of 100 metres or more (Pierson et al., 1996). Lateral migration of channels and river bank erosion can lead to the destruction of buildings, roads and bridges located on local floodplains or alluvial fans.

Lahars are capable of travelling very long distances from the source at high speeds of up to 15 m/s (Pierson et al., 1990). During an eruption of Cotopaxi volcano in Ecuador in 1877 for example, lahars travelled more than 320 kilometres down one valley at an average speed of 27 kilometres per hour (McEwan and Malin, 1989). High-speed flows are also capable of climbing valley walls on the outsides of bends, and their momentum may also carry them over obstacles (e.g. topographical barriers, bridges, dams etc.). Lahars have high bulk fluid densities (e.g. $>1,400 \text{kg/m}^3$, Rodolfo, 2000), high impact forces, and can be initiated with or without an eruption. They can also continue for months, even years, after the eruption – such was the case more than 10 years after the eruption of Mt Pinatubo, where lahars continued on the foothills of the urbanised island of Luzon.

The major hazard to human and animal life from lahars is from burial or impact by boulders and other debris; burns can also result from lahars which carry hot debris or due to the

extremely low pH of the flow. Damage to buildings and infrastructure can include burial, foundation failure, transportation, excessive wall or roof loads, collapse, undermining, and corrosion (Figure 2) (Rodolfo, 2000). Historic eruptions at Vesuvius (AD 79 and 1631), Kelud (1919), Casita (1988) and Soufrière Hills Volcano (1997) have produced lahars which have caused death, injury and/or damage (Spence et al., 2004b).

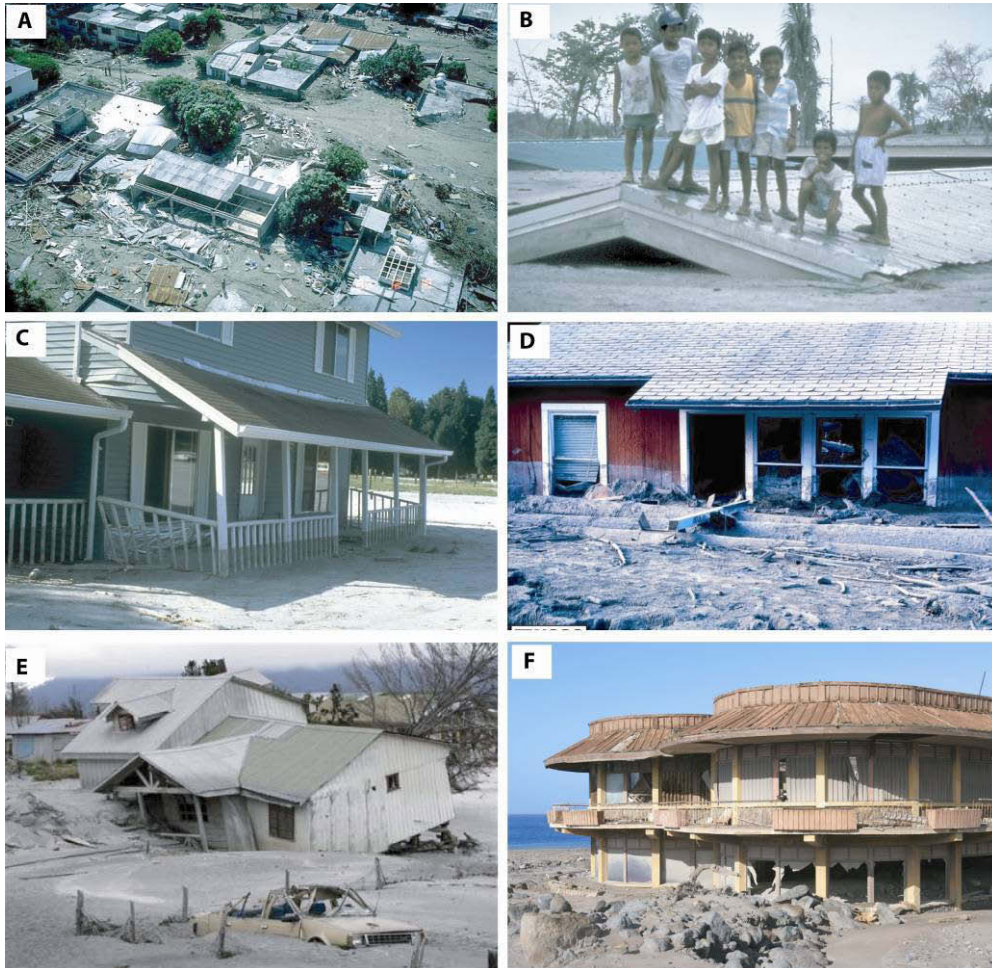


Figure 2: The damage caused by lahars to buildings. A: The only remaining buildings in Armero, Colombia, 72 km downstream from Nevado del Ruiz volcano, destroyed and partially buried by lahars on 13 November 1985 (photograph by N. Banks, 18 December 1985, USGS website). B: this school house was buried by a lahar after the enormous eruption on June 15, 1991 from Mount Pinatubo, Philippines (photograph taken 12 October 1991, USGS website). C: This house is partially buried in a lahar deposit that was formed by the dewatering of a large volcano landslide from Mount St. Helens, USA on 18 May 1980. After it stopped, water from the saturated landslide percolated to the surface and across it to form many lahars that merged as they rushed down the valley (photograph by L. Topinka, 1981, USGS website). D: A home covered in mud and logs from a Mount St. Helens lahar on 18 May 1980. More than 200 homes and 300 kms of roads were destroyed by the 1980 lahars (photograph by L. Topinka, 16 July 1980, USGS website). E: A house destroyed by lahar in Chaitén, Chile, on 26 February 2009 (REUTERS/Victor Ruiz Caballero). F: Store buried in lahar deposits, Plymouth, Montserrat (Photograph taken on January 2006, photovolcanica website).

As mentioned earlier in this introduction, lahars produced during the 1985 eruption of Nevado del Ruiz (Columbia) resulted in the death of more than 23,000 people (Voight, 1990). Baxter (2005) from studies at Montserrat stated that most people would have been killed immediately by the collapse of buildings, flying debris, and burial by the slurry. Bodies would have been driven against stationary objects, or crushed by entrained debris during the initial flow event, and as the flow waned, objects in the flow could cut the skin forming lacerations and the mud could force its way into the eyes, mouth, ears and open wounds (Baxter, 2005). Many of those who survived the initial flow impact, but were severely injured, died while waiting to be rescued. Asphyxiation occurred where people were buried in the mud and as the mud hardened by the third day, rescuing survivors trapped in the mud became increasingly difficult. Hospital records show that 150 people died after their admission to hospital, the majority from infections of lahar-related wounds (Baxter, 2005).

The 1985 Nevado del Ruiz eruption provided an example of the effect of lahars on an unprepared population. Yet, despite the known hazard and resulting damage from lahars, many communities ranging from small villages to large urban areas inhabit lahar-prone areas downstream of volcanoes. For example, 27 communities with a total population of greater than 80,000 are located downstream of Mount Rainier, USA (Wood and Soulard, 2009); 12,000 people are threatened in the Northern Valleys from lahars of Cotopaxi Volcano, Ecuador (McEwan and Malin, 1989); more than 60,000 people could be at risk from lahars during a medium sized eruption of Vesuvius, Italy (Pareschi et al., 2000); and over 120,000 people live in lahar-prone zones at Merapi, Indonesia (Thouret et al., 2000).

Loss of life and property damage from lahars can be reduced if officials and at risk populations understand and manage the risks associated with living and working in these areas. In order for public policies to be developed which minimise the losses due to lahars, methods are needed to evaluate the exposure and vulnerability, and risk to the community. This thesis will present an insight in the effects and impacts of lahars on housing and urban infrastructure and the physical vulnerability of such structures from a lahar.

Assessing the volcanic hazard, vulnerability and risk of communities

Risk assessment is an important topic with a long history across multiple disciplines. Over the last two decades, risk assessment has generated an increased interest from a natural hazard

perspective, and as a result literature relevant to hazard, vulnerability and risk are presented for a range of natural hazards and have been particularly well established for earthquakes, cyclones and floods (e.g. Kelman, 2002; Leger and Tremblay, 2009), and also for volcanic hazards (Tilling, 2005; Chester et al., 2001; and Blong, 2000 for example).

The assessment of volcanic hazard and analysis of the social, political and economical context (outside of the scope of this thesis) are necessary both for the short-term to manage volcanic crises, and for the long-term to reduce volcanic risk. Methods to characterise risk vary to address specific issues (e.g., life loss, structural damage, financial loss) and risk-reduction strategies (e.g., evacuation, mitigation, insurance). Increasingly, studies have become focused on assessing and defining the social and economic conditions that make individuals and communities vulnerable to hazards (Dibben and Chester, 1999; Chester, 2002; and Degg and Chester, 2005).

For volcanic hazard management strategies of communities to be effective, the hazard posed by volcanoes and the vulnerability of the community needs to be well understood in order to comprehend the risk. This section outlines the ways in which past and present studies are gaining a better understanding about volcanic hazards, vulnerability and risk, and how a novel method might improve their approach.

The concepts and definitions of hazard, vulnerability and risk require a more in-depth discussion. A *hazard* is a potentially threatening event, or the probability of a potentially damaging phenomenon occurring within a given time period and area (Fournier d'Albe, 1979; Tilling, 2005). Natural hazards are capable of producing damage to the physical and social space in which they take place not only at the moment of their occurrence, but in the long-term due to their associated consequences (e.g. long-term health effects, food shortage, economic repercussions, unemployment etc.). A *volcanic hazard* describes the physical characteristics of an eruption. An erupting volcano can produce a variety of hazards, such as lava flows, pyroclastic flows, or ash fallout, all having the potential to affect society and goods. Near-vent volcanic hazards tend to be very destructive, while distal hazards may cause damage to structures or disrupt everyday life and have a flow-on effect for not just the community but also the country. Even when a volcano is not in eruption, hazards such as debris avalanches or remobilised secondary lahars can still occur.

A natural hazard (or a natural event) however, only becomes a disaster due to the vulnerability and/or lack of resilience of a community. Chester (1993, p. 232) describes this situation “without people there can be no natural hazards; they are an artifice of the interaction between people and nature. In general, the greater the population density and the higher the economic development, the more severe will be the losses once an eruption occurs.” The type/s of interactions between the hazard and the vulnerable system are illustrated in Figure 3.

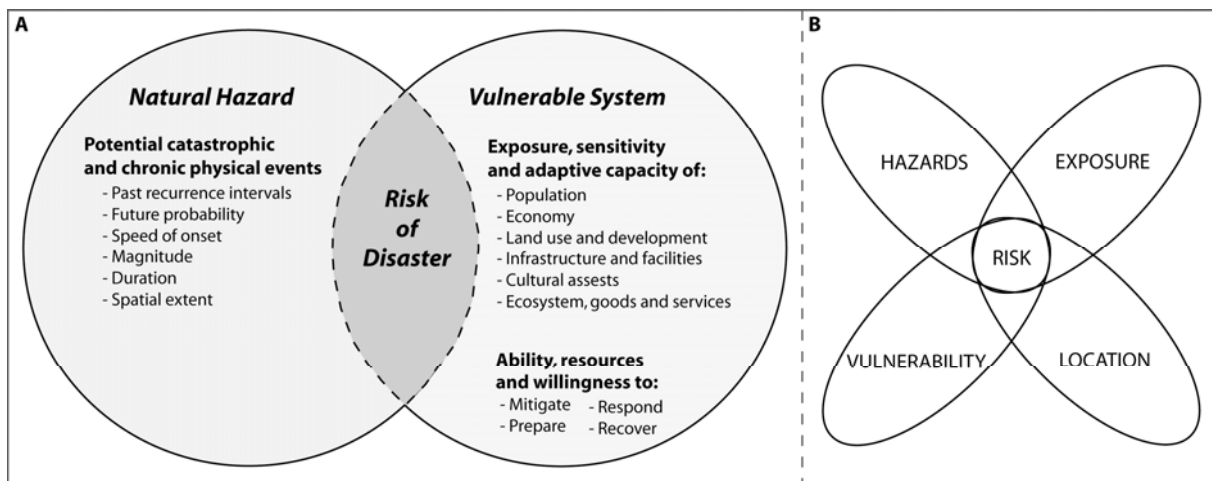


Figure 3: The elements and processes which contribute to risk. A: defines the risk of disaster as a function of natural hazards and the vulnerable human-environmental systems, of which are made up from many and varying elements (from Wood and Salard., 2009). B: A sketch showing a more simplistic approach to the main elements which contribute to risk, such as hazards, exposure and location (accessed from <http://water.usgs.gov/wid/html/HRDS.html>).

Volcanic risk, often misunderstood and confused with *hazard*, has been studied and defined by many authors (e.g. Blong, 2000; Wisner et al., 2004; Tilling, 2005). Risk is the expected number of lives lost, persons injured, damage to property and disruption of economic activity from a particular natural phenomenon; and in the simplest form has been described as the product of hazard, value and vulnerability (Blong, 2000). In reality the risk faced by a population can be complex, and disasters result from the interaction between both hazard and vulnerability (Wisner et al., 2004).

Research in identifying volcanic risk usually focuses on a combination of two major components: 1) the range of volcanic hazards that an area is exposed to, and 2) the identification of elements that are vulnerable. Volcanic hazard assessment has traditionally been conducted using a deterministic approach – based on geological and geomorphological

investigations, determining the magnitude and frequency of eruptions, and using these to define a maximum impacted area (e.g. Blong, 2000; Scott, 1989). One disadvantage of this method of hazard assessment is that the distribution of deposits and age dating are typically incomplete and may be biased. For example, very significant volcanic hazards (such as ash-surge clouds and volcanic blasts) are not well-preserved in the geological record.

Newer methods developed since the 1990's such as geophysical data obtained from volcanic eruptions and analogue or digital modelling have provided more quantitative parameters to estimate the spatial distribution and properties of tephra, pyroclastic flows and lahars (e.g. Vesuvius, Italy, Spence, et al 2004a; Colima, Mexico, Saucedo et al., 2005). Advances in information technology has also permitted the use of numerical codes coupled with GIS and recently, with viewing platforms (Iverson et al, 1998; Gómez-Fernández, 2000a; Sheridan et al, 2005;).

Another type of model that is emerging is that of an 'event tree' scheme to statistically estimate both long- and short-term volcanic hazard. The procedure is based on a Bayesian approach that produces a probability estimation of any possible event in which the researchers are interested in and can make use of all available information including theoretical models, historical and geological data, and monitoring observations. The 'event tree' structure accounts for external triggers (geothermal, seismic) as a source of volcanic unrest and looks at the hazard from different types of magma composition and different vent locations (as opposite to a central vent only) (e.g. Vesuvius, Italy, Marzocchi et al., 2008; Teide-Pico Viejo stratovolcanoes, Tenerife, Canary Islands, Martí et al., 2008b).

Models of volcanic processes are very useful to help identify hazardous areas where historical and geological records are sparse, or where investigations have not been conducted. In these circumstances the use of simulation codes has proved valuable. They are, however, limited by simplifications and incomplete understanding of the physics, and do not take over from the traditional approach.

The second stage of identifying volcanic risk is defining the vulnerability. The study of vulnerability related to natural disasters has been the focus of many different investigations and hence, of several definitions. Westgate and O'Keefe (1976) defined vulnerability as "the degree to which a community is at risk from the occurrence of extreme physical or natural

phenomena”, where risk refers to the probability of occurrence and the degree to which socio-economic and socio-political factors affect the community’s capacity to absorb and recover from extreme phenomena (Alcantara-Ayala, 2002). However, it is the definition of Blaike et al. (1994), which considers different factors affecting or producing the vulnerability of individuals or groups, which is most relevant. These authors identified vulnerability as “the characteristics of a person or group in terms of their capacity to anticipate, cope with, resist, and recover from the impact of a natural hazard. It involves a combination of factors that determine the degree to which someone’s life and livelihood is put at risk by a discrete and identifiable event in nature or society.”

Vulnerability varies from element to element and numerous factors can contribute which may include: houses, commercial and industrial buildings, and other infrastructure (roads, rail, bridges, airports, telecommunications, utilities etc.), crops and other economic activity (Figure 3). Whilst physical vulnerability encompasses the damage to goods and structures; societal vulnerability also plays a role in how at risk a community is from a volcanic hazard because it is the most vulnerable groups that find it hardest to reconstruct their livelihoods following disaster. The key characteristics of variations of impact include class, ethnicity, gender, disability, education and age (Blong, 2000).

Similar to the interaction of elements and processes displayed in Figure 3, Blaike et al., (1994) described the complex role of hazard, vulnerability and risk in a natural disaster by the pressure and release model (PAR) (Figure 4). In this model a natural disaster is described as the intersection of two opposing forces: those processes generating vulnerability on one side, versus physical exposure to the hazard on the other. *Root causes* are those that give rise to vulnerability and include economic, demographic and political processes. The root causes affect the allocation of resources and are connected to the functioning of the political state, which reflects the distribution of power in a society. *Dynamic pressures* are processes and activities that transform the effects of root causes into the vulnerability of unsafe conditions (e.g. rapid population growth and disease). *Unsafe conditions* are specific forms in which the vulnerability of population is expressed in time and space in conjunction with a hazard (e.g. people living in dangerous locations and being unable to afford safe housing). The PAR model encompasses many aspects of social vulnerability, but it provides little detail on how a hazard is related to the consequences.

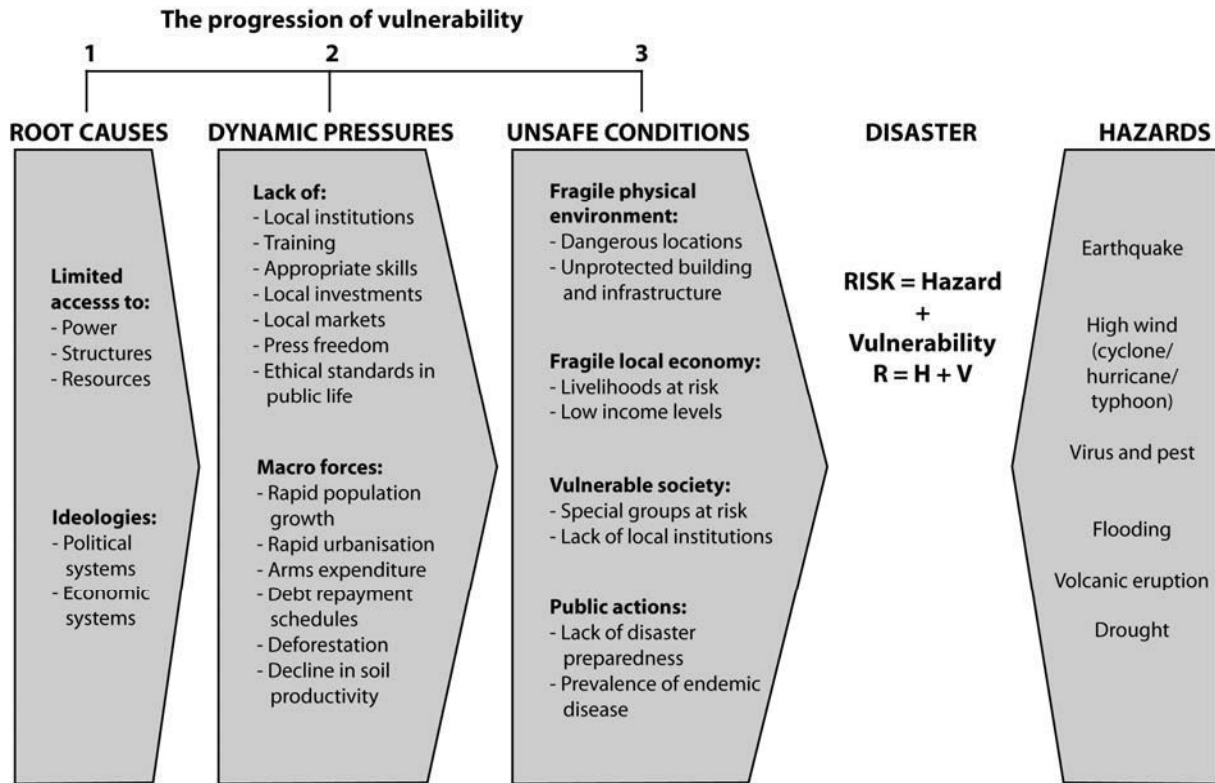


Figure 4: the Pressure and Release Model (PAR) as described by Blaike et al., (1994).

Vulnerability can therefore be defined as the susceptibility of an element due to a natural hazard to suffer different degrees of loss or amount of damage depending on its particular social, economic, cultural, physical and political weaknesses. Thus, in evaluating risk, vulnerability needs to be considered with at least the same degree of as importance that is devoted to understanding and addressing natural hazards. However, the combination of hazard analysis with a thorough consideration of vulnerable elements (i.e. risk analysis) is relatively rare (Blong, 2000).

Within the last decade, and particularly in the last five years, research into the impact of volcanic eruptions within the urban environment has become much more advanced. A summary of some of the key studies are presented in Table 3.

City	Hazard	Tools and methods	Results	References
Auckland, New Zealand	<ul style="list-style-type: none"> • Base surge • Lava fountain • Lava flow • Tephra 	<ul style="list-style-type: none"> • Probabilistic tephra dispersal: ASHFALL computer model • Geologic, meteorological and historic observations • Probabilistic Assessment of vent locations (cluster model and various statistics) 	<ul style="list-style-type: none"> • Isomass maps showing tephra fall dispersal and suggested hazards • Probable vent location • Preliminary geological and statistical assessment of risk 	Johnston (1998); Newnham et al. (1999), Wilson & Stirling (2002), Magill & Blong (2005a,b)
Naples, Italy	<ul style="list-style-type: none"> • Tephra • Pyroclastic flows • Tsunamis • Volcanic earthquakes 	<ul style="list-style-type: none"> • Building stock field survey • Analytical and experimental tests • Computer model for simulation runs 	<ul style="list-style-type: none"> • Physical impact of explosive eruptions on urban setting • Human casualty rate and building vulnerability • Structural resistance of buildings 	Barberi et al. (1990), Luongo et al., (2003), Spence et al., (2004a,b), Baxter et al., (2008), Neri et al. (2008)
Sao Miguel, the Azores	<ul style="list-style-type: none"> • Tephra • Volcanic earthquakes • Bombs • Pyroclastic-surges/flows 	<ul style="list-style-type: none"> • Field survey: type, condition and damage • Calculations on force on buildings except for lahars • Vulnerability analysis of hazards 	<ul style="list-style-type: none"> • Effects of hazards on buildings/people (casualties) • Risk map of island from effects of hazard on building • Methods to reduce the hazard impact 	Baxter et al. (1999), Dibben & Chester (1999), Jones et al. (1999), Pomonis et al. (1999)
Rabaul, Papa New Guinea	<ul style="list-style-type: none"> • Tephra 	<ul style="list-style-type: none"> • Building stock survey • Calculations on tephra loads and strengths of buildings 	<ul style="list-style-type: none"> • Index and categorization of building damage from tephra loads 	Blong, (1994), Blong et al., (2003)
Douala, Buea, Goma, and Limbe, Cameroon	<ul style="list-style-type: none"> • Tephra • Pyroclastic flows • Lava flows • Lahar (small part) • Landslides • Tsunamis 	<ul style="list-style-type: none"> • Identify different hazard components • Elaborate threat matrix by crossing intensity and frequency indices • Mapping the hazards and exposed elements • Vulnerability and risk analysis 	<ul style="list-style-type: none"> • Geological hazard zoning • Qualitative and quantitative inventory of elements at risk • Five risk zoning maps – population, elements at risk, buildings, agriculture, and native environment 	Léone (1995), Kouokam (2001), Thierry et al., (2007)

Table 3: Summary of key vulnerability and risk assessments undertaken at volcanoes world-wide.

The most studied urban areas is the city of Naples (Aspinall et al. 2003; Baxter et al. 2005, 2008; Neri et al., 2008; Spence et al. 2004a,b, 2005a,b; Zuccaro et al. 2008) where a population of nearly one million it is located within 9 km of Mount Vesuvius – best known

for its AD 79 eruption that led to the destruction of Pompeii and Herculaneum. Detailed studies of past eruptions and their products, an event tree and its emergency scenarios, deterministic and probabilistic numerical modelling of pyroclastic density currents and tephra fallout, a database on the built environment, and the mapping of modelled impacts on the buildings and infrastructure, with consequent hypothetical casualties, have been used to develop methods for quantifying risk in case of future explosive eruptions of Vesuvius. Their research utilises an evidence-based and multi-disciplinary approach to decision making adopting formal probabilistic reasoning and statistical decision analysis. Following this research some of these methods have been applied to Teide (Tenerife; Martí et al., 2008) and La Soufrière (Guadeloupe; Spence et al., 2008).

Other studies, as highlighted in Table 3, have concentrated principally on the effects of tephra and pyroclastic flows. Yet, given the evidence from the literature presented in this chapter concerning the destructive nature of lahars and evidence of these impacts such as at Herculaneum (Italy, AD79) and Armero (Colombia, 1985), the consequences for buildings and infrastructure from lahars appears not to have been rigorously examined. Furthermore, good data sets detailing building damage following lahars have not been collected. This lack of information stands in stark contrast to the wealth of data on building damage due to earthquake ground shaking (e.g. Leger and Tremblay, 2009) and the substantial volumes of data on flood (e.g. Kelman and Spence, 2004) and coastal damage (e.g. Reese and Markau, 2002).

Developments have also taken place to account for socio-economic factors in vulnerability and risk assessment – for example at Cotopaxi and Quito (Ecuador; D'Ercole and Metzger, 2004), Mt. Pinatubo (Philippines; Léone and Gaillard, 1999), Ubinas and El Misti (Peru; Degg and Chester, 2005). However, few studies combine results based on traditional geological hazard studies, numerical simulations, regional databases (e.g. on dwellings, land-use, infrastructure), and geotechnical tests on building materials (in situ and laboratory). Only a small number of studies then integrate these results with an analysis of socio-economic vulnerability factors (e.g. Magill and Blong, 2005a,b; Spence et al., 2005a,b).

Volcanic mass flows (lahars, hyperconcentrated flows, flash floods and debris flows) represent destructive and dangerous phenomena which warrant further study in a vulnerability framework. At present, there is lack of studies into the effect of lahars in dense urban

environments - a very real threat for many cities worldwide situated in the vicinity of an active volcano. Furthermore, this impact is greater in developing countries due to the geographical location of urban areas in zones highly susceptible to natural hazards (natural vulnerability), but also due to the various types of economic, social, political and cultural vulnerabilities that exist. As a result of this significant gap in current research an encompassing research project is presented, which takes into account the physical impacts of lahars on the built environment within a developing country.

Much like the city of Naples is to Mt. Vesuvius, Arequipa (southern Peru), with a population of nearly 1 million, is located approximately 17 km SW of El Misti Volcano with suburbs extending as close as 9 km to the summit. El Misti's last major eruption occurred 550 years ago, with smaller eruptions occurring during 17th and 18th centuries. In addition to geological studies identifying lahar volumes ranging from $0.01 \times 10^6 \text{ m}^3$ to $11 \times 10^6 \text{ m}^3$, floods have occurred historically (on average every 10 years) in the Río Chili and Quebradas (Thouret et al., 2001). Previous workers (e.g., Thouret et al., 2001, Delaite et al., 2005; Stinton et al., 2004a; Vargas et al., 2010) have indicated that any volcanic crisis at El Misti volcano will pose a serious threat to the city of Arequipa. Continued development on the volcano's flanks and radial valleys, places an increasing number of the city's population at great risk from explosive activity and mass flows. It is therefore imperative that the risk to Arequipa City from volcanic mass flows be identified.

The purpose of this research is to develop methods to assess the vulnerability of buildings and infrastructure to damage from lahars, hyperconcentrated flows and flash floods. It is anticipated that the methods developed here could be transferable to other volcanoes. Details of this research project are described in the following sections.

Thesis aims and objectives

The main aim of this research project is to develop a method for assessing hazards and risks from volcanic mass flows (lahars, debris flows and hyperconcentrated streamflows) within an urban environment, using the case study of Arequipa and El Misti volcano in Southern Peru. Reaching this aim will aid in the improvement of techniques and tools used in the mitigation of volcanic mass flows. The aim will be achieved by fulfilling the following objectives:

- To model mass flow hazards in Arequipa through the simulation code Titan2D, using a newly enhanced digital elevation model created from Differential Global Positioning System (DGPS) surveys and satellite data.
- To derive mass flow hazard scenarios for the study areas using the simulation code Titan2D and statistically-derived data from previous geological studies.
- To analyse the sensitivity of derived hazard scenarios to the selected model input parameters, such as initial flow properties (volume, sediment-water ratio, internal friction, basal friction, etc), and also to DEM accuracy and resolution.
- To determine the flow effects on building and infrastructure derived from the characteristics of materials collected during surveying, and from geotechnical testing.
- To define the physical vulnerability of elements within cities exposed to risk such as residential and commercial buildings, medical facilities, transport links, and power supplies.
- To prepare a GIS database containing data and information relevant to the generation of lahar hazard and corresponding risk assessment within the study areas. The risk assessment will consider the direct risk to buildings, agriculture, and infrastructure. The risk assessment to the population and quantification of economic losses are outside the scope of this research project.
- To convey knowledge about prevention and risk management at departmental and municipal level, and to display the results using databases, maps, plans, and interactive models.

These objectives are pivotal in achieving the research aim as shown by the following Figure 5.

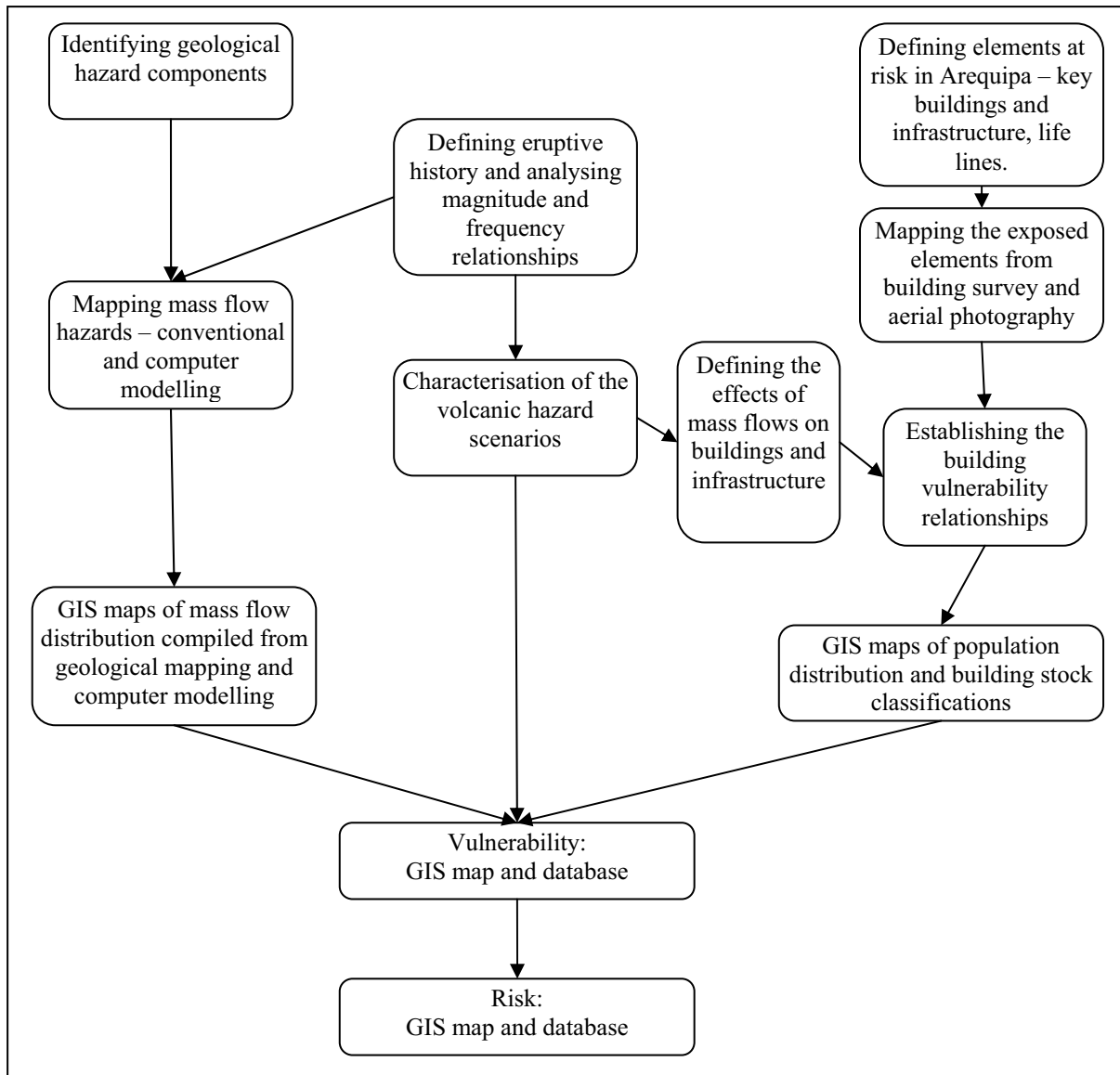


Figure 5: An outline of the processes undertaken to construct a quantitative vulnerability and risk assessment of the city of Arequipa facing volcanic and non-volcanic mass flow hazards.

Firstly, the geological hazard components must be identified using geological studies (Thouret et al. 1999b, 2001), followed by establishment of the eruptive history including magnitude and frequency relationships. The resulting information, along with flow modelling data, is used to characterise volcanic hazard scenarios and to map the volcanic and non-volcanic hazards that potentially affect Arequipa. Identifying the elements at risk is a key part of the research. Distribution of elements at risk combined with geological flow data, hazard scenarios, and the physical effects of flows on structures form the basis for the GIS maps, which in turn are used to form vulnerability and risk assessment for Arequipa.

Case study: Arequipa in south Peru – a large city in the shadow of the active El Misti volcano

Arequipa is the second largest city in Peru, with a population exceeding 860,000, and resembles the city of Naples in Italy, where at least 600,000 and up to 3 million people are exposed to Vesuvius volcanic activity (the number of population affected depends on the eruption type). Arequipa has experienced rapid population growth since the 1940s, after which population multiplied by a factor of 5. From 1970 onwards the urban area grew due to social unrest and related migration from poor rural areas. In 45 years (1970-2005) the built up area grew from 13 km² to roughly 60 km². The current extension of the city's built up area is 400% larger than it was in the 1960's.

Settlements have now expanded onto the southwest flank of the volcano, the Río Chili Valley terraces and on terraces or fans adjacent to tributaries within 9 km of El Misti summit (Figure 6). The small town of Chiguata is located on the Southern flank of the volcano, where 3,000 people live at 11 km from the summit. With the city expanding into more hazardous prone areas it is necessary to assess the vulnerability of buildings and infrastructure in response to the threat posed from volcanic mass flows. Herein follows a short summary of the geologic setting of the case study area; further results, discussion and analysis can be found in Chapter 2.

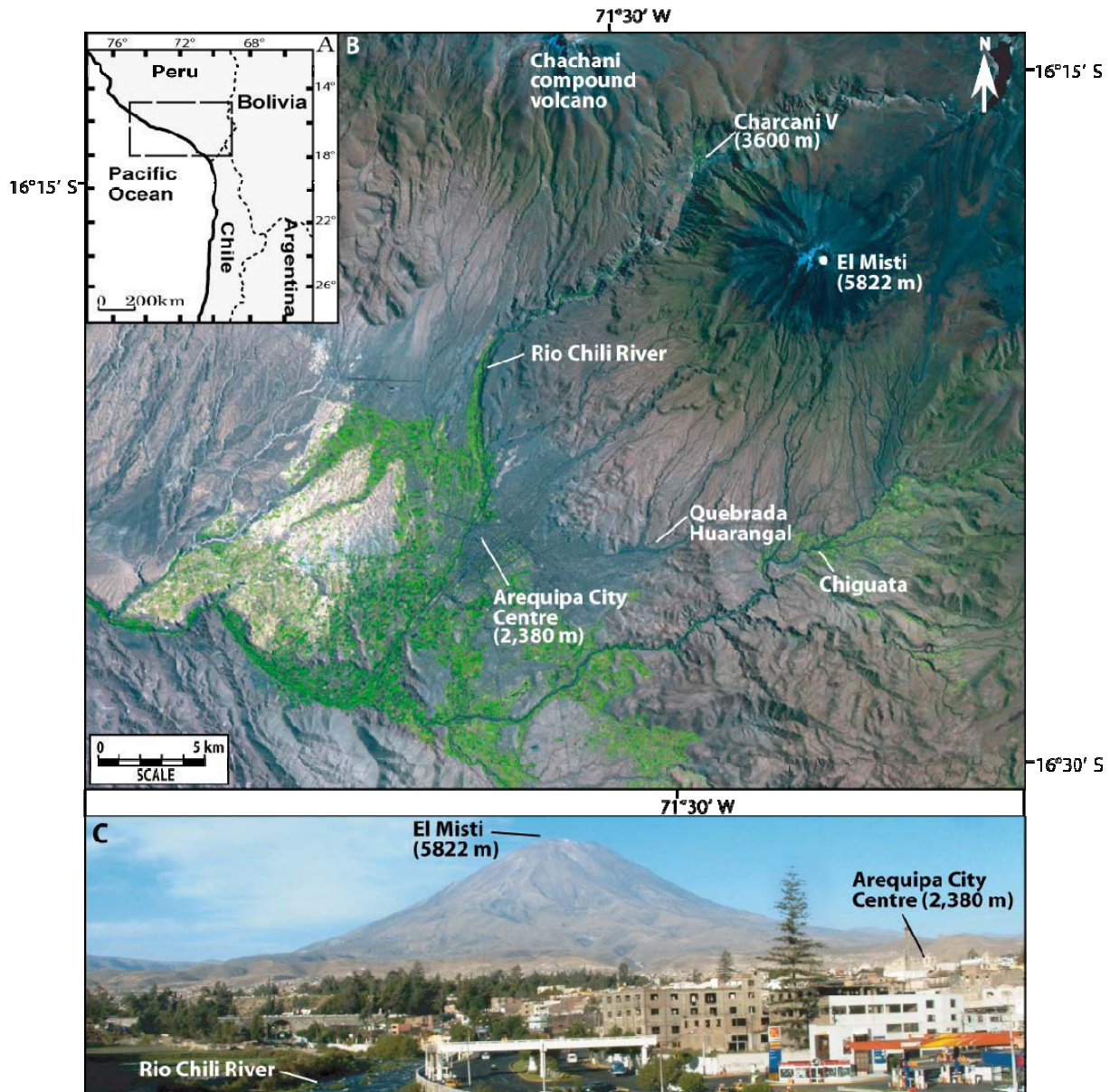


Figure 6 (A): The locality of the study area in South America and in southern Peru. **(B)** Arequipa is situated approximately 17 km the SW of the active El Misti volcano. Increasing population growth has resulted in urban sprawl on the flanks of the volcano and in radial valleys. **(C)** El Misti as viewed from the city centre area of Arequipa adjacent to the Río Chili.

The Andes extends 6000 km from north to southernmost South America and is the result of the subduction of the Nazca oceanic plate under the continental South American plate; a tectonic setting responsible for the seismicity and volcanic activity that affects western South America (Figure 7). Andean volcanism is divided into three active provinces: the Northern Volcanic Zone (NVZ), the Central Volcanic Zone (CVZ) and the Southern Volcanic Zone (SVZ). In Peru, the active volcanic front is located 200 km east of the Peru-Chile trench, and the volcanoes lie on a trench-parallel trend oblique to the E-W convergence. Within the CVZ,

Peru has eight active volcanoes in the Plio-Quaternary volcanic chain: Nevado Sara Sara, Nevado Sabancaya, El Misti, Ubinas, Huaynaputina, Tiscani, Tutupaca and Yucamane (de Silva et al., 2000).

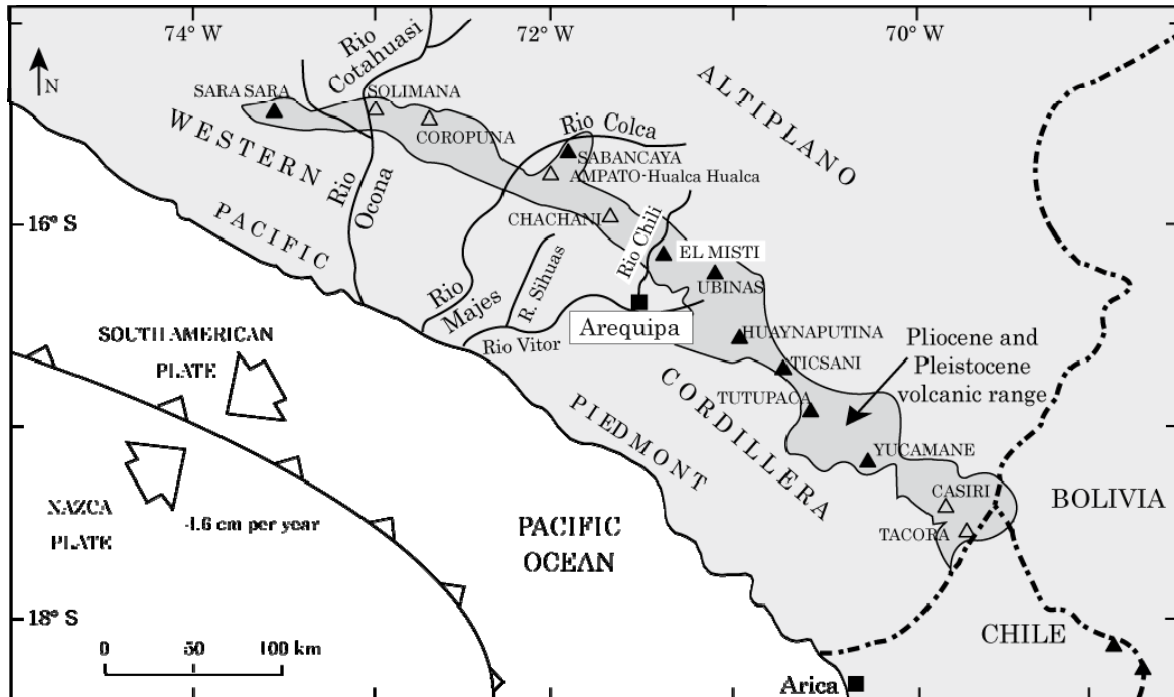


Figure 7: Geological setting of the study area highlighting the plate boundary to the west of the Peruvian coastline and the resulting Plio-Quaternary volcanic chain – active volcanoes are shown with black triangles. Adapted from Thouret et al., (2001).

El Misti is one of the eight active volcanoes within the CVZ; the summit (5824 m amsl.) of which is located 3500 m higher than, and at a distance of only 17 km from the city of Arequipa. El Misti belongs to a group of three volcanoes (with Chachani to the West and Pichu Pichu to the East) which surround the area of Arequipa and its suburbs to the SW as well as Chiguata to the S. The eruptive history of El Misti volcano has been studied by several authors (e.g. Legros, 2001; Delaite et al., 2005; Thouret et al., 1999, 2001). The stratigraphy of the deposits and maps of erupted products have shown that tephra falls, lahars, pyroclastic flows and debris avalanches underlie the entire city area. It can be inferred therefore, that similar hazards would almost certainly affect Arequipa during future eruptions.

El Misti's eruptive behaviour has been established from the eruptive history of the volcano and from the statistical analysis of dated deposits (Figure 8). A ca. 833,000 year-long evolution of the composite edifice in four stages termed Misti 1 through 4 has been recognised (Thouret et

al. 2001; Finizola et al., 2004). Misti 1 and Misti 2 stratocones (833-110 ka) mainly consist of voluminous lava flows with some pyroclastic debris. Pleistocene lava flows of Misti 1 flowed up to 11 km from the vents towards Arequipa. Non-welded dacitic ignimbrites (bulk volume of 4-6.5 km³) resulted from explosive eruptions on Misti 3 that formed large craters, or nested calderas, between 40,000 and 34,000 yr BP. Repeated episodes of growth and destruction of lava domes triggered dome-collapse avalanches and block-and-ash flows, including pyroclastic surges. The dome-building episodes alternated with sub-Plinian eruptions, the tall columns of which collapsed and generated pyroclastic flows. A summit caldera formed between 13,000 and 11,000 years. Misti 4, the most recent summit cone, formed and was active over the Holocene with several tephra falls, and pyroclastic flows and debris flows. Some thick pumice falls were produced by plinian or subplinian eruptions. Within the summit caldera, two nested craters encompass the largest (c.900 m wide) vent attributed to the 2050 yr old-eruption and the smaller vent (250 m deep and c.400 m wide) formed by the 15th century old eruption, and capped by a fumarolic plug today.

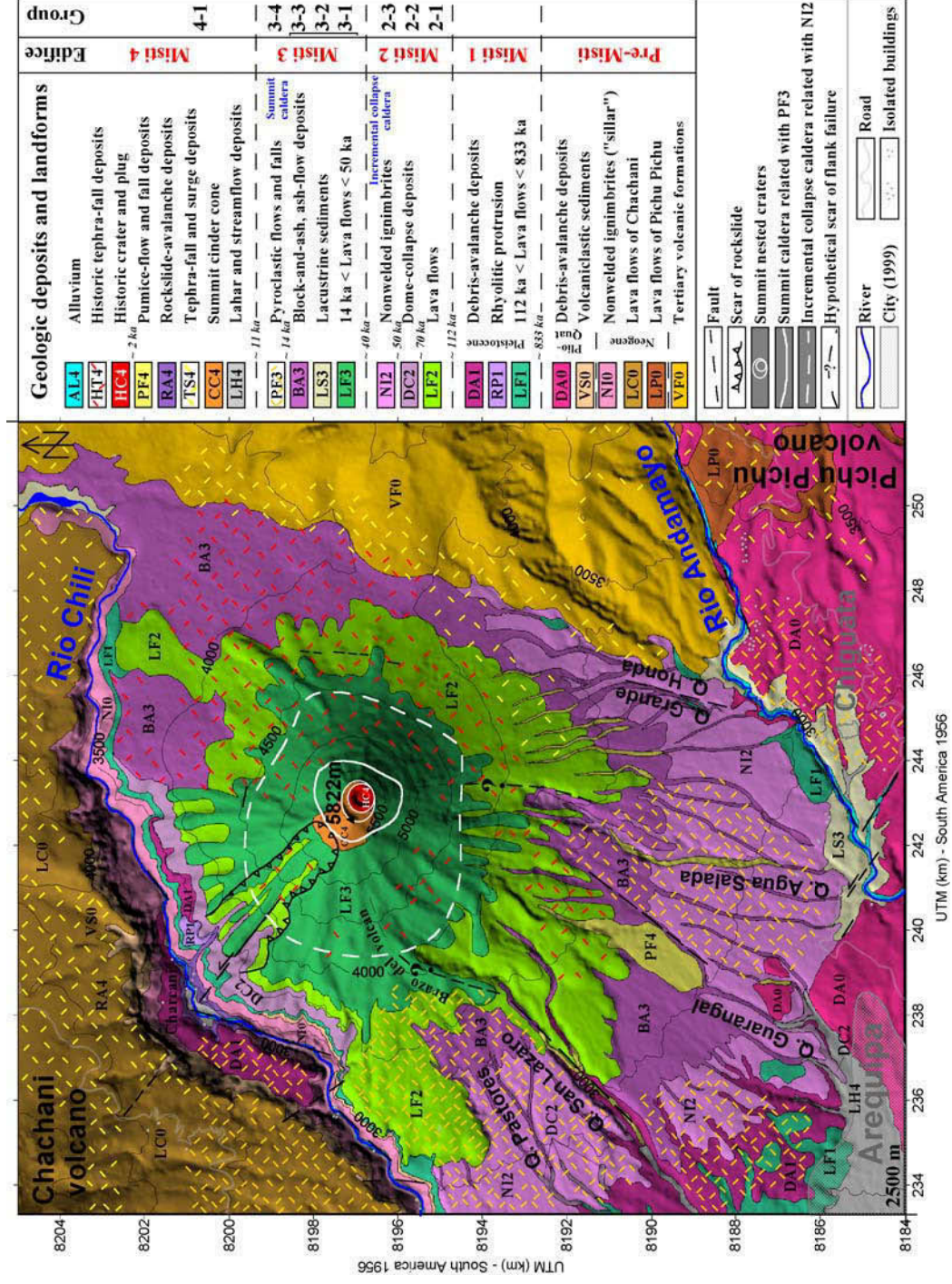


Figure 8: Geological map of El Misti volcano indicating the different stages of growth from pre-Misti to the most recent edifice, Misti 4 (Thouret, et al., 2001).

The last sub-Plinian explosive episode occurred ca. 2030 yr BP (400 BC-340 AD) and produced pumice-fall and flow deposits $\geq 1.24 \text{ km}^3$ in bulk volume. The last eruption occurred AD 1440-1470 (an andesitic plug is still visible in the small crater), and phreatic events were reported in 1677, 1784, and 1787 (Chávez, Chávez 1992; Simkin and Siebert, 1994). The small AD 1440-1470 eruptive episode produced about $6 \times 10^6 \text{ m}^3$ of ashfall deposit that was directed towards the SW and to the North. Persistent, high-temperature fumarolic activity occurs today on the plug inside the youngest crater and on the summit east flank.

Based on the eruptive history and behaviour of Misti 2, 3 and 4 over the past $\sim 110 \text{ ka}$ the pattern of activity has evolved significantly and can be grouped into one of five eruption types (Thouret et al., 2001):

1. Ignimbrite-forming eruptions generated pyroclastic flows of several km^3 (bulk volume) every 10,000 to 20,000 years on average;
2. Growth and destruction of domes generated dome-collapse avalanches and block-and-ash flows occurred several times during the eruptive episodes between 50,000 and 11,000 yr BP;
3. Subplinian eruptions produced pumice-rich flows and fall deposits less than 1 km^3 in volume every 1500 to 5000 years;
4. Vulcanian and phreatomagmatic eruptions produced small-volume ashfall, scoria-flow, and ash-flow deposits at 300 to 1000 year intervals;
5. Lava flows have been produced at El Misti with a large volume and frequency between 110 and 50 ka.

Primary (eruption triggered) and secondary (rain-triggered) lahars have frequently occurred during the Holocene and historical time, even without eruption. For example, lahars swept down the Río Chili valley and its tributaries 1,035 years, 520 years, and 340 years ago. The older flows were likely triggered by melt water generated by pyroclastic debris that flowed over the summit snowfield (an area of $1\text{-}7 \text{ km}^2$ between January and August). The volume of melt water produced this way may be $\sim 2.5 \times 10^6 \text{ m}^3$ and the volume of the channelled debris flows varies from $\sim 5 \times 10^6 \text{ m}^3$ to a maximum of $11 \times 10^6 \text{ m}^3$ (Vargas et al., 2010). The lahar volumes used are based on: the estimated volume of Holocene lahar deposits surrounding El Misti; the approximate amount of material which can be mobilized in channels; rainfall threshold of at least 10 mm per hour (e.g. February 1997), and surface area of the seasonal

(December – July) snowfield on the volcano summit (1 to 4 km², up to 7 km² in case of heavy snowfall) (Vargas et al., 2010).

Hyperconcentrated streamflows also sweep down the five tributaries which cross the city of Arequipa on a 10-year return interval (Nagata, 1999). These narrow ravines are known locally as *quebrada* and remain dry for 6 to 9 months a year, but feature occasional torrential streams. On 25 February 1997 flash floods triggered by approximately 33 mm of rainfall during a three-hour period, transformed into hyperconcentrated streamflows and claimed three victims in the Quebrada Mariano Melgar. About 5 km upstream from Arequipa, a mud-line 10 m high on the walls of the entrance of the Río Chili canyon resulted from a historical flood which deposited metre-scale boulders resting on the low terrace situated 4 m above the present channel.

Large-volume pyroclastic flows triggered lahars distances as far as 10 km from the summit and through the dry valleys across Arequipa and at least 25 km down valley beyond the city in the main Río Chili channel. Near Uchumayo (25 km SW of Arequipa), a 5m thick debris-flow deposit overlies a 10 cm pumice-fall deposit that mantles the middle terrace on the left bank, 15 m above the channel. The coarse ash matrix, rich in pumice, and the underlying tephra-fall layer link this debris flow to a distal ignimbrite, which may be correlated with one of the events of Misti 4 (13,700–11,300 years ago). Closer to Arequipa, a 2 m-thick lahar deposit in Quebrada San Lazaro directly overlies the ca. 2030 yr BP-old pumice fall which covers the low terrace. The lahar must have been derived from the ca. 2030 yr BP-old pyroclastic-flow deposits because it can be traced from the front of these deposits at 2800 m asl (9 km from El Misti's summit) toward the city of Arequipa at 2600 m asl – 3 km down valley (an area which is now populated).

Proposed Eruption Scenarios for El Misti

Three eruption scenarios have been proposed by Delaite et al. (2005) and Thouret et al. (1999, 2001) based on three magnitude/frequency events recognized in the recent history of El Misti:

1. A low-magnitude (VEI 2) / high frequency (500 to 1500 years) eruption such as the AD 1440-1470 vulcanian events;
2. A moderate magnitude (VEI 3) and frequency (1600 to 5000 years) eruption such as the ca. 2030 yr BP-old sub-Plinian explosive episode;

3. A maximum probable eruption resembling the 34,000-30,000 year-old or the 13,000-11,000 year-old ignimbrite-forming eruptive episodes (VEI 3-4) with a low frequency of 10,000 to 20,000 years.

The first eruption scenario (Figure 9) represents the most probable future type of activity at El Misti, based upon low magnitude but high frequency events, modelled on the mid 1400's eruption at El Misti. The effects of such an eruption would resemble those caused by the two most recent events in Peru nearby Arequipa: the 1990-1998 vulcanian and phreatomagmatic activity at Nevado Sabancaya, 70 km NW of Arequipa (Gerbe and Thouret, 2004) and the 2006-2009 eruption of Ubinas, 65 km East of Arequipa (Rivera et al., 2010). Ash falls up to 5 cm thick could be expected in the city of Arequipa from low elevation eruption plumes 3 to 4 km above the vent. Based on the dispersal pattern of the mid 1400's tephra (Thouret et al., 2001), ash falls occurred to the N, the W, and the SW of the cone within a 30 km distance. Prevailing winds 3 to 4 km above the vent would disperse tephra from low columns preferentially toward the NE should the eruption occur during summer, winter and spring, or towards the W should the event happen at autumn. The airport (approximately 12 km WSW of the vent) is likely to be affected by ash fall even in the case of a small-scale eruption.

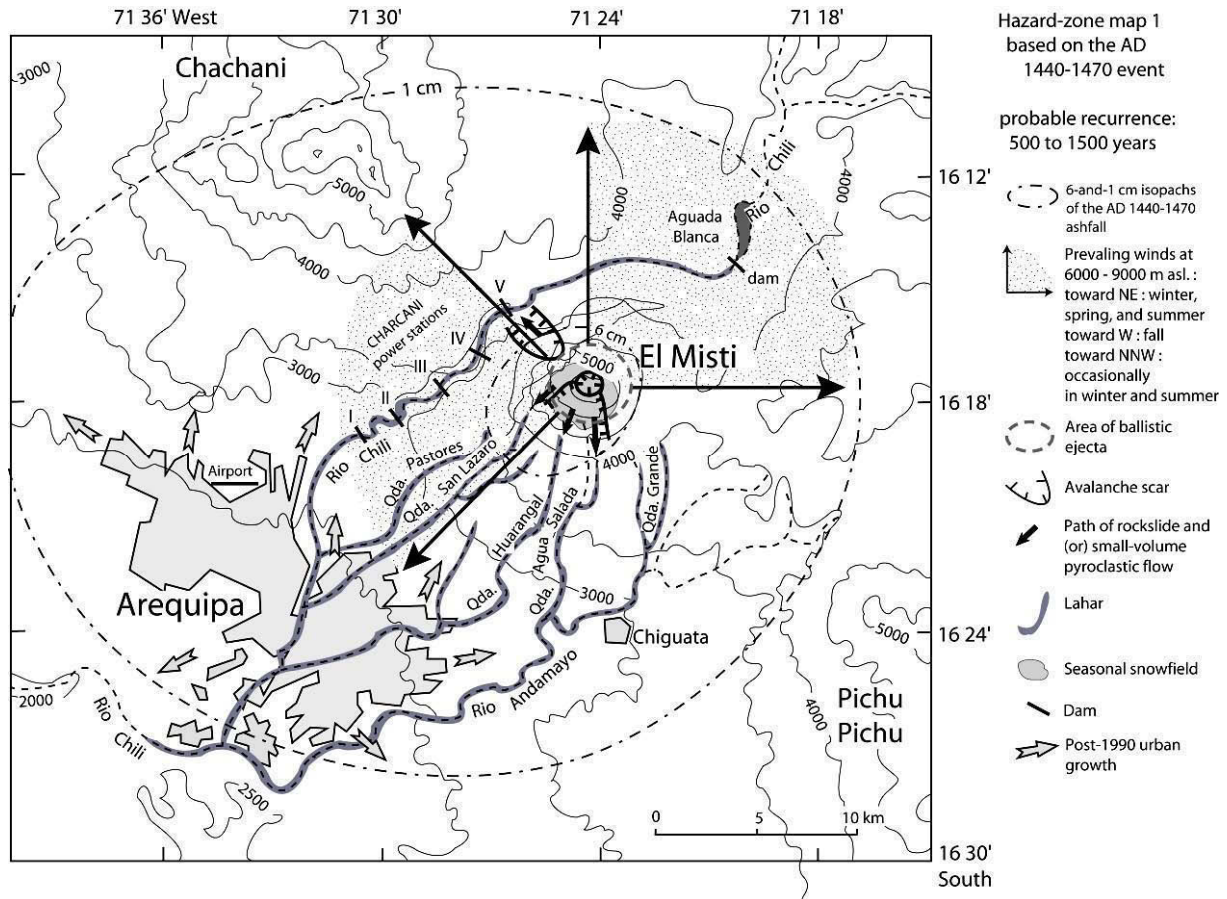


Figure 9: The first eruption scenario based on the AD 1440-1470 vulcanian event with a recurrence interval of 500-1500 years. Even with a small event such as this lahars would be channelled through the city (e.g. Río Chili, Qda. Pastores, and Qda. Huarangal) (Thouret et al., 2001; Delaite et al., 2005).

An area of approximately 3 km in diameter is likely to be mantled by ballistic ejecta due to the disruption of the andesitic plug during this scenario. Phreatomagmatic events may contribute to destabilise the fractured and hydrothermally-altered south rim of the larger crater. Because a 1 km-wide and 4 km-long scar cuts the loosely consolidated material that forms the west flank of the summit (Figures 8 and 9), a consequent rockslide avalanche could dam the Río Chili canyon, where five power stations are located only 5 - 7 km to the W and WSW and 2.8 km below the summit. Dammed-lake breakouts could be destructive down valley toward Arequipa.

Another hazard to consider is the formation of lahars during and shortly after the eruption. The ca. 330, 520, and 1035 yr BP-old lahar deposits that mantle the two lowermost Río Chili terraces represent this phenomenon. Although as little as 100 - 250 mm of rain falls per year in the Arequipa depression, larger rainstorms do occur from December to March higher up in the catchments at 3500 - 5800 m amsl. Lahars triggered by snow melt water could bulk loose

pyroclastic debris both on the bare slopes and in the channels down-valley. Debris flows could also form without an eruption when summer rainstorm-induced runoff incorporates volcanic debris from the stream channels.

The second eruption scenario (Figure 10) is based on the ca. 2030 yr BP (400 BC - AD 340) old sub-Plinian explosive episode. Past events of this type had a relatively moderate magnitude (VEI 3, volume c. 1.3 km^3) and have occurred with a 1600 to 5000 year frequency. One of the major hazards is brought about by the impact of pumice and ash fall load on buildings. This can be seen in 50- and 10-cm isopachs in Figure 10, which show the distribution pattern of the ~2030 yr BP pumice-fall deposit in Arequipa. Prevailing winds during winter and spring would disperse ash and lapilli from 9-20 km-high eruption columns toward the SW. Occasional winds could carry ash toward the W and WSW during autumn and toward the SE during winter and summer. As a result, the airport traffic probably would be engulfed within the 10-cm isopach.

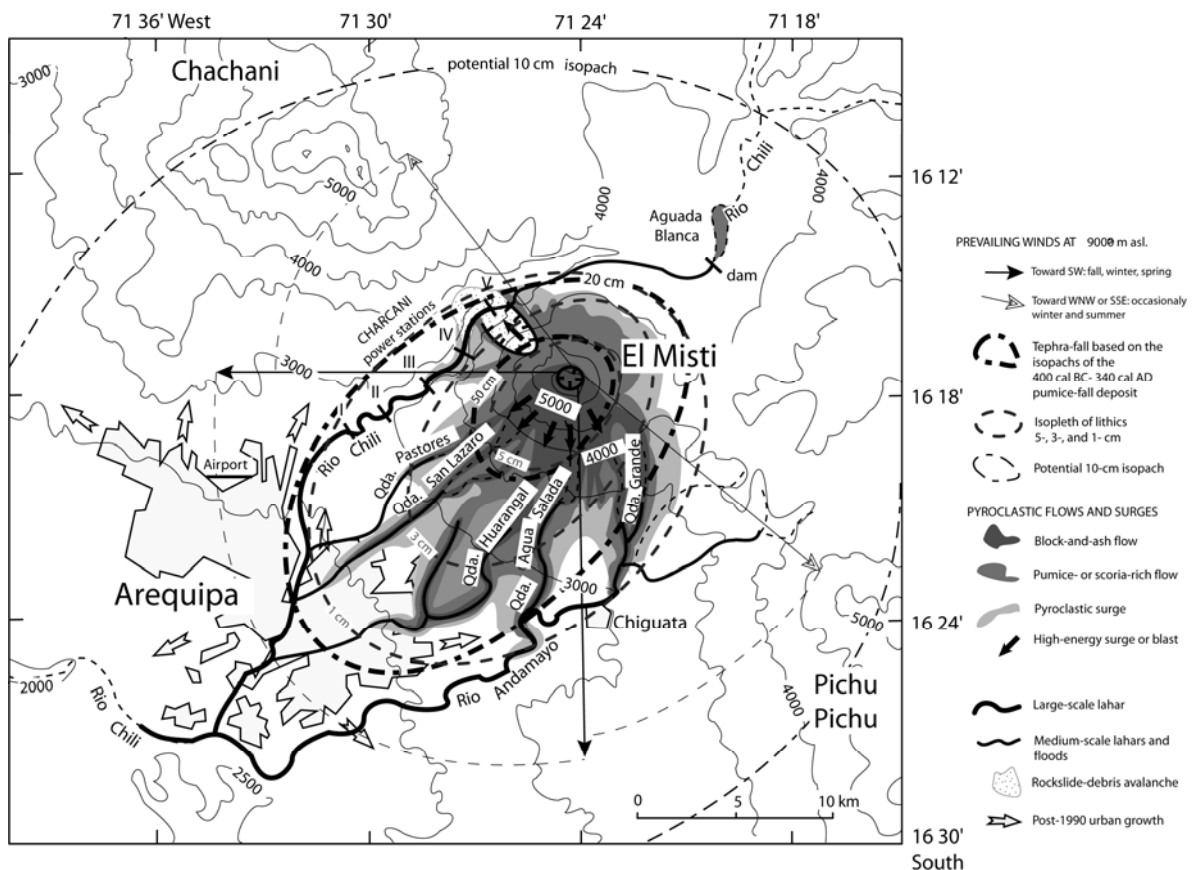


Figure 10: Hazard scenario 2 which is based on the 400 BC – 340 AD eruptive episode, with a probable recurrence interval of 1600 – 5000 years. Large-scale lahars would flow in all drainage channels radiating the volcano (from Thouret et al., 2001; Delaite et al., 2005).

The expected direction of future pyroclastic flows is toward the south, owing to the breached rim of the largest crater above the steep south flank. Should a growing dome overtop the youngest crater rim, block-and-ash flows would spill over the steep slopes of the summit cone and be channelled as far as 6-10 km from the vent area. Such activity would primarily affect the town of Chiguata and farms nearby, as there is evidence of a surge deposit of at least 0.5 m thick 11 km from the vent, 0.5 km before the western entrance of the town of Chiguata and the NE suburbs of Arequipa (Figure 10). Collapse of sub-Plinian eruption columns could produce pumice flows that would travel 10-12 km towards the south, southwest and southeast. Despite their small to moderate volume, pyroclastic flows at Misti acquire a high momentum due to the H/L ratio (2.4 km height versus 6 km distance between the volcano summit and the break-in-slope on the ring plain). Such a momentum provides a long run out distance of 11-13 km, exceeding that usually observed at composite cones (Delaite, 2003).

Rockslide avalanches could occur on the southern and western flanks towards the 0.5 – 1.5 km deep Río Chili valley. Lahars and stream flows have swept down the radial valleys in all directions over the past centuries, as shown by the 1400's, the 1600's, 1035 yr BP and 2090 yr BP-old debris-flow deposits in the Río Chili valley and Quebrada San Lazaro (Figures 6 and 10). New suburbs of Arequipa are spreading upstream in this area. Large-volume lahars in the Río Chili canyon might result from rockslide debris avalanches and dammed-lake breakouts if the steep-sided, unstable west flank were to fail above the major power station at Charcani Grande and the subsequent five dams down-valley.

The third eruption scenario (Figure 11) portrays areas likely to be affected by Plinian and ignimbrite-forming eruptions (VEI 3-5) similar to events that occurred at El Misti 34,000-33,000 yr BP and 13,650-11,280 yr BP. Large-scale eruptions may recur every 10,000 to 20,000 years on average (Thouret et al., 2001). This scenario includes a 10 to 25 km-high Plinian eruption column that would cover the city and surrounding area with at least 50 cm of pumice-fall deposit over the city area and beyond (Figure 11). Arequipa airport, the third largest passenger platform in Peru and a critical link for tourism in southern Peru is likely to be severely damaged by a Plinian pumice-fall deposit of only a few decimetres thick. The prevailing seasonal winds would carry aloft the ash for at least 100 km toward the W and SW in winter and spring, and toward the NW and NE in summer. A radius of 25 km around El Misti is likely to be mantled by at least 10 cm of pumice lapilli. During the Plinian eruption of

Huaynaputina on 19-20 February 1600, 75 km ESE of Arequipa, the area was mantled with 20 to 25 cm, of which 7 to 12 cm of this white, dacitic ash layer was measured in 2000 within Arequipa city (Thouret et al., 2001). Pyroclastic flows, generated by column collapses, can sweep all flanks of the volcano and be channelled for 10 to 15 km along the Río Chili valley and tributaries, as shown by the 40,000 yr BP-old ignimbrite that is 10 m thick on the high Río Chili terrace, 10 km upstream from the city boundary.

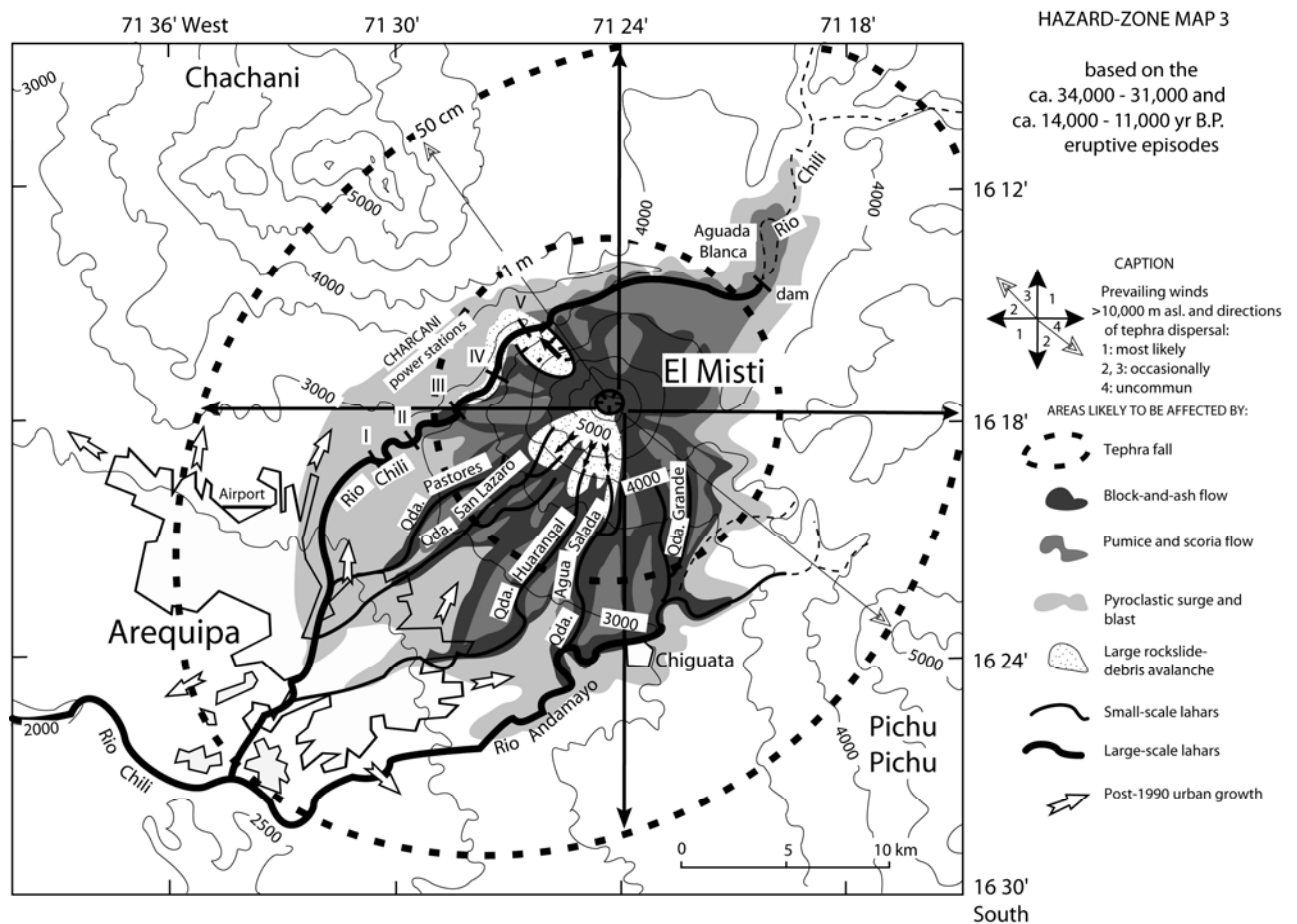


Figure 11: The largest eruption scenario proposed for El Misti (hazard-zone 3) based on the ca. 34,000 – 31,000 and ca. 14,000 to 11,000 yr B.P. eruptive episodes with probable recurrence of 10,000 to 20,000 years (from Thouret et al., 2001; Delaite et al., 2005).

Flank failures could trigger debris avalanches on the south and WNW flanks of El Misti. Resulting debris avalanches and lahars would choke the Río Chili valley and devastate the five power supply dams. Valleys would convey voluminous lahars triggered by rainstorms for several years after the eruption, in particular the Río Chili canyon. Not only would the five power stations be destroyed but also the large Aguada Blanca reservoir 6 km to the north, as well as the cultivated and populated Río Chili valley both to the north and south of the city. A

5 m-thick Holocene lahar deposit located 35 km from the summit that mantles the middle terrace of Río Chili near Uchumayo provides evidence of these voluminous lahars (Chapter 2).

The information above highlights the significant hazards, particularly of volcanic mass flows posed to Arequipa. Previous authors have studied the eruptive history of El Misti, defined the volcanic hazards and made progress towards a vulnerability and risk assessment of the city (e.g. Vargas et al. 2010). However, further research is necessary to precisely delineate areas that could be affected, to map the elements at risk and derive vulnerability functions defining the hazard levels and the magnitude of its impact upon those elements at risk. Another vital need is to evaluate the risks in Arequipa from volcanic mass flows in order to assist the authorities in managing urban development and to make decisions on prevention and elaborate emergency plans in case of disaster. This case-study of Arequipa presents an opportunity to research the effects of mass flows in the urban environment – a threat that is being faced in large cities at volcanoes world-wide (e.g. Kagoshima, Japan; Quito, Ecuador; Yogyakarta, Indonesia; Tacoma, USA; and Naples, Italy).

Study areas in Arequipa

On the basis of geological and geomorphological studies, Thouret et al. (2001) pointed out that the urban areas most likely to be inundated by pyroclastic flows and lahars are located along the Río Chili valley as well as two tributary catchments that originate on the upper slopes of the volcano and cross the centre of the city: Quebrada San Lazaro and Quebrada Huarangal. For this reason, and because a study of the whole city would be much too large for this study, three locations within two main areas, have been chosen as test sites for this case-study. The test sites are the Río Chili River valley (including a smaller study area of Charcani Quinto) and Quebrada Huarangal (Figure 12); discussed in more detail in Chapters 1 and 2.

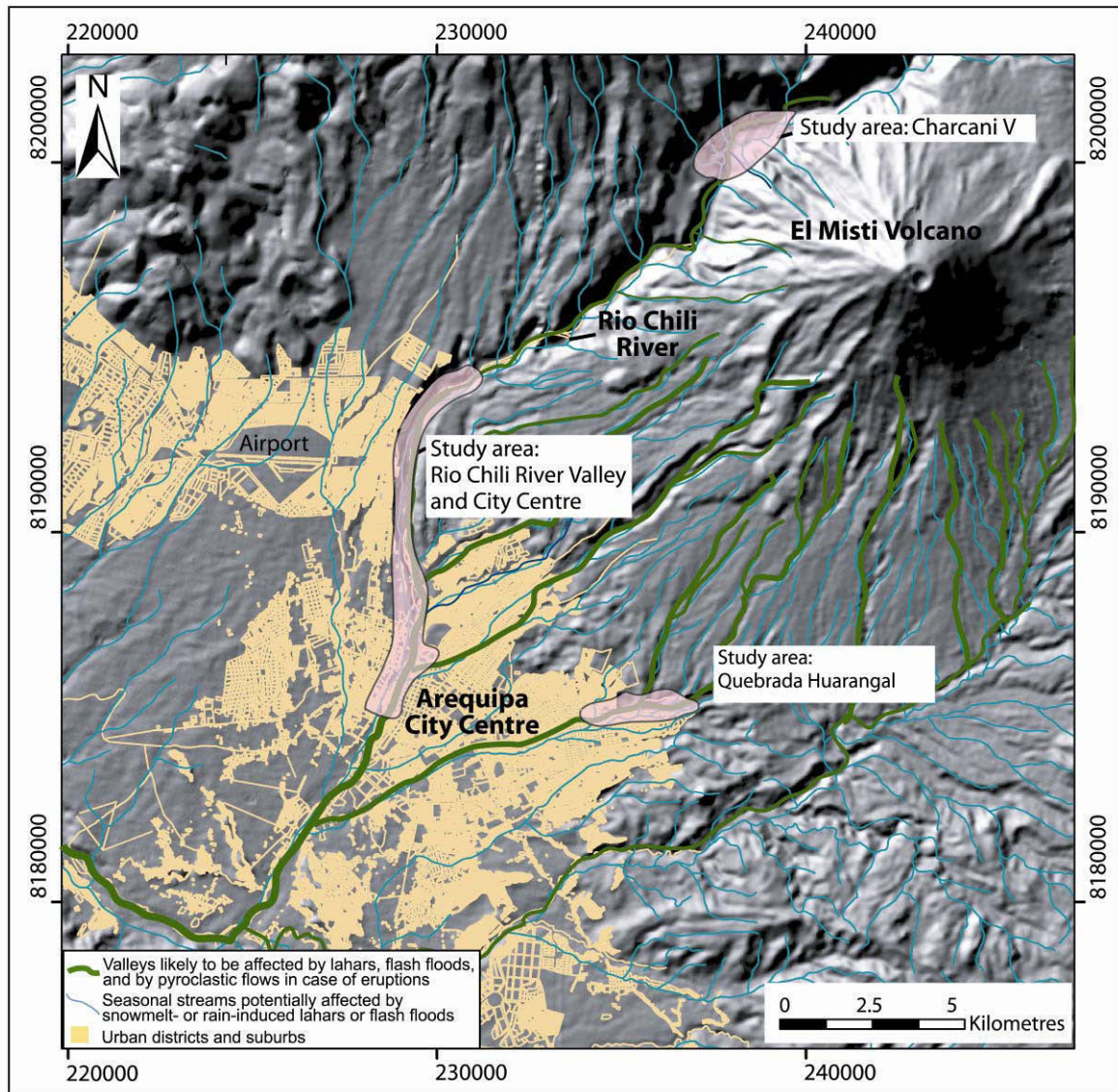


Figure 12: El Misti mass flow hazard-zone map showing areas likely to be affected by lahars and flash floods during eruptions, and seasonal streams potentially affected by snowmelt- or rainfall-induced lahars or flash floods (based on Thouret et al., 2001 and Delaite et al., 2005). Areas chosen for this project are highlighted.

Río Chili Valley

Arequipa city (founded in an oasis around AD 1540) is situated adjacent to the only perennial river, the Río Chili. Many lifelines and critical elements rely on the Río Chili, for example the river supplies the drinking water and hydroelectric power, and provides irrigation for agriculture. However, geological and historical evidence exists for the formation of mass flows within this river. In addition, there is geological evidence of a dammed lake in the upper Río Chili in the recent past (see chapter 2), which suggests the possibility of a dam-break flood scenario.

Quebrada Huarangal and its fan

The fan area along the Quebrada Huarangal is an area of rapidly population to the Northeast of the city centre. Pressure on land has resulted in an expansion of legal and illegal communities, comprising often low quality housing, being built within the Quebrada Huarangal. The Quebrada is dry for most of the year but can become a fast flowing, torrential stream during times of high rainfall. Construction within the channel (buildings, mining operations, channelization etc.) could impede and/or influence the flow path.

Thesis outline

This thesis consists of 5 chapters set out in 3 parts: Part 1. Setting and methods; Part 2. Lahars and flash floods within an urban environment; and Part 3. Vulnerability and risk within an urban setting.

Part 1 begins with the *Introduction*, followed by *Chapter 1* which outlines the methods and rationale used in this research project. *Part 2* consists of *Chapters 2* and *3*. The lahar and flash flood hazards of El Misti are discussed in *Chapter 2* with an analysis of the magnitude and frequency of events, and the elaboration of three hazard scenarios for Arequipa. The geophysical modelling of lahars using Titan2D is covered in *Chapter 3*, where the sensitivity of input parameters is explored and a new lahar hazard map for Arequipa is presented. *Part 3* focuses on vulnerability and risk in large cities on active volcanoes and begins with *Chapter 4*. This chapter focuses on the physical vulnerability of land use, buildings and infrastructure in Arequipa. *Chapter 5* is divided into 2 parts; the first part focuses on the physical effects of lahars and flash floods in the urban environment, and the second part combines the results in previous chapters to determine the physical vulnerability and risk to Arequipa. Finally, a discussion of the results of this project, and the implications for further research is presented in the conclusion.

Chapter One

Methods and Rationale

1.0 Introduction

Natural hazard, vulnerability and risk assessments have been well established for natural phenomena such as earthquakes, cyclones, floods, and more recently tsunamis. In contrast, for volcanoes there has been a lack of vulnerability studies on elements at risk and the incorporation of vulnerability is not well established in risk assessments (Glade, 2003; Douglas, 2007). However, in recent years, the EXPLORIS project (funded by the EU) has promoted vulnerability assessments, adapted from seismic and flood vulnerability studies, to be undertaken in volcanic and urban environment (e.g. Spence et al. 2005b; Baxter et al. 2008; Neri et al. 2008; Marzocchi et al. 2009; Sandri et al. 2009; Zuccaro et al. 2008). The impact of three volcanic phenomena – pyroclastic flows and surges, tephra fall and volcanic earthquakes, on the city of Naples from an eruption of Vesuvius was the main subject of their research, resulting in the development of a probabilistic dynamic model for the volcanic impact evaluation. The results of the EXPLORIS research has also been applied to Teide-Pico Viejo stratovolcanoes (Tenerife, Canary Islands) (e.g. Martí et al. 2008a, 2010). There remains a gap in vulnerability studies related to the physical effects of lahars and other volcanic mass flows in an urban environment. Volcanic mass flows including lahars, hyperconcentrated flows, and flash floods represent destructive and dangerous phenomena which warrant further study on the vulnerability framework of these events.

The case study of Arequipa, Peru, provides a good example for the study of the vulnerability of a large city in close proximity to an active volcano. Arequipa can be likened to the city of Naples, which is located in close proximity to Mt. Vesuvius. Both cities have a population exceeding 900,000 inhabitants, and both are located within 17 km of an active volcano. In Arequipa, rapid population growth and urban expansion of more than 400% in 50 years has led to poorly designed suburbs and illegal settlements, which have expanded onto the southwest flank of the volcano, the Río Chili terraces and adjacent to tributaries within 9 km of El Misti summit. Previous geological and historical studies, including the development of

three possible hazard scenarios, concluded that future eruptions of El Misti (even if moderate in magnitude) will pose a serious threat to Arequipa. It is therefore imperative that a comprehensive vulnerability assessment be undertaken (Thouret et al., 1999; Delaite et al., 2005; Vargas et al., 2010a). It is for these reasons that the case study of Arequipa is appealing for this research project.

Some of the previous research that has been undertaken on El Misti volcano includes: the volcanism of the region (e.g. Bullard, 1962); geochemistry and petrology of the deposits (e.g. Finizola, 2002; Ruprecht et al., 2004; Rivera, 2010); ignimbrite geochemistry and emplacement (e.g. Legros et al., 2001; Paquereau Lebti et al., 2006); volcanic landslide deposit emplacement from Pichu Pichu (e.g. Legros et al., 2000); the tephra stratigraphy (e.g. Legros, 2001); the geology and eruptive stages of El Misti (e.g. Thouret et al., 2001); interferometry analysis of the volcanic structure and fluid circulation (e.g. Finizola et al., 2004; Stevens et al., 2004); satellite analysis of volcanoes in Peru (e.g. Mering et al., 1996), volcanic tremors associated with the volcano (Lesage et al., 2002) and work undertaken by Peruvian colleagues at the Instituto Geofísico del Perú (IGP) and the Instituto Geológico Minero y Metalúrgico (INGEMMET).

More hazard based research conducted at El Misti Volcano includes: the social perception to volcanic hazards in Peru (e.g. Degg et al., 2005); volcanic hazard identification and assessment (e.g. Thouret et al., 2001; Nagata; 1999; Mariño et al., 2007) and lahar hazard and risk assessment (Stinton et al., 2004a; Delaite et al., 2005; Vargas et al. 2010a). Other studies that have been conducted in the region also add to a better understanding of volcanic processes and hazards that could be experienced at El Misti, some of which include: the eruption of Huaynaputina, 75 km east of Arequipa (e.g. Thouret et al., 1999a, 2002), Nevado Sabancaya (e.g. Gerbe and Thouret, 2004; Thouret et al., 2002) and Ubinas (e.g. Thouret et al., 2005; Rivera et al., 2010). The research into lahar hazard and risk assessment conducted by Stinton et al., (2004a), Delaite et al., (2005) and Vargas et al., (2010a), and the established geologic and historical history of the El Misti (in particular Thouret et al. 2001 and Legros, 2001) have provided the basis of this research project.

1.1 Selection of valleys to study in Arequipa

Three areas were chosen for this study (Figure 1.1): 1) the area around Charcani Quinto hydroelectric power station in the upper Río Chili canyon, 2) the Río Chili canyon from the opening of the canyon into cultivated terraces, to the southern boundary of the city and 3) the Quebrada Huarangal fan to the east of the city centre.

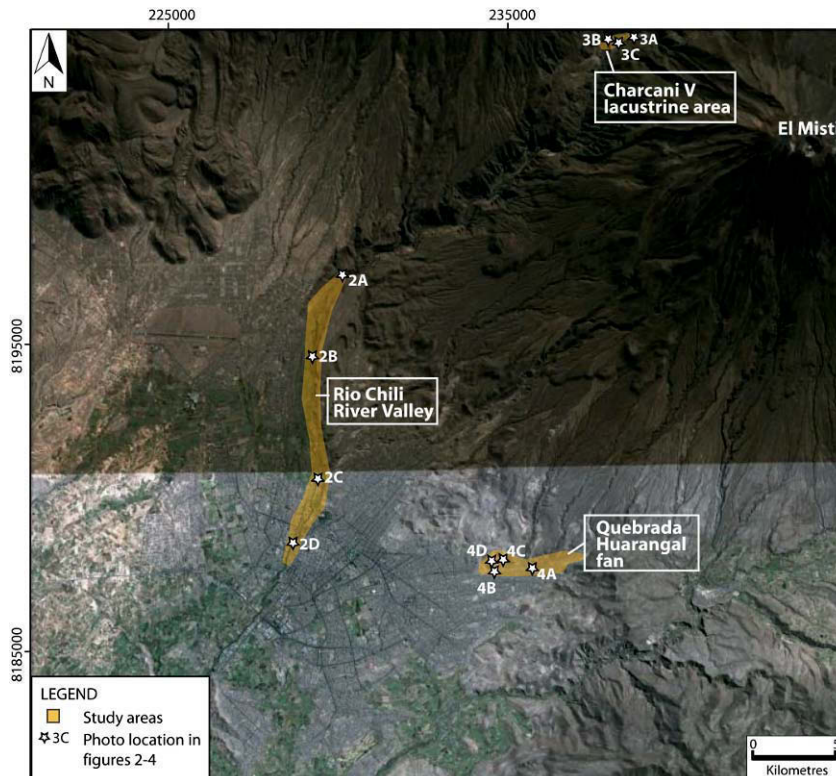


Figure 1.1: The location of the study areas in Arequipa on a Google Earth Image (2010). Stars and numbers (2A – 4D) indicate the location of photographs taken, which are shown in Figures 1.2-

1.1.1 Río Chili canyon

1.1.1.1 Alluvial valley of the Río Chili

The area from the southern entrance of the Río Chili canyon (232116, 8194785) to the southern boundary of the city centre (229410, 8187365), approximately 9.5 km in length and covering an area of 7 km², is the site of this study area (Figure 1.1). At the entrance of the Río Chili Canyon, the river is no longer confined by sheer ignimbrite cliffs but by a series of terraces bordering the river – a valley width of 500 m to 1500 m (Figure 1.2). The point at which the river is no longer confined by the canyon walls is important in terms of flow behaviour and thus is of interest for simulations presented in this study and future volcanic flow hazards in this locality (Chapter 2).

From this point the valley becomes wider, encompassing many heavily cultivated terraces of valuable arable crops. Further south, the agricultural land disappears to make way for urbanisation in the form of houses, commerce, industries (e.g. Egasa main power station), sports clubs, infrastructure and churches etc. The prominent land-use type from the north of the study area to the south changes dramatically and represents a diverse cross-section of the Arequipeño lifestyle. There are three main motives to study this valley (Figure 1.2): 1) previous geologic and geomorphological studies of Holocene and historic lahar, hyperconcentrated flow and flash flood deposits and processes along this channel and terraces, 2) the proximity of the city with respect to the river channel, and including buildings, infrastructure, economic centres, farmland and people, and 3) the importance of the Río Chili for Arequipa, by providing water and power generation, irrigation for agricultural land and tourism.

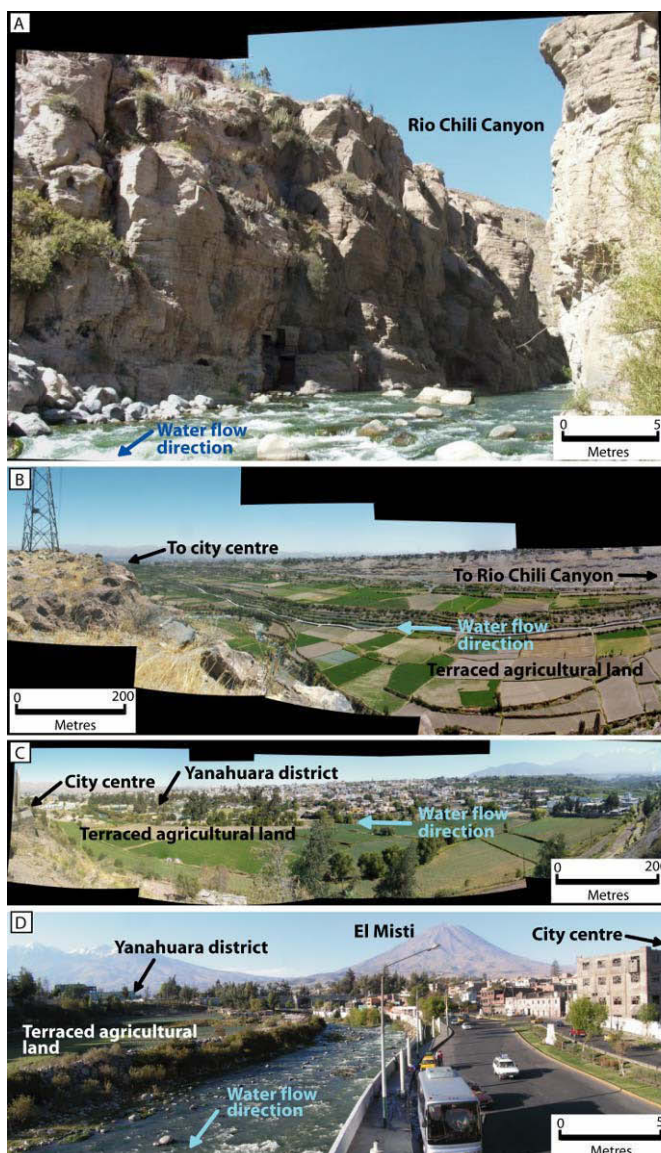


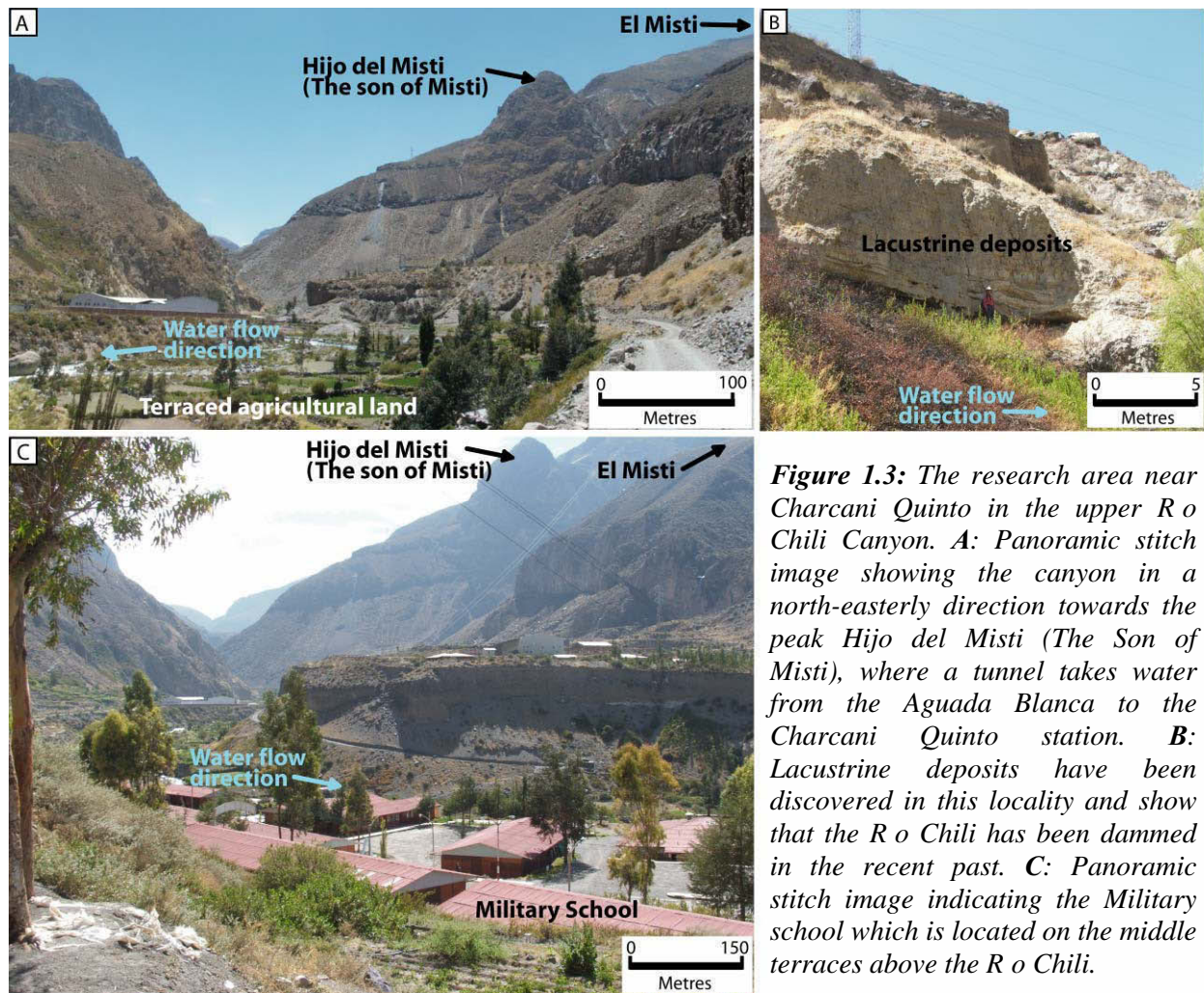
Figure 1.2: The area of research within the Río Chili Valley. **A:** Panoramic stitch image showing the southern entrance of the Río Chili canyon. **B:** Panoramic stitch of the terraces present in the upper part of the study area. The river terraces are heavily cultivated with a variety of agricultural crops, such as broccoli and lucerne. **C:** Panoramic stitch image: closer to the city centre, agriculture becomes less common and buildings take prominence. Urban sprawl encroaches on the agricultural land from the south. **D:** Panoramic stitch image, looking north, showing the entrenched Río Chili channel in the city centre. The main city is to the right of the image, with agricultural land on the left and houses located upon higher terraces.

Based upon geologic and geomorphological studies of Holocene and historical lahar deposits in the study area, Thouret et al. (2001) identified two main drainage systems that originate on the upper slopes of the volcano and pass through the centre of the city (Quebrada San Lázaro and Quebrada Huarangal), together with particular urban areas along the Río Chili that would most likely be affected by lahars. The Río Chili valley favours lahar generation for a number of reasons: 1) a large drainage area with a permanent source of water, 2) a readily available supply of loose material both in the river channel and on the slopes of the volcano, 3) a steep, narrow gorge with constrictions (e.g. six man-made dams), and 4) a direct supply of sediment from the unstable WNW flank of El Misti (Thouret et al., 1999a, 2001; Vargas et al., 2010a).

In addition to lahars, flash floods and hyperconcentrated flows have occurred, including in 1989, 1992, 1997 and 2011 (Chapter 2). Video footage and photographs from 1989 show a hyperconcentrated flow surging through the city centre, uprooting trees and carrying large debris (Chapter 2). Flooding occurred where banks had breached and water overtopped the low, modern Bajo Grau bridge, which was in construction. In February 1992 a Río Chili flood event ($260 \text{ m}^3 \text{ s}^{-1}$) overran Bajo Grau, just downstream of the Puente Grau, and flooded residential areas on the low terrace of the eastern river bank (Vargas et al. 2010a). In February 2011, water levels were dangerously close to overtopping bridges in the city centre and flooded agricultural land downstream (GrupoRPP, Peru: <http://www.rpp.com.pe/>).

1.1.1.2 The area of Charcani Quinto in the Río Chili canyon

The area chosen in the upper Río Chili Canyon is located approximately 19 km upstream of Arequipa City centre and approximately 5.8 km from El Misti's vent, at an elevation of 2990 m (UTM location 238113, 8200820) (Figure 1.3 A and C). Within this locality is Charcani Quinto, one of six EGASA hydroelectric stations built on the Río Chili to supply power to the national grid and to supply most of the potable water to the city (Chapter 4). Facilities (e.g. offices, a chapel) and infrastructure (e.g. bridges, roads) associated with this power station are also located within the study area. An exclusive military school, which controls access in and out of the area, is situated on a middle terrace on the western side of the river. The lower terraces on both sides of the river have been cultivated for agriculture, while rural housing and agricultural storage facilities also exist within the area.



An extensive lacustrine deposit (refer to Chapter 2) of approximately 6-8 m in thickness outcrops on the eastern side of the river; just to the south of the Military school (Figure 1.3 B). The presence of the lacustrine deposit is significant for this research project. The extensive and thick lacustrine deposits provide evidence that a large body of water existed at this location (to be discussed further in Chapter 2). Pyroclastic and debris flows deposits within this locality provide evidence that these eruptive deposits could have dammed the Río Chili. Also, non-eruption related mass movements from the very steep and actively eroding NWN flanks of El Misti could have dammed the Río Chili to form a lake.

Although no evidence of dam-break flood deposits have been discovered downstream, a mud-line and flood cobbles visible at least 10 m high above the channel are present at the entrance of the canyon. While this is not related to the flood event, it is an indication of how powerful floods can feature within this narrow (<0.5 km) and deep (0.5 – 1 km) canyon. The occurrence of the lacustrine deposit at Charcani Quinto presents an interesting and potentially

devastating scenario for future hazards from El Misti. A dam-break flood scenario is important to consider when assessing the vulnerability of the city of Arequipa to mass flows.

1.1.2 Quebrada Huarangal volcaniclastic fan

The Quebrada Huarangal volcaniclastic fan, with an area of approximately 3.5 km², is occupied by dense, low income housing – some of which are constructed within the channel itself (UTM: 235916, 8185133; Figure 1.4). The area is of particular interest because overbanking was observed in this locality in previous Titan2D flow simulations (Stinton et al., 2004a). Previous work has also identified this area as one of the main drainage and fan systems, along with Quebrada San Lazaro, that could be affected by a lahar (Thouret et al. 2001).

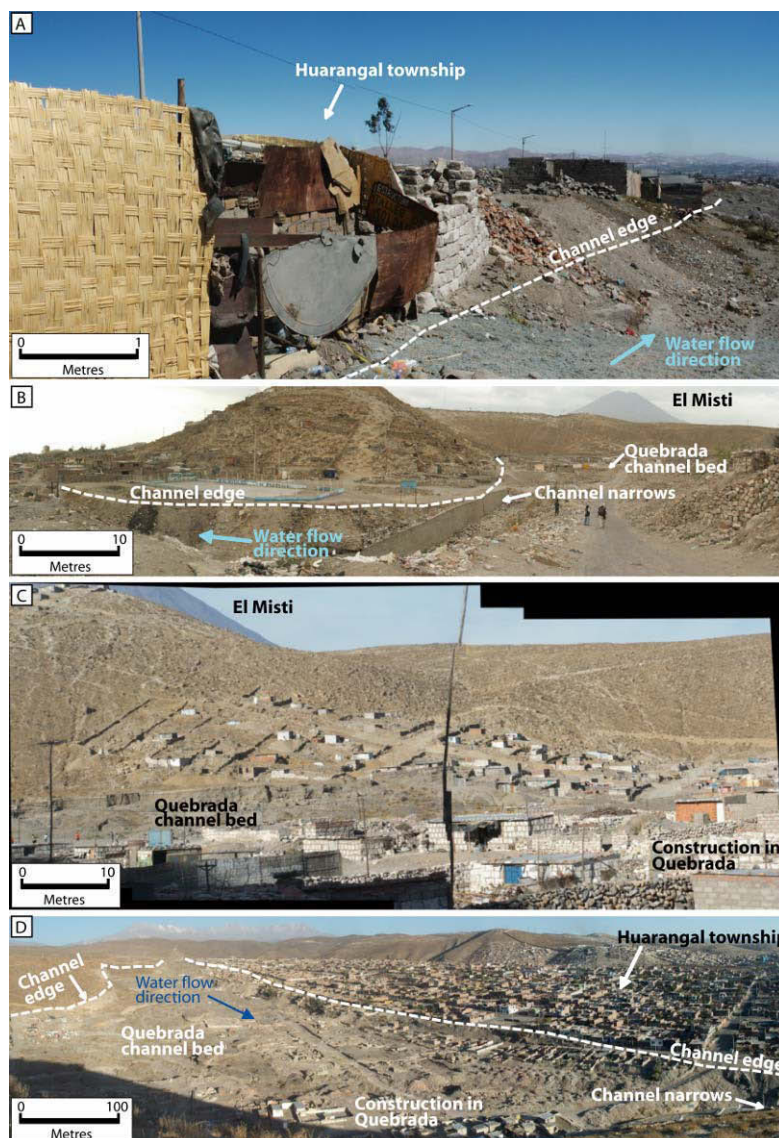


Figure 1.4: The area of research within the Quebrada Huarangal Fan. **A:** Panoramic stitch image showing the southern channel edge of the Quebrada, with an example of the type of housing present in this locality. **B:** Panoramic stitch showing where the Quebrada narrows to a confined channel. **C:** Panoramic stitch image showing the houses on the northern edge of, and within, the Quebrada. **D:** Panoramic stitch image, looking east, showing almost the entire study area. Houses are located on the southern edge of the channel extending south up several terraces. To the north, houses are built within the Quebrada itself.

The study area included the channel and terraces of the Quebrada Huarangal fan starting from a quarry upstream and ending at the downstream bridge of '8 de Octubre' (Chapter 2). The channel geometry changes and becomes narrower downstream due to channel incision into hard rock, ignimbrite or lava flow. This contrasts with the wider channel upstream which is cut into alluvial and volcanoclastic deposits (Figure 1.4 D). To the north of the channel hummocks are present in subdued debris-avalanche deposits. Where the wide channel (varying from 100-500 m across) becomes confined to a very narrow artificial channel (less than 10 m across), floods and lahars may become constricted and overtop the banks. Furthermore, flow acceleration here could cause an associated increase in its erosive power. Observed overbanking in the Titan2D simulations was also a result of the low (<4 m) bank margin of the Huarangal valley near the fan, and to the south.

Discarded household and industrial waste, vegetation, building materials, and the mining of alluvial material within the channel itself, will be a source of bulking for potential flows. In addition, residents of Quebrada Huarangal represent a much poorer socio-economic group than that of the Río Chili Valley. Houses are of poorer quality and those with the lowest quality are located within the Quebrada channel itself (Figure 1.4 C and D). The Quebrada Huarangal fan study area provides an interesting land-form upon which to model volcanic flows. The quality, density and location of housing are in contrast to those in the Río Chili Valley, and will provide an interesting comparison of the effects, vulnerability and risk of different areas within Arequipa to volcanic mass flows.

1.2 Fieldwork conducted in Arequipa

Two field campaigns were undertaken in Arequipa: the first from 16 July 2007 to 13 August 2007 and the second from 11 to 26 September 2008 and from 6 to 27 October 2008. The field campaign provided an insight into the geological, geomorphological and hydrological aspects of the physical environment in which Arequipa is located, and its exposure to natural hazards. Six main objectives were pursued in the field: 1) Lahar and flood deposits within the study areas were observed, described and sampled (Chapter 2). The main purpose was to characterise the types of flows and to understand the potential hazard they pose; 2) The observation, description and sampling of deposits in the upper Río Chili canyon was performed to investigate the possibility of a dam-break flood scenario for the city of Arequipa, and the

possibility of a lake existing in the upper gorge in recent geological time (Chapter 2); 3) The acquisition of high resolution Differential Global Positioning System (DGPS) data within the study areas. The data was used for the creation of an enhanced Digital Elevation Model (DEM) to assist in the identification of hazard-prone areas in the city of Arequipa (Chapter 3); 4) The identification of at-risk elements within the study areas (Chapter 4). Previous vulnerability studies in volcanic and non-volcanic environments were reviewed and a survey of the buildings and infrastructure within the valley and terraces was undertaken. The compilation of a building and infrastructure inventory obtained for the purpose of a vulnerability assessment; 5) A survey of the dominant land-use types was carried out in parallel with the at-risk element identification (Chapter 4); and 6) To understand the damage effects of volcanic mass flows on specific building components, geotechnical laboratory tests were conducted on materials collected in the field, including brick, adobe, concrete and ignimbrite (Chapter 4 and 5).

1.2.1 DGPS surveying

Prior to this study a 30 m DEM existed for Arequipa, however a more precise (<30 m) DEM was required to facilitate more accurate lahar computational modelling. The aim of a GPS survey in Arequipa was to create a better resolution DEM in two main areas, the Río Chili Valley and Quebrada Huarangal. In order to get centimetre to metre precision a Differential GPS (DGPS) positioning system (TOPCON and ASHTECH) was used (Figure 1.5). By using two GPS receivers simultaneously many systematic errors such as satellite (timing and position), atmospheric, multi-path and service availability, are removed thus increasing the accuracy of the location data (Steede-Terry, 2000; Trimble, 2004). GPS data can be corrected in real time using radio signals or through post-processing after data capture using post-processing software (Steede-Terry, 2000).

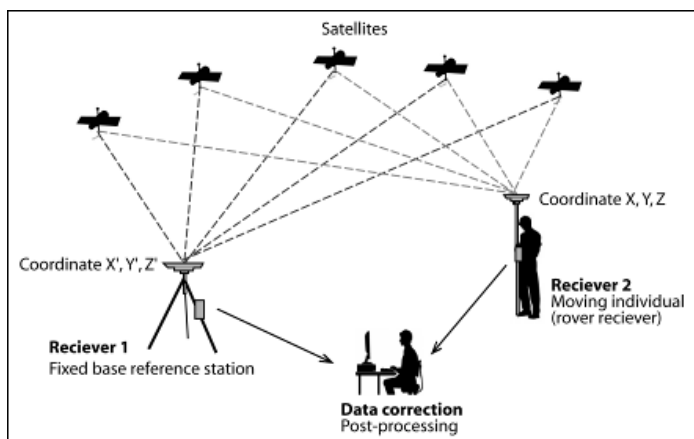


Figure 1.5: The principle of Differential GPS with data processing being undertaken after the data is collected (post-processed), as opposed to real-time-kinetic survey where a radio link corrects the data in real-time. Adapted from <http://www.ngs.noaa.gov/CORS/> and Trimble, (2004).

In 2007 static surveying was undertaken in Arequipa, and a kinematic survey was conducted in 2008 (refer to section 1.2.1.1). Both methods require the data to be post-processed (refer to section 1.4.2.1). *Static surveying* uses a base station fixed on a known point and a rover (a separate receiver) attached to a pole such that it can be carried from point to point. *kinematic surveying* also uses a rover and base station but it measures points approximately every second while the rover is in motion. *Real Time kinematic (RTK) surveying* is preferable in most cases, because RTK removes the need for post-processing by utilising a radio or other communication link between receivers, which allow for computer processing of coordinate differences in real time. RTK surveying could not be applied in this study due to the large distance difference between the base and the rover (up to 20 km), and also the use of radio communication links would require permission from a Peruvian Government Agency. However, each survey method does achieve similar levels of accuracy. The decision regarding which technique is appropriate will depend on factors such as project specifications, the objective of the data, and the sources available for differential correction.

1.2.1.1 DGPS Survey in Arequipa

2007 field survey

The DGPS survey was undertaken using two Topcon GB-1000 DGPS receivers (Topcon Positioning Systems Inc, 2006) acquired from the Technical Division at the National Institute of Sciences of the Universe (Division Technique de L'Institut national des Sciences de l'Univers) in Paris (Figure 1.6).

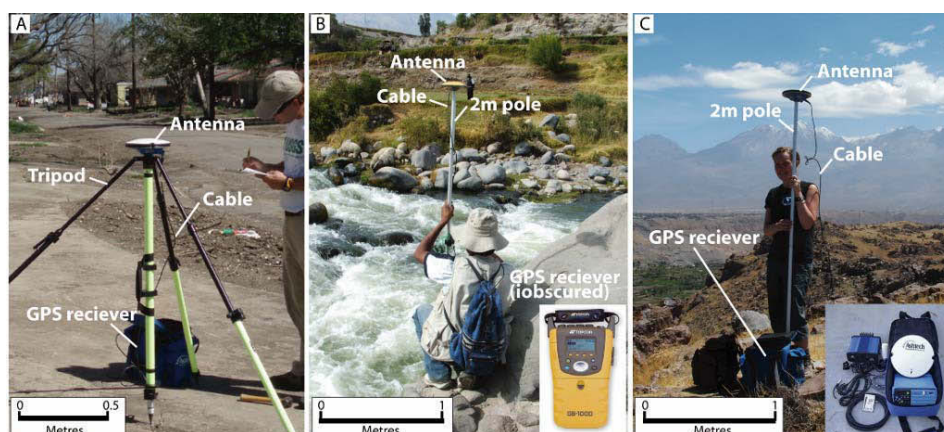


Figure 1.6: The DGPS system. **A:** Base station (generic image downloaded from <http://www.usgs.gov/>), a similar setup was used in Arequipa on the roof of the Samana Hotel (Figure 1.7) using a Topcon GB-1000 GPS receiver in 2007 and an Ashtech - treme GPS receiver in 2008. **B:** Rover using the Topcon GB-1000 receiver (see inset) adjacent to the Río Chili. **C:** Rover using the Ashtech - treme receiver (see inset) on the eastern ridge above the Río Chili Valley.

The detailed topographical survey was concentrated on the four main terraces of the Río Chili Valley. The area surveyed is approximately 4 km², starting at the Military Camp approximately 15 km from the summit (229202, 8188708) moving downstream to the Bolognesi Bridge in the city centre (228533, 8185370), including the confluence of the Río Chili with the tributary Quebrada San Lazaro (Figure 1.7 A; 228855, 8185956). In addition less than 1 km² of the Quebrada Huarangal area, 13 km from the summit, was surveyed (Figure 1.7 B); from the gravel mine at the eastern margin of the study area (236796, 8184796) extending 500 m downstream (236323, 8184796) and inclusive of built terraces.

The DGPS base station was installed on the north balcony of the Hotel Samana (16°23'24,0201", 71°32'44,4451", elev. 2405.2 m asl) in the Yanahuara district of Arequipa. The height of the rover antenna was set at 2 m. The DGPS survey was undertaken in static mode and DGPS measurements (from satellite and GLONAS) were obtained with a sampling rate of 1 second. The survey was undertaken in transects, where possible, with points acquired at intervals of less than 5 metres apart. Longer periods of time were spent acquiring positional data at monuments, bridges, and areas that can be easily identified from the orthophotos, as ground control points (GCPs) for the DEM creation.

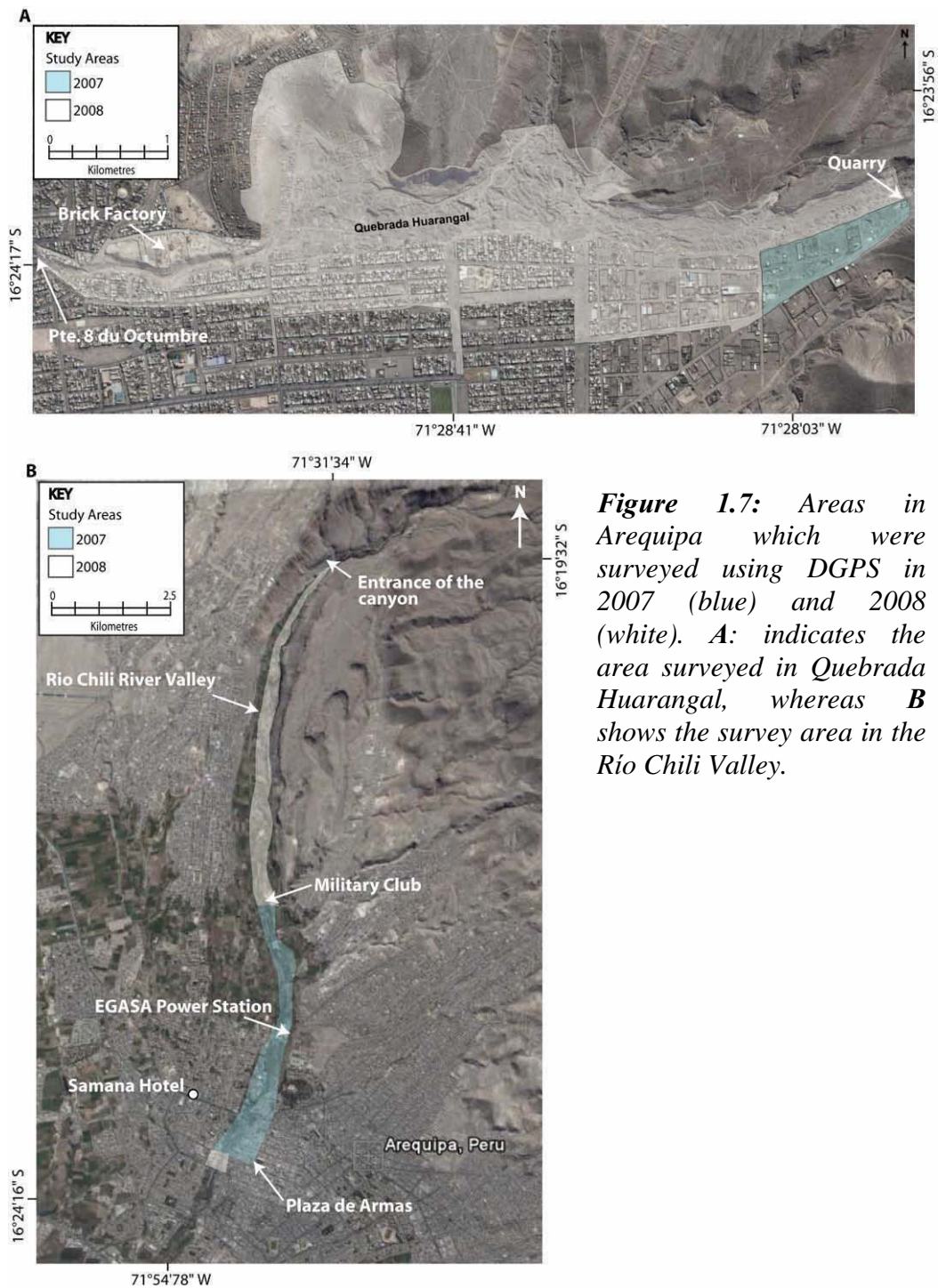


Figure 1.7: Areas in Arequipa which were surveyed using DGPS in 2007 (blue) and 2008 (white). **A:** indicates the area surveyed in Quebrada Huarangal, whereas **B** shows the survey area in the Rio Chili Valley.

2008 field survey

The topographical survey undertaken in 2008 utilised two Ashtech Z-Xtreme GPS receivers (Thales Navigation, 2002) – one used as a base station, and the other in rover mode (Figure 1.6). The survey was undertaken on the four main terraces of the Río Chili Valley from the downstream canyon entrance approximately 12 km from the summit (230113, 8193506) to the Military Camp approximately 15 km from the summit (229202, 8188708), and from the

Bolognesi Bridge (228533, 8185370) to the Quiñones Bridge (228461, 8185151) in the southern part of the city. The survey area was approximately 10 km² (Figure 1.7 B). An opportunity was also made to take additional points in the areas surveyed during 2007. Additionally an area of approximately 4 km² on the Quebrada Huarangal fan area was surveyed; from 500 m downstream of the Quarry in the east (236323, 8184796) to the 8 du Octubre Bridge (233929, 8184659) in the west (Figure 1.7 A). The survey was conducted both within the channel and on adjacent terraces.

The base station was set up on the Samana Hotel (Yanahuara) on the northern balcony (16°23'24.0288"; 71°32'44.445"; 2405 m) and on the roof of the southern balcony (16°23'24.4248"; 71°32'44.466"; 2408.32m). The different locations were taken into account during post-processing. The height of the rover antenna was set at 2 m. Unlike in 2007 the DGPS survey was undertaken in kinematic mode, and DGPS measurements (from satellite) were obtained with a sampling rate of 1 second. Transects were made and where possible points were acquired at intervals of less than 5 m spacing and logged as waypoints. As with the survey conducted in 2007, longer periods of time were spent acquiring positional data at monuments, bridges, and areas that can be easily identified from the orthophotos, as GCPs for the DEM creation.

1.2.2 Surveying the building stock, land use and infrastructure

1.2.2.1 Building survey

Building stock surveys have previously been undertaken in a number of environments, including in volcanic settings for pyroclastic flows, tephra fall and volcanic earthquakes (e.g. Soufrière Hills Volcano, Baxter et al., 2005; Vesuvius, Spence et al., 2004a, b; Soufrière Guadeloupe, Spence et al., 2005a; Rabaul, Blong 2003; and Furnas Volcano, Pomonis et al., 1999), for floods (e.g. Eastern England, Kelman, 2002) and also for earthquakes (e.g. Catania City, Faccioli et al., 1999). Spence et al. (2005a) found from surveys of building stock that there are three main building characteristics of primary importance; 1) the construction materials forming the vertical load-bearing structure, 2) height (as defined by the number of storeys), and 3) age of the structure. Additional characteristics, such as roof type, and presence and types of openings Spence et al. (2005a) assumed as subsidiary, and can be derived from the primary classification.

Adding to the building types identified by Chevillot (2000) in Arequipa, and to surveys conducted by others (e.g. Pomonis et al. 1999; Spence et al.; 2004b, 2005a; Baxter et al. 2005) a descriptive survey was conducted to characterise the building stock according to: 1) the dominant building material (ignimbrite brick, red brick, and adobe); 2) number of floors; 3) building reinforcement; 4) roof type and style; 5) opening type and quantity; and 6) overall building structural integrity (Chapter 4). Signs of disrepair were quantified visually rather than by in-situ testing of the building materials. In-situ testing of wall condition and load bearing capacity could not be undertaken due to time and permission restrictions.

The descriptive building surveys were undertaken in the Río Chili Valley and on the Quebrada Huarangal fan and conducted in parallel with the DGPS survey, thus covering the same area (section 1.2.1.1 and in figure 1.7). The aim of the survey was to assign a building type to individual buildings within the survey area. This was possible as the survey was conducted externally (at street level) and where permitted, within the boundaries of the land-owners properties. However there were some places where access was not granted or the land was inaccessible. Where properties were unable to be viewed, building type surveys were complemented with orthophotos, Google Earth and SPOT5 satellite imagery (Figure 1.8). As the survey progressed, the building type table was modified to better describe the buildings present within the study areas. The results of the survey, along with a vulnerability ranking of the building types with respect to the resistance of the structure, can be found in Chapter 4.

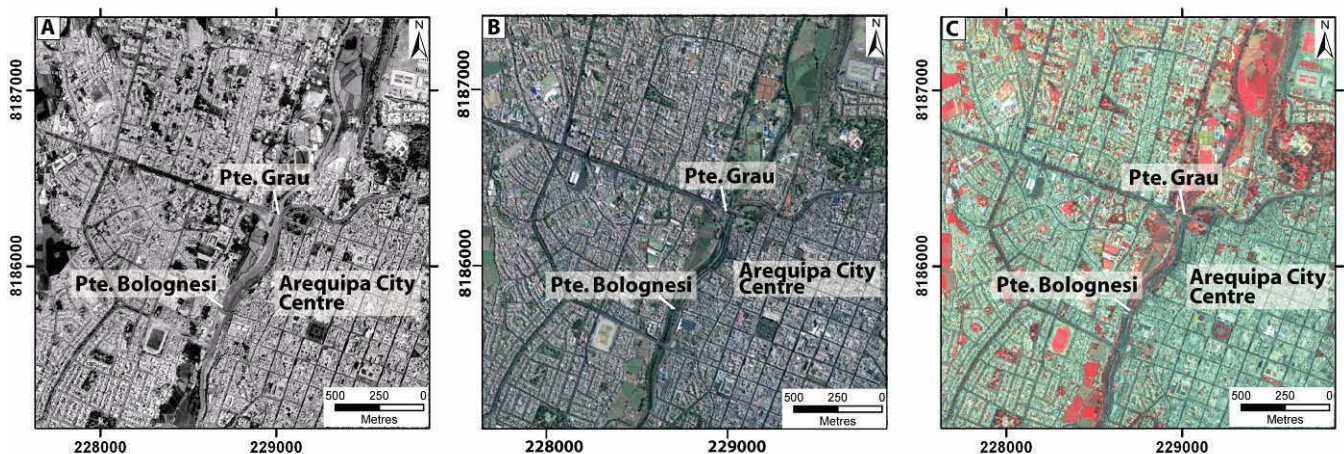


Figure 1.8: Imagery used to complement field surveys of building and infrastructure: (A) orthophotos taken in 2000, (B) Google Earth imagery taken in 2006 and (C) SPOT5 imagery taken in 2008.

1.2.2.2 Land use survey

Land use can be defined as the activities or socio-economic functions for which land is used; the same land is capable of supporting multiple uses. Land use inventories are common for government departments including local and regional councils. However, land use inventories can also be used for various research applications (e.g. Lambin et al., 2003; Gallego et al., 2008). Land use inventories can be used to quantify the amount of rural to urban change, to identify change trajectories, to study land zoning changes, to help understand how change is occurring, to predict future changes and infrastructure development. Three methods exist for identifying urban land use: ground observations (e.g. Fuller et al., 1994), aerial photography (e.g. Donnay et al., 2001) and satellite imagery (e.g. Stefanov et al., 2003).

There is no internationally agreed classification of land use, and they often vary depending on the intent of the research. For example, some surveys are almost entirely of agriculture, thus tend to focus more intently on this aspect (e.g. Fuller et al., 1994), whereas others are focussed within an urban environment thus urban classifications are expanded (e.g. Donnay et al., 2001). Drawing information on land use surveys conducted from various sources (e.g. Fuller et al., 1994; Stefanov and others) and previous studies based in Arequipa (e.g. Chevillot, 2000; ITC ATLAS, 2001; Delaite, 2003; Vargas et al., 2010a) the classification of land-use types for the Arequipa survey was devised before the field campaign. Using a ground-based observation method, descriptive land-use surveys were undertaken in the Río Chili Valley along with Quebrada Huarangal and were conducted in parallel with DGPS and building surveys (section 1.2.1.1 and figure 1.7). Where properties were unable to be viewed, land use surveys were complemented with aerial photographs, Google Earth and SPOT5 satellite imagery (Figure 1.8). The results of the survey, along with a vulnerability ranking (according to their importance, value, cost and occupancy of the land-use types), can be found in Chapter 4.

1.2.2.3 Infrastructure survey

As modern urban functions rely on lifeline systems much more heavily than they used to, infrastructure constitutes a major component of the vulnerability of a city if a disaster strikes. Infrastructure can be defined as the basic physical and organisational structures needed for the operation of a society, or the services and facilities necessary for an economy to function

(Wisner et al., 2004). These can include water supply, sewage, power supply and telecommunications and transportation networks just to name a few.

Infrastructure surveys were undertaken in the Río Chili Valley and on the Quebrada Huarangal fan (Figure 1.7). However, some important and vital infrastructure was taken into consideration outside of these boundaries (e.g. the hydroelectric system). In addition to field surveys, data was gathered from previous surveys (e.g. Delaite, 2003), company information (e.g. water: SEDAPAR, electricity: EGASA), orthophotos, Google Earth and SPOT5 satellite imagery (Figure 1.8). The aim of the surveys was to locate important infrastructure (i.e. transportation links, electricity generation and supply) and then assess the vulnerability of this infrastructure. The results of the survey, along with a vulnerability classification can be found in Chapter 4.

1.2.2.4 Building materials

Besides the type of construction, the quality of building materials and workmanship are factors which also affect the vulnerability of a structure. To compare building materials used in Arequipa with Peruvian and world-wide Building Code Standards, samples of three main building materials (red clay brick, ignimbrite and concrete) were collected for some physical properties to be determined (section 1.3). The samples were collected both in the field and from brick factories within the city centre and the Quebrada Huarangal fan. The properties of the samples were used to calculate the strength of buildings and for determining the threshold at which the building would likely fail in the event of lahar or flood (chapter 5).

1.2.3 Lahar and flood deposits

In order to understand the types and nature of volcanic and non-volcanic flows that pose a potential threat to the city of Arequipa, deposits from earlier events were studied. Photos and notes were taken of the deposits at nine different sites (Figure 1.9), including the locality, description, thickness, and stratigraphic description (i.e. stratigraphic logs). Sample sites A and B correspond to a lacustrine deposit located in the upper Río Chili canyon.

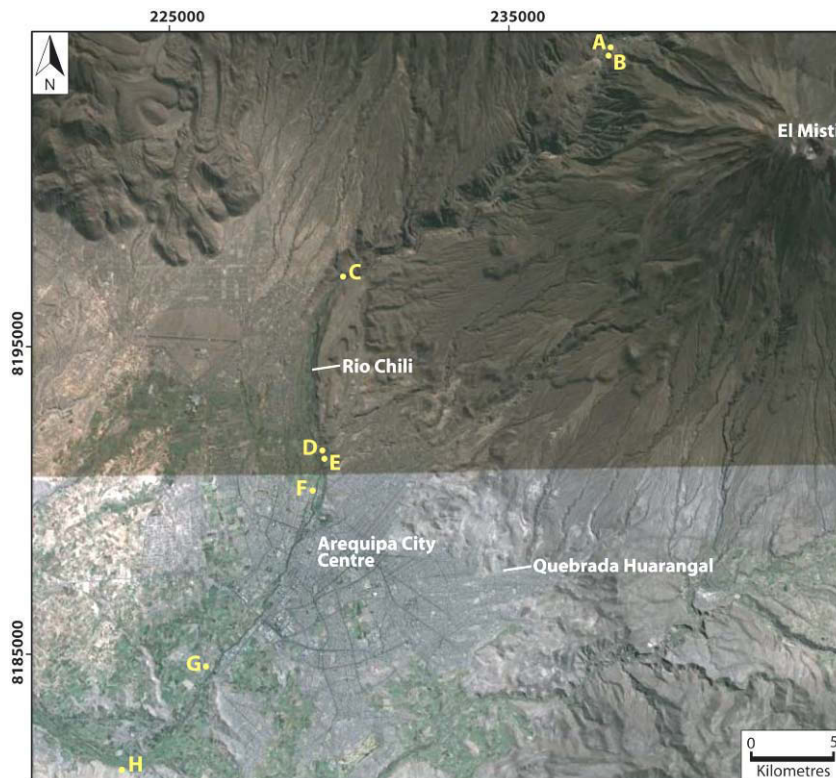


Figure 1.9: The location of lahar deposits studied within Arequipa. Localities A and B are that of a 6-10 m-thick lacustrine deposit located in the upper Rio Chili canyon. Base image from Google Earth.

The description of the sample stratigraphy can be found in Chapter 2.

1.3 Laboratory experiments

Characterisation and measurement of relevant engineering properties of natural materials, either in the laboratory or in-situ, is a fundamental aspect of geotechnical engineering. Geotechnical laboratory testing has also been applied to research in the mining industry, building response, earthquake studies, general construction, road and monument preservation. Geotechnical laboratory analysis was undertaken on eight different types of construction materials present in Arequipa. The purpose of these experiments was to characterise the type, strength, durability, and variability of common construction material in order to assess the vulnerability of different construction materials in buildings in Arequipa. Three experiments were conducted: Ultrasonic Pulse Velocity (UPV), Unconfined Compressive Strength (UCS), and absolute density, all of which are explained below in sections 1.3.1 – 1.3.3.

1.3.1 Unconfined Compressive Strength

Unconfined Compressive Strength (UCS) is defined as the capacity of a material to withstand axially directed compressive forces whereby the material will be crushed when the limit of compressive strength is reached (Hoek and Brown, 1980). The sample is compressed between the plates of a compression-testing machine with a gradually applied load until fracturing is observed. The amount of compressive load a material can bear before fracturing is noted. UCS can be undertaken on a number of different materials such as aggregate, cement, concrete, timber, brick, and rock. In addition, UCS results have long been used to estimate the strength of rocks (e.g. Hoek and Brown, 1980).

The UCS test was undertaken by a technician at ITC (Etudes Ingénierie et Techniques de la Construction) in Clermont-Ferrand. An electrically operated Seidner “Form + Test” compression machine was used for the compressive strength test on eight different types of construction materials collected in the field (Figure 1.10). The machine is controlled by a computer with various pre-defined set-up parameters which fulfil different standards. In addition, it performs semiautomatic density measurements on samples.

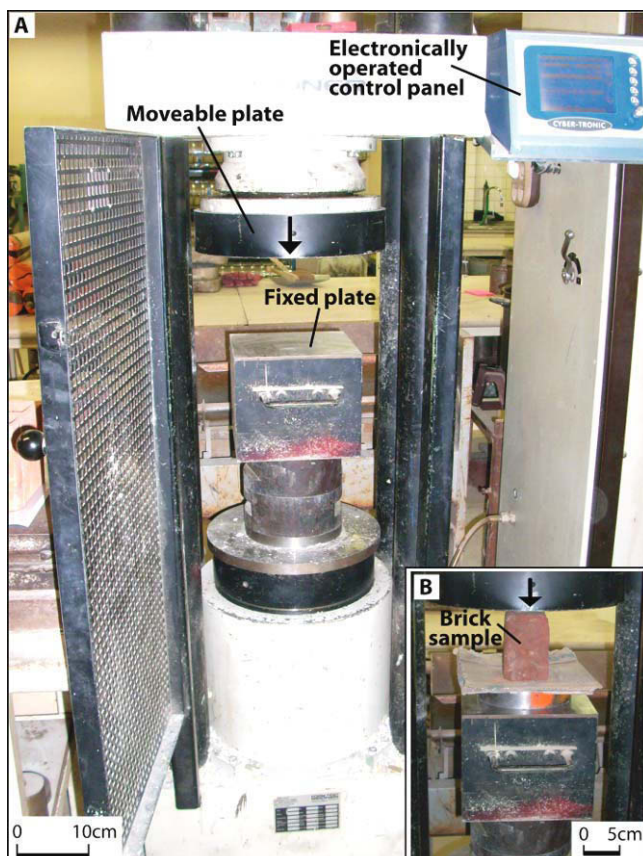


Figure 1.10: *A: The Seidner Form Test unconfined compressive strength machine at ITC, Clermont-Ferrand. B: A brick loaded between the two load plates (the surface protected by card) before the force is applied.*

The “Method of Test for Compressive Strength” is given in the ASTM C 1314-03b, Standard Test Method for Compressive Strength of Masonry Prisms (American Standard for Material Testing 2003). The standard specifies that individual bricks must be arranged with mortar in a stack-bonded prism, with the height of a prism a minimum of three bricks and not less than three times the thickness of the prism (ASTM, 2003). Once cured, the prism is placed in a testing machine and subjected to a constantly applied load over the entire top and bottom surfaces of the specimen. The load at failure is then recorded to the nearest five kN. However, this standard assumes that the bricks being tested are newly manufactured, which is not the case in Arequipa so the test involved applying a constant force to an entire brick. The brick was prepared by covering the surfaces with a cardboard sheet to give a smooth and flat surface on which to apply the load. The sample was then compressed at a constant rate of 0.5 to 1.0 MPa/s until the weight exceeded that of the compressive strength of the sample, causing it to fracture. Peak weight (P) at break was recorded. From the maximum load (F) or load applied in kN and the cross-sectional area (A) of the surface that the load was applied to, the compressive strength (σ) in kN/m² was calculated using the following formula:

$$\sigma = \frac{F}{A}$$

The American Society for Testing and Materials Standard C62 (ASTM, 2008) specifies minimum compressive strength requirements from the average of five bricks: 21 MPa for a severe weather environment, 17 MPa for a moderate weather environment and 10 MPa for a normal weather environment. The strengths of most building stone are well in excess of this. Comparisons between unconfined compressive strengths compiled from different sources and those calculated from the Arequipa samples are made in Chapter 4.

1.3.2 Density and porosity

The density and porosity of building materials are important for determining their use and durability during construction. The density of bricks influences the weight of walls and the variation in weight has implications on structural, acoustical and thermal design of the wall. Raw materials and manufacturing process affects brick density, which could vary between 1300 kg/m³ to 2200 kg/m³ (Hendry, 2001). Highly porous bricks are not as durable as those with lower porosity and density. In addition they can facilitate the absorption of water;

highly porous bricks may remove water from the mortar preventing complete hydration of the cement (Hendry, 2001). Density, volume, and porosity are physical characteristics of solid materials that can be determined by a variety of experimental techniques. However, the value obtained is very likely to be dependent on the technique. This is largely because of the way the measurement technique treats volume in respect to the degree of exclusion of void spaces associated with the sample material.

1.3.2.1 Density

Density (ρ) is the mass of a unit volume of material with the following calculation, where M is the mass of the material measured in grams, and V is the volume occupied by the material measured in centimetres cubed.

$$\rho = \frac{M}{V} \text{ g/cm}^3$$

There are three methods for measuring the density of a rock sample: geometric, water displacement and hydrostatic weighing. The geometric method uses the geometry of the sample to determine the volume. The mass is determined by a precise electronic scale, and the accuracy of the density depends on the precision of the instruments used to measure the sample dimensions, the geometry of the sample and the scale accuracy (CNAM, 2006). The samples that were collected in the field are not perfectly regular in size, and have a heterogeneous texture and therefore it is very difficult to determine the volume of the sample accurately using geometry.

Depending on whether or not the sample has been waterproofed (coating the surface with a water impermeable substance); the water displacement method calculates the bulk density or the specific density of the sample. The density is measured from the mass and volume of the sample, which is determined by the quantity of water that is displaced. The accuracy of this method depends on the equipment used and sample size

The density of samples can be accurately determined using a Hydrostatic Balance. It consists of a rigid support frame, incorporating a water tank mounted on a platform (Figure 1.11). A mechanical lifting device is used to raise the water tank through the frame height immersing the specimen suspended below a balance. By measuring the mass of the sample in water and

above water, the bulk density of the sample is determined (CNAM, 2006). When the sample is weighed out of water, the mass of the sample is determined (M), and the sample is only subject to gravity. When measuring the same sample mass in water (m), the sample is subject to gravity and buoyancy, therefore the mass is equal to the volume of water displaced. The bulk density (ρ_{app}) can be determined by the following calculation, where V is the volume, M is the mass of the sample in air, and m is the mass of the sample in water. M minus the mass of the volume of water displaced is equal to m . The density of water (ρ_w) is 1 gm/cm^3 .

$$\rho_{app} = \frac{M}{(M - m) \cdot \rho_w}$$

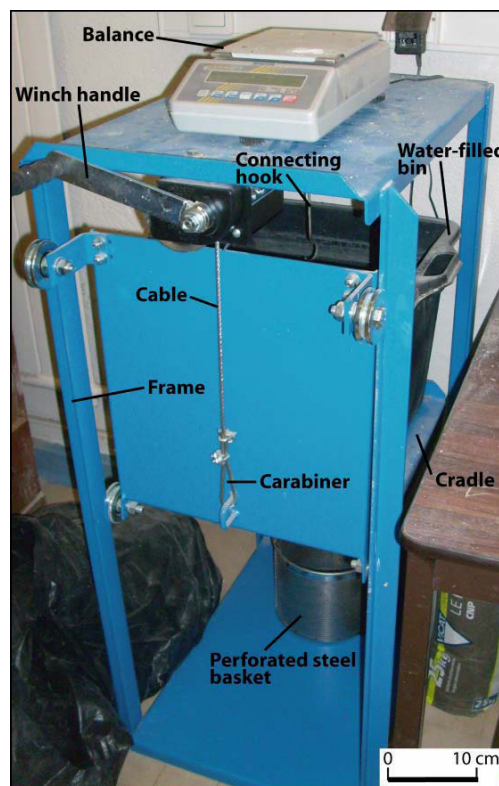


Figure 1.11: The buoyancy balance with dimensions of $510 \times 510 \times 1150$ mm, and a weight of approximately 50 kg.

Using experimental procedure for hydrostatic weighing outlined by CNAM (2006), the density of three types of Arequipa brick samples were determined (Figure 1.11) at the Laboratoire Magmas et Volcans, Clermont Ferrand. The density of brick samples with intentional voids could not be measured. The experiment procedure was as follows: 1) The samples were dried at 100°C for 24 hours to remove all traces of water, and the mass of the dry sample was measured in air using an electronic scale accurate to 0.01g ; 2) The tank was filled with water to a depth approximately 5 cm from the top edge; 3) The water tank was replaced in a high position so that the hanging basket was completely immersed, leaving

space 5 cm below the hanging basket. The scale was zeroed and the sample placed in the basket ensuring it was completely immersed; 4) After approximately one hour the mass (m) of the immersed sample was recorded; 5) The experiment was repeated three times for each sample; and 6) The bulk density of the sample was calculated using the equation outlined above.

In the method outlined above the pore volume is excluded whereby the liquid has completely filled the pores. This method can be restricted as porous samples absorb the water in which they are immersed; if pores are to be included a sealing coating may be applied. The experiment was repeated, but after the samples were dried in the oven they were coated in paraffin to make them impervious to water. Paraffin was melted at temperatures of between 60 and 62°C and applied to the sample covering it with a continuous film. Careful attention was paid so that air bubbles were not trapped and no surface area was exposed where water could penetrate, and subsequently distort the results.

Table 1.1 below provides typical density values for common materials (Prentice, 1990; Duggal, 2008). Comparisons between these values and those calculated from the Arequipa samples are made in Chapter 4.

Sample	Bulk density (kg/m ³)
Limestone or quartz sand	2500
Hard limestone gravel	2500-2600
Basaltic road gravel	2700
Granitic sand	2600
Plain concrete with natural stone aggregate	2300
Plain concrete with natural broken aggregate	2300
Basalt rock	3000
Granite rock	2700
Sandstone rock	2300
Pumice	500-1000

Table 1.1: Typical bulk density values of samples from Duggal (2008).

1.3.2.2 Porosity

Porosity (n) is the degree to which the material is interspersed with pores, and can be calculated from density. As discussed with regard to density, porous materials allow the ingress of water (from nature or mortar) more easily than non-porous, reducing the durability

of the material. Denser materials which possess lower porosity are commonly used in construction requiring high mechanical strength (Duggal, 2008). The porosity of the Arequipa samples was determined using the measurements obtained during hydrostatic weighing, and based upon the calculations used by Rousset Tournier (2001) and Paquereau-Lebti (2006). The porosity of the sample (n) can be expressed by the following calculation, where M is the mass of the sample in air, m is the mass of the sample in water and m' is the mass sample which is covered in paraffin in the water:

$$n = \frac{(M + m) - M}{(M + m) - m'} \times 100$$

Prentice (1990) devised a classification system (class 1-5) of material based upon the relationship between dry density and porosity (Table 1.2). Comparisons between these values and those calculated from the Arequipa samples are made in Chapter 4.

Class	Dry density (Mg/m ³)	Description	Porosity (%)	Description
1	< 1.8	Very low	> 30	Very high
2	1.8 – 2.2	Low	30 – 15	High
3	2.2 – 2.55	Moderate	15 – 5	Moderate
4	2.55 – 2.75	High	5 – 1	Low
5	> 2.75	Very high	< 1	Very low

Table 1.2: Classification of material according to the dry density and porosity (from Prentice, 1990)

1.3.3 Ultrasonic Pulse Velocity (UPV)

UPV is a common non-destructive evaluation technique, adapted from concrete technology for masonry evaluation, to measure the velocity of acoustic waves through a material. The UPV value is governed by the mineral composition, density, porosity, elasticity, and degree of fracturing within a rock mass. It has been reported by several authors (e.g. Hobbs and Wright, 1987; Goodman, 1989) as a useful and reliable non destructive tool for assessing the mechanical characteristics such as the modulus of elasticity and the compressive strength, of concrete and masonry in existing structures. Subsequently these parameters can be used in the safety evaluation of the structure – for example UPV has been used in assessing fire damaged concrete (Chew, 1993) and the masonry of historic buildings (Schuller et al. 1995).

The experiment was undertaken on three different types of material samples – solid red clay brick, concrete block and ignimbrite block. Hollow red clay brick samples were not used due to intentional voids in the brick; the voids would not allow the propagation of waves. UPV measurements of compressional waves were carried out using the Pundit Plus (CNS Farnell Ltd., 2006) at the Laboratoire Magmas and Volcans in Clermont-Ferrand. The Pundit Plus is a low frequency ultrasonic apparatus for field or laboratory use, with data storage and computer output facilities. (Figure 1.12). Two ends of the sample were coated in gel and the transducers placed at either end. The velocity is calculated from the time taken for a pulse of longitudinal vibrations, produced by an electro-acoustical transducer, to pass through a sample. After traversing a known path length (L) through the sample, the received pulse of vibrations is converted into an electrical signal by a second transducer (normally held in contact with the other side of the sample) and electronic timing circuits enable the transit time (T) of the pulse to be measured. Transducers are coupled to the surface with gels for maximum energy transmission. The pulse velocity V (m/s) is given by:

$$V = \frac{L}{T}$$

The average pulse velocity was determined after measuring the velocity taken at each face of the sample.

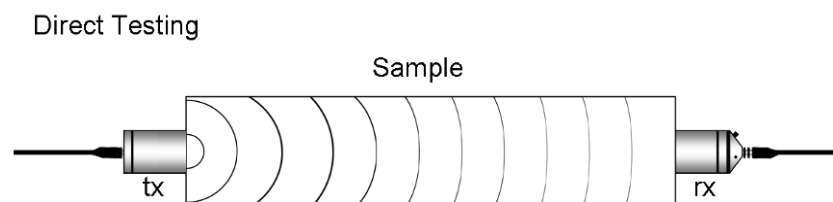


Figure 1.12: The UPV direct testing setup. Transducers (with gel) are fixed at each end of the sample and measurements are read on an electronic panel. Figure adapted from <http://www.cnsfarnell.com/>

The results were compared to velocities published in the literature for similar materials (Goodman, 1989). Goodman (1989) suggested velocity values range from <2500 m/s for very low quality rocks, to >5000 m/s for very high quality rocks (Table 1.3). Browne et al (1983) suggested values <3000 m/s for poor quality concrete and values >4000 m/s for good quality concrete. The results and comparisons can be found in Chapter 4. Previous work (Hobbs and Wright, 1987) also points to the conclusion that UPV gives an indication of the

integrity of a sample, but other parameters should be studied in addition, as described in the following sections.

UPV values for rock		UPV values for concrete	
Velocity (m/s)	Quality	Velocity (m/s)	Quality
< 2500	Very low	< 3000	Poor
2500 – 3500	Low	3000 – 4000	Fair
3500 – 4000	Moderate	< 4000	Good
4000 – 5000	High		

Table 1.3: Suggested values for rock (Goodman, 1989) and concrete (Browne, 1983) that can be used to assess the condition.

1.3.4 Radio-carbon dating

Radio-carbon dating (^{14}C) was undertaken on a charcoal sample (kim0811; 238047, 8200377; 3016 m) calculated by M. Fontugne at the Laboratoire Sciences du Climat et de l'Environnement in France. The sample was taken from a banded pumice-fall layer which is intercalated in a pyroclastic-flow deposit, forming a terrace constructed in the upper course of the Río Chili. The results are presented in Chapter 2.

1.4 Geographical Information Systems

The advance in computer systems over the past 25 years has led to an increase in the use of Geographic Information Systems (GIS); almost replacing the manual processing and production of paper maps. Most definitions of GIS focus on two aspects of the system: technology and/or problem-solving – GIS is a system of hardware, software and procedures designed to “support the capture, management, manipulation, analysis, modelling and display of spatially referenced data for the solution of complex planning and management problems” (Aranoff, 1989).

GIS can be used to identify and model hazards, begin to evaluate the consequences, and can play a major role in hazard and risk assessment and mitigation (Van Westen and Terlien, 1996; Pareschi et al., 2000; Van Westen et al., 2003). The applications are diverse, from the delineation of hazard-zones for land-use planning to identify the best route for evacuation and/or emergency services (Cole et al., 2005). GIS is widely used in landslide hazard

research (e.g. Van Western and Terlien, 1996) but also in the analysis of other natural hazards, such as rockfalls (e.g. Lan et al., 2010), snow avalanches (e.g. Gruber and Bartelt, 2007), floods (e.g. Fernández and Lutz, 2010) and earthquakes (e.g. Pessina and Meroni, 2009).

In the past 20 years GIS has become a useful tool in the field of volcanic hazard and risk research. Recent work includes using GIS as a tool for the assessment of the likelihood of reactivation of vents in the Campi Flegrei caldera using geophysical, geological and geochemical data (e.g. Lirer et al., 2010), the determination of safe areas from potential lava flows on Tenerife (e.g. Gómez-Fernández, 2000b), and the modelling of volcanically-derived flows for hazard assessment (e.g. Sheridan et al. 2010). Where comprehensive information on a volcano exists, the development of a GIS in a broader perspective can be undertaken, including for example all types of hazards, and evaluation of all types of potential risks in terms of damage and mortality (e.g. Alberico et al. 2002). It is difficult to overlook the benefits of GIS for volcanic hazard and risk assessments, and thus forms an integral part of this research project.

1.4.1 Data acquisition and availability

1.4.1.1 GIS software

During this research project a number of GIS programs were used depending on data to be used, and the purpose. The programs used were: 1) ArcGIS 9.1 (ESRI, 2005): georeferencing orthophotos and satellite imagery, making raster and vector layers, investigating interpolation methods, and making and updating databases; 2) Surfer 9 (Golden Software, 2010): manipulation of geographic data from different sources, creating DEMs and contour maps; 3) ILWIS Open 3.6.01 (ITC, 2009): viewing ITC Atlas data and exporting it for use in ArcGIS; and 4) GRASS 6.0 (GRASS, 2007): optimisation of DEM for using in Titan2D.

ArcGIS was the most widely used because it combines several generating functions. ArcMap allows the viewing, editing and analysis of geographical data, to connect and analyse layers of information, and to develop of maps. ArcToolbox is an application of GIS tools which allows for a wide range of data processing. Data can then be organised within ArcCatalog and complex geographic databases can be created. Finally, ArcScene can be used to project the data in 3D. Surfer was found to be much more efficient at dealing with the large volume

of data (GPS and ASTER points), especially during interpolation. Georeferencing SPOT images in ENVI were deemed a lot more user-friendly than the other software programs. The use of ILWIS was specific to the data which had been acquired previously, while GRASS is the only program supported by Titan2D at present.

1.4.1.2 Available data

A multitude of data was available through the Environmental Atlas of Arequipa, produced by ITC (International Institute for Aerospace Survey and Earth Sciences, Enschede, Netherlands). In addition, data was made available from previous students and researchers at the Laboratoire Magmas et Volcans; the data was supplied from various sources originally. Data available and used included: georeferenced images of Arequipa – Landsat; orthophotos of Arequipa; cadastral plan of Arequipa; geological and geotechnical maps; 30 m DEM; road and rail routes; three hazard scenarios; urban and rural land-use identification; and LaharZ and Titan2D simulations

1.4.1.3 Data acquired and/or created during the research project

Additional data was required for this research project, and includes: georeferenced images of Arequipa – SPOT5; georeferenced orthophotos; DGPS data; SRTM DEM; ASTER DEM; enhanced El Misti DEM; land-use types – database and shapefiles; building types – database and shapefiles; bridges – database and shapefiles; updated road and rail routes – database and shapefiles; updated urban and rural land-use identification – database and shapefiles; water canals and hydroelectric power stations – database and shapefiles and Titan2D simulations.

1.4.2 Creating an enhanced DEM for Arequipa

The Earth's surface can be digitally represented in the form of a Digital Elevation Model (DEM) which can be in either a raster or a Triangulated Irregular Network (TIN) format. A raster model consists of a matrix of cells; each cell has a width and a height and is a portion of the entire area represented by the raster. Surfaces are approximated by taking a sample of the values at different points and interpolating the values between these points. Raster models however can oversample smooth areas due to elevations sampled on a regular grid. The alternative is a TIN, in which terrain surfaces are approximated as a network of planar

triangles, and the vertexes are points of known elevation (Pareschi et al., 2000). TINs model terrain using variably sized elements and this variability means that algorithms used to analyse surfaces are complex. The complexity of TIN creation can render a simple surface creation difficult, and the transfer of TINs between software systems is not as simple as with rasters (Pareschi et al., 2000).

For the purposes of geophysical modelling a precise DEM for accurate modelling and subsequent analysis of the results is paramount. The existing DEM for Arequipa (based on digitising 1:25,000-scale topographic maps and on radar interferometry) has a resolution of 30 m which characterises the area well. However many of the features within the channel, which can impact on flow behaviour (e.g. terraces, bridges), are not represented. The absence of these characteristics on an individual valley may have a significant impact on the results of a simulation. DEM resolution has been shown to impact a wide range of characteristics including flow direction, and properties such as channel networks and flows extracted from DEMs (e.g. Wechsler, 2007).

DEM accuracy can be complicated to determine due to the many variables used in DEM creation. Factors affecting accuracy can include the data type and the nature of the algorithms used to compute terrain (Wechsler, 2007). DEM accuracy does however decrease with coarser resolutions while smaller grid cells allow better resolution of complex topography. The selection of an appropriate resolution ultimately depends on characteristics of the study area such as topographic complexity and nature of the analysis (Kienzle, 2004). The following section outlines the methods undertaken to create a new DEM for Arequipa with an enhanced resolution.

1.4.2.1 Data acquired for DEM creation

The main source of data for the creation of a new DEM was the DGPS points collected in Arequipa which were augmented by data obtained from satellite imagery.

Post-processing GPS data

DGPS data acquired in 2007 and 2008 were post-processed, which is a method of removing the both natural and man-made errors that affect GPS measurements (Trimble, 2004). In post-processed DGPS, the post-processing software calculates the error in each GPS measurement

logged by the reference station receiver, and applies the error corrections to measurements in the rover data file. Post-processing can use multiple base observations from before and after the measurement to achieve a better accuracy (Trimble, 2004).

The data collected in 2007 was converted from TPS (Topcon) format to RINEX and then to ASHTECH for post-processing using computer software called WINPRISM. More data points were logged in 2008 and the program Ashtech Solutions handled the large data set much better than WINPRISM. The resulting GPS files were then filtered using a Matlab-based program called FiltreGPS (Bovin, 2008), to disregard points with a low number satellites, high PDOP (accuracy of 3D GPS position, related to the satellite position), high root mean square (rms) error and also duplicated points.

The GPS points were saved as an ASCII grid and imported into ArcGIS for DEM creation. When the points were plotted there were a high number of artificial sinks and high points in the data from both 2007 and 2008. It was discovered that an error was made during the acquisition of the base station location for the post-processing. Initially the base station location was acquired from a GPS point taken at the NASA Arequipa Laser Station. A GNSS monument, an exact known location, was measured by the rover. In order to determine the exact location of the base station at Samana Hotel, the rover point taken from the Laser Station was treated as a base, and the Samana Hotel base as a rover. The file was post-processed using the location of the GNSS monument to give the location of the base station. The files were post-processed using the acquired base station co-ordinates (16°23'24,0201"; 71°32'44,4511"; 2405.32 m). The same procedure was undertaken for the 2007 and 2008 data using slightly different base station locations (see earlier text). To remedy the error, data was obtained from a continuous permanent NASA base station in Arequipa.

RINEX files from 57 days (24 from 2007, 33 from 2008) were downloaded from <ftp://igsceb.jpl.nasa.gov> (Facility Data Group, UNAVCO); and each day included one navigation (.N) and one observation (.O) file. The RINEX files were uncompressed from a compact RINEX file using the CRX2RNX software, and then converted into Ashtech format (the same as the DGPS data files collected in the field) for use in WINPRISM. Using the known fixed coordinates from the NASA base station (16°27'55.8612; 71°29'34.0680; 2489.05 m) and the Samana hotel base station files from 10 days in 2007 and 10 days in 2008,

the location (averaged over the 10 days) of the Samana hotel base station in 2007 and 2008 were determined in WINPRISM. The new locations are given in Table 1.4 below.

Year	Base station	Coordinates in WGS84		Elevation (m)
		Latitude	Longitude	
2007	Samana hotel – northern balcony	16°23'24.0201"	71°32'44.451"	2405.20
2008	Samana hotel – northern balcony	16°23'24.0288"	71°32'44.455"	2405.00
2008	Samana hotel – roof of southern balcony	16°23'24.4248"	71°32'44.466"	2408.32

Table 1.4: Location of the base station used in this study, situated at the Samana Hotel in the Yanahuara district of Arequipa.

The GPS files were post-processed using the newly acquired base station locations in WINPRISM (2007 data) and Ashtech Solutions (2008 data), and then filtered using FiltreGPS. Only 20% of the points were retained, so the MATLAB script was modified to retain 50% of the GPS points, approximately 50,000. The data was then plotted in Excel to remove any outliers in the dataset. The GPS points were saved as an ASCII grid and imported into ArcGIS for DEM creation. When the points were plotted the distribution of points in the Z-axis indicated a problem with data collected in 2007; there were still abundant sinks and high points in the data. Figure 1.13 shows an ArcGIS 3D plot of GPS points collected in Arequipa during 2007 and 2008. Points to the right of the image are gently sloping to the left and represent the Río Chili Valley from the entrance of the canyon and downstream. To the left of the image, these points represent the survey taken in 2007 near the city centre.

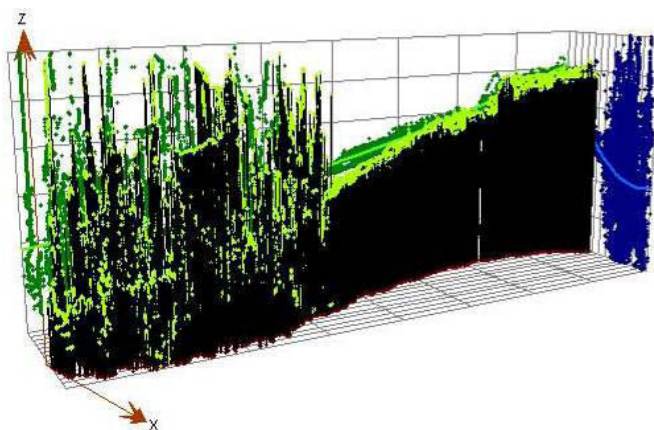


Figure 1.13: A 3D ArcGIS plot of GPS points collected in Arequipa during 2007 and 2008. Points to the right of the image were taken in 2008, points to the left were taken in 2007.

The problem in the 2007 dataset was attributed to the data being collected in static mode and not in kinematic mode (personal communication, J-F., Oehler, 2010a). The data was

reconfigured into kinematic mode using the software Topcon Tools. Post-processing of the base and rover data using the established base station location was also undertaken using Topcon Tools. The 2007 and 2008 GPS points were combined and exported as an ASCII grid, and plotted in ArcGIS to represent the topography of the Río Chili Valley and Quebrada Huarangal fan.

Satellite data used to complement the DGPS data

The DGPS points alone provide excellent coverage of the study areas in the Río Chili valley and the Quebrada Huarangal fan (chapter 5). However a larger area, including the summit of El Misti, was required for subsequent computer modelling. An investigation into the appropriate data to complement the DGPS data was undertaken using the previously created 30 m DEM, ASTER GDEM and SRTM DEM.

SRTM DEM

NASA's Shuttle Radar Topography Mission (SRTM) acquired data in February 2000, from which DEMs have been created (Rabus et al. 2003). A version 2 SRTM DEM for Arequipa was downloaded from NASA (<ftp://e0srp01u.ecs.nasa.gov/srtm/>) with a 90 m resolution. The data was converted into UTM coordinates, and imported into Surfer 8 where a contour plot of the study area was created for comparison with other data available.

ASTER

A Version 1 ASTER (Advanced Spaceborne Thermal Emission and Reflection Radiometer) Global DEM (GDEM) was downloaded from NASA (<https://wist.echo.nasa.gov/api/>). The image is in GeoTIFF format with geographic lat/long coordinates and a 1 arc-second (approximately 30 m) grid. Estimated accuracies for the global product were at 20 m at 95% confidence for vertical data and 30 m at 95% confidence for horizontal data (Fujisada et al. 2005). The data was converted into UTM coordinate, and imported into Surfer 8 where a contour plot was created of the study area for comparison with other data available. The ASTER 30 m DEM was chosen as the best fit for complementing the DGPS points collected in Arequipa for this study because it is more accurate than the 30 m Arequipa DEM and has a better resolution than the SRTM DEM (Chapter 3).

1.4.2.2 Combining DGPS and satellite data

A script was applied in Matlab 7.0 to add more than 50,000 DGPS points to the ASTER GDEM data. The results of the combined data indicated a systematic error in the elevation between the two data sources, whereby the ASTER data was at a continuously lower elevation than that of the DGPS data. One hundred data points were chosen to determine an average difference in elevation of approximately 40 m. The conversion of DGPS elevation points into orthometric height – by subtracting the height of the geoid (with reference to the WGS84 ellipsoid) – approximated to the 40 m height difference between the two data sources. The discrepancy in elevations could also be explained by the difference of vertical accuracy of the two data sources and/or different projections. A Matlab script was applied to subtract 40 m from all DGPS elevation values to account to bring them in line with the ASTER elevation.

The influence of the ASTER points on the DGPS points was also taken into consideration, whereby a buffer zone was created to exclude all ASTER data within the study area. The effect was to ensure that the DGPS data would have the maximum effect on the DEM in those localities. For example, a slight difference in elevation between the DGPS point and surrounding ASTER points could misconstrue a terrace boundary, or an important feature outlined during DGPS surveying. The buffer zone also excluded all ASTER points within a user-defined distance (e.g. 0 – 50 m) of the boundary of DGPS points. The influence and determination of the optimum buffer width was explored once the data had been interpolated (Section 1.5.2.2 and Chapter 3).

1.4.2.3 Data interpolation

The combined DGPS and ASTER data was interpolated to create the final DEM. Interpolation is undertaken using computer driven mathematical algorithms, for which a number of different models exist. Each model makes different assumptions of the data, and certain models are more applicable for specific data. Many studies have shown that the chosen model can influence the accuracy/quality of the surface produced (e.g. Wise, 2007; Huggel et al. 2008), and the choice of model depends upon the surface under investigation, as well as the nature of the data (e.g., source, density and spacing of points) for interpolation.

Detailed reviews and analyses of the various interpolation approaches have been undertaken by other authors (e.g. Yilmaz, 2007) and will be only briefly discussed here.

Interpolation methods can be classified into deterministic and geostatistical. Deterministic interpolation methods use mathematical functions to calculate the values at unknown locations based either on the degree of similarity (e.g. Inverse Distance Weighting: IDW) or the degree of smoothing (e.g. Spline) in relation with neighbouring data points. Geostatistical techniques use both mathematical and statistical methods to predict values at unknown locations and to provide probabilistic estimates of the quality of the interpolation based on the spatial autocorrelation among data points (e.g. Krigging) (Johnston et al. 2001). Data can also be triangulated to create a TIN.

DEMs were created utilising a number of different interpolation techniques to assess which interpolation technique is most favourable for modelling volcanic mass flows. Six different models were used: IDW, Spline, Krigging, Natural Neighbours, and Topo to Raster. Interpolation was undertaken in Surfer 9 for all models with the exception of Topo to Raster which is a model exclusively used in ArcGIS 9.1. Different parameters within the models were investigated and each interpolation method was visualised with shaded relief and contour maps after Wood and Fisher (1993) and Schwendel et al. (2010). The maps were qualitatively examined and interpolation methods that did not represent the surface realistically were excluded from further analysis (Chapter 3).

A grid size of 10 m for the enhanced DEM was chosen to provide a good representation of the overall Arequipa area while not losing any detail in the DGPS surveyed region. The 10 m grid size was deemed suitable to account for small scale variation in densely surveyed areas, but still large enough to avoid the occurrence of artefacts (e.g. Williams, 2008; Schwendel et al., 2010).

1.4.3 Creation and management of GIS data

The purpose of this study is the provision and validation of data necessary for prevention and assessment of volcanic hazards of El Misti over the city of Arequipa. Thus, the GIS created for Arequipa involves compiling a database containing information layers needed for the project. These layers of information are analysed in order to obtain answers to questions

posed by the researchers who address specific problems. The mode of formation of the GIS database must be carefully considered, the available data sources and the format of data integration within the database must be identified. It is essential to update the data regularly, so as to sustain the validity of the database.

A database on the city of Arequipa and El Misti volcano has been established in ArcGIS integrating all documents available. Several layers of information have been created in order to complete the database. Information layers constituting the database (Van Westen et al., 2003) are built around a core consisting essentially of: 1) Hazard maps indicating the probability of occurrence of potentially damaging phenomena within a period of time; 2) A database of elements at risk (buildings, infrastructure, etc.); 3) Analysis of the vulnerability of these elements against the specific hazard; 4) Estimate of the potential damage to these elements; and 5) Multi-hazard risk assessment, such as the creation of risk maps by the combination of several hazards. The formation of these layers and their incorporation into the database are described below.

1.4.3.1 Georeferencing

Georeferencing something means to define the location of an object in space; by establishing a relationship between page coordinates (i.e. x, y) with known real-world coordinates (i.e. longitude/latitude, UTM, etc) (ArcGIS helpdesk, 2009). A relationship can be established between raster or vector images and coordinates by the spatial location of other geographical features. Orthophotos, SPOT5 satellite imagery, and cadastral, transportation and infrastructure maps of Arequipa were georeferenced and rectified using the Georeferencing tool in ArcMap.

1.4.3.2 Building, infrastructure and land use

Data gathered from the building and infrastructure surveys conducted in Arequipa were mapped over a cadastral plan of the city in ArcMap, with most of the information stored in shapefiles (a geospatial vector data format). Polygon shapefiles were created for each building and land-use type, and point or polyline shapefiles (depending on the attribute being mapped) were created for different infrastructure. Additional information, such as geotechnical characterisation of building materials or the derived vulnerability functions

(chapter 4), were added to the attribute table in ArcCatalog. Data gathered from other sources (e.g. ITC Atlas database and city road plans) were either used to create new shapefiles or to add to the attribute table of existing shapefiles.

1.4.3.3 Hazards and flow data

Polygon shapefiles were created based upon the geological map and hazard scenarios of Thouret et al. (2001), Delaite et al. (2005) and this research (Chapter 2). Additional information such as weights were assigned to the lahars according to their magnitude and their recurrence (Section 1.7 and Chapter 2), and were added to the polygons attribute table. A geotechnical map was created by Delaite (2003), which assesses what materials are will likely be remobilised during the passage of a lahar. The geotechnical map was exported from ILWIS and imported into ArcGIS, and additional information was added to the polygons attribute table.

Delaite (2003) also scanned paper maps of the river systems of Arequipa and the region and digitised on screen to produce a polyline. The river vector file was exported from ILWIS and imported into ArcGIS as polyline shapefile layer. In addition, Titan2D simulation output ASCII files were imported into ArcGIS. Pile heights were displayed as point shapefiles, and then interpolated into surfaces (rasters) showing the extent and thickness of flow simulations (section 1.5 and Chapter 3).

1.4.4 Displaying and analysing data

One of the main techniques for combining multiple layers of information within a GIS is the spatial overlay operation. It involves superimposing different levels of information in the study area, georeferenced using the same system of referencing. The principle of this technique is to compare the different characteristics of a region depicted in the different layers, which are assigned tables. Multiple layers which included: information on the flow inundation area, depth and velocity; geotechnical properties of the soils; and information on buildings, land use and infrastructure were combined to develop risk maps based on the three scenarios that could occur if a new eruptive period of El Misti began (Chapters 4 and 5). The resulting maps were processed and displayed using ArcGIS.

1.5 Computer modelling of mass flows

The determination of the total run-out distance, the area affected by the event and the energy along the flow path are all necessary for mass-flow hazard mapping – traditionally undertaken by extrapolating past inundation areas of each type of flow on the present topography. In the last decade or so, advances in computing power and graphical computer interfaces alongside the development of numerical models has greatly aided, in conjunction with conventional techniques, the development of volcanic mass-flow hazard mapping. In addition, outputs of numerical simulations combined with GIS and remotely sensed data allows information to be easily communicated to decision makers.

Numerical simulation and characterisation of mass flows is based on either determining empirical relationships identified from experiments and flow observations, or by comparing physics-based flow models to experimental or natural examples (e.g. Iverson and Denlinger, 2001; Denlinger and Iverson, 2001). Numerous flow models exist today (such as DAN, VolcFLOW, FLO-2D, LaharZ and Titan2D) and many have been useful in gaining a better understanding of mass flow behaviour, forecasting the distribution of mass flows and permitting the development of hazard and risk maps. A summary of some models are described in Table 1.5. All models have their advantages and disadvantages and it is up to the user to decide based upon literature of scientific studies and analysis which model is best for the purpose in question. Reasoning can include the flow type, initiation and deposits, and the physical or statistical model relationships. For this research project, a code was required which could model two-phase flow relationships and provide outputs which could be used in hazard analysis.

Name	Theory	Principles	Reference
LaharZ	Statistical model	Uses an empirical relationship between the planimetric area, cross-sectional area, and volume of debris flows (in the Cascade Range) to map areas that could be potentially covered by future debris flows on a DEM. LaharZ simulates volcanic debris flows providing statistical analysis of deposits.	Schilling (1998)
DAN	Continuum model	A continuum model based on a Lagrangian solution of the equations of motion. DAN allows the selection of a variety of material rheologies, which can vary along the slide path or within the slide mass. The model is 1D and divides the moving mass into constant volume slices perpendicular to the base and keeps track of the forces on each slice. A variety of flow rates are applied to calculate basal resistance.	Hungr (1995)
Flow	Simplified Mathematical Model	Calculates the velocity and simulated flow path over a DEM. Movement of the flow is determined by the initial conditions, gravitational acceleration, and resistance to the motion. Resistance to the motion is described as Coulomb, viscous, or turbulent.	McEwan and Malin (1989)
Flow2D	Mathematical Model	Developed to overcome topographical errors generated with an energy line model. This code assumes that the shear resistance depends on both basal friction and viscosity parameters. Development of Flow2D has been superseded by Flow3D.	Sheridan and Macías, (1995)
Flow3D	Based on Coulomb resistance to a sliding block	The model calculates the changes in velocity as the block slides across a DEM; the block trajectory is traced in small increments of time until it stops. The velocity and position of the block at each time step can be recorded and plotted to show the trajectory and the run-out of a large number of blocks.	Sheridan and Kover, (1996)
VolcFlow	Depth-average approximation	Based on a depth-average approximation, where equations are solved using a shock-capturing numerical method based on a double upwind Eulerian scheme. This depth-average approximation is represented by a topography-linked coordinate system. Various rheologies can be used (frictional, Bingham, viscous) or can be created by modification of the initial code.	Kelfoun and Druitt (2005)
Flo-2D	Volume conservation model	Volume conservation model that distributes a flood hydrograph over a system of square grid elements. It implements the Diffusive Hydrodynamic Model (DHM) created by Hromadka and Yen (1987), which is a simple numerical approach with a finite difference scheme that permits modification of the grid element attributes.	O'Brien et al., (1992)
Titan2D	Based upon a model for an Incompressible Coulomb continuum	Depth-averaged 'shallow water' granular flow model, which assumes a continuum volume, parcels of which are pulled down by gravity. The friction between particles, and the ground resist momentum, and conservation equations are solved using a coulomb type friction term for the interactions.	Pitman et al., (2003)
ArcGIS Hydro	Hydrological models	Vertical variations in flow characteristics (sediment concentration, rheology of material, friction, viscosity etc.) are summarised as vertically averaged values; solving shallow water equations to predict flow levels and depth averaged velocities; solved under a variety of numerical methods, and over a variety of different grids.	ESRI (2007)
Mike 21			DHI
Delft 3D			Delft Inc.

Table 1.5: A summary of some models, and the fundamental theory behind their development, used for modelling mass flows (e.g. floods, pyroclastic flows, lahars). This table is by no means exhaustive, but provides a range of models that have been created and applied. Compiled and adapted from Martelli, 2007 and Procter, 2010.

1.5.1 Introduction to Titan2D

Titan2D is a model based on widely accepted flow physics, which has been used to successfully to model a range of mass flows in both volcanic and non-volcanic environments, and is one of the reasons it was chosen. The other reason is to extend on the work already undertaken using Titan2D at El Misti. The following sections discuss the principles of the model, along with the applications.

Titan2D was developed by the Geophysical Mass Flows Group at SUNY, University at Buffalo for simulating geological flows by combining numerical granular flow codes with digital models of natural terrain (Pitman et al., 2003; Patra, 2005; Titan2D User Guide, 2007). Titan2D is based on models of Savage and Hutter (1989); Iverson (1997); Denlinger and Iverson (2001) and Iverson and Denlinger (2001) for simulating a dry granular flow, or a two-phase fluid plus granular flow (Patra et al., 2005; Pitman and Le, 2005). Titan2D is available publically for use with Linux and Windows platforms (downloaded from <http://www.gmfg.buffalo.edu>).

1.5.1.1 Titan2D “single-phase” Model

The model is a depth-averaged 'shallow water' granular-flow model, which assumes a continuum volume, parcels of which are pulled downslope by gravity. The friction between particles and between particles and ground resist this momentum, and the conservation equations for mass and momentum are solved using a Coulomb-type friction term for the interactions between the granular material and the basal surface. The governing equations (described in Patra et al., 2005 and Pitman and Le, 2005) are solved using a parallel, adaptive mesh, Godunov scheme and The Message Passing Interface (MPI) (Pitman et al., 2003). The MPI allows for computing on multiple processors, which increases computational power, decreases computational time and allows the use of large data sets (Pitman et al., 2003; Patra et al., 2005). In addition, adaptive gridding allows for the concentration of computer power on regions of special interest, with mesh refinement capturing the leading edge of the flow as well as locations where the topography changes rapidly (Pitman et al., 2003).

Titan2D operates in a LINUX environment via a python scripted Graphical User Interface (GUI) (Pitman et al., 2003). Terrain data is entered into the simulation via the GRASS

(Geographic Resources Analysis Support System; U.S. Army Corps of Engineers' CERL) GIS environment and format. Through this interface the user inputs the parameters needed to successfully run the program, which are pile dimensions, starting co-ordinates, internal and bed friction angles, and simulation time. The simulation is then computed on a DEM of the desired region. The outputs of Titan2D are flow momentum, depth, run-up, height, inundation area and dimensional time. The results can be displayed through the TITAN2D viewer utilities, open source GRASS GIS or other visualization software packages (such as Tectplot or ArcGIS).

1.5.1.2 Titan2D “two-phase” Model

The Titan2D two-phase model is “a ‘thin layer’ system of equations modelling the depth-averaged flow of granular material coupled to interstitial fluid, as the two-fluid mix moves over topography” (Pitman and Le, 2005). The Model uses the balance laws of mass and momentum equations for both fluid and solid phases, based upon Savage–Hutter theory (Savage and Hutter, 1989) and Iverson (1997), which are well accepted in fluid mechanics. Each phase is balanced as individual constituents with the two-fluid equations of Anderson and Jackson (1967), and following Anderson et al. (1995), to mathematically explain the description of solids and fluid flow and interaction. The resulting hyperbolic system of equations describes the motion of the two constituent phases and is fully explained in Pitman and Le (2005). The governing equations are solved in the same way as the single-phase model and applied through the Titan2D Toolkit (e.g. via a GRASS environment). This numerical model allows for the simulation of debris flows and lahars.

1.5.1.3 Studies using Titan2D

Many researchers have used Titan2D to model a range of mass flows from debris avalanches to scoria and ash-flows. Table 1.6 below presents a summary of some of these studies. It is by no means exhaustive but gives an indication into the general acceptance of Titan2D.

Phenomenon	Location	Author/s
Lahars	Cotopaxi Volcano, Ecuador	Williams, 2006; Williams et al., 2005, 2008
	Santa Ana Volcano, El Salvador	Bajo et al. 2009
	El Misti, Peru	Stinton et al. 2004a; Delaite et al. 2005; Vargas et al., 2010a
	Popocatepetl, Mexico	Muñoz-Salinas et al., 2004, 2008
	Mt. Ruapehu, New Zealand	Cronin et al., 2004; Procter et al., 2004b, 2010b ; Procter et al, 2010a; Sheridan et al., 2010b
Block- and- ash flows, pyroclastic flows, and debris avalanches	Cerro Machin Volcano, Colombia	Murcia et al., 2008, 2010
	Galeras Volcano, Colombia	Stefanescu et al. 2010
	Arenal Volcano, Costa Rica	Berrocal and Malavassi, 2006
	Tungurahua Volcano, Ecuador	Sheridan et al., 2004
	Santa Ana Volcano, El Salvador	Bajo et al. 2009
	Merapi, Indonesia	Charbonnier and Gertisser, 2008, 2009; Gertisser et al. 2011
	Mt. Etna, Italy	Norini et al. 2007
	Colima Volcano, Mexico	Pitman et al., 2003; Rupp et al., 2003, 2006; Saucedo et al., 2004; 2005; Sulpizio et al., 2010
	El Chichón Volcano, Mexico	Macías et al., 2008
	Nevado de Toluca, Mexico	Capra et al., 2005, 2008; Grieio et al., 2007
	Soufrière Hills Volcano, Monserrat	Hidayat et al. 2007, 2008; Ogburn et al., 2008; Widiwijayanti et al., 2004, 2007, 2010
	Mt. Taranaki, New Zealand	Procter et al., 2004a, 2009, 2010b,c; Procter, 2010
	Mt. Ngauruhoe, New Zealand	Martelli and Cronin, 2006; Martelli, 2007
Mount Rainier, U.S.A	Sheridan, 2005; Stinton et al., 2004b	

Table 1.6: *Compilation of major studies using Titan2D since 2004. Block- and- ash flows, pyroclastic flows, and debris avalanches have been put into the same category because in many cases authors interchanged terms, thus the individual classification becomes difficult. In some instances, both pyroclastic flows and debris avalanches were the focus of an individual study.*

1.5.2 Methods for Titan2D two phase modelling at El Misti

All studies conducted at El Misti using Titan2D concluded that further investigation of the model at this locality is warranted (refer to Chapter 3). This research project focussed on flows which exist in two phases: a solid and a fluid phase, such as lahars, hyperconcentrated flows and flash floods. Thus a model was required that could represent both phases in flow. The Titan2D “two-phase” model was chosen as it is based on recognised and accepted flow physics and has been used to successful model other two-phase flows such as lahars at Mt.

Ruapehu, New Zealand (e.g. Procter et al., 2010a) and Cotopaxi Volcano, Ecuador (Williams et al., 2008).

The Titan2D two-phase model (Version as of July 2007) was acquired from the Geophysical Mass Flow Group, SUNY, University at Buffalo. Firstly, the sensitivity of the 30 m DEM was analysed using changes in the simulation input parameters including: 1) DEM, 2) internal and basal friction angles, 3) volume, 4) starting point, 5) simulation time, and 6) solid fraction, and by assessing the modelled flow features. More than 200 simulations were run in order to get the best correlations with the geological record and previous studies. The most favourable parameters were then selected and applied to the 10 m DEM. Following this comparisons were made between the outputs from the differing DEMs. These results can be found in Chapter 3.

1.5.2.1 Input parameters

Definitions of the input parameters are summarised below, for a more in-depth analysis of the input parameters with relation to the simulations performed at El Misti refer to Chapter 3.

DEM

Titan2D performs flow simulations on a DEM of a desired region and the simulation accuracy and speed is highly dependent on the DEM resolution and quality. The model uses the component of gravity along a terrain as a driving force; therefore accurate slopes derived from DEMs are vital (Capra et al., 2010; Stefanescu et al., 2010). Studies conducted on the effect of DEM resolution for geophysical mass flow modelling (e.g. Titan2D: Capra et al., 2010) have shown that DEM resolution is fundamental for simulation accuracy, i.e. a better resolution and quality DEM leads to more results more faithful to the behaviour of real flows influenced by topography.

Friction angles – basal and internal

Friction angles (internal and bed friction) are one of the more important input parameters in Titan2D modelling. The internal friction angle is a parameter that provides a measure of the strength to the material. This strength can be attributed to two factors: 1) the friction between individual grains and 2) the geometrical interlocking between the particles (Saucedo et al., 2004). The internal friction angle corresponds to the angle of repose, which is a measure of

the natural slope that would form if a cylindrical pile of the granular material was placed on a flat plane and allowed to collapse under its own weight (TITAN2D User Guide, 2007). A slight control on the lateral spread of the simulated flow can be achieved by changing this value in Titan2D. However most authors have shown that the internal friction angle has little effect on the output of the flow models, within a reasonable range of values (Sheridan et al., 2005; Dalbey et al., 2008; Murcia et al., 2010). The basal friction angle corresponds to the minimum slope that an inclined surface must attain before the material placed on it begins to slide from its static position (TITAN2D User Guide, 2007). In contrast to the internal friction angle, the variation of this parameter has been seen to have a strong influence on Titan2D flow dynamics such as acceleration and velocity of the moving mass (Patra et al., 2005; Murcia et al., 2010; Procter, 2010).

Volume

The flow volume is determined by specifying the initial pile volume, derived from the pile's dimensions (height, width and length). The selection of appropriate dimensions is crucial to guarantee reliable results as these pile dimensions, and their relationship to the drainage channel can affect the way in which the flow is modelled.

Starting point

The starting point is the location of the centre of a pile for the initiation of the flow. The starting point can be selected by applying the energy cone relationship (e.g. Delaite et al., 2005), or the point can be selected by taking into consideration the dimensions of the drainage channel in question, and local slope conditions that could lead to the initiation of a volcanic mass flow.

Time

In Titan2D, the maximum number of time-steps and the maximum time (in seconds) must be input into the model as this defines the run time of the simulation. When the job is submitted for processing, the simulation will stop when it has either gone through the time steps or has simulated the specified amount of time. Both the values should be set high enough to ensure that the geologic event being simulated has ended (i.e. the material has come to rest). If either of the values is set too low, the simulation will end with material not having reached static equilibrium. If both these values are set excessively high however, wasted computation will be performed, dynamically simulating the pile whilst it remains in static equilibrium

(Titan2D User Guide, 2007). The number of computed time-steps needed also varies depending on the amount of computational mesh points used, the friction parameters, the use of grid adaptation, the simulation order and the initial pile geometry and location.

Solid fraction

The sediment concentration of a two-phase flow plays an important role in flow behaviour and mechanics, and thus the determination an appropriate solid fraction value to be used in Titan2D is critical (Iverson, 1997; Pierson, 2005). As discussed in the Introduction (see Figure 1 and Table 2) the determination of the appropriate solid content of a lahar can be difficult because a lahar event can transform between one or more flow phases, including a debris flow phase, a transitional or hyperconcentrated flow phase and a streamflow phase, which can vary during the flow event (Vallance, 2000; Dumaisnil et al., 2010). Water floods normally transport mostly fine sediment and in relatively small quantities – containing generally less than 4% by volume (vol.%) or 10% by weight (wt.%) suspended sediment (Pierson, 2005). In contrast, high-discharge debris flows (and/or mudflows) may transport more sediment than water with sediment concentrations in excess of 60 vol.% (80 wt.%) (Pierson and Costa, 1987; Costa, 1998).

1.5.2.3 Output files and examining flow features

Output files

Outputs files show the time slices for travel time and velocity, pile thickness and inundation area, and were visualised in Tecplot and Paraview. To get more useful data, a computer program was written for this research project in C# for Microsoft Windows (“Reform.exe”; Kellman, 2010) to convert tecplot files to ASCII files and to exclude data where pile heights were less than 0.1 m. The ASCII files were then imported into ArcGIS for further analysis (see section 1.4.3.3 and Chapter 3).

Examining flow features

The observation of flow behaviour is important for modelling mass flows and furthermore for assessing their hazards (Sheridan, 2005). Flow features including run out, super-elevation, ponding, flow divergence and convergence were examined to observe if simulations provided realistic results. The analysis of flow behaviour is discussed in Chapter 3.

1.6 Hazard analysis

Hazard identification is the first, and in many ways, the most important step in risk assessment. A volcanic hazard (H) in volcanic risk assessment is defined as the probability of a given area being affected by potentially destructive volcanic processes or products within a given time period. Crandell et al. (1984) summarised that the essential data needed for an adequate hazards assessment should include: 1) complete record of historical eruptions; 2) prehistoric eruptive activity deduced from the geologic record; 3) geologic (especially stratigraphic); petrologic, and geochemical data on the nature, distribution, and volume of the eruptive products; and 4) dating of the volcanic products and events interpreted from them. Acquisition of these data provides key constraints on the types, scales, duration, recurrence, and other characteristics of hazardous processes that have dominated the volcano's eruptive history. All of which provide the basis for assessing potential hazards from future eruptions.

The hazard analysis undertaken for the lahar and flash flow hazard at El Misti (Chapter 2) is based upon an analysis of the geological and historical records of deposits, their extent, thickness and age, from which the magnitude and frequency was determined. Hazard scenarios were then developed and mapped for the two study areas.

1.6.1 Determining the magnitude, frequency and extent

The magnitude, frequency and extent of lahars and hyperconcentrated flows at El Misti have been determined by previous authors (e.g. Legros, 2001; Thouret, 2001; Delaite et al., 2005). An extensive overview into historic flood records was under taken in order to improve the present knowledge. A Gumbel Law distribution (Richards, 1982) was used to calculate the recurrence of flood discharge for the Rio Chili. The equations is as follows, where the n is the maximum annual flow rate and N is the total population.

$$F(Q) = \frac{(n - 0.5)}{N}$$

The terraces of the Rio Chili and the Quebrada Huarangal fan were mapped in order to magnitude and frequency of events, establish hazard scenarios and form the basis for lahar and flash flood hazard zonation maps.

1.7 Vulnerability analysis

A vulnerability analysis has been undertaken based upon: 1) the building, land use and infrastructure surveys conducted in 2007 and 2008, 2) the analysis of reported damage (e.g. Pinatubo, Pierson, 1992; south east England floods, Kelman, 2002; Soufrière Hills volcano, Baxter et al., 2005), 3) techniques of structural engineering (housing, urban infrastructure, basic services and communications), and 4) using methods adapted from Vargas et al. (2010b) and others (e.g. Thouret and Vivian, 2009; Spence et al. 2005a,b; Pomonis et al. 1999). Building types, land use and infrastructure were classified and ranked according to different criteria such as construction materials, essential/critical facilities, and economic repercussions.

1.7.1 Buildings

The influence of different structural components needs to be taken into consideration to determine the most vulnerable building type. Building types were defined, classified and ranked according to the type of frame, wall and roof materials, roof types, storeys, proportion of windows, to name a few. Coefficients, where 0 is not vulnerable/good quality and 1 is very vulnerable/bad quality, were assigned to each building feature, and sub-feature. The mean value was calculated from the coefficient totals to define which building type was the most susceptible to lahars and floods. These values also allowed the ranking of buildings from least to most vulnerable.

1.7.2 Land use

Land use classification for defining element vulnerability is as crucial as the classification of building and infrastructure construction itself, because the consequence of losses depends on the occupancy of the structures (e.g. private dwellings will usually have less people present than in hotels). The *structure* in this research refers to the building and associated land regardless of what its purpose is (e.g. school, dwelling, sports stadium, power station). By defining the dominant land use, one can easily identify structures whose survival is important and vital during a crisis and which are intended to remain operational during and after a volcanic crisis.

Coefficients, ranging from 0 (low importance) to 1 (high importance) were assigned to different categories (such as economic repercussions, population exposure and value) for each land-use type. These coefficient values were added together and averaged to give a value between 0 and 1 for the importance of the particular land use and therefore the vulnerability during a volcanic crisis. The values were normalised to account for subjectivity in assigning the values, normalised minimum and maximum values were obtained from which the mean value of all the criteria was calculated. The results were mapped to show the vulnerability distribution within the study areas (Chapter 4).

1.7.3 Infrastructure

As modern urban functions rely on lifeline systems much more heavily than in the past, infrastructure constitutes a major component of the vulnerability of a city if a disaster strikes. Infrastructure can be defined as the basic physical and organisational networks needed for the operation of a society, or the services and facilities necessary for an economy to function. These can include water supply, sewage, gas distribution, power supply and telecommunications network just to name a few.

The vulnerability analysis included elements such as defining whether the lifeline is critical and/or essential, whether the population would be exposed during the daytime and/or during the night, the economic repercussion in terms of loss of income and the rebuild cost, the age of construction and the type of materials it is constructed from, the energy output (for electrical infrastructure), the distance from the river and the height above the river.

For each infrastructure type coefficients ranging from 0 (low importance) to 1 (high importance) were assigned to the different categories. These coefficient values were added together and averaged to give a value between 0 and 1 for the importance of the particular infrastructure and therefore the vulnerability during a volcanic crisis. The values were normalised to account for subjectivity in assigning the values, normalised minimum and maximum values were obtained from which the mean value of all the criteria was calculated. The infrastructure types were evaluated against one another to determine the most susceptible infrastructure present in Arequipa. The results were mapped to show the vulnerability distribution within the study areas (Chapter 4).

1.8 Risk analysis

Risk is a complex combination of hazard and vulnerability. The hazard is a potentially harmful natural phenomenon. Vulnerability refers to the propensity to suffer from damages in the event of the occurrence of a given hazard, or in other terms the social condition which makes it possible for a hazard to become a disaster.

The risk of inundation and/or damage to buildings, land and infrastructure was assessed by combining a number of tools: hazard assessments, flow characteristics and effects, and element vulnerability. The calculations were undertaken in a GIS allowing for the spatial expression of the risk element, which is an attractive method for communicating information to decision makers and the community alike. Another advantage of using a GIS is that databases can be readily updated when new information becomes available, thus allowing for the analysis of data in quasi real-time.

1.9 Conclusion

This research combined a number of techniques in order to define the physical vulnerability, namely of buildings and infrastructure, in urban areas threatened by lahars and flash floods. Using the case study of Arequipa, Peru, vulnerable areas were identified from former and current geological studies; conventional and computer-aided mapping of volcanoclastic and fluvial deposits; numerical flow modelling (Titan2D); field surveys of buildings and infrastructure; statistical analysis including multivariate analysis for the building and infrastructure surveys; GIS; and geotechnical characteristics of building materials (including mechanical tests). These methods have allowed for a multi-faceted study which in particular highlights the capabilities and limitations of diagnostic tools such as GIS and Titan2D in the application to the assessment of volcanic hazards, vulnerability and risk.

**PART TWO:
LAHARS AND FLASH FLOODS IN AN URBAN
ENVIRONMENT**

Chapter Two

Mass-flow hazards from El Misti Volcano

2.0 Introduction

The definition of the mass flow hazard (lahars and flash floods) from El Misti volcano is an important part of this research project. As discussed in the introduction, the eruptive history of El Misti volcano has been studied by several authors (e.g. Bullard, 1962; de Silva and Francis, 1990; Thouret et al., 1999, 2001; Delaite et al., 2005). Their research has culminated in the development of three eruptive scenarios for El Misti and subsequent hazard maps. For the analysis of the hazards posed by lahars and/or flash floods, the available data (geologic maps, flood photographs, etc.) has been revised to verify the flow volumes, scenarios and the mass flow hazard to Arequipa.

2.1 The mass-flow hazard at El Misti volcano

The current El Misti composite edifice comprises an eroded stratovolcano designated Misti 1, partially overlapped by two stratovolcanoes termed Misti 2 and Misti 3, and a summit cone, Misti 4 (Thouret et al., 1999, 2001). Lava flows and debris avalanche deposits make up Misti 1 (833 to 112 k.y.) while Misti 2 (112 to 40 k.y.) is characterised by lava flows and dome-collapse deposits. Non-welded ignimbrites 3-5 km³ in volume, were erupted at the end of Misti 2 (ca. 50 to 40 k.y.) and are likely to be related to the formation of a cluster of nested craters. Misti 3 (40 to 11 k.y.) is characterised by lava flows, block-and-ash, and ash-flow deposits, with pyroclastic deposits marking the formation of a summit caldera towards the end of Misti 3.

Pyroclastic flow, fall and debris-avalanche deposits are associated with the eruptive stage of Misti 4 (11 k.y. until the present), which involved the growth of the summit cinder cone and the formation of two summit craters. The larger summit crater is 950 m wide and the smaller 550 m across and 200 m deep. Thouret et al (2001) suggested that the larger crater could have been formed during the c.2030 yr BP eruptive episode. The inner crater cuts historic domes and contains a 130 m wide and 15 m high andesitic plug. There have been no major eruptions

since the colonisation of Arequipa in 1540, with only a few phreatic events in 1677, 1784 and 1787. Fumarolic activity continues to the present day inside the inner crater and on the uppermost northeast flank of the edifice.

To analyse the type, magnitude and frequency of mass flows which have been generated from El Misti a table (Table 2.1) was constructed from the literature (e.g. Thouret et al., 1999, 2001) and from dated deposits. The table summarises the main depositional units in each Misti stage along with the date, thickness and extent, dominant type of activity at the time of eruption, the corresponding VEI rank and an estimate of the eruptive frequency.

Edifice	Sub	Period	Depositional unit	Average thickness / Volume	Dated samples	Dominant activity	Magnitude range	Frequency (years)		
Misti 4 Summit Cone	4-1	Historic	Ballistics and thin ash fall	Scattered	1677, 1784 and 1787 chronicles	Phreatic, fumarolic	VEI 1 (2?)	Frequent		
		Historic	XVth century ashfall	5-10 cm (city)	AD 1440-1460 chronicle	Vulcanian, intermittent	VEI 2	c. 400 - 1000		
	4-2	2030 yr BP	Pumice fall and PFs	Pumice fall 30-50 cm, volume 0.35 km ³ . PF volume 1 km ³	2030 yr BP= 420 BC-340 AD	Subplinian transition to Plinian	VEI 4	2000 to 4000		
			Several ash falls and pumice falls	Each layer is 20-50 cm thick, totalling 2 - 4 m	Holocene < 10,000 yr	Vulcanian / subplinian / Plinian	VEI 2 to 4	2000 to 4000		
	3-4		SAF* deposits interbedded with pumice-fall and pyroclastic surges	Several metres thick when confined. Volume <0.5 km ³	11,300 - 13,700 yr	Vulcanian and phreatomagmatic	VEI 3	5000-10,000		
		13,000-14,000	Welded SF* and fall	Several metres	ca. 13,000 yr	Summit caldera-forming eruption	VEI 3 - 5	10,000 - 15,000?		
	Misti 3 Stratovolcano		> 14,000	Reworked tephra, debris-flow and stream-flow deposits (upper radial valleys)	Several metres thick when confined or in fans (Huarangal, San Lazaro)	Upper Pleniglacial	Reworked by meltwater from ice fields capping Misti and Chachani during the 2nd Glacial maximum (ca. 25,000 - 20,000 yr BP)			
				Interbedded BAF*, SF* and ash deposits with phreatomagmatic bombs	Each unit is several metres thick	20,000 - 25,000 yr	Dome growth and collapse intercalated with vulcanian events	VEI 3 to 4	3000 - 5000?	
		3-3	ca. 21-20,000	Pumice-fall deposit interspersed in BAFs*	Most voluminous Plinian fall unit 1-3 m thick, 9-13 km from vent	Youngest in Misti 3-3 erupted at ca. 21 ka. Pumice cobble from second pumice layer ca. 20.3 ka (TL*).	Plinian		VEI 4	4000 - 5000
			ca. <25,000 - 20,000 yr BP	Andesitic succession with at least 5 BAF* units	Several confined units 5-20 m thick each		Growth and destruction of Misti 3 domes built up between 25,000 - 20,000 yr BP	VEI 3 to 4	10,000-20,000?	
3-2			Yellow greenish PF* and tephra-fall deposits interbedded with group 3-2	10-15 m thick		Vulcanian and subplinian/plinian	VEI 3 to 4	5000?		
			Pumice-fall layers included within PF deposits	20-40 cm thick at least 12 km from the summit	c. 24,000-25,000 yr BP	Plinian	VEI 4	4000-5000?		
	ca. <30,000 - 25,000 yr BP	Dacitic BAF*s and lithic-rich PF deposits	30-50 m thick		Growth and destruction of domes built up of Misti 3 between <30,000 - 25,000 yrs BP	VEI 3 to 4	5000-10,000?			

Table 2.1: A summary of the age, extent, frequency, and dominant activity present at the time of eruption, for deposits at El Misti Volcano. Data based upon the literature (e.g. Thouret et al. 1999, 2001; Legros, 2001) and dated samples. *Note in the table BAF = block-and-ash flow, PF = pyroclastic flow, SF = scoria flow, SAF = scoria-and-ash flow, DA =debris avalanche and TL = thermal luminescence.

Misti 2 Stratovolcano	3-1	>31,000 to 33,000 - 34,000 yr BP	Yellow dacite pumice-fall and tephra-fall deposit overlies one dacitic lava and interbedded with groups 2-3 and 3-1	Pumice fall and ash fall decimetres thick; lava flow 10 m thick and 6 km long	Pumice cobble (TL*) 36.1 +/- 6.8 ka	Plinian and one effusive event	VEI 3-4	PF* 5000? Lava flow, one in c.35,000 yr						
			Large PF* deposit	Volume >1.5 km ³	ca. >31,300 yr BP (top of dacite)	Large explosive episode	VEI 4 to 5	Twice over 50 ka						
	2-3		Pumiceous and lithic PFs intercalated with pumice fall layers		>38,300 yr BP			VEI 5						
		2-3B	Between 38,300 and 49,000 yr BP	Non-welded ignimbrites forming groups 2-3A and 2-3B	30-40 m thick. Bulk volume of 3-5 km ³ .	49,000 - 43,000 yr BP	Formation of incremental caldera collapse or cluster of large craters	VEI 5	2 distinct ignimbrite-forming eruptive episodes					
	2-2	2-2A		Stream-flows and laharic deposits (in Quebradas) intercalated between groups 2-2 and 2-3	10-20 m thick		Period of erosion between groups 2-2 and 2-3 may reveal decrease in volcanic activity							
			> 43,000 yr BP	Bread crust bombs in scoriaceous deposit (from Charchani) interbedded with glacial and laharic deposits			Hydromagmatic interactions	VEI 2-3						
			ca. 70 - 50 ka	Andesite and dacite dome block, (matrix-poor) flow 10-20 m thick	10 m thick		Dome collapse flow	VEI 3?	Twice over 70 ka					
				Scoriaceous pumiceous PF* deposits interbedded with lava flows				VEI 2-3	At least three times over 50 ka					
	Misti 1	2-1	ca. 112 - 70 ka	Lava flows	Volume several to tens of km ³	112-70 ka	Effusive activity		Frequent at base of Misti 2					
			ca 112 ka	Several PFs* interbedded with lava flows	Several tens of metres thick	112-70 ka	Effusive and pyroclastic activity	VEI 3	Frequent in period 2-1					
		ca 835 - 112 ka	Lava flows	Hundreds of metres thick	Poorly constrained		Effusive activity							
		Closer to 112 than to 835 ka	DA deposits	10-100 m thick when confined. Volume of several km ³	Poorly constrained	Flank collapse towards the west		2 debris avalanche deposits known at Misti						

Table 2.1: Continued.

From the table of deposits at El Misti it is clear to see that mass flows have featured fairly frequently in the geological history of this volcano. Eruptive and post-eruptive lahars/mass flows were formed during the last significant eruption of El Misti in the fifteenth century (AD 1440-1460) when a Vulcanian eruption resulted in tephra 5-10 cm thick blanketing the city (Thouret et al., 2001). Furthermore, debris flows with an estimated volume of 1.5 to 3 million m³ were deposited in the Rio Chili valley and Quebrada San Lazaro. Additionally, lahars have swept down the Rio Chili valley and tributaries approximately 1,000 yr BP, 500 yr BP and as recently as the 1600s (Thouret et al., 2001).

Lahars formed during and following the major Plinian eruption of 2030 yrs BP. The collapse of a 21 km-high eruption column produced lithic and pumice-rich pyroclastic flows 0.7 km³ in volume (Thouret et al., 2001). Pyroclastic-flow and debris-avalanche deposits were transformed into lahars which flowed in the Rio Chili valley and in quebradas surrounding the volcano (e.g. 2030 yrs BP-old debris-flow deposits in the Rio Chili valley and Quebrada San Lazaro).

Dome growth and subsequent collapse during Misti stage 3 led to the formation of block-and-ash and pyroclastic flows, depositing sediment several metres thick down many valleys surrounding the volcano (e.g. Misti 3-3, ca. 21,000 to 20,000 yrs BP and Misti 3-2, ca. 30,000 to 25,000 yrs BP). Volcaniclastic sediment and melt water from ice fields that capped Misti during the second glacial maximum (ca. 25,000-20,000 yrs BP) also generated mass flows (Thouret et al., 2001). Reworked tephra, debris flow and stream flow deposits (>14,000 yrs BP) are several metres thick in upper radial valleys of Quebradas Huarangal and San Lazaro.

The volcano has also produced some particularly large events; ignimbrites deposits (e.g. 34,000 yrs BP, 25,000 yrs BP and 14,000 yrs BP) can be found at least 15 km from the crater, and pyroclastic-surge deposits up to 11 km to the south (Thouret et al., 2001). Calderas were formed between 50,000 to 40,000 yrs BP depositing ignimbrites with a volume of 3-5 km³ to the south-east, south and south-west of the volcano. It was during this time period that hydromagmatic interactions generated lahars.

Debris avalanches feature in the geological history of this volcano (e.g. during Misti stages 1 and 4). A frightening scenario is the formation of a lake due to waterway blockage by debris avalanche. This could lead to sudden dam bursts where voluminous mass flows could be

generated. While no evidence of dam-break flood deposits have been discovered as yet, lake deposits are present in the upper Rio Chili canyon (section 2.1.2 and figure 2.3) presenting the possibility of dam-break flood generation. Mass flows can also be generated from debris-avalanche deposits, given sufficient water availability.

The voluminous eruptive deposits (e.g. Plinian pumice-fall deposit, ca. 21-20,000 yrs, up to 3 m thick 13 km from the vent) provide evidence for an adequate debris source for mass flow formation, not only during the eruptive period but also many years or decades later. Snow meltwater or rainstorms can bulk loose volcanoclastic sediment on the slope of the volcano or in channels generating mass flows. Their formation is dependent on water availability however, snow cover is not permanent at El Misti and rain storms only occur from December to March. Nevertheless, the snowfield can cover an area of up to 7 km² in August or between December and May, with an estimated volume of 2.5 million m³ (Delaite et al., 2005). Furthermore, rainstorms with intensities greater than 10 mm per hour are common between December and March and can trigger flash floods and hyperconcentrated stream flows.

This geological history provides many credible scenarios for mass flow generation during a future eruption of El Misti.

2.2 Field studies of lahar and flood deposits

Stratigraphic sections and exposed deposits were studied to characterise the type, extent and magnitude of past flow events, focussing on two main areas (Figure 2.2):

- 1) Charcani Quinto: In the vicinity of one of the hydroelectric power stations (refer to figure 4.47, chapter 4 for a more detailed explanation) one of the EGASA hydroelectric stations situated ~5.8 km from the vent at an elevation of 2990 m (238113, 8200820). In the bottom of the 1.5 km deep gorge, a terrace system includes lacustrine deposits towards the base. This presents an interesting scenario for a possibility of a dam-break flood scenario for El Misti.
- 2) Rio Chili Valley: From the entrance of the canyon (232116, 8194785) to the southern boundary of the city centre (229410, 8187365), an area of ~8 km². The valley opens out from the entrance of the canyon into a series of agriculturally cropped terraces into dense urban areas built up on either side of the river.

Eight stratigraphic sections were studied along the Rio Chili Valley (Figures 2.2 – 2.6), and one sample was taken for ^{14}C dating (Figure 2.7 and Table 2.2).

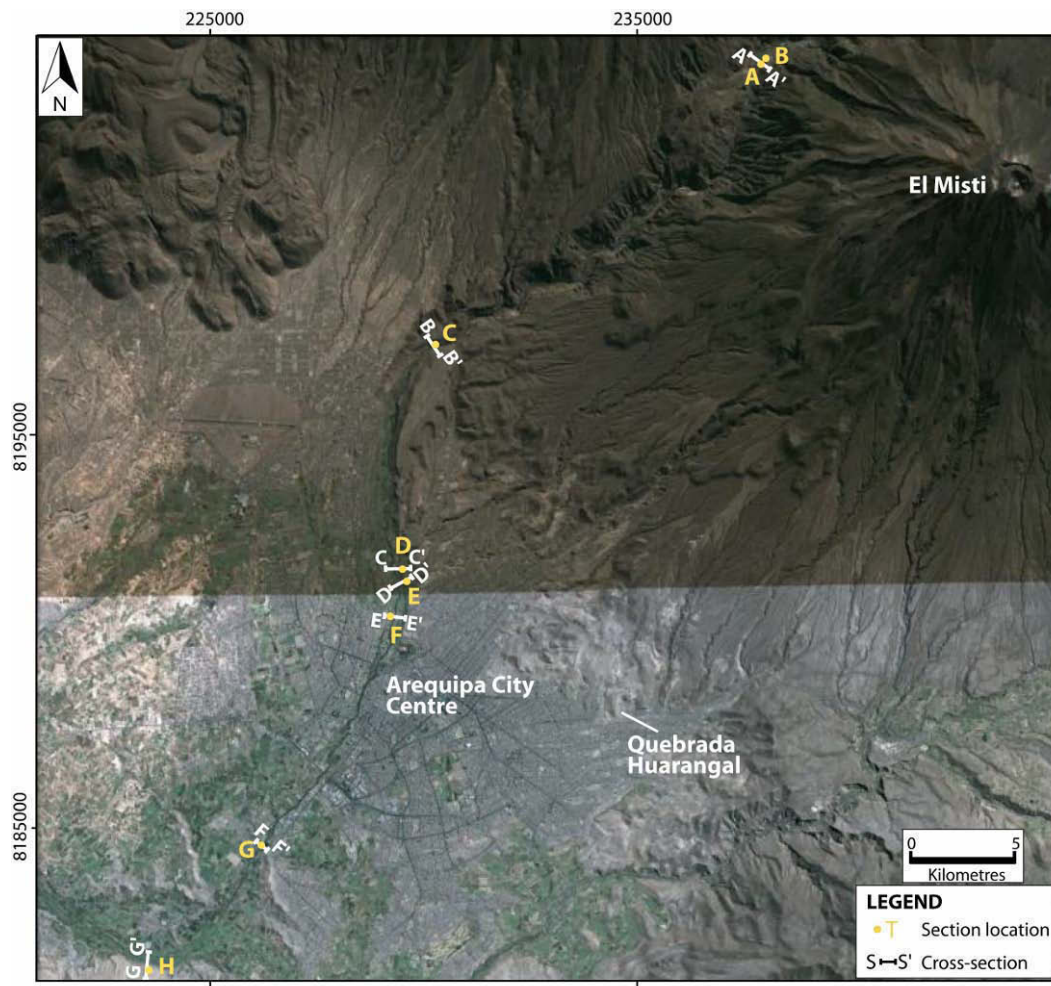


Figure 2.1: The location of deposits studied along the Rio Chili marked by a yellow point and letter. Cross-sections within the vicinity of the deposits are marked with white letters. Image from Google Earth.

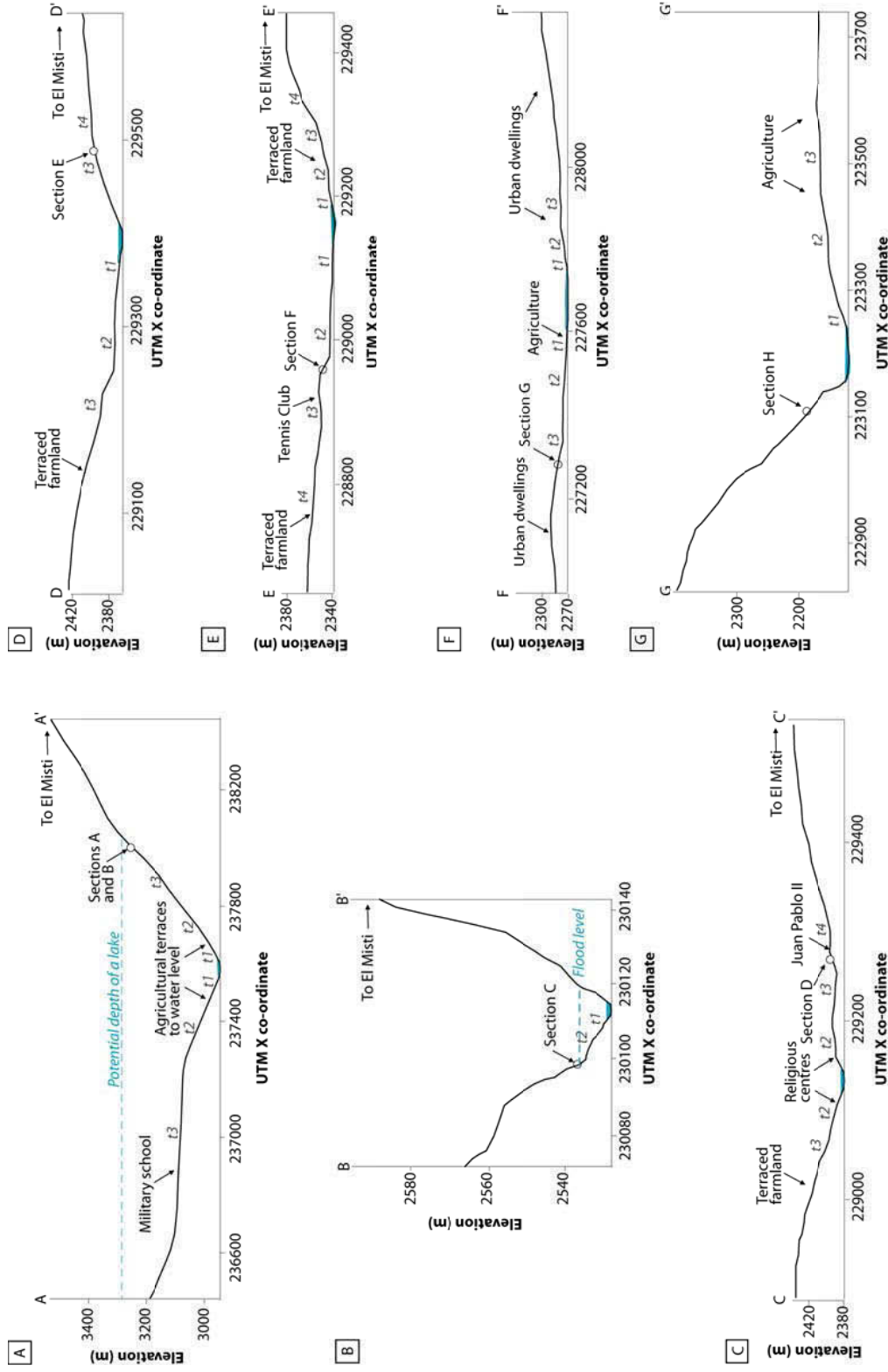


Figure 2.2: Cross-sections across the Rio Chili (refer to Figure 2.1 for the location) where sections were studied and samples taken. The symbol t_n denotes the terrace level. A: the upper Rio Chili where a thick lacustrine deposit suggests a lake was present for some time in this location. B: the entrance of the Rio Chili canyon, a flood level is marked by an alluvial deposit ~10m above river level. C – F: shows the relatively flat topography, truncated by river terraces, of the lower Rio Chili. G: A cretaceous batholith makes up the hill to the left of this section.

2.2.1 Sections A and B: Charcani Quinto

Sections A and B are located 19 km upstream of the Arequipa City centre and approximately 5.3 km downstream from the 'altiplano', near the Aguada Blanca lake, at an elevation of 2990 m (Figures 2.2 A and 2.3). Within this area is Charcani Quinto, one of 6 EGASA hydroelectric stations built within the Rio Chili valley to supply power to the national grid, a military school and agricultural terraces. The sections form part of a 15 m-high terrace (t2) located on an inside bend of the river. The objective of section A was to obtain an age constraint for lacustrine deposits and to decipher what occurred in the canyon below El Misti in recent times (i.e. Holocene). Charcoal (kim0811; 238047, 8200377; 3016m) was taken from a banded pumice-fall layer which is intercalated in a pyroclastic-flow deposit; this forms a terrace constructed in the upper course of the Rio Chili. A ^{14}C age of 2085 yr old (cal 1981 yr) was attained, which falls within the range of ages obtained earlier for the c. 2030 yr BP Plinian eruption of El Misti.

Section B features an extensive lacustrine deposit at the base of the mentioned terrace, which varies between 6 and 10 m in thickness depending on location. The deposit comprises mainly of silts with some clay; some iron and magnesium weathering product, and intercalated organic layers. Fine alluvial layers are located near the base, with dark-coloured fine sand and gravel derived from the underlying block-lava flow deposit (as indicated in the products below). An undulated boundary separates the block-lava flow at the base from the lacustrine deposit. A coarse fluvial deposit overlies the lacustrine deposit, followed by approximately 8m of hyperconcentrated flows. A reworked pyroclastic flow (~8m) represents the top of the section.

The young ^{14}C age may suggest that the river was dammed by the pyroclastic and debris-flow sequence of deposits as a probable result of the c. 2030 yr BP Plinian eruption of El Misti. The damming effect is evidenced by the thick lacustrine deposits (Figure 2.3). Evidence of dam-break flood deposits have not been discovered yet, however a dam-break flood scenario is not irrelevant. There are flood deposits (a mud-line) at least 10 m high above the channel at the entrance of the canyon. While this is not related to that particular event, it is an indication of how powerful floods can get in this narrow (<0.5 km) and deep (0.5 – 1 km) canyon. Consideration of a dam-break flood scenario therefore, is vital when assessing the vulnerability of the city of Arequipa to mass flows.

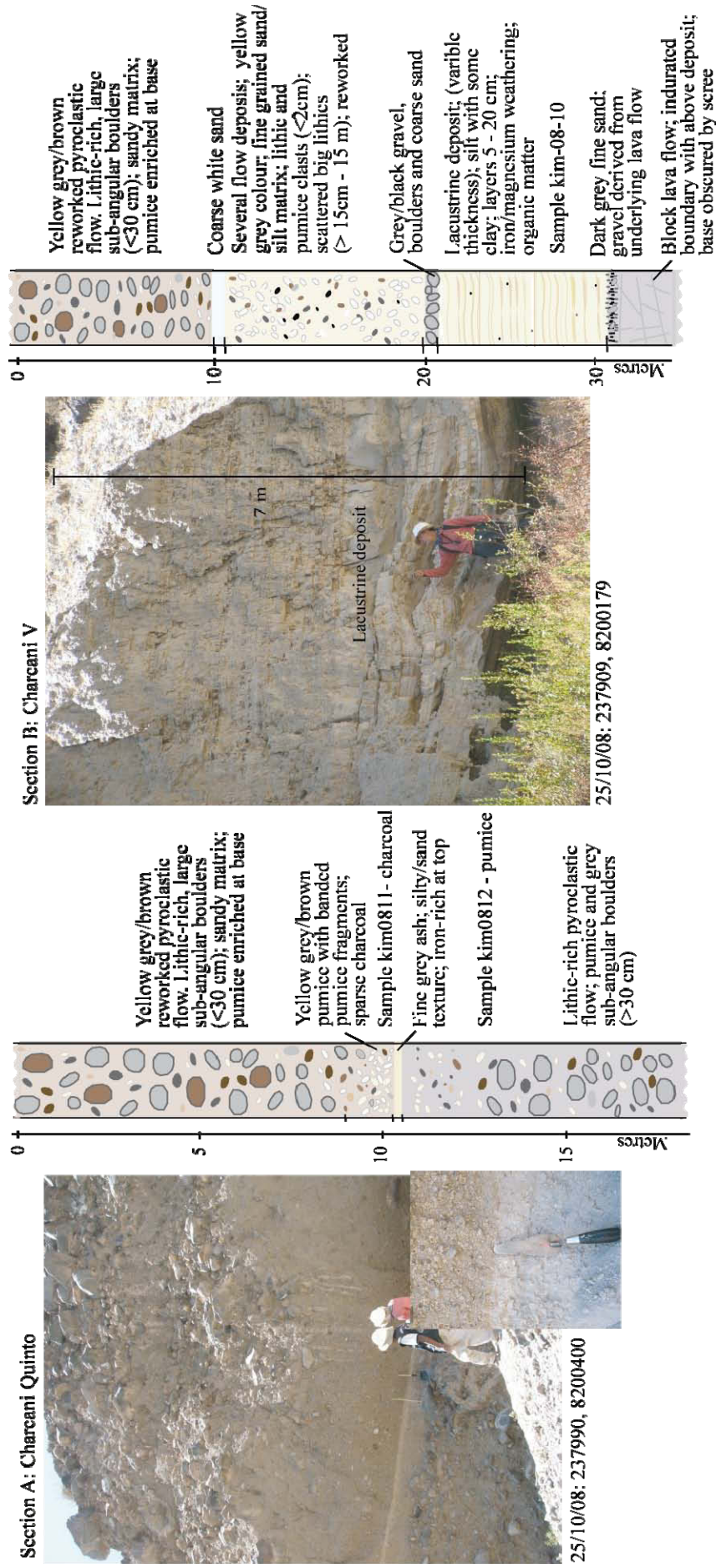


Figure 2.3: Stratigraphy of lahar and pyroclastic deposits located near the Charcani Quinto power station (location of sections can be found in Figure 2.1). Section A: the location where a charcoal sample was taken for ¹⁴C dating (inset image). Section B: thick lacustrine sediments in the upper Rio Chili Canyon.

2.2.2 Sections C: Rio Chili Canyon Entrance

This section is located at the entrance of the Rio Chili canyon, approximately 11 km from Arequipa city centre and 12 km downstream of the ‘altiplano’ (Figures 2.2 B and 2.4; location Figure 2.1). The focus of this section was the mud-tide mark located 8 to 10 metres from normal the Rio Chili river level. The age of the mud-line is unknown but it is thought to be young and may be related to large boulders strewn on the terrace t1 about 1 km down valley on the western side. The ignimbrite is a yellow brown, partially welded, irregular jointed ignimbrite which belongs to the La Joya ignimbrite which is 4.9 Ma (Paquereau-Lebti et al., 2006).

2.2.3 Sections D: Chilina

This section (Figures 2.2 C and 2.4; location Figure 2.1) is situated below the Juan Pablo II church and makes up the terrace t3, located approximately 5 km from Arequipa city centre and 18 km downstream of the ‘altiplano’.. A yellowish grey lahar deposit lies directly below a thin brown cultivated soil. The 70 cm-thick lahar deposit contains lithic and pumice clasts (> 1 cm) with few scattered big lithics (> 5 cm) in a fine grained sand/silt matrix. The top 5-10 cm of the lahar deposit has been reworked and contains charcoal due to intense cultivation practices on the above terrace. Below the lahar deposit there are pyroclastic surge deposits, and alternating layers of scoria flow and fallout deposits. At the base of the section there are fluvial deposits – layered black and grey sands – which overly boulders of terrace t2’.

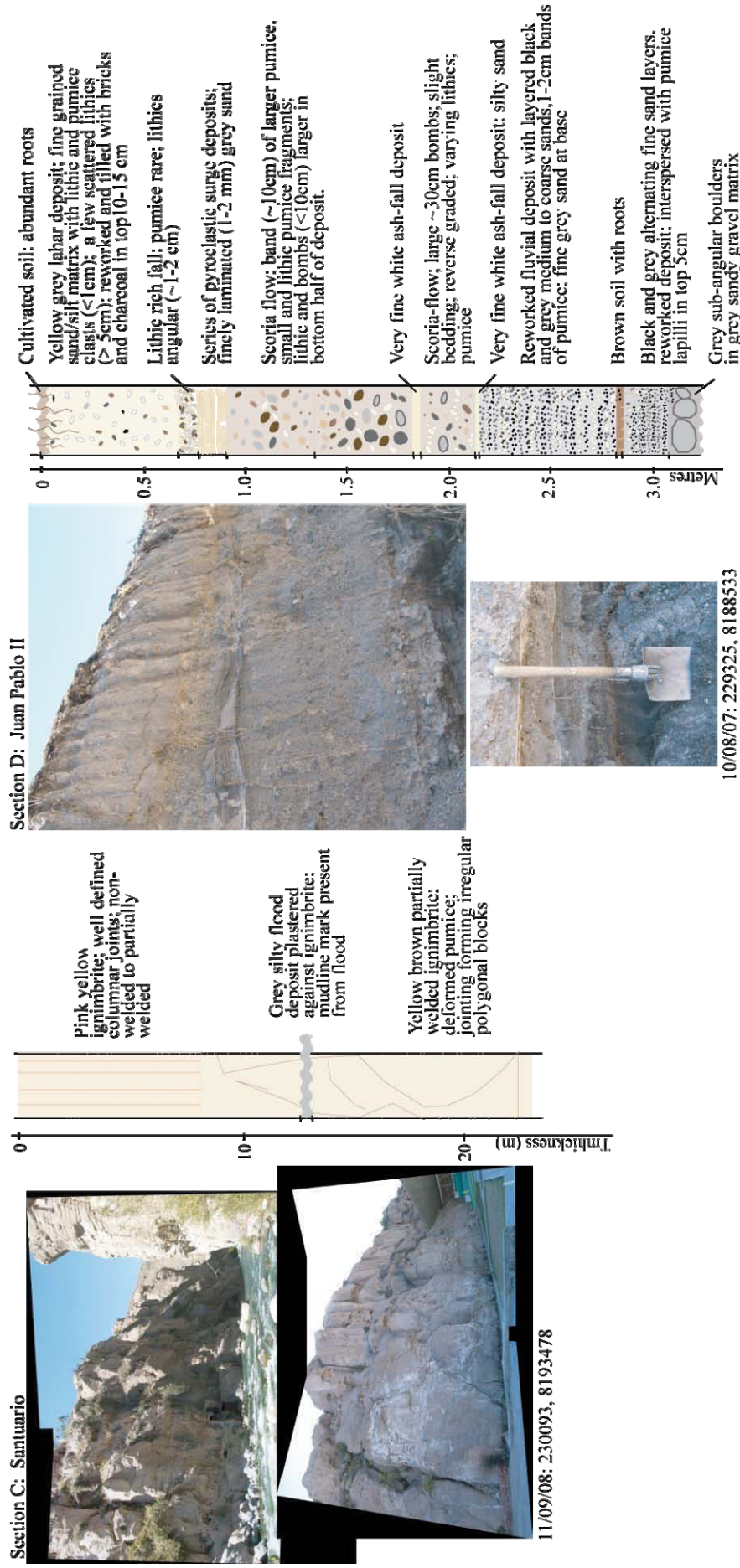


Figure 2.4: Stratigraphy of deposits in the Rio Chili Valley (location of sections can be found in Figure 2.1). Section C: flood deposit located at the entrance of the Rio Chili canyon. Section D: Lahar, ash-fall, pyroclastic deposits located near Juan Pablo II.

2.2.4 Section E: Chilina

This lahar deposit (sample K.Mis.07-01a) is part of a terrace (t3) which the church Juan Pablo II sits upon in Chilina, located approximately 5 km from Arequipa city centre and 18 km downstream of the 'altiplano' (Figures 2.2 D and 2.5; location Figure 2.1). The lahar deposit is two metres thick, grey in colour with lithic and pumice clasts up to 1 cm in diameter within a sandy silt matrix. It has been dated at 1035 ± 45 yr B.P. and it is the same deposit as in Section D (Delaite, 2003). The incorporation of some charcoal and brick is apparent in the upper 50 cm of lahar deposit due to cultivation practices over the centuries. The deposit is overlain by a thick, cultivated, dark brown soil. Underlying the lahar is a whitish grey brown lithic-rich pumice-fall deposit which directly overlies boulders of terrace t2'

2.2.5 Section F: Tennis court lahar

Located approximately 3.5 km from Arequipa city centre and 19.5 km downstream of the 'altiplano' (Figures 2.2 E and 2.5; location Figure 2.1). This section comprises of four sub-units within two lahar deposits totalling 2.2 m in thickness. At the top of the section, the *academia de tennis* is situated on a refill from a former filled terrace. This forms a wavy boundary with the upper lahar deposit, which is a white-grey deposit. Overall, the lithic and pumice size clasts are smaller than those in the lower deposit (<1 cm). The lower lahar deposit (sample K.Mis.07-02a) is white-pink in colour with an abundance of lithic and pumice clasts less than 2 cm in diameter, including some reworked ignimbrite clasts. The lahar deposit has a ^{14}C age of 520 ± 25 yr B.P (Delaite, 2003) and sit upon boulders of the t1' terrace.

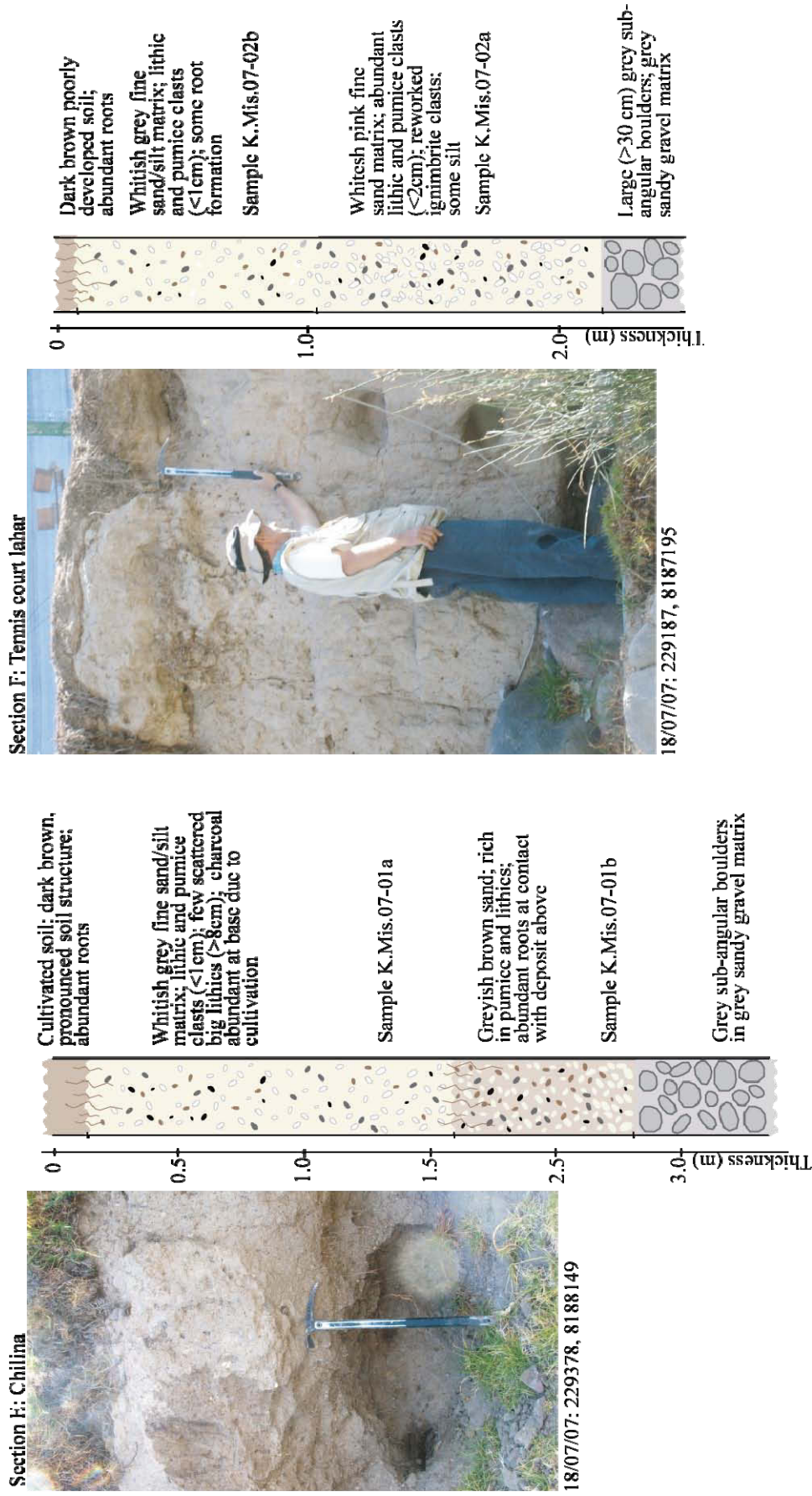


Figure 2.5: Stratigraphy of lahar deposits located near the Chilina and the Tennis Club (eastern and western sides of the river respectively). Refer to Figure 2.1 for location. Section E: a lahar deposit located near Juan Pablo II which correlates to the deposit in section D. Section F: four deposits within two lahars deposits.

2.2.6 Section G: Downstream Rio Chili

Located approximately 10 km downstream of Arequipa city centre and 32 km downstream of the 'altiplano' is a 2.5 m-thick lahar deposit (sample K.Mis.07-03b) (Figures 2.2 F and 2.6; location Figure 2.1). This lahar deposit is white-yellow in colour with an abundance of yellow weathered pumice which is weathered and mineral rich. The top of the section is obscured and the deposit overlies dark brown silty clay (20 cm thick). The clay overlies a pumice fall-deposit, which is possibly related to the 2030 yr BP eruption. Boulders within a sandy alluvium make up the bottom of the section and are related to the t3 terrace.

2.2.7 Section H: Uchumayo

The lahar deposit at Uchumayo is located approximately 17 km downstream of Arequipa city centre and 39 km downstream of the 'altiplano' (Figures 2.2 G and 2.6; location Figure 2.1). Despite the distance from the vent this deposit is very thick (almost 6 metres) and probably large ignimbrite-eruption related. The lahar deposit may be related to the pyroclastic flow (ignimbrite) deposits, which are prior to Holocene, observed at the Rio Andamayo catchment in the lowermost course of Quebrada Honda y Grande on the south flank of El Misti. Unlike the other lahar deposits, this deposit is fairly well cemented with very high lithic and pumiceous block content. Some lithics are greater than 50 cm in diameter, most of which are andesite and ignimbrite. The Uchumayo deposit overlies a pumice fall deposit and lacustrine deposits with alluvium.

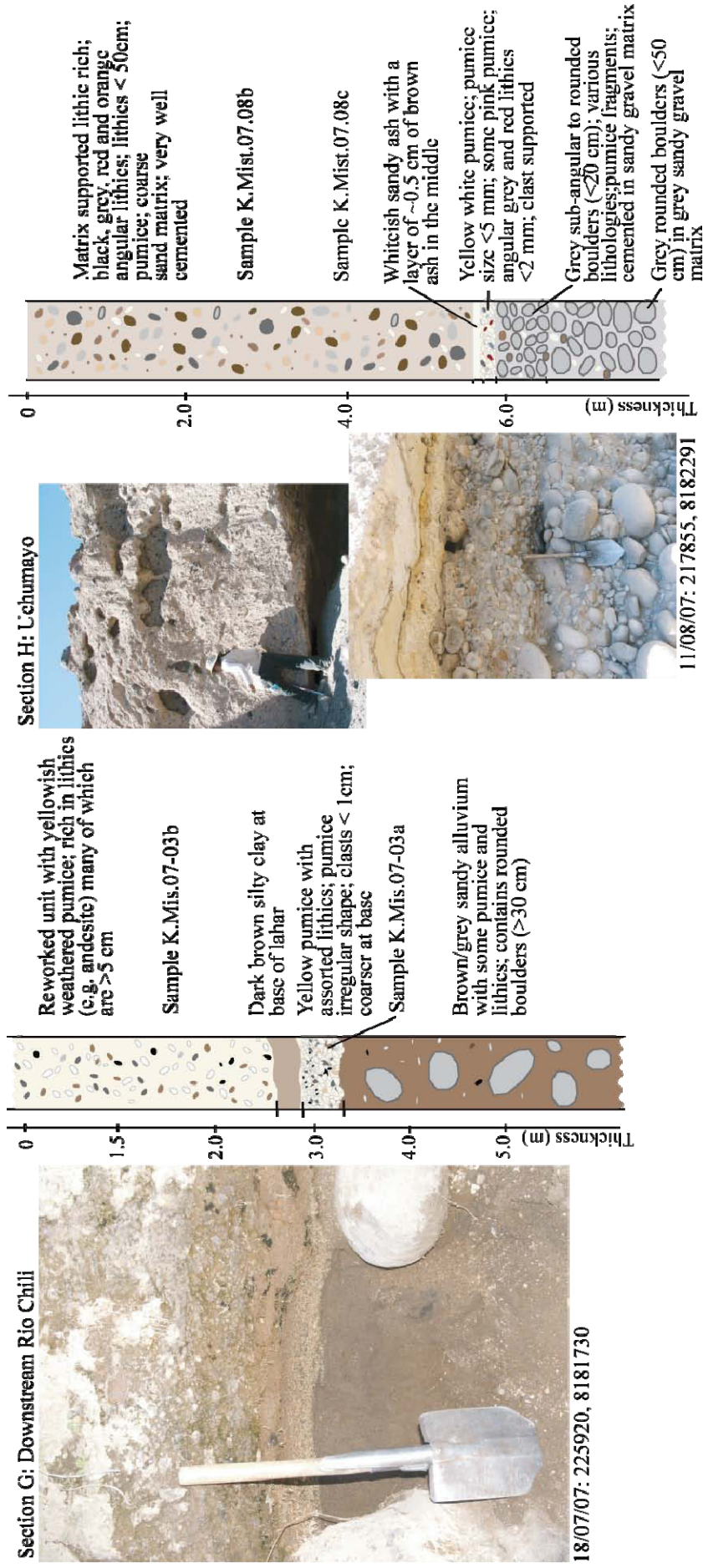


Figure 2.6: Stratigraphy of deposits downstream of Arequipa City Centre along the Rio Chili. Section G: a lahar deposit located on the western side of the river. Section H: a 5.5 m-thick lahar deposit located 25 km from El Misti's vent. The location of the sections is given in Figure 2.1.

2.3 Flash flood occurrence in Arequipa based on historical events

Throughout history, the city of Arequipa has been hit many times with heavy rainfall, leading to flooding which has caused serious destruction and claimed lives. Nagata (2000) summarised flood events which have affected the city from the 17th Century until 1997, with information gathered from press articles, eye witness accounts, scientific and government agency reports. Cuentas (2007) further refined the summary of events concentrating on the Mariano Melgar district of Arequipa. In both cases the data is most complete for the last 50 to 100 years.

Using the information from Nagata (2000), Cuentas (2007), and reports from INDECI and SENAMHI (civil defence and meteorological groups), events for the last 100 years were analysed (Appendix A), and a summary of the large magnitude events for the last 50 years is shown in Table 2.3.

Date		Rainfall Intensity (mm)	Damage
1961	25 January	Unknown	<ul style="list-style-type: none"> - Water <u>levels recorded at 1 metre.</u> - District without power. - <u>Two men died.</u> - More than <u>200 houses destroyed/damaged.</u> - Large number of roads destroyed and tramline affected. - Izuchcha Bridge collapsed and irrigation canals damaged.
1972	15 January	Unknown	<ul style="list-style-type: none"> - Water height <u>reached 8 metres</u> in Qda. San Lazaro. - <u>Three fatalities</u> - Roads, <u>homes (130)</u> and crops destroyed. - Water mains destroyed.
1973	12-15 January	Unknown	<ul style="list-style-type: none"> - <u>Rio Chili 200 m³/s</u>, water exceeding retaining wall to height 3.5 m. - City without power. - No telephone systems or transportation services - <u>10 people injured</u>, 42 homes destroyed, 90 families affected. - Crops and roads damaged, foundations of Pte. Bolognesi affected.
1989	8-9 February	37.7	<ul style="list-style-type: none"> - Pte Bajo Grau acting as a dam. - <u>5 people killed</u> and 300 families affected. - Houses, vehicles, roads and utility networks were destroyed. - 20 m retaining walls destroyed and foundation damage to Puente Bolognesi. - City without water for 20 days; drainage system defective.
1994	21-24 February	34.33	<ul style="list-style-type: none"> - The rise of the <u>Rio Chili flow to 200 m³/s</u> - Bolognesi Bridge weakened, also Ptes Grau, San Martin, and Tingo. - More than a thousand hectares of farmland destroyed a dozen isolated villages, access roads blocked. - <u>Four people dead.</u>
1997	25 February	45.43	<ul style="list-style-type: none"> - Storm left <u>5 dead in Arequipa.</u> - Rio Chili capacity <u>130 m³/s.</u> - No services in action. - Crops, farmland and homes damaged.
1999	14 March	29.97	<ul style="list-style-type: none"> - <u>Destruction of homes</u> on channel edges. - Foundations and bridge abutments undermined; destruction of bridges and water pipeline crossing waterways. - Storm water obstruction added to flooding; destroying roads.
2001	19 March	34.10	<ul style="list-style-type: none"> - Floods including significant debris <u>destroyed homes</u>, roadways and bridges. - Avenues became waterways moving stranded vehicles.
2011	21 February	Unknown	<ul style="list-style-type: none"> - <u>25 homes destroyed</u>, 6100 homeless. - 85% city without water. - Crops, farmland, water canals and roads damaged/destroyed. - Rio Chili capacity <u>236 m³/s.</u>

Table 2.3: Damage caused by historical flood events in Arequipa (adapted from INDECI and Nagata, 2000; rainfall intensity calculated from the SENAMHI rainfall records by Cruz Cuentas, 2007).

A comprehensive analysis of video and photographic documentation of historical floods in Arequipa was undertaken. This not only provided further information on both the type and extent of these flow events but moreover revealed evidence of the resulting aftermath on the people and communities within the city. This work is summarised below.

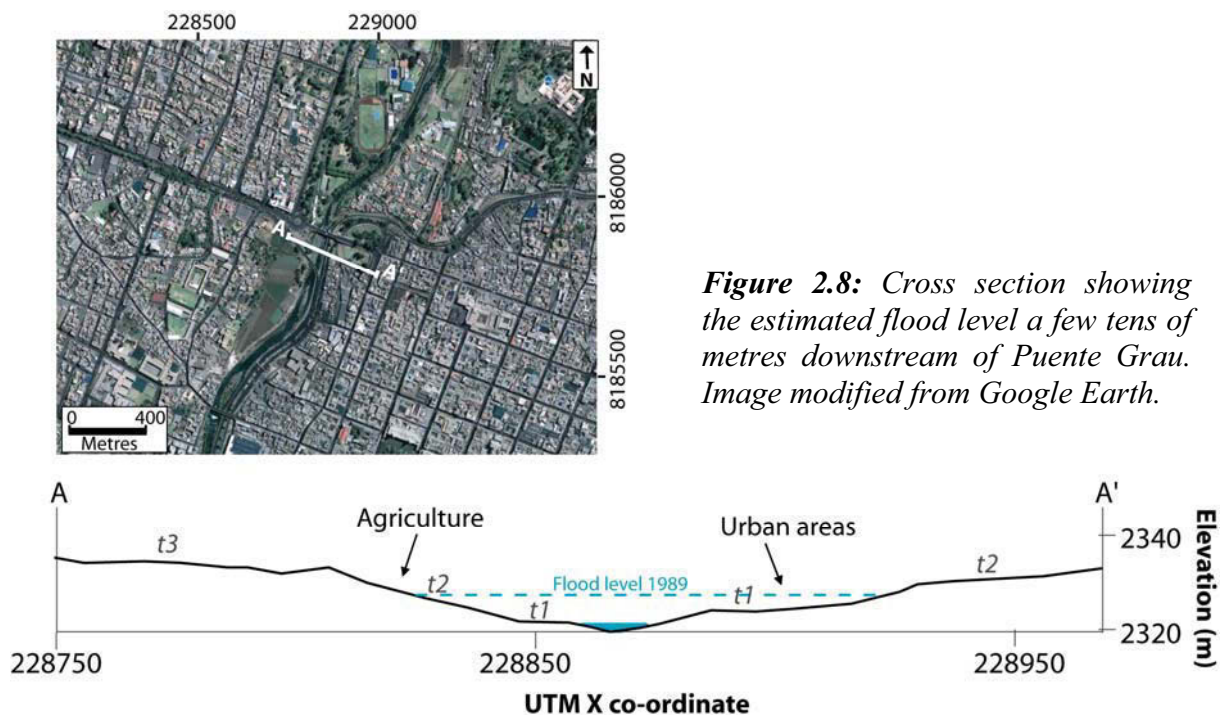
2.3.1 8-9 February 1989

The 1989 flood was one of the larger events recorded and from analysis of video (Figure 2.7) and photographic evidence (Figure 2.9), flow characteristics were determined. The video shows the flow to be dense, sediment and debris rich, and capable of moving large objects in the flow path. A large tree including the root base, approximately 5 to 10 metres in length, was observed within the flow, downstream of Puente Grau –20 km downstream from the Charcani V power station. In addition, two trees on the western edge of the Rio Chili (a few tens of metres downstream of Puente Grau) were observed being uprooted, pushed over, and transported in the flow. A car on the eastern side of the river was pushed down slope from terrace two (*t2*) to terrace one (*t1*) (refer to the terrace maps in Figures 2.18 and 2.19) by the force of the flow moving through buildings and the streets (Figure 2.7 E and F).



Figure 2.7: Frames taken from film footage showing the events and damage caused by the 8-9 February 1989 flood in Arequipa. A and B: Flow in and around the Puente Grau Bridge in the centre of the city. C and D: the flow height around a house on the eastern side of the Rio Chili, downstream of the Puente Grau Bridge. E and F: An increase in flow depth can be observed between the two snapshots. A car has also been carried away by the flow. G and H: the flow within the Rio Chili channel can be observed. The height of the flow is above the retaining walls which are usually 3.5 m above normal flow. The effects of the flow on buildings can also be observed in snapshot H. Snapshots are obtained from unedited film from the local regional TV channel (Channel 8) viewed on “Youtube”.

Flood depths of approximately 1.5 to 2 m flowed around and through buildings on the eastern side of the river (35 to 40 metres from the river edge), downstream of Puente Grau (Figures 2.7 C and D; and 2.8). The flow depth is estimated to be 6 to 7 metres higher than normal Rio Chili flow level as calculated from the height of the water observed on the Puente Grau piers (Figure 2.7 A and B, and 2.8). A flow velocity of 6-8 m/s near Puente Grau was calculated from a tree transported in the flow. Standing waves are observed in the channel, downstream of bridge piers and at the confluence of Quebrada San Lazaro and the Rio Chili.



Flooding in the vicinity of Puente Grau was enhanced by the construction of Puente Bajo Grau; the bridge acted as a barrier to normal flow forcing water around the bridge (overflow and avulsion) and into adjacent streets and buildings. Evidence shows the powerful force of the flow, for example wooden power poles on a lean (Figure 2.7 C and D), the destruction of the weir downstream of Puente Bolognesi (Figure 2.9 D and E) alongside damaged foundations. Retaining walls built to contain the river flow adjacent to the Rio Chili were destroyed allowing the flood to ingress onto Avenue Marina and into adjacent buildings (Figure 2.9 A).

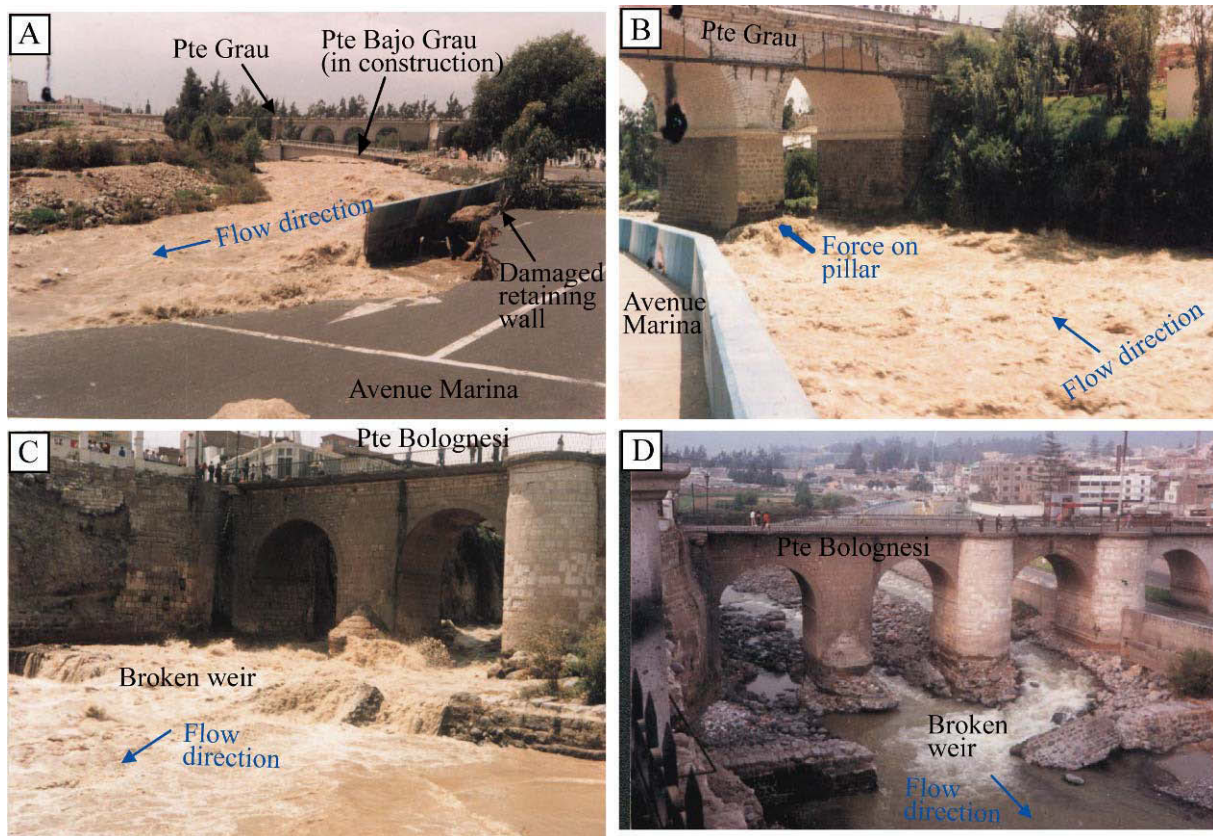


Figure 2.9: Events and damage caused by the February flood in Arequipa. A: Broken retaining wall of the Rio Chili allowing flood water onto Avenue Marina. B: Upstream of the bridge, note the force of the flow on the pillars. C: Downstream of Puente Bolognesi, the destroyed weir in the flood waters of the Rio Chili. D: The wrecked weir, obvious after flood waters receded. Photographs obtained from Victor Rodriguez.

Hydraulic characteristics suggest that the flow behaviour observed from this event would be likened to that of a hyperconcentrated flow at least, rather than a normal streamflow. The sediment concentration is relatively high, but not high enough to be classified as a debris flow i.e. the sediment concentration would be greater than 4% vol.% but less than 60 vol.% falling into an intermediate range which is attributed to hyperconcentrated flows ((Pierson and Costa, 1987). The flood line and calculated flow velocity attest to floods $> 200 \text{ m}^3/\text{s}$.

2.3.2 25 February 1997

The flood of 25 February 1997 was a similar event to that of 1989. Reports suggest a hyperconcentrated flow ($200 \text{ m}^3/\text{s}$) capable of scouring channel banks, bridge abutments and building foundations, with photographs (Figure 2.10) confirming its destructive nature.

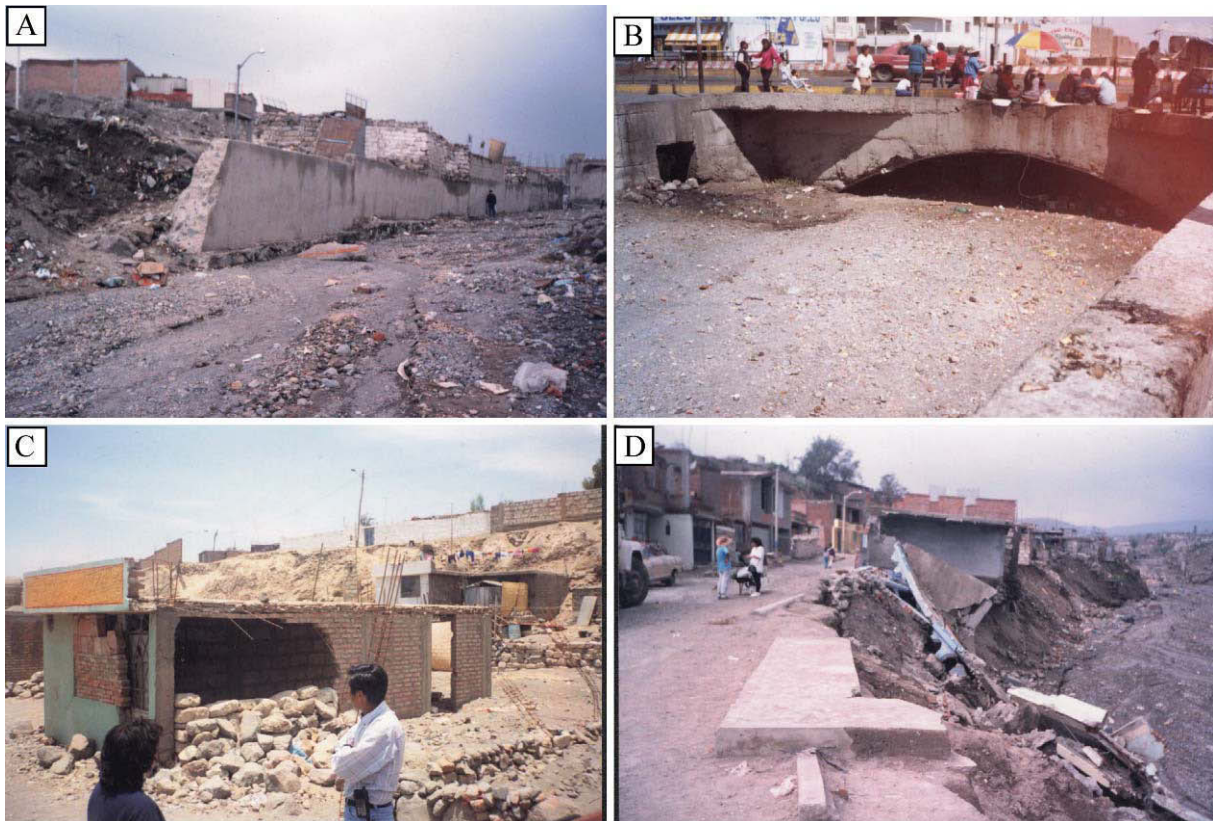


Figure 2.10: A: Destruction of a retaining wall. B: Inundation of Puente Avenue Jesus from Quebrada Mariano Melgar. C: A house damaged by the hyperconcentrated flow debris in the district of Mariano Melgar. D: Houses collapsed into Quebrada Mariano Melgar after channels were undermined by the hyperconcentrated flow. Photographs obtained from Victor Rodriguez.

Most damage was concentrated in the suburb of Mariano Melgar where retaining walls, and as high as 3-4 m), adjacent to the quebrada were destroyed (Figure 2.10 A), channel beds were filled with sediment (Figure 2.10 B) and buildings collapsed into the quebrada (Figure 2.10 C) as the channel banks were undermined, claiming three lives. The quebradas are often used as dumping areas, adding sediment to bulk up the flow, as well as reducing the channel capacity. The effect of reduced channel capacity was most pronounced at bridges where the flow was impeded, overflowing into neighbouring suburbs flooding homes, business and streets (Figure 2.10 C).

In the Rio Chili channel, flood waters (discharge $>200 \text{ m}^3/\text{s}$) inundated the newly constructed Puente Bajo Grau and flooded homes, businesses and streets of the city centre's eastern bank.

2.3.3 February 2011

Heavy rainfall in the Arequipa region during February 2011 resulted in flooding within various suburbs around the city. Intense rainfall in one hour on 10th February led to flooding of 12 homes in Alto Selva Alegre and 9 in Miraflores, while a landslide left several families homeless in the same area (GrupoRPP, 2011). More than 6 km of roads were affected when city streets were flooded, preventing the normal movement of vehicles and pedestrians.

Further rainfall on 11th February resulted in flooding of 25 homes in San Jeronimo (part of the study area in Quebrada Huarangal). It appears that the flow was funnelled through a 2-3 metre channel to the north of the quebrada channel bed (chapter 1 and Figure 2.11). Where this channel abruptly ends the flow made a path across the wide and unconfined quebrada channel bed to where it became confined once more. Where the flow was not confined within a channel, it inundated poorly-built dwellings and destroyed homes. Figure 2.12 shows the likely routes that the flow took based upon the knowledge of the channel morphology and also from photographs of the aftermath. One of the reasons this quebrada was chosen for the study was due to the increasing and seemingly uncontrolled presence of poorly constructed houses within the channel bed. This flow event highlights the danger posed to people living within this area.

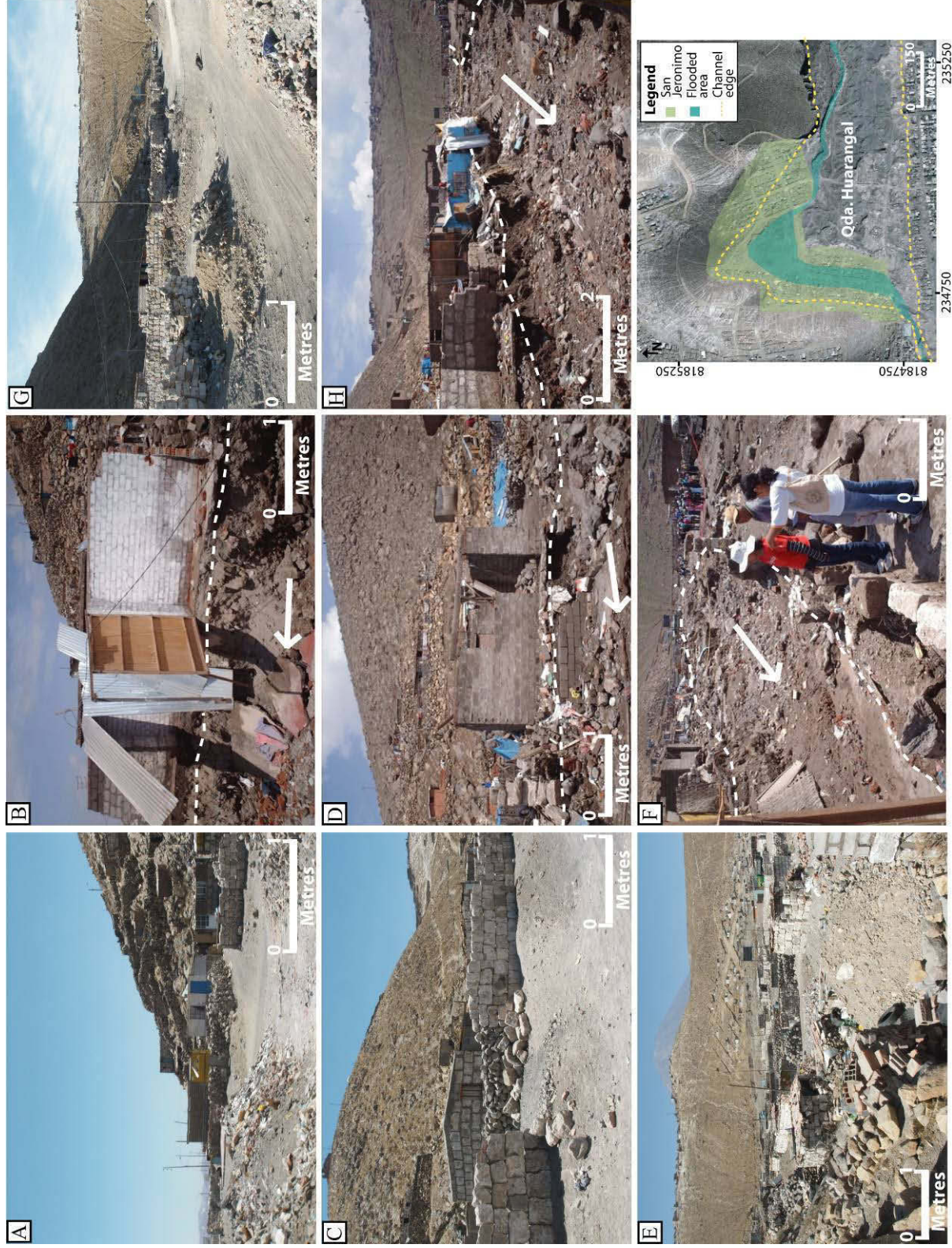


Figure 2.11: Damage from the February 2011 flow event in San Jeronimo. A, C, E and G were photographs of the area taken during the field campaign in 2008. Photographs B, D, F and H were taken in the same area in 2011. The damage and collapse of houses from the erosion of the house foundations can be clearly seen in B, D and H. The width and depth of the flow is evident from F and H. Photographs from 2011 were obtained from GrupoRPP (www.rpp.com.pe)

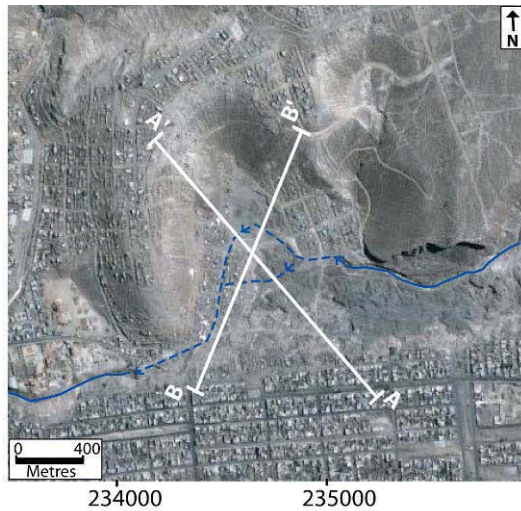
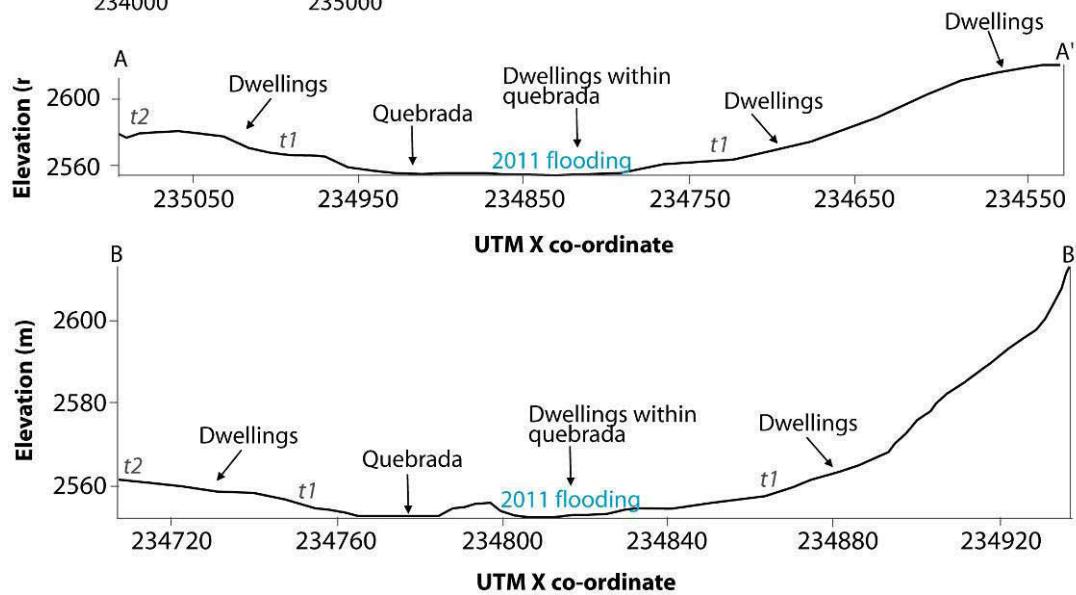


Figure 2.12: Cross-section lines through the flooded area of Quebrada Huarangal. The filled blue lines represent the path the flow took, and the dashed blue lines show the likely path that the flow took based upon channel morphology and photographs. The cross-sections show the wide flat channel bed of this quebrada, the area where many dwellings are present. Image from Google Earth.



Comparisons of photographs taken in San Jeronimo during the field campaign in 2008 were made with news report photographs (GrupoRPP, 2011) of the flow aftermath from February 2011 (Figure 2.11). The photographs show that the flow was approximately 6 metres wide and 0.5 to 1 metre in depth where it passed through the housing estate (Figure 2.11 E and H). It appears that the flow was confined to the road and followed a path between houses. Houses adjacent to the channel were damaged as shallow foundations were eroded causing the buildings to collapse overflowing water also caused water damage.

In the Mariano Melgar district, flows carried more debris (Figure 2.13); large boulders, miscellaneous debris and thick mud are evident in the photographs. As mentioned in the 1997 floods, debris is readily available due to the dumping of household and industrial rubbish into the quebradas. Houses were also damaged due to the erosion of shallow foundations (Figure 2.13).

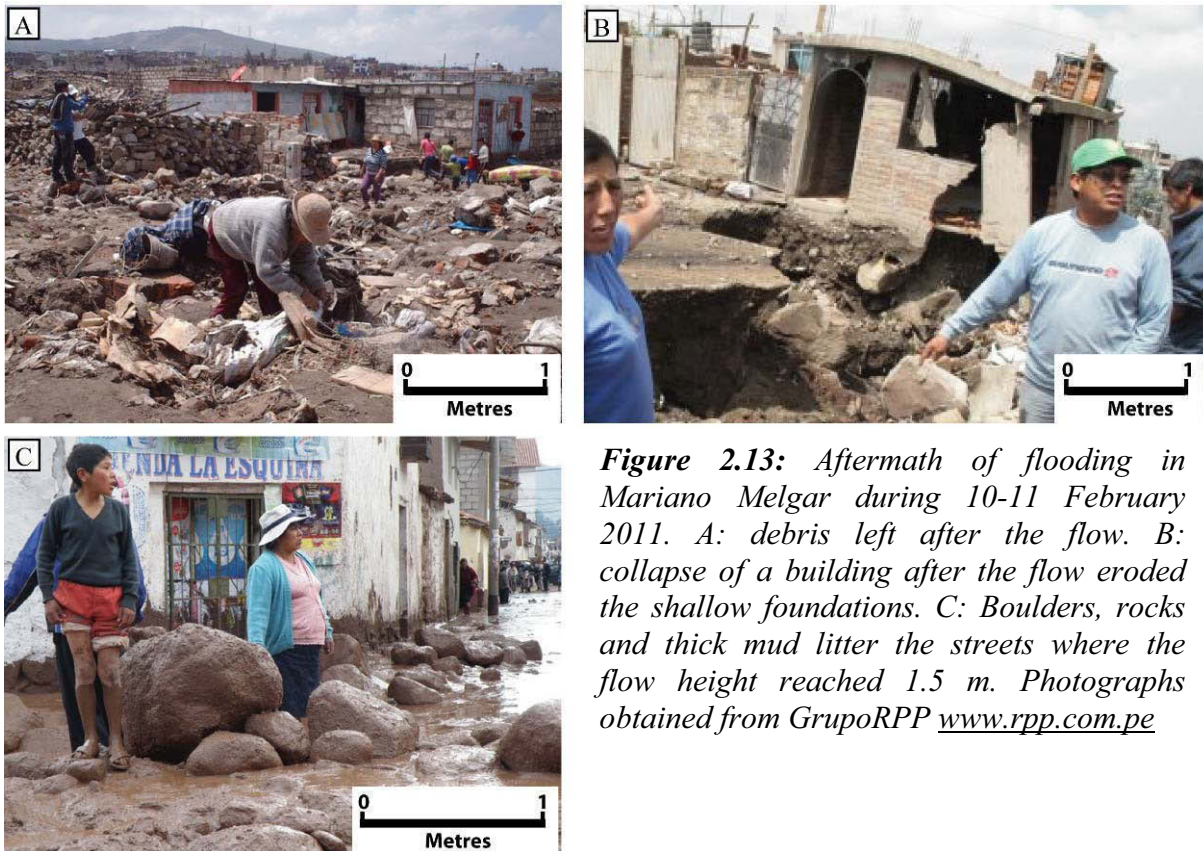


Figure 2.13: *Aftermath of flooding in Mariano Melgar during 10-11 February 2011. A: debris left after the flow. B: collapse of a building after the flow eroded the shallow foundations. C: Boulders, rocks and thick mud litter the streets where the flow height reached 1.5 m. Photographs obtained from GrupoRPP www.rpp.com.pe*

Heavy rainfall also filled the Aguada Blanco dam to maximum capacity and water had to be released into the Rio Chili. By the 23rd February the normal Rio Chili flow (7 to 24 m³/sec) had increased to 236 m³/sec, a figure not seen in 14 years (INDECI). Main bridges (Puentes Grau, Bajo Grau, Bolognesi, San Martín, Fierro and Tingo) in the city were closed to vehicular and pedestrian traffic, while pedestrians were also prevented access to Avenue Marina. No damage to the bridges were reported, however the flow was very close to reaching the Puente Bajo Grau deck height of 5 metres (Figure 2.14 B and D). Photographs indicate that this event in the Rio Chili is more likely to be a muddy streamflow, rather than a hyperconcentrated flow or debris flow, due to the significant lack of sediment and debris within the flow (Figure 2.14).



Figure 2.14: Before and after photographs of the flooding in the Rio Chili – before photos are taken in 2007 and 2008, and after photos were taken on 23 February 2011 (obtained from GrupoRPP www.rpp.com.pe). A and C show the channel and bridge height of Puente Grau during normal river flow while B and D show the height of the flow (just under the bridge deck) and absence of terraces as can be viewed in C. E and F are downstream of Puente Bolognesi, again the absence of islands can be noted in F. Also the level of the river is noticeably higher in F than E.

The release of such a large amount of water into the Rio Chili resulted in over 10 hectares of farmland and crops being flooded to the south of the city (e.g. Uchumayo). The Zamacola canal which supplies the water to the water treatment plant was closed due to an increase of debris in the canal, and as a result 80% of people in Arequipa were without potable water for more than 24 hours. In addition to a lack of water, many sewer pipes failed within the city.

It has been estimated that in the Arequipa district more than 6000 people were made homeless and more than 22,000 people were affected by the February 2011 flooding. The majority of victims were people who “invaded” hills and streams in the districts of Alto Selva Alegre, Mariano Melgar, Paucarpata, Hunter and Miraflores (INDECI).

2.4 Dam-break floods in Arequipa?

A dammed lacustrine deposit less than 2030 yrs BP is located in the upper Rio Chili canyon, approximately 5.8 km W of El Misti’s vent, and approximately 19 km upstream of the city centre (Figure 2.3, Section B). Deposits located in the vicinity provide compelling evidence for lake formation and subsequent dam-break floods. Debris avalanche, block-and-ash flow and rockslide avalanche deposits are all located within and at the confluence of a WNW elongated scar with the Rio Chili valley (Figure 2.15 A). The rockslide avalanche scar is approximately 3 km long and 2.5 km wide.

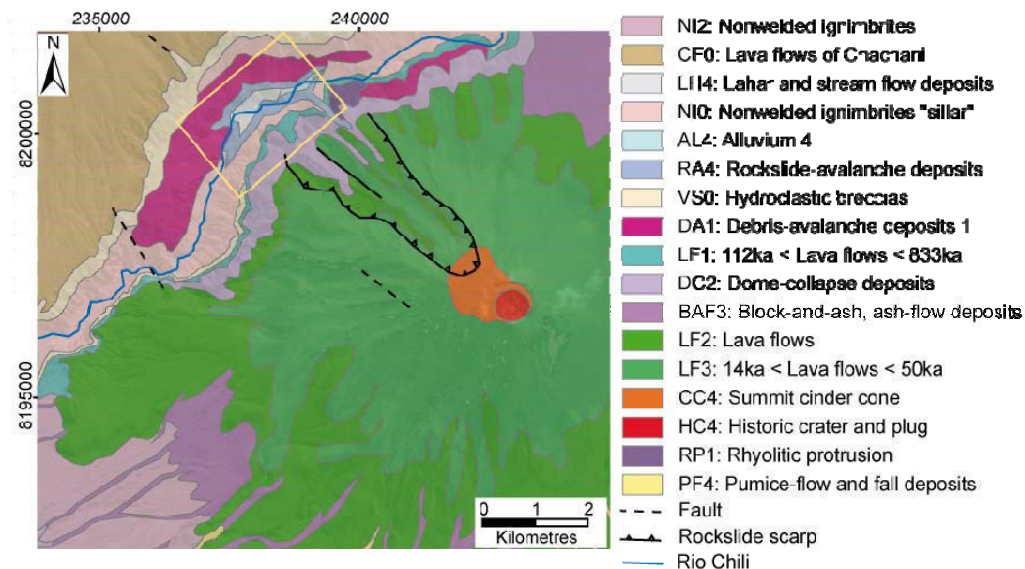


Figure 2.15: Geological map of El Misti focussing on the area near where a lake could form in the upper Rio Chili canyon (near Charcani V, as indicated by the yellow square). The deposits in this area indicate that the Rio Chili could become blocked in the future (e.g. debris avalanche deposits, block and ash flow deposits). Geological map modified from Delaite (2003) and overlapped on a Google Earth image.

Debris flows and rockslides can occur before an eruption (e.g. due to deformation of the cone destabilising the flank and/or material on the flank); during (e.g. collapse of dome growth and/or other flows generated by an eruption such as pyroclastic flows); and after (e.g. material

dislodged by heavy rainfall). Movement can also be generated by an earthquake; the gully and elongated scar are parallel to an active fault (Thouret et al., 2001) Movement of fault lines could result in a significant amount of sediment dislodged into the Rio Chili from the steep slopes of El Misti. In addition, seismic surveys since 2005 (IGP) point to swarms of if shallow (2.5 – 5 km) low magnitude volcanoclastic events. If the canyon becomes blocked, a lake could form behind it. Over time this lake could burst, sending potentially large volumes of water down the Rio Chili. The occurrence of a dam-break flood in the Rio Chili will be discussed further in sections 2.5.3 and 2.6.

2.5 Flow magnitude and frequency of lahars, dam-break and flash floods

2.5.1 Lahars

The generation of lahars has been associated with each of the four eruption types (either syn- or post-eruption). The estimated flow volumes of dated deposits range from $1.5 \times 10^6 \text{ m}^3$ (e.g. Chilina deposit) to $30 \times 10^6 \text{ m}^3$ (e.g. Uchumayo deposit). The Uchumayo lahar deposits are 0.1 to 0.2 km wide, 2 to 5 m thick and extend 8 km to more than 30 km from the volcano. Lahars such as the Chilina deposit are estimated to have a recurrence interval of 300 to 1000 years, and the Uchumayo lahar, a recurrence interval of approximately 20,000 years (Thouret et al., 2001).

Depending on the eruption type, flow volumes from $0.5 \times 10^6 \text{ m}^3$ to $11 \times 10^6 \text{ m}^3$ have been determined by Delaite et al. (2005) from the estimated volume of Holocene lahar deposits surrounding El Misti, the approximate amount of material which can be mobilised in channels, rainfall threshold of at least 10 mm per hour, and surface area of the seasonal (December – July) snowfield on the volcano summit (1 to 4 km², up to 7 km² in case of heavy snowfall).

2.5.2 Floods

Smaller hyperconcentrated flows and flash floods have also occurred without an eruption, as shown in section 2.3. Data available for the past 100 years (e.g. Nagata, 2000; Cuentas, 2007; INDECI and SENAMHI) was analysed and classified depending on the extent, magnitude, deaths/injuries and destruction caused (refer to Appendix A). Annual precipitation data was

then compared with the flood events to see if there was any correlation. However, there was little correlation between flood events and annual rainfall data. This is because floods are initiated in Arequipa during periods of intense rainfall (>15 mm/hr). For example, the 25 February 1997 floods were initiated when approximately 60 mm of rainfall fell over 3 hours (Nagata, 2000; Vargas et al., 2010). Rainfall is concentrated during the rainy season and these periods of intense rainfall can lead to large runoffs of sediment.

Using the maximum annual Rio Chili river flow data from 1937 to 1989, the recurrence interval for flood discharge was calculated using a Gumbel-Law distribution (after Richards, 1982) (Figure 2.16, Table 2.4).

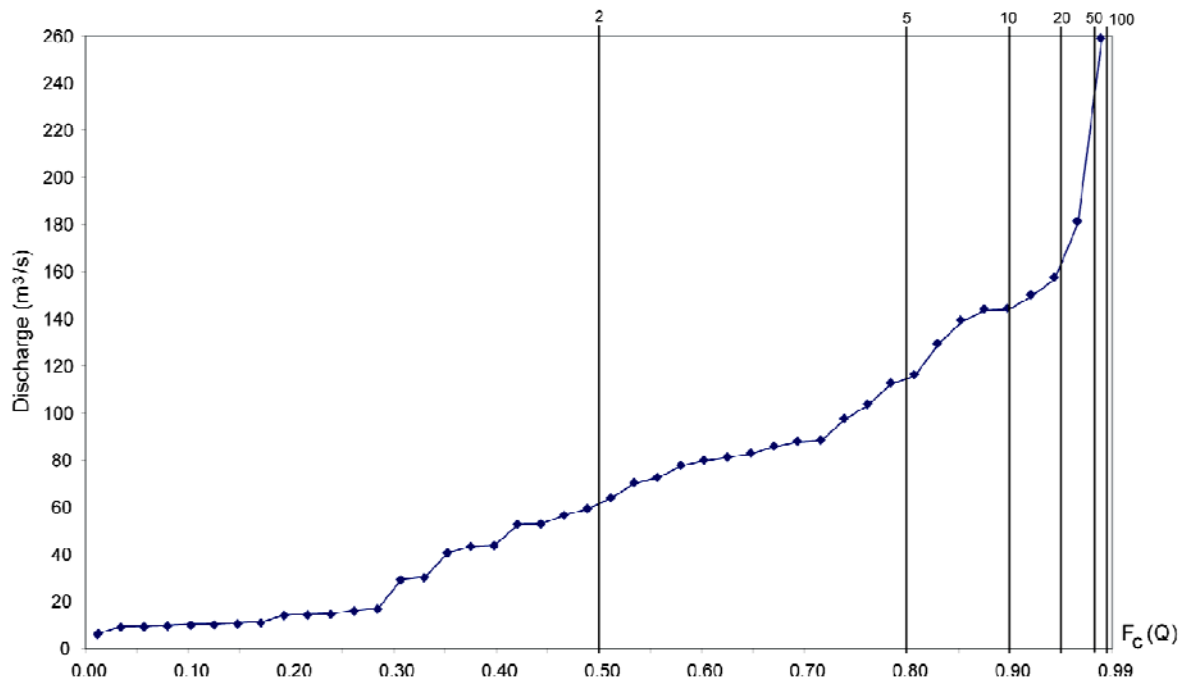


Figure 2.16: Adjustment of maximum annual flood for the Rio Chili using a Gumbel distribution.

	Recurrence interval (years)				
	2	5	20	50	100
Discharge (m ³ /s)	62	110	142	238	260

Table 2.4: Maximum annual flood discharge and recurrence intervals for floods in the Rio Chili.

The calculation of maximum annual flood and recurrence intervals are lower than what would be expected. For example, the discharge of the Rio Chili in February 2011 was 263 m³/sec,

and reported as a figure not seen in 14 years, whereas as this corresponds to a 100 year recurrence interval with this Gumbel distribution. However, the classification table of Appendix A indicated that over a period of 100 years, floods ranging from less than $0.01 \times 10^6 \text{ m}^3$ to $0.1 \times 10^6 \text{ m}^3$ have occurred with a recurrence interval of 2 to 10 years. These will be the volumes and recurrence intervals for the hazard scenarios created (section 2.7).

2.5.3 Dam-break floods

From the analysis of the geomorphology near where the lacustrine deposits are located, the area covered by a potential lake can be approximated (Figure 2.17). A small (light blue) and moderate (darker blue) sized lake outline, based on lacustrine outcrops and canyon landforms, is shown in Figure 2.17.



Figure 2.17: area where a lake could form in the upper Rio Chili canyon (near Charcani V). The lighter blue represents the likely area where a smaller lake would form, the darker blue representing the likely area flooded by a moderate sized lake. Image from Google Earth.

The surface area represented by the smaller lake is approximately 0.32 km^2 while the larger is 0.58 km^2 . The volume of water held can be determined from the approximated depth of the lake. The depth of the lake is approximated because the thickness of the lacustrine deposit alone does not represent how deep the lake would have been. The size and depth of the lake is related to the sediment supply and a balance between water supply and loss through evaporation. These variables also control the sedimentation rate (related to the thickness of the deposit). Cross-sections through the basin indicated that there is an elevation difference of approximately 5-10 m from the current river level to the edge of the small lake, and 15-20 m different for the larger lake. Therefore the estimated volume of water that could be stored is between 1.6 and $11.6 \times 10^6 \text{ m}^3$.

Of course this volume would be increased significantly by the volume of dam sediment incorporated by the flow and sediment entrained on path. For example, $1.3 \times 10^6 \text{ m}^3$ of water was released from Mt Ruapehu's crater following a break of the crater wall on 18 March 2007 (Procter et al., 2010). After 5 km the flood had mobilised a net value of $2.5 - 3.1 \times 10^6 \text{ m}^3$ of boulders, gravel and sand to form a lahar with a volume of at least $4.4 \times 10^6 \text{ m}^3$ (Procter et al., 2010). A lake-breakout flood from the crater of Mt St Helens, USA, on 19 March 1982 was initiated by the complete drainage of a transient meltwater lake having a volume of approximately $4 \times 10^6 \text{ m}^3$ (Pierson and Scott (1985). Within the first 5 km (average gradient 18%), the water flood transformed fully to a debris flow, and rough volume estimates indicated a bulking factor of about 3.0 for this reach (Pierson & Scott (1985). The bulking factor increased from 4.5 – 5.0 as the flow became more erosive, and also as additional water was ingested with the eroded sediment. If a bulking factor of 3.0 to 4.0 is taken into consideration for potential dam-break floods at El Misti, the estimated volume of the mass flow (debris flow to hyperconcentrated flow) would be range from approximately 5 to $50 \times 10^6 \text{ m}^3$.

2.6 Extent of lahars and flash floods

The determination of areas which are likely to be inundated by lahars and floods is important in hazard analysis and evaluation. Terraces of the Rio Chili and Quebrada Huarangal were mapped based upon measured terraces and aided by aerial photographs, satellite imagery and DEMs (Figures 2.18 and 2.19) (Thouret et al., *in press*).

Thouret et al. (*in press*) describes the terraces of the Rio Chili as follows (Figure 2.18):

- Terraces t3 and t4 are the oldest terraces along the Rio Chili, located 20-25 m above the present channel. An age has not been established for these terraces; however they are older than dated pumice-flow deposit (ca. 40,200 yr BP) that they overlay or erode. They should be younger than 100 ka, the age of the base of Misti 3.
- Terraces t2 and t2a, are located approximately 10-15 m above the channel, and are composed of pyroclastic-flow, lahar and hyperconcentrated-streamflow deposits. The terraces are Holocene in age and are covered by lahar deposits dated at ca. 1035 and

520 yr BP (e.g. lahar deposit of the Tennis Club). Historical lahar deposits of ca. 320 yr B.P., mantle the t2a terrace 9.5 m above the channel in the Yanahuara district.

- Terrace t1 is 3-4 m above the channel and is thought to be of Pre-Colombian historical age because the deposits contain Inca or pre-Inca archaeological fragments. A lahar runout deposit, dated at approximately 340 yr BP, mantles t1. Terrace t1a is 2-3 m above the channel and consists of two or three steps cut into the t2 terrace, which are younger than 300 years. This terrace (t1a) has been frequently inundated by recent floods (i.e. 10 year interval).
- Terrace t0 is <1 m above the ‘minor’ or river channel. It is commonly flooded when ordinary discharge is reached – at least once a year during the rainy season. This terrace corresponds to the ‘major’ channel that can be flooded almost every year in the rainy season.

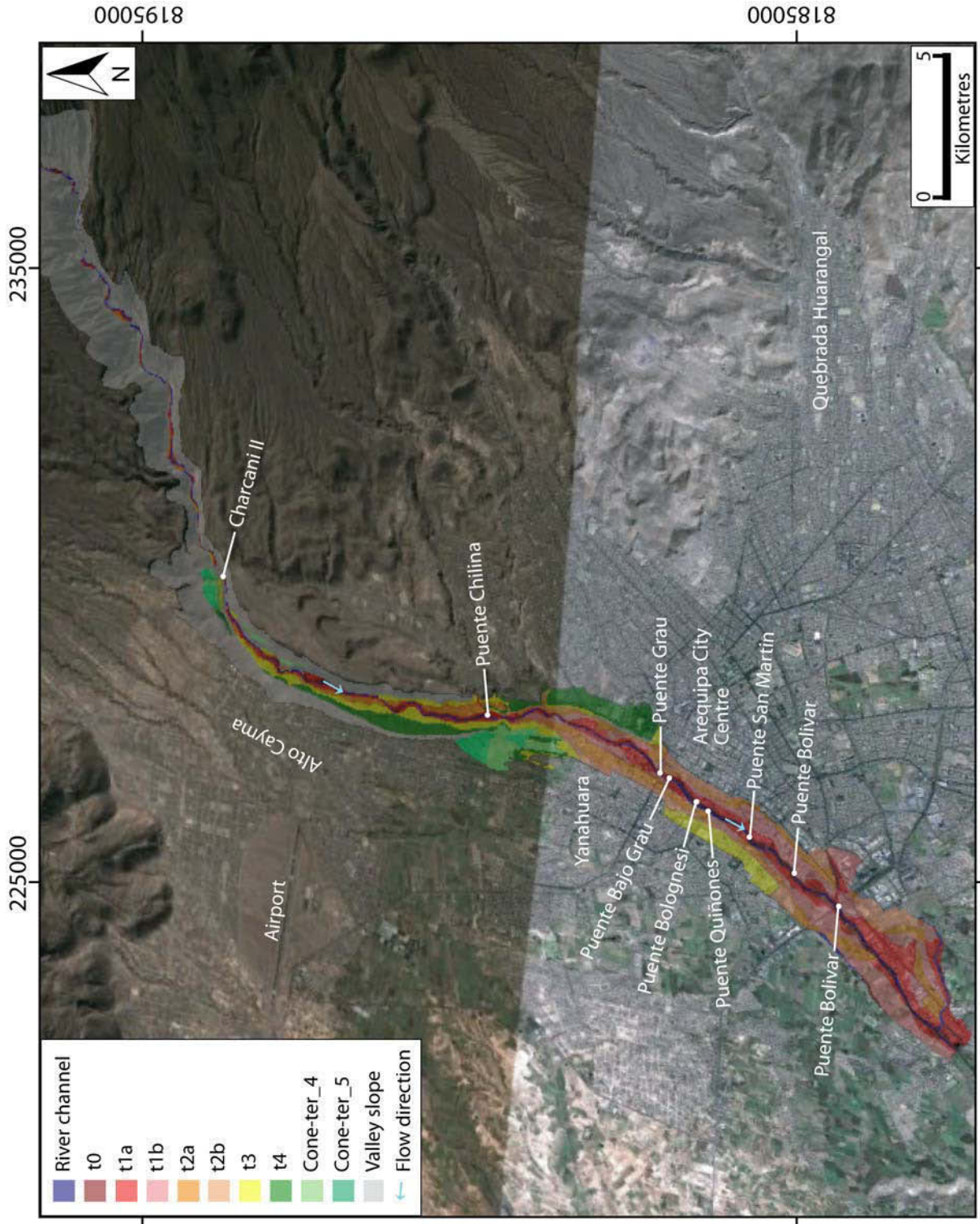


Figure 2.18: Terraces in the Rio Chili Valley based upon field mapping, geological and historical data, and aided by aerial photographs, satellite imagery and DEMs. Image from Google Earth (Modified from Thouret et al., in press).

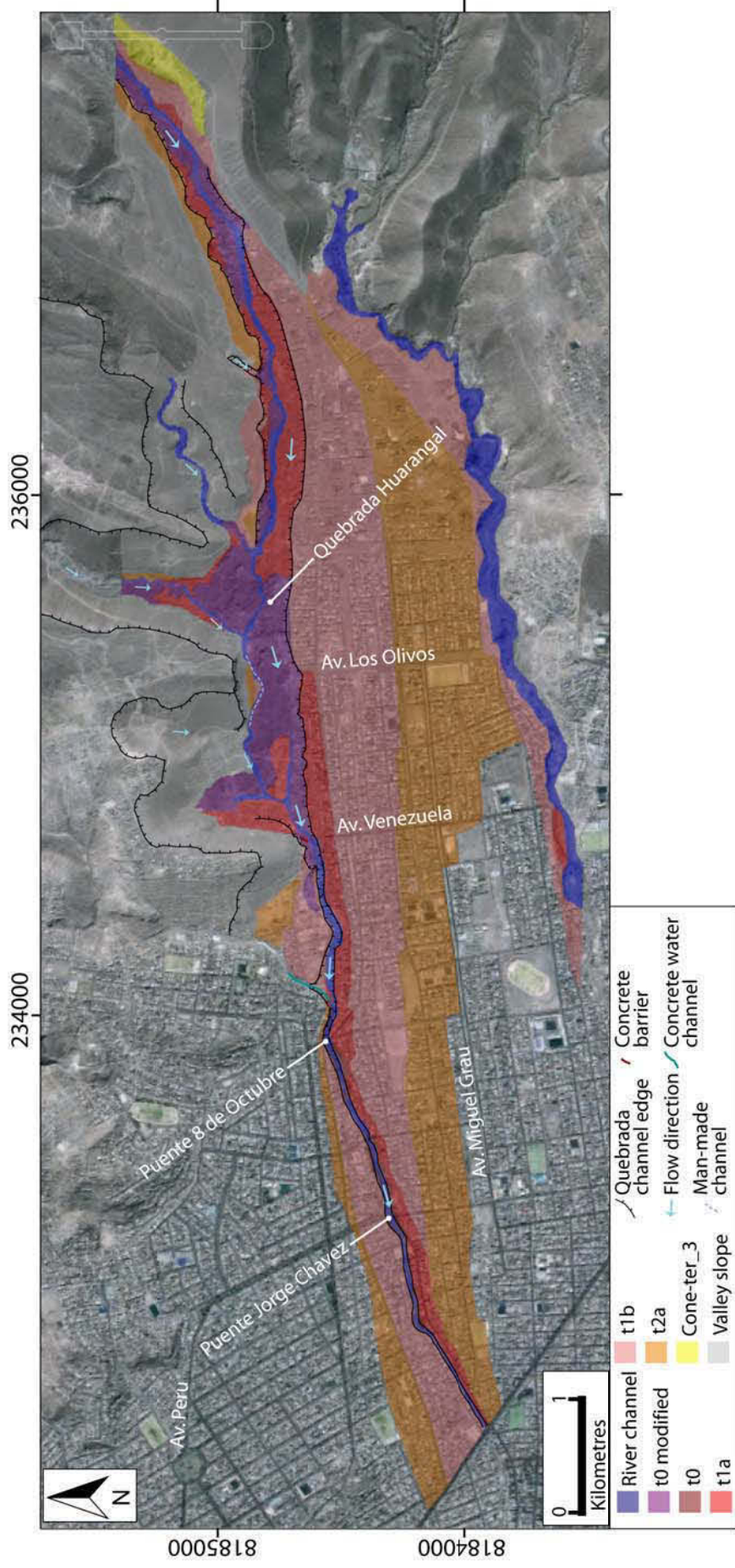


Figure 2.19: Terraces and fan terrace (cone terrace) of the Quebrada Huarangal fan based upon field mapping, geological and historical data, aided by aerial photographs, satellite imagery and DEMs. Sharp-like ridges are outlined and formed in subdued debris-avalanche deposits. Volcaniclastic fans in the upper right of the map form a conspicuous high scarp looking south. The scars on the upper part of the map are small tributary watersheds, but in most part are scars from old landslides. Image from Google Earth (Modified from Thouret et al., in press).

It is more difficult to determine the ages for the terraces of the Quebrada Huarangal fan due to a lack of dateable deposits when compared to the Rio Chili valley. However the terraces are described by Thouret et al. (*in press*) as follows (Figure 2.19):

- Terrace t2a is mantled by flow deposits with an average recurrence interval of between 100 and 1000 years.
- Terrace 1b has been inundated by flows which have a recurrence interval of 50 to 100 years, and represent moderate eruption events.
- The terraces of t0 and t1 are often inundated by smaller volume ($0.01 \times 10^6 \text{ m}^3$ to $0.1 \times 10^6 \text{ m}^3$), frequent (1.2 per 10 years) flood and hyperconcentrated flow events (e.g. 1997 and 2011 flash floods). The larger magnitude of these frequent floods also affects terrace t1a. In summary, the recurrence interval for terrace t1a is 5 to 10 years, t0 is 1 to 5 years and the channel is flooded at least once a year.

The terraces described in Figures 2.18 and 2.19 will be related to hazard scenarios in the following section.

2.7 Hazard scenario evaluation

2.7.1 Determination of scenarios for lahars, dam-break and flash floods

The hazard scenarios proposed by Thouret et al. (2001), Delaite et al. (2005) and Vargas et al. (2010) cover the range of mass flows generated by eruptive processes and rainstorms/snowmelt. Vargas et al. (2010) proposed three scenarios which directly related to lahar generation: 1) non volcanic, small to moderate size and frequent (2 to 10 years); 2) moderate and probable (300 to 1000 years), even if a small eruption; and 3) large but infrequent (1000 to 5000), with a large eruption. However, given the lacustrine deposit present in the upper Rio Chili canyon, a scenario for a dam-break flood must be considered – triggered by an eruption, an earthquake or a landslide. Little is known about the recurrence interval for these events but as discussed in previous sections Arequipa is threatened by lake breakouts originating in the upper Río Chili canyon.

The volumes and recurrence intervals of the scenarios proposed by the other authors have been validated against the data gathered, compiled and analysed for this research project. In addition the scenario for a dam-break flood has been added. The scenarios for lahars and floods are presented in Table 2.5.

Scenario for mass flow generation		Minimum volume (x 10 ⁶ m ³)	Maximum volume (x 10 ⁶ m ³)	Recurrence interval (years)
Eruption triggered	Non eruption triggered			
1.	Small to moderate size frequent floods	0.01	0.5	1.2 times/10 years
2. Moderate size lahars, probable during small eruption	Moderate to very large size, infrequent floods	0.5	4.0	>50 to 300
3. Large but infrequent lahars, generated by large eruption		4.0	11.0	>100 to 2 000
4. Very large lahars but very infrequent generated by large eruption		11.0	30.0	5,000 to >10,000

Table 2.5: The scenarios for lahar and flash flood generation in Arequipa. Scenarios 2-4 also consider the formation of a flow from a dam-break flood scenario. Adapted from Vargas et al. (2010).

Scenario 1 relates to small to moderate volume frequent floods, which are generated by heavy rainfall and/or snowmelt, such as the floods in 1989, 1997 and 2011. For the generation of moderate to very large floods, *scenario 2* would involve exceptional rainfall. Scenario 2 also relates to moderate sized lahars produced during a small eruption, such as the AD 1440-1470 vulcanian events where the VEI is 2. *Scenario 3* accounts large lahars that are produced during a moderate magnitude eruption (i.e. VEI 3) such as the ca. 2030 yr BP-old sub-Plinian explosive episode; and *Scenario 4* lahars are very large and generated based on an eruption resembling the 34,000-30,000 year-old or the 13,000-11,000 year-old ignimbrite-forming eruptive episodes (VEI >3).

The dam-break flood scenario will not be considered with floods and lahars as the dam-break flood can occur during all scenarios outlined above, and more (e.g. earthquakes, landslides). The dam-break flood is more likely to correspond with the flow volumes of scenarios 2 to 4 – 4 to 47 x 10⁶m³. The recurrence interval is harder to define due to the lack of knowledge of these events at El Misti, but is likely to occur because of a 1) a deep and narrow canyon; 2) active faults and 3) debris-avalanche deposits are present at El Misti. However, the occurrence of a dam-break flood originating in the Rio Chili canyon will be considered as a separate scenario for the purposes of Titan2D modelling (Chapter 3) to determine the magnitude, extent and effect of such a flow being released within this fluvial system.

2.7.2 Hazard zone maps

Hazard zone maps were created for the Rio Chili valley and the Quebrada Huarangal fan based upon the geological and historical history, terrace maps and developed hazard scenarios for floods and lahars (Figures 2.20 and 2.21). A high hazard class was assigned to the terraces where deposits from frequent and low magnitude events (i.e. Scenario 1) were mapped. Similarly very large and very infrequent events, representing the upper terraces, were given a very low hazard class. Even though the events of a very low hazard class are of an exceptional magnitude, they are very infrequent (5,000 to 10,000 years) and thus are less hazardous to the population at a smaller time-scale, when compared to much more frequent (2 to 10 years) smaller magnitude events.

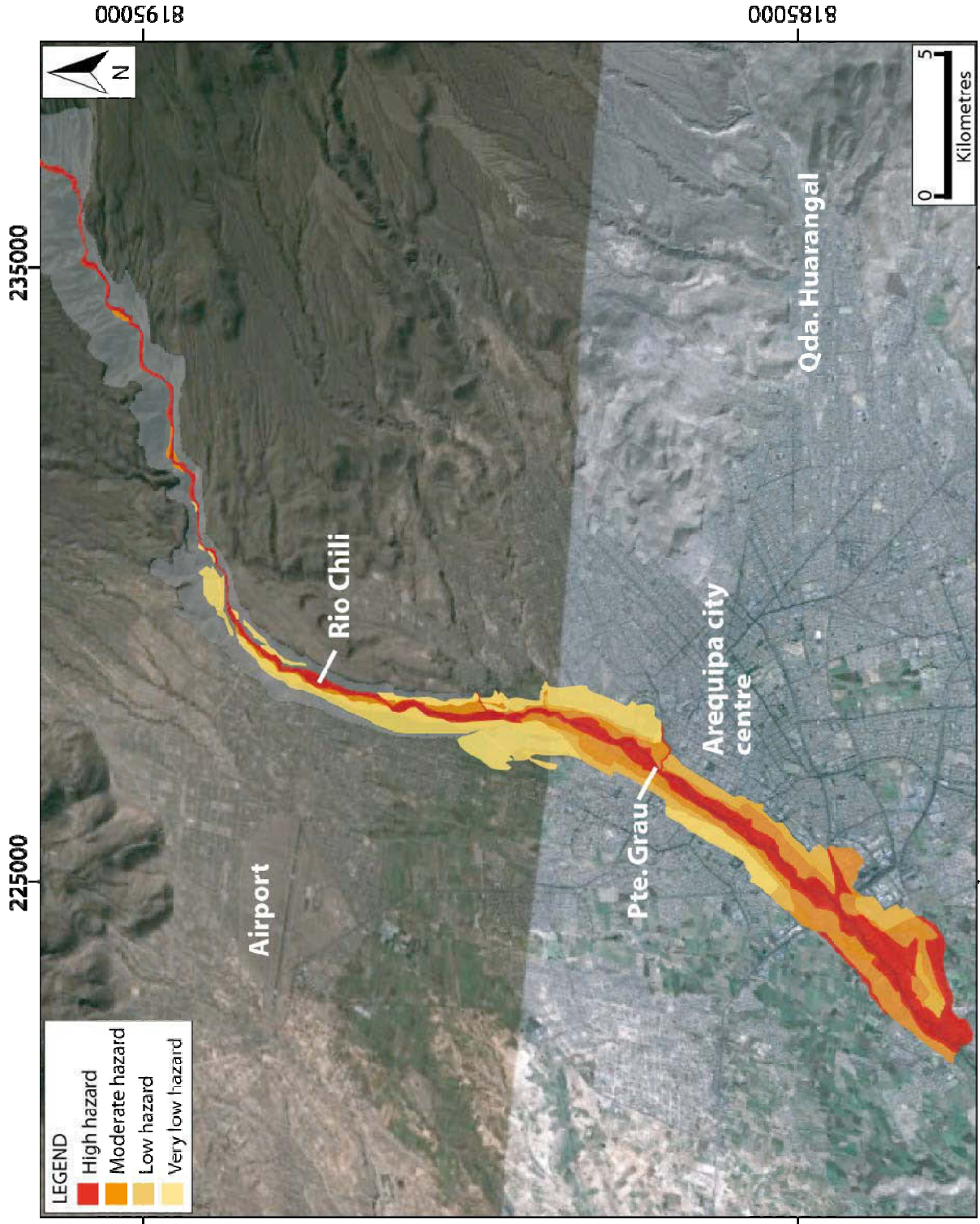


Figure 2.20: Mass flow hazard map for the Rio Chili valley based upon field mapping, geological and historical data, and terrace maps. Image from Google Earth.

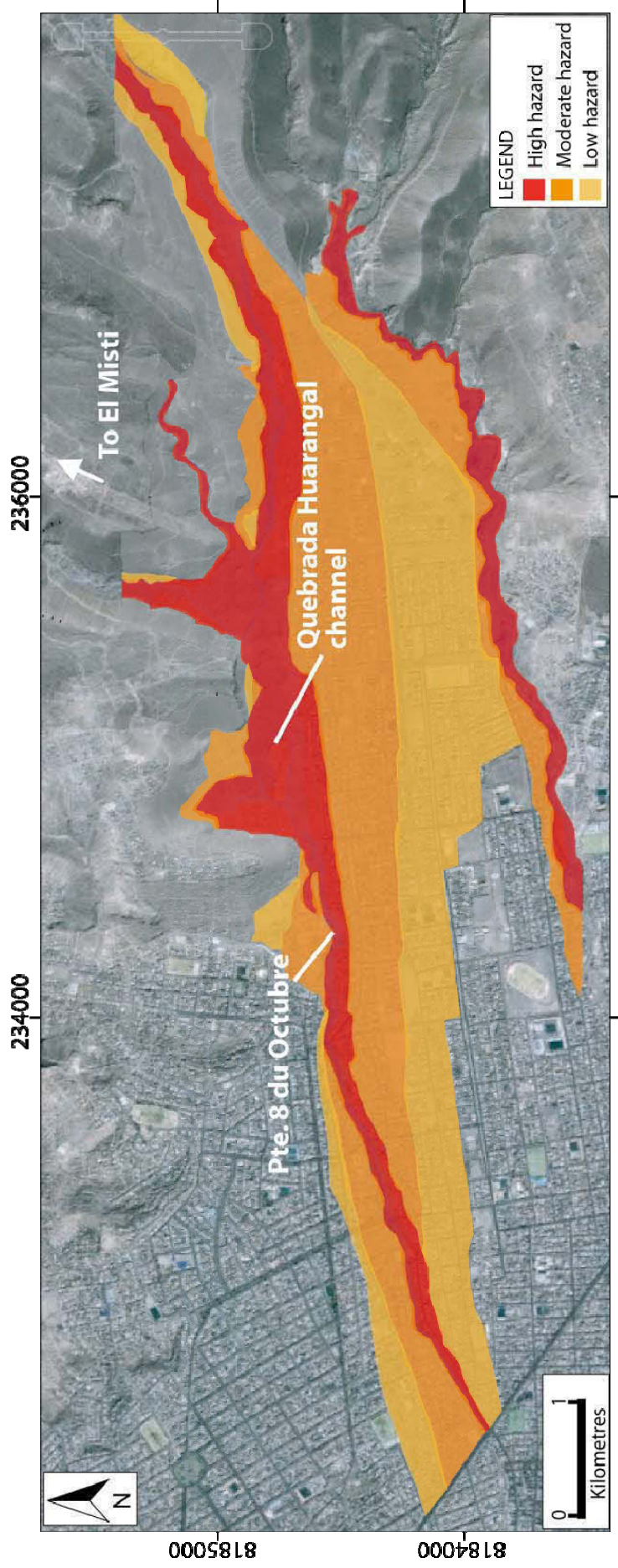


Figure 2.21: Mass flow hazard map for the Quebrada Huarangal fan based upon field mapping, geological and historical data, and terrace maps. Image from Google Earth.

For the purposes of hazard evaluation weights are assigned to the different hazard classes based upon the blind weighting method (Van Westen, 1997). Using this method the high hazard class has a weighting of 35, moderate hazard class a weighting of 20, low hazard class 10, and very low hazard class a weighing of 5. The weightings are applied when establishing the risk to Arequipa with respect to the vulnerability of the population (Chapter 5).

2.8 Discussion and conclusion

The hazard zone map for the Rio Chili Valley (Figure 2.20) highlights greater *high hazard* areas to the south of the city centre than higher up in the fluvial system. The gradient in this region has decreased sufficiently for deposition, 2.5% slope gradient across the most populated area, and the topography is more subdued. This has considerable implications in that the areas of highest hazard are confined to the most populated areas along the Rio Chili. Historical accounts of smaller magnitude ($0.01-0.5 \times 10^6 \text{ m}^3$) but frequent (2 to 10 years) mass flows in the Rio Chili have described flooding to be more pronounced in the city centre where banks are overtopped and retaining walls fail, but also where flatter, widespread farmland is located at the southern extremity of the city. In the upper river the flows are more confined and therefore by nature less hazardous.

The highest hazard on the Quebrada Huarangal fan represents frequent low magnitude mass flows (e.g. flash floods of 1997 and 2011) which inundate the modified channel bed and the lowermost terraces t0 to t1 (Figure 2.21). Of deep concern is that the poorest quality and most vulnerable housing occupy the highly hazardous channel bed itself (chapter 4). Wide flat terraces (t0 – t1') which represent moderate and low hazard classes occupy the land to the south of the channel bed; these areas are the most densely populated in the area. However, in general, the quality of building is superior to that located within the channel bed (chapter 4).

Based upon geological and historical evidence mass flows will be generated from El Misti regardless of an eruption (e.g. during an eruption, seismic crisis, and/or no unrest) if a sufficient rainfall threshold ($>15 \text{ mm/hr}$) and/or snowmelt conditions are reached. In addition, a dam-break flood scenario is plausible as suggested by dammed-lake deposits forming a 15 m-high terrace in the upper Rio Chili canyon. Debris avalanches and rockslides occurring on the steep slopes of the WNW flank of El Misti's cone, where an active fault is

located and new seismic activity has been recorded at a shallow depth since 2005, are capable of blocking the narrow canyon, leading to lake formation.

The results of this chapter clearly highlight that floods and lahars, even if moderate in magnitude will affect Arequipa. The most vulnerable populations are located within the most hazardous zones, with urban expansion leading to an increasing number of people inhabiting the highly hazardous areas. In addition essential infrastructure (e.g. the hydroelectric power system of five dams located in the upper Rio Chili canyon) is located within the canyon and the failure of such could have dire consequences to the population of Arequipa (e.g. no electricity or clean drinkable water supply). The vulnerability of infrastructure is the focus of Chapter 4 and will be evaluated with regard to the hazard maps in Chapter 5.

Chapter Three

Modelling lahars using Titan2D

3.0 Introduction

The computational modelling of mass flows has become an important tool in volcanic hazard assessment; numerical simulations help to assess quantitatively the rheological behaviour of flows, improve estimations of run-out distances, and to delineate expected inundation zones (Sheridan et al., 2005). Many different flow models exist (e.g. Flow2D, DAN, Flo-2D, VolcFLOW) and have been used with varying degrees of success to delineate hazard zones at volcanoes throughout the world (refer to Chapter 1, table 1.5). El Misti volcano is no exception; mass flow inundation zones have been further refined on El Misti's flanks, ring plain, and in the city of Arequipa with the aid of computational modelling. LaharZ (Schilling, 1998) was used by Toyos (2000), Van Gorp (2002), Delaite (2003) and Delaite et al., (2005) to identify areas prone to lahar inundation in the Río Chili Valley, and the Quebradas San Lazaro, Huarangal and Agua Salada. Stinton et al., (2004a) compared the LaharZ results obtained by Delaite (2003) with Titan2D single phase (Patra et al., 2005) simulations. Vargas et al., (2010a) took the research further by using the two-phase Titan2D model (Pitman and Le, 2005) to simulate lahars and compare the results with LaharZ simulations obtained by Delaite (2003).

Stinton et al., (2004a) and Vargas et al., (2010a) noted several differences between the results from the two models including: 1) LaharZ run-out distances were consistently longer than those achieved in Titan2D simulations, for example even the largest volume Titan2D flows ($11.0 \times 10^6 \text{ m}^3$) did not extend further than the smallest volume ($1.5 \times 10^6 \text{ m}^3$) LaharZ simulated flows; 2) common flow features that are present in reality, such as superelevation on river bends, overbanking on low relief fans and flow divergence and convergence around hills or terraces, were observed in Titan2D simulations but not with LaharZ; and 3) Titan2D simulations reacted to the underlying topography, for example where changes in the slope and channel occurred, more faithful to topographic variations than did the LaharZ simulations.

The results of their studies concluded that LaharZ simulations represent more closely the spatial distribution and extent of past deposits; however Titan2D simulates the behaviour of debris flows more realistically than LaharZ. The discrepancies in the results are due to the underlying differences between the two models – LaharZ is a statistical and semi-empirical code, whereas Titan2D takes into account the physical aspects of lahar flow.

LaharZ is a semi-empirical code which models and calculates the area covered by lahars, operating within the GRID module of ArcInfo (ArcGIS). Schilling (1998) developed the model from mathematical and statistical relationships derived from 27 lahars at 9 volcanoes in the world, using two equations for estimating the surface and planimetric cross-section of a lahar in a valley, depending on its volume. For a more detailed description of the model relationships the reader is referred to Iverson et al., (1998) and Schilling (1998). The program simultaneously performs a calculation on values including the volumes of lahars, a DEM and a value of H / L . H and L are respectively the height and basal radius defining a break-in-slope where the energy line intersects the volcano flank profile. LaharZ calculates the development of flood zones from a limited proximal hazard defined by the intersection of this cone of energy with the ring plain of the volcano. The modelled results are dependent on the accuracy of the input parameters. Delaite (2003) noted that an enhanced DEM optimised LaharZ simulations at El Misti, when compared with the result from a less accurate DEM used by Toyos (2000) and Van Gorp (2002).

In contrast, Titan2D is a depth-averaged model for an incompressible Coulomb continuum, a “shallow-water” granular flow suitable for simulating a variety of geophysical mass flows. Conservation equations for mass and momentum are solved with a Coulomb-type friction term for the interactions between the grains and between the granular material and the basal surface. For a more detailed description of the model relationships the reader is referred to Chapter 1 (section 1.5.1) of this manuscript, Patra et al., (2005) and Pitman and Le, (2005). The input parameters are internal and basal friction angles, starting pile location and flow volume, detail topographic data base of the volcano (DEM), and solid fraction in the case of “two-phase” model. A precise DEM is a critical input for the Titan2D simulation algorithm and for the accuracy of the results. Capra et al., (2010) showed that topographic resolution significantly affects the flow path and run out of Titan2D simulations. In addition, flow paths, areas, and the thickness of simulated flows differed when the DEM resolution was varied but all other input parameters (such as basal friction angle) remained the same.

As outlined above, LaharZ and Titan2D are different models used for distinct purposes and it is therefore difficult to make a direct comparison between the two models and their results. LaharZ can be viewed as a first delineation of lahar-prone zones, whereas Titan2D explores the relationship between the topography and the flow physics (Vargas et al., 2010a). Stinton et al., (2004a), Delaite et al., (2005), and Vargas et al., (2010a) all concluded that further investigation into modelling at El Misti is warranted, and particular with the creation of a better resolution DEM for simulations.

Little research has been conducted at El Misti using the Titan2D “two-phase” model (Chapter 1, section 1.5.1.2); a model based on recognised and accepted flow physics and successful in modelling other two-phase flows such as lahars at Mt. Ruapehu, New Zealand (e.g. Procter et al., 2010a) and Cotopaxi Volcano, Ecuador (Williams et al., 2008). Consequently, this research utilises the Titan2D “two-phase” model for the delineation of lahar hazard zones at El Misti, and also to investigate the effect of DEM resolution on the simulations.

3.1 New Titan2D simulations at El Misti Volcano, Arequipa

3.1.1 The effect of input parameters

Simulations were performed on a 30 m DEM, based upon digitised 1:25,000 scale topographic maps and on radar interferometry (Delaite, 2003) using expected flow scenario volumes ranging from $0.01 \times 10^6 \text{ m}^3$ to $11 \times 10^6 \text{ m}^3$ (refer to Chapter 2), down the Río Chili Valley and Quebrada Huarangal. Successive runs of Titan2D were conducted varying the input parameters (e.g. starting point, internal and bed friction angles, and solid fraction) in order to constrain the simulations.

The input parameters were calibrated against historic and geologic evidence of past events, and by examining the impact of flow features. Flow features occur as a response to the surrounding topography and can include: 1) *Superelevation*, which occurs when a high energy flow changes direction, such as on river bends; 2) *Ponding* is where a ‘pond’ occurs usually due to an obstacle in the path or where the channel becomes restricted; 3) *Overbanking* occurs where the flow encounters low relief fans; 4) *Flow divergence* and *convergence* happens

when the flow reaches an obstacle (e.g. hills, terraces) and moves around it, converging on the other side; and finally 5) *Run-out*, which is the longitudinal extent of the flow.

The results of simulations were compared with the mapped deposits, and the parameters used were validated against the literature. Once the input parameters were determined as appropriate for simulations at El Misti, successive runs varying only the flow volume were undertaken on an enhanced resampled 10 m DEM (refer to section 3.1.1.6). These simulations were to determine the run-out zones for typical flows. These run-out zones then in-turn define areas that could be inundated during future mass flow events. A summary of input parameters is shown in Table 3.1. A full explanation of the parameters used, and the results, follows in successive sections of this chapter and also in Chapter 1 (section 1.5.2.1).

Input parameter	Value
Internal friction angle (°)	20-30
Basal friction angle (°)	8-25
Solid ratio	0.4-0.7
Volume ($\times 10^6 \text{ m}^3$)	0.5, 1.5, 4, 9, 11

Table 3.1: *Input parameters used for the modelling of volcanic mass flows in Titan2D two-phase. Basal and internal friction values were chosen based on previous work using Titan2D simulations (Sheridan et al. 2005) and from the literature (e.g. Pierson, 2005). In addition, the basal friction angles are within range of values often used for glacial and fluvial deposits (Stinton et al. 2004a). Solid fraction covers the range of values that define hyperconcentrated flows (e.g. Pierson, 2005). Volumes are discussed further in Table 3.3.*

3.1.1.1 Starting location

The starting point is where the central point of the initial material pile is located. The starting point can be difficult to determine because source starting locations are poorly known in many cases (Sheridan et al., 2010). The starting point can be selected either by applying the energy cone relationship (e.g. Delaite et al., 2005), or by taking into consideration the dimensions and dynamics of the drainage channel and local slope conditions that could lead to the initiation of a volcanic mass flow (e.g. Stinton et al., 2004a). For this study a catchment analysis was performed using ArcGIS (e.g. Procter et al., 2009) where catchments were identified based on channel morphology and the slopes angle. Two points were identified for each catchment; the centre point, which corresponds to the break in slope, and the upper point which is the top of the catchment (Figure 3.1). A more detailed description of, and the

rationale for choosing, these valleys for Titan2D simulations can be found in the Introduction chapter and Chapter 1, section 1.1.

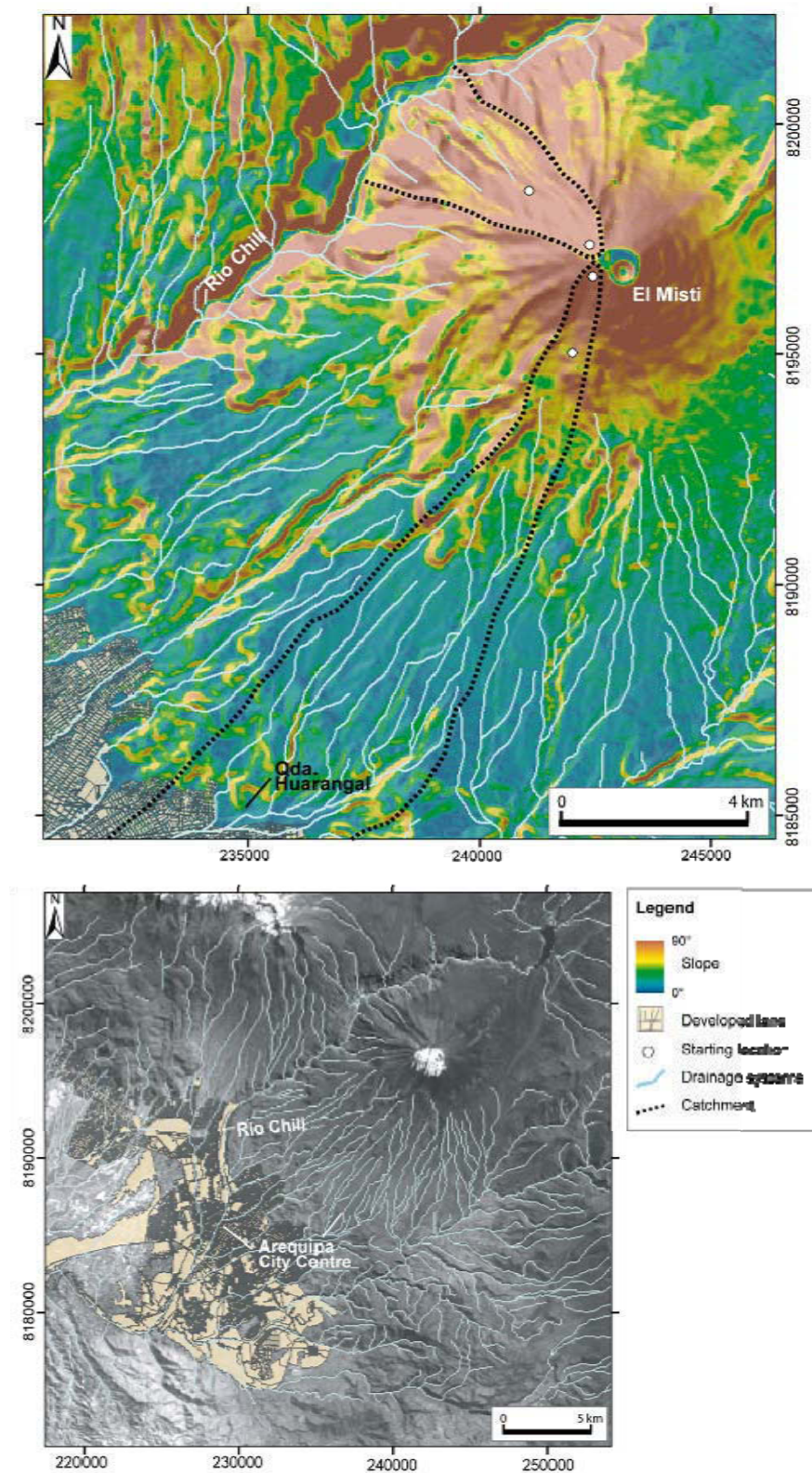


Figure 3.1: Starting point locations for Titan2D pile . Flow starting point locations based on piles at top of cone and at break in slope in the respective catchment areas of the Rio Chili Valley and Quebrada Huarangal. The figure on the right gives an indication to the slope angle on El Misti and the location of drainage into the study area from the cone.

The catchments identified for the Río Chili and Quebrada Huarangal correspond to the most probable location for flow initiation according to the catchment analysis. Details of the catchments and the location of the starting points are presented in Table 3.2.

Catchment	Catchment size (km ²)	Starting point for Titan2D simulations			
		Location	UTM coordinates	Elevations (m)	Slope angle (°)
Río Chili Canyon	9.4	Upper point	241089, 8198584	5577	33
		Centre point	242345, 8197422	4373	26
Quebrada Huarangal	36.0	Upper point	242298, 8196748	5538	33
		Centre point	241928, 8195050	4515	25

Table 3.2: Starting point locations for Titan2D pile . Locations based on piles at top of cone and at break in slope in the respective catchment areas.

For both the Río Chili and Quebrada Huarangal drainage channels, the upper starting points are located on the cusp of the summit cinder (Misti) cone and 14 – 50 ka lava flows, an area of unconsolidated to consolidated rock (after the Unified Soil Classification System) at a slope angle of approximately 33°. The lower starting points are situated within the channel, the break-in-slope at a slope angle of approximately 25°, in areas of consolidated to unconsolidated 14 – 50 ka lava flows which down slope become more unconsolidated (e.g. dome collapse deposits), gravely (e.g. non-welded ignimbrite deposits) and sandy (e.g. pumice-flow and fall deposits and alluvium) deposits. Lava flow ridges commonly mark the channel boundaries; wherein the case of the Río Chili starting points, simulated flows can take one (or all) of three possible channels, controlled by the lava ridges, downstream of the starting point before reaching the Río Chili valley (Figure 3.1). The Río Chili starting locations also located within a debris avalanche scar, which comprises a considerable amount of loose sediment that accumulated at the bottom of the steep gullies.

Due to the current configuration of the nested craters on the volcano's summit, the formation of lahars on the SE – SSW sector of the cone could be considered more probable in a lahar-forming event, which does not modify the current crater configuration. This is because the SE – SSW sector is not protected by an outer crater rim as is the case with the other sectors of the cone. The starting points for the Quebrada Huarangal simulations are situated on the S – SW sector in a valley controlled by lava flow ridges on either side (Figure 3.1). Deep gullies have been formed in softer sediments (e.g. pumice flow and fall, block-and-ash flow and non-welded ignimbrite deposits) which funnel the flows towards the Quebrada Huarangal fan. As

with the Río Chili starting location, a considerable amount of loose sediment is available within the gullies for incorporation into future flows.

The upper and central starting locations for both channels were explored in Titan2D; however the centre point, or the break in slope, was considered more likely to be the point at which flows would initiate. This is because above the break in slope, the slope is too steep for the significant accumulation of loose material. Therefore, further simulations using an enhanced 10 m DEM were carried out using the centre starting point located at the break in slope.

3.1.1.2 Maximum time and number of time steps

Shallow-water models, such as Titan2D, are essentially diffusion processes and the boundary conditions of the examined flow must be artificially defined at a reasonable scale. In Titan2D, the maximum number of time steps and the maximum time (in seconds) must be input to set a run time for the simulation. When the job is submitted for processing, the simulation will stop when it has gone through the time steps or has simulated the specified amount of time. Both the values should be set high enough such that the geologic event that is being simulated has ended (i.e. the material has come to rest). If either of the values is set too low, the simulation will end with material not having reached static equilibrium. If both these values are set excessively high however, wasted computation will be performed dynamically simulating the pile in static equilibrium (GMFG, 2007).

The selection of the appropriate time to run the simulations was determined by trial and error and in the case of El Misti, also based also upon the time used by previous researchers (e.g. Stinton et al., 2004a; Delaite et al., 2008 and Vargas et al., 2010a). The number of computed time steps needed to simulate a geologic event will vary depending on the amount of computational mesh points used, the friction parameters, the use of grid adaptation, the simulation order and the initial pile geometry and location. For simulations on El Misti 500 seconds were adequate.

3.1.1.3 Friction angles – internal and basal

Friction angles (internal and basal friction) are one of the more important input parameters in Titan2D modelling because they control the acceleration and velocity of the moving mass and

also allow a subtle control on the lateral spread (refer to Chapter 1, section 1.5) (GMFG, 2007; Procter, 2010). Approximately 200 simulations were run using a constant initial volume and location with different combinations of internal and basal friction parameters at intervals of 2-5° (refer to Table 3.1).

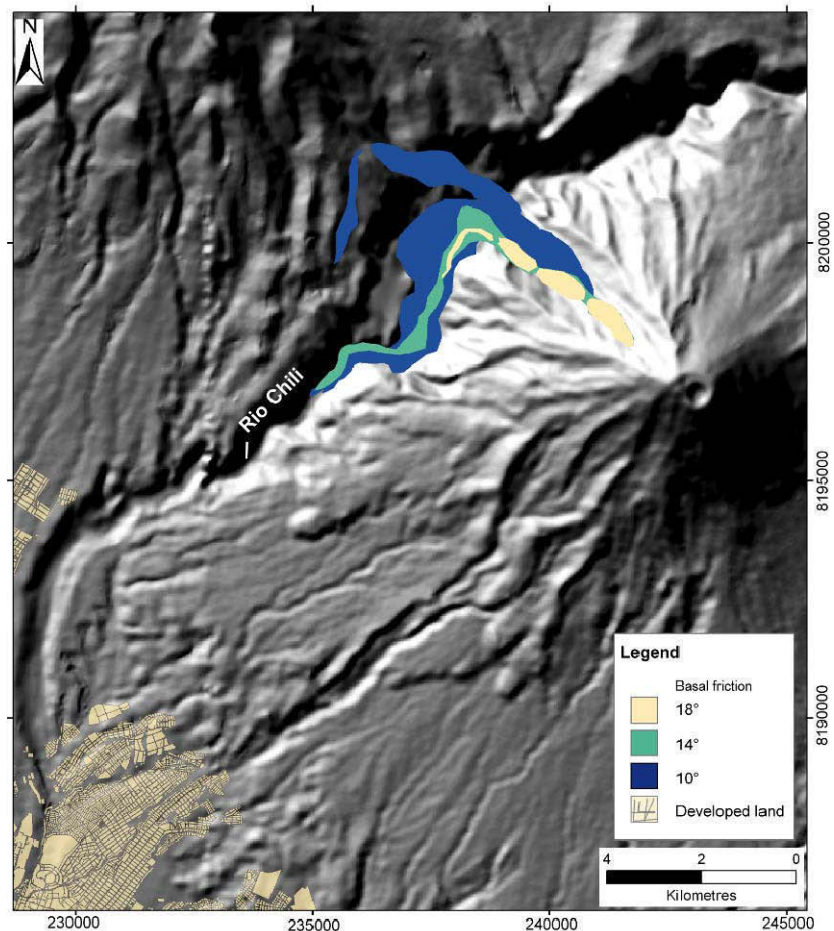
The internal friction angle is a parameter that provides a measure of the strength to the material. This strength can be attributed to two factors; the friction between individual grains and the geometrical interlocking between the particles (Pouliquen and Renaut, 1996; Saucedo et al., 2004). Generally speaking changing the internal friction angle has little to negligible effect on the flow, and the most influential angle is that of the basal friction angle which corresponds to the minimum slope that an inclined surface must obtain before the material placed on it begins to slide from its static position (GMFG, 2007). Many authors (e.g. Stinton et al., 2004b; Sheridan et al., 2005; Williams et al., 2008; Procter et al., 2009; Murcia et al., 2010) have shown that a reduction in the basal friction parameter has a significant effect on increasing run-out lengths, whereas changes in internal friction angle have shown less dramatic effect or no noticeable effect in the mid-value ranges.

For this study the best results were obtained using internal friction angles between 25°-33°. This is close to the angle of repose of typical El Misti Volcano debris flow sediment (gravel – coarse sand) on the cone, and is consistent with values used by other authors (e.g. Pitman et al. 2003; Stinton et al. 2004b; Bursik et al. 2005; Sheridan et al. 2005; Rupp et al. 2006; Macías et al. 2008; and Procter, 2009) in a variety of volcanic settings for debris flows and pyroclastic flows. While this parameter has a minor effect on the final inundation area and run out of flow, it appears to play a more important role in affecting the velocity outputs of the simulation at particular points in time (discussed further in section 3.2).

As discussed above, the simulations are highly sensitive to the basal friction value (Figure 3.2) and basal friction angles allowed a level of control of the acceleration and velocity of the moving mass (discussed further in section 3.2). The best results were found using angles between 8-12°. Extremely low basal friction values (<8°) resulted in flows that accelerated rapidly and unrealistically down slope. In addition, low basal friction values resulted in the simulated flow ‘unrealistically’ flowing up the canyon wall near the military school. While debris flows have deposited within this locality, they have not flowed this far up the canyon wall.

Debris avalanches worldwide also show that the lower the basal friction angle the further the distance travelled (Hayashi and Self, 1991). At the opposite end of the spectrum basal friction values of greater than 18° resulted in flow run-outs less than 1 km from the initial starting location. Figure 3.2 clearly shows that the lower the basal friction angle the further the simulated flow travels. As a result of the repeated simulations, varying the basal friction angle, a basal friction angle of 12° was used in the final simulations on an enhanced 10 m DEM of the region (refer to section 3.1.1.6).

Figure 3.2: Simulations carried out with Titan2D on a 30 m DEM using the R o Chili flow scenario. The basal friction value was varied using a constant flow volume of $4 \times 10^6 \text{ m}^3$, internal friction of 25 and solid ratio of 0.4. The basal friction angles that were used are 10 , 14 , and 18 .



The range of basal friction values determined in this study are consistent with angles used by other authors (e.g. Williams et al., 2008; Procter et al., 2009) for lahars. Williams et al., (2008) found that a basal angle of 10° was best suited for Titan2D simulated lahars in two valleys on Cotopaxi, Ecuador. However Williams et al., (2008) did state that in-depth analysis into this parameter was outside the scope of their study and thus utilised a value within an accepted range for fluvial and glacial deposits (after Stinton et al., 2004b). Similarly, Procter et al., (2009) found that basal friction angles ranging from 9° to 12° suited Titan2D simulated lahars down the Whangaehu Valley, Mt. Ruapehu, New Zealand. However, in terms of

Titan2D modelled pyroclastic flows, block-and-ash flows, debris avalanches etc. a wide range of basal friction angles exist. Bursik et al., (2005) and Rupp et al., (2006) used values of 20–28° for Colima Volcano, Mexico; Macías et al. (2008) used values of 10–12° for El Chichón Volcano, México; and Murcia et al., (2010) used a basal friction angle of 15° for Cerro Machín Volcano, Colombia.

Stinton et al. (2004b) in an application to Little Tahoma Peak Avalanches, USA, demonstrated the importance of using variable bed friction values, depending on the substrate, because the distribution of the deposits changed greatly with the variation of the bed friction. Variable bed friction values can be introduced into Titan2D with a GIS-based surficial material map, where changes in the surface morphology results in a change in the basal friction angle. While the range of basal friction values determined for this study correlate well with previous studies and with aspects of the topography, one value cannot be viewed as representative of the changes in basal friction experienced along a flow path. The addition of a material map, derived from geotechnical and geological maps of the region, would be highly recommended for further research into Titan2D simulations at El Misti.

3.1.1.4 Solid ratio

Sediment concentration plays a fundamental role in flow behaviour and mechanics (Iverson, 1997; Pierson, 2005), and is an important parameter in the Titan2D “two-phase” model (refer to the Introduction for further information). Water floods normally transport mostly fine sediment and in relatively small quantities – containing generally less than 4% by volume (vol.%) or 10% by weight (wt.%) suspended sediment (Pierson, 2005). In contrast, high-discharge debris flows (and/or mudflows) may transport more sediment than water with sediment concentrations in excess of 60 vol.% (80 wt.%) (Pierson and Costa, 1987). A hyperconcentrated flow is often applied to intermediate flows. However these values cannot be regarded as definitive because the solid concentration is highly variable even within one debris flow event and along the path of the propagating flow, other criteria such as grain size and the physical characteristics of the material play a part (Dumaisnil et al. 2010). This is one aspect, a varying sediment concentration, which cannot be altered in Titan2D.

The appropriate solid fraction for El Misti lahars was determined from a literature review and from geological and historical evidence (Figure 3.3). Williams et al. (2008) used a range of

solid concentrations, from 0.4 to 0.7, to cover the spectrum of values that define debris flows (after Pierson, 1985; and Scott, 1988). The solid fraction of lahars at Cotopaxi was unknown however thought to be towards the upper end of scale (Williams et al., 2010). In contrast, field studies at El Misti suggest that lahars are characterised more as hyperconcentrated flows and therefore represent the lower to middle end of the debris-flow scale (e.g. Chapter 2; Thouret et al., 2001; and Vargas et al., 2010a).

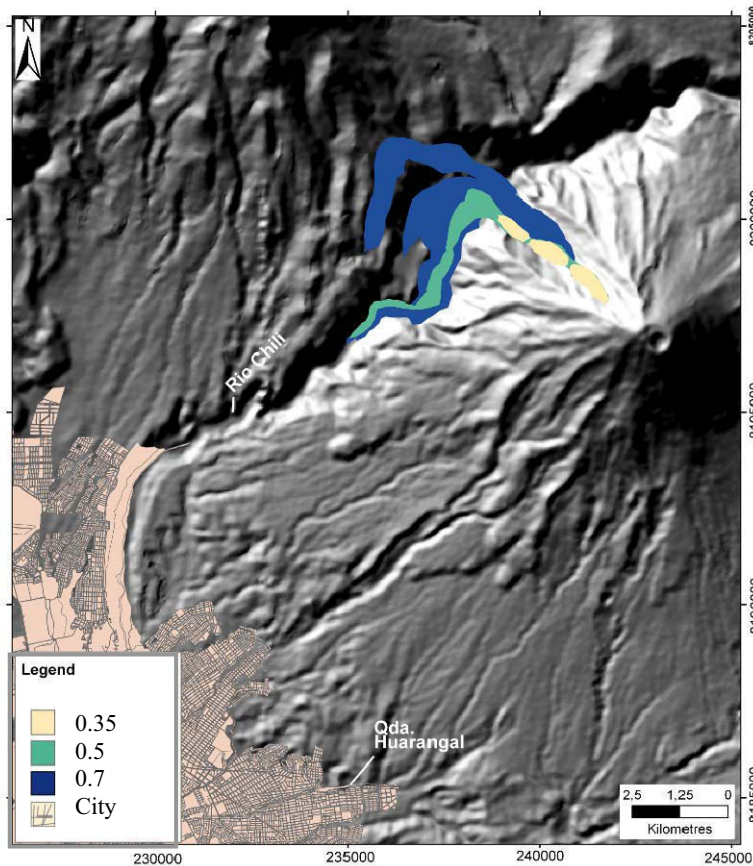


Figure 3.3: Simulations carried out with Titan2D on a 30 m DEM using the Rio Chili flow scenario. The solid ratio was varied from 0.35 to 0.7 using a constant flow volume of $4 \times 10^6 \text{ m}^3$, internal friction of 25 and basal friction of 12 .

Based on this evidence, Titan2D simulations were undertaken varying the solid concentration from 0.35 to 0.7 at 0.1 intervals. Titan2D is unstable using values above and below these limits. Successive runs were undertaken varying this value to investigate the effect of a changing the solid fraction on the simulations. Solid fractions towards 0.7 resulted in the flow stopping and not flowing, rather leaving “hops” or small mounds in on the slope (Figure 3.3). Solid fractions below 0.4 are either unstable or the extent and run out is very long. In the case of El Misti “unreasonable” flow run up and direction is observed towards Charcani when the solid fraction is below 0.4. It was found that a solid fraction of between 0.4 and 0.5 was adequate for modelling of lahars at El Misti (Figure 3.3).

3.1.1.5 Flow volume

The flow volume is determined by specifying the initial pile volume derived from the pile's dimensions; an ellipsoid by a height (z) and an elliptical base defined by radii in the x and y planes (Sheridan et al., 2005). The selection of appropriate pile dimensions is crucial to guarantee reliable results, because the dimensions of the pile and relationship to the drainage channel can also affect the way in which the flow is modelled. In this study the pile height did not exceed 15 m, and the pile dimensions were in accordance with the geomorphology of the drainage channel; the longest side of the ellipsoid is parallel to the channel rather than across.

The volume of material used in this study corresponds to flow volumes derived from geological studies, and from volcanic events and hazard scenarios described for El Misti volcano based on the magnitude and frequency of events (Thouret et al. 1999; Stinton et al., 2004a; Delaite et al. 2005; Vargas et al., 2010a; and this study, see Chapter 2). The calculated lahar volume estimations also take into account an estimate of the amount of material which could be mobilised into the channels, a rainfall threshold (e.g. 61 mm in 3 hours), and the area of the seasonal snowfield on the volcano summit (Delaite et al., 2005; Stinton et al., 2004a). Table 3.3 gives the estimated lahar volumes for three hazard scenarios along with the flow volumes used in Titan2D simulations.

Scenario for generation of lahars	Minimum lahar volume ($\times 10^6 \text{ m}^3$)	Maximum lahar volume ($\times 10^6 \text{ m}^3$)	Recurrence interval (years)	Volume used in Titan2D simulations ($\times 10^6 \text{ m}^3$)
1. Non volcanic, small to moderate size, frequent	0.01 to 0.1	0.1 to 0.5	2 to 10	0.5
2. Moderate and probable, small eruption	0.5 to 1.5	1.5 to 4.0	300 to 1 000	1.5, 4.0
3. Important but rare, only if large eruption	4.0 to 9.0	9.0 to 11.0	1 000 to 5 000	9.0, 11.0

Table 3.3: Lahar volumes are based on the estimated volume of Holocene lahar deposits surrounding El Misti, a rainfall threshold of at least 15 mm per hour (e.g. February 1997), and surface area of the seasonal (December – July) snowfield on the volcano summit (up to 7 km in case of heavy snowfall) (Delaite et al., 2005 and Vargas et al., 2010a).

Parameters for internal friction angle (25°), basal friction angle (12°), solid ratio (0.40) (discussed in the following sections) remained constant on the 30 m DEM to evaluate the flow

run-out length and inundation area for the volumes ranging from $0.5 - 11.0 \times 10^6 \text{ m}^3$, as shown in Figure 3.4. The map illustrates that even the largest volume flow does not reach the city limits, and barely makes it out of the Canyon, which is in agreement with the observations made by Stinton et al., (2004a), Delaite et al., (2005) and Vargas et al. (2010a). These run outs are much shorter than past deposits and the LaharZ derived inundation areas of Delaite et al. (2005). The shorter run out of Titan2D simulated flows is most likely due to a weakness inherent of all 2-D thin-layer models where acceleration and momentum are not calculated in the vertical (z) direction; diffusion is only considered in the horizontal (x and y) directions. When there are very steep slopes or run-up of canyon walls, the flow energy is lost and the flow stops much too early. The differing results highlight the need to understand the model limitations, because without this understanding there could be serious implications for hazard assessments.

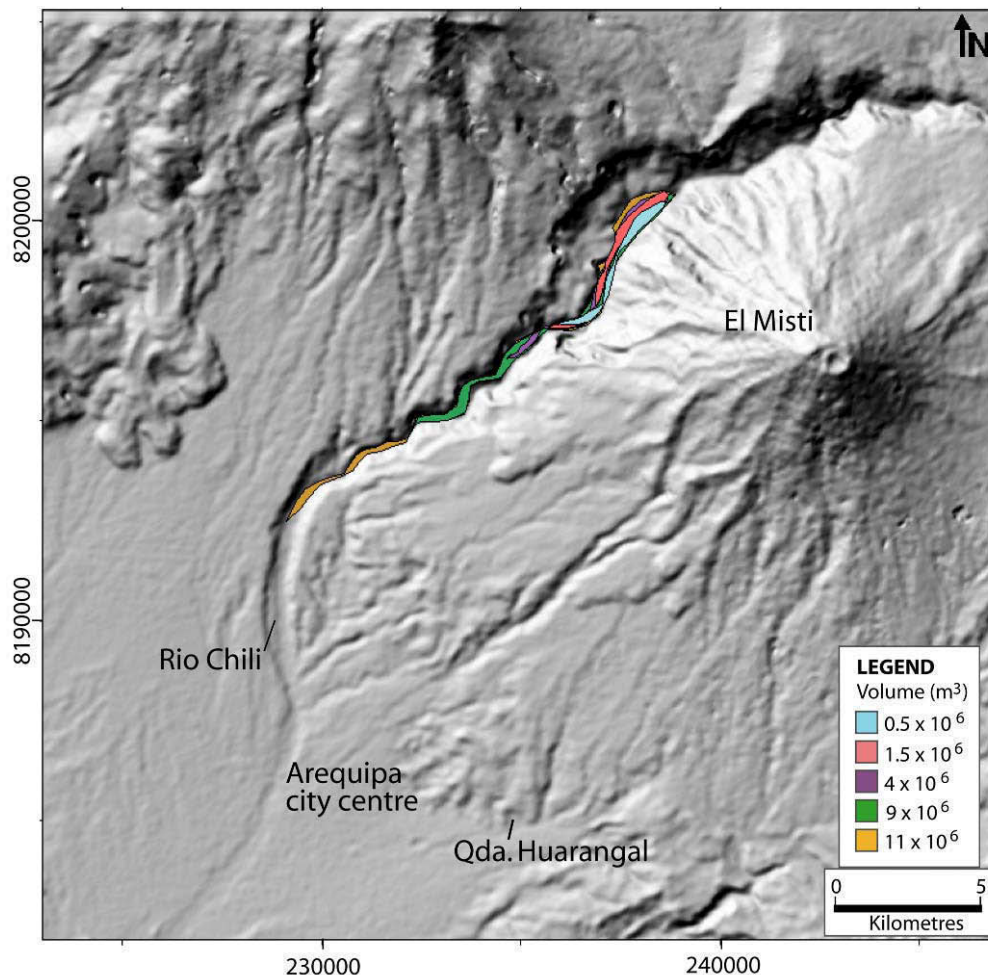


Figure 3.4: The results of a Titan2D simulation in the Rio Chili using the new enhanced DEM. Volumes ranging from $0.5 - 11.0 \times 10^6 \text{ m}^3$ were used with an internal friction angle of 25° , a basal friction angle of 12° and a solid ratio of 0.40.

3.1.1.6 DEMs

Previous studies have shown the importance of DEM resolution on computational routines for reconstructing different paths, velocities and extents of various flows, and for correctly estimating the areas and levels of hazards associated with future volcanic activity (e.g., Stevens et al. 2002; Pitman et al. 2003). Prior DEMs used at El Misti were of low resolution which could be a factor in the subsequent ‘unrealistic’ results. To investigate the effect of DEM accuracy on simulated results an enhanced DEM was computed using Differential GPS and ASTER data and compared to a pre-existing 30 m DEM (Delaite et al., 2005).

Detailed topographical data was acquired during a DGPS survey of an area of ~12 km² in 2007 and 2008. After post-processing the DGPS points, a DEM was created by interpolating (kriging) ASTER 30 m data with ~50,000 DGPS points (Chapter 1). This was then resampled at 10 m to create an enhanced DEM for Arequipa. DEM creation was carried out in Surfer and later converted into GRASS GIS raster formats for Titan2D simulations. Merging the DGPS data with the ASTER data was a necessary step for two reasons. Firstly the DGPS data did not cover the entire study area and secondly, the ASTER data does not accurately represent river channels and terraces due to poor resolution in the 30 m DEM. Merging the data allowed for potentially more accurate simulations.

The decision to use the ASTER DEM over other DEMs is twofold, 1) the ASTER DEM represents the best resolution publically accessible DEM, and 2) it is more accurate than the 30 m DEM of Delaite (2003) (henceforth called the previous DEM). A comparison made between the contours of the two DEMs showed that while the shape of the contour is similar, there is an approximately 500 to 800 metres horizontal offset between the ASTER DEM contours and that of the previous DEM (Figure 3.5b). In contrast, there is a good agreement between the contours of the ASTER DEM and a 90 m SRTM DEM (Figure 3.5c). The quality of the previous 30 m DEM is called into question. The difference could be due to the different data used to create the DEMs; radar interferometry and the digitising of 1:25,000-scale topographic maps versus satellite derived data.

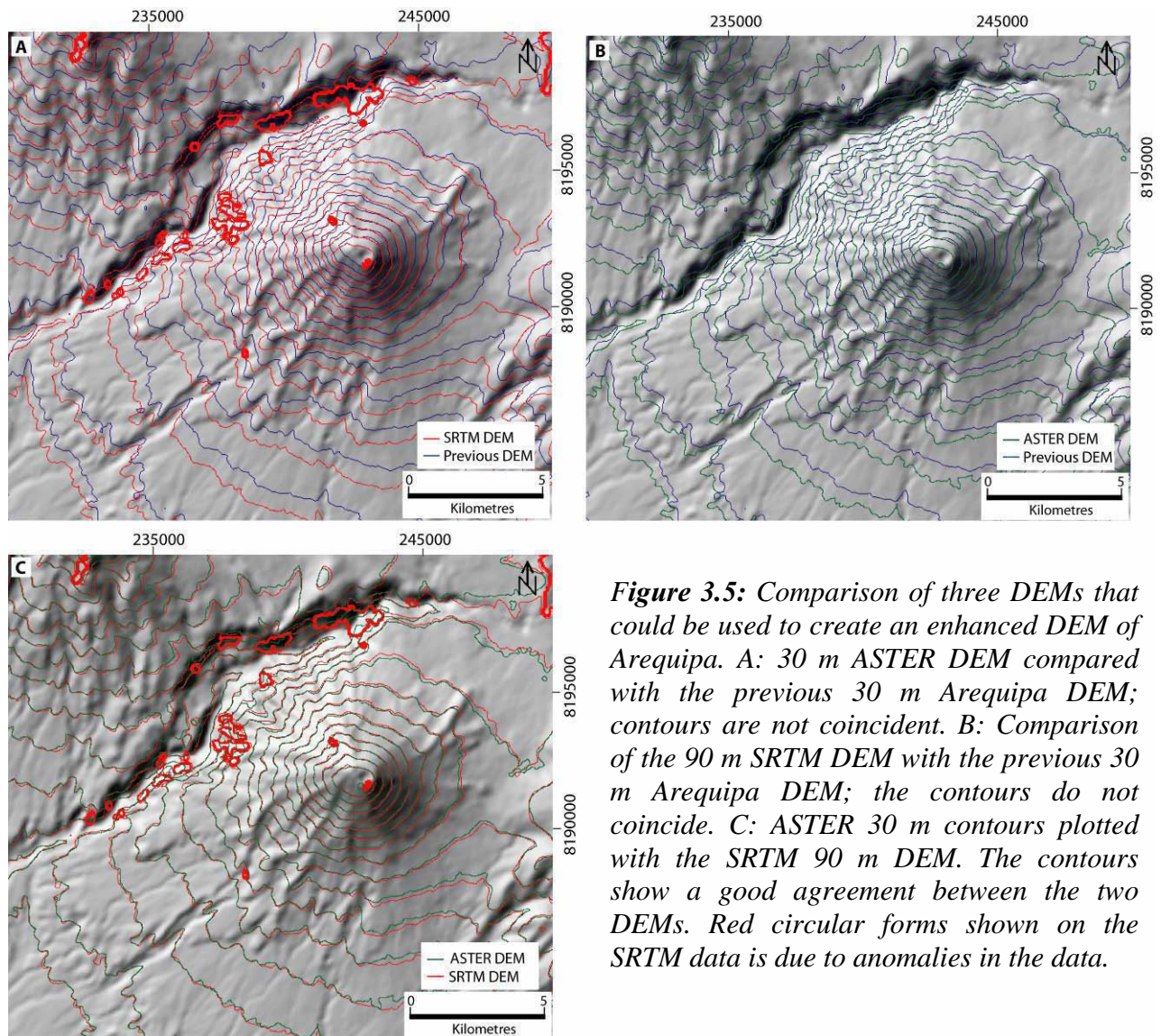


Figure 3.5: Comparison of three DEMs that could be used to create an enhanced DEM of Arequipa. A: 30 m ASTER DEM compared with the previous 30 m Arequipa DEM; contours are not coincident. B: Comparison of the 90 m SRTM DEM with the previous 30 m Arequipa DEM; the contours do not coincide. C: ASTER 30 m contours plotted with the SRTM 90 m DEM. The contours show a good agreement between the two DEMs. Red circular forms shown on the SRTM data is due to anomalies in the data.

More than 50,000 DGPS were added to the ASTER DEM where a systematic error in the elevation between the two data sources was observed; the ASTER data was at a continuously lower elevation than that of the DGPS data. One hundred data points, taken throughout the two study areas, were chosen and the average difference in elevation was determined to be 40 m. The discrepancy in elevations could be explained by the difference of vertical accuracy of the two data sources, but also due to differences in geometric and orthometric heights. The DGPS elevation data was converted into orthometric height by subtracting the height of the geoid, with reference to the WGS84 ellipsoid, in the area of interest.

However with merging the two datasets a slight difference in elevation between the DGPS point and an adjacent ASTER point could misconstrue a terrace boundary, or an important feature outlined during DGPS surveying. In order to maximise the topography represented

by the DGPS points a buffer was created to exclude ASTER data in close proximity of the DGPS points. The influence and determination of the optimum buffer width was explored after the data had been interpolated (Chapter 1, section 1.4.2.3), and a buffer of 20 m was chosen.

The merging and interpolation of DGPS and ASTER data has resulted in a DEM of higher resolution (~10m) than used previously for the simulation of mass flows at El Misti (Figure 3.6). The Río Chili channel is much better defined in the new DEM where DGPS surveying was more regular and unhindered by construction and/or lack of access. However, in Quebrada Huarangal the detail of the channel and terrace banks are not as well represented for a number of reasons. Firstly, construction on the terrace is very dense and access for DGPS surveying was limited mostly to roads which are not closely spaced. Additionally, gaining access to private properties was much more difficult than it was in the Río Chili Valley. Secondly, field work time spent in this area was much more limited than in the Río Chili Valley. Thirdly, changes in topography are much more subtle than in the Río Chili, especially with active mining occurring in the channel disturbing the natural channel bed. Finally, many DGPS points collected possessed a high RMS error which meant they were removed from the dataset; they were concentrated in a similar area and perhaps the error could be explained by an interference of the DGPS with large overhead power pylons and lines. The inset of Quebrada Huarangal in Figure 3.6 shows the areas where DGPS data is missing and as a result the DEM is less representative of the topography in this locality.

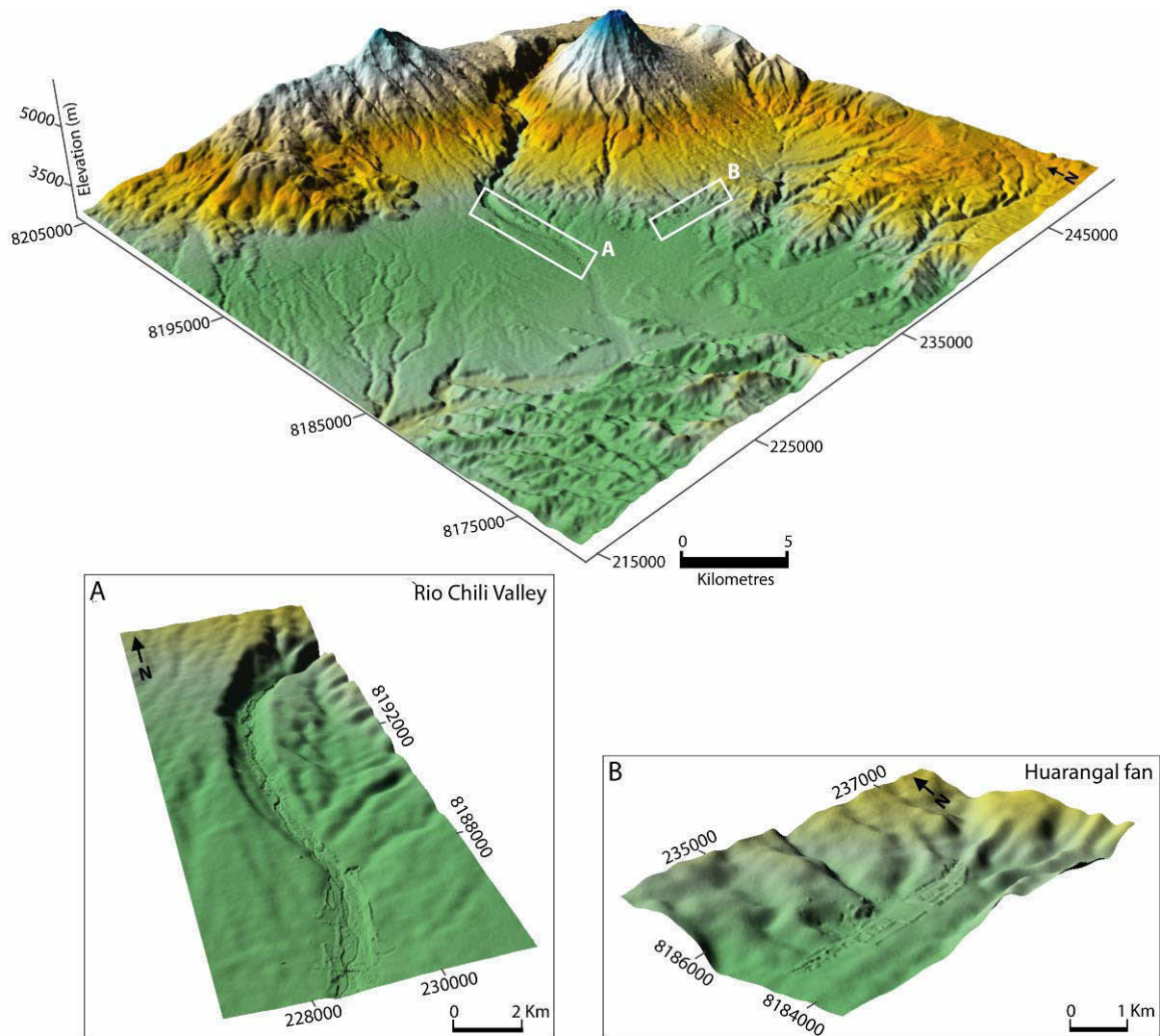
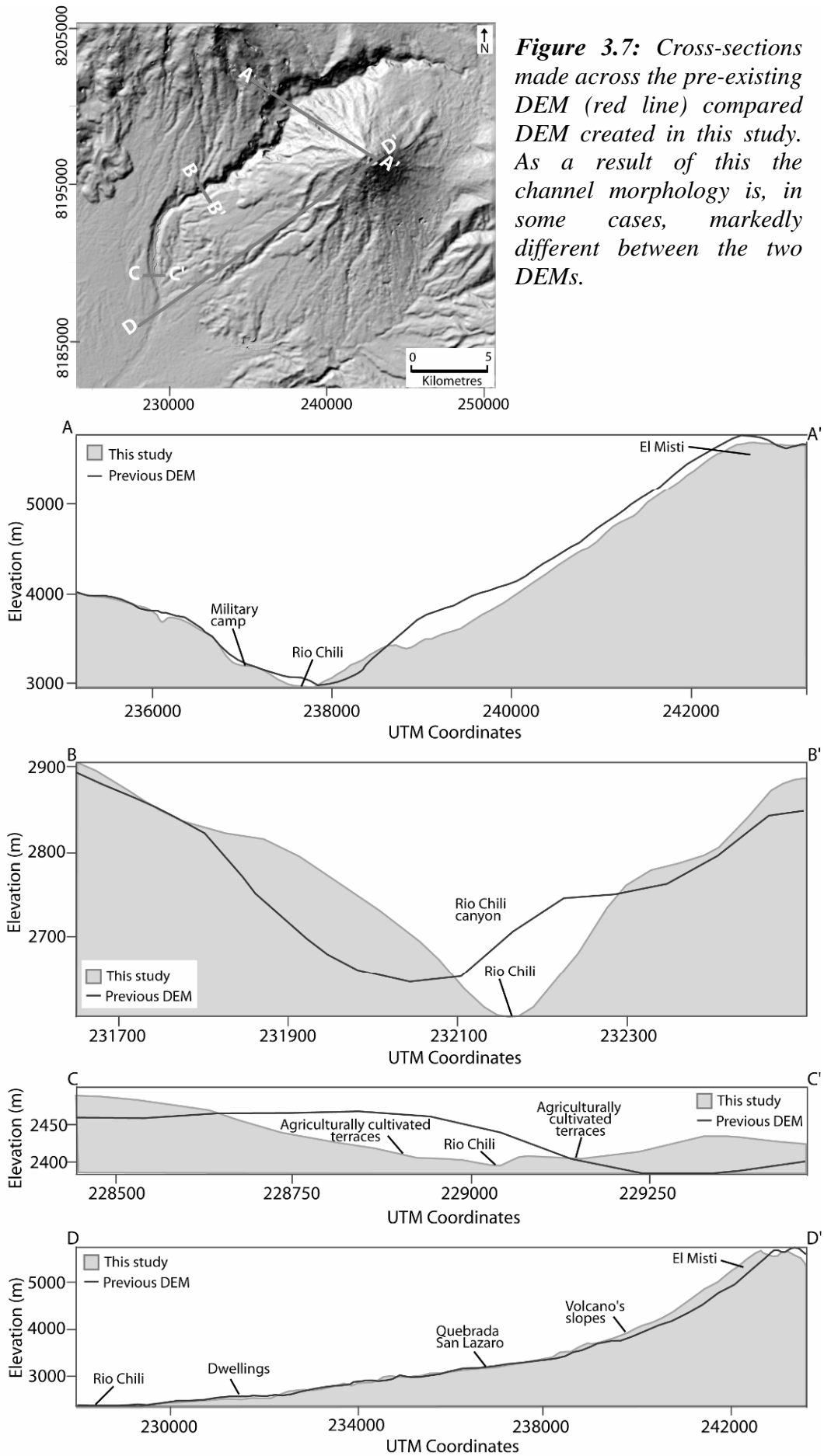


Figure 3.6: 3D view of the new enhanced DEM created for Arequipa by the interpolation of ASTER and DGPS data. The overall DEM shows more detail and is of higher resolution than earlier DEMs used in the region. The close up view of the Rio Chili Valley shows clearly the detail of the river and river terraces which were not apparent in previous DEMs (see **Figure 3.8**).

Figure 3.7 illustrates the difference in topography, in cross-section, between the new enhanced DEM and the previous DEM. Most notable is level of detail observed, particularly closer to the channel, on the new DEM. Smaller changes in topography, such as terrace levels, are much better represented – this can be seen especially in the A-A' and D-D' cross sections in Figure 3.7. The position of the channel between the previous DEM and the new DEM has changed in cross sections B-B' and C-C' (Figure 3.7) which is likely to result to have implications on the run out and extent of Titan2D modelled flows between the two DEMs.



The level of detail achieved in the new DEM is quite remarkable when making a comparison to other DEMs of the region, as shown in the enlargement of a portion of the Río Chili Valley study area from four DEMs in Figure 3.8. Channel detail in the 90 m SRTM DEM channel detail is not recognisable and the image is very pixellated. The previous 30 m DEM and the 30 m ASTER DEM possess the same resolution and as a result the images are quite similar. Overall the ASTER DEM appears to have more clarity, although the south east section of the previous DEM is more detailed than in the ASTER DEM. This could be due to the more detailed digitisation of contours than what could be interpolated from satellite imagery or it could be an artificial artefact. The ASTER and DGPS data combined produces a significantly higher quality DEM than ever previously produced. Channel detail and terraces can be clearly identified and is in far more detail than both the ASTER and previous DEM.

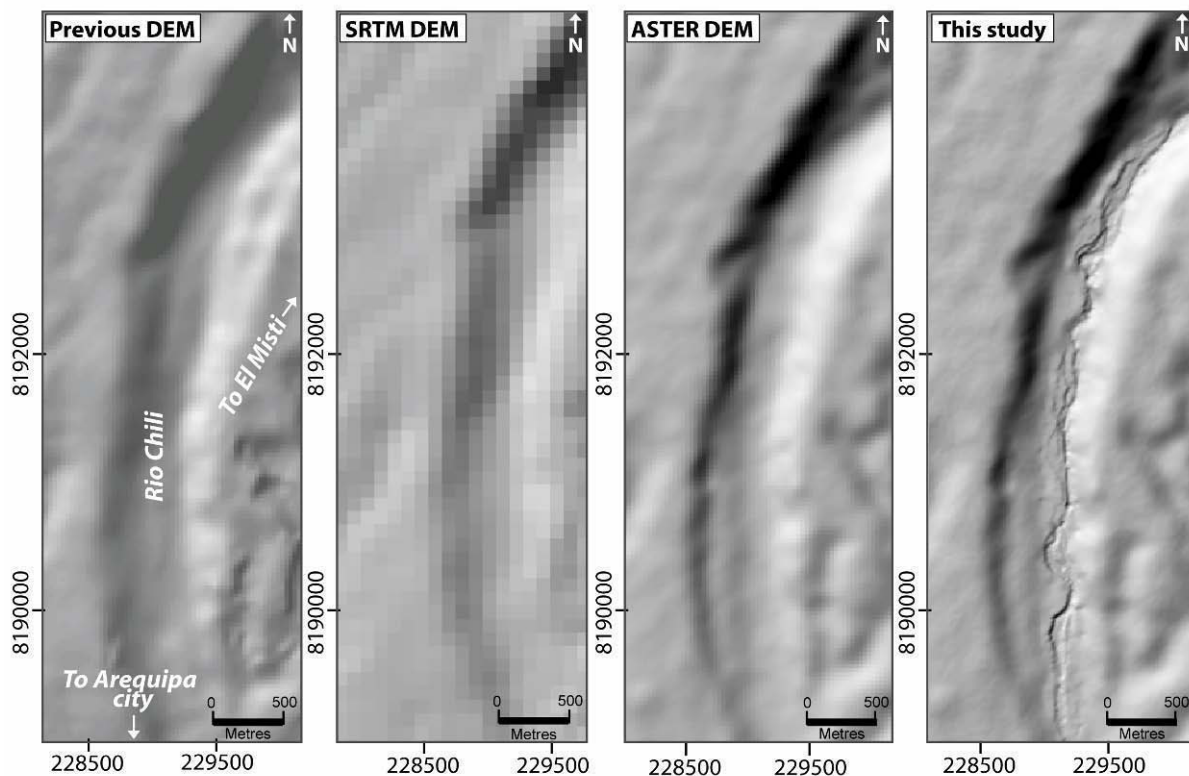


Figure 3.8: A comparison of DEMs using a subset of the Río Chili Valley. The previous DEM (created from digitised 1:25,000-scale topographic maps and from radar interferometry) was used for earlier Titan2D simulations and is similar in resolution and detail to the ASTER DEM. The 90m SRTM DEM has a very coarse resolution where even the channel is not very clearly defined. The new enhanced DEM can be seen clearly as an improvement over other DEMs of this region.

The accuracy of channel and terrace features, especially within the Río Chili Valley, has been vastly improved for this study resulting in important implications for Titan2D flow simulations, particularly on the run-out length and inundation area.

Implications for Titan2D modelling

Comparisons of simulations using the differing DEMs are shown in Figures 3.9 and 3.10. Simulations using constant input parameters (internal friction angle of 25°, a basal friction angle of 12° and a solid ratio of 0.40) were undertaken on the previous 30 m and the enhanced 10 m DEMs varying only the volume of simulated flows

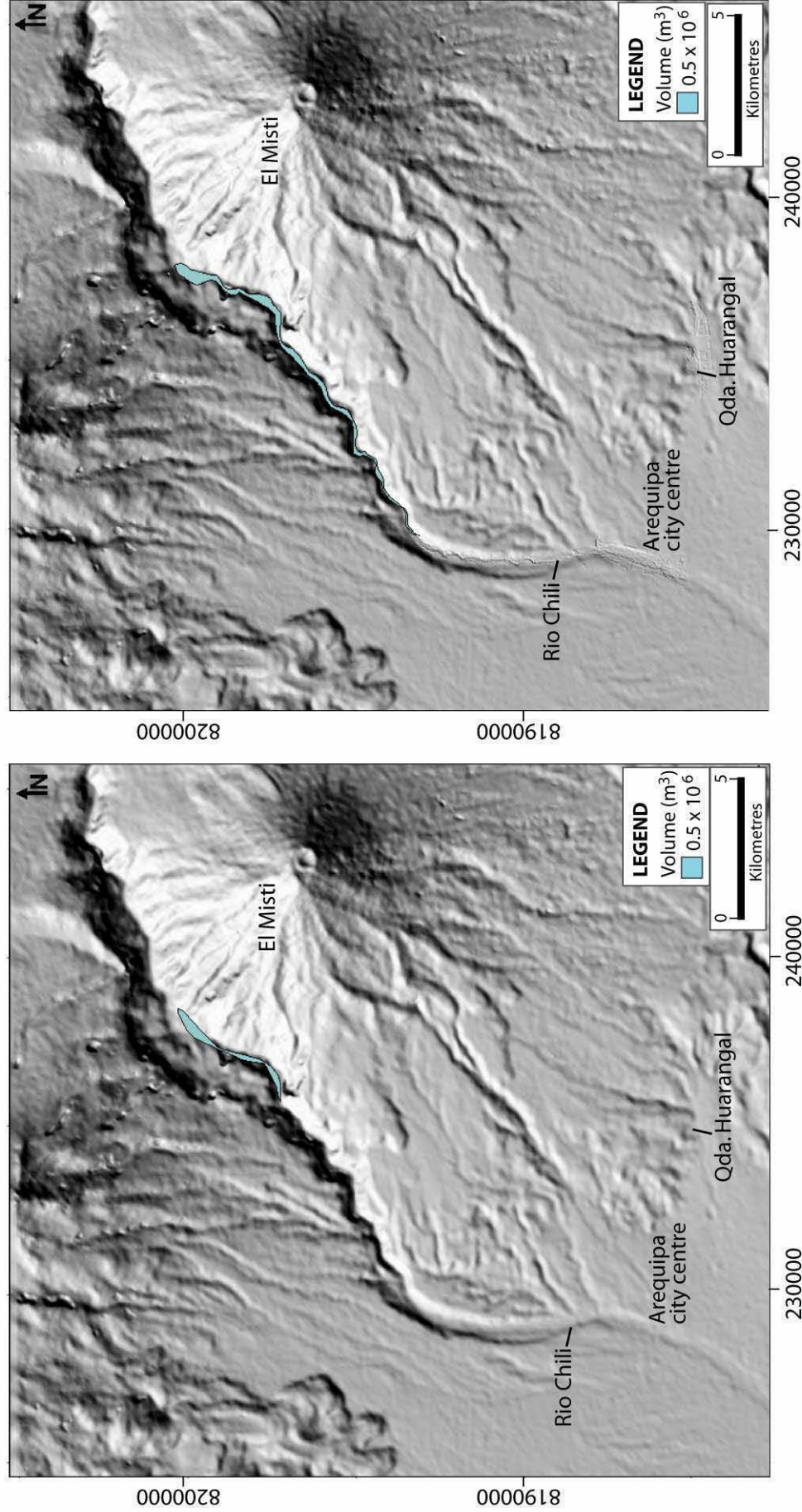


Figure 3.9 The results of a Titan2D simulation in the Rio Chili River using the 30m previous DEM (left) and the 10m enhanced DEM (right). The flow is $0.5 \times 10^6 \text{ m}^3$ in volume simulated with an internal friction angle of 25°, a basal friction angle of 12° and a solid ratio of 0.40. From the diagram it can be seen that a longer flow run-out is achieved using the enhanced DEM.

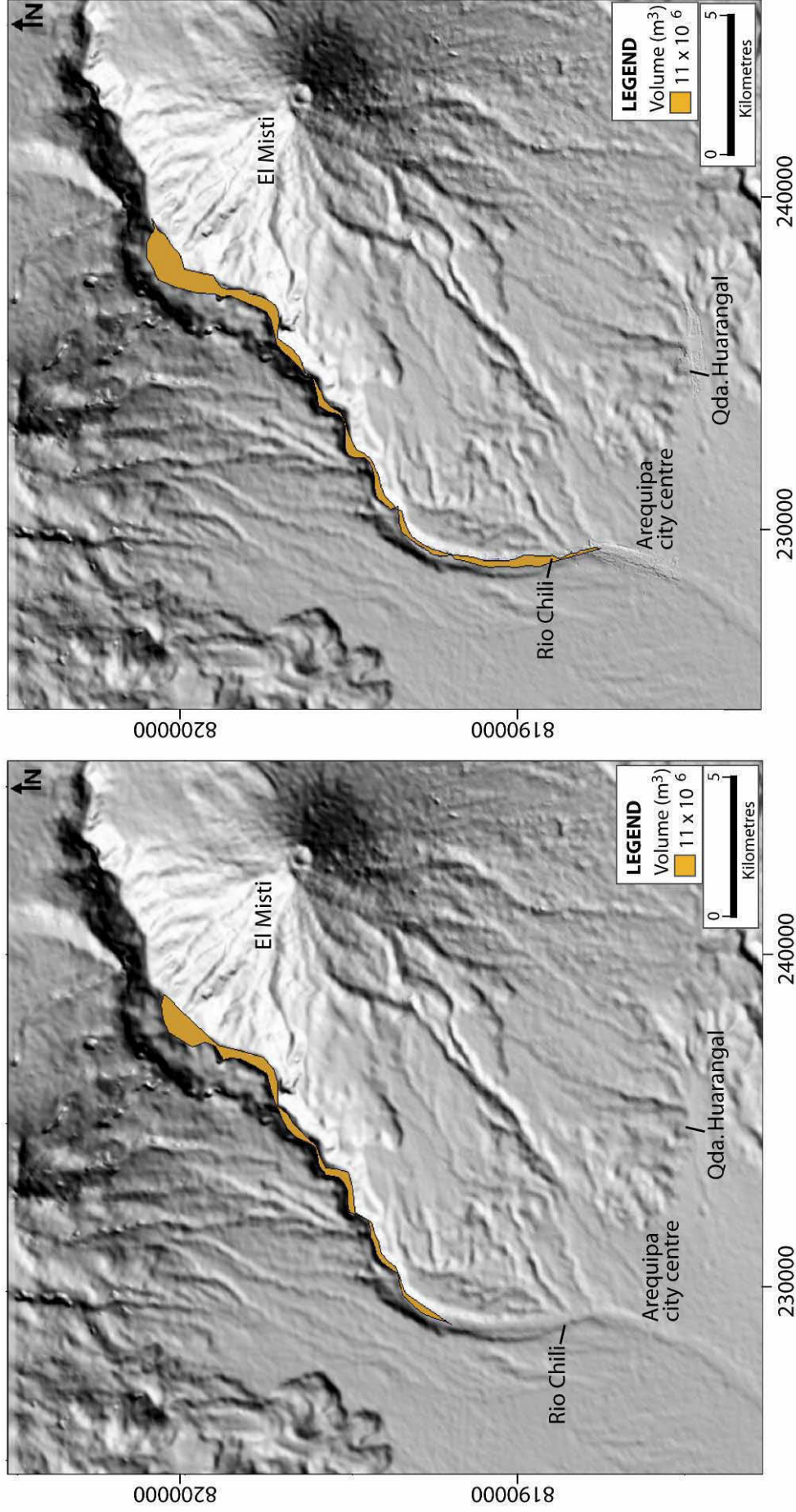


Figure 3.10: The results of a Titan2D simulation in the Rio Chili River using the 30m DEM (left) and the 10m DEM (right). The flow is $11 \times 10^6 \text{ m}^3$ in volume simulated with an internal friction angle of 25 , a basal friction angle of 0.40. The map illustrates that the largest volume flow reaches the city with the new DEM, whereas the flow is 5 km from the city with the 30 m DEM.

The figures show that topography differences clearly affect the run-out and inundation area of simulated flows – simulations undertaken on the 10 m DEM feature longer run-out than those of the 30 m DEM. Furthermore, the 10 m DEM resolves earlier issues encountered with the 30 m DEM where flows tended to pond in the Río Chili upper canyon, a location where the width of the channel is confined by sheer cliffs (at least 500 m high). The increased resolution of the 10 m DEM has allowed simulated flows to move through the canyon featuring less unrealistic ponding, resulting in longer run-out lengths. Highly detailed channel and terraces featured on the 10 m DEM also allows simulated flows to move faster through the river valley (past the high walls and confining nature of the canyon) resulting in the longer run-out.

As with the studies of Stinton et al., (2004a) Delaite et al., (2005), and Vargas et al., (2010a) the run-out and inundation of the simulated flows in this study, even on the new enhanced DEM, do not conform to the previous deposits in the Río Chili Valley. This could be due to the inadequate DEM resolution of the Río Chili canyon. The DEMs used cannot sufficiently represent the narrow (<10 m to 60 m across) and deep Río Chili Canyon bed which funnels flows to the middle and lower valley, 20 m to >500 m in width. The poor DEM resolution results in the artificial ponding, and run-up of the flows on the western side of the canyon, in the uppermost part of the valley near the military school and Charcani Quinto. While there is geological evidence for lake formation in the upper Río Chili Canyon (refer to Chapter 2) where Titan2D simulations pond, there is also geological evidence that small to medium volume lahars reach the city, which is not the case in the Titan2D simulations.

As discussed in section 3.1.1.5, an improved DEM resolution may not necessarily improve computer flow modelling; a shorter run-out of simulated flows could be related to the Titan2D modelling program itself. T-D models only consider diffusion in the x and y directions, so flow energy is lost where there are very steep slopes or run-up of canyon walls. This is problematic for computer modelling using a steep volcano such as El Misti. Although, many studies (e.g. Capra et al., 2008; Muñoz-Salinas et al., 2008; Williams et al., 2008; and Procter et al., 2010a) have proven that Titan2D has been successful for modelling geophysical mass flows in a range of different volcanic environments (e.g. eruption type, flow initiation, volcano height/slope). The addition of a GIS-based surficial material map, an optional Titan2D input to define the zones in the region where changes in the surface morphology results in a change in the basal friction angle, may aid in the better simulation of lahars and

other flows at El Misti and should be investigated during future Titan2D simulations at El Misti.

3.2 Titan2D outputs and flow behaviour

Using software such as Tectplot, the time-step outputs from Titan2D simulations can be spliced to provide an animated visualisation of simulations in 3D allowing for immediate validation of the model flow behaviour within expected ranges. Analysis of the multi-simulations revealed several flow characteristics were modelled by Titan2D such as superelevation, flow divergence and convergence, ponding and uphill flow, and overbanking.

Obstacles in the path of a flow can affect the behaviour of the flow, such as where a flow is diverted around a hummock or similar obstacle. At abrupt changes in channel direction, particularly where the Río Chili canyon opens out from a steep sided gorge to a wide river valley (near the Chacani hydro-electric dam), the flow forms temporary ponds or even ceases to move altogether. This is especially apparent in Figure 3.11, in which the flow ponds where the river channel is narrow and/or changes direction. As the flow moves through the narrow gorge it is apparent that it is clearly affected by the topography, and thus the run out is shorter than would have been expected for a flow of that volume. Superelevation also occurs in the upper Río Chili canyon where the flow has made an impact on the channel wall due to the velocity of the flow travelling around a bend.

In Figure 3.12, we can see ponding of the Titan2D simulated flow; this is especially apparent where the flow has descended the steep slopes of El Misti and enters into the main fan. At this point the direction of the channel changes quite abruptly from a SE to SW, resulting in ponding of the flow in this location. Overbanking of the southern terrace, the location of the Huarangal settlement, is more prominent in Titan2D simulations (Figure 3.12 and 3.14) than in LaharZ. The Titan2D simulation spreads out at the mouth of the Quebrada Huarangal (where the topography becomes flatter moving into the Arequipa Basin) and overtops the current channel resulting in the deposition of the flow in a broad area. Conversely, the LaharZ inundation zone stays is more limited to the confines of the channel. It is fair to assume that overbanking would be a realistic occurrence in this locality due to the seemingly abrupt change in the channel direction, and also because the terrace bank is <4 m high.

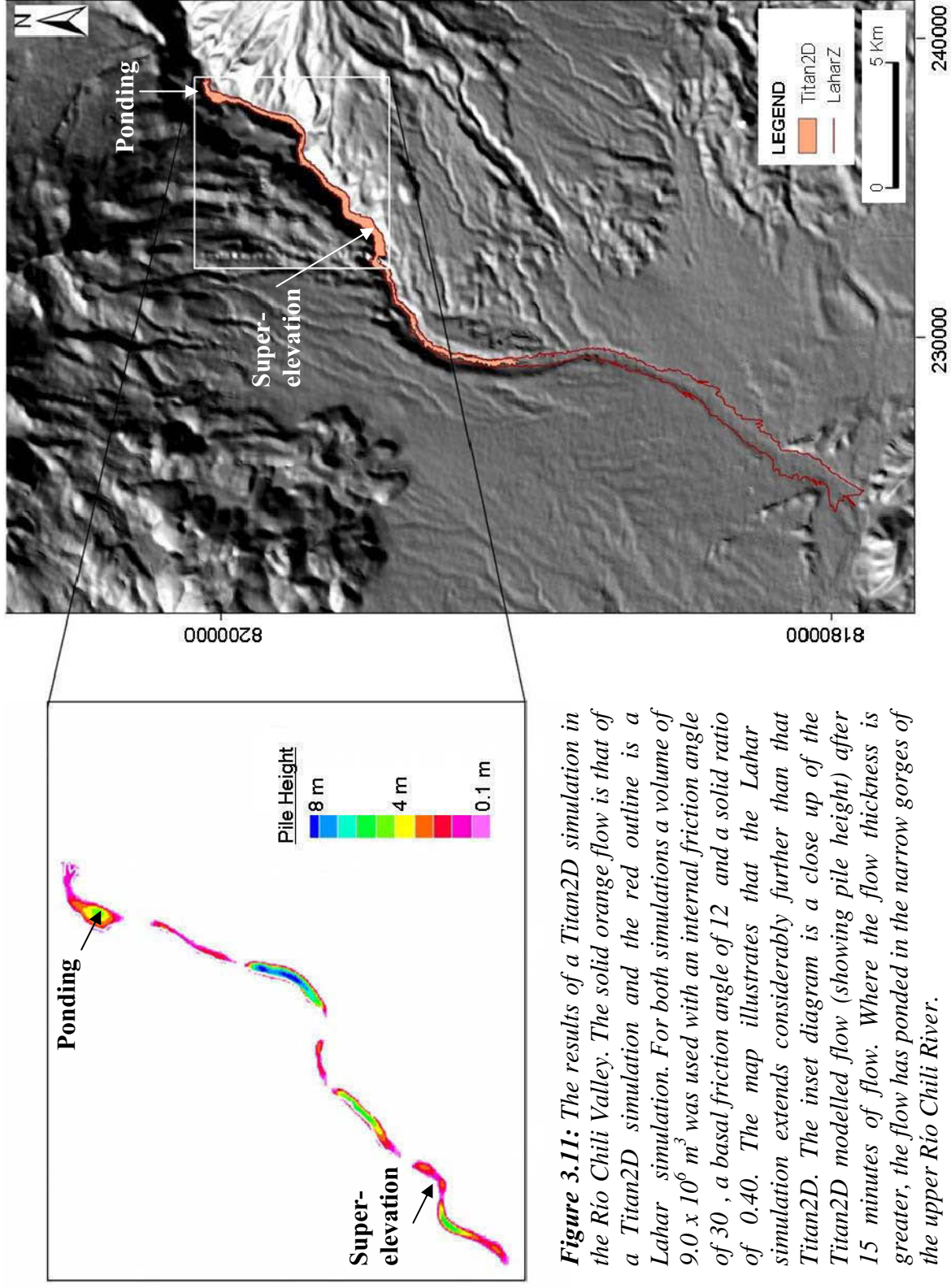


Figure 3.11: The results of a Titan2D simulation in the Rio Chili Valley. The solid orange flow is that of a Titan2D simulation and the red outline is a Lahar simulation. For both simulations a volume of $9.0 \times 10^6 \text{ m}^3$ was used with an internal friction angle of 30° , a basal friction angle of 12° and a solid ratio of 0.40 . The map illustrates that the Lahar simulation extends considerably further than that of Titan2D. The inset diagram is a close up of the Titan2D modelled flow (showing pile height) after 15 minutes of flow. Where the flow thickness is greater, the flow has ponded in the narrow gorges of the upper Rio Chili River.

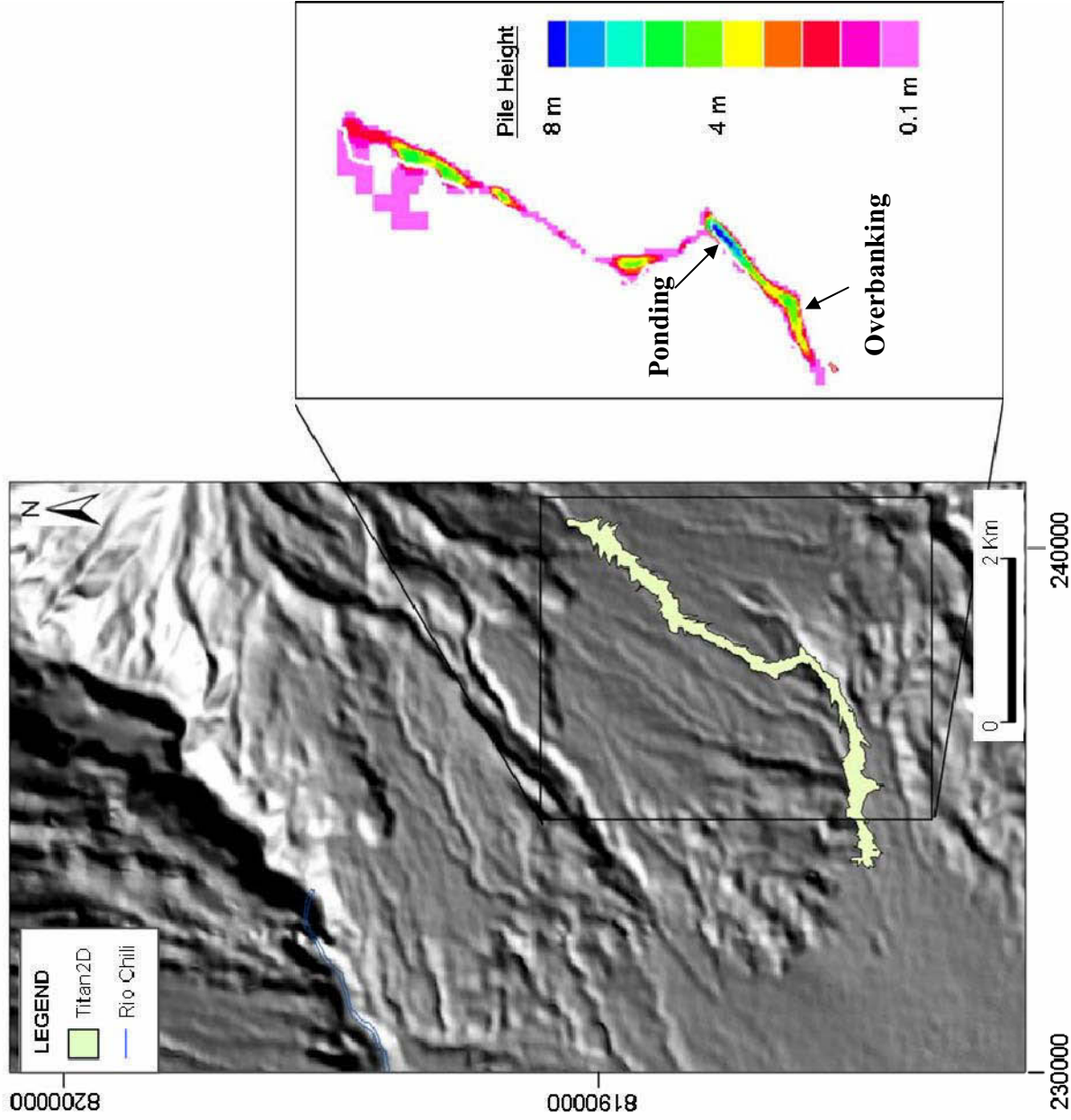


Figure 3.12: The results of a Lahar simulation in the Quebrada Huarangal, indicated by the solid green flow shape. The inset diagram is a Titan2D simulation using the same volume and starting point as the Lahar simulation. A volume of $4 \times 10^6 \text{ m}^3$ was used, an internal friction angle of 30° , a basal friction angle of 12° and a solid ratio of 0.40. There is not a lot of difference between the two models. Overbanking of the Titan2D flow is prominent in the upper catchment.

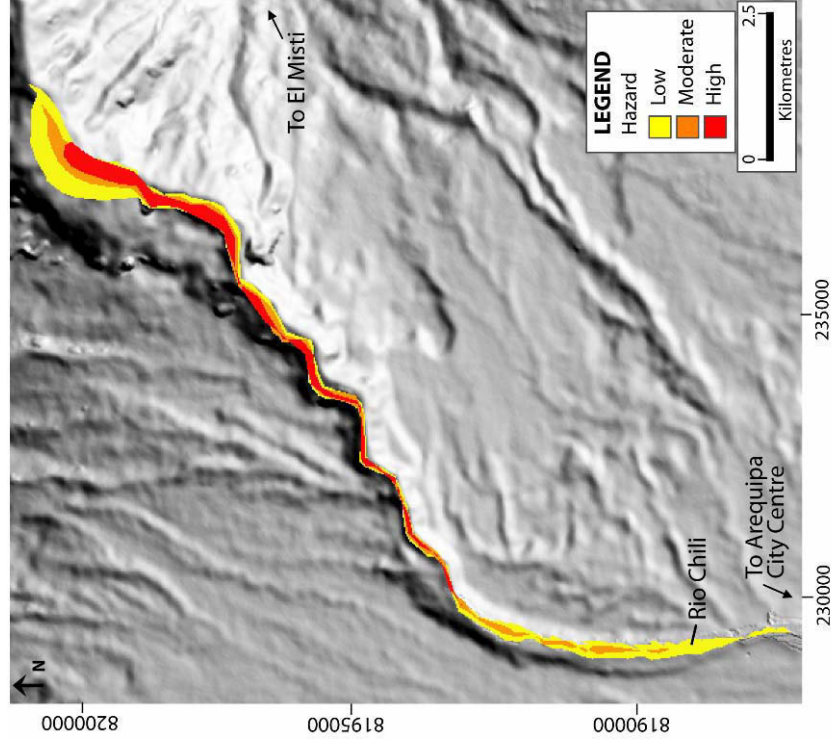
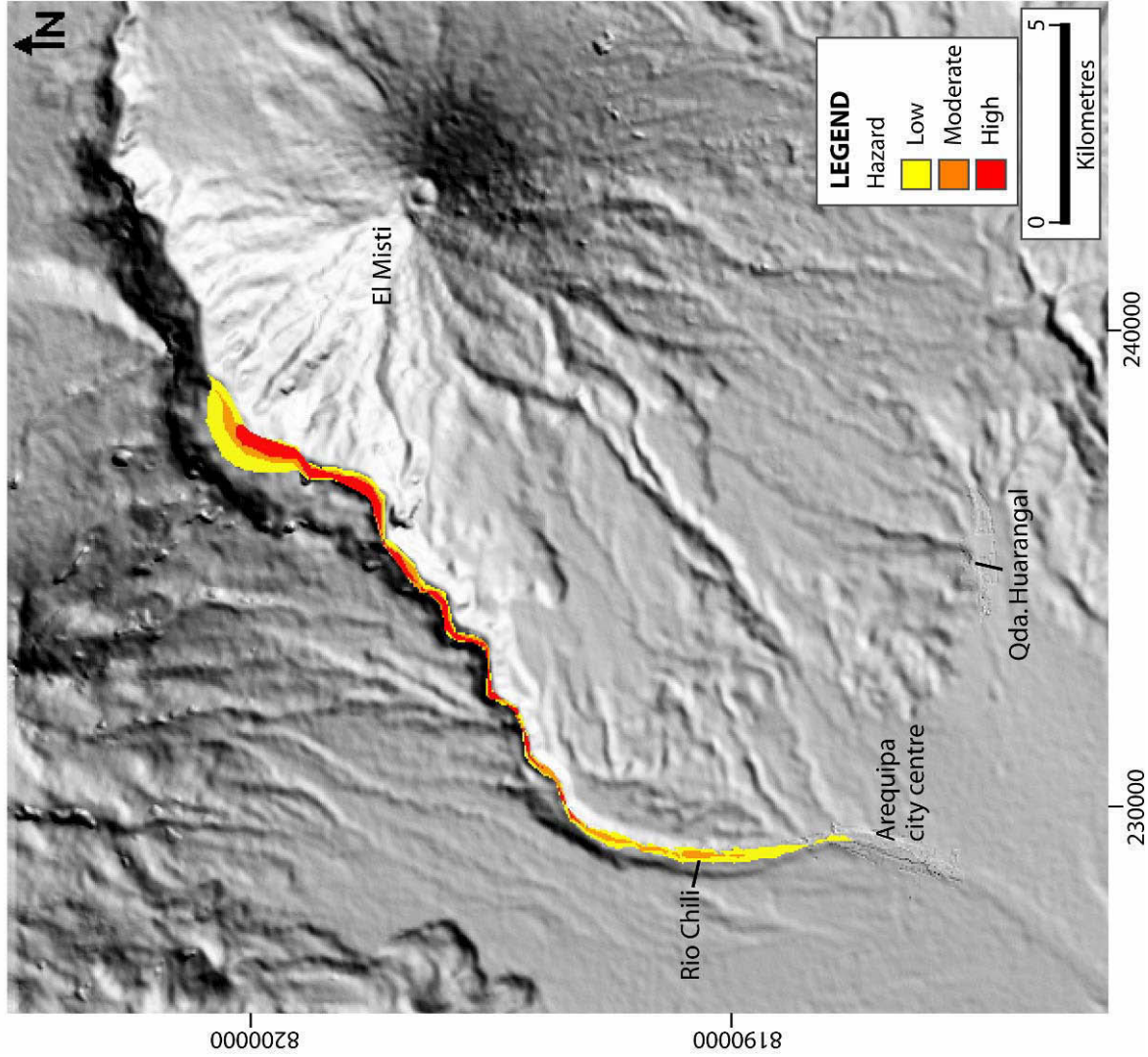
In addition to the observation of several flow features common to lahars, the simulated velocity and depth of the flows were used to aid in the validation of the parameters tested. The average velocities are computed by considering the velocity of various computational cells, which on average range from 4-7 m/s. It must be noted that these velocities do not correspond to those recorded at the flow front, but can be compared to the minimum velocities determined at flow run-up onto obstacles perpendicular to the flow direction and superelevation along the outside of bends in confined channels. The average flow depth for the simulations range from 2.5 to 5 m, this is consistent with what is known of the thickness of lahar deposits at El Misti (refer to Chapter 2).

Overall the analysis of flow features indicated that Titan2D is very sensitive to changes of the input parameters, especially the location of the starting point and the basal friction value. A small change in the basal friction angle, of less than 5° , had a noticeable effect not just on the flow distribution, run out and the flow path direction, but the type and extent of common flow features observed. The analysis of the flow features aided in the validation of the parameters and provided an interesting comparison with studies conducted by the previous authors using LaharZ (e.g. Delaite et al., 2005) whereby flow features are not observed. This is due to the fact that Titan2D simulated flows react better to underlying topography than flows modelled with LaharZ, which will be addressed further in the discussion (section 3.4).

3.3 Lahar inundation zones

Zones susceptible to lahar inundation were identified in Titan2D simulations undertaken in the Río Chili valley (Figure 3.13) and on the Quebrada Huarangal fan (Figure 3.14). Volumes from $0.5 \times 10^6 \text{ m}^3$ to $11 \times 10^6 \text{ m}^3$, corresponding to the previously identified hazard scenarios, were modelled using an internal friction angle of 30° , a basal friction angle of 12° and a solid ratio of 0.40 on the enhanced 10 m DEM. Inundation outlines were delineated based upon a stopped simulated flow where the pile height is greater than 0.1 m. The *high hazard* corresponds to the low volume but frequent lahars, *moderate hazard* to the moderate volume and frequency lahars and the *low hazard* for the large volume but infrequent events (refer to Table 3.3 for magnitude and frequencies).

Figure 3.13: Hazard map for the Rio Chili derived from Titan2D simulations on a 10 m DEM. Volumes from $0.5 \times 10^6 \text{ m}^3$ to $11 \times 10^6 \text{ m}^3$ were modelled using an internal friction angle of 30° , a basal friction angle of 12° and a solid ratio of 0.40. A close up of the inundation zones are given in the image below where the largest volume flows reach the upper reaches of the city centre.



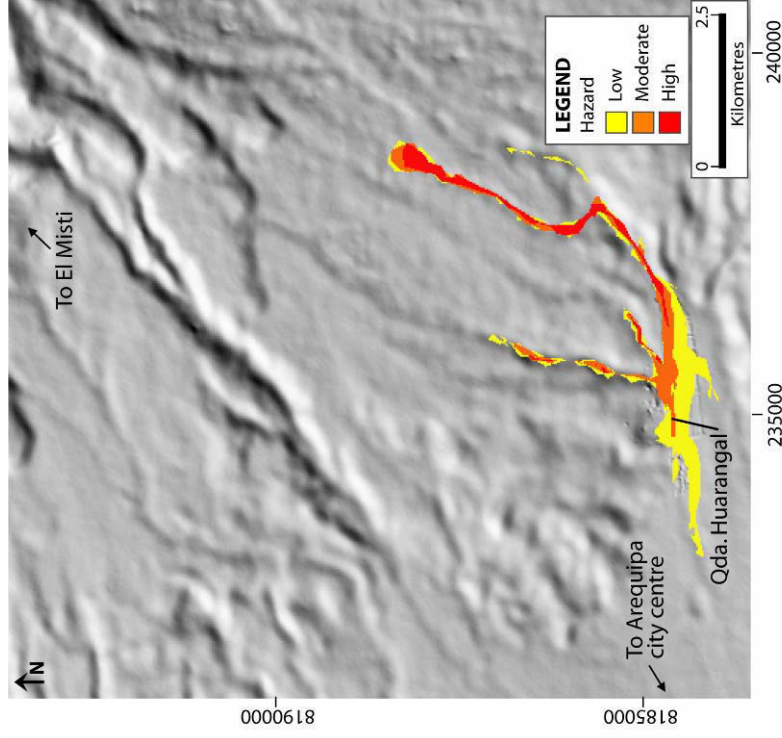
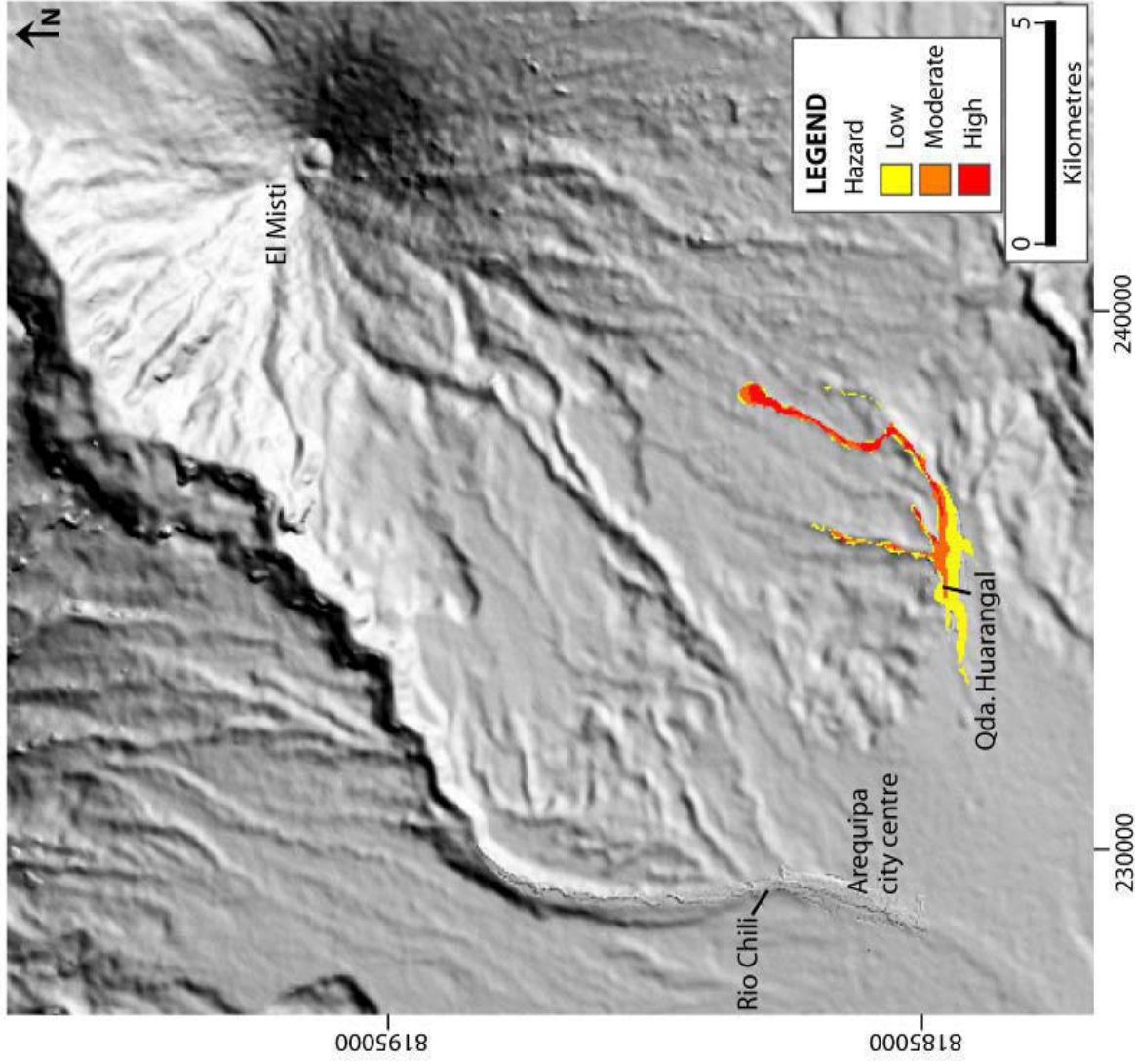


Figure 3.14: Hazard map for the Quebrada Huarangal fan derived from Titan2D simulations on a 10 m DEM. Volumes from $0.5 \times 10^6 \text{ m}^3$ to $11 \times 10^6 \text{ m}^3$ were modelled using an internal friction angle of 30° , a basal friction angle of 12° and a solid ratio of 0.40. A close up of the inundation zones and largest volume flows inundate the populated areas of the fan.

Titan2D flow inundation in the Río Chili Valley and on the Quebrada Huarangal fan are both larger in extent and run out than previous Titan2D studies by Stinton et al., (2004a) and Vargas et al., (2010a). For example, the largest flow of $11 \times 10^6 \text{ m}^3$ in the Río Chili reaches approximately 12 km further downstream than in previous simulations. Similarly for the same volume flow on the Quebrada Huarangal fan the simulated run out length is 2.5 km longer for this study. However, as with studies of Stinton et al., (2004a) and Vargas et al., (2010a), the Titan2D simulations are still shorter in run-out length than the LaharZ run-outs of Delaite et al., (2005). The Titan2D simulation run-out for the largest volume flow in the Río Chili is 9.5 km shorter than LaharZ simulation run-out, and on the Quebrada Huarangal fan the Titan2D simulation run-out is 4.8 km shorter. Also, the lahar inundation map generated by Titan2D does not compare with the lahar and flash flood inundation map created from geological and geomorphological evidence (Chapter 2). This will be discussed further in section 3.4. Despite the differences between the Titan2D and LaharZ inundation areas, and the inundation areas derived from mapped deposits, this Titan2D derived lahar inundation map still has significant implications for the Río Chili Valley and Quebrada Huarangal fan (refer to chapter 5).

3.4.1 Río Chili Valley

The high hazard zone, corresponding to small volume but frequent flows, is confined to the Río Chili canyon (Figure 3.13). There are very few private dwellings compared to further downstream, however the affect of an event in this area is much wider reaching. This is due to the location of five hydroelectric power stations, the main electricity generation for all of Arequipa, within the high hazard zone (Chapter 4, figures 4.47 and 4.53). The loss of electricity to a city with nearly 1 million people for a significant period of time would be devastating, and is discussed in depth in Chapter Four. Fortunately the largest electricity output is generated from the Charcani Quinto hydroelectric station which is located just outside the high hazard zone. The water supply for the city and irrigation is also drawn from the Río Chili; even these small volume flows can affect the water supply for the city and agriculture production (Chapter 2).

The moderate hazard zone, corresponding to moderate volume flows of a moderate frequency, affects the upper reaches of Río Chili Canyon and extends out of the canyon into the terraced Río Chili valley, 3.5 km upstream of the Puente Grau Bridge in the city centre (Figure 3.13). In addition to the effects described for the high hazard zone above, a significant portion of

agricultural land would be affected along with the military school in the upper Río Chili canyon. The majority of the military school would be affected apart from the administrative offices located on an upper terrace. The Charcani Quinto hydroelectric power station is outside of the moderate hazard zone. At the downstream entrance of the canyon the *Santuario de la Virgen de Chapi*, an important religious monument, would be affected along with the intake of the Zamácola canal which conveys water to the water treatment plant and to irrigation canals. Agricultural land of the lower terraces, t0 to t2, would be inundated and the t3 terrace inundated in some localities. Some rural housing would also be affected. The location and vulnerability of structures and land use in the moderate hazard zone are described in detail in Chapter four.

The low hazard zone, corresponding to large volume flows of a lower frequency, encompasses the upper reaches of Río Chili Canyon and extends out of the canyon into the terraced Río Chili valley, 1.9 km upstream of the Puente Grau Bridge in the city centre (Figure 3.13). In addition to the concerns described for the moderate and high hazard zones above, agricultural land of the lower terraces, t0 to t2, would be inundated. The inundation of these terraces would also affect a number of rural dwellings. In addition to inundation affecting the supply of water to the irrigation canals, damage to the canals would also influence the irrigation supply in non-inundated areas downstream. The suburb of Chilina, 2 km upstream of Puente Grau, would also be inundated. There are a number of dwellings and businesses (e.g. the popular restaurant *La Chocita*) in this locality along with a military recreation camp and large religious establishments (e.g. *Casa de Retiro de Chilina* and *Juan Pablo II*). The location and vulnerability of structures and land use in the low hazard zone are described in detail in Chapter 4.

3.4.2 Quebrada Huarangal Fan

The high hazard zone, corresponding to small volume but frequent flows, is confined to the small upper channels which feed into the main Quebrada Huarangal fan (Figure 3.14). No established dwellings are located within the inundation zone, however the gravel mining plant and operations are located at the extremity of this zone, 2.5 km upstream of the *8 du Octubre* bridge. A few makeshift dwellings, situated within the channel, are located in this high hazard zone.

The moderate hazard zone, corresponding to moderate volume and moderate frequency flows, encompasses the upper quebradas, the Quebrada Huarangal channel and the lower (t0 to t2) developed terraces on the southern bank, less than 1 km upstream of the *8 du Octubre* bridge (Figure 3.14). In addition to the effects described for the high hazard zone above, a significant number of private dwellings and small businesses in this hazard inundation zone would be affected. The southern terraces are heavily developed with some of the most poorly constructed dwellings located on the lower terraces and within the channel itself (Chapter 4). Mining operations within the channel would also be impinged upon. The location and vulnerability of structures and land use in the low hazard zone are described in detail in Chapter 4.

The low hazard zone, corresponding to large volume flows of a lower frequency (Table 3.3), encompasses the Quebrada Huarangal channel and fan extending approximately 1 km beyond the *8 du Octubre* bridge (Figure 3.14). The low hazard inundation zone covers the vast majority of the Quebrada Huarangal fan study area. In addition to the affects described for the high and moderate hazard zones above, private dwellings and businesses located within the channel and on the southern terraces of t0 through to t3 (Chapter 2) would be inundated. Brick factories located on northern terrace, approximately 10 m upstream of the *8 du Octubre* bridge, would also be inundated. The location and vulnerability of structures and land use in the low hazard zone are described in detail in Chapter 4.

3.4 Discussion

Some of the problems encountered using a 30 m DEM for Titan2D “two-phase” modelling at Arequipa were overcome using an enhanced 10 m DEM. For example, at abrupt changes in channel direction the modelled flows temporarily cease to move on the 30 m DEM, resulting in shorter run out lengths than expected. Conversely, simulations on the enhanced DEM feature longer flow run out lengths because simulated flows can move more easily through the channels due to the better definition in the 10 m DEM. Despite this, the run out lengths of Titan2D simulations are still much shorter than LaharZ simulations and the mapped deposits. This could be due to the inability of 2-D models to deal with vertical channel walls which are inevitable in El Misti simulations. This inability leads to simulated flows losing momentum and dying out earlier than it would naturally. Eventually 3-D codes are needed to deal with

steep slopes, narrow channels and waterfalls. The shorter than expected run out lengths can also have significant implications for a hazard assessment because the resulting lahar inundation areas differ. A way of dealing with this would be to start the model further downstream, assuming that the ponded material seems unrealistic, by decreasing the initial flow volume. By avoiding the steep narrow channels, and unrealistic ponding, the simulated flows would reach Arequipa and be beneficial for hazard and risk assessments.

This study and previous studies (e.g. Stinton et al., 2004a and Vargas et al., 2010a) have shown that Titan2D models the behaviour of lahars adequately; while the run out of LaharZ simulations is more comparable to mapped deposits (Delaite et al., 2005). The discrepancies in the results are due to the underlying differences between the models. LaharZ is a statistical and semi-empirical code, whereas the experimental Titan2D model takes into account the physical aspects of lahar flow.

The physical parameters used for the simulation, or the conditions at the time of flow generation, can also be responsible for the differences observed between the two models and the actual deposits. Perhaps the most important characteristic of a lahar for hazard management is its inherent variability. Lahars often comprise several distinct phases within a single event and consequently flow properties and flood impacts vary considerably in time and space (Procter, 2010; Dumaisnil et al., 2010). This is the primary limitation of Titan2D, and any existing 2-D flow model, for modelling lahar hazards – its inability to replicate erosion or deposition, including any variation in topography relating to this and any resulting changes in flow rheology. However, it may be another decade before the models and computational capacity can address these features.

Even though more favourable results were obtained following the creation of a 10 m DEM, additional refinement in the Río Chili canyon would be beneficial for further analysis of the lahar hazard for Arequipa using Titan2D. A DEM could be computed from commercially available satellite data, if it exists, or from an airborne LIDAR (Laser Detection and Ranging) survey. An airborne LIDAR survey conducted of the Whangaehu River (Mt. Ruapehu, New Zealand) resulted in a high quality DEM used in Titan2D simulations (Procter et al., 2010). However both suggestions are expected to be expensive.

Further DGPS measurements of the Quebrada Huarangal fan would improve the DEM in this region. In particular DGPS measurements would be beneficial where significant ponding is observed (Figure 3.12); this is the location that the channel gradient is significantly reduced and direction of the channel changes. In addition, more closely spaced DGPS measurements across the channel bed would be valuable. Further DGPS measurements of the developed terraces, especially in the area highlighted in section 3.1.1.6, would hopefully resolve the hummocky nature of the DEM in this locality.

3.4 Concluding remarks

Despite the differences outlined above and provided the user understands the limitations of the models, simulations are extremely valuable in understanding flow behaviour, defining flow inundation areas expected on current DEMs and identifying hazard zones. The simulation results of this study have been used to create a lahar inundation map which provides a basis for the assessment of the vulnerability of the city in the event of lahar. Alongside the lahar inundation map derived from conventional methods (Chapter 2) the lahar prone zones, combined with expected deposit thicknesses and flow velocities, will define the expected damage states of buildings inundated by volcanic mass flows (Chapter 5).

PART THREE:
VULNERABILITY AND RISK ASSESSMENT WITHIN AN
URBAN SETTING

Chapter Four

Elements at risk: land, building stock and infrastructure in Arequipa

4.0 Introduction

Whilst modelling of the runout and extent of volcanic mass flows is important to identify the areas which could be affected during a future mass flow event, it is equally important to identify the elements that could be at risk during such an event, such as buildings and infrastructure. Damage from mass flows has often been observed, such as the burial of the town of Amero (Columbia) following lahars from Nevado del Ruiz in 1985 which resulted in the deaths of approximately 23,000 people (Voight, 1990); in 1953, 151 people died following the destruction of the Tangiwai Rail Bridge (Mt Ruapehu, New Zealand) by a lahar (Conly and Stewart, 1991), and Emperor Augustus' villa was buried by post-79 AD lahar and stream flows at Vesuvius (Italy) (Perrotta et al., 2006). The physical damage from lahars and flash floods can include burial, foundation failure, debris impact, transportation, excessive wall or roof loads, collapse, undermining and corrosion. However the impact from lahars and floods are not just limited to the direct physical effects; long-term disruption can be common in the aftermath of such phenomena as summarised in Table 4.1.

	Tangible	Intangible
Direct	Physical damage to: <ul style="list-style-type: none"> • Housing, structure and assets • Infrastructure and public utilities • Agriculture • Tourism 	<ul style="list-style-type: none"> • Loss of life* • Health effects • Environmental damages
Indirect	<ul style="list-style-type: none"> • Temporary relocation • Cleaning and sanitation • Loss of income and employment • Industrial production losses • Loss of 'attractiveness' 	<ul style="list-style-type: none"> • Societal disruption • Increased vulnerability of survivors • Severe and protracted loss of GDP in less developed countries leading to economic depression

***Table 4.1:** An overview of different types of damage/consequences from lahars and floods (adapted from Mekong River Commission, 2009). The damage is divided into tangible and intangible damage, depending on whether or not the losses can be assessed in monetary values. *Recent studies (Sandri et al., 2010) have included estimates of the cost of death/injury for an eruption in Auckland, New Zealand.*

This research will only focus on the direct tangible effects resulting from lahars and flash floods due to the difficulty in assessing intangible effects. Direct tangible effects include damage to building stock: such as private dwellings, commercial and industrial buildings, schools, emergency services and offices. It is important to quantify the damage to buildings not only for determining the economical loss, but also for people living in these buildings who could be killed by a collapse. Another tangible effect is the potential damage to infrastructure: such as transportation links (rail, road and air) and lifelines (e.g. the supply and distribution of electricity and water). This information would also lead to the determination of available resources (e.g. shelter, command centre, emergency services) in case of volcanic crisis, in turn these resources might be evaluated according to potential damage if they are located in harms way. Damage to the agricultural industry must also be considered, agriculture plays a vital role in Arequipa's economy and as food supply. This industry is reliant on the irrigation system derived from the Río Chili – a pathway for future lahars. The city of Arequipa is recognised as a UNESCO World Heritage site and every year tourism brings around 1 million visitors to the region. The potential loss of income from dropping tourist numbers would be devastating to the region.

To quantify the damage, the failure mechanisms initiated by the flow events must be understood; and which failure mechanism will depend on both the flow and building factors (Roos, 2003). Influencing flow factors can include: flow depth, velocity, duration and timing, and also debris impact (discussed in Chapters 3 and 5). Building factors depend on the structural components of the building (e.g. height, number of storeys and openings, building material and structural system, etc.) and how they interact with one another (Nicholas et al, 2001; Kelman, 2002; Soetanto and Proverbs, 2004). It is also crucial to identify the land use patterns (e.g. agriculture, industry, urbanisation, recreational facilities, etc.) and population distribution in order to estimate the potential economic losses, environmental damage and loss of human lives.

Using methods adapted from Chevillot (2000) and others (Pomonis et al. 1999; Kelman, 2002; Spence et al. 2004a,b, 2005a,b; Baxter et al. 2005) to identify elements at risk, a descriptive survey was conducted to characterise the land use patterns (section 4.3), building stock (section 4.4), and key infrastructure (section 4.5) present within the two study areas – the Río Chili Valley and Quebrada Huarangal (for further detail on the methods refer to Chapter 1). Different classes of building, land use patterns and key infrastructure were

identified to define the probability of a building and other assets being in a particular state, given the intensity level of the particular hazard concerned.

4.1 Arequipa: A rapidly expanding city

Arequipa was founded in 1540 and remained small until the 1960s (population of 86,000) when the city experienced rapid population growth (Thouret et al., 2001). From 1970 onwards the urban area grew substantially due to social unrest and related migration from rural areas, mainly in the form of poorly designed suburbs and illegal settlements. Since 1995 the population has grown by as much as 5% with settlements now occupying 2/3 of the oasis area and volcaniclastic fans. Additionally in the last 50 years the overall population of Arequipa has increased by more than 400% (Figure 4.1 c). Urban expansion is easily identifiable from the photographs in Figure 4.1 (a and b) which show development of land in 2006 that was otherwise undeveloped in 1947. Of note are the volcaniclastic fans, marked by A and B in both photographs, which show no urban expansion in these areas in 1947 compared to the urbanisation of them by 2006.

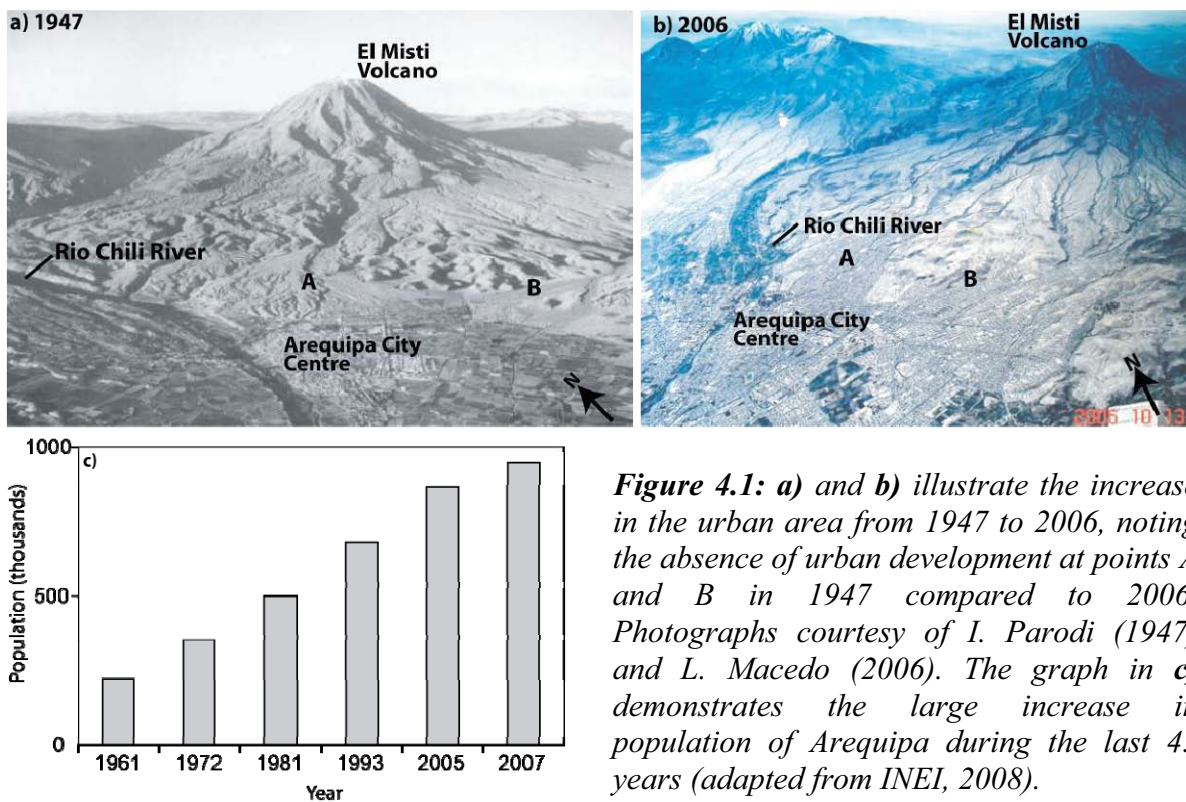


Figure 4.1: a) and b) illustrate the increase in the urban area from 1947 to 2006, noting the absence of urban development at points A and B in 1947 compared to 2006. Photographs courtesy of I. Parodi (1947) and L. Macedo (2006). The graph in c) demonstrates the large increase in population of Arequipa during the last 45 years (adapted from INEI, 2008).

The growth of the city is also well demonstrated in Figure 4.2, where aerial photographs and satellite have been used to define the urban area from 1944 to 2007 and to classify parcels of land as urban, tilled and non-constructed. In over 50 years the built up area has grown from 13 km² to approximately 70 km². The classification of land use from 2007 SPOT5 imagery shows that even in 10 years tilled and non-constructed areas have rapidly declined in favour of construction.

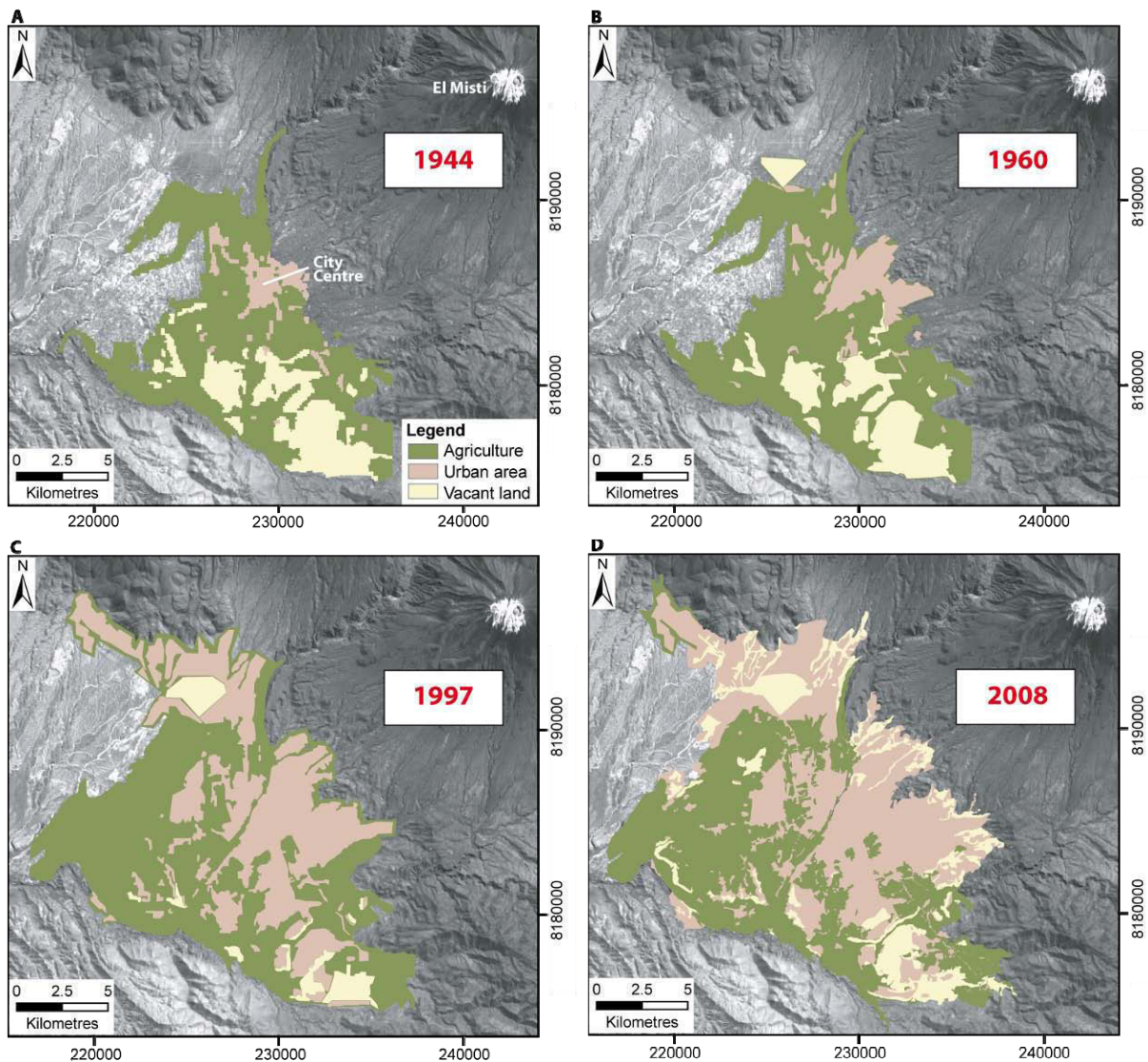


Figure 4.2: Growth of Arequipa from 1944 to 2007. From 1944 (A) to 1960 (B) the extent of the city did not increase dramatically but the urban area increased to the NE. By 1997 (C) the Arequipa grew substantially, the agriculture to the SW increased and much of the original agricultural land became urbanised. In 2007 (D) much of the existing agricultural land became urbanised and urban area increased up the slopes of the volcano's cone to the NW. The classification of land from 1944 and 1960 is based upon aerial photography (adapted from Delaite, 2003). The 1997 and 2007 classifications are based on SPOT satellite imagery (1997 data adapted from Delaite, 2003). The land classifications are draped over a Landsat image.

Urban planning as known within the Western world is unheard of in some developing countries, and where there is urban planning it is often poorly enforced by the authorities, as is the case in Arequipa. In Arequipa the rapidly increasing population is encroaching onto land on the volcano's flanks (Figure 4.2 D), at least 7 % growth of the outer margins from 1997 to 2008, and also within and adjacent to fluvial channels which drain the cone. Unfortunately many of these houses are 'tolerated' and therefore are of poorer quality than those within planned urban settlements. Within the 'tolerated' or 'overlooked' settlements there exists some self- and community-regulated control pertaining to the location and size of individual plots, but there is no control over the structural quality of the dwelling despite government regulations stipulating the code to which the dwelling must adhere to (e.g. Peru National Building Code E.030, 2003). Another result of this uncontrolled expansion is that little planning has been undertaken to create efficient infrastructure (e.g. roadways, bridges) which would prove vital in the case of crisis evacuation. This chapter aims to expose the most vulnerable areas of the city and could serve as planning advice for further development of the city.

4.2 Land-use classification

4.2.1 Introduction

Land use classification for defining element vulnerability is as crucial as the classification of building and infrastructure construction itself, because the consequence of losses depends on the occupancy of the structures (e.g. private dwellings will usually have less people present than in hotels). The *structure* in this research refers to the building and associated land regardless of what its purpose is (e.g. school, dwelling, sports stadium, power station). By defining the dominant land use, one can easily identify structures whose survival is important and vital during a crisis and which are intended to remain operational during and after a volcanic crisis. These essential facilities can include and are not limited to: medical care centres, power stations and police headquarters. However, if medical care centres and/or police stations are damaged, resources such as town halls, schools, churches and/or stadiums can be used as temporary facilities for the relocation for some essential services, and also as temporary evacuation shelters and communication centres.

Most building codes throughout the world including Peru require the use of an occupancy category and/or the *importance* factor in a building's structural design for the primary intent of protecting the life and safety of the public. These occupancy categories and/or *importance* factors relate to the intended use of the structure. For example, seismic codes require that resilient structures be designed by increasing the seismic design coefficients by an *importance* factor (i.e. an elevated *importance* factor creates proportionally higher design loads; García-Pérez et al., 2005). This factor is set intuitively or arbitrarily and always independent of the design coefficients of ordinary structures.

Building occupancy classifications refer to categorising structures based on their usage and are primarily used for building and fire code enforcement but also for the purposes of applying flood, wind, snow, earthquake, and ice provisions. In the International Building Code (International Code Council, 2006) the occupancy categories range from I to IV, where Occupancy Category I represents buildings and other structures with a low hazard to human life in the event of failure, and whilst Occupancy Category IV represents essential facilities. Essential or critical facilities are those intended to remain operational during and after an extreme environmental event, such as a hurricane or snowstorm.

In some cases, the *importance* is determined by the value of the content (e.g. certain public buildings or schools), or by the risk imposed by the consequences of a failure (e.g. industrial buildings where harmful substances are managed) as well as by the cultural significance of the structure (e.g. monuments, museums, cathedrals). A higher *importance* Factor and Building Occupancy classification improves the reliability, and therefore safety factor, of the structure. This helps to protect its occupants as well as its function (e.g. hospital) during and after a major environmental event. The concept of *importance* factor and Occupancy Category will form the basis for the land use classification at Arequipa presented in this report.

In the Peruvian National Building Code for Earthquake-resistant design E.030 (Permanent Technical Committee of Earthquake-Resistant Design, 2003) buildings are divided into four categories: A, B, C, and D, in terms of *importance*. Category A buildings represent essential facilities where their function cannot be interrupted immediately after an earthquake, such as hospitals, communication centres, fire-fighter and police headquarters. These buildings can be used as shelter after the event and are assigned an *importance* coefficient for earthquake resistant design of 1.5. Category B buildings include important facilities such as places for

meetings (e.g. theatres, town halls, stadiums etc.) or for valuable patrimony (e.g. museums, libraries etc.) and important storage facilities for supplies (e.g. grain depot). Category C buildings are common facilities whose collapse would cause intermediate losses such as dwellings, offices, hotels, restaurants etc. Category D buildings are minor facilities whose failure causes small losses (e.g. low fences and small temporary houses or sheds).

In theory, most essential services (Category A) in Arequipa should have been designed or retro-fitted to comply with the seismic building code and essentially should withstand higher loads than buildings of Category C for example. However, since it cannot be assumed that all buildings within Arequipa have been built adequately according to the Seismic Code (see section 4.4.3), dominant land use within in Arequipa has been located and identified along with essential key elements that are more vulnerable during a lahar or flood event.

4.2.2 Land-use classification in Arequipa

During the survey conducted in Arequipa in 2007 and 2008 (Chapter 1), twenty different land-use types were identified (Table 4.2, Figures 4.3 to 4.5) varying from non-built intensive agriculture to dense urban areas.

GIS ID	Land use	GIS ID	Land use
1	Urban dwelling	11	Other commercial*
2	Rural dwelling	12	Administration
3	Commercial with dwelling	13	Industry/handicraft
4	Accommodation	14	Service station
5	Medical centre	15	Carpark
6	Police	16	Agriculture
7	Religious establishment	17	Monument
8	Education establishment	18	Abandoned
9	Public area/sports area	19	No construction
10	Restaurant	20	Unknown

Table 4.2: *Predominant land-use types identified for the areas surveyed in Arequipa. The classification of 'unknown' was assigned to areas which were unseen, and where permission to access the land was not granted. *Other commercial corresponds to commerce does not have dwellings attached, such as supermarkets, larger stores etc.*

These land use types were then assessed and ranked according to their *importance*, value, monetary cost and occupancy (see Chapter 1 for the methods) in Section 4.3.3.

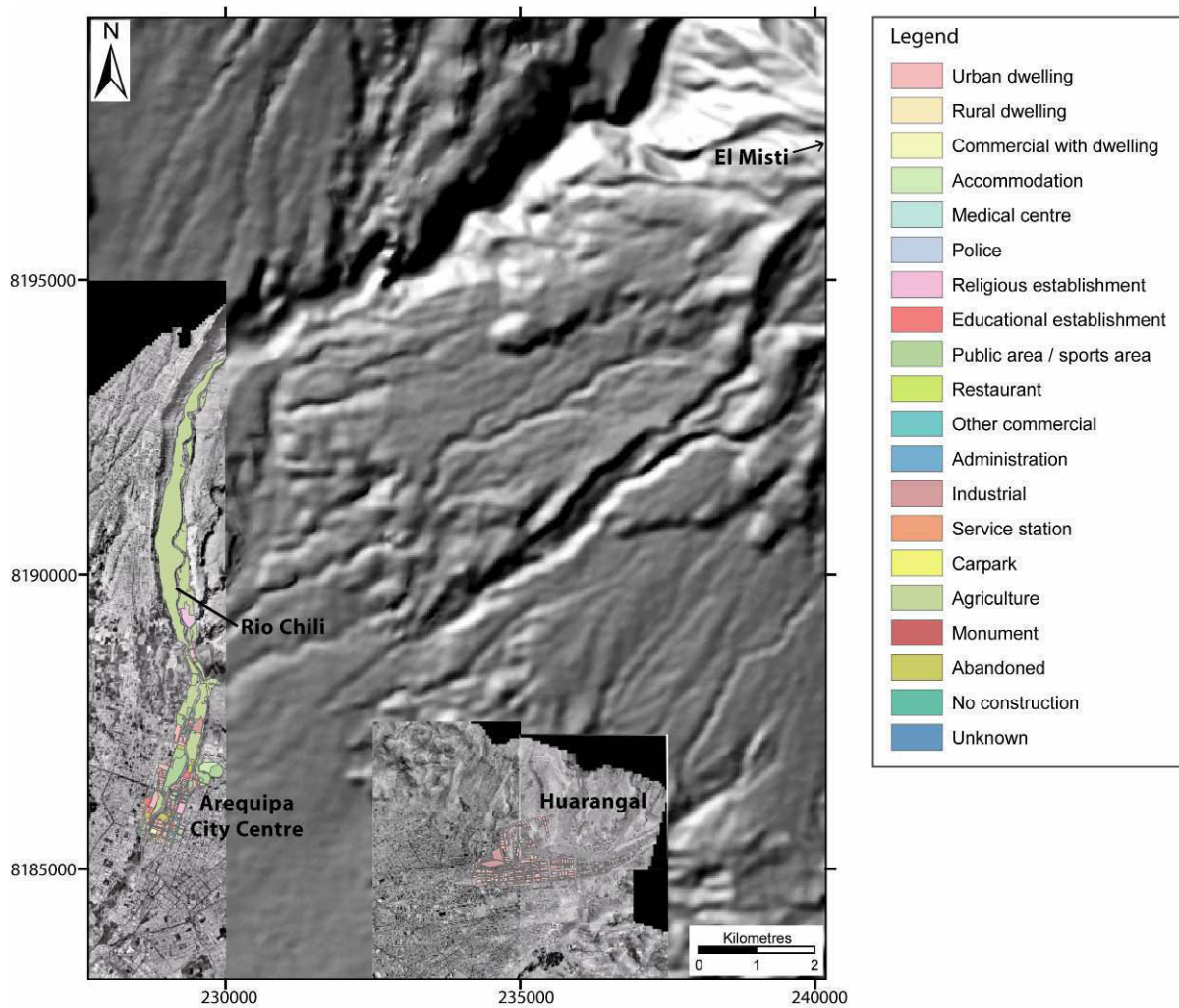


Figure 4.3: Predominant land use in the two main survey areas shown over orthophotos and a DEM of the Arequipa area. Agriculture is the predominant land use to the north of the city, along the Río Chili Valley, whilst urban dwellings are more predominant within the Quebrada Huarangal area.

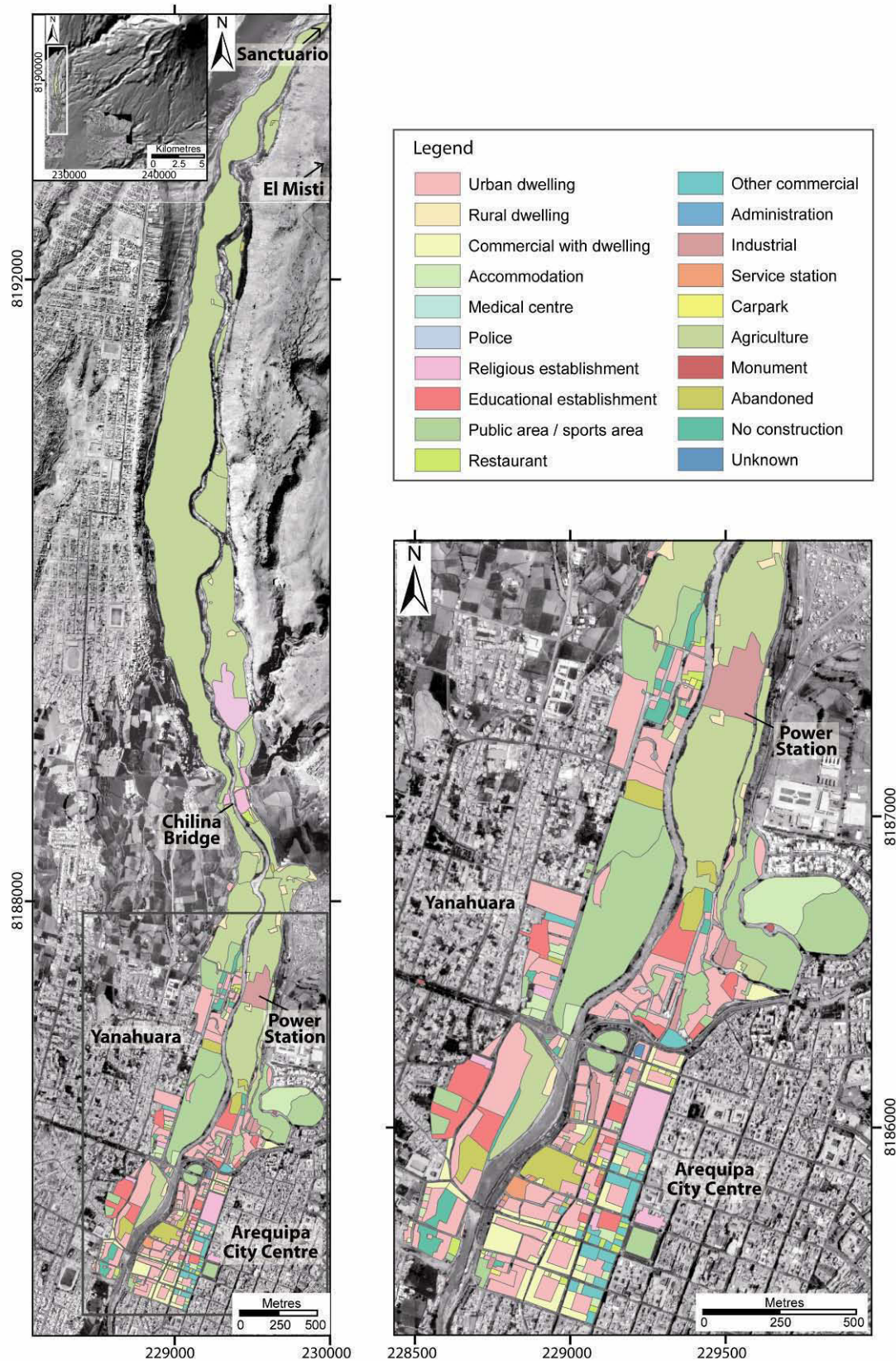


Figure 4.4: The predominant land use in the Río Chili Valley study area from the Quiñones Bridge to the military school in the upper Río Chili canyon. The southern part of the study area is largely for commercial, industrial and residential use. In contrast, the northern part of the study area is cultivated (valuable arable crops) with very few rural dwellings.

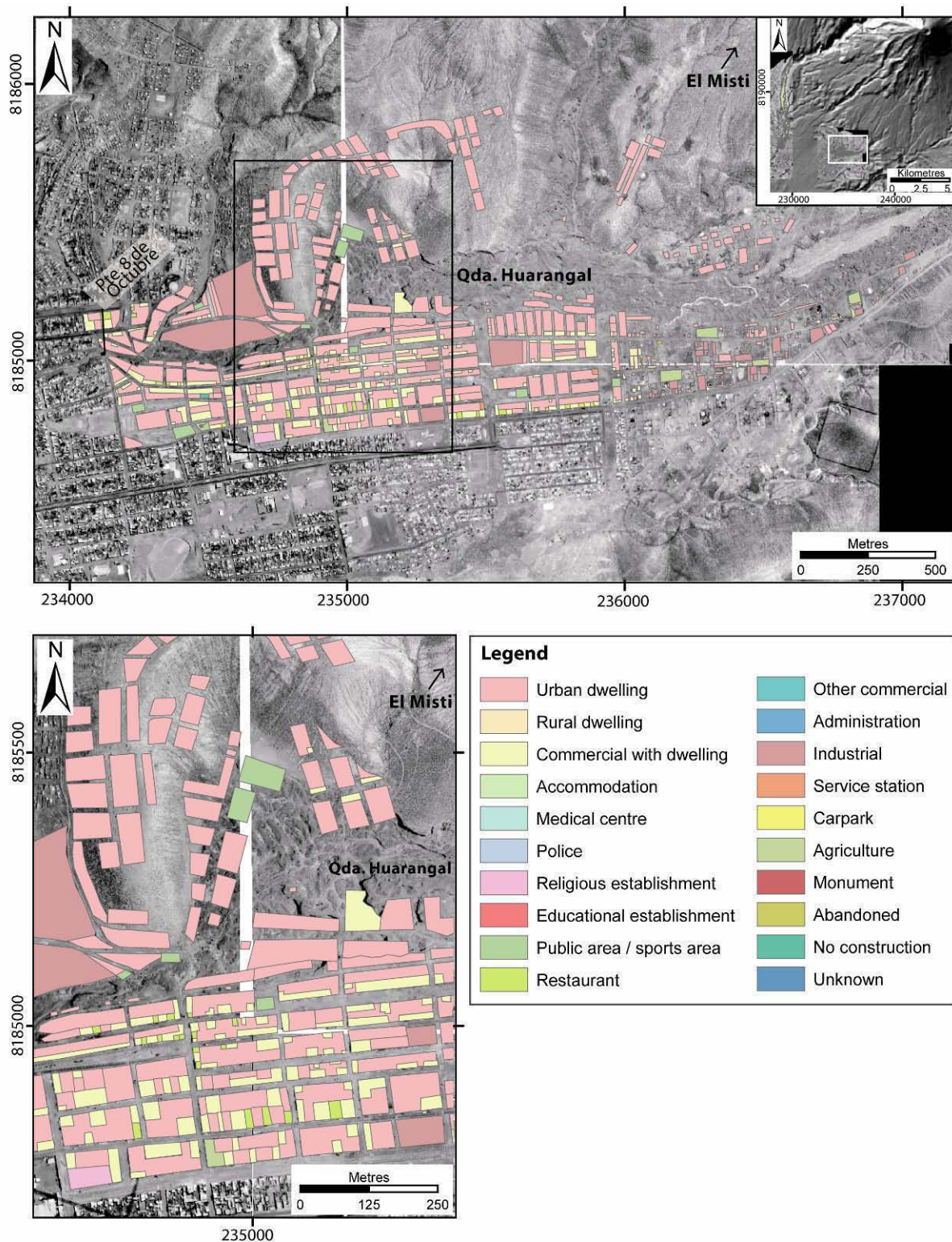


Figure 4.5: The predominant land use in the Quebrada Huarangal study area from the Bridge 'Puente 8 de Octubre' in the west to a Quarry in the east. Land use is not so varied within this fan area compared to that of the Río Chili Valley. There is no agriculture, some industry (e.g. mining, automotive mechanics, factories), and commercial stores which serve as urban dwellings too. The most predominant land use within this area is private urban dwellings.

4.2.2.1 Introduction

Spatial contrasts of land use in Arequipa

The proportion of land use types vary widely from the Río Chili valley to the Quebrada Huarangal fan, the differences of which can be seen clearly in Table 4.3. Agricultural land occupies the most area within the Río Chili valley, whereas private urban dwellings are more common on the Quebrada Huarangal fan. In both study areas medical and police facilities are not present, with administrative facilities and monuments occupying the least land in the Río Chili valley and Quebrada Huarangal fan respectively.

Land-use	Area (x10 ⁻³ m ²)			Land-use	Area (x10 ⁻³ m ²)		
	Río Chili	Huarangal	Total		Río Chili	Huarangal	Total
1	292.86	468.42	761.28	11	33.17	0.00	33.17
2	33.73	4.01	37.81	12	0.45	0.00	0.45
3	63.49	98.52	162.01	13	48.68	92.48	141.16
4	57.05	0.00	57.05	14	4.94	0.86	5.80
5	0.00	0.00	0.00	15	2.07	0.00	2.07
6	0.00	0.00	0.00	16	1858.67	10.33	1868.99
7	52.87	2.93	55.80	17	1.10	0.09	1.19
8	64.41	0.00	64.41	18	56.61	0.31	56.92
9	336.98	14.11	351.09	19	31.60	0.71	32.31
10	16.78	8.04	24.82	20	1.67	0.00	1.67

Table 4.3: The area of each type of land use occupied in the Río Chili valley and Quebrada Huarangal fan.

Agricultural land occupies just over half of the land studied (51%) followed by private urban dwellings (21%), public/sports areas (10%) and industry (13%). Administrative facilities, car parks, monuments and abandoned lots each occupy less than 0.5% of the studied area.

Río Chili Valley

Generally speaking agricultural land, which represents 63% of land surveyed (Table 4.3, Figure 4.4), becomes much more common towards the Charcani Santuario in the upper Río Chili Valley (12 km upstream of the Arequipa City centre) where extensive crops occupy lower (t1, t1') and middle terraces (t2-t3) of the Río Chili. Poorly built rural private dwellings, representing 1% of the surveyed land, generally occupy these tilled terraces (discussed further in Section 4.4.4); however newer housing developments are being built as pressure for land increases.

The second most predominant land type is represented by public/sports areas (11% of the survey area) such as parks and squares, followed by private urban dwellings (10%). Police stations and medical centres are not present within the study area, therefore monuments (e.g. statues) and administrative buildings occupy the smallest area within this study at <0.1%. A hotel (La Posada del Puente), a sports club (Club Internacional), tourist restaurants (La Choceta and Sillustani), a University (Universidad Católica San Pablo) and a power station (Egasa) are some of the larger and more well established businesses located on the lower terrace (t1, t1'). Hydroelectric power stations also occupy the Río Chili Canyon from Charcani Santuario up to Charcani Quinto (more details of which are in Section 4.5.5), near a military school (19 km upstream of the Arequipa City centre and ~5.8 km west of El Misti's vent).

Southwards, towards Arequipa City, building density increases as does the heterogeneity of land use, ranging from private urban dwellings to churches (<1% of survey area) and schools (2%). Agricultural land within this vicinity is sparse. A number of important cultural monuments and buildings such as the cathedral and the Santa Catalina Monastery exist within the city centre – reflecting the UNESCO World Heritage status.

Quebrada Huarangal Fan

In contrast to the Río Chili Valley, little to no agricultural land exists (<2% of survey area), with the exception of a pig farm (Figure 4.5, Table 4.3). This is due to the lack of flowing water within the valley, where water for domestic use is drawn from wells. The Quebrada's channel bed is predominately used for mining, with the exception of the western end where dwellings and small commercial stores are being rapidly built. At the downstream reach of the Huarangal valley new housing developments, of predominantly poorer quality, are being created by the infilling of the channel.

Private urban dwellings (67% of surveyed area) are the most predominant followed by industrial areas (13%) such as brick factories. Accommodation, educational establishments, administration, commerce without urban dwellings, police stations, car parks and medical centres are not present within the study area, therefore monuments (<0.1% of surveyed area), service stations (0.1%) and abandoned lots (<1%) occupy the smallest area within this study.

Within the western boundary of the Huarangal fan land use is almost entirely limited to private urban dwellings, whereas to the south of the fan rising up one to two terraces an increasing number of small commercial operations exist – mainly in the form of general stores (14% of the surveyed area), markets and restaurants (1%). Some industry exists on the higher terraces such as automotive repair and small factories (e.g. brick manufacturing). Very few public sport or open areas exist (2%) and there is one large police station on the very top terrace (just outside of the study area).

4.2.3 Vulnerability of land use in Arequipa

Using methods adapted from the International Building Code (International Code Council, 2006), the Peruvian National Building Code for Earthquake-resistant design (Technical Standard of Building E.030, 2003) and the New Zealand Standard NZS 1170.5:2004 (Standards New Zealand, 2004) the vulnerability of land use in Arequipa was assessed. Coefficients, ranging from 0 (low *importance*) to 1 (high *importance*) were assigned to different categories (such as economic repercussions, population exposure and value) for each land-use type (the method and rationale is discussed in chapter 1). These coefficient values were added together and averaged to give a value between 0 and 1 for the *importance* of the particular land use and therefore the vulnerability during a volcanic crisis (Table 4.4). The values were normalised to account for subjectivity in assigning the values, normalised minimum and maximum values were obtained from which the mean value of all the criteria was calculated. Reasoning for the assignment of the coefficient values are based on a literature review including Kelman, 2002, Spence et al. 2004a,b to name a few, and is rationalised in Appendix C.

The land-use types were evaluated against one another to determine the most vulnerable land use type present in Arequipa. The results were mapped to show the vulnerability distribution within the study areas (Figures 4.6 and 4.7). Furthermore, a GIS database was created so that the land-use and building type vulnerabilities could be combined to show an overall vulnerability for the study areas (Figure 4.8).

Land-use	Criteria (coefficient (0 - low importance/vulnerability, 1 - high importance/ vulnerability)										Totals				
	Facility used during a crisis		Population exposure		Value		Economic repercussion		Total maximum	Total maximum normalised	Total minimum	Total minimum normalised	Mean	Rank	
	Emergency facilities (administration, accommodation)	Ensuring emergency supplies	People exposed during the day	People exposed during the night	Place of community importance (cultural/social)	Value to the individual	Loss of income	Cost of rebuilding							
1- Dwelling	0.10	0.00	0.30	0.90	0.10	0.60	0.00	0.20	2.20	1.80	0.45	0.40	0.10	0.28	13
2- Rural dwelling	0.10	0.00	0.50	0.90	0.10	0.60	0.10	0.20	2.50	1.80	0.45	1.15	0.29	0.37	11
3- Commercial with dwelling	0.10	0.10	0.90	0.80	0.10	0.60	0.70	0.30	3.60	2.30	0.58	1.30	0.33	0.45	7
4- Accommodation	0.50	0.00	0.50	0.90	0.10	0.20	0.80	0.50	3.50	2.40	0.60	1.10	0.28	0.44	8
5- Medical centre	1.00	1.00	1.00	0.80	1.00	1.00	0.20	0.80	6.80	3.80	0.95	3.20	0.80	0.88	1
6- Police	1.00	1.00	1.00	0.70	1.00	1.00	0.10	0.50	6.30	3.50	0.88	2.80	0.70	0.79	2
7-Religious establishment	0.80	0.10	0.90	0.10	0.90	0.70	0.10	0.90	4.50	3.50	0.88	1.00	0.25	0.56	3
8- Educational establishment	0.80	0.00	0.90	0.00	0.70	0.50	0.50	0.80	4.20	3.20	0.80	1.00	0.25	0.53	5
9- Public area	0.70	0.00	0.90	0.10	0.30	0.30	0.10	0.30	2.70	2.20	0.55	0.50	0.13	0.34	12
10- Restaurant	0.00	0.20	0.80	0.70	0.10	0.10	0.80	0.50	3.20	1.90	0.48	1.30	0.33	0.40	10
11- Other commercial	0.10	0.10	0.90	0.10	0.10	0.10	0.80	0.50	2.70	1.90	0.48	0.80	0.20	0.34	12
12- Administration	0.10	0.10	0.90	0.10	0.10	0.10	0.80	0.50	2.70	1.90	0.48	0.80	0.20	0.34	12
13- Industry	0.10	0.70	0.90	0.50	0.20	0.20	0.90	0.80	4.30	2.70	0.68	1.60	0.40	0.54	4
14- Service station	0.00	0.80	0.90	0.10	0.10	0.20	0.80	0.50	3.40	2.70	0.68	0.70	0.18	0.43	9
15- Carpark	0.30	0.00	0.70	0.10	0.00	0.00	0.10	0.30	1.50	1.30	0.33	0.20	0.05	0.19	14
16- Agriculture	0.10	0.50	0.90	0.10	0.00	0.50	0.90	0.80	3.80	2.80	0.70	1.00	0.25	0.48	6
17- Monument	0.00	0.00	0.90	0.10	0.90	0.70	0.10	0.80	3.50	2.60	0.65	0.90	0.23	0.44	8
18- Abandoned	0.00	0.00	0.10	0.10	0.00	0.00	0.00	0.00	0.20	0.10	0.03	0.10	0.03	0.03	15
19- No construction	0.20	0.00	0.00	0.00	0.00	0.00	0.00	0.00	0.20	0.20	0.05	0.00	0.00	0.03	15
20- Unknown	0.00	0.00	0.00	0.00	0.00	0.00	0.00	0.00	0.00	0.00	0.00	0.00	0.00	0.00	16

Table 4.4: Classification of the land use vulnerability in Arequipa. Land-use types are assigned coefficients from 0 to 1 (0 least important/susceptible, 1 most important/susceptible) according to the importance of the particular land use potentially exposed during a crisis, how many of the population will be affected, the value of the land and the economic repercussions during a volcanic crisis. The mean gives the value of the land use on the same 0 to 1 scale of susceptibility with the various land-use types ranked to show the most and the least susceptible.

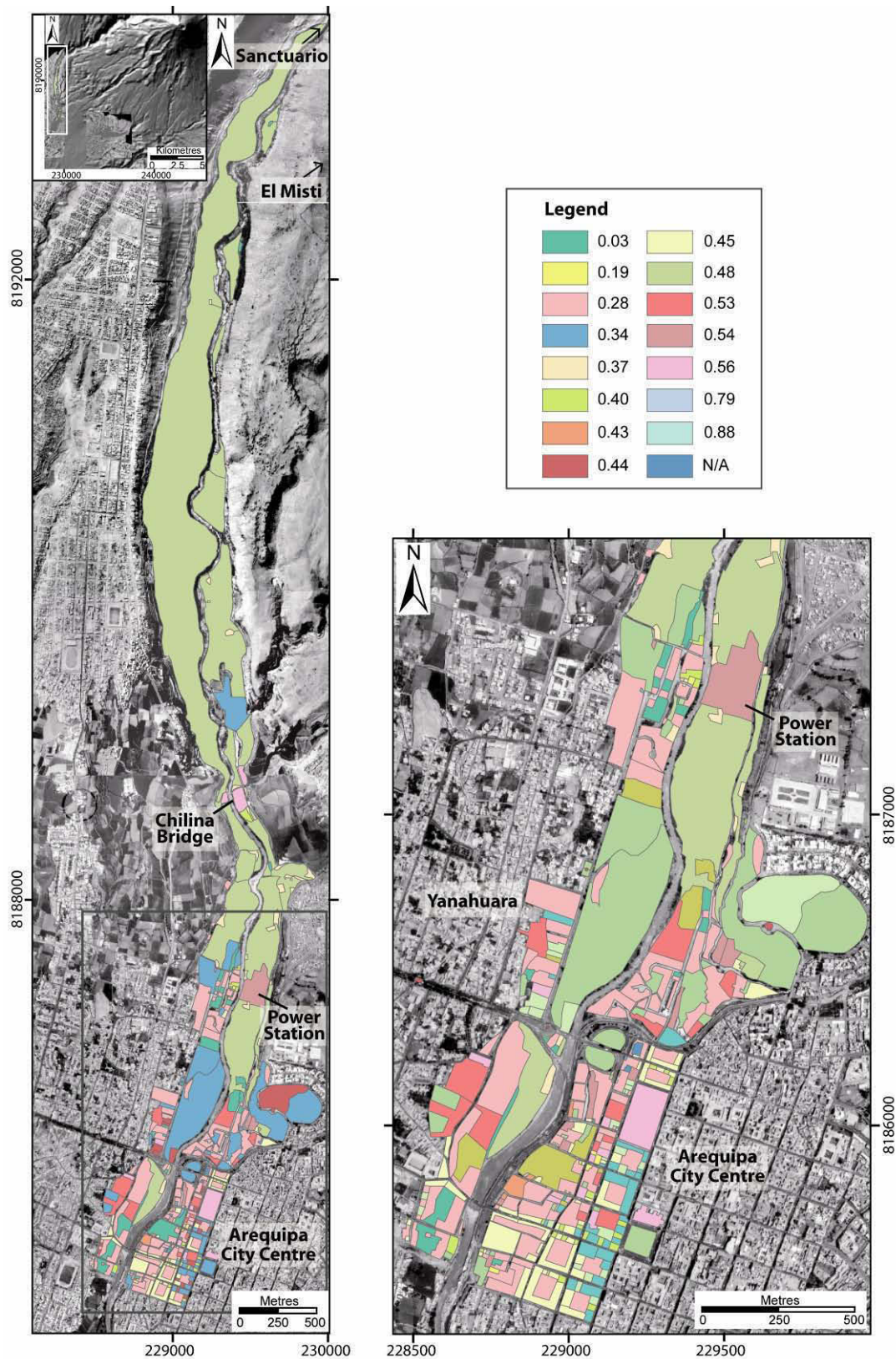


Figure 4.6: The vulnerability of land use in the Río Chili Valley study area. The most vulnerable land use within this area is represented by high coefficient values. Agriculture (coefficient 0.48) is the most widespread land-use type and is closer to the volcano than other vulnerable land uses such as factories (0.54), located within the Arequipa City Centre.

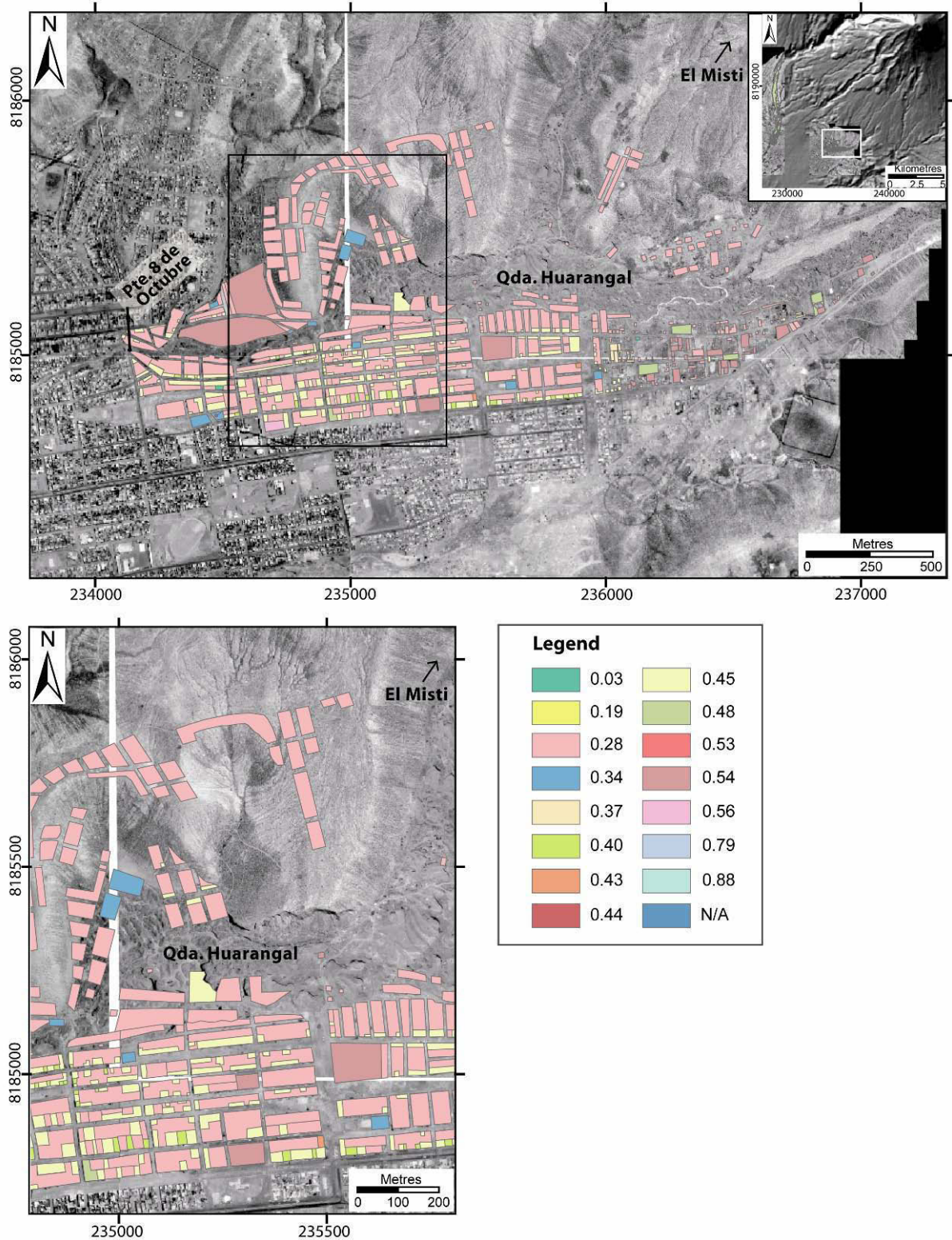


Figure 4.7: The vulnerability of land use in the Quebrada Huarangal study area. The most susceptible and vulnerable land-use within this area is represented by high coefficient values. The majority of the land use represented in the Huarangal fan is of a low vulnerability value. However, within and on the banks of the channel more vulnerable land-use areas have been identified, such as factories or commercial buildings with dwellings.

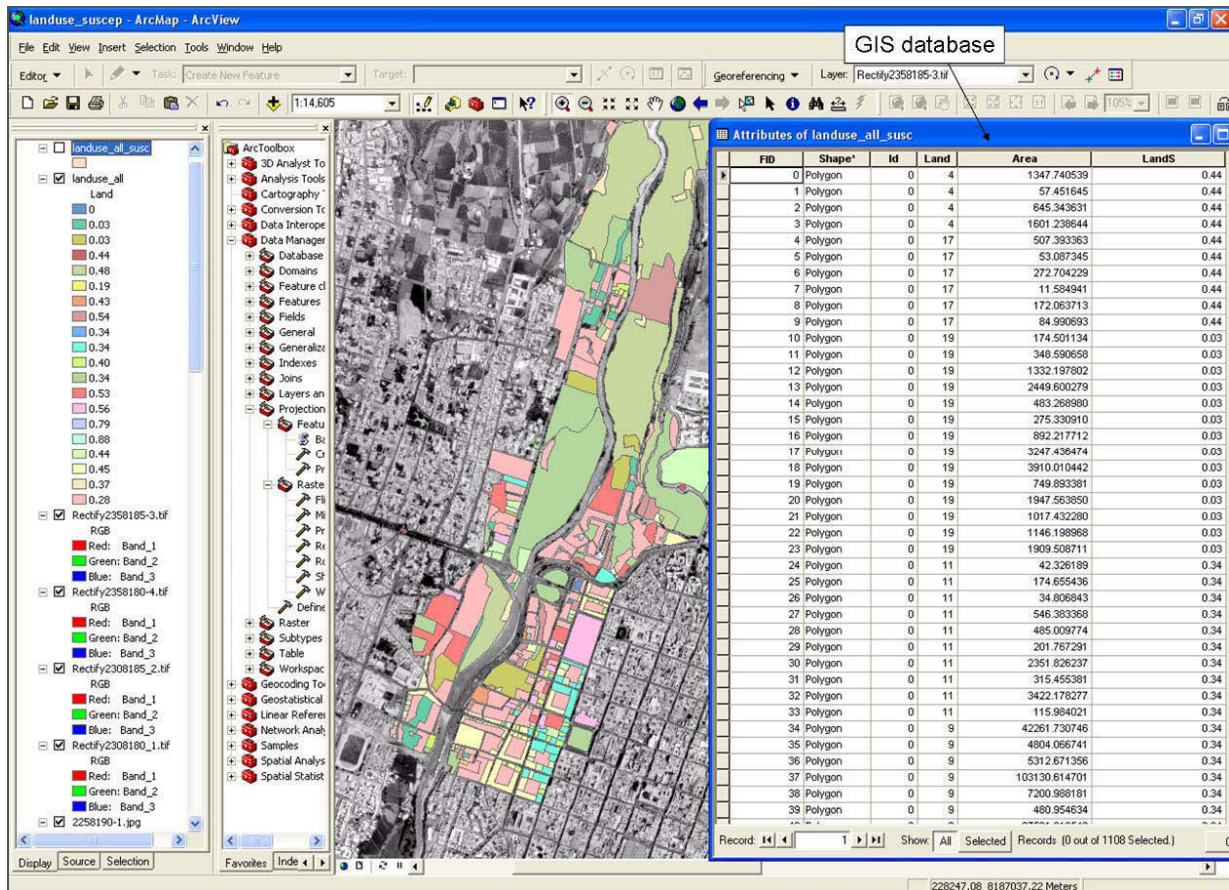


Figure 4.8. Database created in ArcGIS showing the predominant land use within the study areas. Assigned with the land uses are the vulnerability categories and coefficients.

4.2.3.1 Summary

The vulnerability analysis of land use indicates that police stations, medical centres, religious establishments and industrial enterprises are the most vulnerable land-use types. However, both police stations and medical centres are not present within the study area, but are nearby such as the large police station just outside the Huarangal fan. The least vulnerable land-use types according to the vulnerability analysis (Table 4.4) are ‘unknown’, unconstructed and abandoned lots. Private urban dwellings, despite having a high occupancy during night-time hours are considered low in vulnerability (rank 13) due to the lower replacement cost, no lost income, and they are not considered as essential and/or critical buildings during a volcanic crisis. This is quite a contentious outcome, however in terms of the variables used in the ranking, private dwellings were considered low.

Agriculture is considered financially vulnerable (rank 6) due to the potential loss of income and the use of agriculture as a food supply during a volcanic crisis. Agricultural land can also

be used as an open area for the construction of evacuation shelters. Alarming, agriculture in Arequipa is at higher risk during a lahar or flood event than some of the other land-use types such as religious centres and businesses with private dwellings. This is due to its location adjacent to the Río Chili channel and the lowermost flood-prone terraces (t0, t1), which are up to 3-5 m above the river bed (t1'). Similarly one of the major industries (rank 4) and lifelines - the Egasa power station, is located on the low eastern terrace (t1') of the Río Chili Valley just to the north of the city centre.

Dominant land use is not the only important factor in determining the vulnerability of a city to lahars and floods, land use goes hand-in-hand with the type of building construction/materials and the vulnerability of this type of building to damage during a flow event.

4.3 Building stock classification

4.3.1 Introduction

The descriptive building surveys were undertaken in the Río Chili Valley and on the Quebrada Huarangal fan with the aim of assigning a building type to individual buildings within the survey area. The results of the survey, along with a vulnerability ranking of the building types with respect to the resistance of the structure, are presented in the following sections.

4.3.2 Construction types and building materials used in Arequipa

Building types in Arequipa differ from Peru as a whole (Figure 4.9); adobe is much less common at 1.7% compared to 34.8% in Peru. This could be due to devastating earthquakes (e.g. 1600, 1687, 1868, 1958, 1960, 2001; The Associated Press, 23 June 2001) or because ignimbrite blocks have been the most accessible type of building material in Arequipa. Despite the major earthquakes, many 17th- and 18th-century buildings built from ignimbrite have survived. The prevalence of clay soils and volcanic ash has also facilitated red clay bricks to be used for building material.

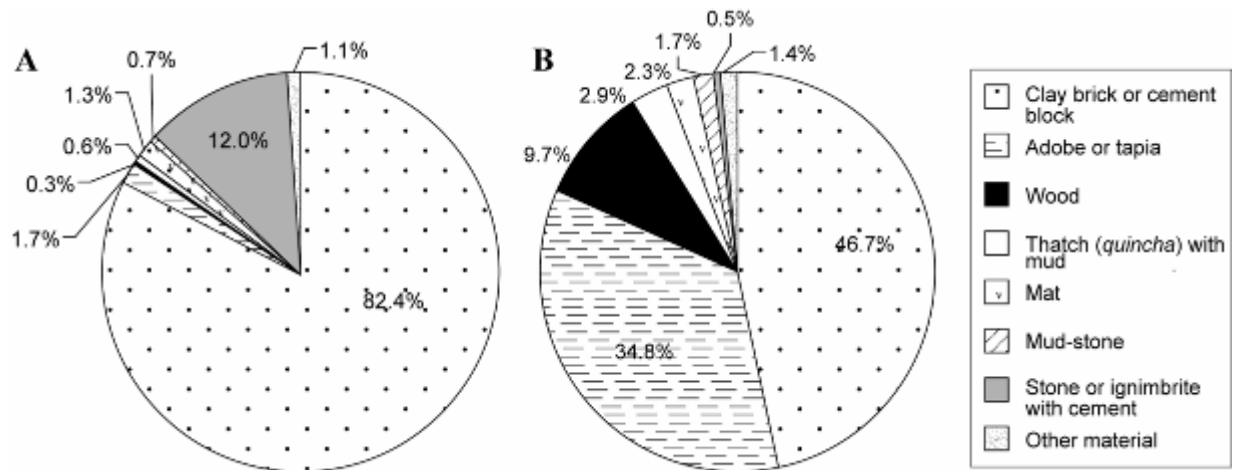


Figure 4.9: Types of material used in construction in Peru from the 2007 census (INEI – National Census 2007). *A*: Predominant construction type in Arequipa compared to *(B)* the predominant construction type in Peru as a whole.

4.3.2.1 Confined masonry – red clay brick

In terms of masonry, the most common in the study areas is red clay brick confined masonry construction. This construction type is the most common single-family housing construction practice in both urban and rural areas of Peru in the last 45 years (Loaiza and Blondet, 2003a,b). In Arequipa more than 70% of buildings are built as confined masonry systems.

Red volcanically-derived clay is mixed with sand (volcanic ash in Arequipa) and water, and pressed by hand into moulds (Figure 4.10). Once moulded, the brick is left to dry in the sun, and then fired in a coal powered kiln. Alternatively, bricks can be manufactured by machine, although in Arequipa this is less common. In construction, masonry walls (of unreinforced perforated or solid clay bricks) are erected first and reinforced concrete confinements are constructed afterwards (Figure 4.11). Vertical confinements are cast directly against the masonry walls and then horizontal confinements, anchored on the previous ones, are placed together with the slab. This construction sequence produces an integral system of all the involved elements.

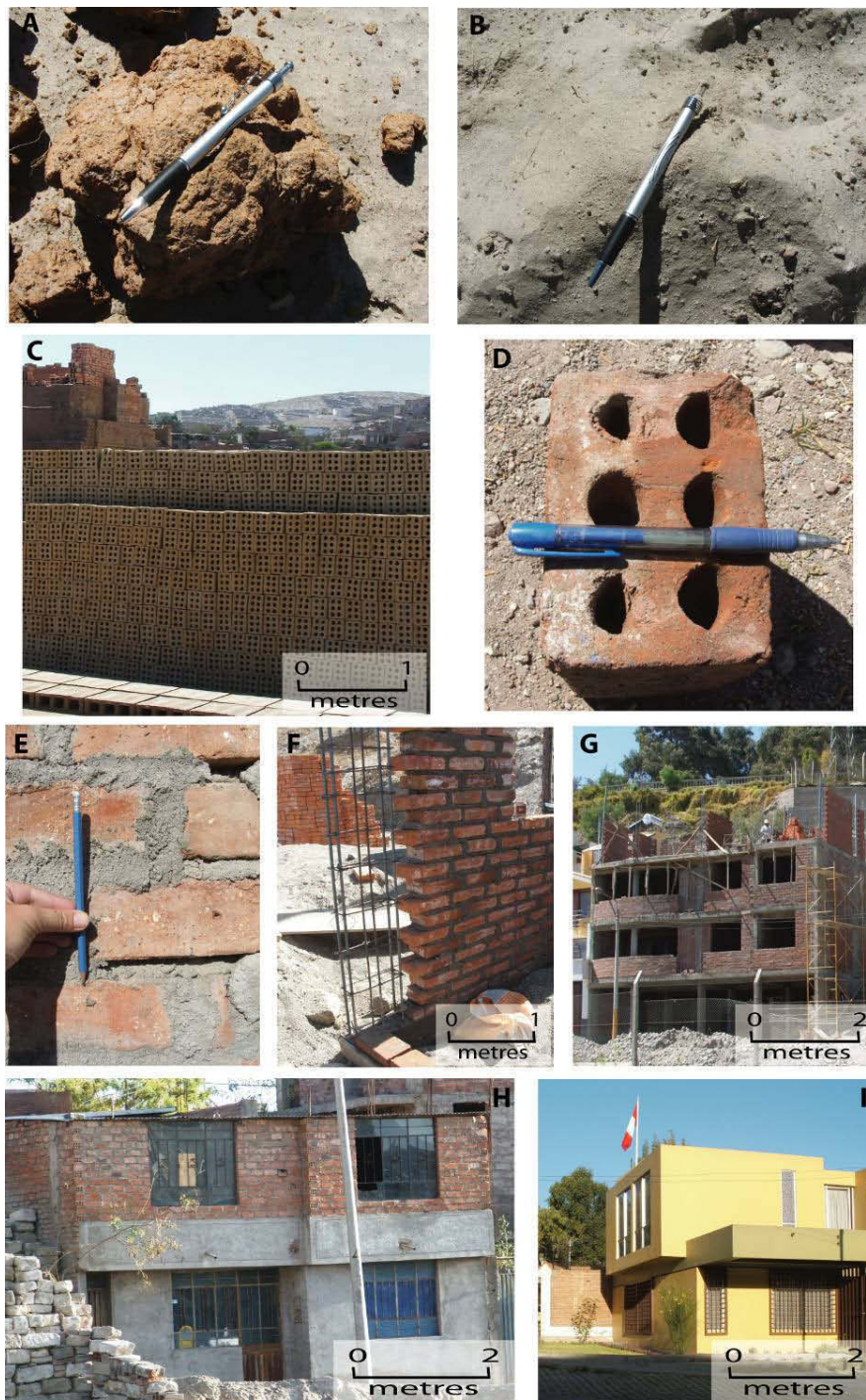


Figure 4.10: Typical confined masonry buildings present in Arequipa. **A:** Red clay used in brick making. **B:** Sand used in brick making. **C:** Bricks left to dry in the sun. **D:** A Pandareta-style red clay brick. **E:** Photograph of a house in the Río Chili Valley where the brick and mortar are not laid well (cf. the right top of image). **F:** Construction of a masonry wall against the reid bar of the corner column. **G:** Construction of a masonry house in the Río Chili Valley. **H:** Confined masonry home in Quebrada Huarangal – the bottom floor has a concrete façade; with a brick second storey which was probably built some time after the first storey. **I:** A well finished and maintained confined masonry home in an affluent housing compound adjacent to the Río Chili near the Arequipa City centre.

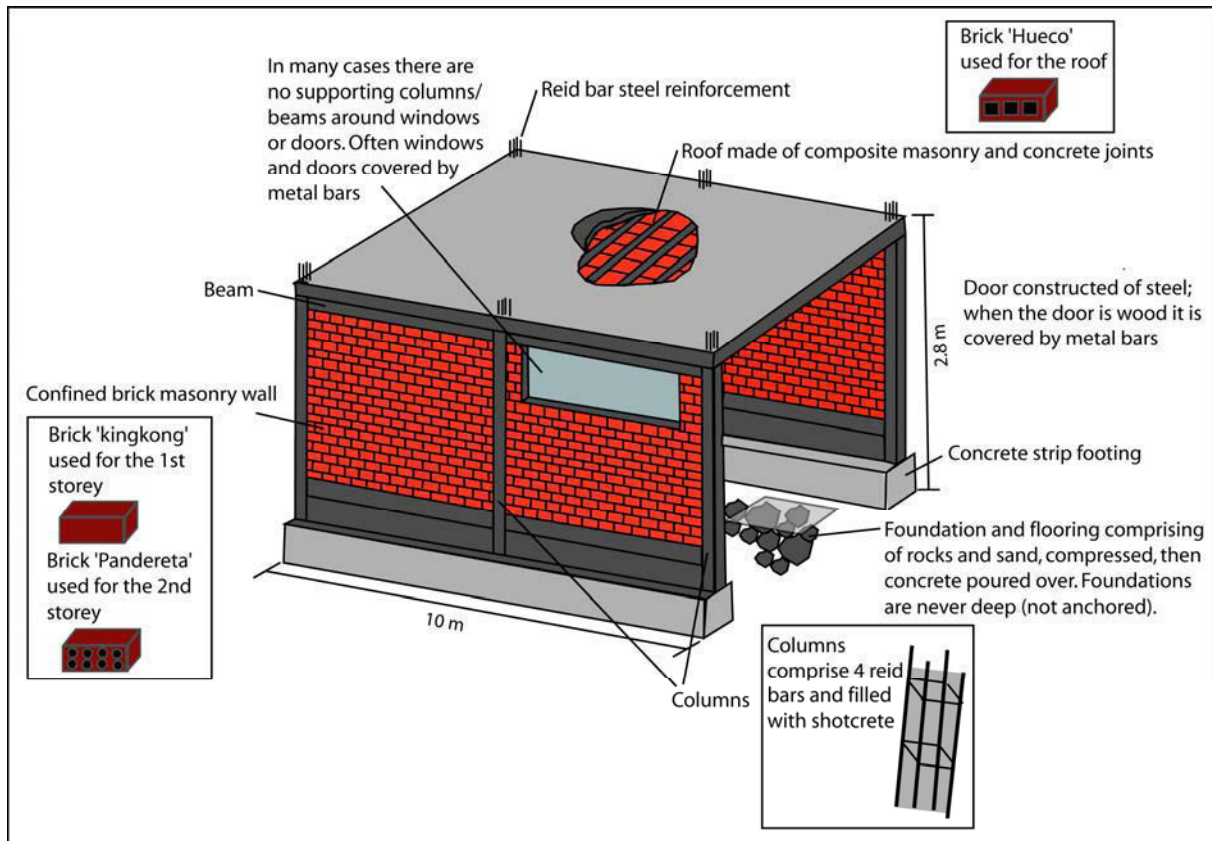


Figure 4.11: Typical structure of a confined masonry building as observed in Arequipa. Three different types of bricks are used in construction with subsequent storeys constructed using pandereta (modified from Loaiza and Blondet, 2003a).

A typical confined masonry house is between 10-15 m in length and 10-15 m in width, with 2-3 storeys (storey height 2.60-2.80 m). In Arequipa it is not uncommon to start a house with one storey and when the family grows, to add further storeys; these are often not well proportioned and distributed and can cause a loss in structural integrity. Most houses have 6 to 10 windows per floor, windows and doors rarely possess shutters, and most on lower floors have steel bars. The positions of the openings can be variable, but usually approximately 0.8 to 1.0 m from floor level in rooms and from 1.8 to 2.0 m in bathrooms; often there are no reinforced columns and beams around openings. Typical houses have a good wall density with only 2-7% of voids and a typical thickness of 150-250 mm (Loaiza and Blondet, 2003a). Most foundations are shallow and constructed from rubble stone (fieldstone) with strip footing. The floor and roof system typically comprise composite masonry and concrete joint, however corrugated iron sheet roofs are also common.

Confined masonry buildings used for purposes other than private dwellings possess a slightly different plan. Buildings are typically a rectangular shape (20 m x 12 m) with 3 to 4 windows

(typically 1-2 m wide). Most buildings have on average 4-6 storeys, with a typical storey height of 2.5-2.5 m. The typical structural wall has a larger void index of up to 5% (Loaiza and Blondet, 2003b). Shallow foundations consist of reinforced-concrete strip footing, and usually the foundation is of plain (unreinforced) concrete unless the soil is clay or silt.

4.3.2.2 Unconfined masonry – red clay brick

Unconfined red clay brick masonry is common in the margins of Arequipa city, on the tilled agricultural terraces of the Río Chili Valley, and on the Huarangal fan (Figure 4.12). Buildings are either rectangular or square in shape, with a typical length of 9 m, width of 8 m and one storey high (typically 3-4 m in height). Normally they comprise one door or window opening per wall. Typical houses have a good wall density with only 2-7% of voids a typical thickness of 150-250 mm (Loaiza and Blondet, 2003a,b).



Figure 4.12: Unconfined masonry dwellings in Arequipa. Dwellings **A** and **B** are constructed of red clay brick with mortar, whereas dwellings **C** and **D** are constructed from a mixture of ignimbrite and red clay brick with no mortar.

There are two types of unconfined red brick masonry – those with mortar (e.g. Figure 4.12 A and B) and those without (e.g. Figure 4.12, C and D). Both types do not possess reinforced columns as confined masonry does; buildings with mortar have very vulnerable wall corners or junctions, and in the case of structures with no mortar, all parts of the building are vulnerable. Figure 4.12 (A and B) shows a building where bricks and mortar are well bonded but there are no lateral supporting beams. The roof is a concrete and masonry composite; there is no mortar or lateral and horizontal reinforcement. There is one window and door and the corrugated iron roof is held in place with loose bricks. In Figure 4.12 (C and D) the dwelling has been constructed from ignimbrite blocks and an assortment of red clay bricks, but there is no mortar between bricks, or lateral or horizontal confinement. The dwelling in Figure 4.12 D is lacking windows, the door is made from fabric, and the roof consists of plastic with wooden sheets strewed across. In each case, the buildings have a shallow foundation often without a rubble stone strip footing, and many cases without a floor or a foundation at all. These buildings have little regard to construction principles (especially those without mortar) and reinforcement.

4.3.2.3 Unconfined masonry – ignimbrite/concrete block

This type of construction is the second most common in Arequipa and has been used since the last third of the XVIth century (Figure 4.13); extensive use of the whitish stone in the historic city has resulted in the international reputation as the “White City” and a UNESCO World Heritage status (Kusunoki, 2002). The stone is pearl or pink, inexhaustible, soft, light, thermal, aesthetic and waterproof, and has emerged as a seismic structural solution in some cases (Kusunoki, 2002). However, well-known examples of ignimbrite architecture have been damaged in earthquakes, including the Basilica Cathedral of Arequipa which was founded in 1612 and subsequently damaged and rebuilt several times after a fire and several earthquakes. Following the 23 June 2001 M_L 8.4 earthquake one of the bell towers collapsed. The Santa Catalina Monastery, founded in 1579, was heavily damaged during the 1868 and 2001 earthquakes (Kusunoki, 2002).

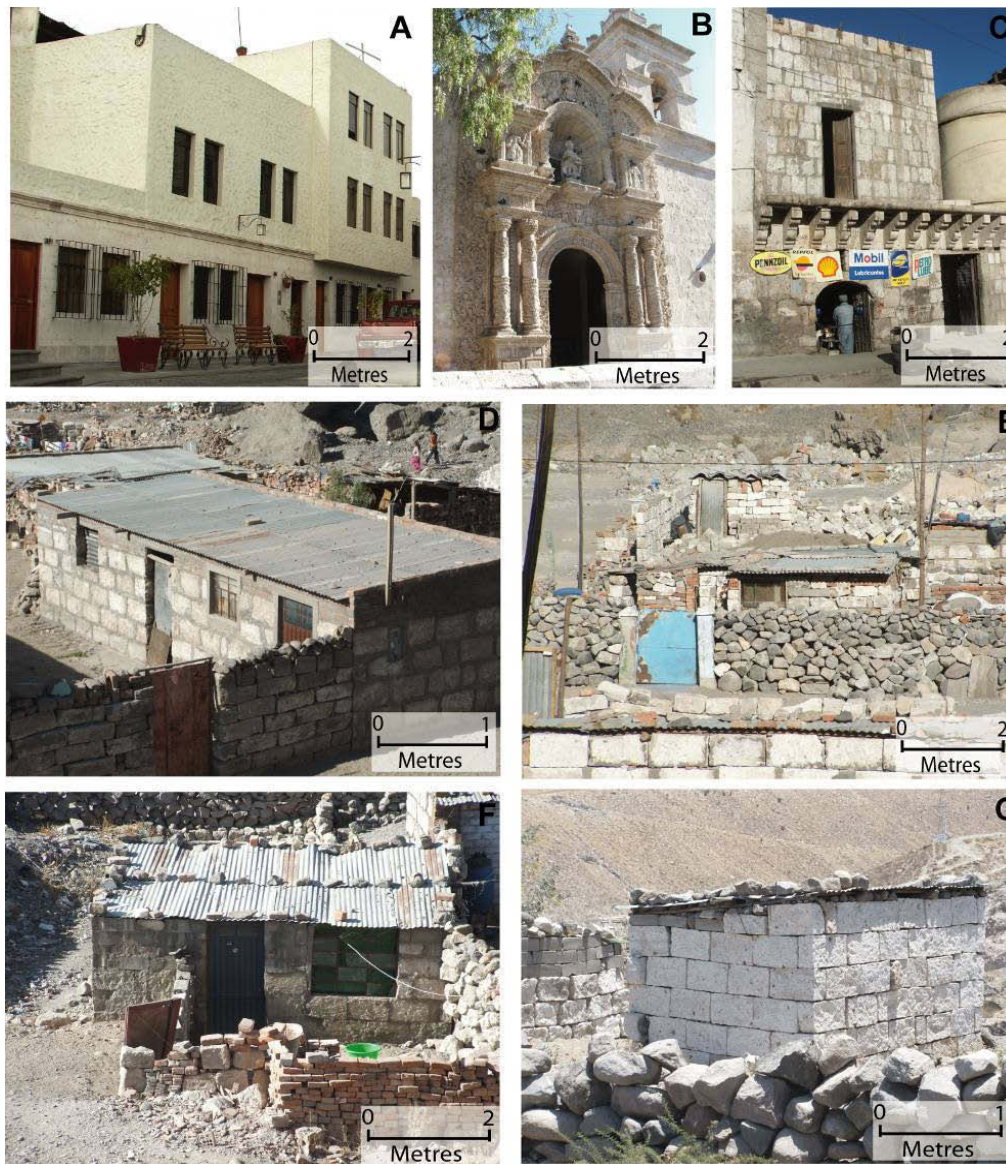


Figure 4.13: The range of ignimbrite block construction in Arequipa. **A:** New, well built and finished ignimbrite private dwellings **B:** An example of a ignimbrite church, the San Juan Bautista. **C:** A business building constructed from ignimbrite blocks. Behind this store private dwellings were being (re)constructed with ignimbrite. **D:** An ignimbrite block masonry dwelling within Quebrada Huarangal. **E:** and **F:** Similar dwellings situated within Quebrada Huarangal. **G:** A dwelling on the southern bank of Quebrada Huarangal.

These buildings are perhaps the most variable in plan, ranging from tens to hundreds of square metres, and have an unpredictable number of openings. Ignimbrite bricks are typically large in size (up to 0.5m x 0.2m), usually have a low bulk density, and are bonded with a calcareous mortar. The buildings often do not possess any vertical reinforced confinements but some have reinforced horizontal beams. Houses shown in Figure 4.13 (E and F) do not appear to have a good bond between the bricks and mortar. The doors go from the base to the roof, openings are relatively large, the dwelling lacks structural elements, and the corrugated

iron roofs are held in place with rocks. Figure 4.13 (G) provides a good example of the types of dwellings present on the southern bank of Quebrada Huarangal. The dwelling possesses no mortar between bricks and instead the bricks are just stacked upon one another, the only opening is a door. The dwelling lacks any structural elements and the sloping corrugated iron roof is held in place with stones. Where ignimbrite buildings have been well constructed, roofs are generally constructed from concrete beams and slabs, which include the majority of 3+ storey buildings in the city centre, and historical monuments (e.g. Figure 4.13 B, Church San Juan Bautista in Yanahuara built in 1750). A typical problem associated with this type of masonry construction is due to their very dense walls, often without mortar or pillars, which can collapse during earthquakes.

4.3.2.4 Adobe

Adobe has been a typical earth construction in Peru since the XIVth Century Incaic Period (Loaiza et al., 2003c) (Figure 4.14). Walls are constructed from adobe blocks (sun-dried bricks composed of mud and straw) laid in mud mortar (Figure 4.15). The roof structure is usually made from wood; consisting of timber beams and planks covered with mud mortar. Traditionally this is overlaid with clay tiles, but in Arequipa corrugated iron sheets are much more common. Corrugated iron sheets are normally held in place with steel nails but it is not unusual for sheets to be held crudely in place by rocks, wood and other heavy objects. A good example of this type of construction is shown in Figure 4.15 (F) - a rural dwelling, which also houses animals and machinery. The adobe bricks form thick walls, and where the adobe has fallen away, stones are put in to secure the structure. The roof is corrugated iron sheets held in place by nails and rock/blocks of wood, situated on top of timber beams, which have been incorporated into the upper part of the adobe walls.

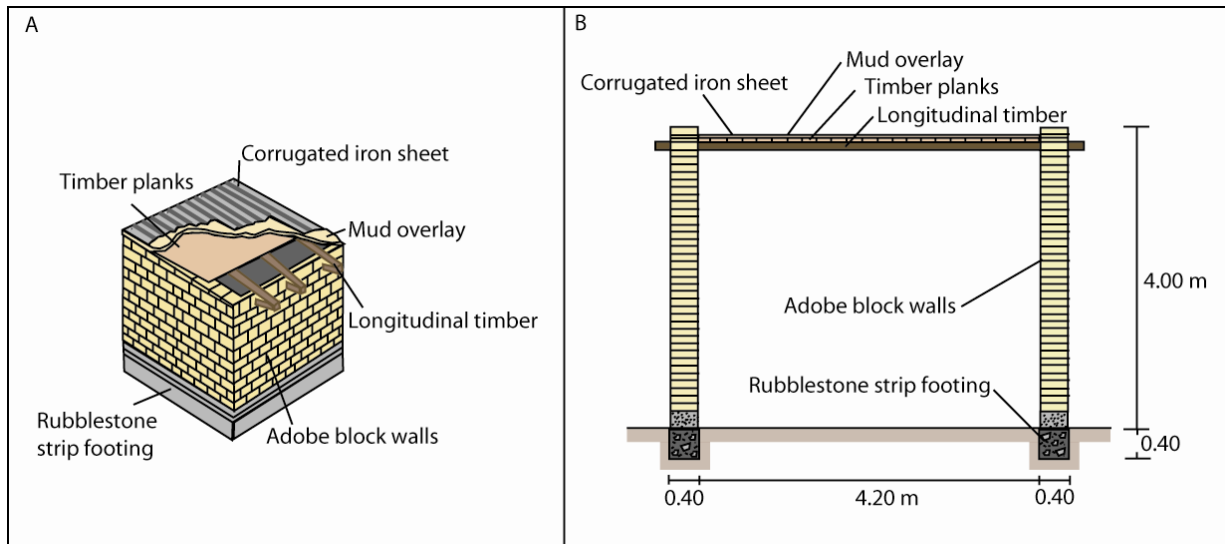


Figure 4.14: Typical adobe structure as observed in Arequipa. **A:** The main constructional materials used in adobe buildings (dimensions of the house are the same as in **B**). **B:** Structural components of adobe construction (modified from Loaiza et al., 2003c)



Figure 4.15: Making adobe bricks – **A:** a big pit is made and water added to make the ‘mud’, mud is then scooped up (**B**) and put into moulds (**C**), bricks are then turned out (**D**) and left to dry (photos obtained from Victor Rodriguez). **E:** An adobe brick from Arequipa – note the muddy texture with bits of straw. **F:** An adobe dwelling on the lower terrace side of the western side of the Río Chili in the city centre.

Typically adobe buildings are regular in shape – either rectangular or square, with a typical length of 9 m, width of 8 m and one storey high, typically 3-4 m in height. Normally they comprise one door or window opening per wall. Typical wall thicknesses are 300-800 mm and quite low densities as the index ratio is 20 to 40% (Loaiza et al., 2003c). The building does not possess reinforced columns as confined masonry does, thus wall corners (junctions) are the very vulnerable parts of the structure. The building has a shallow foundation, often without footing and rubble stone strip footing.

In most cases the construction is carried out by future inhabitants, with little or no knowledge of the basic construction principles; methods of construction vary widely and this introduces some variations in the strength of adobe housing. It is not common practice in Peru to invest in house maintenance, therefore it may be expected that the vulnerability inherent to unreinforced adobe construction is worsened by aging. Taucer et al. (2007) found that during the 2007 Pisco earthquake, 80% of adobe houses within the affected zone collapsed. Collapse was due to heavy mass; very low strength with respect to the density of the material; failure of material in a brittle matter; low quality of construction, especially of mortar; slender walls and long unsupported lengths; large percentage of openings; unstaggered brick arrangements at corners; flexible roofs and /or floors; and heavy roofs (Taucer et al., 2007).

4.3.2.5 Makeshift construction

Makeshift buildings are those constructed from a multitude of different building materials, mainly occupying rural land to the north of the city centre, city margins or illegal squatting (Figure 4.16).

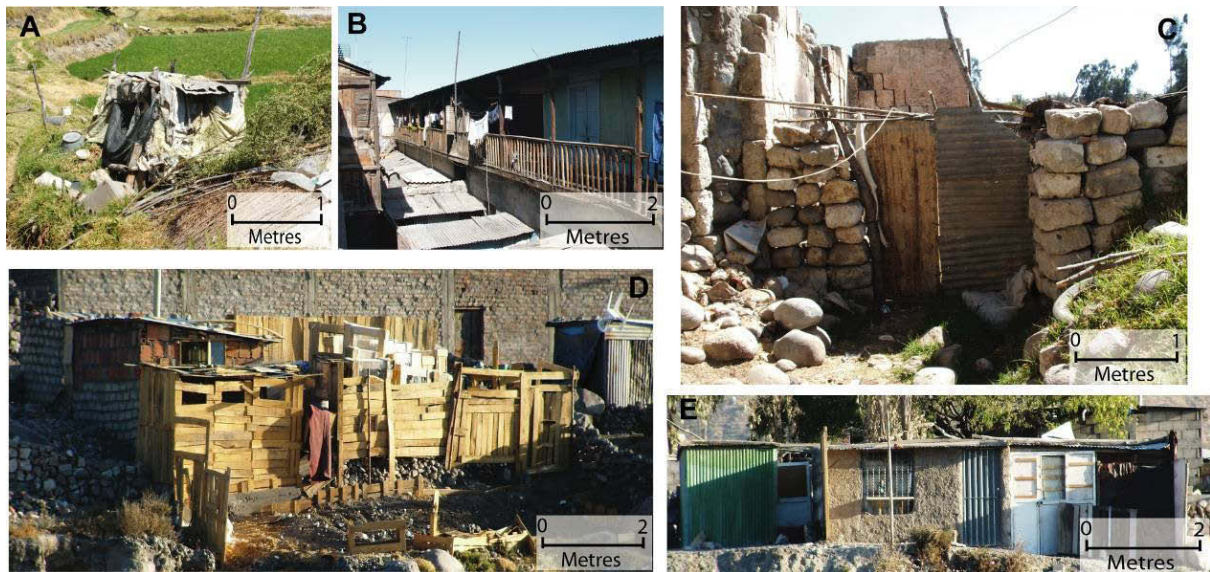


Figure 4.16: Makeshift buildings in Arequipa. *A:* Common shelter in agricultural land in the Río Chili Valley. *B:* A ‘shanty-town’ of homes located in Arequipa City Centre. *C:* A rural dwelling located on the eastern side (terrace t2) of the Río Chili Valley. *D* and *E:* Dwellings on the southern bank of Quebrada Huarangal.

Make-shift homes are common throughout agricultural land in Arequipa (Figure 4.16 A). These dwellings are made from plastic, wood, material and sticks, and whilst nobody lives in these shelters permanently they can be occupied throughout the day, providing shelter for owners while their animals graze. “Shanty-town” construction is also common in old abandoned buildings, in courtyards and on rooftops in the city centre (e.g. Figure 4.16 B) where large numbers of people live in a make-shift community. Another example of make-shift dwellings occupying existing buildings is shown in Figure 4.16 C where a rural dwelling located on the eastern side of the Río Chili Valley is constructed against one wall of an old and disused ignimbrite dwelling. The dwelling itself is constructed, un-engineered, from many different materials. These make-shift homes are common along the banks of, and in the channel of Quebrada Huarangal. Figure 4.16 (D and E) gives an indication of the material used in these dwellings, such as wood, ignimbrite blocks, stacked (without mortar) red clay bricks, adobe bricks, rock, and a corrugated iron roof held in place by rocks, nails and wood.

These homes often have no windows or sound strong doors, are without power (or illegally tapped) and running water. These buildings have no regard to construction principles and reinforcement (there are no reinforced columns or beams to supply structural support). They are considered the least sturdy of all constructions in Arequipa.

4.3.3 Physical properties of building materials

The survey undertaken of the building stock highlights the heterogeneous nature of the construction in Arequipa, where there is a range of construction types often within the same city block. Besides the type of construction, the quality of building materials and workmanship are factors which affect the vulnerability of a structure.

The National Service for Training for the Construction Industry (SENCICO) has developed regulations for building design and construction technologies that aim at improving quality and reducing cost; codes such as wooden structures (NTE E.010; SENCICO, 2006a), masonry (NTE E.070; SENCICO, 2006b), Adobe (NTE E.080, SENCICO, 1999), soils and foundations (NTE E.050, SENCICO, 1997), and reinforced concrete (NTE E.060 SENCICO, 2009) are some that have been enacted. However standards are poorly adhered to, and in practice many buildings do not comply with the building codes. For example, it has been estimated that between 50% and 80% of buildings in Lima do not comply with National Building Codes (Johansson et al., 2007). These authors suggested that the reason building codes are not adhered to is that obtaining the license for construction is very lengthy and costly, and municipalities are often understaffed. In many cases self construction is favoured, and the building is completed in a piecemeal fashion by the dweller without proper training.

To compare building materials used in Arequipa with Peruvian and world-wide Building Code Standards, samples of three main building materials (red clay brick, ignimbrite and concrete) were collected and some physical properties were determined (refer to Chapter 1 for methods). The properties of the samples will also be used to calculate the strength of buildings for determining the threshold at which the building is likely to fail in the event of a lahar or flood (Chapter 5).

4.3.3.1 Construction material samples

Red clay brick

Six different types of red clay bricks were collected in the field and subjected to various laboratory tests (Chapter 1). Only solid red clay bricks were assessed in terms of bulk density and velocity due to intentional voids present in other bricks.

The red clay brick (Figure 4.17) is comprised of reddish orange brown clay (derived from the weathered Pichu Pichu debris-avalanche deposit that outcrops east of the city) mixed with very fine light grey sand derived from volcanic ash. The raw clay fragment is a weathered clay loam soil, with a moderate fine-medium sub-angular blocky to granular texture. There are few very small to small stones and common roots. Coarse grains correspond to volcanic components including andesitic lava, pumice or ignimbrite fragments and free crystals such as feldspar, quartz and biotite.



Figure 4.17: Red clay brick sourced from handmade brick factory in Quebrada Huarangal, Arequipa.

The texture of the brick is very coarse with many natural voids due to either loss of organic material once fired, or air bubbles formed during the mixing process. Individual grains present in the sample are up to 1 cm in size with the majority of visible grains 1-2 mm in size. A darker red tinge is visible on the outer edge of the brick as a result of the firing process.

Ignimbrite

Ignimbrite blocks (Figure 4.18) were collected in the field and subjected to various geotechnical tests (Chapter 1). Two main quarries are utilised for ignimbrite building stone in Arequipa, with the majority of ignimbrite blocks quarried from the white unit of the 1.65-Ma-old Arequipa Airport Ignimbrite (AAI), a whitish lithic-rich massive lapilli-tuff (Paquereau Lebti et al., 2006).



Figure 4.18: Ignimbrite block sourced from a brick factory in Arequipa.

The non welded ignimbrite shows a vapour-phase facies, and is called ‘Sillar’ locally (Degg and Chester, 2005). The indurated block consists of a white to grey ashy matrix with grey to yellow fibrous pumice, which is fragile and highly vesiculated. Fragile weathered pumice, some of which are as large as 3 cm, can lead to large voids forming within the building material (see the bottom right corner of Figure 4.18). The brick is also rich in small lithic fragments (up to 25%) consisting of sub-rounded oxidised andesite fragments of free crystals of plagioclase, biotite, and magnetite and of glass (e.g. obsidian) (Vatin-Perignon et al., 1996). The texture of the brick is smooth and is reasonably hard apart from softer areas and pitting caused by the high vesiculated and fragile pumice.

Concrete block

Concrete blocks (Figure 4.19) were collected in the field and subjected to various laboratory tests (Chapter 1).



Figure 4.19: Concrete block sourced from a disused building in Arequipa. Note the concrete stucco facing to the bottom of the image.

The concrete block is a breccia, comprising a multitude of different clasts within a very fine cream matrix (a microbreccia itself), which also includes smaller broken fragments. Sub-rounded to angular basaltic-andesite, andesite, and dacite clasts are common with some ignimbrite, and red-clay brick fragments. Individual clasts are up to 5 cm across in length, with 0.5 cm clasts the most common. Small (<1 mm) holes are present throughout the block where smaller clasts have fallen out, organic material has been lost, or where the concrete has not been mixed thoroughly. The outer, non-cut, edge of the block is rough and uneven. The concrete stucco layer is medium to coarse-grained grey sand with a yellow painted outer layer.

4.3.3.2 Experimental results

Laboratory experiments (unconfined compressive strength, dry density, and velocity/porosity) were undertaken on red clay bricks, ignimbrite and concrete blocks from Arequipa (see methods discussed in Chapter 1). Whilst all bricks have broadly similar uses their properties differ in important respects (Table 4.5) due to the raw materials used and the method of manufacture.









Sample		Dimensions										Results of geotechnical laboratory tests							
ID	Type	Photo	Original dimensions				Cut dimensions						Bulk density		Velocity (m/s)				
			length (cm)	width (cm)	height (cm)	volume (cm ³)	Surface area (cm ²)	Other	length (cm)	width (cm)	height (cm)	volume (cm ³)	surface area (cm ²)	UCS (MPa)	Dry	Wet	Face 1	Face 2	Face 3
	Ignimbrite - AAI		30.0	20.0	15.0	9 000.0	2 700.0		10.0	10.0	10.0	1 000.0	600.0	12.00	1.3	1.9	1 714.0	1 648.0	1 738.0
B	Red clay brick "hueco"		29.0	15.0	14.0	6 090.0	2 102.0	8 squares at 5.8cm x 5.8cm each	14.5	14.0	11.0	2 233.0	1 033.0	12.00					
C	Red clay brick "hueco"		22.0	14.0	10.0	3 080.0	1 336.0	6 squares at 3cm x 3.8cm each	14.0	9.0	10.0	1 260.0	712.0	13.00					
D	Red clay brick "hueco"		29.0	28.0	11.0	8 932.0	2 878.0	3 squares at 5.9cm x 6.5cm each	10.0	10.0	10.0	1 000.0	600.0	10.00					
E	Red clay brick "ling kong"		23.0	14.0	6.5	2 093.0	1 125.0		10.0	9.0	6.5	585.0	427.0	1.00	1.6	2.0	2 132.0	1 954.0	1 972.0
F	Red clay brick "pandereta"		24.0	14.0	10.0	3 360.0	1 432.0	17 holes with 3.0cm diameter	10.0	10.0	10.0	1 000.0	600.0	17.00					
G	Red clay brick "pandereta"		21.0	14.0	10.0	2 940.0	1 288.0	6 holes with 2.5cm diameter	9.5	9.5	10.0	902.5	560.5	6.00					
H	Concrete brick "bloqueta"		28.0	15.0	10.0	4 200.0	1 700.0		10.0	10.0	10.5	1 050.0	620.0	9.00	1.9	2.1	991.0	1 136.0	1 189.0

Table 4.5: Properties of the main types of construction material present in Arequipa. All samples were collected in the field during the 2007 and 2008 field trips. B density and velocity tests were not undertaken on samples D-H because voids in the bricks render the tests invalid.

Unconfined compressive strength

By definition, the compressive strength of a material is that value of uniaxial compressive stress (the capacity of a material to withstand axially pushing forces) without lateral restraint, reached when the material fails completely (Table 4.5). The compressive strength of brick is an important mechanical characteristic for structural applications. The quality of the bricks depends on the material that forms them, and specific materials have distinct geochemical properties which make them suitable as raw materials for industrial bricks. Most bricks in Peru however are not produced in factories, and thus hand-made bricks do not have the appropriate resistance according with national technical standards (Zavala et al., 2004).

The compressive strength of building material tested from Arequipa are below the average brick compressive strength from various building codes including British (BS EN 771; British Standards Institute, 1999, 2003), Australian/ New Zealand (AS/NZ 4455; Standards New Zealand, 2008), and French (NFP12-021/ NF EN 771-1; La norme NF, 2005) (Figure 4.20). Peruvian building codes could not be compared with the results at this stage as compressive strengths are only given for masonry units (brick and mortar) not just brick.

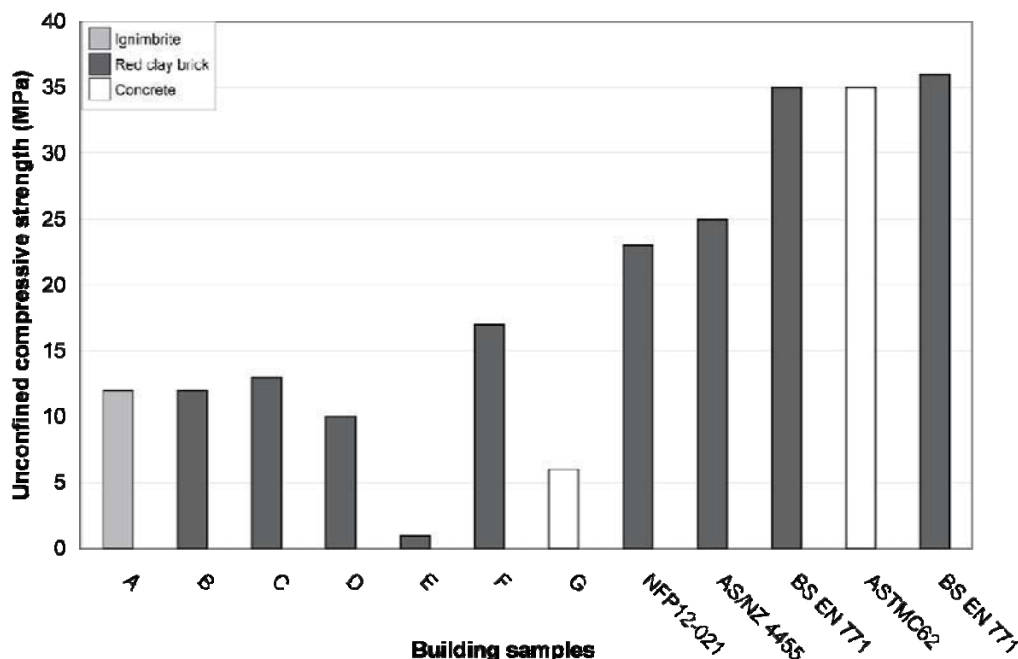


Figure 4.20: Unconfined compressive strength of samples of building material (red clay brick, ignimbrite and concrete block) collected in Arequipa. The strength of these building materials is less than the normal requirements stipulated in building codes from other countries. BS-EN-771 – British Building Code, ASTM C62 – American Building Code, AS/NZ 4455 Australian/New Zealand Building Code and NFP12-021 – French Building Code.

Clay bricks can have strengths up to 100 MPa but strengths between 20 and 40 MPa are generally sufficient for domestic buildings; the strengths of the Arequipa samples were between 1 and 17 MPa. The result for brick type E is very low, and perhaps not truly representative of this type of brick. Concrete blocks generally have a compressive strength of between 2.8 to 35 MPa, with ignimbrite blocks (stone blocks) generally possessing similar compressive strength requirements as concrete (Hendry, 2001). The concrete sample from Arequipa was tested at 6 MPa, whereas the ignimbrite sample was 12 MPa; both in low to mid range of values. Figure 4.20 indicates that the building materials collected and analysed from Arequipa do have low compressive strengths when comparing to building codes from other countries. Many more samples would have to be collected and tested to make a solid conclusion about the strength of bricks in Arequipa.

In terms of the bricks internal structure, cracking was observed along the ridgelines, but also due to the internal structure – pockets of clay and air. These pockets are the result of poor manufacturing, and would certainly influence the low compressive strength of the analysed materials.

Bulk density and porosity

The density and porosity of building materials are important for determining their use and durability during construction. Highly porous bricks are not as durable those with lower porosity and lighter density. In addition they can facilitate the absorption of water; highly porous bricks may remove water from the mortar preventing complete hydration of the cement (Hendry, 2001). Bulk density was calculated for the Arequipa building materials (Table 4.5 and Figure 4.21), the methods of which are described in Chapter 1. The porosity of the samples were calculated using the results obtained during hydrostatic weighing.

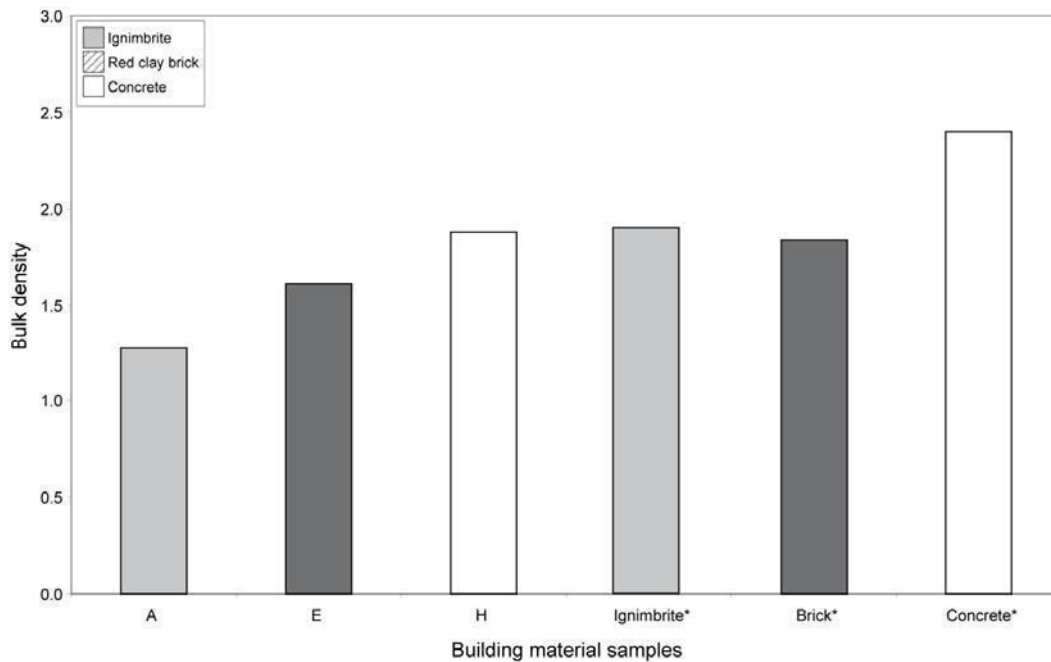


Figure 4.21: Bulk density of sample A (ignimbrite), E (red clay brick) and H (concrete). Note: samples indicated by * are typical apparent density values of the building materials.

Building materials in Arequipa have a much lower bulk density than the typical values of the same material (Figure 4.21). The typical bulk density of ignimbrite (1.8 – 2.5) is much higher than what was calculated for the Arequipa sample, 1.27. Similarly, the calculated apparent density of concrete and red clay brick was 1.61 and 1.88, compared to 1.75-2.5 and 1.4 – 2.4, respectively.

The reason for much lower bulk density values calculated for Arequipa is due to the samples being a lot less dense than ‘normal’ samples of the similar material. As mentioned previously in section 4.2.3.1, voids were clearly visible in all samples, due to poor manufacturing in the cases of the red clay brick and concrete block. However, the calculated porosities for the red clay brick and concrete block were moderate at 9.8% and 8.4% respectively. The non welded vapour-phase facies ignimbrite has a low bulk density because it contains mostly (indurated) ash and pumice with a low lithic content. A porosity of 31.3% was calculated for this sample, which is considered as a very high porosity (Prentice, 1990). The porosity of the ignimbrite brick is consistent with the porosity values Paquereau-Lebti (2006) measured for the same ignimbrite; the Arequipa Airport Ignimbrite (AAI).

Velocity

Ultrasonic Pulse Velocity (UPV) data can be used along with the strength data to estimate the engineering properties of rocks, and thus was used to evaluate the samples taken in Arequipa (Figure 4.22). Ultrasonic scanning is a non-destructive evaluation test to qualitatively assess the homogeneity and integrity of a material. UPV utilises measurements of compression waves using a high-energy pulse-receiver on the driving side and a 2-channel digital storage oscilloscope on the receiving side for the measurement of travel time (see Chapter 1 for a more detailed explanation of the methods).

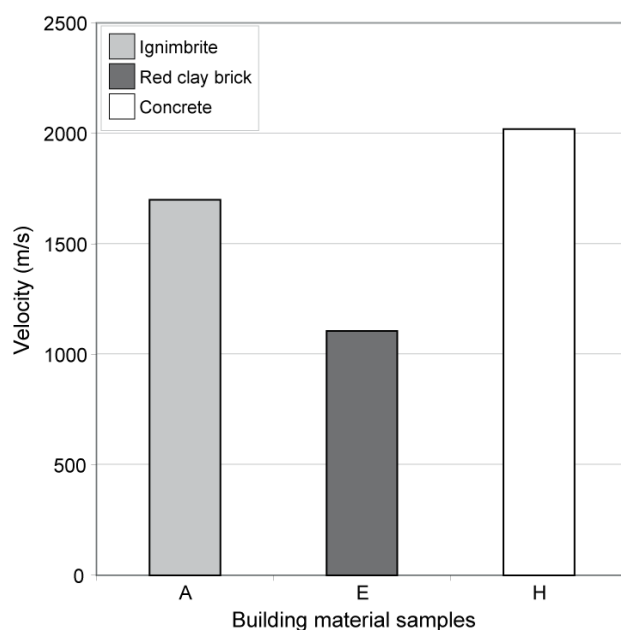


Figure 4.22: Ultrasonic pulse velocity (UPV) for the Arequipa building material samples.

The ultrasonic pulse velocity depends on the density and elastic properties of the material being tested. Cracks, voids and other defects will cause variations in the measured pulse velocity. For example, the diffraction of a wave pulse around an internal air void will cause an increase in the time of propagation for a path through the void centre, and the apparent velocity will decrease. However, only large cracks and voids, generally larger than the transducer contact face, will cause measurable reduction in velocity, which is the case for the brick samples.

As with the other geotechnical tests undertaken on the Arequipa building materials, the values obtained for this experiment are lower than the 'typical' values. Normally for concrete, values of >4000 m/s are considered excellent quality, whereas <3000 m/s is considered a poor

quality concrete with the loss of integrity (Ben-Zeitun, 1986). To compare, the Arequipa concrete sample only measures 1180 m/s. Ignimbrite and clay bricks should have velocities >2500 m/s, whereas the Arequipa samples have velocities of 2019 m/s and 1700 m/s, respectively. These low velocities indicate the Arequipa materials are of low quality and contain many voids, as evidenced in previous sections.

4.3.3.3 Summary

Geotechnical experiments undertaken on the samples of Arequipa building materials indicate that they are of a quality lower than world-wide building code requirements. The samples not only have low to moderate compressive strengths, they have a low specific density and contain many voids, thereby compromising the structural integrity of the brick.

Although the aforementioned tests give some indication to the strength properties of the building material in Arequipa, it is not accurately representative of the strength of a wall or building. This is because the building acts as a complete structural system, which takes into account the strength and quality of the mortar; the number of openings and their placement; and reinforcement type, quality and placement; just a few of the variables to take into account when calculating the strength of a wall or building. In addition, many more brick samples would have to be collected and tested to make a solid conclusion about the strength and condition of bricks. However, the values determined do provide an indication into the type and quality of building materials present in Arequipa.

4.3.4 Classification of building types in Arequipa

Using methods adapted from Chevillot (2000) and others (Pomonis et al. 1999; Kelman, 2002; Spence et al. 2004a,b, 2005a,b; Baxter et al. 2005) building surveys of the two study areas in Arequipa were conducted externally (at street level) and where permitted, within the boundaries of the land-owners property (further details can be found in Chapter 1). Initially nine construction types were identified (Table 4.6, Figures 4.23-24) and defined according to: the dominant building material, number of floors, building reinforcement, roof type and style, opening type and quantity, and overall building structural integrity. The wall condition and its load bearing capacity could not be assessed with in-situ testing, and houses with visible signs of disrepair were quantified instead. These building types will be classified and ranked

according to their strength in section 4.2.5. Further photographs of the building types can be found in Appendix B






Type A	
<p>Structure: Confined masonry Masonry panels, typically 1-2m in each direction. Wall material generally consists of perforated clay bricks or concrete blocks that are un-reinforced. Cast-in-situ reinforced concrete frames (horizontal and vertical). Generally reinforced with four No.3 (9mm) bars and traverse ties of heavy-gauge wire.</p> <p>Height: 1-3 storeys.</p> <p>Floor: Commonly in-situ filler block floors.</p> <p>Roof: Roof is mostly flat or pitched built of reinforced concrete masonry composite slabs.</p> <p>Openings: Large glass windows throughout the building, often with aluminium framing and lower windows secured with steel bars. Doors are generally solid and wooden, with steel security screen/bars.</p> <p>Maintenance: Some covered with stucco which may increase the strength and stiffness. Overall building is well finished with paint, fencing and security. The building and surrounds are well-kept.</p>	
Type B	
<p>Structure: Confined masonry The same structural components as Type A buildings, however the structure <u>has not been completed</u> (even though occupied). Often the ground storey is lived in but not completed to the same standard as Type A buildings; structure built slowly one storey at a time. With incremental building the vulnerability of the structure increases due to inadequate connections with the existing structure, as well as asymmetrical configuration.</p> <p>Height: 1-3 storeys.</p> <p>Floor: Same as A.</p> <p>Roof: Same as A</p> <p>Openings: Same as A</p> <p>Maintenance: The overall evolution of the structure is positive and the house is well finished with paint, fencing, and security. The building and the surrounds are well-kept.</p>	
Type C	
<p>Structure: Confined masonry Same structural components as Type A buildings, however the structure <u>has not been completed</u> (even though occupied). Ground floor often painted with subsequent storeys unpainted.</p> <p>Height: 2-4 storeys. Vertical extension unfinished and some material that has been used are unstable.</p> <p>Floor: Same as A.</p> <p>Roof: Same as A, however some may be constructed with corrugated iron.</p> <p>Openings: Same as A.</p> <p>Maintenance: Overall long-term evolution will be positive. Environment and building not well kept. Body of building fenced.</p>	
Type D	
<p>Structure: Confined masonry Same structural components as Type A buildings, however building characteristics similar to Type B with incremental and <u>unfinished</u> construction practices.</p> <p>Height: 2-4 storeys. Vertical extension unfinished and some material that has been used are unstable.</p> <p>Floor: Same as A</p> <p>Roof: Same as A.</p> <p>Openings: Same as A.</p> <p>Maintenance: The overall evolution of the structure is positive and the house is well finished with paint, fencing, and security. The building and the surrounds are well-kept.</p>	
Type E	
<p>Structure: Confined masonry Same structural components as Type A buildings, however, building is <u>typically colonial</u> style and constructed from ignimbrite brick and/or adobe.</p> <p>Height: 1-2 storeys.</p> <p>Floor: Same as A.</p> <p>Roof: Same as A.</p> <p>Openings: Same as A, however windows tend to be smaller than newer houses constructed in Types A-C.</p> <p>Maintenance: The upkeep of the building is poor and can appear 'shabby'. Parts of the building are likely to be unstable. The overall evolution of the structure is positive and the house is well finished with paint, fencing, and security. The building and the surrounds are well-kept.</p>	

Table 4.6: shows classification of buildings in Arequipa according to the main structural components and overall appearance (adapted from Chevillot, 2000). In general, structural condition worsens from Type A to Type I.





Type F		
<i>Structure:</i>	Confined masonry The same structural components as Type A buildings, however the structure is <u>degraded and unstable</u> . The building is often unfinished or constructed poorly, or has been damaged (e.g. earthquake) and not remedied.	
<i>Height:</i>	1-2 storeys.	
<i>Floor:</i>	Same as A.	
<i>Roof:</i>	Roofing is the same as Type A or constructed of corrugated iron. The overall quality is poorer than that of Types A-C. The corrugated iron roofing is often held in place by objects such as rocks and pieces of wood if not nailed in place.	
<i>Openings:</i>	Windows are often small and few with aluminium or wood framing. It is not uncommon for the windows to have no glass or to be boarded up. Security bars not as common as buildings of Types A-C. Doors are constructed of mainly tin/aluminium, and are somewhat flimsy and with or without security.	
<i>Maintenance:</i>	Ground floor and 1st storey constructed from brick with no stucco or paint. Overall long-term evolution of the structure will be negative, and the environment and building are not well kept.	
Type G		
<i>Structure:</i>	Unconfined masonry The building generally comprise of an old base constructed from stones and ignimbrite. The walls are constructed from ignimbrite, brick or adobe and are not confined by either reinforced horizontal or vertical cast-in-situ concrete, and in many cases appear quite unstable.	
<i>Height:</i>	One storey.	
<i>Floor:</i>	Same as A, or no floor.	
<i>Roof:</i>	Typically constructed with corrugated iron placed on wooden rafters and held in place by rocks, bricks, wood etc. In some cases they are nailed into place.	
<i>Openings:</i>	Openings (however it is not uncommon <u>for there to be no windows</u>) are the same as F. Ground floor and 1st storey constructed from brick with no stucco or paint.	
<i>Maintenance:</i>	Overall long-term evolution of the structure will be negative, and the environment and building are not well kept.	
Type H		
<i>Structure:</i>	Make-shift housing Building construction a composition of heterogeneous objects, such as bricks (red, ignimbrite, and adobe), rocks, plastic, wood, straw, iron etc. Little to no structural integrity.	
<i>Height:</i>	One storey.	
<i>Floor:</i>	No constructed floor (ground, plastic etc.).	
<i>Roof:</i>	Roof is constructed out of any material available.	
<i>Openings:</i>	No windows or doors. Often a piece of fabric or plastic as a door.	
<i>Maintenance:</i>	Slum environment with construction mainly by 'illegal squatters'. Overall long-term evolution will be negative. Environment and building not well kept.	
Type I		
<i>Structure:</i>	Unconfined masonry Abandoned and destroyed housing.	
<i>Height:</i>	1-3 storeys.	
<i>Floor:</i>	All types if floor still exists.	
<i>Roof:</i>	Typically mostly flat or pitched built of reinforced concrete masonry composite slabs if roof still exists.	
<i>Openings:</i>	Variable, often with no glass remaining in windows.	
<i>Maintenance:</i>	Some buildings destroyed in the 2001 earthquake and never rebuilt or cleared. Unsafe, unstable, common with squatters.	

Table 4.6: continued.

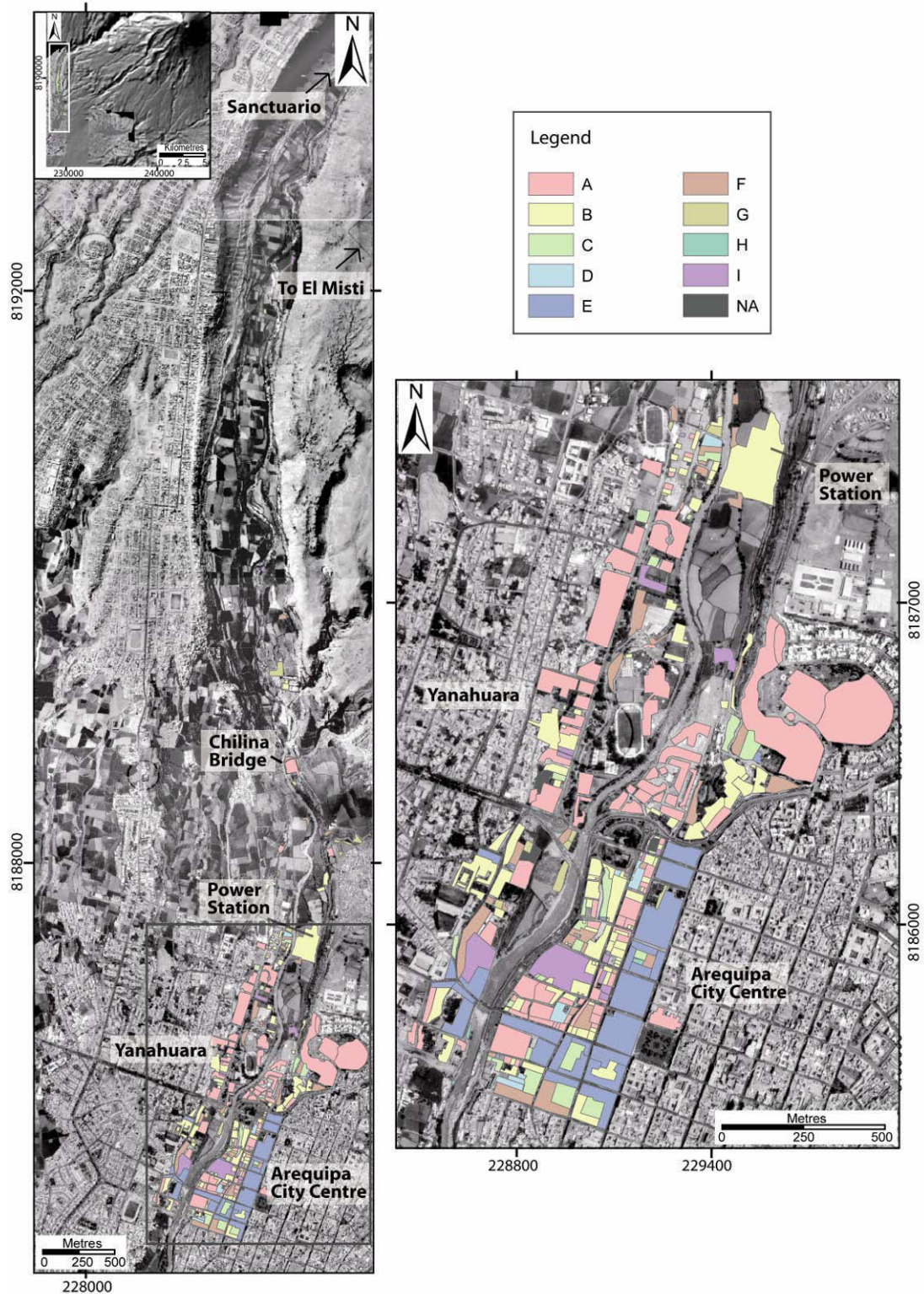


Figure 4.23: This map shows the predominant building types in the Río Chili valley from the Quiñones Bridge up to opening of the canyon. **A:** Close-up map of the study area from the Quiñones Bridge, southern boundary of the city (229410, 8187365), to the entrance of the canyon (232116, 8194785). This valley is heavily cultivated (valuable arable crops) and in close proximity to the EGASA main power station, clubs, factories and some housing. Housing in cultivated areas is usually confined to rural type dwellings. Within this area, the building types are largely for commercial, industrial and residential use. **B:** Close-up map of the predominant building types in the city centre.

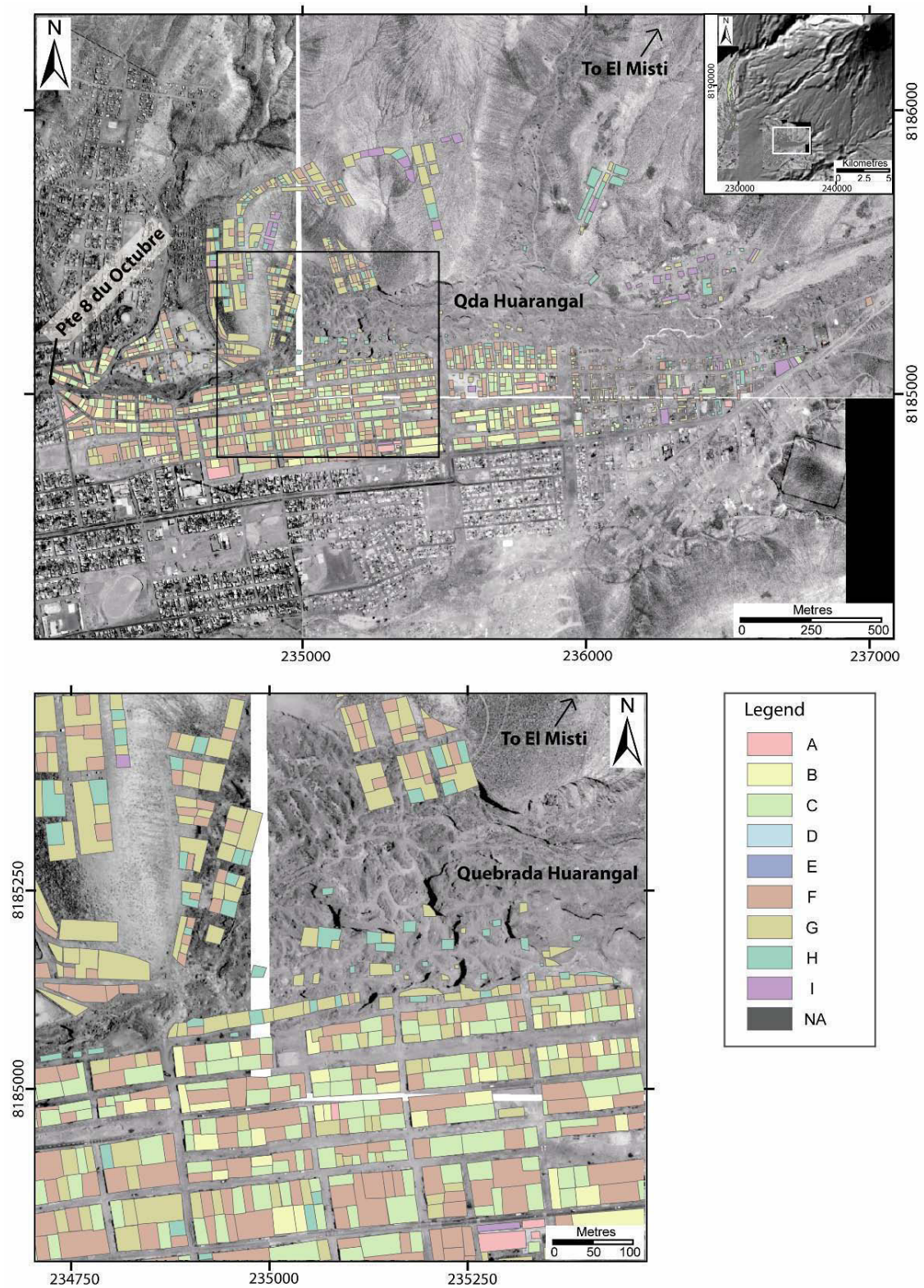


Figure 4.24: This map shows the predominant building types on the Quebrada Huarangal fan from the Bridge 'Pte. 8 de Octubre' in the west (233931, 8184658) to a Quarry in the east (236790, 8185007) of the study area. The second image is a close up of an area of the fan. Building types are not so varied within this study area, with some industry (e.g. mining, automotive mechanics, factories) and commercial stores, which also serve as dwellings. The most predominant building types in this area are private dwellings of type F.

4.3.4.1 Observations of construction types in Arequipa

Río Chili Valley

In the study area most new construction consists of unreinforced masonry panels (perforated red brick and mortar) with cast-in-situ reinforced concrete frames (horizontal and vertical) and flat or pitched reinforced concrete slab roofs – a system called confined masonry construction. Large glass windows are throughout with aluminium or wood framing and often secured across the glass with steel bars. Doors are solid and wooden with steel security screen/bars. Type A buildings represented 38% of buildings surveyed (Figure 4.25). Conversely, Type G construction comprises old stone/ignimbrite base with unreinforced masonry panels (ignimbrite, brick or adobe, with poor quality mortar). The walls are not confined by either reinforced horizontal or vertical cast-in-situ concrete, and in most cases appear unstable. Wooden rafters support corrugated iron roofs, secured with heavy objects such as rocks. These buildings represent 3% of those surveyed, and more commonly situated on the lower terraces (t1, t1' and t2) of the Río Chili Valley and associated with agricultural lifestyle blocks.

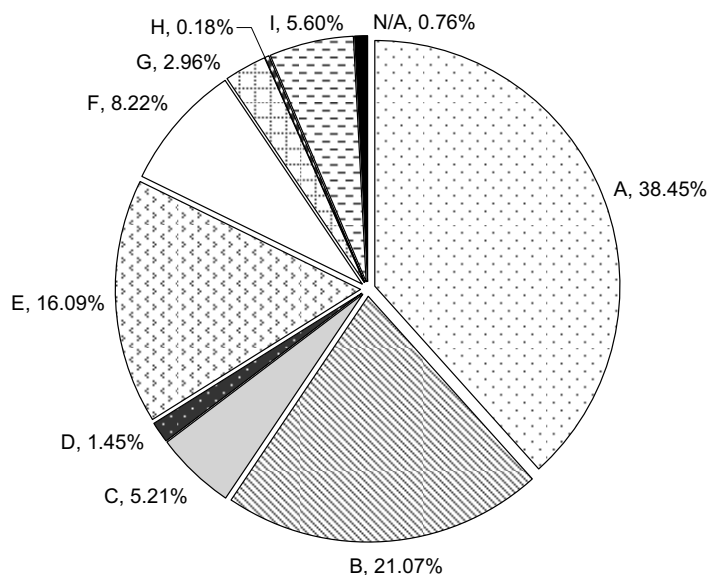


Figure 4.25: Building types within the Río Chili Valley study area. The letter corresponds to the building type, and the second is the percentage of building types within the study area.

Less than 50% of the population surveyed resides in dwellings less resistant than those of Type C. However, the majority of those are situated in more hazardous (e.g. Río Chili lower terraces) areas. Housing of poorer quality is often situated in the most vulnerable areas upstream of the city and within the river channels, the flood-prone terrace t0 for example

(apart from type A housing located on the confluence of the Río Chili and Quebrada San Lazaro).

Quebrada Huarangal fan

Building types present in the Quebrada Huarangal volcaniclastic fan differ to those in Río Chili Valley. The most popular housing type in this study is Type F (33%) – confined red brick masonry with a flat concrete slab/red brick roof and large aluminium framed windows (Figure 4.26). These dwellings are often constructed in a piece meal fashion, where often the bottom floor is finished but further storeys are unfinished and added slowly depending on the demand of the family and finances.

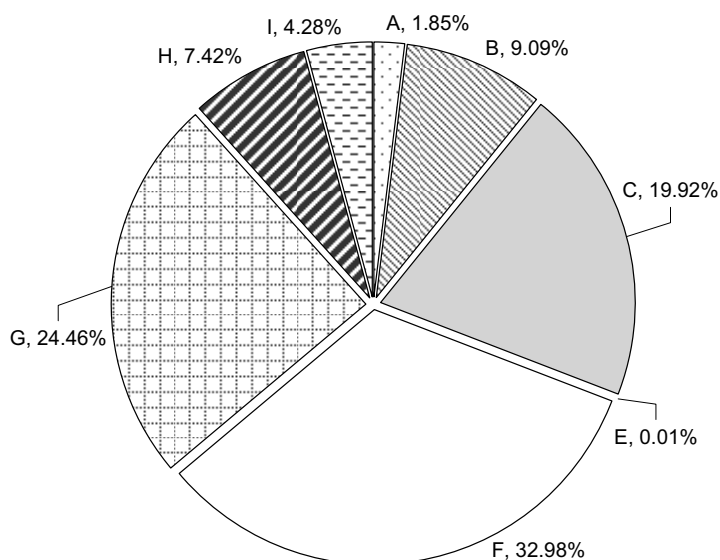


Figure 4.26: Building types within the Quebrada Huarangal fan. The letter corresponds to the building type, and the second is the percentage of building types within the study area.

Also in contrast to the Río Chili Valley building stock, building type A only corresponds to <2% of buildings surveyed. Unconfined masonry (Building Type G) is also more prevalent in Quebrada Huarangal, 25 % compared to 3% on the Río Chili terraces. Unconfined masonry – constructed with or without mortar – is common in the poorer areas on the Huarangal fan. Buildings are being constructed rapidly within the Quebrada channel, the majority of which corresponds to Building Type G, one of the poorest quality construction located in one of the most vulnerable localities for future lahars and flash floods. Approximately 70% of the population in this area lives in buildings less resistant than Type C.

4.3.5 Vulnerability of building types in Arequipa

Up until this point building descriptions were purely based on face value, and building types A to I have not been ranked in order according to structural integrity. However, the influence of different structural components needs to be taken into consideration in order to determine the most vulnerable building type. Using methods adapted from Vargas et al. (2010b) and others (Prevot, 2009; Palhol, 2008; Spence et al. 2004a,b, 2005a,b; Baxter et al. 2005; Kelman, 2002; Pomonis et al. 1999) building types defined in Table 4.7 were classified and ranked according to frame materials, wall materials, roof types, roof material, storeys, proportion of windows, type of window frames and foundation type. Coefficients, where 0 is not vulnerable/good quality and 1 is very vulnerable/bad quality, were assigned to each building feature, and sub-feature. The values were normalised to account for subjectivity in assigning the values, normalised minimum and maximum values were obtained from which the mean value of all the criteria was calculated. These values also allowed the ranking of buildings from least to most vulnerable. Reasoning for the assignment of the coefficient values are based on a literature review including Kelman, 2002, Spence et al. 2004a,b, 2005a,b; Baxter et al. 2005 to name a few, and is rationalised in Appendix C.

Criteria	Class									Coefficient 0 = very good, 1 = very bad
	Type A	Type B	Type C	Type D	Type E	Type F	Type G	Type H	Type I	
Frame Materials										
1. Steel										0.1
2. Concrete - Reinforced Cement Concrete (RCC)	0.1	0.1	0.1	0.1	0.1	0.1				0.1
3. Wood										0.1
4. No frame							1.0	1.0		1.0
Wall materials										
1. Concrete (RCC)										0.1
2. Concrete	0.3	0.3	0.3	0.3		0.3				0.3
3. Bricks (red clay)	0.4	0.4	0.4	0.4		0.4	0.4			0.4
4. Ignimbrite (thick walls)					0.5					0.5
5. Ignimbrite with no mortar							0.8	0.8		0.8
6. Adobe					0.7					0.7
7. Adobe with no mortar							1.0	1.0		1.0
8. Wood								0.7		0.7
9. Stone with no mortar							1.0	1.0		1.0
10. Makeshift (plastic, stone, others)								1.0		1.0
Roof Type										
1. Flat	0.2	0.2	0.2	0.2	0.2	0.2	0.2	0.2		0.2
2. Pitched	0.4	0.4	0.4							0.4
Roof material (weight)										
1. Concrete slab	0.1	0.1	0.1	0.1						0.1
2. Brick and concrete	0.2	0.2	0.2	0.2		0.2				0.2
3. Tile	0.2	0.2	0.2		0.2	0.2	0.2			0.2
4. Wood					0.3		0.4	0.4		0.4
5. Makeshift materials							0.8	0.8		0.8

Table 4.7: Vulnerability coefficients assigned to various building components, such as pitched roof, for the purpose of determining the most vulnerable buildings in Arequipa (adapted from Vargas et al., 2010b; Prévot, 2009 and Palhol, 2008).

Storeys									
1. One story	0.7	0.7	0.7		0.7	0.7	0.7	0.7	0.7
2. 2 stories	0.5	0.5	0.5		0.5	0.5			0.5
3. =>3 stories	0.1	0.1	0.1	0.1					0.1
Proportion of windows (1 -2^t floors)									
1. 0-5%									0.1
2. 5-20%					0.3	0.3	0.3	0.3	0.3
3. 20-50%	0.5	0.5	0.5	0.5					0.5
4. >50%								0.7	0.7
Type of window									
1. Aluminium frame	0.2	0.2	0.2	0.2	0.2	0.2			0.2
2. Wood frame					0.6	0.6	0.6		0.6
Foundations and depth									
1. Piled				0.1					0.1
2. Solid wall	0.3	0.3	0.3	0.3	0.3	0.3			0.3
3. Slab	0.4	0.4	0.4						0.4
4. Fill					0.6	0.6			0.6
5. No foundation							1.0	1.0	1.0
Totals									
Total maximum	2.90	2.90	2.90	2.00	3.50	3.10	5.60	5.40	
Total maximum normalised	0.36	0.36	0.36	0.25	0.44	0.39	0.70	0.68	
Total minimum	1.80	1.80	1.80	1.60	2.30	2.10	4.40	4.30	
Total minimum normalised	0.23	0.23	0.23	0.20	0.29	0.26	0.55	0.54	
Total mean	2.46	2.46	2.46	1.90	3.04	2.73	5.28	5.12	
Total mean normalised	0.31	0.31	0.31	0.24	0.38	0.34	0.66	0.64	
Rank	2	2	2	1	4	3	6	5	

Table 4.7: Continued.

Type D buildings came out as the least vulnerable building to lahars and floods, followed by Types A, B and C with the same vulnerability index. Type G buildings are the most vulnerable, followed closely by type H buildings. Type E buildings are also more vulnerable to lahars and flash floods than type F buildings. Confined masonry buildings were the least vulnerable (e.g. Type A), whereas unconfined and buildings without mortar were more vulnerable. Type H buildings (make-shift) were less vulnerable than Type G because there were less structural components in the vulnerability assessment and therefore no coefficients for certain building criteria could be added to the calculation.

4.3.5.1 Vulnerability in the Río Chili Valley

Figure 4.27 shows the vulnerability of buildings within the Río Chili Valley study area. The most vulnerable buildings are located within the downtown city area, whereas the least vulnerable buildings are located towards the north of the study area (north of the yellow star in Figure 4.27) and also adjacent to the Río Chili Valley. There are a few more vulnerable buildings located adjacent to the river (e.g. an adobe building with a vulnerability value of 0.66, indicated by the yellow star).

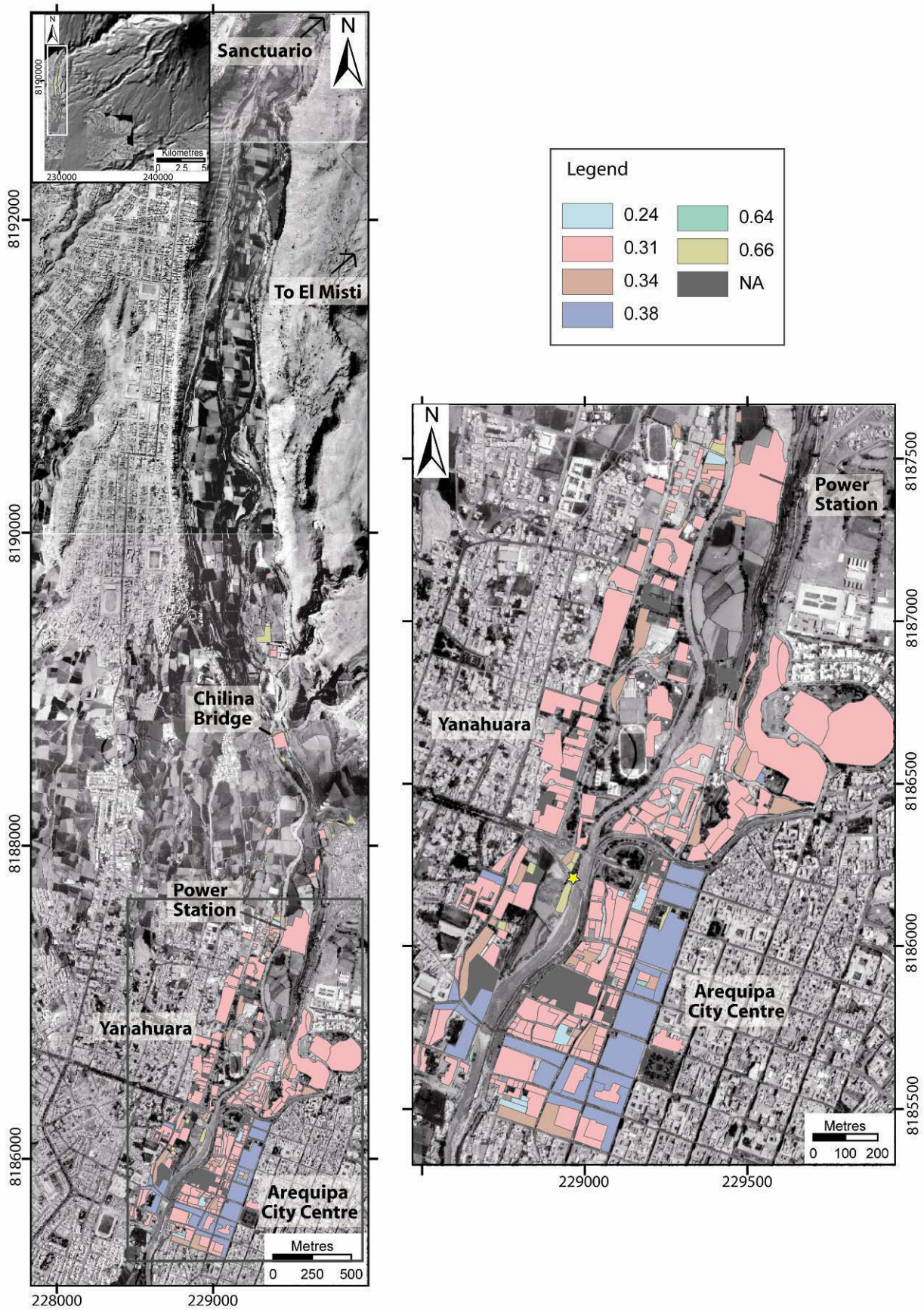


Figure 4.27: Vulnerability map for buildings in the Río Chili Valley, where 0 is the least susceptible and 1 is the most.

The majority of buildings (64%, Figure 4.28) within this study area has a vulnerability of 0.31 and corresponds to building types A to C. More than 15% of buildings (Type E) have a vulnerability index of 0.38, with less than 1% of buildings (Type H) corresponding to a 0.64 vulnerability value.

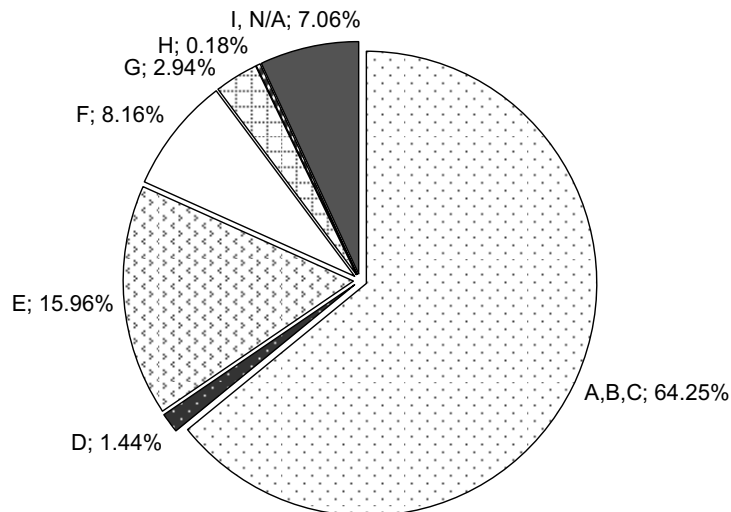


Figure 4.28: Distribution of vulnerable building types in the Río Chili Valley.

4.3.5.2 Vulnerability in the Quebrada Huarangal fan area

Vulnerability of buildings to lahars and floods for the Quebrada Huarangal fan is indicated on Figure 4.29. Buildings within this study are by large more vulnerable to those located in Río Chili Valley. Alarmingly, the most vulnerable buildings are located within close proximity to, or within, the Quebrada channel (vulnerability index 0.64 and 0.66). The most vulnerable buildings are also located primarily to the north of the study area. On the southern side of the Quebrada the buildings are primarily a mix of 0.31 and 0.34 vulnerability values.

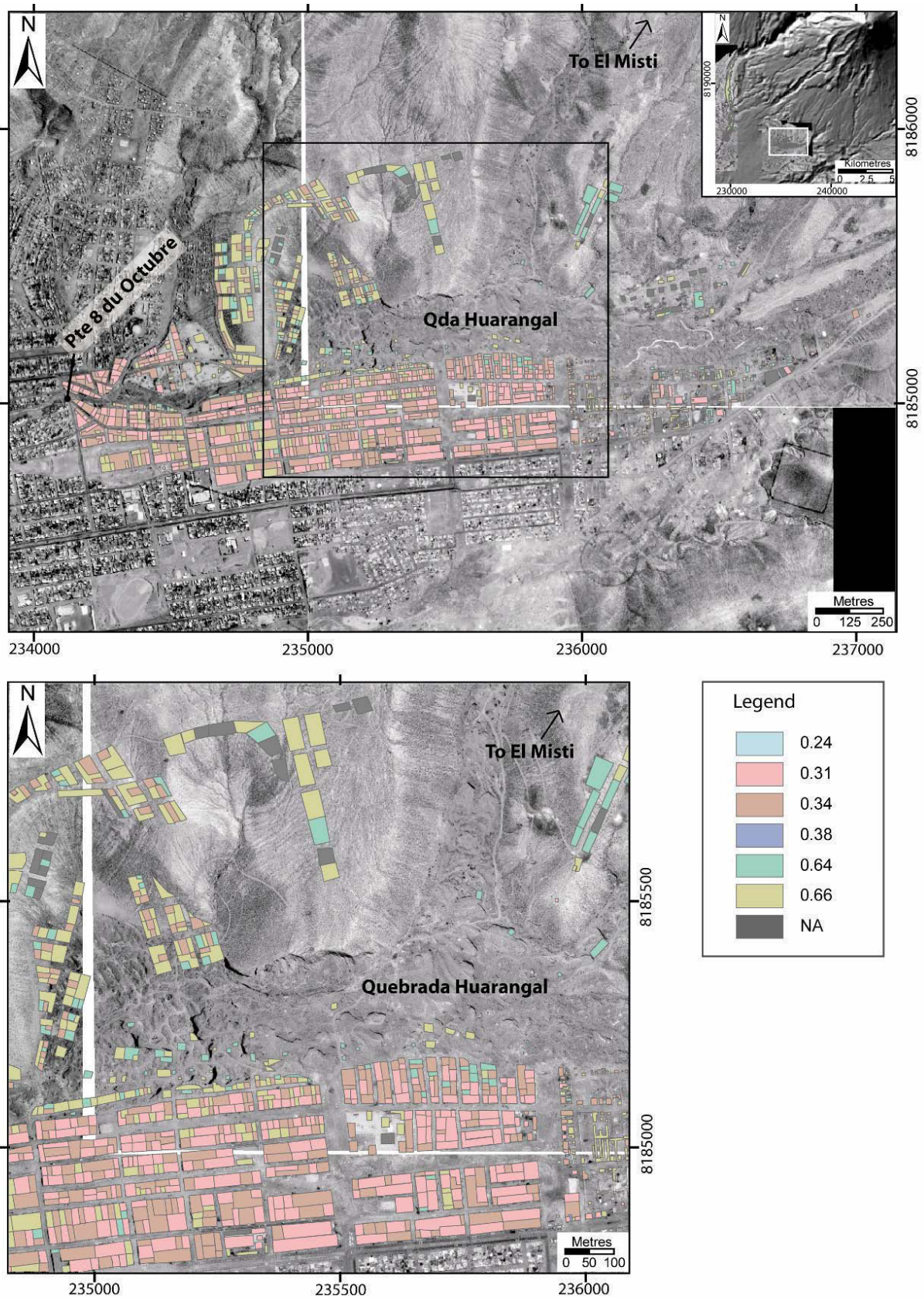


Figure 4.29: Vulnerability map for buildings in the Quebrada Huarangal study area, where 0 is the least susceptible and 1 is the most.

There is an almost equal distribution between buildings with a vulnerability of 0.31 (type A, B and C), 0.34 (type F) and 0.66 (type G), representing just over three quarters of the buildings present (Figure 4.30). The other quarter of vulnerability types is made up of house types D (0.01%), I, N/A (4%) and H (7%).

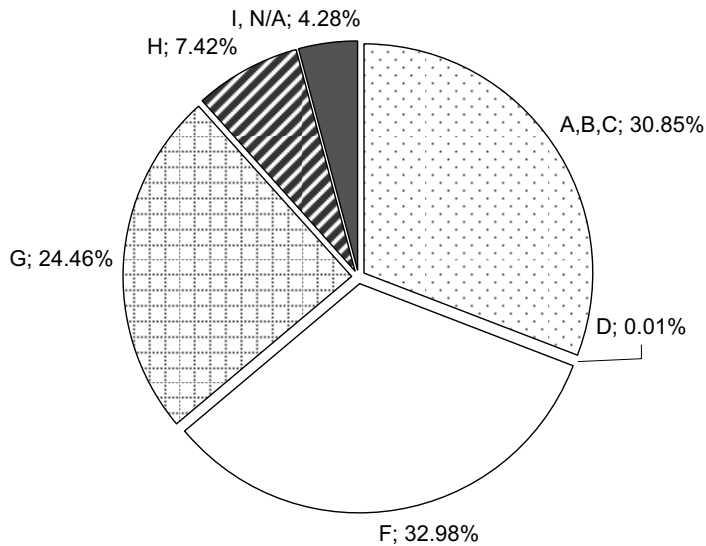


Figure 4.30: Distribution of vulnerable building types on the Quebrada Huarangal fan.

As discussed above, the contrast between building types, heterogeneity, and therefore vulnerability index can be seen quite clearly between the two study areas. This could be related to the type of population living in the areas and their socio-economic standing; people living in the Río Chili Valley are generally from wealthier backgrounds than those who inhabit Huarangal. This is reflected in the type and quality of construction.

4.4 Vulnerability of building types and land use in Arequipa

In order to get one value to determine the vulnerability of the buildings in Arequipa, the land-use vulnerability index was combined with the building vulnerability index to give a single vulnerability value. This value represents the vulnerability of the building combined with the influence of the land use on the vulnerability. The method for combining these values has been discussed in Chapter 1, and the results can be seen in Table 4.8, and Figures 4.31 and 4.32.

Building Type	A		B		C		D		E		F		G		H		I	
	Sum of A-land-use	Mean A-land-use	Sum of B-land-use	Mean B-land-use	Sum of C-land-use	Mean C-land-use	Sum of D-land-use	Mean D-land-use	Sum of E-land-use	Mean E-land-use	Sum of F-land-use	Mean F-land-use	Sum of G-land-use	Mean G-land-use	Sum of H-land-use	Mean H-land-use	Sum of I-land-use	Mean I-land-use
1	0.59	0.30	0.59	0.30	0.59	0.30	0.52	0.26	0.66	0.33	0.62	0.31	0.94	0.47	0.92	0.46	0.28	0.14
2	0.68	0.34	0.68	0.34	0.68	0.34	0.61	0.31	0.75	0.38	0.71	0.36	1.03	0.52	1.01	0.51	0.37	0.19
3	0.76	0.38	0.76	0.38	0.76	0.38	0.69	0.35	0.83	0.42	0.79	0.40	1.11	0.56	1.09	0.55	0.45	0.23
4	0.75	0.38	0.75	0.38	0.75	0.38	0.68	0.34	0.82	0.41	0.78	0.39	1.10	0.55	1.08	0.54	0.44	0.22
5	1.19	0.60	1.19	0.60	1.19	0.60	1.12	0.56	1.26	0.63	1.22	0.61	1.54	0.77	1.52	0.76	0.88	0.44
6	1.10	0.55	1.10	0.55	1.10	0.55	1.03	0.52	1.17	0.59	1.13	0.57	1.45	0.73	1.43	0.72	0.79	0.40
7	0.87	0.44	0.87	0.44	0.87	0.44	0.80	0.40	0.94	0.47	0.90	0.45	1.22	0.61	1.20	0.60	0.56	0.28
8	0.84	0.42	0.84	0.42	0.84	0.42	0.77	0.39	0.91	0.46	0.87	0.44	1.19	0.60	1.17	0.59	0.53	0.27
9	0.65	0.33	0.65	0.33	0.65	0.33	0.58	0.29	0.72	0.36	0.68	0.34	1.00	0.50	0.98	0.49	0.34	0.17
10	0.71	0.36	0.71	0.36	0.71	0.36	0.64	0.32	0.78	0.39	0.74	0.37	1.06	0.53	1.04	0.52	0.40	0.20
11	0.65	0.33	0.65	0.33	0.65	0.33	0.58	0.29	0.72	0.36	0.68	0.34	1.00	0.50	0.98	0.49	0.34	0.17
12	0.65	0.33	0.65	0.33	0.65	0.33	0.58	0.29	0.72	0.36	0.68	0.34	1.00	0.50	0.98	0.49	0.34	0.17
13	0.85	0.43	0.85	0.43	0.85	0.43	0.78	0.39	0.92	0.46	0.88	0.44	1.20	0.60	1.18	0.59	0.54	0.27
14	0.74	0.37	0.74	0.37	0.74	0.37	0.67	0.34	0.81	0.41	0.77	0.39	1.09	0.55	1.07	0.54	0.43	0.22
15	0.50	0.25	0.50	0.25	0.50	0.25	0.43	0.22	0.57	0.29	0.53	0.27	0.85	0.43	0.83	0.42	0.19	0.10
16	0.79	0.40	0.79	0.40	0.79	0.40	0.72	0.36	0.86	0.43	0.82	0.41	1.14	0.57	1.12	0.56	0.48	0.24
17	0.75	0.38	0.75	0.38	0.75	0.38	0.68	0.34	0.82	0.41	0.78	0.39	1.10	0.55	1.08	0.54	0.44	0.22
18	0.34	0.17	0.34	0.17	0.34	0.17	0.27	0.14	0.41	0.21	0.37	0.19	0.69	0.35	0.67	0.34	0.03	0.02
19	0.34	0.17	0.34	0.17	0.34	0.17	0.27	0.14	0.41	0.21	0.37	0.19	0.69	0.35	0.67	0.34	0.03	0.02
20	0.31	0.16	0.31	0.16	0.31	0.16	0.24	0.12	0.38	0.19	0.34	0.17	0.66	0.33	0.64	0.32	0.00	0.00

Table 4.8: Combination of land use and building vulnerability.

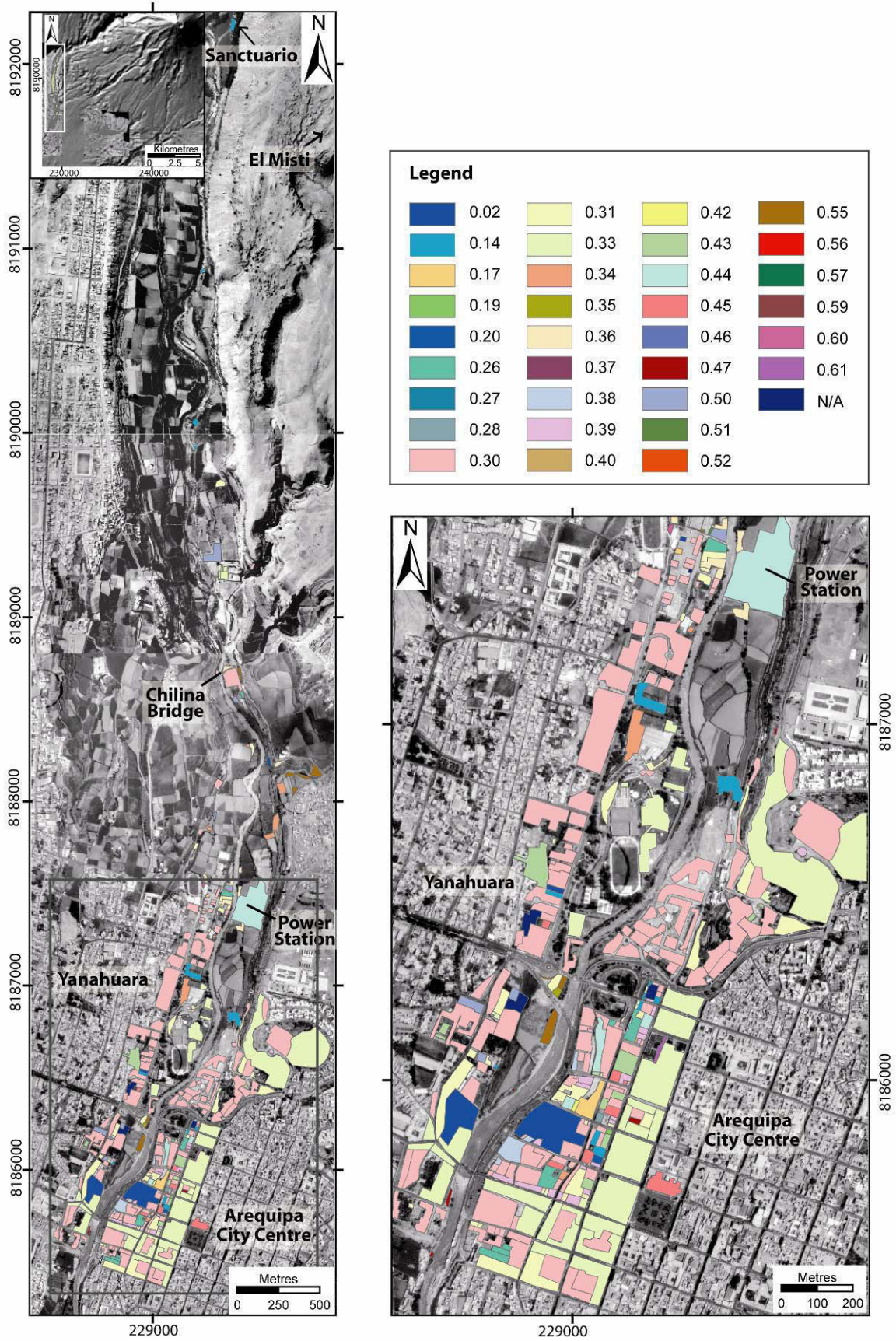


Figure 4.31: Building and land use vulnerability map for the Rio Chili Valley, where 0 is the least susceptible and 1 is the most.

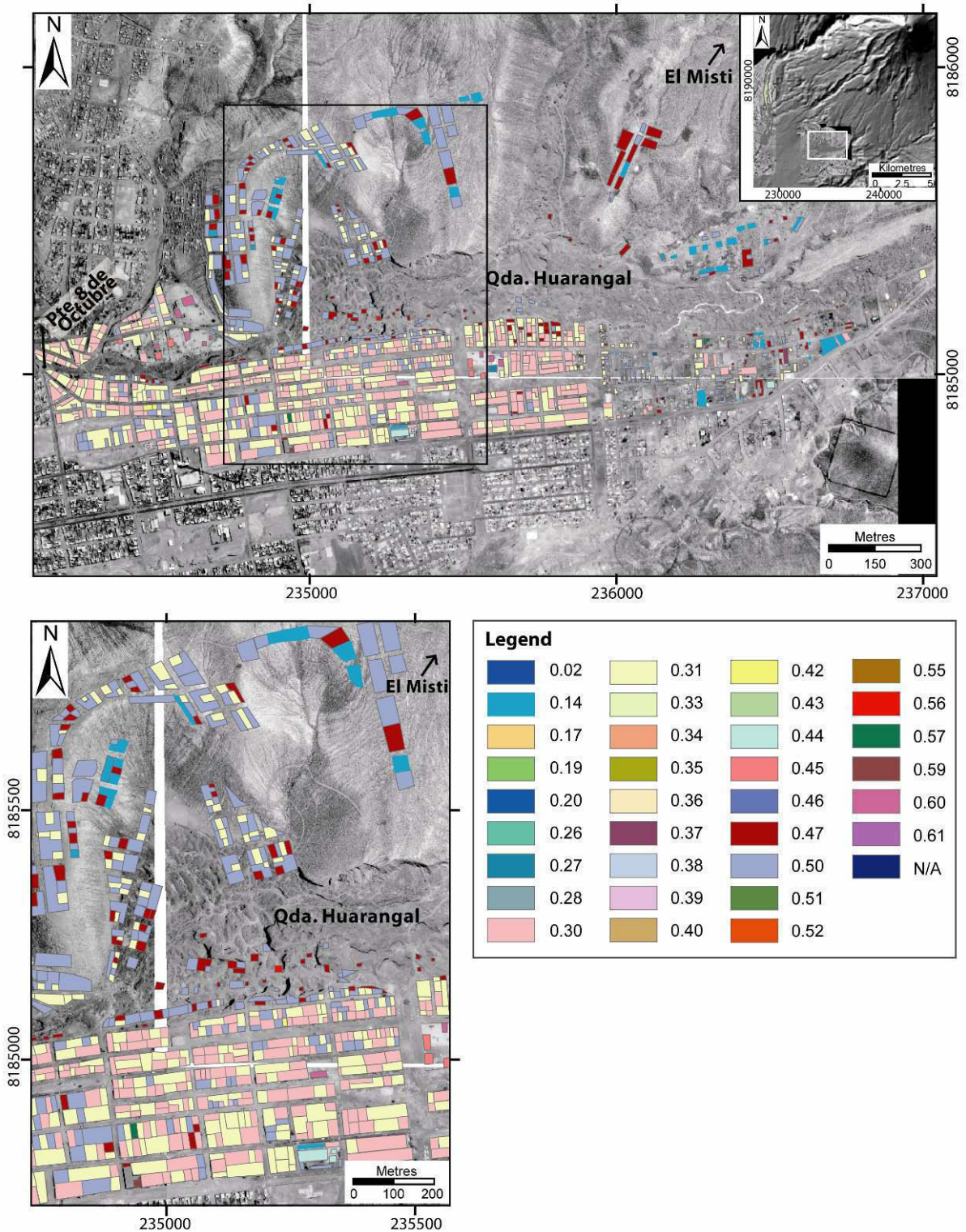


Figure 4.32: Building and land-use vulnerability map for the Quebrada Huarangal fan, where 0 is the least susceptible and 1 is the most.

The building and land use vulnerability map for the Río Chili Valley shows a region with an overall low vulnerability when compared to the Quebrada Huarangal fan. However, the distribution of vulnerability appears to be more evenly distributed on the Quebrada Huarangal fan where most of the highly vulnerable buildings are confined to the north of the study area and within the Quebrada channel, whereas vulnerability in the Río Chili Valley is much more contrasted. It is perturbing that the most vulnerable buildings in the Quebrada Huarangal fan are located within and adjacent to the temporary stream. With regards to a lahar or flood event these buildings, which are already considerably vulnerable due to their location, are further endangered by their construction type and dominant land use.

The results of the building and land-use vulnerability assessment were saved into a GIS database for use in Chapter 5 (Figure 4.33).

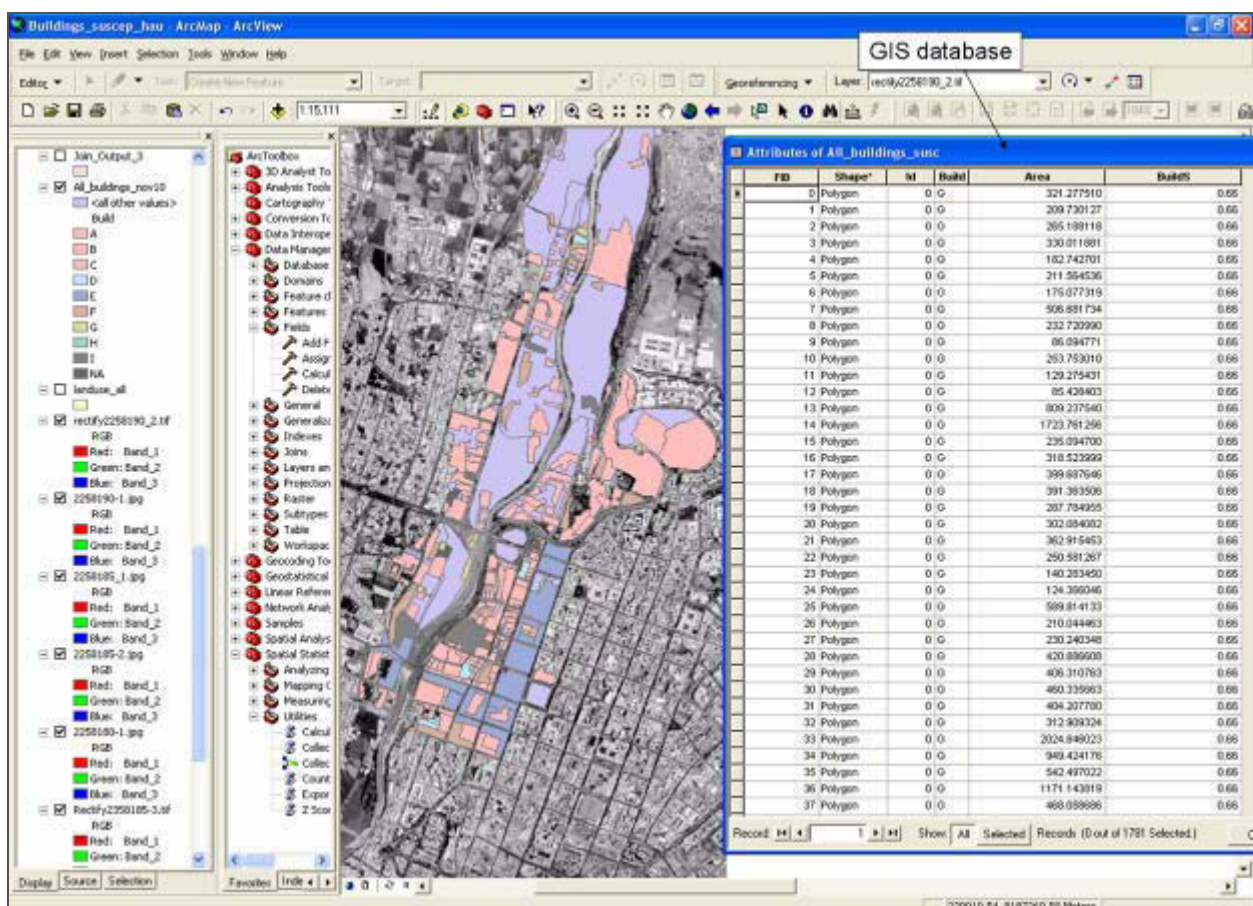


Figure 4.33: Database created in ArcGIS showing the predominant building types within the Río Chili Valley.

4.5 Infrastructure classification

4.5.1 Introduction

As modern urban functions rely on lifeline systems much more heavily than they used to, infrastructure constitutes a major component of the vulnerability of a city if a disaster strikes. Infrastructure can be defined as the basic physical and organisational networks needed for the operation of a society, or the services and facilities necessary for an economy to function. These can include water supply, sewage, gas distribution, power supply and telecommunications network just to name a few; a more exhaustive list of vulnerable infrastructure in cities is presented in Table 4.9.

Infrastructure	Systems	Specific elements
Transport network	Roadways Railways Bridges Airport	Highways, roads, streets, tracks and footpaths Road, rail and foot
Lifelines	Energy supply systems Water supply systems Disposal supply systems Telecommunication systems	Electricity, oil, gas and steam source, supply and distribution (including fuel storage facilities, underground pipes and cables, overhead lines, transformers and substations) Potable and industrial water source, supply and distribution (including underground pipes and storage tanks) Sewer, garbage and waste treatment (including pipelines) Telephone, facsimile, and digital data communication (including underground cables, overhead lines, and antennas/towers)
Emergency services	Medical systems Police systems Fire systems Rescue systems	Health buildings (clinics and other non-hospital facilities) and public hospitals Communication centre, law enforcement, prisons, police stations and equipment Communication centre, fire stations and fire fighting equipment Communication centre, rescue station and equipment
Civil engineering protection works	Waterway and flood protection systems	Dams, culverts, pipes, and runoff areas
Educational	Educational systems e.g. schools and universities	Buildings, land, equipment and facilities, e.g. sports area, swimming pools and teaching materials
Government/economy centre	Government systems e.g. councils and public services Banking and finance systems	Buildings, land, equipment and facilities e.g. public records and books. Banks, equipment and facilities e.g. public records and financial records
Nutrition	Food and agriculture systems	Production (e.g. farmland), storage and distribution
Commodities	Iron, steel, aluminium etc.	Production, storage and distribution

Table 4.9. Vulnerable infrastructure and lifeline systems in cities (compiled from Blaikie et al., 2001; Hellstrom, 2007; Kroger, 2008; van Westen et al., 2008).

Infrastructure and services are not independent of one another and a breakdown in one element can have role in the effects to other infrastructure, services and lifelines. For example, the transportation sector is dependent on a number of different infrastructure sectors, including electric power, telecommunications, government, natural gas/fuel and water. Electric power is relied upon for the operation of traffic lights and counter flow systems. Both land and air transport is dependent upon a supply of fuel, and public transit systems would be substantially affected by a disruption to fuel supply.

The health care sector is dependent on transportation for the movement of human resources and supplies – health workers rely on land transportation to reach hospitals and laboratories, and if personnel cannot reach their workplace, services could be disrupted. In addition, ambulances and emergency crews rely on roads to transport injured people to hospitals or to transfer patients if a specific site is damaged by a disaster event. Hospitals and other sites also require a range of medical supplies and food. Water services are necessary for drinking water and to support a healthy workforce, while the water sector relies on transportation for the delivery of chemicals such as chlorine for water treatment. Breakages in the water and wastewater sectors can also undermine roads and bridges.

The transportation network, telecommunications, lifelines and emergency services are regarded as essential infrastructure because they need to be operational to cope during and immediately after a disaster. Educational, government and economy services, nutrition and commodities are regarded as important infrastructure/services within a city because while they are important to the city, they are not essential to saving and/or protecting human life during a disaster.

4.5.2 Infrastructure present in Arequipa

In Arequipa much of the essential infrastructure (e.g. bridges, power lines, water pipes and power stations) are primarily concentrated across and in close proximity to the Río Chili, and also within the city centre. Emergency services and important infrastructure (civil engineering protection works, educational, government and economy services, nutrition and commodities) were addressed in the land use section of this chapter; therefore the following sections will cover transportation networks and lifelines.

4.5.2.1 Transportation network

Roading

The main highways, roads and railroads in Arequipa are shown in Figure 4.34. Within the city centre main roads are situated adjacent to the Río Chili River (Avenue de la Marina, Figure 4.35) where bridges link these routes and Arequipa City Centre with suburbs to the west of the river (e.g. Yanahuara).

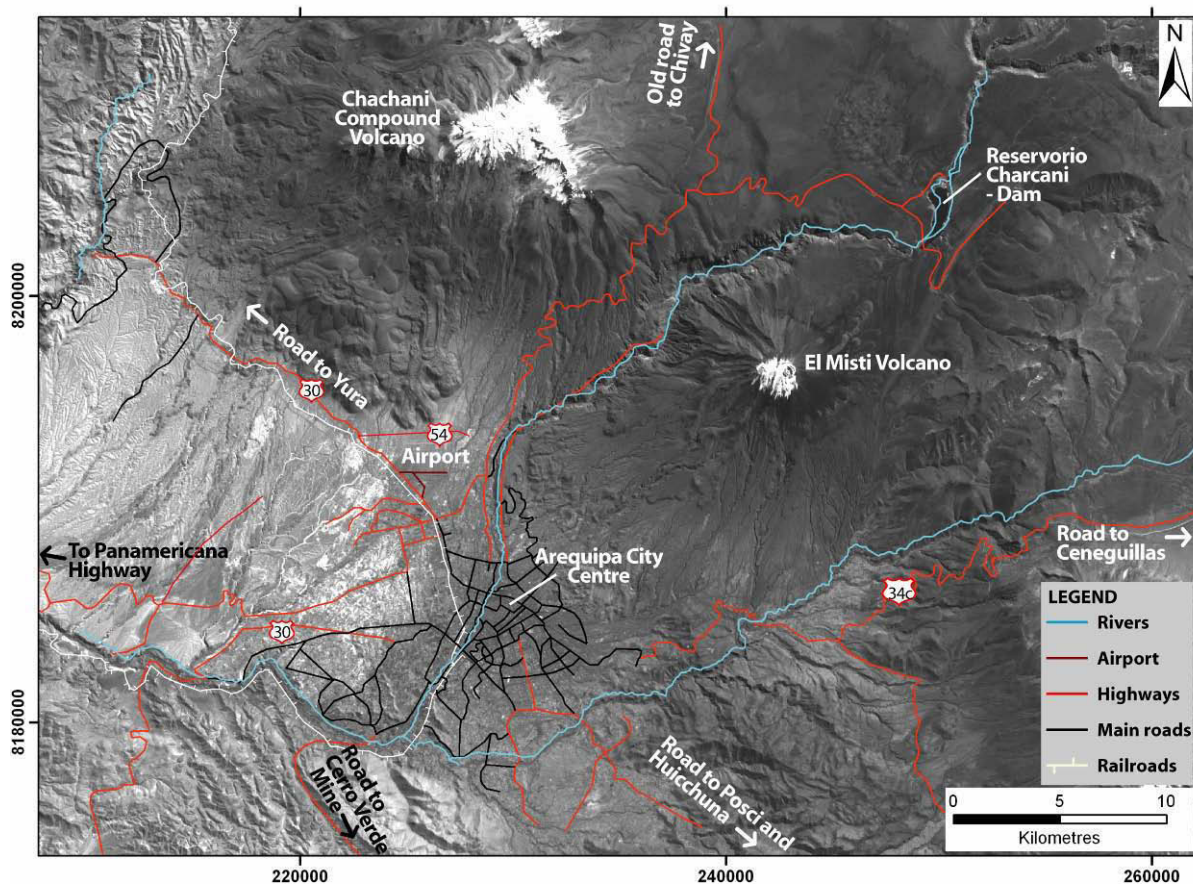


Figure 4.34: The main transportation network in Arequipa showing the highways, main roads, railroads and the airport. Main roads providing a link from the east to the west of the city, and vice versa, cross over bridges across the Río Chili. Adapted from vector files of Delaite (2003) draped over a Landsat image.

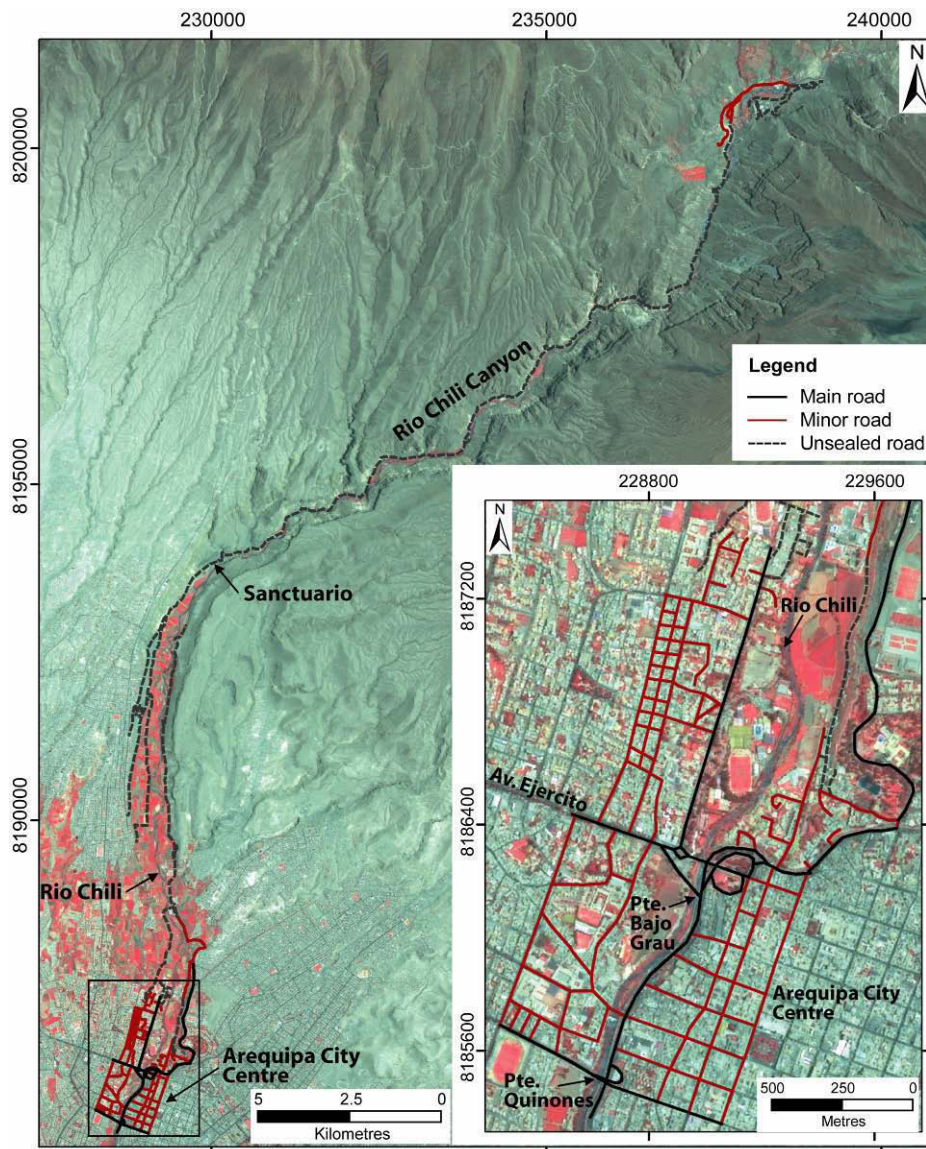


Figure 4.35: The road network, including main, minor and unsealed roads, within the Rio Chili Valley study area. Inset image is a close up of the city centre area showing the bridges which connect traffic flow from one side of the city to the other. Vector files derived from Google maps and draped over a 2008 SPOT5 image.

The main arterial route (Avenida de la Marina) links the southern city centre with the north and is adjacent to the Río Chili River. As discussed in Chapter 2 historical floods have affected the road network, and this section of road especially during the 1989, 1992 and 1997 flood events where the flow broke through the eastern bank of the Río Chili flooding streets, homes and businesses, overtopping the low Bajo Grau Bridge and causing structural damage to other bridges. The bridges represent a weak point in the network, because without their full functionality access between the east and the west is seriously compromised.

Within the Huarangal area roads are of poorer quality and are poorly maintained, apart from the dual carriageways (main roads highlighted on the Figure 4.36). The minor and unsealed roads are not routinely improved and/or repaired. Bridges link Huarangal to suburbs to the north and south; these bridges are also weak points in the network due to their low clearance height (e.g. 2-4 m) and the poor maintenance of channels. Sediment and rubbish are not cleared routinely and therefore limit the channel capacity increasing their vulnerability to flooding even during small-scale flood events. Roads within and adjacent to the Quebrada were flooded in February 1997 and roads crossing the Quebrada flooded in 2011.

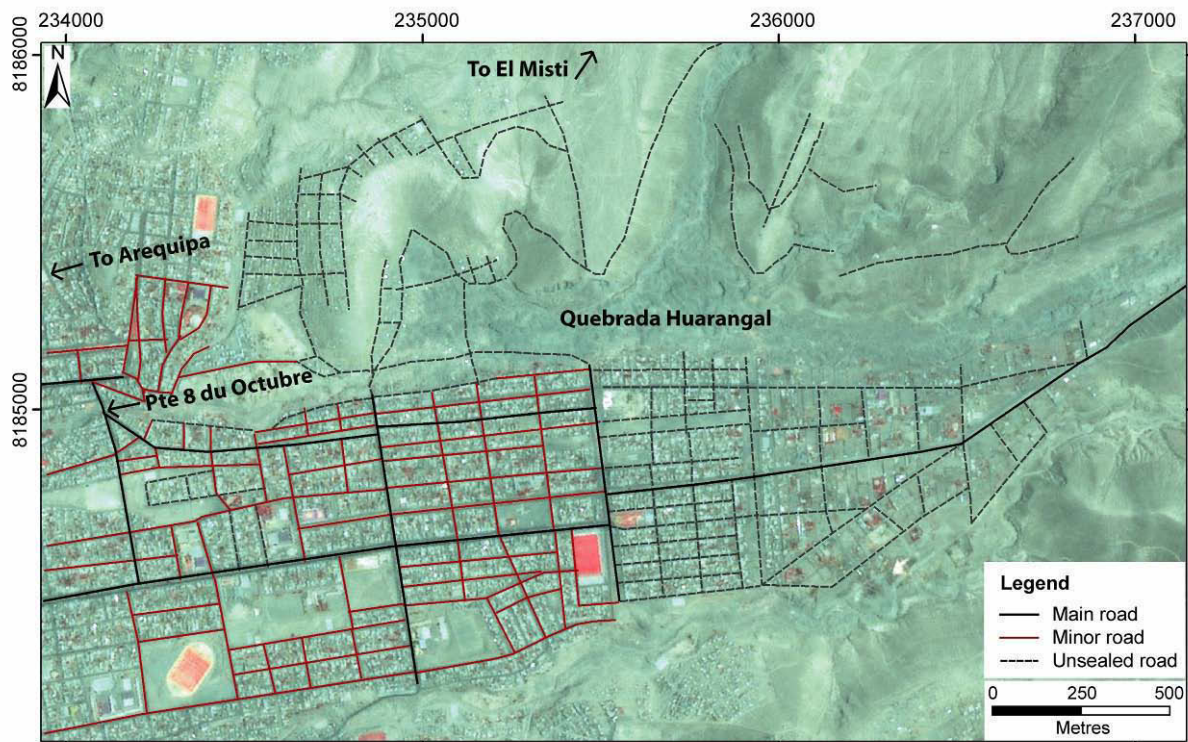


Figure 4.36: The transportation network in Quebrada Huarangal fan showing the main roads, minor roads, and the unsealed roads. Vector files derived from Google maps and draped over a 2008 SPOT5 image.

The roads are not only affected by burial, but also by scouring of the channel bank, which can undermine the stability of the road. In addition, flood waters can affect the integrity of the road surface as can the impact of debris, while damage to bridges can result in isolated roads and a disruption of the road network.

Railways

There is not an extensive railway network in Arequipa (Figure 4.34). Railway lines are located to the south of the City Centre for passenger and freight transportation between the coast and the mountains. Only an uncommon and exceptionally large magnitude flow event may affect railway bridges to the south of the city and moderate magnitude flows may affect the railway station located in the southern city centre. The network will be considered in terms of disruption to essential supplies during a crisis; however the network is located outside of the study area and will not be studied in great detail for the vulnerability analysis.

Bridges

Bridges located across the Río Chili and Quebrada Huarangal are prone to debris accumulation due to their low deck height (2 to 12 m) and narrow arch spans (4 to 10 m), and also to scouring around the pillars and the abutments (Figure 4.37). During floods in 1989, 1992 and 1997 debris accumulated behind the bridges, and subsequently overtopped the Río Chili channel flooding nearby homes and businesses (e.g. flood level of 1 to 2 m) on the eastern bank in the city centre (refer to Chapter 2). If bridges, such as Pte. Bolognesi and Pte. Quiñones, are destroyed access from one side of the city to the other will be severely limited. Water pipes and power lines are often located at bridges, and are thus equally vulnerable to damage. Figure 4.37 shows the location of bridges in the study areas.

Flood- and debris flow-related damage on bridges results from a variety of factors including the following (in order of importance in Arequipa): scour around piers and abutments, debris impact on structure, clogging due to debris causing redirection of flow, erosion of embankment due to overtopping flow, erosion along the toe of highway embankment due to along-embankment flow and the horizontal migration of stream banks (Melville and Coleman, 2000). The effects of a mass flow on the bridges will be discussed further in Chapter 5.

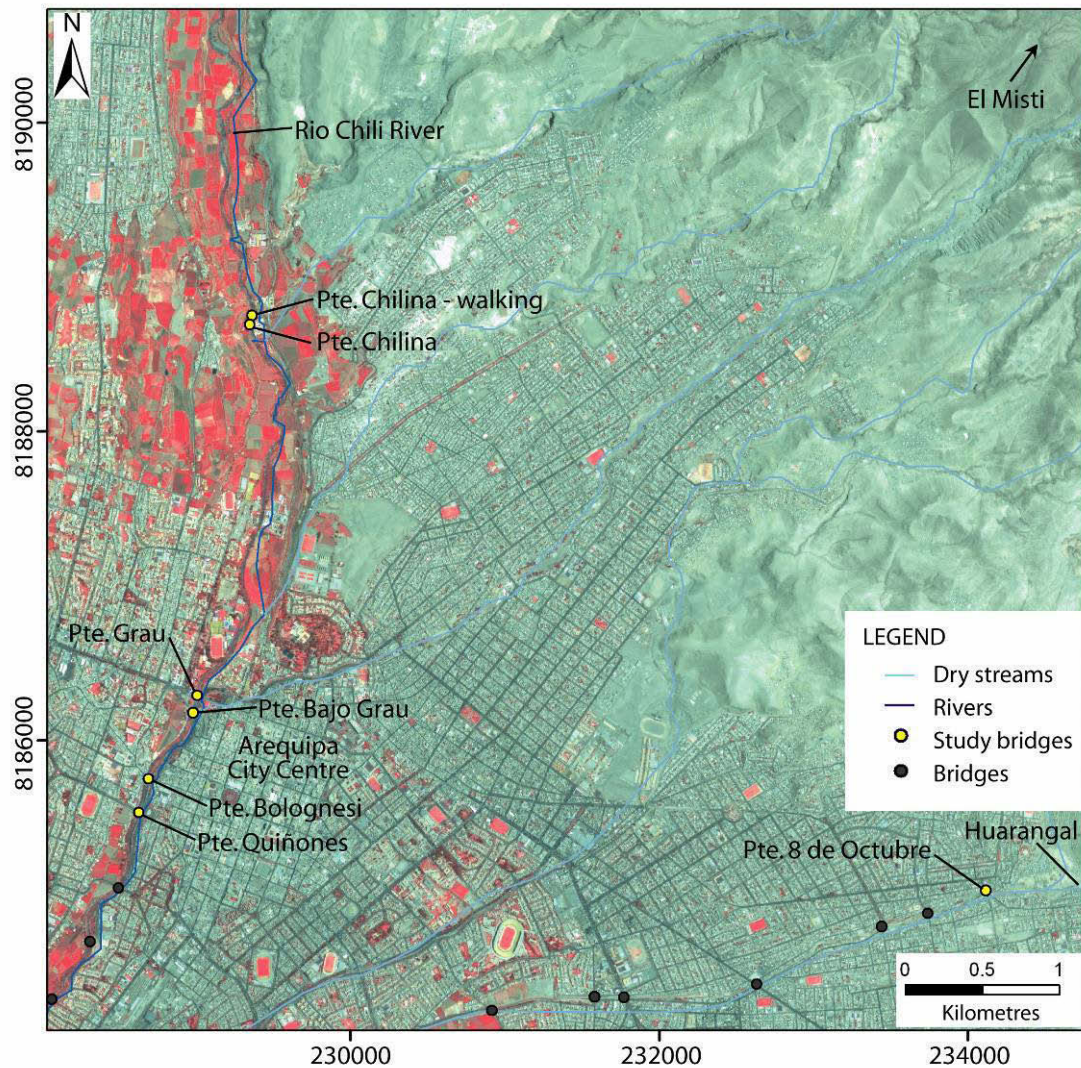


Figure 4.37: The location of bridges which cross the Río Chili and Quebrada Huarangal within, and in the vicinity of, the study areas. The bridges that were studied are highlighted in yellow.

Within the city centre there are four bridges crossing the Río Chili. Puentes Grau and Bolognesi are old, large colonial arch-style bridges constructed from ignimbrite bricks, whereas Bajo Grau and Puente Quiñones are new modern bridges constructed from concrete. Puente Consuelo does not cross the river, and directs traffic on and off Avenida de la Marina from Pte. Quiñones. There are two bridges in Chilina, one for light traffic and the other for foot traffic. Puente Chilina is constructed from ignimbrite and concrete whereas the walking bridge is constructed from iron with concrete abutments and wooden planks. At the western margin of the Huarangal fan there is a low clearance (3 m) concrete bridge – Puente 8 de Octubre. Bridges located outside of the study area will not be included in the vulnerability.

Chilina walking bridge

The Chilina walking bridge is situated a few tens of metres upstream of the Chilina Bridge (Figure 4.38). This bridge existed before September 2007 but it was in a state of disrepair; it was completed by September 2008. The structure is only used for minor foot traffic, and is located on private land.



Figure 4.38: *A: Looking upstream at the Chilina Walking Bridge. This bridge connects private land from one side of the river to the other. B: Reinforced cast in-situ concrete east abutment; the steel truss is bolted onto the concrete. C: Reinforced cast in-situ concrete west abutment built flush into the river bank. D: The steel frame truss with wooden plank bridge span.*

The bridge is constructed of a lightweight steel frame truss, a wooden deck and concrete abutments. The western abutment is a very poor concrete design and is sited on rock with no other reinforcement, and the eastern abutment is a mass reinforced concrete block. The bridge is very prone to damage/loss from any floating debris, and as the structure is lightweight with poor abutments, it would not take a lot of force for the bridge to fail. Analysis of the potential effect of a flow on this bridge is discussed in Chapter 5. A concrete wall constructed on the eastern wall of the river is prone to damage if the flood level rises above the wall. Scouring

could also undermine the wall causing damage to adjacent land and possibly the Chilina Bridge 25 m downstream.

Puente Chilina

This bridge links the Chilina community with farmland on the western side of the Río Chili supporting minor vehicular traffic (including farming machinery) and moderate foot traffic (including animals) (Figure 4.39). The bridge appears to be a rebuild as the abutments comprise ignimbrite masonry but the bridge span is cast in-situ reinforced concrete, suggesting that the original bridge has collapsed at some point and has since been replaced (Figure 4.39 B). The bridge is in poor condition. The foundations appear to be built on rock and unlikely to fail from scour, although masonry blocks will be prone to being plucked out of the wall, which could lead to failure.

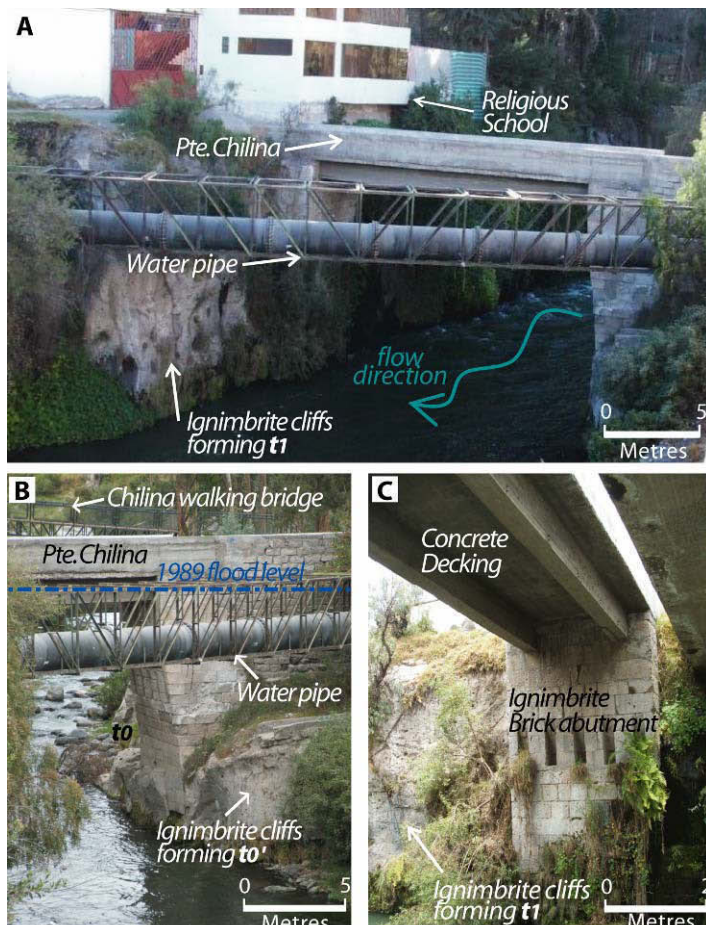


Figure 4.39: The ignimbrite masonry and cast in-situ reinforced concrete bridge at Chilina (North of Arequipa City). **A:** Downstream view of the bridge and pipeline from the Eastern bank. **B:** Downstream view of the bridge and a large pipe encased in a steel truss from the western bank. **C:** The underneath of the bridge with ignimbrite masonry abutments and concrete bridge span. To the right of the photograph is the reinforced concrete casing of the upstream pipe.

Downstream of the bridge is a pipeline, which is supported by a single span steel truss (Figure 4.39, A and B). If a flow was high enough to touch the truss, or if it was hit by floating debris, there would be serious damage to the truss and pipeline. However, the structure is protected to

some degree by the concrete/masonry bridge immediately adjacent. Upstream of the bridge is another pipeline which is enclosed in an in-situ reinforced concrete frame (Figure 4.39, C). At this locality the waterway is considerably smaller than upstream (the river narrows at this point) and likely to cause constriction depending on flood severity, leading to flooding of low to middle terraces with buildings.

Puente Grau

This is the main, and iconic, bridge of Arequipa City with construction beginning in 1884 and completed by 1898 (Zamacolya and Auregui, 1958) (Figure 4.40). This is a major bridge in Arequipa with heavy vehicular traffic in one direction connecting the historical part of the city in the city centre with communities on the west side of the river, such as Yanahuara.



Figure 4.40: The iconic colonial-style ignimbrite masonry multiple span arch bridge ‘Puente Grau’. Note the gradient of the road sloping away from the river. **A:** Downstream view of the bridge crossing the Río Chili. **B:** Upstream view of the large pillars and footings constructed from dacite lava masonry from the western side of the river. **C:** The upstream view of the bridge, from the eastern side, at the confluence with Quebrada San Lázaro.

The bridge is a closed spandrel, stone masonry, multiple span arch in the 'Centro Histórico' part of Arequipa (Young, C; 2009, pers. comm.). The bridge was constructed in a similar manner to the ancient Roman bridges – a stone pier supporting a cut stone arch with bossed facing stones. The stone walls have buttresses to hold back the soil that supports the roadway. There is also a water main connected to the upstream side of the bridge.

The bridge span is at a sufficient height above the river (~16 m); however historical floods have broken through the east bank, flooding the road and houses. The arches make the bridge vulnerable during flood events because if the flood event is carrying large enough quantities of debris the pillar in the river is vulnerable to impact loads in addition to the build up of material behind the arches. This can cause overtopping of water or a build up of pressure causing the river to change course. Alternately the whole bridge could topple over due to the static forces. Scour and undercut of the foundations at this bridge would cause substantial damage, while blocks in the bridge can be prone to plucking out from the wall which could eventually cause failure. Analysis of the potential effect of a flow on this bridge is discussed in Chapter 5. The bridge has sustained a fair amount of damage resulting from both earthquakes and simply as a result of its age. The 2001 earthquake displaced stone blocks used for the balustrade; caused ripples in the road surface; cracked the surface; loosened a joint in the upper arch; loosened between the surface of the arch and other stone masonry; and formed a crack in the arch (Kusunoki, 2002).

Bajo Grau

Bajo Grau was constructed in 1989 and is a relatively new bridge compared to others in the region (Figure 4.41). It is a single span cast in-situ reinforced concrete structure with a single half arch of the bridge (Figure 4.41, A – to the right of the image) cast in place and the deck elements may have been precast.



Figure 4.41: *A: Puente Bajo Grau, a one-way bridge connecting the Yanahuara district on the western side of the Río Chili River with the city centre. Note the different terraces on the western channel edge. B: Downstream view of Bajo Grau showing the slope of the bridge deck to the east. C: Curvature of the bridge to the south directing one-way traffic onto Avenue de la Marina. D: View of the bridge westwards towards Yanahuara, face-on to traffic, and Pte. Grau in the background. Note the pipe running under the bridge deck.*

When the bridge was in construction in 1989 it was flooded and was also instrumental in causing flooding to the adjacent road and properties on the east bank (Chapter 2). Water was redirected and debris piled up behind the bridge causing it to be overtopped and forcing the flow through the eastern channel bank where flow heights of 4-5 m were recorded on the lower terrace (t1).

The waterway is substantially less than the upstream Pte. Grau Bridge, the channel width is ~12 m compared to ~22 m upstream. However, due to the absence of mid-river piers, the bridge allows unobstructed flow until the deck height of 4.5 m is reached. The low abutment (eastern side) will be prone to scour, and at present the river is showing a tendency towards undercutting this bank. This could be due to the whole area being modified to build the road

with the original waterway filled in, and also due to the traverse slope of the river bed (and valley) towards and east. If the bridge has not been piled sufficiently and if the protection wall does not reach to an adequate depth, scouring will cause a lot of damage to this bridge.

Puente Bolognesi

Puente Bolognesi is the oldest bridge in Arequipa with construction beginning in 1577 and completed in 1608 (Figure 4.42) (Kusunoki, 2002). Puente Bolognesi is buttressed masonry arch bridge constructed from ignimbrite and consisting of five spans over the busy Avenida de la Marina and the Río Chili (Young, C; 2009, pers. comm.).

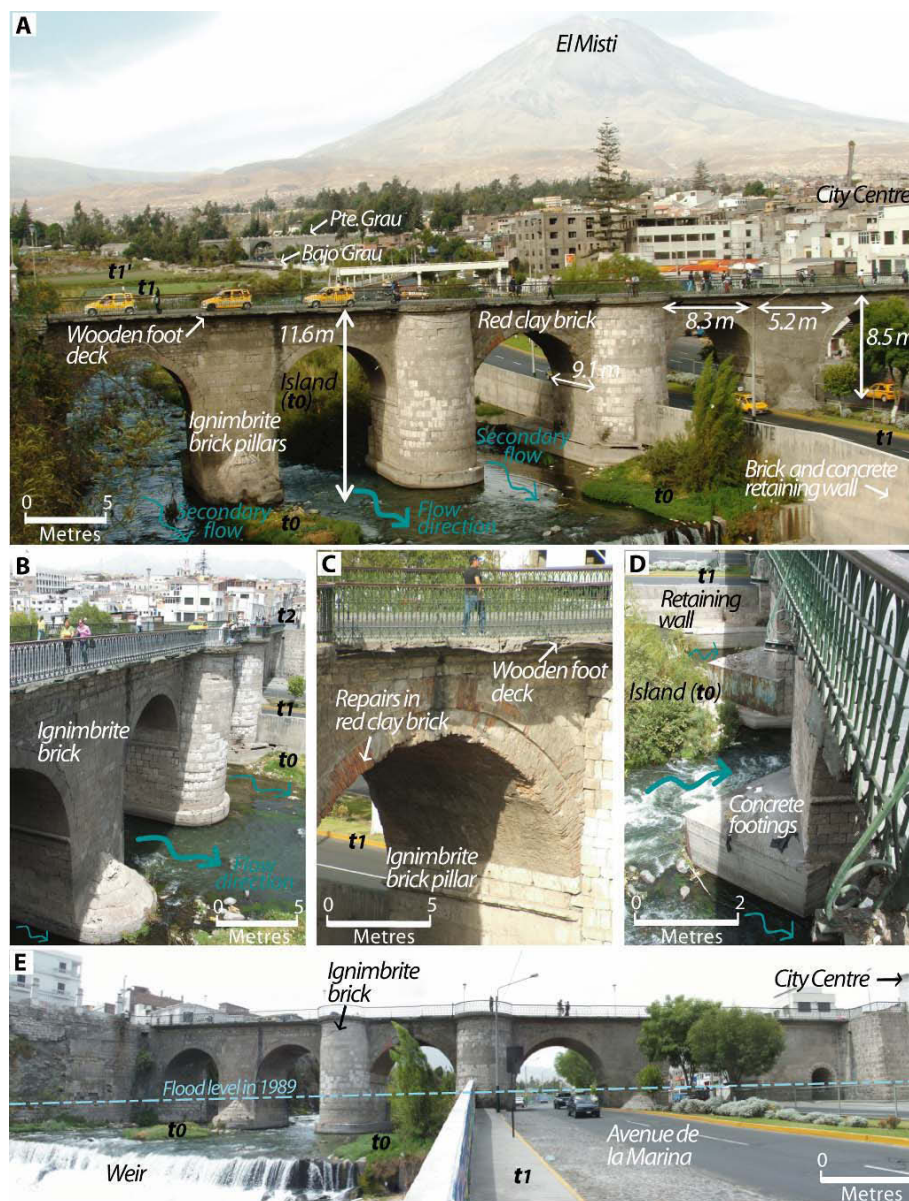


Figure 4.42: A: Downstream view of the bridge and its five arches over the river and highway. B: Downstream view of the bridge. C: Damage and poor repair of the river arch closest to the road, and the uneven footpath which is constructed from wood. D: The large pillars of the upstream side of bridge. E: Downstream view of the bridge at road level, the weir is on the left side of the photograph.

The bridge appears to be underpinned on the upstream side to prevent, or to reduce, scour effects on the stone work. However, the stone itself will probably be prone to loss of section through abrasion from harder volcanic rocks. The weir downstream is likely to have been built specifically to protect the foundation of the bridge, which means it will be critical to the survival of the bridge. Although, photographs from the 1989 flood (Chapter 2) show significant damage to the weir; the weir is constructed from masonry which is easily ‘plucked’ by floodwaters. Lahar/fluvial deposits on the western side of the river are prone to erosion and could lead to foundation failure.

There are round turrets between the arches with iron railing along the edge of the deck, and a wooden footpath. It appears as if a concrete deck has been cast upon the existing bridge, and probably reinforced. The middle arch has sustained some damage in the past (Figure 4.42, C) and it has been poorly repaired with red clay brick. Whilst Pte. Bolognesi has a high deck height (11 m); the arches can be vulnerable to debris impact and the build up of debris in a flow event. In addition the bridge is in a poor state of repair adding to its vulnerability. Analysis of the potential effect of a flow on this bridge is discussed in Chapter 5.

Puente Quiñones

Puente Quiñones and Puente Consuelo are a pair of bridges that connect Abelardo Quinones to Consuelo Streets across the Río Chili with ramps on and off Avenida de la Marina (Figure 4.43). Puente Quiñones is a large multi span post-tensioned reinforced concrete bridge with a low deck height featuring a highly contoured soffit (instead of a typical column design) where the soffit dips to take the shape of the column (Young, C and Henry, C, 2009, pers. comm.). The bridge was most probably cast in-situ, however some aspects may have been precast and abutments are of cast in-situ concrete.



Figure 4.43: *A: Looking downstream to Pte. Quiñones and Pte Consuelo. B: Looking downstream at Pte. Quiñones. C: The western abutment of Pte. Quiñones. D: The middle pier between the Río Chili and Avenida de la Marina on the eastern side of Río Chili*

As this bridge is of relatively recent construction it is likely to be piled, which should have been designed for scour, along with the concrete wall on the western abutment. Expansion joints (a flexible system to allow the bridge to expand and contract in the heat) are present at the ends of the bridge, however many observed cracks in the pavement suggest that this system is not working sufficiently. This is likely because of poor detailing (i.e. a good bridge design concept but not applied properly). This structure has a low deck height (~8 m), especially as it curves towards Avenida de la Marina, however the open streamlined nature of the deck soffit would minimise damage to the bridge.

Puente 8 du Octubre

Located at the western extremity of the Huarangal fan area, this bridge is a single span, semi arch, reinforced cast in-situ concrete structure (Figure 4.44).



Figure 4.44: Upstream of Pte. 8 du Octubre in Huarangal. Of note is the amount of debris (including sediment, rock, building materials, rubbish) present in the channel. The GPS antenna is 2 m in height.

This bridge has an exceptionally low deck height of ~4.5 m with a clearing of <2 m above the detritus. This Quebrada is used as a dumpsite and contains a lot of artificial debris in the channel, which would add to sediment in a flow.

Airport

The Alfredo Rodríguez Ballón International Airport is located in the district of Cerro Colorado, approximately 12 km northwest of the city at an altitude of 2561 m. Domestic and international flights accounted for more than 930,000 passengers in 2010 alone, a 50% increase on the previous year. The airport provides a link to the southern cities from Lima and is a popular way for tourists to travel to Arequipa, and then onwards to Cusco or Juliaca.

The airport is located too high (~150 m) above the Río Chili channel to be affected by volcanic mass flows from El Misti, but could be affected by exceptional runoff from the slopes of Charcani. The airport is also vulnerable to tephra fall depending on the wind direction (discussed in the Introduction). The airport will be considered in terms of disruption to the distribution of essential supplies during a crisis; however the airport is not affected directly by mass flows and is located outside of the study area therefore will not be studied in great detail for the vulnerability analysis.

4.5.2.2 Utility services

Utility systems (e.g. potable water, waste-water, telecommunication, electric power) are vital for the community as they supply energy and fresh water, treat the waste water and provide communication services to inhabitants. They are the basic requirement of most communities and are critical and essential elements during and after a crisis.

Electricity supply

Power stations

Electricity is fundamental to any large city, and power supplied to Arequipa originates from both hydroelectric and thermal power systems (Figure 4.45). The construction of the hydroelectric power stations began in 1895 with the original Charcani I (0.4 MW) which provided electricity to Arequipa. As the city grew more power stations were built, including Charcani V which was constructed in 1989 and is located inside El Misti Volcano. There are six hydroelectric dams and stations in total (Charcani I-VI), positioned in the upper Río Chili gorge (0.5 to 1 km deep), and covering a distance of approximately 14 km from the upper to the lower dam. The uppermost dam (i.e. Charcani V) is located approximately 20 km upstream of the city centre, and the lowermost dam (i.e. Charcani II) is approximately 10 km from the city centre (Figure 4.45 A). The thermal power station is located on the eastern low terraces (t1 – t2) of the Río Chili approximately 1.5 km upstream of the city centre (Figure 4.45 B). The characteristics of the power stations are summarised in Table 4.10.

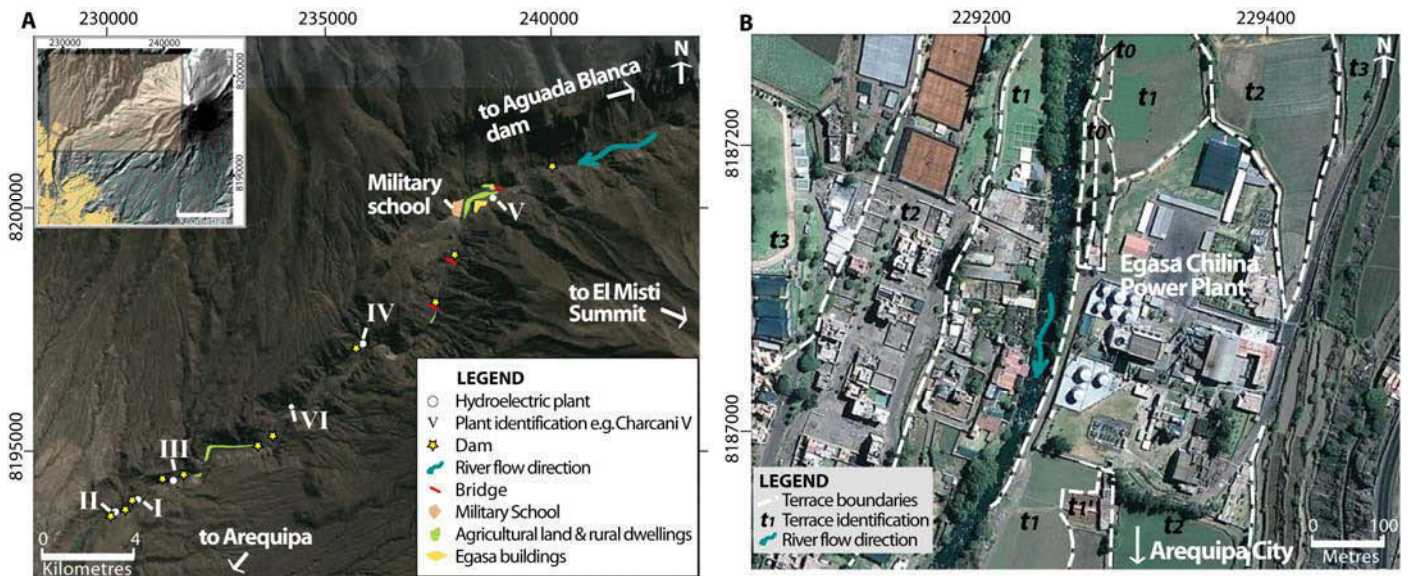


Figure 4.45: *A: The system of hydroelectric dams and stations in the upper Río Chili canyon. B: The thermal power plant located on the eastern bank of the Río Chili.*

	Power Station	Construction Date	No. of turbines	Capacity (MW)	Design Flow (m ³ /s)	Net Fall (m)	Additional information
Hydroelectric	Charcani I	1905	2	1,47	7.6	26.85	Shops, shelters, church and sports fields are built on site.
	Charcani II	1912	3	0,79	6	18.70	Water is taken directly from the discharge of Charcani I and passes through a sand trap.
	Charcani III	1938	2	4,56	10	57.50	Features remote monitoring from the Control Centre in Chilina.
	Charcani IV	1959 - 1970	3	14.4	15	117.35	Modernised in 1993.
	Charcani V	1989	3	153.87	24,9	706.4	Operates using the water from the Aguada Blanca dam (3650 m.a.s.l.) which flows through a 10 km long pressure tunnel inside Misti. The water's declination starts through a forced conduct (>900 m long) located inside the Hijo del Misti (or "son of Misti"), accessing the power house station and moving three generating units.
	Charcani VI	1976	1	8,96	15	69	Modernised in 1995.
Thermal	Chilina	1955-1982	4	39.69			This power plant has three water-tube boilers and one diesel powered boiler to generate the steam for electricity.

Table 4.10: *Characteristics of the power generation systems in Arequipa, including hydroelectric and thermal power generation (Egasa, 2009).*

These hydroelectric and thermal power installations are very vulnerable to inundation and impact from even small volume mass flows, due to the location within, and adjacent to, the main fluvial channel. Flood deposits can be found approximately 10 m up the canyon walls at

the entrance of the Río Chili canyon (Chapter 2), providing evidence of a moderate- to large-volume flash flood which is likely to have caused damage to at least the Charcani II dam and power station located at the canyon entrance. In addition a sizeable debris flow deposit with the large boulders (>1m) is located on the western lower terraces (up to t1') 2.5 km downstream of the canyon entrance and 4.6 km upstream of the thermal power plant, and provides evidence of the carrying capacity of smaller volume events and the potential for small volume debris flows to impact lower terraces. This is particularly concerning as the thermal power plant is located on the t1 to t2 terraces where nine large (approximately 9 m in diameter and 20 m high) diesel storage tanks and a radio control tower are adjacent to the river. Not only would the damage to these diesel tanks led to a disruption and/or rupture of the power supply but it could also result in detrimental environmental effects on the Río Chili – the source of potable water and irrigation for the city.

The power installations are also threatened by debris avalanches and landslides (Figure 4.45); deposits within the Río Chili canyon provide evidence for the possibility of these events in the future originating from the steep slopes of El Misti and Chachani (Chapter 2). Debris avalanches and landslides can cause damage by their impact alone, but also from the development of secondary flows. With the addition of sufficient water, lahars and/or hyperconcentrated flows can form and damage the power systems, not only by impact but as the abrasive sediments damage the turbines. Debris avalanches and landslides into the river can also initiate a dam-break flood scenario if the channel becomes blocked and water can no longer be held behind a temporary dam. All of these scenarios could have a devastating effect on the power supply to Arequipa.

Damage to hydroelectric power stations from mass flows is not uncommon; for example syn- and post-eruptive lahars from the 1996-97 eruptions of Mount Ruapehu (New Zealand) caused almost US \$17 million worth of damage to the Rangipo hydroelectric power station (Cronin et al., 1997). Sediment from lahars caused considerable turbine wear, affected the operation of a hydroelectric power station, and it closed for many months for repairs. Enough power could be generated from other power sources to compensate for the temporary loss of the Rangipo station, whereas Arequipa is reliant on both the hydroelectric and thermal power stations located within and adjacent to the Río Chili for power supply to the city. Arequipa was left without power for several days in August 1967 when an avalanche in the Río Chili gorge cut water supply to the Charcani IV hydroelectric station. Even a small magnitude

event, such as this in the Río Chili, could cause severe disruption to the electrical supply of the city, with a follow-on effect for lifeline services such as hospitals and other emergency services during a crisis.

Powerlines

Information of the location of the powerlines in Arequipa could not be obtained, however the majority of power is distributed by overhead lines as evidenced by notes and photographs taken in the field (Figure 4.46). Power poles constructed from reinforced concrete line the main, and most minor, roads within Arequipa. Wooden power poles support the lines on smaller roads, lanes, and rural areas (if power is accessible). Power is passed from building to building on wooden poles as can be seen in the figure below; notably the lines can be chaotically distributed within dense urban areas. The 2007 census determined that 21% of private dwellings within the Arequipa province are without electricity (INEI, 2008).



Figure 4.46: *The majority of power is distributed overhead in Arequipa where lines are held up by reinforced concrete and wooden power poles.*

A sustained flow can result in power poles being pushed over and therefore cutting the power supply. A snapshot taken from video footage of the 1989 hyperconcentrated flow event (Chapter 2) show a reinforced concrete power pole in the city centre being forced over by the strength of the flow. The impact from debris in the flow also threatens the stability of power poles. The variables to power pole strength include construction material and quality, height and width of pole, line load and the foundation depth and quality. The failure of just one pole can result in power outages across a city block or even further afield. As discussed earlier, power supply is an essential and critical element not only for the population but in emergency response. For the vulnerability assessment the distribution of powerlines will be assumed to

be present on all roadways with the exception of rural areas and in the north-eastern extremity of the Quebrada Huarangal fan where utility services are very limited or non-existent.

Water

The main water supply for Arequipa is sourced from reservoirs in the highlands surrounding Arequipa. The last reservoir is the Aguada Blanca, located approximately 35 km upstream of the city centre with a capacity of $28.59 \times 10^6 \text{ m}^3$ (EGASA, 2009). The management of this reservoir, and upstream reservoirs, primarily determines the water availability in the Río Chili. The outlet to the dam is controlled to regulate water supply to the hydroelectric power system, this amount of water varies depending on the season (e.g. rainfall is concentrated over four months from December to March) and therefore water availability. The water supply is used for many different purposes including energy production, domestic water, small industry, untreated waste water transport, city drainage, agriculture and mining. Notably, downstream of the dams, water from the river is tapped to supply a large irrigation scheme – essential for agricultural production in this semi-arid environment.

Water is drawn into the Zamácola canal near the Santuario, at the entrance of the canyon, after it is used in the hydroelectric power generation (Figure 4.47). The Zamácola canal transports water along the western side of the Río Chili where 1650 l/s of water is drawn into secondary and tertiary irrigation canals, and a further 1500 l/s is taken into the Tomila Water Treatment Plant for the city's water supply (SEDAPAR, 2009). Water is also taken from via the Zamácola canal to irrigate the agricultural areas of Acequia Alta Cayma (i.e. 550 l/s) to the west and Alto Cural (i.e. 520 l/s) to the south west respectively (SEDAPAR, 2009).

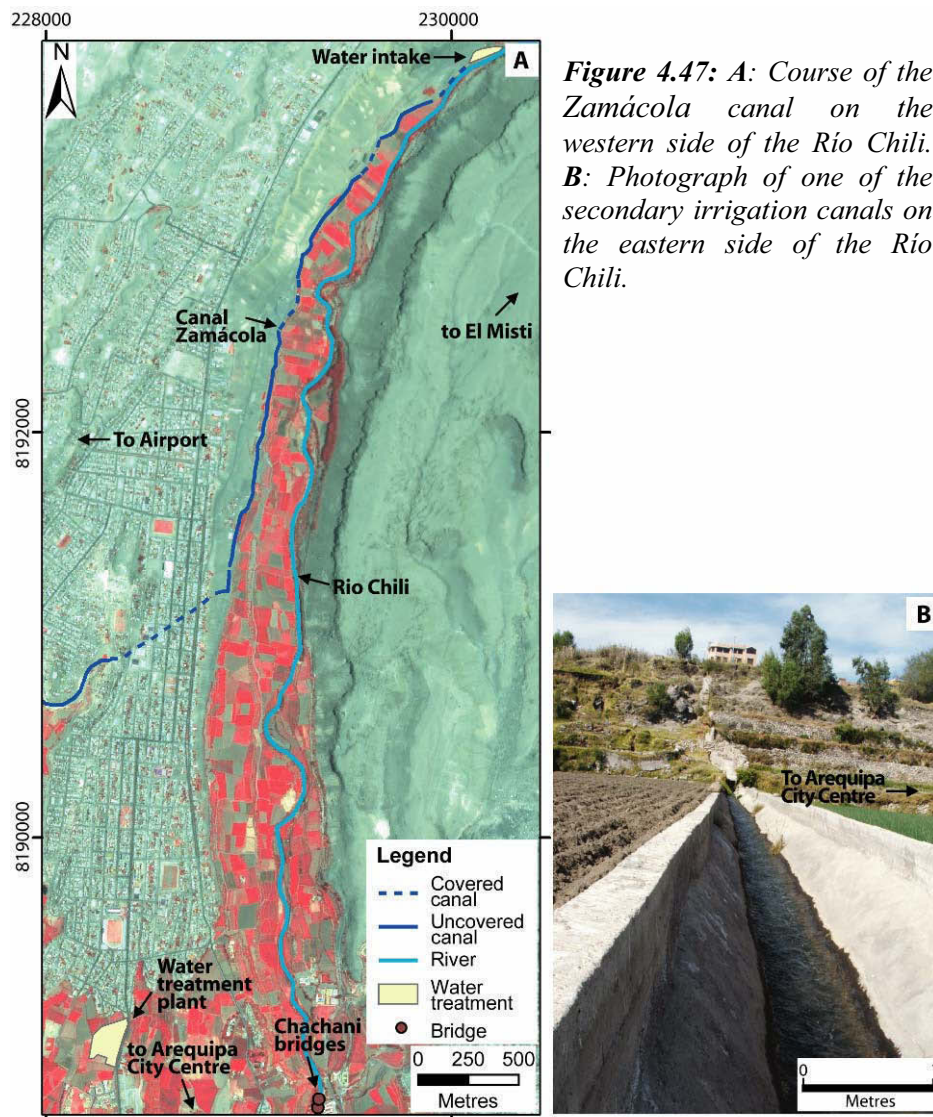


Figure 4.47: A: Course of the Zamácola canal on the western side of the Río Chili. B: Photograph of one of the secondary irrigation canals on the eastern side of the Río Chili.

Information of the precise location of the water pipes in Arequipa could not be obtained, however water is distributed throughout the city by underground pipelines. The exception being at the eastern end of the Quebrada Huarangal fan where water is not piped into buildings; residents take untreated water from pumps situated in the suburb. The 2007 determined that 24% of private dwellings within the Arequipa district are without water (INEI, 2008). The precise location of all secondary and tertiary irrigation canals could not be determined; however they are present along the agriculturally cultivated terraces (t0' to t3) at spacings of between approximately 30 to 90 m, as determined from Google Earth imagery. The irrigated area of the Río Chili is approximately 441 ha with an average farm size of 2.17 ha in 2007; the 794 plots are irrigated by 1.20 l/s per ha of water (Koopman, 2009). The irrigation water is also used for cleaning taxis, washing textiles, bathing and withdrawals for public use.

Also an increase of sediment and debris in the canal system can lead to blockages. During the floods of 8 February 1989 the entire city was left without water for 20 days as the canal was damaged (Fernández-Dávila et al., 2001). The canal system for the agricultural sector was also destroyed and thus in the following months there was a shortage of food. An increase in the Río Chili water level was increased from 7-24 m³/sec to 236 m³/sec in February 2011 led to an increase in sediment and debris in the canal system and the eventual shutdown of the Tomila Water Treatment Plant. Approximately 80% of the city was left without potable water for at least 2 hours (www.rpp.com, 2011). The water system in Arequipa is vital for many aspects of daily living, yet one of the most threatened elements during future flow events. For the vulnerability assessment the distribution of water pipes will be assumed to be present on all roadways with the exception of rural areas and in the north eastern extremity of the Quebrada Huarangal fan.

Waste water/sewer system

The functioning of a waste water and sewer system is imperative during, and immediately after, a crisis as a poor hygiene service can lead to health epidemics such as gastroenteritis. Health epidemics were recorded in parts of the city after waste water and sewer systems were damaged during the February 1989 floods (Fernández-Dávila et al., 2001). Information of the precise location of the waste water and sewer pipes in Arequipa could not be obtained, however waste water and sewerage is led away from the city underground pipelines. The exception being at the eastern end of the Quebrada Huarangal fan because waste water and sewerage systems do not exist. The 2007 census determined that 22% of private dwellings in the Arequipa District are without a sewerage system (INEI, 2008). For the vulnerability assessment, waste water and sewerage pipe distribution will be assumed to coincide with all roadways with the exception of rural areas and in the north eastern extremity of the Quebrada Huarangal fan.

Telecommunication system

Telecommunication systems are vital in case of volcanic crisis, from individuals' calls to emergency services to government organisation of aid and relief. These systems can also facilitate the distribution of critical information (e.g. the location of clean drinking water and food, evacuation and medical centres, etc.) to the population. As with some of the other

services overhead telecommunication lines will be assumed to coincide with roadways with the exception of rural areas and the NE area of the Quebrada Huarangal fan.

4.5.3 Vulnerability of infrastructure in Arequipa

Using methods adapted for the analysis of the vulnerability of land-use and buildings in Arequipa, the vulnerability of infrastructure was assessed. Coefficients, ranging from 0 (low *importance*) to 1 (high *importance*) were assigned to different categories (such as economic repercussions, population exposure and value) for each infrastructure type (the method and rationale for assigning the coefficients is discussed in chapter 1). These coefficient values were added together and averaged to give a value between 0 and 1 for the *importance* of the particular infrastructure and therefore the vulnerability during a volcanic crisis (Table 4.11). The values were normalised to account for subjectivity in assigning the values, normalised minimum and maximum values were obtained from which the mean value of all the criteria was calculated. Reasoning for the assignment of the coefficient values is based on the literature (e.g. Baxter et al. 2005, Kelman et al, 2002; to name a few) and is rationalised in Appendix C. The infrastructure types were evaluated against one another to determine the most vulnerable infrastructure present in Arequipa. The results were mapped to show the vulnerability distribution within the study areas (Figures 4.48 to 4.51).

Elements		Criteria: Coefficients from 0 (low importance) to 1 (high importance)											Totals						
		Lifeline	Population exposure		Economic repercussion		Construction		Other			Total	Total maximum normalised	Total minimum normalised	Mean	Rank			
			Day	Night	Loss of income	Rebuild cost	Age	Materials	Energy output	Distance from river	Height above river								
Roadways	Highway	0.9	0.8	0.4	0.7	0.6	0.2	-	0.1	-	0.1	0.2	-	0.1	3.7	0.54	0.44	0.49	11
	Main road	0.7	0.7	0.3	0.5	0.4	0.4	-	0.5	-	0.4	0.4	-	0.5	3.5	0.56	0.46	0.51	9
	Minor road	0.5	0.5	0.2	0.3	0.3	0.5	-	0.5	-	0.5	0.4	-	0.5	2.8	0.46	0.4	0.43	15
	Unsealed road	0.1	0.2	0.1	0.1	0.1	0.8	-	0.7	-	0.8	0.38	-	0.7	2.1	0.38	0.36	0.37	17
Bridges	Chilina walking	0.1	0.2	0.1	0.1	0.1	0.8	0.1	0.8	0.8	0.8	0.8	0.9	0.8	3.2	0.42	0.24	0.33	18
	Chilina	0.3	0.3	0.1	0.2	0.2	0.4	0.4	0.4	0.8	0.4	0.4	0.9	0.8	3.6	0.42	0.36	0.39	16
	Grau	0.8	0.8	0.4	0.6	0.8	0.7	0.5	0.9	0.3	0.5	0.8	0.9	0.3	5.8	0.8	0.52	0.66	1
	Bajo Grau	0.8	0.7	0.3	0.4	0.4	0.2	0.3	0.9	0.8	0.3	0.62	0.9	0.8	4.8	0.62	0.5	0.56	5
	Bolognesi	0.7	0.6	0.2	0.6	0.8	0.7	0.5	0.9	0.3	0.5	0.74	0.9	0.3	5.3	0.74	0.46	0.6	2
	Quinones	0.9	0.7	0.3	0.4	0.7	0.2	0.3	0.9	0.6	0.3	0.7	0.9	0.6	5	0.7	0.48	0.59	3
	8 du Octubre	0.5	0.7	0.2	0.2	0.1	0.2	0.4	0.9	0.9	0.4	0.54	0.9	0.9	4.1	0.54	0.38	0.46	12
	Railways	0.5	0.6	0.2	0.5	0.6	-	0.2	-	0.3	-	0.44	-	0.3	2.9	0.44	0.34	0.39	16
Other transport	Airport	0.9	0.8	0.1	0.7	0.7	0.3	0.2	0.1	-	0.56	-	0.1	3.8	0.56	0.4	0.48	11	
Hydroelectric power stations	Charcani I	0.8	0.2	0.1	0.5	0.7	0.6	0.3	0.1	0.9	0.3	0.64	0.9	4.2	0.64	0.36	0.5	10	
	Charcani II	0.8	0.2	0.1	0.5	0.7	0.6	0.3	0.1	0.9	0.3	0.64	0.9	4.2	0.64	0.36	0.5	10	
	Charcani III	0.8	0.2	0.1	0.5	0.7	0.5	0.3	0.2	0.9	0.3	0.62	0.9	4.2	0.62	0.38	0.5	10	
	Charcani IV	0.8	0.2	0.1	0.5	0.7	0.3	0.3	0.4	0.9	0.3	0.58	0.9	4.2	0.58	0.42	0.5	10	
	Charcani V	0.8	0.2	0.1	0.5	0.9	0.2	0.1	0.9	0.9	0.3	0.6	0.9	4.6	0.6	0.48	0.54	6	
	Charcani VI	0.8	0.2	0.1	0.5	0.7	0.3	0.3	0.6	0.9	0.3	0.58	0.9	4.4	0.58	0.46	0.52	8	
Hydroelectric dams	Hydroelectric dams	0.8	0	0	0.1	0.5	-	0.2	-	0.9	0.48	-	0.9	2.5	0.48	0.4	0.44	14	
Other power	Power station	0.8	0.7	0.3	0.7	0.7	0.2	0.1	0.6	0.8	0.64	0.6	0.8	4.9	0.64	0.5	0.57	4	
Power poles and lines	Wood	0.8	0	0	0.7	0.4	-	0.8	-	0.5	0.56	-	0.5	3.2	0.56	0.5	0.53	7	
	Concrete	0.8	0	0	0.7	0.6	-	0.3	-	0.5	0.46	-	0.5	2.9	0.46	0.44	0.45	13	
Water supply systems	Water canal open	0.8	0.3	0.1	0.7	0.5	-	0.2	-	0.7	0.54	-	0.7	3.3	0.54	0.46	0.5	10	

Table 4.11: Infrastructure vulnerability in Arequipa. Infrastructure are assigned coefficients from 0 to 1 (0 least important/susceptible, 1 most important/susceptible) according to a number of different criteria. The mean gives the value of the infrastructure on the same 0 to 1 scale of susceptibility with the different infrastructure ranked to show the most and the least vulnerable.

Elements		Criteria: Coefficients from 0 (low importance) to 1 (high importance)											Totals			
		Lifeline		Population exposure		Economic repercussion		Construction		Other			Total	Total maximum normalised	Total minimum normalised	Mean
Critical/essential		Day	Night	Loss of income	Rebuild cost	Age	Materials	Energy output	Distance from river	Height above river						
Water supply systems	Water canal covered	0.8	0	0	0.7	0.6	-	0.1	-	0.7	-	2.9	0.46	0.44	0.45	13
	Irrigation canals	0.7	0.3	0.1	0.7	0.6	-	0.7	-	0.7	-	3.8	0.62	0.56	0.59	3
	Water treatment plant	0.8	0.7	0.1	0.6	0.7	-	0.2	-	0.1	-	3.2	0.5	0.36	0.43	15
	Water pipes	0.8	0	0	0.7	0.6	-	0.3	-	0.5	--	2.9	0.46	0.44	0.45	13
Waste water supply systems	Waste water and sewerage pipes	0.8	0	0	0.6	0.6	-	0.3	-	0.5	-	2.8	0.44	0.56	0.5	10
Telecommunications	Telecommunication lines	0.8	0	0	0.6	0.6	-	0.3	-	0.5	-	2.8	0.44	0.56	0.5	10

Table 4.11: Infrastructure vulnerability in Arequipa continued.

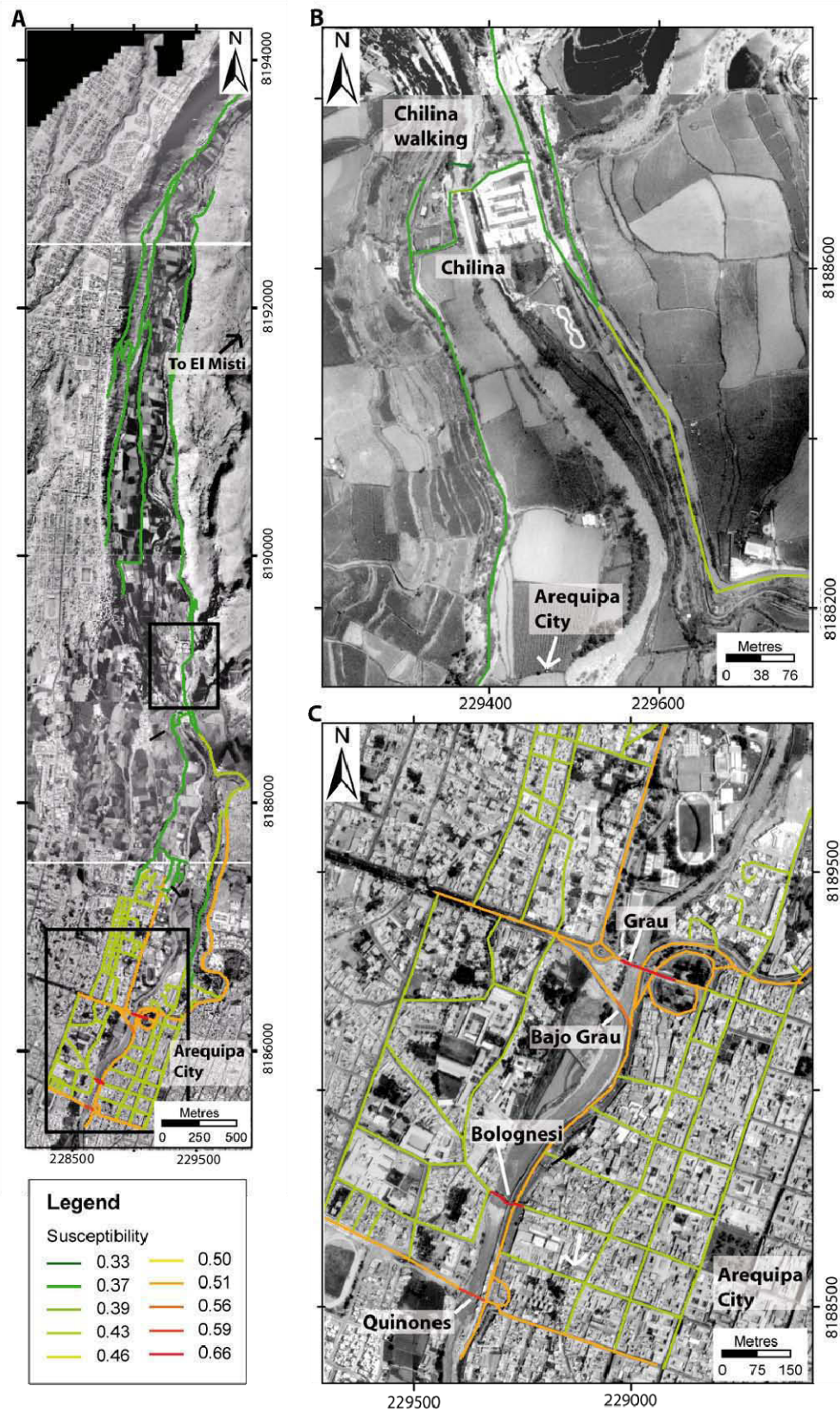


Figure 4.48: Vulnerability analysis map for roadways and bridges in the Río Chili valley, where 0 is the least susceptible and 1 is the most. **A:** Overview of the vulnerability of the transportation network. **B:** The walking and road bridges in Chilina. **C:** Vulnerability of the transportation network in Arequipa city centre, highlighting the main bridges crossing the river.

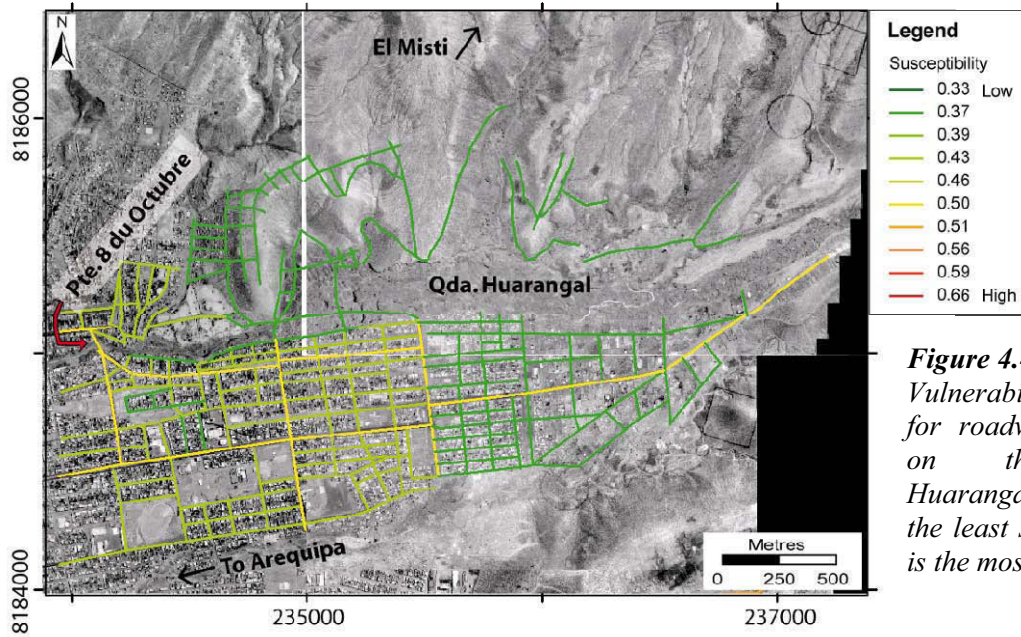


Figure 4.49: Vulnerability analysis map for roadways and bridge on the Quebrada Huarangal fan, where 0 is the least susceptible and 1 is the most.

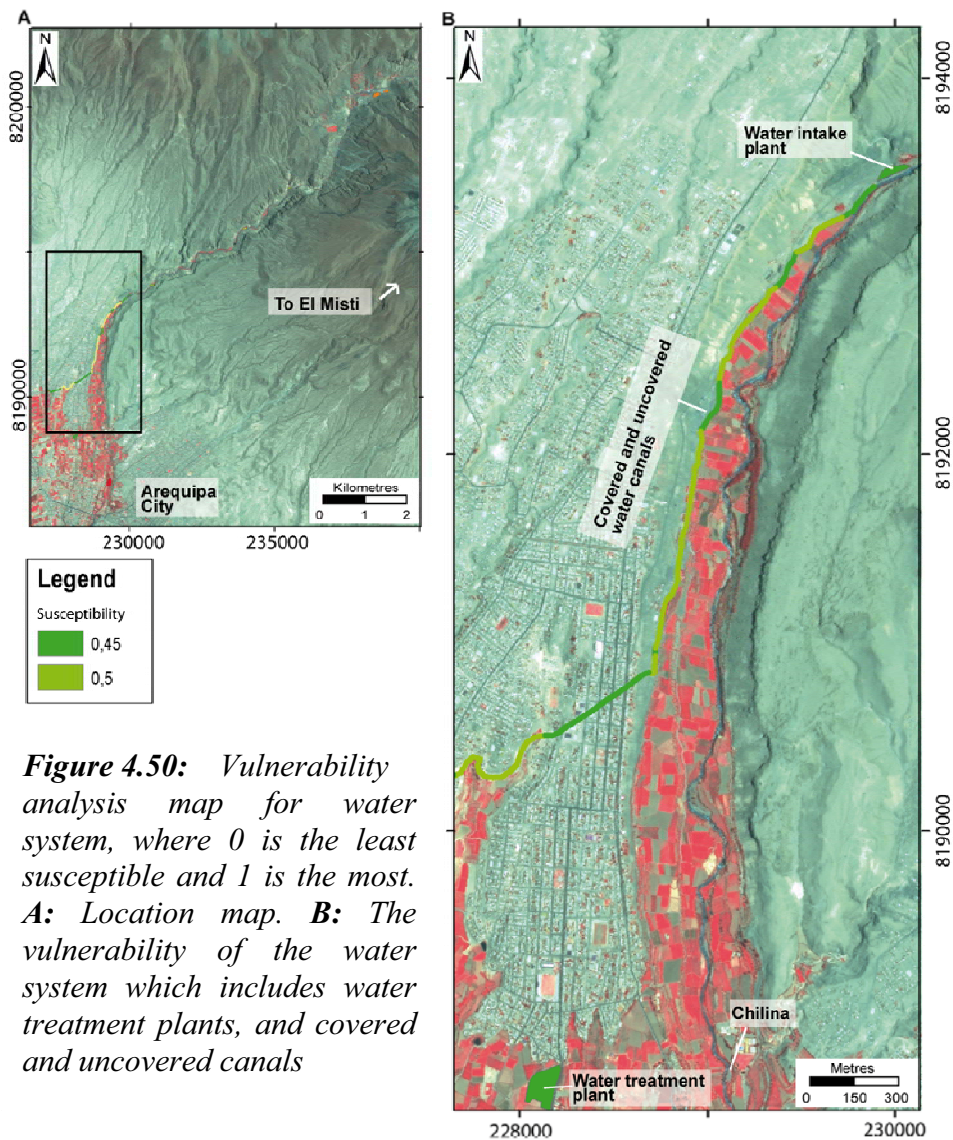


Figure 4.50: Vulnerability analysis map for water system, where 0 is the least susceptible and 1 is the most. **A:** Location map. **B:** The vulnerability of the water system which includes water treatment plants, and covered and uncovered canals

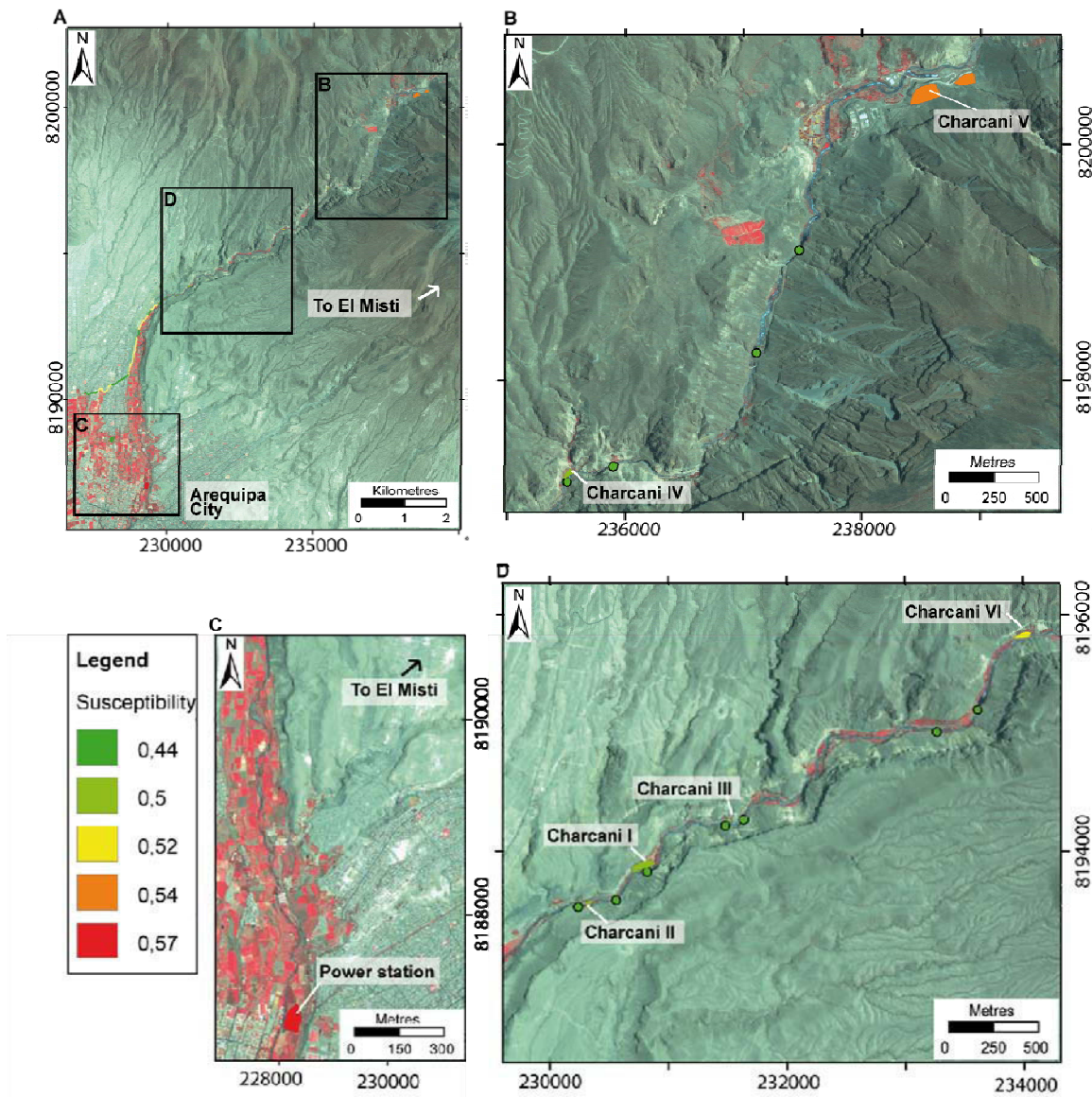


Figure 4.51: Vulnerability analysis map for roadways and bridges in the Río Chili valley, where 0 is the least susceptible and 1 is the most. **A:** Overview of the vulnerability of the transportation network. **B:** The walking and road bridges in Chilina. **C:** Vulnerability of the transportation network in Arequipa city centre, highlighting the main bridges crossing the river.

The vulnerability analysis of infrastructure indicates that Puente Grau is the most vulnerable in Arequipa, followed by Puentes Bolognesi and Quiñones and the irrigation canals. This is not surprising given the relevance of these bridges as major transportation links across the city. In addition Puentes Grau and Bolognesi are the oldest bridges, and perhaps most important with regards to transportation, food supply and tourism in the city. The least vulnerable infrastructure according to the vulnerability analysis are the Chilina walking bridge, unsealed roads, railways and the Chilina bridge. The Chilina walking bridge is situated on private land and is used rarely; the likelihood of people being on the bridge during

a mass flow is low and the immediate need for the bridge after a mass flow event is very unlikely. Both the Chilina bridges have very low traffic volumes and are not considered as vital to the transportation network in Arequipa. Similarly unsealed roads have a much lower traffic volume than sealed roads, and despite being often in poorer condition than minor and main roads, they are cheaper and easier to replace after an event. The low vulnerability rating of the railway networks is due to the railway being situated outside of the study area. The railway network in Arequipa is not extensive because other modes of transportation are more utilised.

The irrigation canals are vital to agriculture in Arequipa; in this semi-arid environment crops would not survive without irrigation. Additionally crops will provide nutrition for the community during and after a crisis. The power stations are also very vulnerable within the top ten most vulnerable infrastructures. The thermal power station is more vulnerable than they hydroelectric due to the higher electricity output, larger number of employees and visitors at the station, and also the reliance of the transportation on diesel fuel for power generation. Charcani Quinto is the most vulnerable hydroelectric power station due to its location, the high electricity output and the rebuild cost (i.e. a large tunnel system taking water through the side of the volcano).

4.6 Summary of the vulnerability of land use, buildings and infrastructure in Arequipa

The most vulnerable land, buildings and infrastructure in Arequipa have been identified in this chapter. The results of the building and infrastructure survey identified a range of construction types, and often within the same city block. The poorest quality houses (and not structurally sound) are often located closest to the river channels with the most vulnerable area identified as within, and adjacent to, the temporary stream of Quebrada Huarangal. Without the vulnerability analysis the buildings are considered vulnerable just due to their location; however the vulnerability analysis confirmed that they are further endangered by their construction type and the dominant land use.

The city is reliant on the Río Chili for power, water and food, and yet if a mass flow event is to occur, these essential services are indeed most vulnerable. Transportation links are vital during a crisis and the analysis of infrastructure highlighted that the bridges, which cross the

Río Chili in the city centre are the most vulnerable. If bridges are destroyed, access from one side of the city to the other will be severely limited and in addition water pipes and power and telecommunication lines are often located at bridges, and are thus equally vulnerable to damage. Services such as the Egasa power station and the hydro-electric dams are also vulnerable, possibly resulting in the severe disruption of power supply to the city, and having a flow-on effect for lifeline services such as hospitals and other emergency services.

Chapter Five

The risk facing the city of Arequipa

5.0 Introduction: the effects of lahars and flash floods on buildings and infrastructure

As part of identifying the risk of inundation and/or damage to buildings, land and infrastructure from lahar and flash floods, the physical effect of the flows and their potential damage must be understood. The damage caused to buildings and infrastructure is influenced by flow characteristics and forces, but is also depends on building factors (e.g. orientation, form, construction quality). Kelman, 2002 identified water depth, flow velocity, bed shear stress, dynamic forces (flow momentum, stream power, depth times speed), rate of flood rise, and debris potential of the landscape as the most important factors when estimating the damage caused by floods. Other parameters which can be considered are corrosion due to chemical contaminants, changing hydrostatic pressure due to waves, pressure from breaking waves, lift due to the buoyancy of the property and scour undermining the foundations. These parameters, most notably flood depth, have continued to be imperative when conducting flood risk analysis (e.g. Kelman, 2002).

Zanchetta et al. (2004) proposed that the destructive power of lahars is due to the action of three main forces: (1) hydrodynamic (i.e. the dynamic overpressure due to the frontal impact, the drag effect exerted by the flow running along the sides of a structure, etc.); (2) hydrostatic, which accounts for the weight of the flow; and (3) collisional, due to the individual objects carried by the flow. These forces mainly depend on peak discharge, velocity, volumes, sediment-water ratio and grain-size distribution flows.

During a flood or lahar event, there are three major failure mechanisms that would make a building unsafe (Kelman, 2002): 1) the building fills with water to a depth which is unsafe for the people inside. Windows and doors are assumed to be the weakest elements are most likely to be damaged by floodwaters. The building is considered unsafe if the depth of water

inside reaches 1.5 m above the floor of the top storey; 2) the flow may cause structural damage leading to the collapse of the building and injury/death to the occupants; and 3) the buoyant and lateral force of the water may overcome the strength of the anchors and the weight of the building holding on to the foundation. The resistance to buoyancy is provided by the weight of the house and the strength of bolts anchoring it to the foundation.

The main forces (and their effects) driving against buildings and infrastructure from lahars are summarised in Table 5.1 below.

Action		Description	Parameters	Direct Processes	Indirect Processes	Effects
Hydrodynamic Pressure	Lateral component	The action of the lahar flowing and moving around a building. As the flow velocity and depth increases then these forces will also increase.	$p_s = 1/2 C_D \rho v^2$ $F_s = p_s d$ In which: ρ = density of lahar g = acceleration of gravity d = depth of flow (m) C_D = drag-coefficient (between 0 and 2, in this case 0.82) v = velocity (m/s)	<ul style="list-style-type: none"> - Ductile deformation - Fragile deformation (cracks) 	<ul style="list-style-type: none"> - Fragile deformation - Rupture - Fissuration - Disaggregation, - Transport of material. - Lateral displacement, - Collapse 	<ul style="list-style-type: none"> - Fragile deformation and breaking if ductile threshold exceeded. - Wall deformation. - Following building deformation, material is removed and transported by lahar. - Wall and roof frame displacement via crack formation.
	Vertical component			<ul style="list-style-type: none"> - Ductile deformation - Fragile deformation - Crack formation 	<ul style="list-style-type: none"> - Fragile deformation - Disaggregation - Vertical displacement - Collapse 	<ul style="list-style-type: none"> - Roofs subside absorbing deformation up to a 'plastic' threshold. Blocking of doors and windows – hindering evacuation. - Cracks in roofs leading to disaggregation. - Downward displacement of roof and floor. - Displacement and cracks leading to roof collapse.
Hydrostatic Pressure	Lateral	The effects on a building of lateral and uplift pressure forces due to the hydrostatic pressure of surrounding lahar and saturated ground.	The hydrostatic force, F_s , due to a lahar acting on a wall are determined from: $F_s = \int \rho g h dA$	<ul style="list-style-type: none"> - Ductile deformation 	<ul style="list-style-type: none"> - Fragile deformation 	<ul style="list-style-type: none"> - Deformation of load bearing walls and deformation propagation to other edifice elements. - Crack propagation through load bearing walls may lead to collapse.
	Capillary rise	Lateral pressures concentrated at bottom of wall, and also drawn up into porous material by capillary rise.	where: ρ = mass density of flow; g = gravitational acceleration; h = depth of flow; A = surface area of the wall in contact with flow	<ul style="list-style-type: none"> - Fragile deformation 	<ul style="list-style-type: none"> - Disaggregation 	<ul style="list-style-type: none"> - Material water content may exceed plasticity threshold.
Debris impact	Static (accumulation of lahar material)	Static debris actions occur due to sediment accumulating externally or internally to a residence.	<i>-Case of deposits on roof:</i> Pressure $P = F / S$ depends on force and surface on which it is exerted $F = m \cdot g$ m mass of elements deposited on roof <i>-Case of deposits on edges of edifices:</i> These exert an oblique force (due to wall-buttressing) dependent on lahar deposit thickness.	<ul style="list-style-type: none"> - Burial 	<ul style="list-style-type: none"> - Flat roofs are more likely to be affected, corrosion - Change in topography - Water soaking 	<ul style="list-style-type: none"> - Burial, blocking doors preventing-evacuation. - Infiltration of material makes structure more resistant but may corrode metal making it less stable. - May avulse stream and rainfall water towards edifice; can remove deposits surrounding edifice. - Slow protracted supply of water to edifice leading to rot.

Table 5.1: The actions and effects of lahar on buildings and infrastructure (modified from Palhol, 2007, Prevot, 2008 and adapted from elman, 2002)

Dynamic	Dynamic debris actions occur when debris moved by the lahar impacts a residence.	$F_i = wV/gt$ F_i = impact force w = weight of the object V = velocity of water g = gravitational constant t = duration of impact in seconds	<ul style="list-style-type: none"> - Ductile deformation especially if continuous impact. - Crack propagation due to discrete or continuous impacts with high energy. 	<ul style="list-style-type: none"> - Fragile deformation - Rupture - Collapse 	<ul style="list-style-type: none"> - Roof and wall deformation due to continuous block impacts. - Wall displacement and/or collapse due to numerous or continuous impacts. - Block impacts creating cavities in edifice may lead to collapse. - Fallen elements from edifice can become blocks in lahar.
	Erosion/scour	Erosion can be caused by lahar flowing around the building or by the actions of waves lapping at a building.	<p>Lahar flow can undercut edifice or soil under it.</p> <p>Lahar density, velocity, solid concentration, channel constriction and terrace material type.</p>	<ul style="list-style-type: none"> - Lateral erosion and undercutting of substrate under building - Removal - Crack propagation due to discrete or continuous impacts with high energy. - Removal 	<ul style="list-style-type: none"> - Deformation, cracks, vertical displacement, collapse - Rupture - Destabilisation of the structure - Collapse
Bouyancy	Water displaced by a building causes a vertical <i>buoyant force</i> upwards on the building.	The buoyant force, F_B , acting on the bottom area, A_b , is determined as follows: $F_B = \int \rho g h dA_b$	<ul style="list-style-type: none"> - Removal 	<ul style="list-style-type: none"> - Vertical displacement, collapse, - Destabilisation of the structure 	<ul style="list-style-type: none"> - Floating of residence, or parts of it. - Risk that the buoyant force may overcome the resistance of the building and lift it from the foundation.
Soil deformation		Soil deformation (ϵ), induced by shrinking or swelling soil mechanism. Pore pressure, soil porosity, soil permeability.	<ul style="list-style-type: none"> - Ductile deformation 	<ul style="list-style-type: none"> - Fragile deformation 	<ul style="list-style-type: none"> - Deformation due to changes in soil or substrate. - Cracks may lead to collapse.
Temperature of hot lahars		Heat transfer from lahar flow to housing elements and furniture: $T < 100^\circ\text{C}$, heat loss from lahar, area of contact on housing (S_b), at ground level (S_l), and exposed to air (S_e). Thermal conductivity and heat capacity of material hit by lahar.	<ul style="list-style-type: none"> - Melting - Slow burning 	<ul style="list-style-type: none"> - Weakens materials. 	<ul style="list-style-type: none"> - Burning of flammable material. - Increase in temperature-affecting material strength. - Increase in temperature affecting material strength. - Slow burning of materials-by hot material infiltration.

Table 5.1 continued.

The main force acting against buildings and infrastructure is that of lateral hydrodynamic pressure. Kelman (2002) calculated that typical United Kingdom masonry walls would begin to fail between 5 to 10 kPa, and a 10 kPa base pressure would equal a 0.7 m flood at 3.5 m/s. Other studies have shown complete failure at 0.6 m with significant damage occurring around 0.3 m (Proverbs et al., 2001).

5.2 Arequipa case study: risk assessment

The risk of inundation and/or damage to buildings, land and infrastructure was assessed by combining a number of tools: hazard assessments, flow characteristics and effects, and element vulnerability (refer to Chapter 1 for the method). The calculations were undertaken in a GIS allowing for the spatial expression of the risk element, which is an attractive method for communicating information to decision makers and the community alike (Figure 5.1). Another advantage of using a GIS is that databases can be readily updated when new information becomes available, thus allowing for the analysis of data in quasi real-time. The risk posed to buildings, land use and infrastructure in Arequipa from lahars and flash floods is discussed in the following sections.

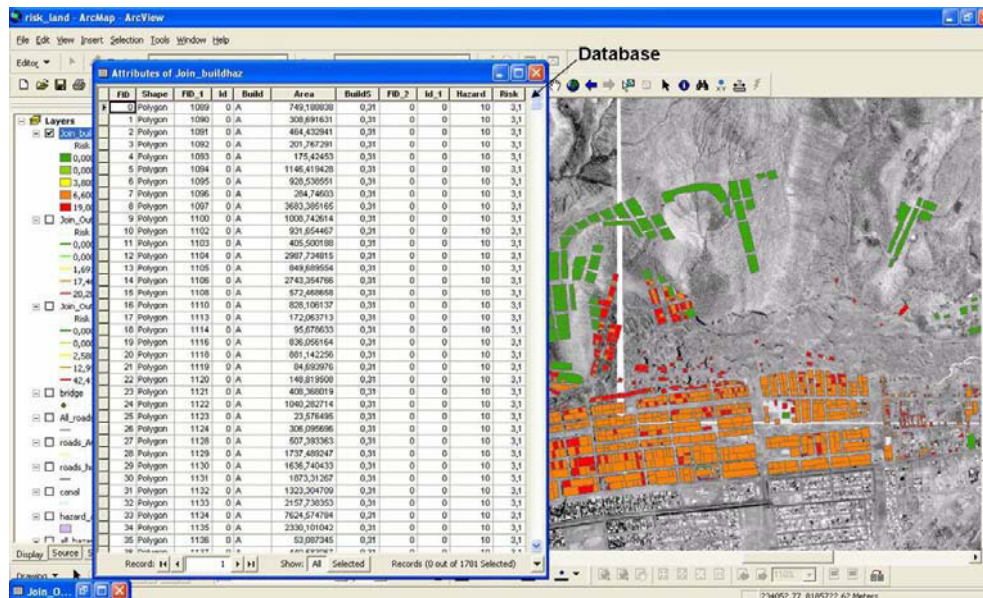


Figure 5.1: Database created in ArcGIS to combine various layers including hazard and vulnerability.

5.2.1 Building Risk

The risk of inundation and/or damage to buildings, depending on their individual vulnerability (refer to chapter 4), from lahars and flash floods are shown in Figures 5.2 and 5.3 below. Figure 5.2 was created using the conventionally-derived hazard assessment and indicates that

the level of risk in the Río Chili Valley is quite low despite the frequency and magnitude of small- to medium-sized flash floods which occur every 2 to 10 years on average. Buildings in the city centre area which are identified as *high* risk relate to poor quality adobe-constructed private dwellings. An ignimbrite building located on the western rivers edge is identified as *high* risk. This building corresponds to a wedding and reception venue where buildings and land adjacent to the river serve this purpose. In addition the military camp and the La Choceta restaurant near Chilina were also identified as *high* risk.

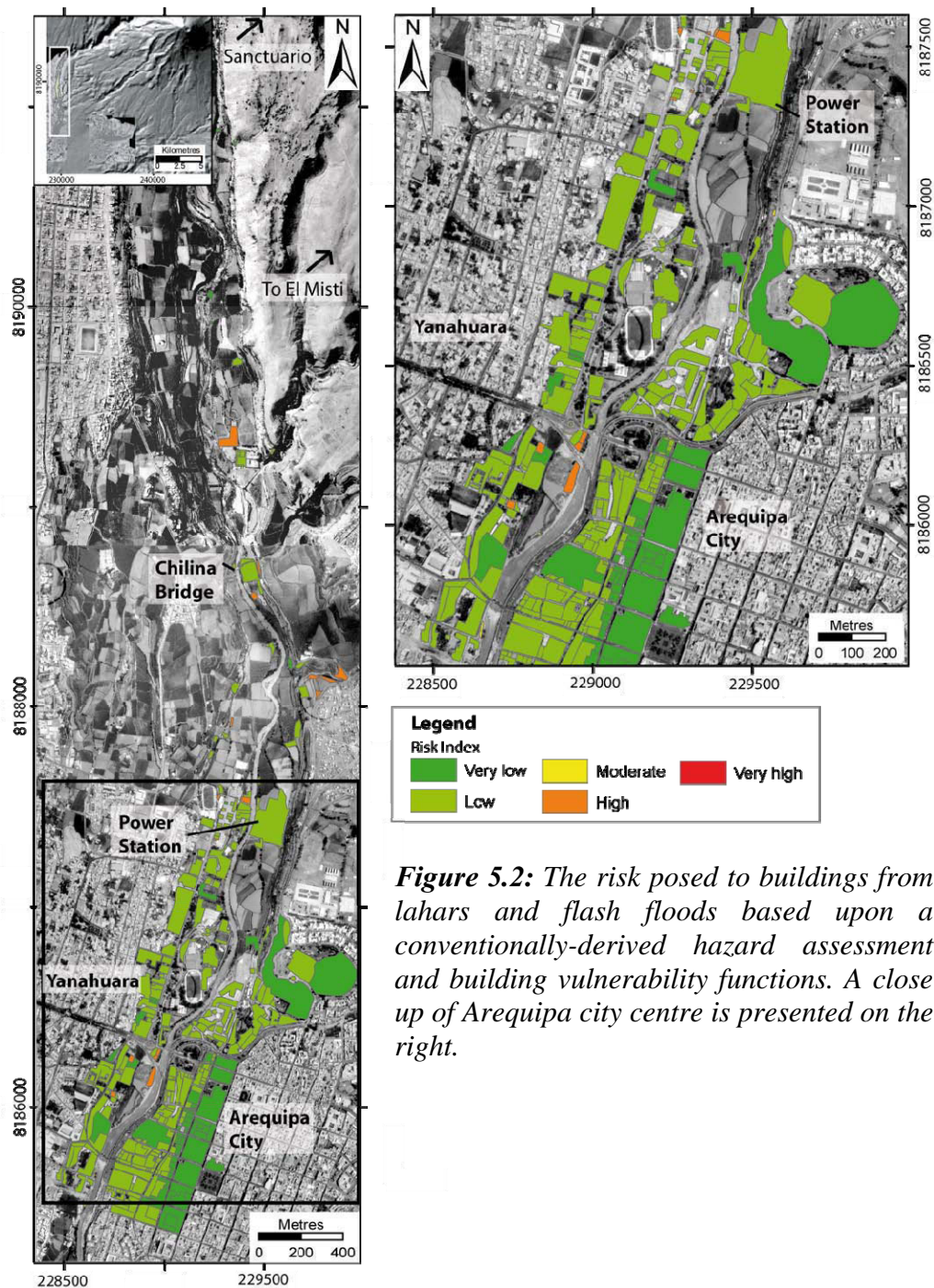


Figure 5.2: The risk posed to buildings from lahars and flash floods based upon a conventionally-derived hazard assessment and building vulnerability functions. A close up of Arequipa city centre is presented on the right.

These risk estimates only relate to the risk calculated from the conventionally-derived hazard maps. The difference in the level of risk between the two methods of hazard assessment can be clearly seen in Figure 5.3; where all of the buildings in the Río Chili valley are considered *low* risk. This is because the Titan2D flow run out length did not reach Arequipa city. The La Choceta, a popular tourist restaurant situated on the eastern bank of the Río Chili in Chilina, is identified as *high* risk in the Titan2D developed risk maps as well as the conventionally developed map.

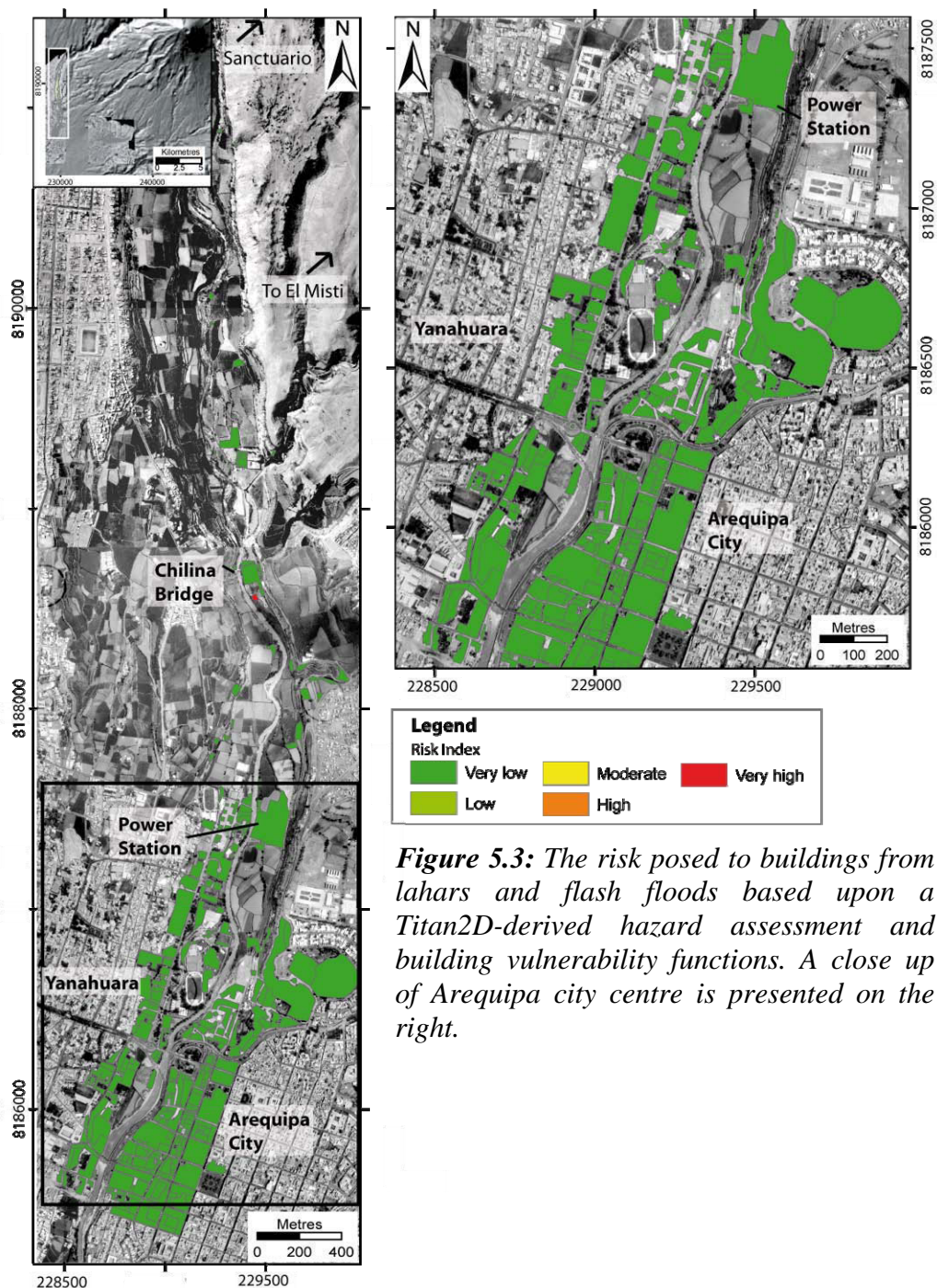


Figure 5.3: The risk posed to buildings from lahars and flash floods based upon a Titan2D-derived hazard assessment and building vulnerability functions. A close up of Arequipa city centre is presented on the right.

A larger number of buildings are identified as at risk on the Quebrada Huarangal fan using both methods of hazard assessment. Figure 5.4 (left) shows the risk of building damage and/or inundation as calculated from the conventionally-derived hazard assessment, whereas Figure 5.4 (right) is based upon the Titan2D-derived hazard map. The main difference between the two assessments is that a larger number of buildings fall into higher risk categories in the conventionally developed risk map. In both maps the highest concentration of *very high* risk buildings are located within in the Quebrada Huarangal channel, and especially in the San Jerinomo suburb which was flooded in February 2011 (Chapter 2). The majority of these buildings are private dwellings with a small number of commercial premises. In addition they are the lowest ranked in building vulnerability in the vulnerability assessment.

Overall the risk assessments indicate that the majority of buildings located within the Quebrada Huarangal channel are considered *high* to *very high* risk from the inundation of lahars and flash floods. Although very few buildings are considered as *high* risk in the Río Chili Valley. This could be due to existence of more structurally sound buildings and also buildings are not sited within the river channel itself as in the case of Quebrada Huarangal.

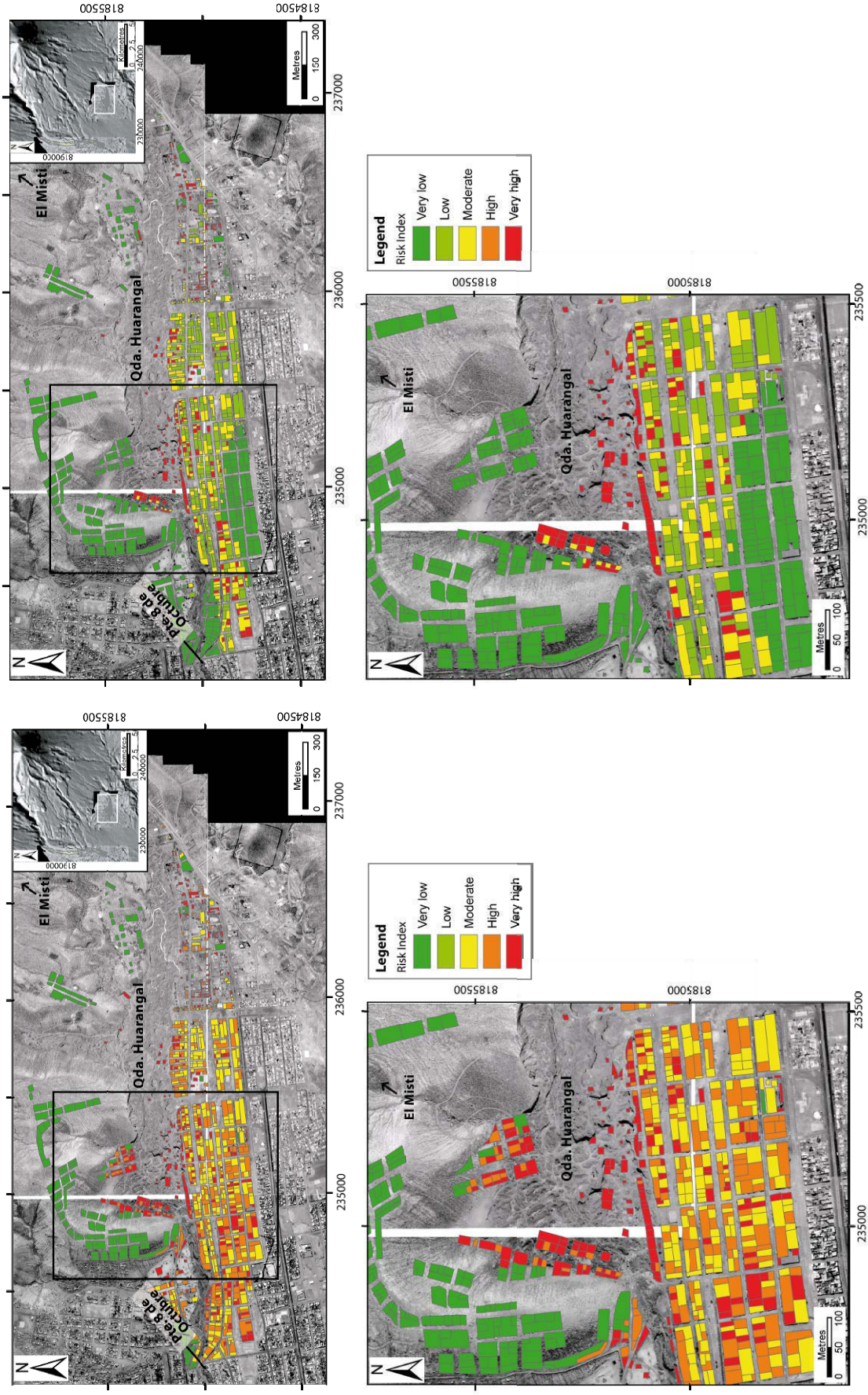


Figure 5.4: The risk posed to buildings from lahars and flash floods based upon hazard assessment and land use vulnerability functions on the Quebrada Huarangal fan. The risk calculated from a conventional hazard assessment is presented to the left of the figure, in contrast the Titan2D based risk assessment is presented on the right.

5.2.2 Land use risk

The level of risk posed to land use in Arequipa from lahars and flash floods is presented in Figure 5.5. Again differences between the two different methods of hazard assessment are especially apparent when comparing the Río Chili valley risk maps. In the conventionally derived risk map the majority of land use in this area is identified as *moderate* risk, whereas the vast majority of land use is identified *very low* risk using the Titan2D hazard assessment. Land use identified as *moderate* risk in the Río Chili valley is not only limited to one or two different land use types, but covers the spectrum from private dwellings to agriculture. In contrast many businesses and factories (e.g. the brick factories located on the northern bank of the channel) within and adjacent the Quebrada Huarangal channel are considered as *high* to *very high* risk. There are not considerable differences in the level of risk on the Quebrada Huarangal fan identified using the two different methods.

Overall the risk assessments indicate that the majority of land use located within the Río Chili valley is considered as at *moderate* risk of inundation and/or damage from lahars and flash floods. Small commercial premises and factories are considered as *high* to *very high* risk during inundation on the Quebrada Huarangal fan.

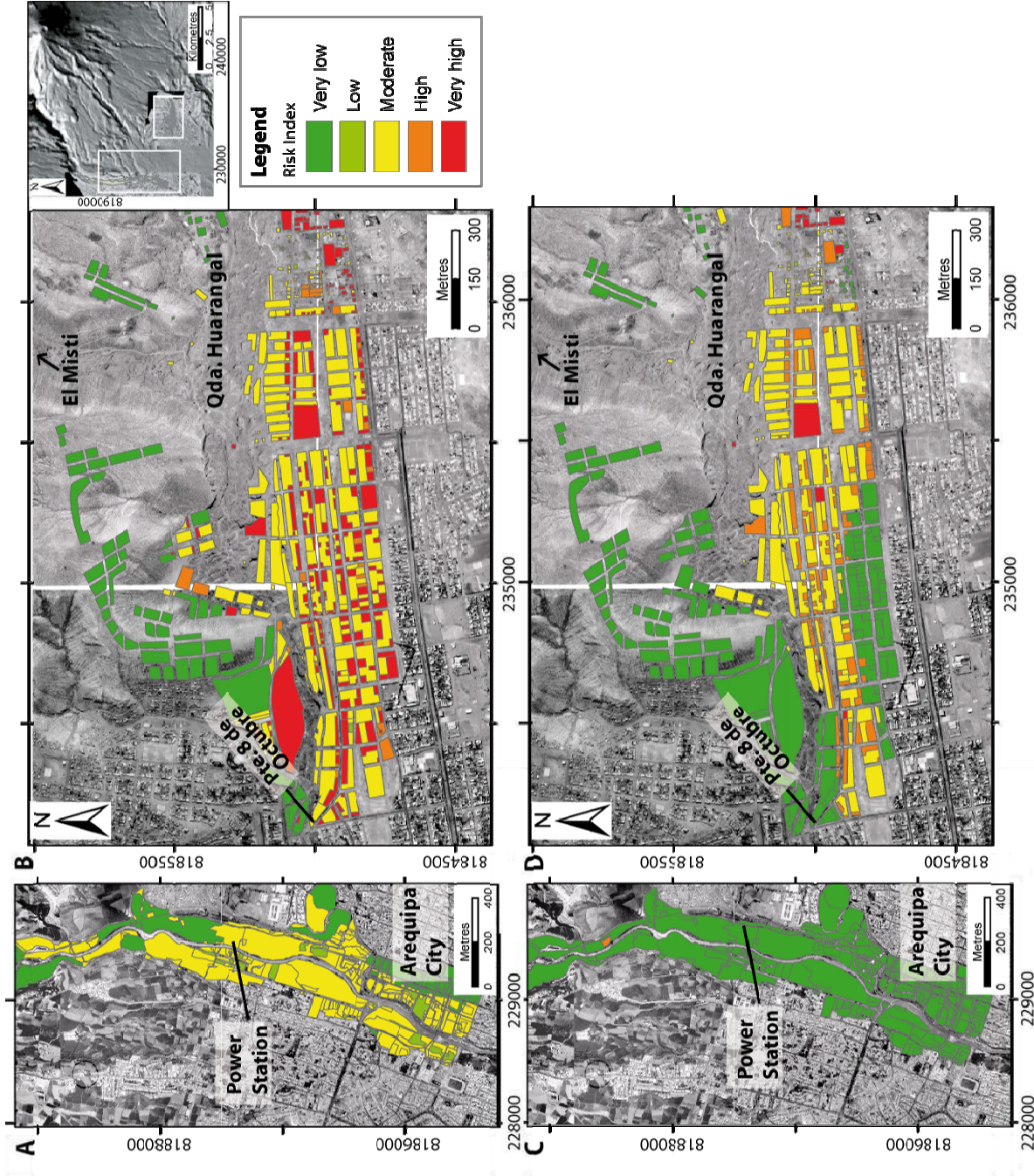


Figure 5.5: The risk posed to land use from lahars and flash floods based upon a conventionally-derived (A and B) and Titan2D-derived (B and C) hazard assessments and building vulnerability functions. The R o Chili valley is represented by images A and C, and the Quebrada Huarangal fan in images B and D.

5.2.3 Combined building and land use risk

The risk has been determined from the combined building and land use vulnerability and the hazard assessments for each of the reference scenarios (Figures 5.6 to 5.11).

5.2.3.1 Scenario one – low magnitude/high frequency

The level of risk to the Río Chili valley from small magnitude ($<0.5 \times 10^6 \text{m}^3$) and frequent (2 – 10 years) floods are given in Figure 5.6 below. The risk of damage and/or inundation for the majority of properties in the Río Chili valley is *very low*, apart from some areas directly adjacent to the river channel when calculated from the conventionally-derived hazard map (Figure 5.6 A). In contrast, all surveyed buildings and land uses are considered *very low* risk in the Titan2D derived assessment (Figure 5.6 B). This is because the Titan2D simulated low volume flow did not extend into the surveyed area.

In the conventionally derived assessment map *very high* risk corresponds to the private adobe dwellings situated on the western channel edge (t0 and t1', refer to Chapter 2, Figures 2.18 and 2.19) in the city centre. The *La Choceta* restaurant, a confined brick single storey building with a thatched-style roof and large pane glass windows, is also at *very high* risk of damage/inundation during a flow event. The restaurant is located approximately 2 km upstream of the city centre on the eastern low terrace (t1') of the Río Chili. Some areas of the *Club Internacional* sports club, on the western low terrace of the Río Chili approximately 200 m upstream of Puente Grau, are considered as *high* risk. *High* risk properties are also identified approximately 500 m upstream of the club on the western low terrace (t1 and t1'). The properties are private dwellings, a small commercial property and a popular tourist restaurant, all constructed from confined brick masonry. Two unconfined masonry rural properties on either side of the river are considered *high* risk.

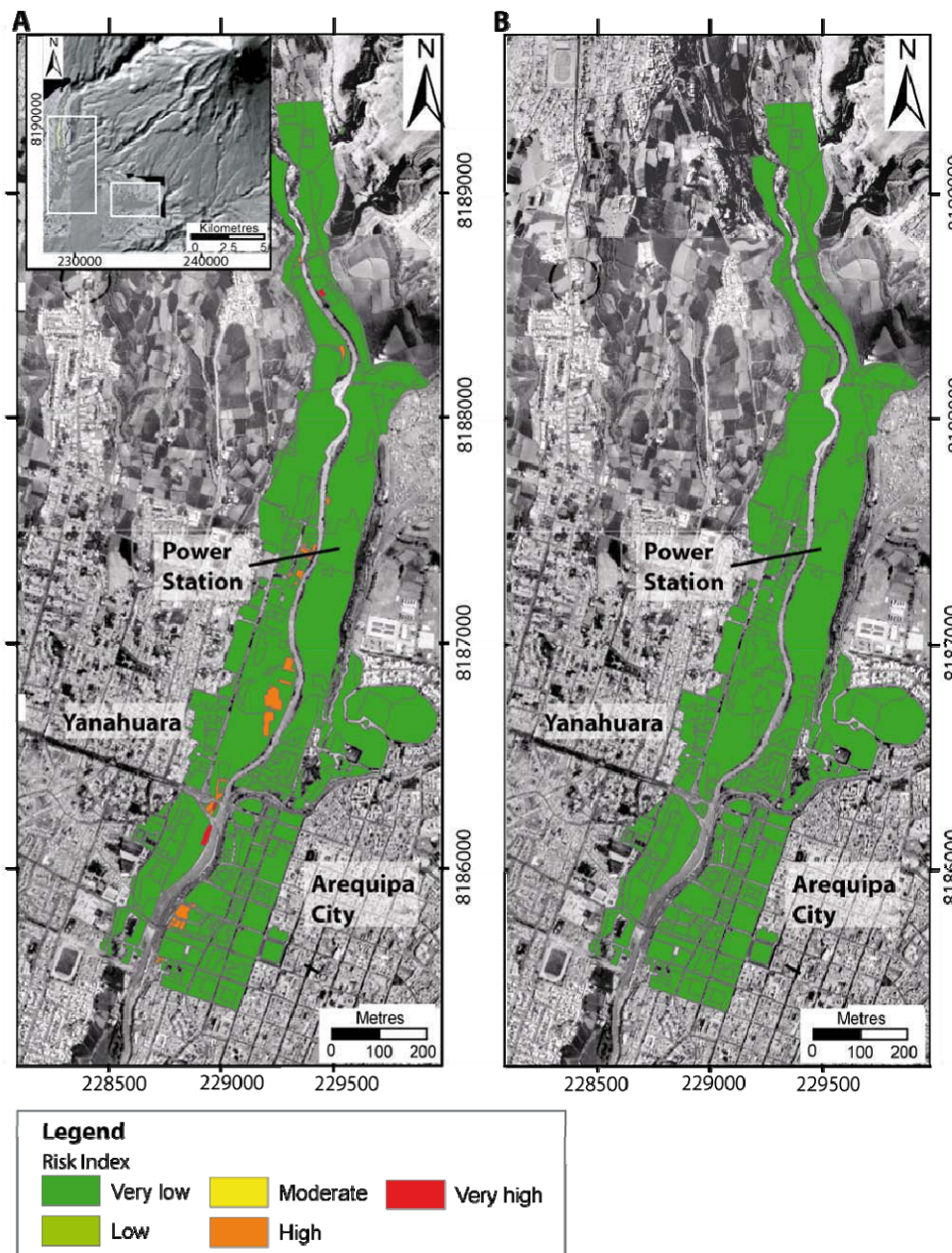
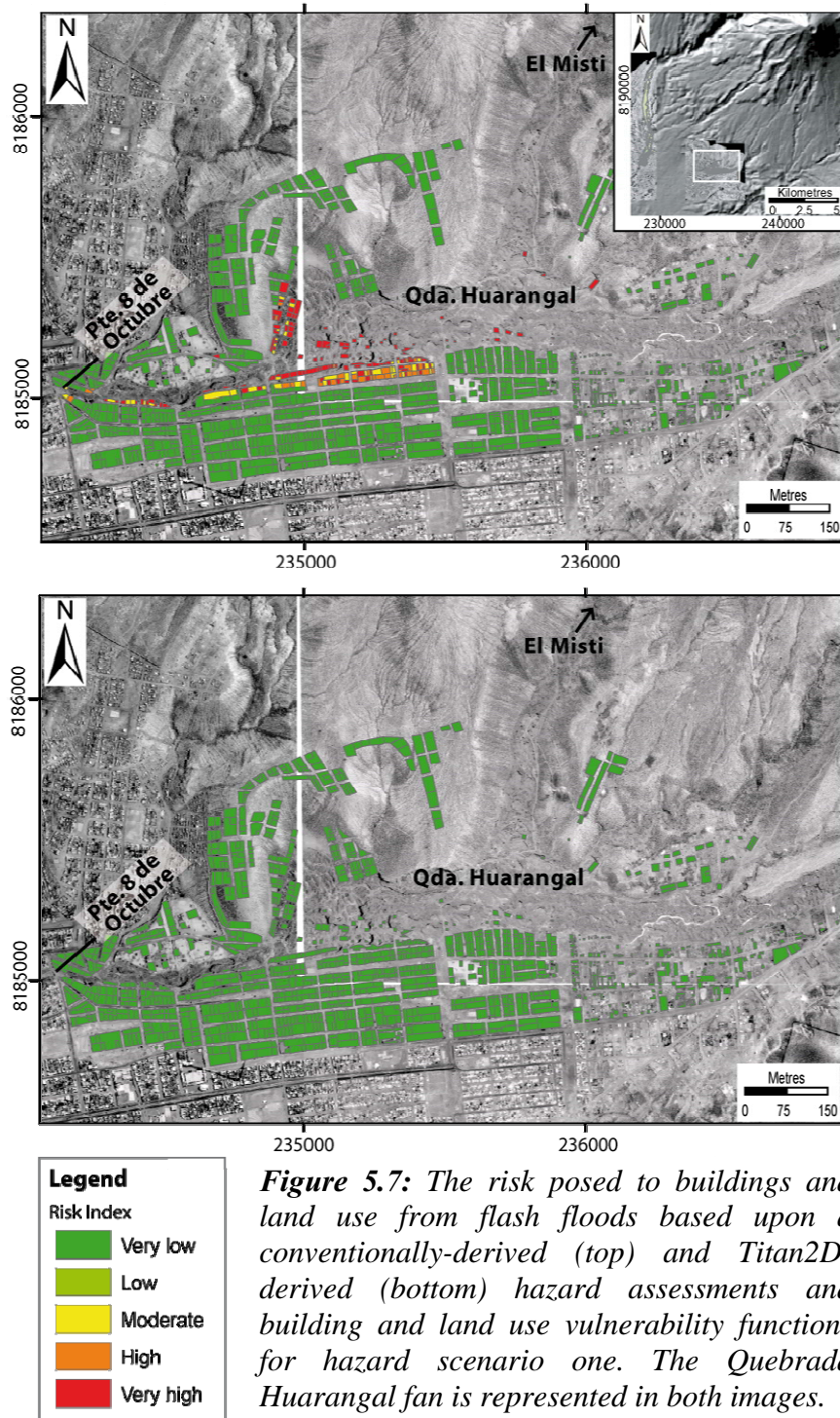


Figure 5.6: The risk posed to buildings and land use from flash floods upon a conventionally-derived (A) and Titan2D-derived (B) hazard assessments and building and land use vulnerability functions for hazard scenario one. The Ro Chili valley is represented in images A and B.

Overall, the risk of damage and/or inundation to property is *very low* when calculated from the conventionally-derived hazard map on the Quebrada Huarangal fan (Figure 5.7, upper image). *Moderate*, *high* and *very high* risk properties are concentrated within, and adjacent to, the channel on the southern lower terrace (t1). In contrast, all surveyed buildings and land uses are considered *very low* risk of damage and/or inundation in the Titan2D derived assessment (Figure 5.7, lower image). This is because the Titan2D simulated low volume flow did not extend into the surveyed area.



In the conventionally derived assessment map the majority of *very high* risk properties are private dwellings and small businesses located within the channel, particularly in the San Jerinomo suburb. The buildings are poorly built confined and unconfined masonry, constructed from brick, ignimbrite, stone, concrete block or a combination of all four. The buildings are situated in an area where ponding is likely, as the flow attempts to navigate the drastically narrowing channel to the east of the study area. While some properties located on

the low terraces (t0', t1) are considered to be of *very high* risk to inundation and/or damage from flows, the majority of properties are of *moderate to high* risk. In general the buildings are of better quality construction than those located within the channel.

5.2.3.2 Scenario two – moderate magnitude and frequency

The level of risk in the Río Chili valley from moderate magnitude ($<0.5 \times 10^6 \text{m}^3$ to $4.0 \times 10^6 \text{m}^3$) and moderate frequency (50 – 300 years) lahars is given in Figure 5.8 below. The risk of damage and/or inundation to the majority of the surveyed area is *very low*, and in the case of the map derived from the Titan2D hazard assessment the entire survey area is of *very low* risk (Figure 5.8 B). This is because the Titan2D simulated low volume flow did not extend into the surveyed area.

The *very low* risk areas of the map calculated from the conventionally-derived hazard assessment mostly represent agricultural land upstream of the city centre, and properties situated on upper terraces ($>t2'$) downstream of the Grau bridge (Figure 5.8 A). The properties on the upper terraces are of mixed land uses and building types, although they possess considerably better quality than the majority of buildings located on the Quebrada Huarangal fan. As with hazard scenario one, *high* risk properties are private adobe dwellings located on the western low terraces (t0 to t1') immediately downstream of the Grau Bridge.

Buildings on the western, lower to middle terraces (t0 to t2) downstream of the Grau Bridge are considered *high* risk. The main land uses are private dwellings, commercial centres and factories with a range of building types. More *high* risk properties are located on terraces t1 to t2 just upstream of the confluence of the Río Chili with Quebrada San Lazaro. The properties are private dwellings of building type A and B situated in an upmarket building compound. Many *high* risk properties are also located on the low to moderate terraces (t1 – t2) approximately 1.8 km upstream of the Grau Bridge. Properties in close proximity to the Grau Bridge comprise of upmarket hotels and commercial buildings of building types A and B. Much of the constructed property located within Club Internacional is *high* risk. As with hazard scenario one, *high* risk properties are identified approximately 500 m upstream of the club on the western low terrace (t1 and t1') and rural properties on either side of the river are also *high* risk. The dwellings, sports fields and arenas of the military camp upstream of the

Chilina Bridge are at *high* risk of damage/inundation during a moderate magnitude and frequency lahar or hyperconcentrated flow event.

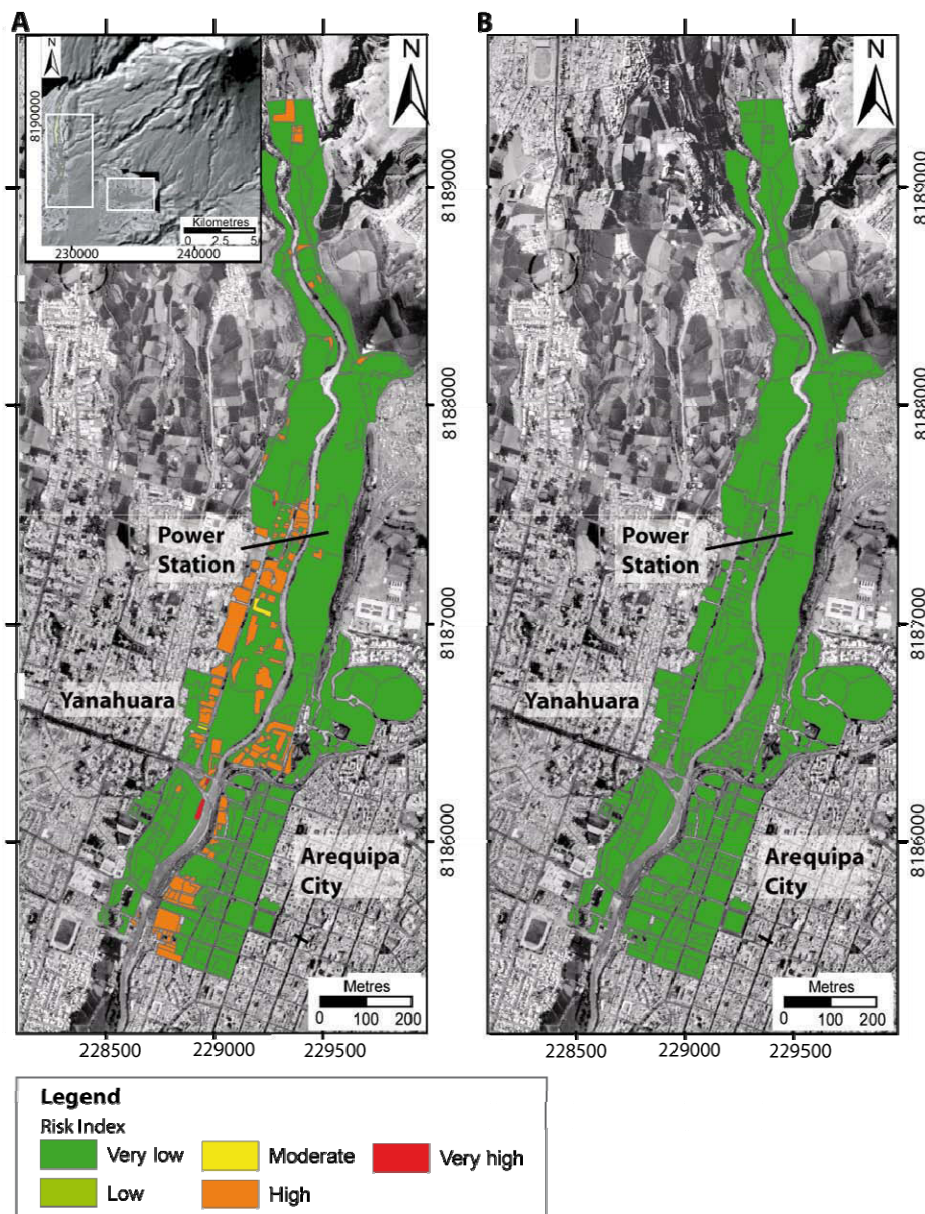
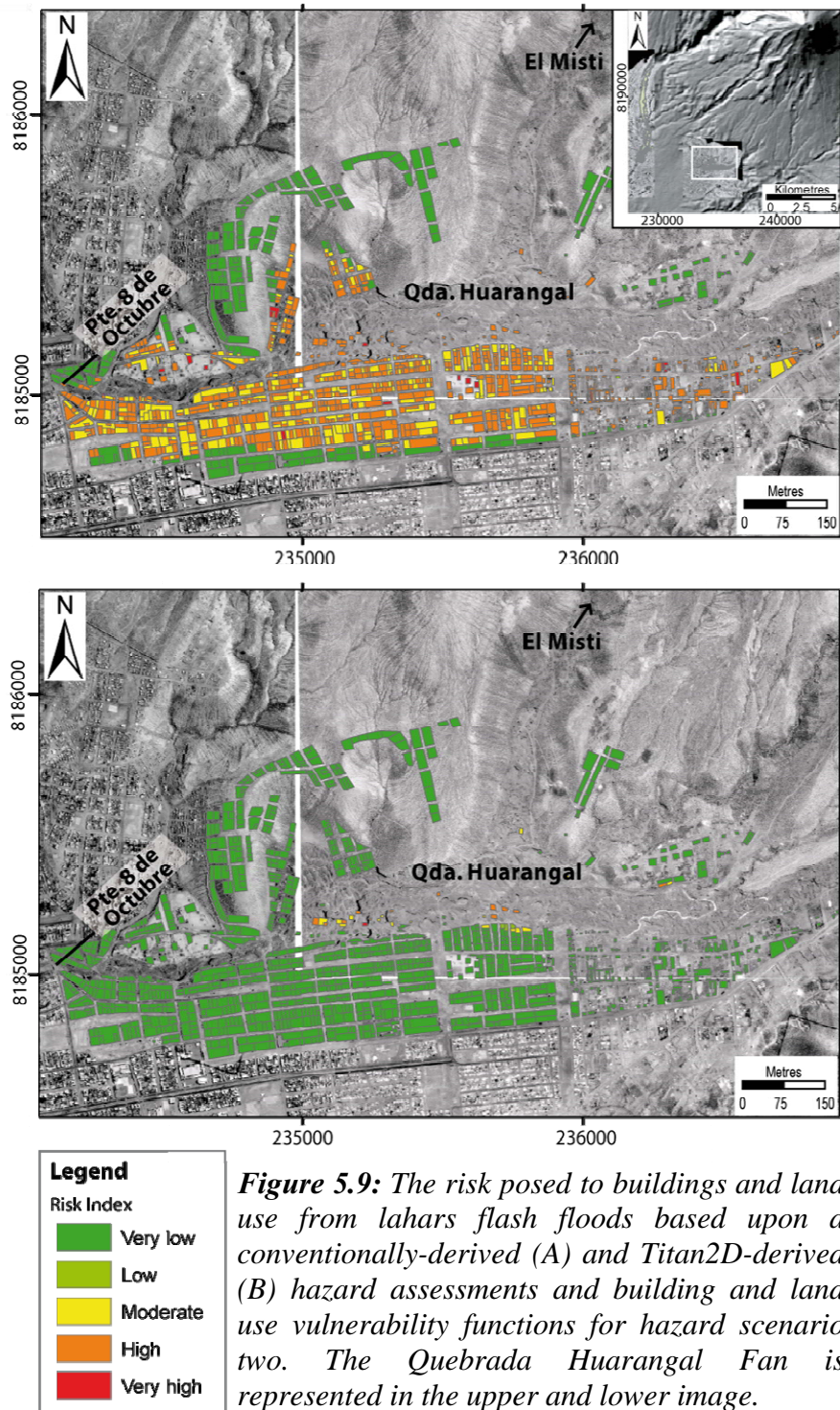


Figure 5.8: The risk posed to buildings and land use from lahars based upon a conventionally-derived (A) and Titan2D-derived (B) hazard assessments and building and land use vulnerability functions for hazard scenario two. The Río Chili valley is represented in images A and B.

On the Quebrada Huarangal fan the risk of damage and/or inundation for the majority of properties is *moderate* to *high* when calculated from the conventionally-derived hazard map (Figure 5.9, upper image). The majority of surveyed buildings and land uses are of *very low* risk when derived from Titan2D (Figure 5.9, lower image). As with the Río Chili Valley study area, this is because the Titan2D simulated low volume flow did not extend into the surveyed area.



On the map constructed from the conventional hazard assessment (Figure 5.9, upper image), moderate, high and very high risk properties are located within the channel, and also on much of the constructed area of the lower to moderate terraces ($t_0 - t_1'$), particularly on the southern side of the channel. As with scenario one, the buildings located within the channel are mostly private dwellings with some small businesses. Buildings are single storey and represent types

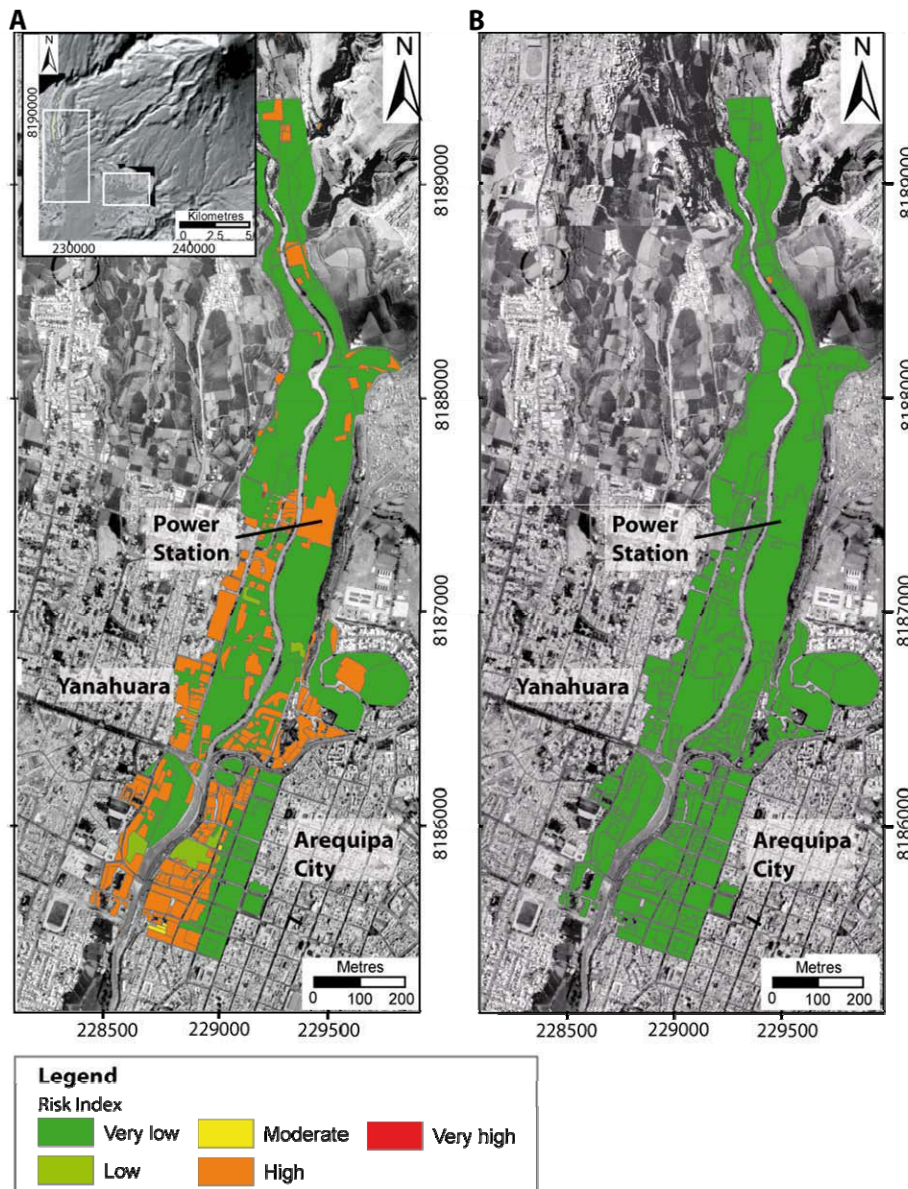
F to H (confined and unconfined masonry and make-shift buildings) which are amongst the lowest ranked (Chapter 4, Table 4.8). They are mostly *high* to *very high* risk.

High and *moderate* risk properties located on the southern terraces mostly consist of building types B, C, F and G. Land use is predominately private dwellings with an equal percentage of commercial properties and factories. The sparse properties located on the south-west side of the terraces are of *high* to *very high* risk due to both their location on the lower terraces and poor quality of construction (building types F to H). *Very low* risk properties are not of any higher quality construction to those located on the terraces; however their position is further from the channel and is unlikely to be inundated by a moderate volume flow.

The majority of properties surveyed are considered *very low* risk in the Titan2D derived assessment (Figure 5.9, lower image), this is because the Titan2D simulated low volume flow did not cover much of the surveyed area. In the channel and adjacent to the channel boundary, where the Titan2D flows reached, properties are of *moderate* to *very high* risk. These properties represent private dwellings of low quality construction.

5.2.3.3 Scenario three – high magnitude/low frequency

The level of risk to the Río Chili valley from large magnitude ($4.0 \times 10^6 \text{m}^3$ to $>11.0 \times 10^6 \text{m}^3$) but infrequent (100 – 2000 years) lahars and hyperconcentrated flow events are shown in Figure 5.10. The risk of damage and/or inundation to the majority of the surveyed area, derived from the conventional hazard assessment, is *very low*, *low* and *high* (Figure 5.10 A). The entire survey area of the map derived from the Titan2D hazard assessment is of *very low* risk with the exception of the La Choceta restaurant near Chilina (Figure 5.10 B) which is a *high* risk property. The extremities of the Titan2D simulated flow at this magnitude was within the vicinity of the restaurant.

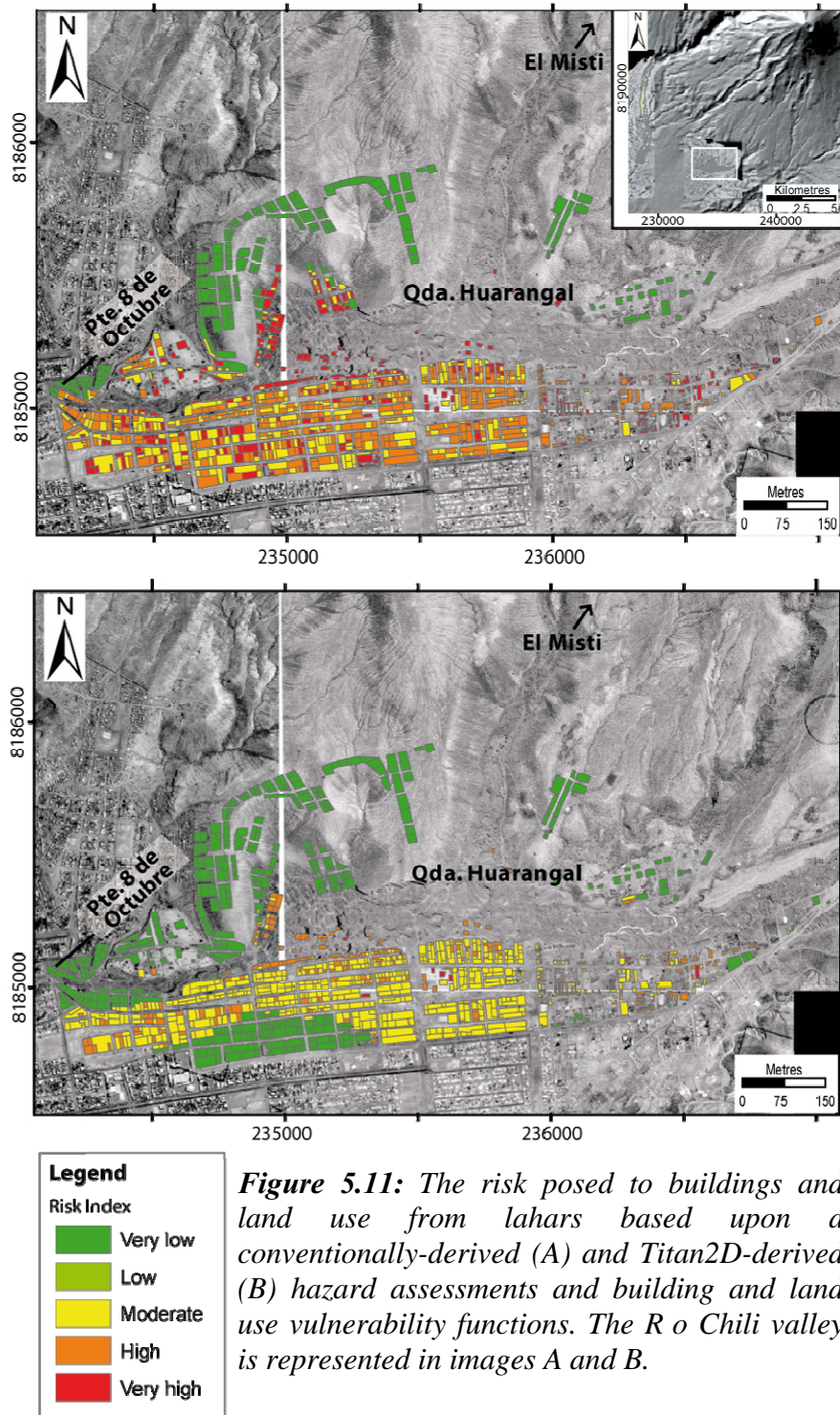


As with scenario two, the *very low* risk areas of the map calculated from the conventionally-derived hazard assessment is agricultural land upstream of the city centre. Properties situated on the eastern upper terraces ($>t_2'$) on the downstream of the Grau bridge are also *very low* risk (Figure 5.10 A). The properties on these upper terraces are of mixed land use and building types.

As with hazard scenario one, *high* risk properties are private adobe dwellings located on the western low terraces (t_1 to t_1') immediately downstream of the Grau Bridge. Buildings located on the western, lower to middle terraces (t_0 to t_2) downstream of the Grau Bridge are considered to be *high* risk. The main land uses are private dwellings, commercial centres and

factories which are of a range of building types. More *high* risk properties are located on terraces t1 to t2 just upstream of the confluence of the Río Chili with Quebrada San Lazaro. The properties are private dwellings of building type A and B sited in an upmarket building compound. Many *high* risk properties are also located on the low to moderate terraces (t1 – t2) up to approximately 1.8 km upstream of the Grau Bridge. The properties in close proximity to the Grau consist of upmarket hotels and commercial buildings of building types A and B. Much of the constructed property located within Club Internacional is *high* risk; excluding however, the open areas which are *very low* risk. As with hazard scenario one, *high* risk properties are identified approximately 500 m upstream of the club on the western low terrace (t1 and t1') and rural properties on either side of the river are also considered *high* risk.

On the map constructed from the conventional hazard assessment for the Quebrada Huarangal fan (Figure 5.11, upper image), the majority of properties located within the channel are considered to be at *high* risk. The buildings are types F to H constructed of confined and unconfined masonry, and make-shift materials (Chapter 4, Table 4.8). The constructed area of the lower to moderate terraces (t0 - t1'), particularly on the southern side of the channel and on the northern side of the channel, are *high* to *very high* risk. *Very low* risk properties are located far from the channel. In contrast to scenario one and two Titan2D derived risk assessments, the majority of properties in scenario three are *moderate* to *high* risk (Figure 5.11, lower image). *Moderate* to *high* risk properties are sited where Titan2D simulated flows “overbanked”, have not navigated the narrowed channel and broken out onto the southern bank. The property types are heterogeneous and represent a range of building and land-use types.



5.2.4 Infrastructure risk

5.2.4.1 Transportation

Scenario one – low magnitude/high frequency

The level of risk posed to the roadways and bridges in Arequipa from lahars and flash floods of small magnitude, and high frequency (i.e. hazard scenario one), is presented in Figure 5.12. On the map calculated from the conventional hazard assessment a road running adjacent to Quebrada San Lazaro is deemed to be at *very high* risk of inundation and/or damage during future flash flood and lahar events. This road is considered *very high* risk because of the propensity of Quebrada San Lazaro to flood and the importance of this transportation link in Arequipa (Figure 5.12A). The Bajo Grau bridge is considered *very high* risk. This is because the bridge has a very low deck height, which was instrumental in the flooding of buildings on the eastern side of the Río Chili in 1989. The Bolognesi bridge is *high* risk and the Chilina bridge and Chilina walking bridge are considered *moderate* risk which is not surprising given their low deck height. All other roads and bridges are of *very low* risk. In addition, a small section of road accessing the military school and Charcani Quinto is of *very high* risk on the map created using a Titan2D derived hazard assessment (not shown).

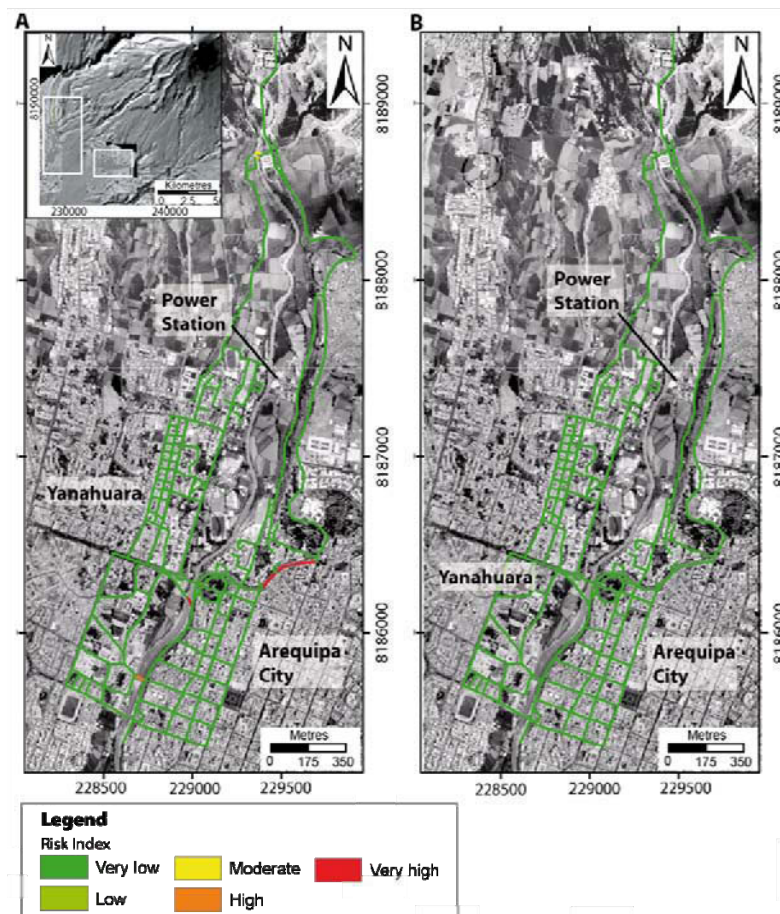


Figure 5.12: The risk posed to roadways and bridges from flash floods based upon a conventionally-derived (A) and Titan2D-derived (B) hazard assessments and building and land use vulnerability functions for hazard scenario one. The R o Chili valley is represented in images A and B.

On the Quebrada Huarangal fan a small area located within the channel, the suburb of *San Jerinomo*, is considered of *moderate to high* risk of inundation (Figure 5.13 upper image). *San Jerinomo*, and surrounds, floods at least every two years (last in February 2011). The map also indicates that the 8 du Octubre bridge, a low deck bridge with poor clearance, is considered to have a *very high* risk of inundation. The rest of the road network is considered to be of *very low* risk for inundation during hazard scenario one. In contrast, the entire road network is considered as *very low* risk using the Titan2D hazard assessment (Figure 5.13 lower image).

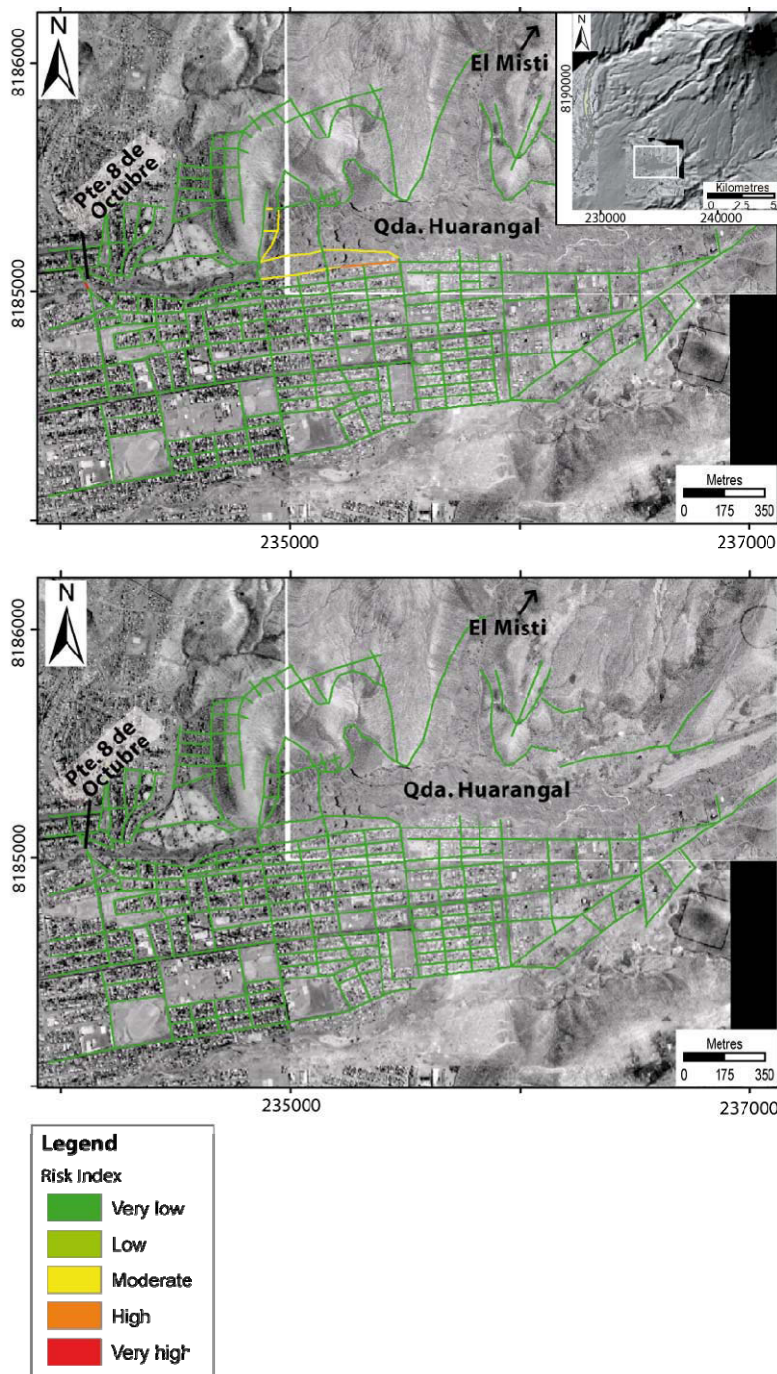


Figure 5.13: The risk posed to roadways and bridges from flash floods based upon a conventionally-derived (A) and Titan2D-derived (B) hazard assessments and building and land use vulnerability functions for hazard scenario one. The Quebrada Huarangal fan is represented in the upper and lower image.

Scenario two – moderate magnitude and frequency

The risk of inundation and/or damage from lahars in Arequipa city in hazard scenario two, is shown in Figure 5.14. All the bridges in the conventionally derived risk map are of varying degrees of risk (Figure 5.14A). The Chilina bridges, and Puente Bolognesi are of *moderate* risk, and Puentes Grau, Bajo Grau and Quinones are all considered *high* risk. *Moderate* risk roadways are located in a residential compound, comprising type A and B buildings, upstream of the confluence with Quebrada San Lazaro. *Moderate* risk roadways are also located in and around the tennis club on the western side of the river, approximately 2.5 km upstream of the Grau bridge. The road which connects the Tennis club with the Grau bridge across the Río Chili is considered *high* risk. The remaining roadways are considered *very low* risk, as with the entire roadways and bridges from the Titan2D-derived map (Figure 5.14B).

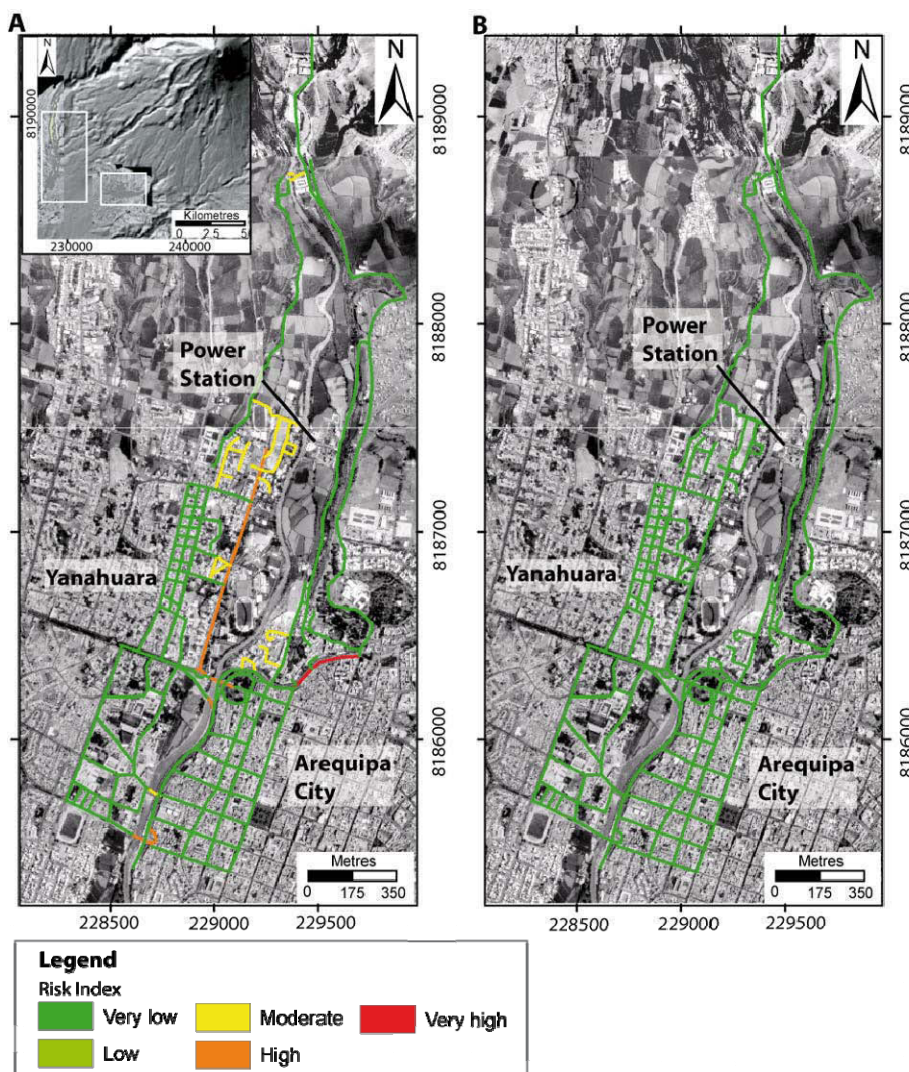


Figure 5.14: The risk posed to roadways and bridges from lahars based upon a conventionally-derived (A) and Titan2D-derived (B) hazard assessments and building and land use vulnerability functions for hazard scenario two. The R o Chili valley is represented in images A and B.

Roads located within the channel and on the lower southern terraces (t0-t1) of the Quebrada Huarangal fan are considered *moderate* risk on the conventionally derived map (Figure 5.15 upper image). The main road connecting the Huarangal centre with suburbs to the north is of *high* risk of inundation and/or damage because the bridge has a very low deck height and clearance. This is mostly due to the large amount of debris/rubbish in the channel. In contrast the roadways and bridge in the Titan2D-derived map are all considered *very low* risk from inundation and/or damage from lahars (Figure 5.15 lower image). This is because the run out of Titan2D simulations for this scenario did not extend into the channel or onto the constructed terraces.

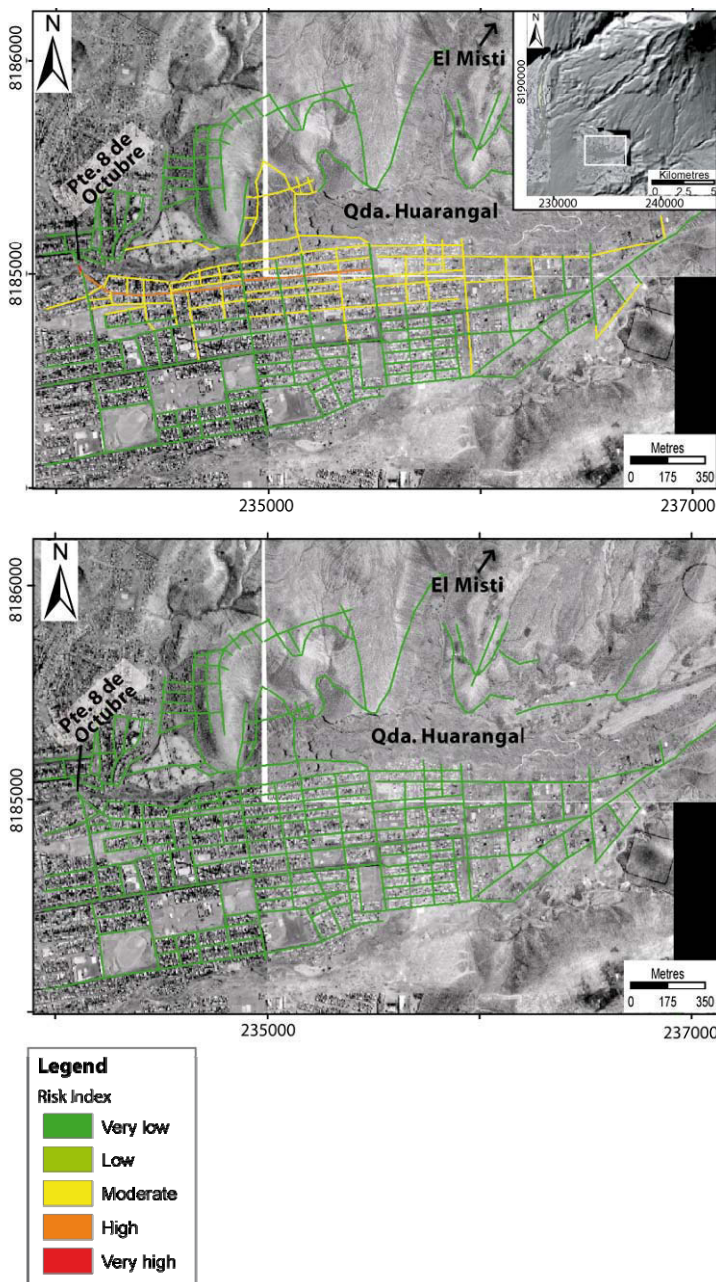


Figure 5.15: The risk posed to roadways and bridges from lahars based upon a conventionally-derived (A) and Titan2D-derived (B) hazard assessments and building and land use vulnerability functions for hazard scenario two. The Quebrada Huarangal fan is represented in the upper and lower image.

Scenario three – high magnitude/low frequency

The level of risk posed to roads and bridges in Arequipa from lahars is presented in Figure 5.16. On the risk map constructed from conventional hazard assessment, all bridges are at *moderate* risk from inundation except for Puente Grau which is considered *high* risk (Figure 5.16A). Puente Grau is particularly vulnerable due to its age, construction and importance for the economy – both in terms of transportation and tourism. The road which runs adjacent to Quebrada San Lazaro is considered to be *very high* risk of inundation. Roads of the lower to middle terraces (t_0 to t_2') are all considered at *moderate* risk of inundation during a lahar formed during scenario three. Roads on the higher terrace ($>t_3$) possess *very low* risk. Conversely, the majority of roads and bridges in the Titan2D-derived map are considered *very low* risk (Figure 5.16B). However, the road accessing the military school in the upper Río Chili canyon (Charcani Qunito) is at *high* risk of inundation, as with the Chilina bridge. The Chilina walking bridge has a *moderate* risk due to low traffic. The Titan2D derived risk map is of considerably lower risk than the conventionally derived risk map, due to the Titan2D simulated flows not extending into the city centre.

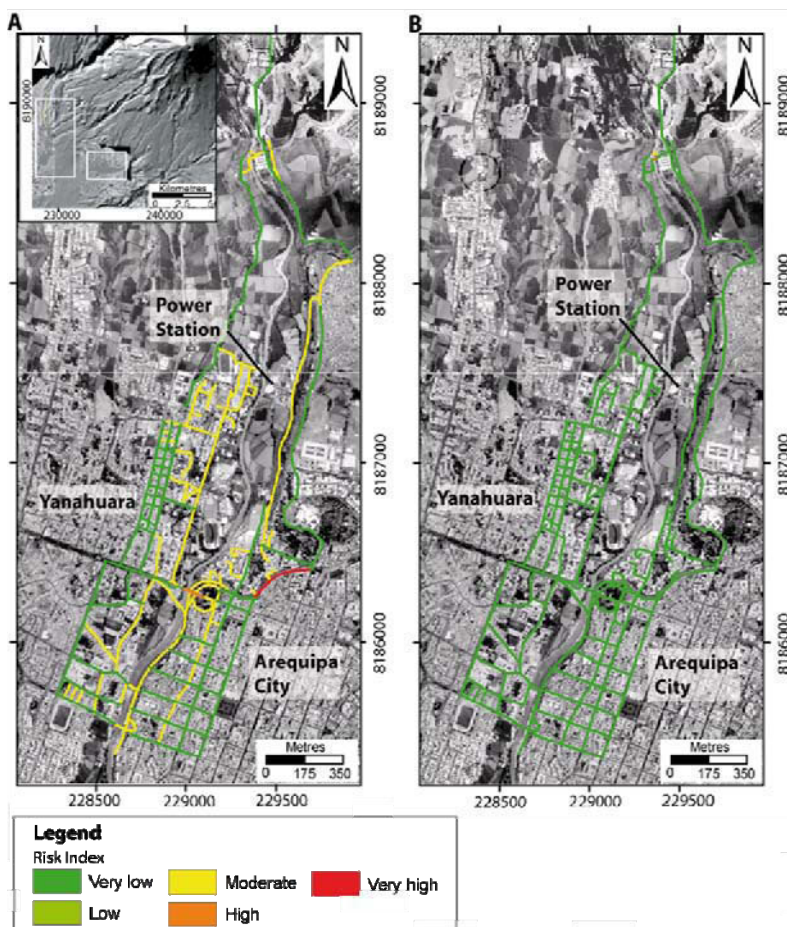


Figure 5.16: The risk posed to roadways and bridges from lahars based upon a conventionally-derived (A) and Titan2D-derived (B) hazard assessments and building and land use vulnerability functions for hazard scenario three. The Río Chili valley is represented in images A and B.

The majority of the Quebrada Huarangal fan is considered to be of *high* risk of inundation in the risk map derived from conventional hazard assessment (Figure 5.17 upper image). The main roads which connect the fan to other parts of Arequipa are at the most risk. Roads of *very low* risk are confined to the higher terraces (>t2) on the southern side of the channel and the volcano's flanks to the north of the channel. At risk areas are featured on the Titan2D-derived map, including a *very high* risk main road running parallel to the channel, a few blocks back from the channel edge (Figure 5.17, lower image). *Moderate* risk roads are located on the southern portion of the channel bed and lower terraces (t0-t1). The majority of roads are of *very low* risk to inundation and/or damage from lahars including the bridge *8 du Octubre*.

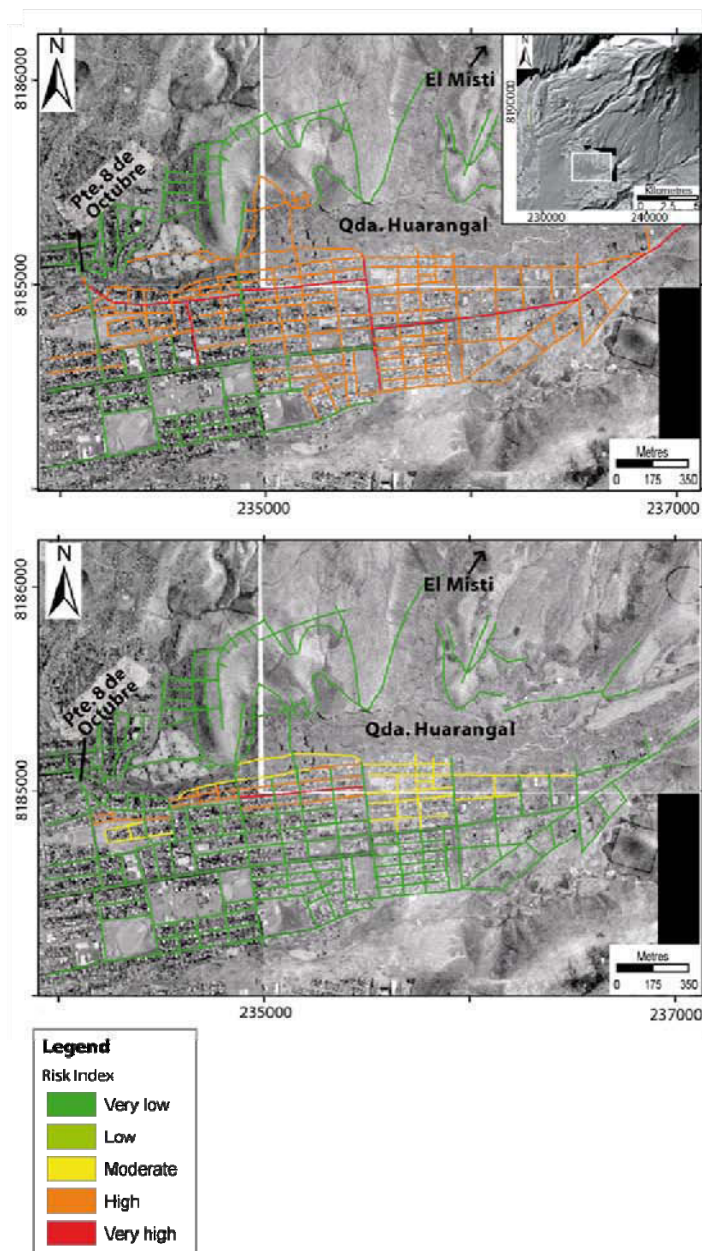


Figure 5.17: The risk posed to roadways and bridges from lahars based upon a conventionally-derived (A) and Titan2D-derived (B) hazard assessments and building and land use vulnerability functions for hazard scenario three. The Quebrada Huarangal fan is represented in the upper and lower image.

5.2.4.2 Electricity

The risk to the electricity generation and supply for Arequipa was assessed based upon the hazard scenarios, and land use, building and infrastructure vulnerability. An overview of the hydroelectric power stations and dams are presented in Figure 5.18, with the risk posed to the stations and dams from floods and lahars shown in Table 5.2.

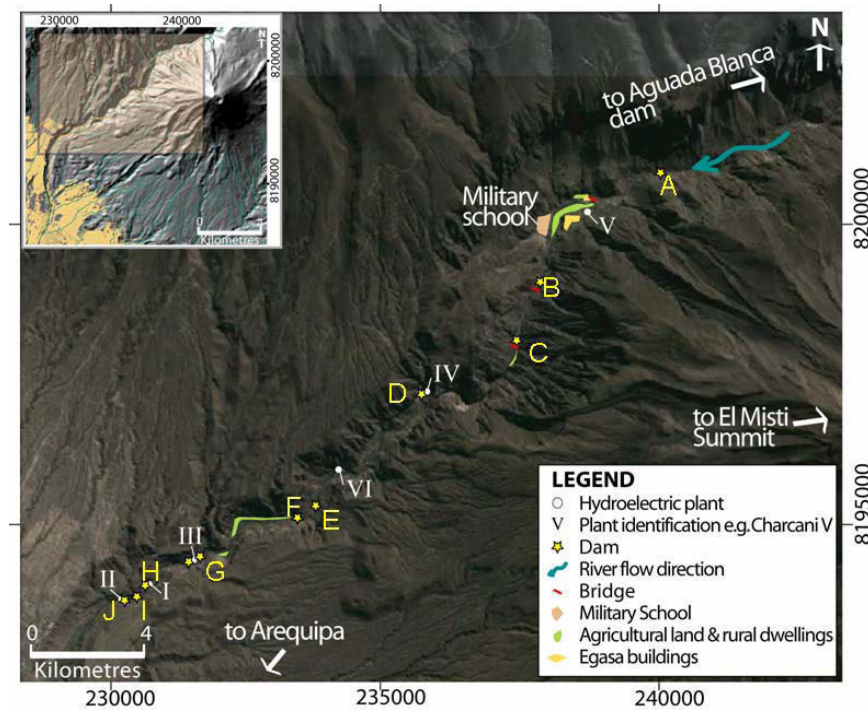


Figure 5.18: The location of hydroelectric stations (I – VI) and dams (A – J) in the Rio Chili canyon.

Element		Risk assessment based on conventional hazard assessment			Risk assessment based on Titan2D-derived hazard assessment		
		Scenario 1	Scenario 2	Scenario 3	Scenario 1	Scenario 2	Scenario 3
Hydroelectric power systems	Charcani I	Moderate	Moderate	High	Very low	Very low	Low
	Charcani II	Moderate	Moderate	High	Very low	Low	Moderate
	Charcani III	Low	Moderate	Moderate	Very low	Low	Moderate
	Charcani IV	Low	High	Very high	Very low	Moderate	High
	Charcani V	Low	High	High	Very low	Moderate	High
	Charcani VI	Low	High	Very high	Very low	Low	Moderate
	Dam A	Low	Moderate	High	Low	Moderate	High
	Dam B	Moderate	High	High	High	High	High
	Dam C	Low	Moderate	High	Low	Low	Moderate
	Dam D	Low	Low	Moderate	Low	Low	Moderate
	Dam E	Low	Low	Moderate	High	High	High
	Dam F	Moderate	High	High	Low	Low	Low
	Dam G	Low	Low	High	High	High	High
	Dam H	Low	Low	Low	Low	Low	Low
Dam I	Very high	Very high	Very high	Low	Low	Moderate	
Dam J	Low	Low	Low	Low	Low	Low	
Other power	Chilina station	Moderate	High	Very high	Low	Low	Low

Table 5.2: The risk posed to the power generation and supply systems in the upper R o Chili valley for the three different hazard scenarios is presented. A comparison is made between the risk calculated using conventional hazard assessment and using Titan2D hazard assessment.

Overall the risk to the dams is the highest for power-related infrastructure, this is due to their location in the river rather than adjacent to. The power stations that are at the most risk are Charcani IV, V, and VI and Chilina, due to both their location and importance (i.e. electricity output) to Arequipa. In general the risk posed to dams is the highest for the Titan2D based assessment.

This assessment highlights that, even during small magnitude flood events, key infrastructure for the generation and supply of electricity to Arequipa is at risk from inundation and/or damage. The level of risk posed to this infrastructure during a volcanic crisis (i.e. scenario two and three) is of concern, especially when electricity is a vital lifeline.

5.2.4.3 Water

The risk to the water supply for Arequipa was assessed based upon the hazard scenarios, and land use, building and infrastructure vulnerability. The risk to the water supply for the hazard scenario three, derived from both conventional and Titan2D hazard assessment, is presented in Figure 5.19. In addition, the risk posed to water supply and treatment plants from floods and lahars for all three hazard scenarios is shown in Table 5.3.

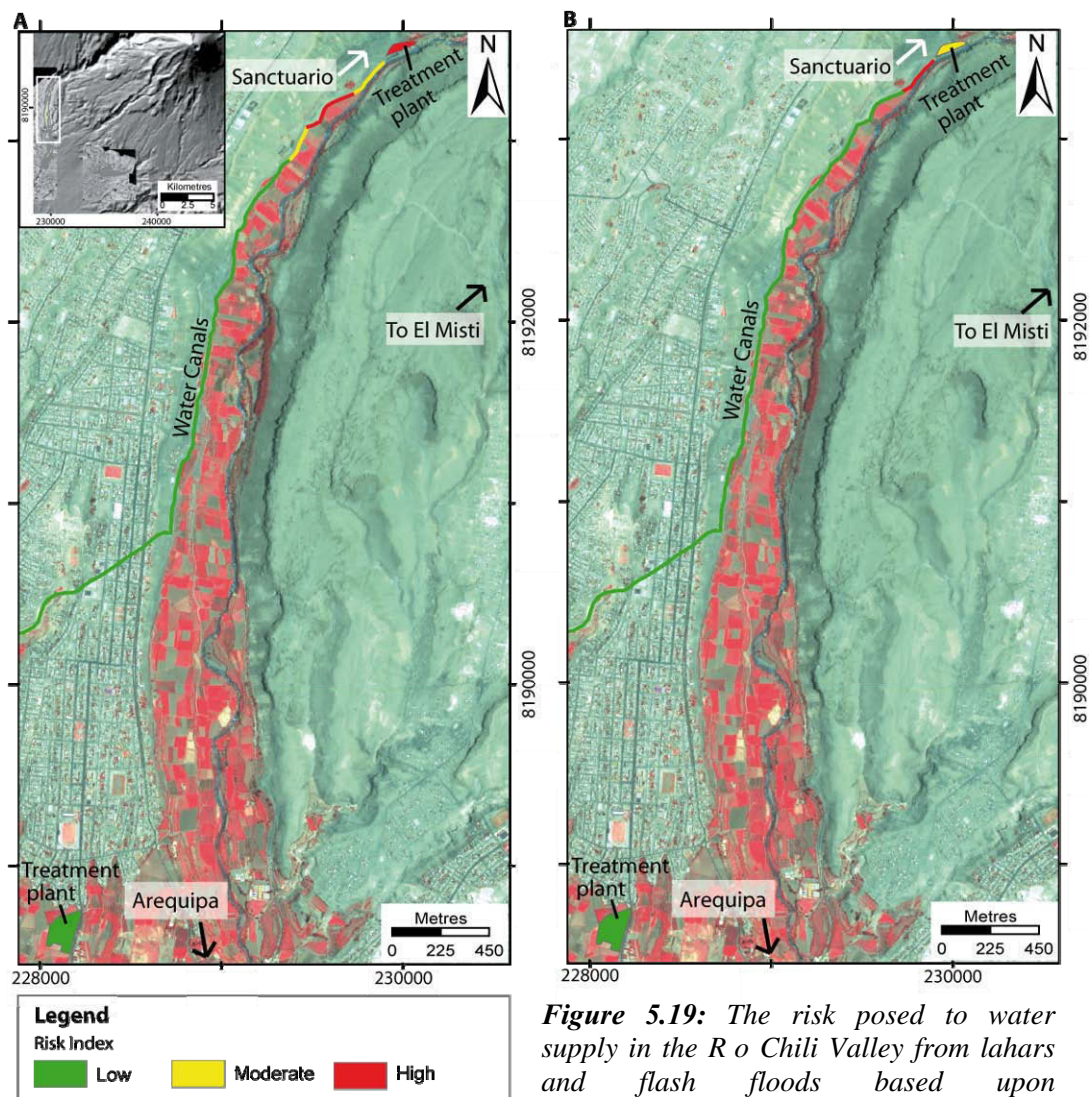


Figure 5.19: The risk posed to water supply in the R o Chili Valley from lahars and flash floods based upon conventionally- (A) and Titan2D- (B) derived hazard assessments and infrastructure vulnerability functions.

Element	Risk assessment based on conventional hazard assessment			Risk assessment based on Titan2D-derived hazard assessment		
	Scenario 1	Scenario 2	Scenario 3	Scenario 1	Scenario 2	Scenario 3
Covered water channel	Very low	Very low	Very low	Very low	Very low	Very low
Covered water channel	Very low	Very low	Very low	Very low	Very low	Very low
Uncovered water channel	Low	Moderate	Moderate	Very low	Very low	Very low
Uncovered water channel	High	High	Very high	Very low	Very low	Very low
Uncovered water channel	Moderate	Moderate	Moderate	Very low	Very low	Very high
Upstream water treatment plant	Very low	Very low	Very high	Very low	Very low	Moderate
Downstream water treatment plant	Very low	Very low	Very low	Very low	Very low	Very low

Table 5.3: The risk posed to the power generation and supply systems in the upper R o Chili valley for the three different hazard scenarios is presented. A comparison is made between the risk calculated using conventional hazard assessment and using Titan2D hazard assessment.

The risk to the water treatment plant at the entrance of the Rio Chili canyon is *very high* for scenario three of the conventionally derived risk assessment. This is the point where water from the Rio Chili is taken into the canals for potable water and irrigation. The risk to the water supply system for Arequipa is negligible with the Titan2D-derived hazard assessment. Floods and lahars in the Rio Chili may have an affect on the supply and quality of water taken into the canals, even if the infrastructure is not inundated. During the February 2011 floods Arequipa was without potable water for 24 hrs because of high sediment water being drawn into the water canals for purifying at the water treatment plant. The treatment plant can clean water of a high sediment and/or debris content, but the debris can cause blockages and damage to the canals, pipelines and water treatment plant.

This assessment indicates that during small to large floods and lahars, portions of the water canal system and water treatment plant could be affected. The risk map indicated that the

highest risk pipelines were located closest the river. Damage to the canals at this point (i.e. close to intake) would compromise the supply to the rest of the canal, affecting not only the potable water supply but the irrigation supply too – essential to agriculture in Arequipa.

5.3 Discussion of risk for future volcanic and hydrologic crises in Arequipa

Depending on the magnitude and frequency of the flood and/or lahar, *high* risk properties cover much of the lower (t0 to t2) to middle terraces in the Rio Chili valley area. There exists a mix of land use but not building type, reflecting the homogeneous nature of the Rio Chili valley. The majority of the Quebrada Huarangal fan (t0 to t2) is *moderate* to *very high* risk. There is little pattern to the spread, reflecting the heterogeneous nature of the building types in Quebrada Huarangal. Overall the risk posed to properties in the Rio Chili valley is a lot less than for the Quebrada Huarangal fan. This is likely due to better quality buildings, building position, and channel geomorphology in the Rio Chili valley.

The risk to the Rio Chili valley road network is significant in terms of mobility during and after a volcanic crisis – with all bridges considered to have some degree of risk to inundation and/or damage. This has serious implications for providing access from one side of the city to the other; particularly when trying to evacuate people and access roads to essential facilities. The assessment of the Quebrada Huarangal fan concluded that there is significant risk posed to roads located within the channel of the quebrada, and especially on the southern terraces (t0-t2). This is due to the overbanking of flows in this locality. For the conventionally derived risk assessment the evacuation of the SE to S portion of the Quebrada Huarangal fan could prove difficult, especially from the east to the west (i.e. towards Arequipa city centre). This is because all the roads on the SE to S portion of the fan are *high* risk, with one main road at *very high* risk.

In terms of risk reduction, credible and rehearsed evacuation plans should be put into place, as well as restricting construction within the Quebrada Huarangal channel bed. In addition, a study should be undertaken into the short- and long-term effects of disruption and/or damage to the hydroelectric power stations and water supply. Alternative methods of energy and water should be investigated, even if to supply the city for the first 72 hours (while waiting for government and international aid) after the event occurs.

CONCLUSIONS AND RECOMMENDATIONS

Conclusions

This research combined a number of techniques in order to define the physical vulnerability, namely of buildings and infrastructure, in urban areas threatened by lahars and flash floods. Using the case study of Arequipa, Peru, vulnerable areas were identified from former and current geological studies; conventional and computer-aided mapping of volcanoclastic and fluvial deposits; numerical flow modelling (Titan2D); field surveys of buildings and infrastructure; statistical analysis including multivariate analysis for the building and infrastructure surveys; GIS; and geotechnical characteristics of building materials (including mechanical tests).

An overview of the geological history from the deposits of El Misti volcano provided several credible scenarios for lahar generation during a future eruption. In addition, information gathered from press articles, eye witness accounts, scientific and government agency reports support the occurrence of one to two flash floods every ten years. The scenarios for lahar and flash flood initiation of Thouret et al. (2001), Delaite et al., (2005) and Vargas et al., (2010) were updated and are summarised below:

- *Scenario 1* relates to small volume (0.01 to $0.5 \times 10^6 \text{ m}^3$) but frequent floods which are generated by heavy rainfall and/or snowmelt, such as the floods in 1989, 1997 and 2011. The recurrence interval is one to two times every ten years.
- *Scenario 2* can occur during a small eruption (VEI 2), such as the AD 1440-1460 vulcanian events, generating lahars 0.5 to $4.0 \times 10^6 \text{ m}^3$ in magnitude. Scenario two can also relate to a non-volcanic event which generates moderate to large flash floods. The recurrence interval for lahars is >50 to 300 years.
- *Scenario 3* accounts for a moderate magnitude eruption (i.e. VEI 3) such as the ca. 2030 yr BP-old (sub)Plinian explosive episode; generating lahars 4.0 to $11.0 \times 10^6 \text{ m}^3$ in magnitude. The recurrence interval for generation of this magnitude lahar is >100 to 2000 years.
- *Scenario 4* is based on an eruption resembling the 34,000-30,000 year-old or the 13,000-11,000 year-old ignimbrite-forming eruptive episodes (VEI 4 to 5); generating

lahars 11.0 to $30.0 \times 10^6 \text{ m}^3$ in magnitude. The recurrence interval for a lahar this magnitude is $5\,000$ to $> 10\,000$ years

- The dam-break flood scenario in the Rio Chili Valley was not considered as a completely different scenario as the flood can occur during all the scenarios outlined above. The dam-break flood however is more likely during scenarios 3 to 4 with volumes ranging from 4 to $47 \times 10^6 \text{ m}^3$. The recurrence interval is harder to define due to the lack of knowledge of these events at El Misti.

The scenarios were used to develop lahar and flash flow hazard maps for Arequipa. The conventionally-derived hazard map for the Rio Chili Valley – our first pilot study area – indicates high-hazard areas are larger to the south of the city centre than higher up in the fluvial system. This is where the gradient in this region, the centre of at the confluence of two perennial rivers: Chili and Anadamayo, has decreased sufficiently for deposition with 2.5% slope gradient across the most populated area. The highest hazard on the Quebrada Huarangal fan – our second pilot area – represents frequent low magnitude flash floods (e.g. flash floods of 1997 and 2011), which inundate the modified channel bed and the lowermost terraces. In contrast, the Titan2D-derived hazard maps cover a much smaller area; for example the high-hazard zone of the Rio Chili valley is confined to the upper canyon. Similarly, the high-hazard zone of the Quebrada Huarangal fan is very small in area and confined to the valleys which feed into the main quebrada. While the hazard zones derived from computer simulations are much smaller in area than the conventionally-derived zones, the Titan2D simulation results of this study do feature longer flow run out lengths than previous Titan2D simulations of Stinton et al. (2004) and Vargas et al. (2010) due to the refinement of the DEM resolution.

The topography of the Rio Chili valley from the canyon entrance to the southern boundary of the city centre was well represented by the DGPS data, and the topography of upper canyon was better represented by the ASTER data than in previous DEMs. The enhanced 10 m DEM allowed for the simulated lahars to be funnelled more precisely through the narrow canyon. However, the simulations do become stalled within the upper Rio Chili canyon. This is because the canyon is narrow and the walls are steep, geomorphological (or topographical) characteristics which are difficult accurately represented with satellite data, and which induce runoff and superelevation of lahars. An intrinsic problem with 2-D models is their failure to resolve in the z, this creates problems in steep sided valleys such as at El Misti. While better resolution satellite data or LIDAR measurements of the upper Rio Chili canyon would greatly

improve the DEM, it may not be so beneficial for further Titan2D simulations. A solution could be to initiate lower volume Titan2D simulated flows further downstream, where the river and terrace topography are much better represented on the new DEM, where the influence of steep sided topography would be much less pronounced.

Whilst the DEM resolution of the Quebrada Huarangal fan was improved, further DGPS surveying would greatly enhance the quality of the DEM in this area. Difficult access and external interference meant DGPS points were not collected in a regular pattern, resulting in “patchy” data. The significance of the “patchy” data meant that data interpolation was not as successful as in the Rio Chili Valley. The topography, while better refined than in the 30 m DEM, could be better represented with the collection of further DGPS in this region particularly concentrating on the channel bed. The channel bed is not flat due to continuous mining operations and many closely-spaced measurements are recommended to overcome the “patchy” data to generate a good quality DEM in this region.

Although the new Titan2D simulations are shorter than the LaharZ simulations of Delaite et al. (2005), this study and the previous Titan2D studies have shown that Titan2D models the behaviour of lahars adequately; whilst the run out of LaharZ simulations is more comparable to mapped deposits. The two models cannot be compared because their input parameters are completely different and represent dissimilar outcomes. LaharZ is a statistical code to identify (roughly outline) areas of lahar inundation whereas Titan2D is based upon physics which include rheological and hydraulic parameters such as friction angle and solid ratio, and therefore more closely linked with observed flow behaviour. The physical parameters used for the simulation or the conditions at the time of lahar flow generation are also responsible for the differences observed between the two models and the actual deposits. Lahars often comprise several distinct phases within a single event and consequently flow properties and impacts vary considerably in time and space. This is an important characteristic of a lahar for hazard management and has been the subject of many studies including Procter et al. (2010).

The difference between the results of the two models and the mapped deposits for lahar inundation zones highlights the importance of understanding the limitations, and also the implications, of different methods for hazard assessment. Perhaps the best way to view the data is to regard the Titan2D simulation outputs as the absolute minimum areas likely to be inundated by a lahar, whereas the LaharZ simulation outputs or runs represent the maximum

areas. Either way, the simulations have been, and are, extremely valuable in understanding flow behaviour, defining flow inundation areas expected on current DEMs and identifying hazard zones.

In this study the most vulnerable land, buildings and infrastructure in Arequipa have been identified. Twenty different land-use types were identified varying from non-occupied intensive agriculture to dense urban areas. Agricultural land occupies just over half of the land studied (51%) followed by private urban dwellings (21%), public/sports areas (10%) and industry (13%). However, the proportion of land use types varies widely from the Río Chili Valley to the Quebrada Huarangal study areas. Agricultural land occupies the most area within the Río Chili Valley, whereas private urban dwellings are more common in the Quebrada Huarangal area. The vulnerability analysis of land use indicates that police stations, medical centres, religious establishments and industrial enterprises are the most vulnerable land use types. Agriculture is also considered financially vulnerable (rank 6 out of 16) due to the potential loss of income and as a staple food supply during a volcanic crisis. Agricultural land can also be used as an open area for the construction of evacuation shelters.

Building surveys identified nine construction types defined according to: the dominant building material, number of floors, building reinforcement, roof type and style, opening type and quantity, and overall building structural integrity. In the Río Chili study area 38% of buildings surveyed fall into the Type A category building, a confined masonry construction system. An unconfined masonry construction system, Type G, represents 3% of the buildings surveyed. Conversely Type A buildings only correspond to less than 2% of buildings present on the Quebrada Huarangal fan, with the most abundant building type belonging to category F (33%) – confined red brick masonry. Category F dwellings are often constructed in a piece-meal fashion, where often the bottom floor is finished but further storeys are unfinished and added slowly depending on the demand of the family and finances.

The survey highlighted the heterogeneous nature of construction in Arequipa, with building types and construction materials varying even within the same city block. In addition, geotechnical experiments undertaken on the samples of Arequipa building materials indicate that they are of a much lower quality than the minimum building code requirement world wide. The samples not only have low compressive strengths, they have a low apparent bulk density and contain many voids, thereby compromising the structural integrity of the building

material. The vulnerability analysis of the building types, based upon the building components such as roof type and pitch, wall material and height, etc., indicated confined masonry buildings were the least vulnerable (e.g. Type A), whereas unconfined buildings without mortar were more vulnerable. Surprisingly, Type H buildings (make-shift) were not the most vulnerable. This is because there were less structural components taken into the vulnerability assessment and therefore no coefficients for certain building criteria could be added to the calculation. This could represent a flaw in the analysis because common sense would dictate that a building with no structural integrity whatsoever would be the most vulnerable during a lahar and/or flash flood. The poorest quality houses (and not structurally sound) are often located closest to the river channels with the most vulnerable area identified as within, and adjacent to, the temporary stream of Quebrada Huarangal. Type G buildings are more commonly situated on the lower terraces (t1, t1' and t2) of the Río Chili Valley and associated with agricultural lifestyle blocks.

Infrastructure represents an important element in vulnerability assessments, and the results of this study highlighted just how vulnerable key infrastructure in Arequipa is. Transportation links are vital during a crisis and the analysis highlighted that the bridges which cross the Río Chili in the city centre are the most vulnerable infrastructure. If bridges are destroyed, access from one side of the city to the other will be severely limited. In addition, water pipes, power and telecommunication lines are often located at bridges, and are thus equally vulnerable to damage. The vulnerability analysis also indicated that the bridge *Puente Grau* is the most vulnerable, followed by *Puentes Bolognesi* and *Quiñones* and the irrigation canals. *Charcani Quinto* located just below the steep and eroded NW flank of El Misti is the most vulnerable hydroelectric power station due to its high electricity output and the reconstruction cost (i.e. a large tunnel system intake through the side of the volcano). The services such as the *Egasa* power station and the hydro-electric dams are vulnerable, and their damage could possibly result in the severe disruption of power supply to the city as in 1961 and 1973. This would have a flow-on effect for lifeline services such as hospitals and other emergency services.

Urban expansion is resulting in an ever increasing number of people inhabiting these highly hazardous areas – as defined by conventional- and simulation-derived data. In addition essential infrastructure, such as power stations and potable water supply, are located within these hazardous areas and the failure of such infrastructure could have dire consequences to the population of Arequipa. Agriculture in Arequipa is at higher risk during a lahar or flood

event than some of the other land-use types. This is due to its location adjacent to the Río Chili channel and the lowermost flood-prone terraces (t0, t1 and t1') which are within 1 to 5 m only above the river bed. Similarly one of the major industries and lifelines - the Egasa power station, is located on the low eastern terrace (t1') of the Río Chili Valley just north of the city centre. The hydroelectric power system, which consists of five dams, is located in the high hazard area of the upper Rio Chili canyon. This hydroelectric power system supplies electricity to the city as well as to the national grid, and failure would have dreadful consequences.

To highlight the areas of Arequipa which are most at risk of inundation and/or damage from lahars and flash floods, the lahar inundation zones, derived from conventional and computer simulation methods, were combined with flow characteristics and element vulnerability. The results of the assessment indicated that the most vulnerable populations, infrastructure and assets are located within the most hazardous zones, such as the San Jerinomo suburb. This suburb, is located within the Quebrada Huarangal channel, was flooded as recently as February 2011. The only evacuation route out of many of the 'at risk' areas is by using roads which have been highlighted in this study as a high to very high risk. The Rio Chili valley was less at risk for smaller magnitude flows but the assessment highlighted a moderate to very high risk to the city's bridges, which are the main access, and possible evacuation, routes across the city. The hydroelectric power system was again highlighted as critical and essential infrastructure which is at moderate to very high risk of inundation and/or damage during even small magnitude events.

Using a GIS in the field of volcanic hazard, vulnerability and risk assessment has shown its capabilities in terms of preparation of maps and information requests from a solid database. The capabilities and limitations of diagnostic tools such as GIS and Titan2D were tested in the application to the assessment of volcanic hazards, vulnerability and risk. A georeferenced database on the El Misti region, including Arequipa city, has been compiled by the acquisition of information layers. New layers of information have been included, such as optimised lahar and flood-hazard scenarios eruptions; building, land use and infrastructure vulnerability maps, etc. This study has shown that the use of dedicated GIS analysis of volcanic hazards and risks is an extremely powerful tool to manage a study of a preventive nature in volcanic hazards, vulnerability and risk.

Recommendations to reduce the risk in Arequipa

This study highlights areas, in particular the Rio Chili valley and quebrada channels, which need to be protected by the Peruvian authorities to ensure the safety of the population in the event of lahars and/or flash floods in Arequipa. Of the utmost importance is the creation, and adherence to, a stringent land-use plan which forbids or limits development in areas of high risk outlined by this study and others (e.g. Vargas et al., 2010). The city limits have been expanding onto the slopes of El Misti and also in, and adjacent to, channels which drain the volcano. While many of the settlements are deemed as “illegal” (i.e. without planning permission) there appears to have been very little management and/or policing to ensure that construction is not continued in at risk areas. However, this year, the City Hall has taken steps to control expansion in to hazardous areas. A law was passed that makes it illegal to build beyond the suburbs on El Misti’s flanks – an area that has been outlined in the 2007 hazard map of El Misti. This is a positive step in reducing the risk to the population.

This study also highlighted the vulnerability of much of the key infrastructure in Arequipa, and alarmingly many of the lifelines (e.g. electricity, water and transportation) are the most vulnerable infrastructure in the case of a lahar and/or flash flood. Strategic risk planning needs to be undertaken by local authorities to identify the limitations on infrastructure and lifelines in case of a crisis, and contingency plans need to be put in to place to deal with a serious loss of the main infrastructure. For example, should the water become contaminated, is there an alternative water source available to supply potable water to the city? If the bridges crossing the Rio Chili are damaged, is there a way to transport the potable water from one side of the city to the other? What will be the effects of no potable water supply on emergency services? Another example is the loss of power; how long would power be lost to the city? How long would it take to repair? Keeping in mind that the hydroelectric power stations are located within the high-hazard zones close to El Misti and across the Rio Chili canyon. How long would the hospitals be able to run on a backup generator? Could fuel be delivered to the hospital if transportation routes are severely damaged? Could patients be evacuated? Many questions need to be answered so that the risk to the population from lahars and/or flash floods is reduced to an acceptable level for the population of Arequipa. A comprehensive risk analysis of the entire infrastructure is recommended to identify and highlight obstacles or weak points in case of a volcanic crisis. For example, in terms of emergency management, it

is imperative to have an operational road network for co-ordinating relief efforts and reaching those people in need.

Some resistance measures (e.g. building a bund, levee or deflection structure) could be employed to minimise the impact of lahars and flash floods directly affecting buildings and giving occupants more time to relocate. Avoidance measures include not building in lahar and/or flash flood risk areas where possible, raising the ground or floor level of buildings, and the construction of local bunds to protect groups of buildings from inundation. Bridges could be built with larger spans and higher free boards to help in cases where a large volume of debris is anticipated.

Public education and awareness is paramount. During the 2008 field campaign discussions with residents of the San Jerinomo suburb, located within the channel of Quebrada Huarangal, revealed that they were unaware of the level of risk posed from lahars and flash floods in their area. Furthermore, the residents of the dwellings and businesses situated within the Quebrada Huarangal channel were under the impression (from the authorities) that the risk of flooding was non-existent to very low. It would have come as a surprise then, when flash floods swept through the suburb flooding 22 homes on 11 February 2011. The public and local authorities need to be educated on the risk posed to Arequipa from lahars and/or flash floods (e.g. evacuation simulation in 2010, Luisa Macedo). In addition, the education needs to be consistent, correct and verified by scientists and other professionals in order to ensure that everyone receives the same information and are well informed.

Finally, emergency shelters and evacuation routes need to be clearly identified, communicated and ensured during a crisis – such as the contingency plans developed for the Ubinas crisis (Rivera et al., 2010). Vargas et al. (2010) suggested that the evacuation route towards the SW be improved to allow for four lanes of traffic to join the Panamericana highway, rather than the two lanes which currently exist. Another route could be constructed towards the pass and Cerro Verde through the mining area south of Arequipa. In addition the road to the SE should be improved all the way to the Rio Tambo, 30 km SSE of Arequipa, and linked to the Panamericana road towards Moquegua. An advantage of establishing an adequate and reliable SE evacuation route is that it would allow the evacuation of people into an area where there is no direct evidence of erupted deposits from El Misti in this area (Vargas et al., 2010). Vargas et al., (2010) also suggested that shelters should be built near the villages of Yarabamba and

Quequeña at the SE end of the depression, (in addition towards the west beyond the town of Yura.).

Recommendations for further research

This project has revealed major gaps in the research, and additional investigation is recommended to further develop the study into lahar hazard, vulnerability and risk assessments within an urban setting, and also in Arequipa. Additional research is recommended in the following areas:

- Magnitude/frequency relationships for lahars and flash floods need to be further explored within a statistical framework, using Bayesian Event Trees (BET) for example. The probability of every possible lahar and/or flash flood initiation could be determined thereby aiding hazard, vulnerability and risk studies. BET is currently being explored for El Misti by the Laboratoire Magmas et Volcans with INGV-Bologna collaboration (L. Sandri, R. Constantinescu and J.C. Thouret, 2011, in prep.).
- While the new DEM is a great improvement over the 30 m DEM, optimisation of the enhanced 10 m DEM is recommended. This would include further research to improve the DEM calculated by DGPS data, including a smooth transition between the DGPS and the satellite data.
- An improved resolution DEM could also be computed entirely, or in conjunction with the DGPS measurements, from higher resolution commercially available satellite data, or from an airborne LIDAR survey. This would be recommended to enhance the resolution of the DEM in the Rio Chili canyon area.
- Further DGPS measurements of the Quebrada Huarangal fan would improve the DEM in this region. Including more closely spaced DGPS measurements across the channel bed and of the developed terraces which would hopefully resolve the hummocky nature of the DEM in this locality.
- Further evaluation of the lahar initiation mechanisms would greatly aid in using computer simulations. The evaluation would include defining more accurately the parameters used in computer modelling.
- A better resolution DEM and enhanced initiation parameters for new simulations would improve the quality of the hazard and corresponding risk map. This would provide the authorities with a reliable lahar-hazard map.

- Titan2D modelling can be lengthy and difficult process, and an overall recommendation for the developers would be to make the program more user-friendly. For example, early on in this research there were installation problems and it took some time before the program was running smoothly. In addition, the model would greatly benefit by having an output that could be easily visualised in popular GIS software (e.g ArcGIS). While the user can choose to output files to a GIS supported file, GRASS does not have many functions or the user support of many other GIS programmes. To get the output Tectplot files into a format for input into ArcMap is a tedious process. Other output formats exist for viewing the movement of the flow and flow path down the cone, but are not very useful for analysing the details of the flow.
- Given the scenario of dam-break floods possibly being generated from the upper Rio Chili canyon (and two artificially dammed lakes upstream), the use and testing FLO-2D for the simulation of dam break floods would be recommended. FLO-2D has been successful in modelling dam break floods and would be useful in gaining a better insight into possible inundation areas in Arequipa.
- A building's wall strength was determined from the unconfined compressive strength of Arequipa masonry using a calculation from the Eurocode 6. However, further investigation into all aspects of building construction and strength is recommended. This would include determining the strength of a building as an entire structural unit, from the foundation through to the roof, and including walls, windows, framing etc. This is currently being undertaken within the ANR RiskNat 'LaharRisk' project framework by the Laboratoire Magmas et Volcans and Clermont'Polytech.
- Part of determining the strength of the entire structural system would involve further geotechnical tests both in the laboratory and in-situ. The laboratory tests on the strength of materials would also validate a classification of material resistance to physical over pressure. This is currently being carried out within the ANR 'LaharRisk' project framework as outlined above.
- In addition to quantifying the structural components, further analysis into the flow effects on the structural system as a whole is recommended, including taking into account the range of forces that come into play.
- The main limitation of the vulnerability analysis is the difficulties of taking into account all of the parameters. It would also be useful to further investigate and validate the parameters used in the vulnerability analysis.

REFERENCES

- Alberico, I., Lirer, L., Petrosino, P., Scandone, R., 2002. *A methodology for the evaluation of long-term volcanic risk from pyroclastic flows in Campi Flegrei (Italy)*. Journal of Volcanology and Geothermal Research 116: d63-78.
- Alcantara-Ayala, I. 2002. *Geomorphology, natural hazards, vulnerability and prevention of natural disasters in developing countries*. Geomorphology 47: 107–124
- American Society for Testing and Materials Standard 2008. *ASTM C62: Standard Specification for Building Brick (Solid Masonry Units Made From Clay or Shale)*. ASTM International, West Conshohocken, PA. Pp. 4
- Anderson, T. B., Jackson, R. 1967. *A fluid mechanical description of fluidized beds: equations of motion*. Industrial and Engineering Chemistry Fundamentals 6: 527–539.
- Andritsanos V.D., Fotiou A., Paschalaki E., Pikridas C., Rossikopoulos D. and Tziavos I.N., 2000. *Local Geoid Computation and Evaluation*. Physics and Chemistry of the Earth 25: 63-69
- Aronoff, S. 1989. *Geographic information systems: A management perspective*. WDL, Ottawa.
- Aspinall, W. P., Woo, G., Voight, B., and Baxter, P.J. 2003. *Evidence-based volcanology: application to eruption crises*. Journal of Volcanology and Geothermal Research 128: 273-285.
- Australian/New Zealand Standard. 2008. *AS/NZS 4455.1:2008 Masonry units, pavers, flags and segmental retaining wall units - Masonry units*. Standards Australia, Sydney.
- Bajo, J.V., Martinez-Hackert, B., Escobar, C.D., Gutierrez, R. E. 2009. *Titan2D Based Pyroclastic Flows Hazard Maps for Santa Ana Volcano, El Salvador*. American Geophysical Union, Spring Meeting 2009, abstract #V71B-06
- Baldi, P., Cenni, N., Fabris, M., Zanutta, A. 2008. *Kinematics of a landslide derived from archival photogrammetry and GPS data*. Geomorphology, 102: 435-444
- Barberi, F., Macedonio, G., Pareschi, M. T., and Santacroce, R. 1990. *Mapping the Tephra Fallout Risk: An example from Vesuvius, Italy*. Nature, 44: 142-144.
- Baxter, P. J., Baubron, J. C., and Coutinho, R. 1999. *Health hazard and disaster potential of ground gas emissions at Furnas volcano, São Miguel, Azores*. Journal of Volcanology and Geothermal Research. 92: 95-106.
- Baxter, P. J., Boyle, R., Cole, P., Neri, A., Spence, R. J. S., Zuccaro, G. 2005. *The impacts of pyroclastic surges on buildings at the eruption of the Soufrière Hills volcano, Montserrat*. Bulletin of Volcanology 67: 292-313.
- Baxter, P.J., Aspinall, W.P., Neri, A., Zuccaro, G., Spence, R.S., Cioni, R. and Woo, G. 2008. *Emergency planning and mitigation at Vesuvius: A new evidence-based approach*. Journal of Volcanology and Geothermal Research 178: 454-473.
- Ben-Zeitun, A.E. 1986. *Use of pulse velocity to predict compressive strength of concrete*. International Journal of. Cement Composites and Lightweight Concrete, 1: 51-59.

- Berrocal, M., Malavassi, E., 2006. *TITAN2D models of Arenal pyroclastic flows*. Cities on Volcanoes 4 Conference, Quito, Ecuador.
- Berry, P.A.M., Smith, R.G., Freeman, J.A., Benveniste, J. 2008. *Towards a New Global Digital Elevation Model*. In: (eds) Sansò, F., Sideris, M.G. *Observing our Changing Earth*. International Association of Geodesy Symposia 133: 431-435. Springer Berlin Heidelberg.
- Blaikie, P., Cannon, T., Davis, I., and Wisner, B., 1994. *At Risk: Natural Hazards, People's Vulnerability, and Disasters*. London: Routledge
- Blong, R. 1984. *Volcanic Hazards: A Sourcebook on the Effects of Eruptions*. Academic Press, London.
- Blong, R. 2000. *Volcanic hazards and risk management*. In: Sigurdsson, H., Houghton, B., McNutt, S.R., Rymer, H., Stix, J. (Eds.). *Encyclopedia of Volcanoes*. Academic Press, San Diego. Pp. 1215-1227.
- Blong, R. 2003. *Building damage in Rabaul, Papua New Guinea*. *Bulletin of Volcanology* 65: 43-54.
- Boggs, S. 2001. *Principles of sedimentology and stratigraphy*. 3rd edition. Prentice Hall Inc., New Jersey. Pp 726.
- British Standards Institute. 1999. *Specifications for Masonry Units – Part 3: Aggregate Concrete Masonry Units (Dense and Lightweight aggregates)* BS EN 771-3-1999.
- British Standards Institute. 2003. *Specification for Masonry Units — Part 1: Clay Masonry Units* BS EN 771-1:2003.
- Browne, R.D., Geoghegan, M.P., Baker, A.F. 1983. *Analysis of Structural Condition for Durability Results, Corrosion of Reinforcement in Concrete Constructions*, A.P. Cron. Ellis Horwood Ltd. Pp. 193-222.
- Bullard, F.M. 1962. *Volcanoes in history, in theory, in eruption*. University of Texas Press, Austin, USA. Pp. 441.
- Bursik, M., Patra, A., Pitman, E.B., Nichita, C., Macias, J.L., Saucedo, R., Girina, O. 2005. *Advances in studies of dense volcanic granular flows*. *Reports on Progress in Physics*, 68: 271–301
- Capra, L., GropPELLI, G., Lunghi, R., Norini, G. 2004. *Volcanic hazards assessment of Nevado de Toluca volcano (Mexico)*. *32nd International Geological Congress, Florence, Italy*. Pp. 84.
- Capra, L., GropPELLI, G., Norini, G., Lunghi, R. 2005. *Preliminary Volcanic Hazard Maps of Nevado de Toluca Volcano (Mexico)*. *Geophysical Research Abstracts* 7.
- Capra, L., Norini, G., GropPELLI, G., Macias, J.L., Arce, J.L. 2008. *Volcanic hazard zonation of the Nevado de Toluca volcano, Mexico*. *Journal of Volcanology and Geothermal Research* 176: 469-484.
- Castruccio, A., Clavero, J., Rivera, A. 2010. *Comparative study of lahars generated by the 1961 and 1971 eruptions of Calbuco and Villarrica volcanoes, Southern Andes of Chile*. *Journal of Volcanology and Geothermal Research* 190: 297-311.
- CEN. 1995. *Eurocode 6: design of masonry structures. Part 1-1 General rules for buildings. Rules for reinforced and unreinforced masonry*. (ENV 1996-1-1), Brussels.

- Charbonnier, S., Gertisser, R. 2008. *Computational modelling of pyroclastic density currents using the TITAN2D simulation code: examples from Merapi Volcano, Indonesia*. Geophysical Research Abstracts, Vol. 10, EGU2008-A-02860, 2008, EGU General Assembly 2008, SRef-ID: 1607-7962/gra/EGU2008-A-02860
- Charbonnier, S.J., Gertisser, R. 2009. *Numerical simulations of block-and-ash flows using the Titan2D flow model: examples from the 2006 eruption of Merapi Volcano, Java, Indonesia*, Bulletin of Volcanology 71: 953–959
- Chávez and Chávez A. 1992. *La erupcion del volcan Misti. Pasado, Presente, Futuro*. -1mpr. Zenit, Arequipa, 158 pp.
- Chester, D. 1993. *Volcanoes and Society*. London: Routledge
- Chester, D., 2002. *Volcanoes and society*. In: Marti, J., Ernst, G.J. (Eds.), *Volcanoes and the Environment*. Cambridge University Press, Cambridge.
- Chester, D., Degg, M., Duncan, A.M., Guest, J.E. 2001. *The Increasing Exposure of Cities to the Effects of Volcanic Eruptions: A Global Survey*. Global Environmental Change Part B: Environmental Hazards 2: 89-103.
- Chevillot B. 2000. *Rapport de mission a Arequipa (sud Pérou) 26 julliet - 15 août 2000. Objet: mise en oeuvre d'un S.I.G. appliqué aux risques hydrologiques et volcaniques*. Rapport., Lab. De traitement de données géographiques ENITA de Clermont-Ferrand, Pp. 44.
- Chew, M.Y.L. 1993. *The assessment of fire damaged concrete*. Building and Environment 29: 97-102.
- CNAM. 2006. *Travaux pratiques - Géotechnique*. Chaire de Géotechnique, Conservatoire National des Arts et Métiers, Paris, France. Pp. 80.
- Cole, J.W., Sabel, C. E., Blumenthal, E., Finnis, K., Dantas, A., Barnard, S., Johnston, D.M. 2005. *GIS-based emergency and evacuation planning for volcanic hazards in New Zealand*. Bulletin of the New Zealand Society for Earthquake Engineering 38.
- Conly, G., Stewart, G. 1991. *New Zealand Tragedies on the Track: Tangiwai and Other Railway Accidents*. Revised edition. Grantham House, Wellington, New Zealand. P. 6-7.
- Costa, J.E., 1988. *Rheologic, geomorphic, and sedimentologic differentiation of water floods, hyperconcentrated flows, and debris flows*. In: Baker, V.R., Kochel, R.C., Patton, P.C. (Eds.), *Flood Geomorphology*. Wiley, Chichester, UK, pp. 113– 122. Chapter 7.
- Cronin, S., Procter, J., Patra, A., Sheridan, M.F., Dalbey, K. 2004. *Evaluating a 2-D granular-flow numerical model for prediction of lahars from Crater Lake at Ruapehu*. Geological Society of New Zealand, New Zealand Geophysical Society, 26th New Zealand Geothermal Workshop.
- Cronin, S.J., Neall, V.E., Lecointre, J.A., Palmer, A.S., 1997. *Changes in Whangaehu River lahar characteristics during the 1995 eruption sequence, Ruapehu volcano, New Zealand*. Journal of Volcanology and Geothermal Research 76: 47–61.
- Daag, A., Van Westen, C.J., 1996. *Cartographic modelling of erosion in pyroclastic flow deposits of Mount Pinatubo, Philippines*. ITC Journal 1996-2: 110-124.
- Dalbey, K., Patra, A. Pitman, E., Bursik, M., Sheridan, M. 2008. *Input uncertainty propagation methods and hazard mapping of geophysical mass flow*. Journal of Geophysical Research, 113: 5203–5219.

- De Silva S.L., Alzueta, J., Salas, G. 2000. *The socioeconomic consequences of the 1600 AD eruption of Huaynaputina, southern Peru*. In: McCoy F, Heiken G (eds) *Volcanic disasters in human antiquity*. Geological Society of America Special Paper 345
- Degg, M.R., Chester, D.K. 2005. *Seismic and volcanic hazards in Peru: Changing attitudes to disaster mitigation*. The Geographical Journal: 171: 125-145.
- Delaite, G. 2003. *Méthodes pour le Diagnostic des Risques Volcaniques Fondées sur les Systèmes d'Information Géographique et le Code de Simulation LAHARZ* (M.Sc. thesis): Clermont-Ferrand, Laboratoire Magmas et Volcans, Department of Geology, Université Blaise-Pascal. Pp. 55.
- Delaite, G., Thouret, J.-C., Sheridan, M. F., Stinton, A., Labazuy, P., Souriot, T., and van Westen, C., 2005. *Assessment of volcanic hazards of El Misti and in the city of Arequipa, Peru, based on GIS and simulations, with emphasis on lahars*. Zeitschrift für Geomorphology N.F., suppl.140: 209-231.
- Denlinger, R.P., Iverson, R.M., 2001. *Flow of variably fluidized granular masses across three dimensional terrain, 2. Numerical predictions and experimental tests*. Journal of Geophysical Research 106: 533-566.
- D'Ercole, R. and Metzger, P. 2004. *La vulnerabilidad del distrito metropolitano de Quito*. IRD & Municipio del Distrito Metropolitano de Quito, Pp. 496.
- Dibben, C., and Chester, D.K. 1999. *Human vulnerability in volcanic environments: the case of Furnas, São Miguel, Azores*. Journal of Volcanology and Geothermal Research 92: 133-150.
- Donnay, J-P., Barnsley, M.J., Longley, P.A. 2001. *Remote sensing and urban analysis: GISDATA*. Taylor & Francis, London. Pp 268.
- Douglas, J., 2007. *Physical vulnerability modelling in natural hazard risk assessment*. *Natural Hazards and Earth System Sciences* 7: 283-288.
- Duggal, S.K. 2008. *Building Materials*. New Age International Pvt Ltd Publishers. New Delhi, India. Pp. 542.
- Dumaisnil, C., Thouret, J.-C., Chambon, G., Doyle, E.E., Cronin, S.J., Surono. 2010. *Hydraulic, physical and rheological characteristics of rain-triggered lahars at Semeru volcano, Indonesia*. *Earth Surface Processes and Landforms*, 35: 1573-1590.
- Elliot, J.L., Larsen, C.F., Freymueller, J.T., Motyka, R.J. 2010. *Tectonic block motion and glacial isostatic adjustment in southeast Alaska and adjacent Canada constrained by GPS measurements*. Journal of Geophysical Research 115.
- Faccioli E., Pessina V., Calvi G.M., Borzi B. 1999. *A study on damage scenarios for residential buildings in Catania City*. Journal of Seismology 3: 327-343.
- Fernández, D.S., Lutz, M.A. 2010. *Urban flood hazard zoning in Tucumán Province, Argentina, using GIS and multicriteria decision analysis*. *Engineering Geology* 111: 90 - 98.
- Finizola A. 2002. *Etude de systèmes hydrothermaux de volcans actifs: Misti (Pérou) et Stromboli (Italie); Approches géophysiques et géochimiques*. PhD thesis, Université Blaise Pascal, Clermont-Ferrand II, Pp. 205.

- Finizola, A., Lénat, J.F., Macedo, O., Ramos, D., Thouret, J.C., and Sortino, F. 2004. *Fluid circulation and structural discontinuities inside Misti volcano (Peru) inferred from self-potential measurements*. Journal of Volcanology and Geothermal Research 135: 343-360.
- Fournier d'Albe, E., 1979. Objectives of volcanic monitoring and prediction. Journal of Geological Society 136, 321–326.
- Fujisada, H., Bailey, G.B., Kelly, G.G., Hara, S., Abrams, M.J. 2005. *ASTER DEM performance*. Transactions on Geoscience and Remote Sensing 43: 2707-2714.
- Fuller, R.M., Groom, G.B., Wallis, S.M. 1994. *The availability of Landsat TM images for Great Britain*. International Journal of Remote Sensing 15: 1357-1362.
- Gallego, J., Bamps, C. 2008. *Using CORINE land cover and the point survey LUCAS for area estimation*. International Journal of Applied Earth Observation and Geoinformation 10: 467-475.
- García-Pérez, J., Castellanos, F., Diaz, O. 2005. *Occupancy importance factor in earthquake engineering*. Engineering Structures. Vol 27, issue 11: 1625-1632
- Gerbe M.C., and Thouret, J-C. 2004. *Role of magma mixing in the petrogenesis of tephra erupted during the 1990-98 explosive activity of Nevado Sabancaya, southern Peru*. Bulletin of Volcanology 66: 541-561.
- Gertisser, R., Charbonnier, S., Troll, V., Keller, J., Preece, K., Chadwick, J., Barclay, J. Herd, R. 2011. *Merapi (Java, Indonesia): anatomy of a killer volcano*. Geology Today 27: 57–62. doi: 10.1111/j.1365-2451.2011.00786.x
- Glade, T. 2003. *Landslide occurrence as a response to dramatic land use change*. Catena 51: 297-314.
- GMFG. 2007. *TITAN2D User Guide*, 2007. Release 2.0.0, 2007.07.09 Geophysical Mass Flow Group (GMFG). State University of New York at Buffalo, USA. http://www.gmfg.buffalo.edu/software/titan_userguide.pdf
- Gómez-Fernández, F. 2000a. *Contribution of geographical information systems to the management of volcanic crisis*. Natural Hazards 21:347-360
- Gómez-Fernández, F. 2000b. *Application of a GIS algorithm to delimit the areas protected against basic lava flow invasion on Tenerife Island*. Journal of Volcanology and Geothermal Research 103: 409-423.
- Goodman, R.E. 1989. *Introduction to rock mechanics*. Second edition. John Wiley & Sons, New York. Pp. 552.
- Grieco, F., Capra, L., Groppelli, G., Norini, G. 2007. *TI: Numerical Modeling of Debris Avalanches at Nevado de Toluca (México): Implications for Hazard Evaluation and Mapping*, AGU Joint Assembly, Acapulco, México.
- Gruber, U., Bartelt, P. 2007. *Snow avalanche hazard modelling of large areas using shallow water numerical methods and GIS*. Environmental Modelling and Software 22: 1472 - 1481.
- Hayashi, J.N., Self, S., 1992. A comparison of pyroclastic flow and debris avalanche mobility. Journal of Geophysical Research 97: 9063– 9071.

- Hendry, A.W. 2001. *Masonry walls: materials and construction*, Construction and Building Materials 15: 323-330.
- Henry, C. 2009. *Personal communication with Christopher Henry, Civil Engineer, Opus International Consultants Ltd.*, Dunedin, New Zealand. Email correspondence 8 October 2009.
- Hidayat, D., Widiwijayanti, C., Voight, B., Patra, A., Pitman, B. 2008. *TITAN2D Based Modeling of Dome-collapse Pyroclastic Flows for Crisis Assessments on Montserrat*, IAVCEI General Assembly, Reykjavik, Iceland.
- Hidayat, D., Widiwijayanti, C., Voight, B., Patra, A., Pitman, E. 2007. *TITAN2D Analyses of Dome-Collapse Pyroclastic Flows on Montserrat*. American Geophysical Union, Fall Meeting 2007, abstract #V31B-0499
- Hill, L.L. 2006. *Georeferencing*. The MIT Press. Pp. 272.
- Hirano, A., Welch, R., Lang, H. 2003. Mapping from ASTER stereo image data: DEM validation and accuracy assessment, *ISPRS J. Photogramm. Remote Sens.* 57: 356-370.
- Hoek E., Brown E.T., 1980. *Underground excavations in rock*. Institution of Mineralogy and Metallurgy, London, UK. Pp. 527.
- Hoffmann, D., Niesel, K., 1995. *Quantifying the effect of air pollutants on renderings and also moisture-transport phenomena in masonry including its constituents (Bundesanstalt für Materialforschung und-prüfung)*. An expanded English version of BAM (Federal Institute for Materials Research and Testing) Research Report No. 209, Berlin, Germany. Accessed from http://www.bam.de/a_vii/moisture/transport.html on 24 October 2000.
- Huelman, P., Corrin, D., 1997. *Drying Walls After a Flood*. Document no. 267 in INFO-U of the University of Minnesota Extension Service, accessed at <http://www.extension.umn.edu/info-u/household/BK267.html> on 3 June 2002.
- Huggel, C., Schneider, D., Julio Miranda, P., Delgado Granados, H., Kääh, A. 2008. *Evaluation of ASTER and SRTM DEM data for lahar modeling: A case study on lahars from Popocatepetl Volcano, Mexico*. *Journal of Volcanology and Geothermal Research* 170: 99-110.
- Hungr, O 1995. *A model for the runout analysis of rapid flow slides, debris flows, and avalanches*. *Canadian Geotechnical Journal* 32: 610–623.
- Instituto Nacional de Estadística e Informática (INEI). 2007. *XI Censo de Población y VI de Vivienda – Arequipa: resultados definitivos de los censos nacionales*. Pp. 3220. Accessed 20 December 2009: <http://www.inei.gob.pe/>
- International Code Council (ICC). 2006. *International building code*. Falls Church, Virginia, USA. Pp. 637.
- Iverson, R. M. 1997. *The physics of debris flows*. *Reviews of Geophysics* 35: 245-296.
- Iverson, R. M., Schilling, S. P., and Vallance, J.W. 1998. *Objective delineation of lahar-inundation hazard zones*. *Geological Society of America Bulletin* 110: 972-984.
- Iverson, R.M., Denlinger, R.P. 2001. *Flow of variably fluidized granular masses across three-dimensional terrain 1. Coulomb mixture theory*. *Journal of Geophysical Research* 106: 537-552.

- Johansson, J., Mayora, P., Torres, T., Leon, E., 2007. *A reconnaissance report on the Pisco, Peru, earthquake of August 15, 2007*. Peru Earthquake reconnaissance team. Pp. 109. Accessed 14 June 2009: http://shake.iis.utokyo.ac.jp/Peru2007/JSCE_JAEE_Report/Index.htm
- Johnston, D.M. 1998. *Modelling ash distribution for Auckland scenarios*. Institute of Geological and Nuclear Sciences Client Report 71770D.10A. Institute of Geological and Nuclear Sciences, Lower Hutt, New Zealand. Pp 1-12
- Johnston, K., Ver Hoef, J.M., Krivoruchko, K., Lucas, N. 2001. *Using ArcGIS™ Geostatistical Analyst*. ESRI Press, USA. Pp.300
- Jones G., Chester D.K., Shooshtarian F. 1999. *Statistical analyses of the frequency of eruptions at Furnas Volcano, Sao Miguel, Azores*. Journal of Volcanology and Geothermal Research 92: 31-38.
- Kelfoun, K., Druitt, T. H. 2005. *Numerical modeling of the emplacement of Socompa rock avalanche, Chile*. Journal of Geophysical Research 110, B12202, doi:10.1029/2005JB003758.
- Kelman, I. 2002. *Physical Flood Vulnerability of Residential Properties in Coastal, Eastern England*. PhD Thesis, University of Cambridge, UK. Available from: <<http://www.ilankelman.org/phd.html>>.
- Kelman, I. and Spence, R. 2004. *An Overview of Flood Actions on Buildings*. Engineering Geology. 73: 297-309.
- Kienzle, S. 2004. *The effect of DEM Resolution on First Order, Second Order and Compound Terrain Derivatives*. Transactions in GIS 8: 83-111.
- Koopman, E.E., 2009. *The influence of hydraulics and spatial differences on the daily practice within an irrigation system: A case study in Arequipa, Perú*. October, 2009. Delft University of Technology Master thesis, Faculty of Civil Engineering and Geosciences, October, 2009. The Netherlands. Pp. 127.
- Kouokam, E. 2001. *Monitoring of Mount Cameroon impact risk assessment-site response analysis (Muea-Bokova-Buea-Bakingili-Ngame area) 1st campaign*. Cameroon ministry of mines, water and energy report, Pp. 105
- Kusunoki, K. 2002. *Report on the damage investigation of the 2001 Atico Earthquake in Peru*. Building Research Institute of Japan. Pp. 27.
- La norme NF EN 771-1. 2005. *Spécifications pour éléments de maçonnerie - Partie 1 : briques de terre cuite de février 2004 et de son amendement 1 de novembre 2005*, (Indice de classement : P12-021-1)
- La norme NF EN 771-3/CN. 2007. *Spécifications pour éléments de maçonnerie - Partie 3 : éléments de maçonnerie en béton de granulats (granulats courants et légers) - Complément national à la NF EN 771-3:2004 et son amendement A1:2005*, (indice de classement : P12-023-1).
- Lan, L., Martin, D.C., Chenghu, Z., Chang, H.L. 2010. *Rockfall hazard analysis using LiDAR and spatial modelling*. Geomorphology 118: 213 - 223.
- Larson, K. M., Poland, M., Miklius, A. 2010. *Volcano monitoring using GPS: Developing data analysis strategies based on the June 2007 Kilauea Volcano intrusion and eruption*. Journal of Geophysical Research 115:

- Leger, P., Tremblay, R. 2009. *Earthquake Ground Motions for Seismic Damage Assessment and Re-Evaluation of Existing Buildings and Critical Facilities. Damage Assessment and Reconstruction after War or Natural Disaster*. NATO Science for Peace and Security Series I: 193-219.
- Legros F., Cantagrel J.M., Devouard B. 2000. *Pseudotachylite (frictionite) at the base of the Arequipa volcanic landslide deposit (Peru): Implications for emplacement mechanisms*. *Journal of Geology* 108: 601-611.
- Legros, F. 2001. *Tephra stratigraphy of Misti volcano, Peru*. *Journal of South American Earth Sciences* 14: 15-29.
- Léone, F. 1995. *Concept de vulnérabilité appliqué à l'évaluation des risques générés par les phénomènes de mouvements de terrain*. Doctoral thesis, Joseph Fourier University, Grenoble (France). Pp. 274
- Léone, F., Gaillard, J.-C. 1999. *Analysis of the institutional and social responses to the eruption and the lahars of Mount Pinatubo Volcano from 1991 to 1998 (Central Luzon, Philippines)*. *GeoJournal* 49: 223-238.
- Lesage, P., Glangeaud, F. and Mars, J. 2002. Applications of autoregressive and time-frequency analysis to the study of volcanic tremor and LP events, *Journal of Volcanology and Geothermal Research* 114: 391–417.
- Lirer, L., Petrosino, P., Alberico, I., Postiglione, I. 2001. *Long-term volcanic hazard forecasts based on Somma-Vesuvio past eruptive activity*. *Bulletin of Volcanology* 63: 45-60.
- Loaiza, C., Blondet., M. 2003. *World Housing Encyclopedia Report on Confined Masonry Building, Peru*. World Housing Encyclopedia. .
http://www.eeri.org/lfe/pdf/peru_confined_masonry_building.pdf
- Loaiza, C., Blondet., M. 2003. *World Housing Encyclopedia Report on Confined Masonry House, Peru*. World Housing Encyclopedia. http://www.eeri.org/lfe/pdf/peru_confined_masonry_house.pdf
- Loaiza, C., Blondet., M., Ottazzi, L. 2003. *World Housing Encyclopedia Report on Adobe House, Peru*. World Housing Encyclopedia. http://www.eeri.org/lfe/pdf/peru_adobe_house.pdf
- Luongo, G., Perrotta, A., and Scarpati, C. 2003. *Impact of the AD 79 explosive eruption on Pompeii, I. Relations amongst the depositional mechanisms of the pyroclastic products, the framework of the buildings and the associated destructive events*. *Journal of Volcanology and Geothermal Research* 126: 201-223.
- Macías, J.L., Capra, L., Arce, J.L., Espíndola, J.M., García-Palomo, A., Sheridan, M.F. 2008. *Hazard map of El Chichón volcano, Chiapas, México: constraints posed by eruptive history and computer simulations*. *Journal of Volcanology and Geothermal Research* 175: 444–458.
- Magill, C., Blong, R., 2005a. *Volcanic risk ranking for Auckland, New Zealand. I: Methodology and hazard investigation*. *Bulletin of Volcanology* 67: 331-339.
- Magill, C., Blong, R., 2005b. *Volcanic risk ranking for Auckland, New Zealand: II. Hazard consequences and risk calculation*. *Bulletin of Volcanology* 67: 340-349.
- Mariño, J., Rivera, M., Cacya, L., Thouret, J.C., Macedo, L., Salas, G., Tilling, R.I., Sheridan, M., Siebe, C., Zuñiga, S. 2007. *Mapa de Peligros del Volcán Misti*. Instituto Geológico Minero y Metalúrgico, Lima, Perú.

- Martelli K.M., Cronin, S.J. 2005. *Forecasting of pyroclastic flow hazards from Ngauruhoe on the Tongariro Crossing*. Report to Department of Conservation, New Zealand. SAF Ref No. 2006/02. Pp.7.
- Martelli, K.M. 2007. *Computer Modelling of the Potential Hazard from Scoria and Ash Flows on Mt. Ngauruhoe, Tongariro Volcanic Centre, New Zealand*. MSc thesis, Massey University, Palmerston North, New Zealand. Pp. 172.
- Martí, J., Aspinall, W.R., Sobradelo, R., Felpeto, A., Geyer, A., Ortiz, R., Baxter, P., Cole, P.D., Pacheco, J., Blanco, M.J., Lopez, C. 2008b. *A long-term volcanic hazard event tree for Teide-Pico Viejo stratovolcanoes (Tenerife, Canary Islands)*. Journal of Volcanology and Geothermal Research 178: 543-552.
- Martí, J., Felpeto, A. 2010. *Methodology for the computation of volcanic susceptibility: An example for mafic and felsic eruptions on Tenerife (Canary Islands)*. Journal of Volcanology and Geothermal Research 195: 69-77
- Marzocchi, W., Sandri, L., Selva, J. 2008. *BET_EF: a probabilistic tool for long- and short-term eruption forecasting*. Bulletin of Volcanology 70: 623-632
- McEwen, A.S., Malin, M.C. 1989. *Dynamics of Mount St. Helens' 1980 pyroclastic flows, rockslide-avalanche, lahars, and blast*. Journal of Volcanology and Geothermal Research 37: 205–231.
- Mekong River Commission Secretariat. 2009. *The flood management and mitigation programme, component 2: structural measures and flood proofing in the lower Mekong Basin*. Draft final report - best practise guidelines for flood risk assessment. December 2009.
- Melville, B.W., and Chiew, Y.W. 1999. *Time Scale for Local Scour at Bridge Piers*. Journal of Hydraulic Engineering 125: 59-65.
- Mering C., Huaman-Rodrigo D., Chorowicz J., Deffontaines B., Guillande R. 1996. *New data on the geodynamics of southern Peru from computerized analysis of SPOT and SAR ERS-1 images*. Tectonophysics 259: 153-169.
- Muñoz, E., Palacios, D., Namikawa, L., Sheridan, M., Renschler, C. 2004. *Contrast between computer simulations and field observations of Popocatepetl lahars*. Geophysical Research Abstracts 6, p. 04599 European Geosciences Union.
- Muñoz-Salinas, E., Renschler, C., Palacios, D., Namikawa, L.M. 2008. *Updating channel morphology in digital elevation models: lahar assessment for Tenenepanco-Huiloac Gorge, Popocatepetl, Mexico*. Natural Hazards 45: 309–320.
- Murcia, H., Sheridan, M., Macias, J., Cortes, G. 2010. *TITAN2D simulations of pyroclastic flows at Cerro Machin Volcano, Colombia: Hazard implications*. Journal of South American Earth Sciences, 29:161–170.
- Murcia, H.F., Sheridan, M.F., Macías, J.L., 2008. *TITAN2D Pyroclastic Flows Simulations at Cerro Machin Volcano – Colombia*. IAVCEI General Assembly, Reykjavik, Iceland.
- Nagata, M. 1999. *Una introduccion a las inundaciones en el area urbana de Arequipa, Informe sobre las Torrenteras en Arequipa* INDECI-IGP-ORSTOM. Pp. 99.

- Neri, A., Aspinall, W.P., Cioni, R., Bertagnini, A., Baxter, P.J., Zuccaro, G., Andronico, D., Barsotti, S., Cole, P.D., Esposti Ongaro, T., Hincks, T.K., Macedonio, G., Papale, P., Rosi, M., Santacroce, R., Woo, G. 2008. *Developing an event tree for probabilistic hazard and risk assessment at Vesuvius*. Journal of Volcanology and Geothermal Research 178: 397-415.
- Newnham, R.M., Lowe, D.J., Alloway, B.V. 1999. *Volcanic hazards in Auckland, New Zealand: a preliminary assessment of the threat posed by central North Island silicic volcanism based on the Quaternary tephrostratigraphical record*. In: Firth, C.R., McGuire, W.J. (eds). Volcanoes in the Quaternary. Special Publication 161, Geological Society Publishing House: Bath; 27-45.
- Nicholas, J., Proverbs, D.G. and Holt, G.D. 2001. *An investigation into factors influencing the assessment of UK flood-damaged domestic properties*. In Proceedings of RICS COBRA 2001 Conference, Glasgow Caledonian University, 3–5 September, pp. 660–669.
- Norini, G., Andronico, D., de Beni, E., Polacci, M., Grieco, F. 2007. *November 16th 2006 Lateral Collapse of South-East Crater on Mount Etna Volcano and Hazard Implication*. American Geophysical Union, Spring Meeting 2007, abstract #V33C-05
- O'Brian, J.S., Julien, P.Y., Fullerton, W.T., 1992. *Two-dimensional waterflood and mudflow simulation*. Journal of Hydraulic Engineering. 119: 244-261
- Oehler, J-F. 2010a. *Personal communication with J-F Oehler*. Ingénieur Géophysicien ALTRAN OUEST-Atlantide, Brest, France. Email correspondance 21 June 2010.
- Ogburn, S., Calder, E., Dalbey, K., Ryan, G. 2008. *Modeling Pyroclastic Flow Hazards in the Belham Valley, Soufrière Hills Volcano, Montserrat*, IAVCEI General Assembly, Reykjavik, Iceland.
- Palhol, H. 2008. *Méthodes d'étude de l'endommagement induit par les effets des lahars au bâti ; le cas de la ville d'Arequipa, Pérou*. Master 1: Rapport du Travail d'Etude et de Recherche. Laboratoire Magmas et Volcans, Université Blaise Pascal, France. Pp. 24.
- Paquereau-Lebti P., Thouret J.C., Wörner G., Fornari M. 2006. *Neogene and Quaternary ignimbrites in the area of Arequipa, Southern Peru: Stratigraphical and petrological correlations*. Journal of Volcanology and Geothermal Research 154: 251-275.
- Pareschi, M.T., Cavarra, L., Favalli, M., Giannini, F., Meriggi, A. 2000. *GIS and volcanic risk management*. Natural Hazards 2: 361- 379.
- Patra, A.K., Bauer, A.C., Nichita, C.C., Pitman, E.B., Sheridan, M.F., Bursik, M., Rupp, B., Webber, A., Stinton, A.J., Namikawa, L.M., Renschler, C.S. 2005. *Parallel adaptive simulation of dry avalanches over natural terrain*. Journal of Volcanology and Geothermal Research 139: 1–22.
- Permanent Technical Committee of Earthquake-Resistant Design. 2003. *Technical Standard of Building E. 030 earthquake resistant design*. Lima, Peru. Accessed 27 July 2007: http://iisee.kenken.go.jp/net/seismic_design_code/peru/NTE-030-PERU.pdf
- Perrotta, A., Scarpati, C., Luongo, G. 2006. *Volcaniclastic resedimentation on the northern slope of Vesuvius as a direct response to eruptive activity*. Landslides Vol. 3, No. 4: 295-301
- Pessina, V., Meroni, F. 2009. *A WebGis tool for seismic hazard scenarios and risk analysis*. Soil Dynamics and Earthquake Engineering 29: 1274 - 1281.

- Pierson, T.C. 2005. *Hyperconcentrated flow; transitional process between water flow and debris flow*. In: Jakob, M., Hungr, O. (Eds). Debris-flow hazards and related phenomena. Springer. Berlin, Federal Republic of Germany.
- Pierson, T.C., Costa, J.E., 1987. *A rheologic classification of subaerial sediment-water flows*. In: Costa J.E., Wieczorek G.F. (Eds). Debris flows/ avalanches; process, recognition, and mitigation. Reviews in Engineering Geology. Geological Society of America (GSA), Boulder, CO, United States. Pp. 1-12.
- Pierson, T.C., Janda, R.J., Thouret, J.C., Borrero, C.A. 1990. *Perturbation and melting of snow and ice by the 13 November 1985 eruption of Nevado del Ruiz, Colombia, and consequent mobilization, flow, and deposition of lahars*. Journal of Volcanology and Geothermal Research 41:17-66.
- Pierson, T.C., Janda, R.J., Umbal, J.V., Daag, A.S. 1992. *Immediate and long-term hazards from lahars and excess sedimentation in rivers draining Mount Pinatubo, Philippines*. U.S. Geological Survey Water-Resources Investigations Report 92-4039, Pp. 41.
- Pierson, T. C., A. S. Daag, P. J. D. Reyes, M. T. M. Regalado, R. U. Solidum, and B. S. Tubianosa. 1996. *Flow and deposition of post-eruption hot lahars on the east side of Mount Pinatubo, July–October 1991, in Eruptions and Lahars of Mount Pinatubo, Philippines*. In: Newhall C. G. and Sparks, R. S. Punongbayan, pp. 921– 950, Univ. of Wash. Press, Seattle.
- Pierson, T. C; Scott, K. M. 1985: *Downstream dilution of a lahar: transition from debris flow to hyperconcentrated streamflow*. Water Resources Research 21: 1511-1524
- Pitman, E.B., Le L. 2005. *A two-fluid model for avalanche and debris flows*. Philosophical Transactions of the Royal Society A: Mathematical, Physical and Engineering Sciences. 363: 1471-2962
- Pitman, E.B., Patra, A.K., Bauer, A., Sheridan, M.F., Bursik, M.I. 2003. *Computing debris flows and landslides*. Physics of Fluids 15: 3638–3646
- Pomonis, A., Spence, R.J.S., Baxter, P.J. 1999. *Risk assessment of residential buildings for an eruption of Furnas Volcano, São Miguel, the Azores*. Journal of Volcanology and Geothermal Research 92: 107-131.
- Pouliquen, O., Renaut, N. 1996. *Onset of Granular Flows on an inclined Rough Surface: Dilatancy Effects*. Journal of Physics II France 6: 923-935.
- Prentice, J.E. 1990. *Geology of construction materials*. Topics in the Earth Sciences 4. Chapman and Hall, London. Pp.202.
- Prevot, T. 2009. *Lahars de la Soufrière (Basse-Terre, Guadeloupe) : étude des impacts potentiels sur le bâti. Master 1: Rapport du Travail d'Etude et de Recherche*. Laboratoire Magmas et Volcans, Université Blaise Pascal, France. Pp. 29.
- Procter, J.N. 2010. *Towards Improving Volcanic Mass Flow Hazard Assessment at New Zealand Stratovolcanoes*. PhD thesis, Massey University, Palmerston North, New Zealand.
- Procter, J., Cronin, S., Patra, A., Dalbey, K., Sheridan, M., Platz, T. 2004a. *Utilising TITAN2D to Forecast Dome-collapse Block-and-ash flow (bafs) Hazards from Mount Taranaki – New Zealand*, IAVCEI General Assembly, Pucón, Chile

- Procter, J., Cronin, S., Sheridan, M., Patra, A. 2004b *Application of Titan2d Mass-flow Modelling to Assessing Hazards from a Potential Lake-breakout Lahar at Ruapehu Volcano, New Zealand*, IAVCEI General Assembly, Pucón, Chile
- Procter, J., Cronin, S., Zernack, A. 2010c. *Emplacement of the Opua Debris Avalanche Deposit from Mt Taranaki, New Zealand: Titan2D simulation compared to sedimentology and GIS analysis*. Geophysical Research Abstracts. Vol. 12, EGU2010-7588, 2010. EGU General Assembly 2010
- Procter, J.N., Cronin, S.J., Fuller, I.C., Sheridan, M.F., Neall, V.E., Keys, H. 2010a. *Lahar hazard assessment using Titan2D for an alluvial fan with rapidly changing geomorphology: Whangaehu River, Mt. Ruapehu*, *Geomorphology*, Volume 116: 162-174
- Procter, J.N., Cronin, S.J., Platz, T., Patra, A., Dalbey, K., Sheridan, M., Neall, V.E. 2010b. *Mapping block-and-ash flow hazards based on Titan 2D simulations: a case study from Mt. Taranaki, NZ*. *Natural Hazards* 53: 483-501
- Procter, J.N., Cronin, S.J., Zernack, A.V. 2009. *Landscape and sedimentary response to catastrophic debris avalanches, western Taranaki, New Zealand*. *Sedimentary Geology* 220: 271-287
- Rabus, B., Eineder, M., Roth, A., Bamler, R. 2003. *The shuttle radar topography mission a new class of digital elevation models acquired by spaceborne radar*, *ISPRS Journal of Photogrammetry and Remote Sensing* 57: 241-262
- Reese, S., Markau, H.-J., 2002. *Risk handling and natural hazards, new strategies in coastal defense-a case study from Schleswig-Holstein, Germany*. In: *Proceedings of the Solutions to Coastal Disasters Conference*, American Society for Civil Engineers (ASCE), San Diego, California, pp. 498-510 24-27 February 2002.
- Richards, K. 1982: *Rivers: form and process in alluvial channels*. London: Methuen. xi + 358 pp
- Rivera, M., Thouret, J-C., Marino, J., Berolatti, R., Fuentes, J. 2010. *Characteristics and management of the 2006-2008 volcanic crisis at the Ubinas volcano (Peru)*, *Journal of Volcanology and Geothermal Research* 198: 19-34.
- Rodolfo, K.S. 2000. *The hazard from lahars and Jökulhlaups*. In: Sigurdsson, H (Ed). *Encyclopedia of Volcanoes*, Academic Press, San Diego, CA. Pp. 973-996.
- Roos, W. 2003. *Damage to Buildings*. TNO Bouw, Delft Cluster, No. DC1-233-9, Holland.
- Rousset Tournier, B. 2001. *Transferts par capillarité et évaporation dans des roches - rôle des structures de porosité*. Doctoral thesis, Strasbourg 1 - Université Louis Pasteur. Pp. 305.
- Rupp, B., Bursik, M., Patra, A., Bauer, A., Nichita, C., Saucedo, R., Macias, J. 2003. *Simulation of pyroclastic flows of Colima Volcano, Mexico, using the Titan2D programme*. *Geophysical Research Abstracts* 5.
- Rupp, B., Bursik, M.I., Namikawa, L., Webb, A., Patra, A.K., Saucedo, R., Macías, J.L., Renschler, C.S. 2006. *Computational modeling of the 1991 block and ash flows at Colima Volcano, Mexico*. In: Siebe, C., Macías, J.L., Aguirre-Díaz, G.J (eds) *Neogene-Quaternary continental margin volcanism: A perspective from México*. *Geological Society of America Special Paper* 402:237–252

- Ruprecht, P., Wörner, G. 2007. *Variable regimes in magma systems documented in plagioclase zoning patterns: El Misti stratovolcano and Andahua monogenetic cones*. Journal of Volcanology and Geothermal Research 165: 142-162.
- Sandri, L., Guidoboni, E., Marzocchi, W., and Selva, J. 2009. *Bayesian Event Tree for Eruption Forecasting (BET_EF) at Vesuvius, Italy: a retrospective forward application to 1631 eruption*. Bulletin of Volcanology 71: 729-745.
- Sandri, L., Jolly, G., Lindsay, J., Howe, T., Marzocchi, W. 2010. *Combining probabilistic hazard assessment with cost-benefit analysis to support decision making in a volcanic crisis from the Auckland Volcanic Field, New Zealand*. Geophysical Research Abstracts Vol. 12, EGU2010-2337. EGU General Assembly 2010, Vienna, Austria.
- Saucedo, R., Macías, J.L., Bursik, M.I. 2004. *Pyroclastic flow deposits of the 1991 eruption of Volcán de Colima, Mexico*, Bulletin of Volcanology 66: 291–306
- Saucedo, R., Macías, J.L., Sheridan, M.F., Bursik, M.I., Komorowski, J.C. 2005. *Modeling of pyroclastic flows of Colima Volcano, Mexico: implications for hazard assessment*. Journal of Volcanology and Geothermal Research 139:103–115
- Savage S.B., Hutter, K 1989. *The motion of a finite mass of granular material down a rough incline*. Journal of Fluid Mechanics 199: 177-215.
- Schilling, S.P. 1998. *LAHARZ: GIS programs for automated delineation of lahar-hazard zones*. US Geological Survey, Open-file Report 98–638. Pp. 84
- Schuller, M. P, Atkinson, R. H., Noland, J. L. 1995. *Structural Evaluation of Historic Masonry Buildings*. APT Bulletin 26: 51-61.
- Scott, K.M. 1988. *Origins, behavior, and sedimentology of lahars and lahar-runout flows in the Toutle-Cowlitz River system, Mount St. Helens, Washington*. U.S. Geological Survey Professional Paper 1447-A. Pp. 74.
- Scott, K.M. 1989. *Magnitude and Frequency of Lahars and Lahar-Runout Flows in the Toutle-Cowlitz River System*. US Geological Survey Professional Paper 1447-B
- Servicio Nacional de Capacitación para la Industria de la Construcción (SENCICO). 1997. *NTE E.050 - Norma Técnica E.050 Suelos y Cimentaciones*. Normas Técnicas del Reglamento Nacional de Edificaciones. Pp. 22.
- Servicio Nacional de Capacitación para la Industria de la Construcción (SENCICO). 1999. *NTE E.080 - Norma Técnica de edificación E.080 Adobe*. Normas Técnicas del Reglamento Nacional de Edificaciones. Pp. 22.
- Servicio Nacional de Capacitación para la Industria de la Construcción (SENCICO). 2006a. *NTE E.010 - Normas de materiales y procedimientos citados - Anexo 2 – Madera*. Normas Técnicas del Reglamento Nacional de Edificaciones. Pp. 439.
- Servicio Nacional de Capacitación para la Industria de la Construcción (SENCICO). 2006b. *NTE E.070 - Norma Técnica E.070 Albañilería*. Normas Técnicas del Reglamento Nacional de Edificaciones. Pp. 58.

- Servicio Nacional de Capacitación para la Industria de la Construcción (SENCICO). 2009. *NTE E.060 - Norma Técnica de edificación E.060 E.060 Concreto Armado*. Normas Técnicas del Reglamento Nacional de Edificaciones. Pp. 193.
- Sheridan M.F., Stinton, A.J, Burkett, B., Patra, A., Nichita, C.C., Pitman, E.B. 2004. *Application of Titan2D mass-flow model to potential hazards at Tungurahua Volcano, Ecuador*. Geophysical Research Abstracts 6.
- Sheridan, M. F., Cordoba, G., Pitman, E., Cronin, S. J., Procter, J. 2010. *A New Two-phase Flow Model Applied to the 2007 Crater Lake Break-out Lahar, Mt. Ruapehu, New Zealand*; American Geophysical Union, Fall Meeting 2010, abstract #NH13C-07.
- Sheridan, M. F., Stinton, A. J., Patra, A., Pitman, E. B., Bauer, A., Nichita, C. C. 2005. *Evaluating Titan2D mass-flow model using the 1963 Little Tahoma Peak avalanches, Mount Rainier, Washington*. Journal of Volcanology and Geothermal Research 139: 89- 102.
- Sheridan, M.F, Patra., A.K., Dalbey, K., Hubbard, B. 2010. *Probabilistic digital hazard maps for avalanches and massive pyroclastic flows using TITAN2D*. In: (eds) Groppelli, G., Viereck-goette, L. Stratigraphy and Geology of Volcanic Areas. Geological Society of America Special Paper. Pp. 291.
- Sheridan, M.F., Kover, T. 1996. *FLOW3D: A computer code for simulating rapid, open-channel volcanic flows*. Proc. UJST workshop on the Technology of Disaster Prevention against Local Severe Storms, Norman OK. 155-163.
- Sheridan, M.F., Macías, J.L. 1992. *PC software for 2-dimensional gravity-driven flows: Application to Colima and El Chichón Volcanoes, México*. Second International Meeting on Volcanology, Colima, México. p. 5.
- Simkin, T., Siebert, L. 1994. *Volcanoes of the World*. Geoscience Press, Tuscon. Pp. 368.
- Small, C., Naumann, T. 2001. *The global distribution of human population and recent volcanism*. Global Environmental Change Part B: Environmental Hazards 3: 93-109.
- Soetanto, R., Proverbs, D.G. 2004. *Impact of flood characteristics on damage caused to UK domestic properties: the perceptions of building surveyors*. Structural Survey 22: 95 - 104
- Spence, R., Kelman, I., Baxter, P., Zuccaro, G., Petrazzuoli, S., 2005a. *Residential building and occupant vulnerability to tephra fall*. Natural Hazards and Earth Systems Sciences 5: 477-494.
- Spence, R., Kelman, I., Calogero, E., Toyos, G., Baxter, P., Komorowski, J.-C., 2005b. *Modelling expected physical impacts and human casualties from explosive volcanic eruptions*. Natural Hazards and Earth Systems Sciences 5: 1003-1015.
- Spence, R.J.S., Baxter, P.J., Zuccaro, G. 2004a. *Building vulnerability and human casualty estimation for a pyroclastic flow: a model and its application to Vesuvius*. Journal of Volcanology and Geothermal Research 133: 321-343
- Spence, R.J.S., Zuccaro, G., Petrazzuoli, S., Baxter, P.J. 2004b. *The resistance of buildings to pyroclastic flows: analytical and experimental studies and their application to Vesuvius*. Natural Hazards Review 5: 48-59.
- Standards New Zealand. 2004. *NZS 1170.5:2004 Structural Design Actions Part 5: Earthquake actions – New Zealand*. Wellington, New Zealand. Pp. 50.

- Steede-Terry, K. 2000. *Integrating GIS and the Global Positioning System*. ESRI Press. Pp. 112.
- Stefanescu, E.R., Bursik, M. I., Cordoba, G., Patra, A.K., Pieri, D.C., Sheridan, M.F. 2010. *Impact of DEM uncertainty on TITAN2D flow model output, Galeras Volcano, Colombia*. 2010 International Congress on Environmental Modelling and Software. Modelling for Environment's Sake, Fifth Biennial Meeting, Ottawa, Canada.
<http://www.iemss.org/iemss2010/index.php?n=Main.Proceedings>
- Stefanov, W.L., Ramsey, M.S., Christensen, P.R. 2001. *Monitoring urban land cover change: an expert system approach to land cover classification of semiarid to arid urban centers*. *Remote Sensing and the Environment* 77: 173-185.
- Stefanov, W.L., Ramsey, M.S., Christensen, P.R. 2003. *Identification of fugitive dust generation, transport, and deposition areas using remote sensing*. *Environmental and Engineering Geoscience*, 9: 151-165.
- Stevens, N.F., Garbeil, H., Mouginiis-Mark, P.J. 2004. *NASA EOS Terra ASTER: Volcanic topographic mapping and capability*. *Remote Sensing and the Environment* 90: 405-414.
- Stevens, N.F., Manville, V., Heron, D.W., 2003. *The sensitivity of a volcanic flow model to digital elevation model accuracy: experiments with digitised map contours and interferometric SAR at Ruapehu and Taranaki volcanoes, New Zealand*. *Journal of Volcanology Geothermal Research* 119, 89–105.
- Stinton, A., Delaite, G., Burkett, B., Sheridan, M., Thouret, J.-C., and Patra, A.. 2004a. *Titan2D simulated debris flow hazards: Arequipa, Peru*: Abstracts, International Symposium on Environmental Software Systems (ISESS), U.S.A.
- Stinton, A.J., Sheridan, M.F., Patra, A., Dalbey, K., and Namikawa, L.M. 2004b. *Integrating variable bed friction into Titan2D mass-flow model: application to the Little Tahoma Peak avalanches, Washington*, *Acta Volcanologica* 16: 153-163.
- Sun, G., Ranson, K.J., Kharuk, V.I., Kovacs, K. 2003. *Validation of surface height from Shuttle Radar Topography Mission using Shuttle laser altimeter*. *Remote Sensing and the Environment* 88: 401-411
- Taucer, F., Alarcon, J., So, E., 2008. *2007 August 15 magnitude 7.9 earthquake near the coast of Central Peru*. EUR 23359 EN - Joint Research Centre - Institute for the Protection and Security of the Citizen. EUR - Scientific and Technical Research series - ISSN 1018-5593. Luxembourg: Office for Official Publications of the European Communities. Pp. 72.
- Thierry, P., Stieltjes, L., Kouokam, E., Ngueya, P., Salley, P. M. 2007. *Multi-hazard risk mapping and assessment on an active volcano: the GRINP project at Mount Cameroon*. *Natural Hazards* 45: 429-456.
- Thouret J.C., Juvigne E., Gourgaud A., Boivin P., Davilla J. 2002. *Reconstruction of the AD 1600 Huaynaputina eruption based on the correlation of geologic evidence with early Spanish chronicles*. *Journal of Volcanology and Geothermal Research* 115: 529-570.
- Thouret J.C., Rivera M., Wörner G., Gerbe M.C., Finizola A., Fornari M., and Gonzales K. 2005. *Ubinas: the evolution of the historical most active volcano in southern Peru*. *Bulletin of Volcanology* 67: 557-589.

- Thouret, J.-C., Davila, J. and Eissen, J.-P., 1999a. *Largest explosive eruption in historical times in the Andes at Huaynaputina volcano, A.D. 1600, southern Peru*. *Geology* 27: 435-438.
- Thouret, J.C., Finizola, A., Fornari, M., Legeley-Padovani, A., Suni, J. Frechen, M. 2001. *Geology of El Misti volcano near the city of Arequipa, Peru*. *Geological Society of America Bulletin* 113: 1593-1610.
- Thouret, J.C., Suni, J., Eissen, J-Ph., Navarro, P. 1999b. *Assessment of volcanic hazards in the Arequipa area bases on the eruptive history of Misti volcano, southern Peru*. *Zeitschrift für Geomorphologie* 114: 89-112.
- Thouret, J-C., Lavigne, F., Kelfoun, K., Bronto, S. 2000. *Toward a revised hazard assessment at Merapi volcano, Central Java*. *Journal of Volcanology and Geothermal Research* 100: 479-502.
- Thouret J., Vivian H. 1997. *Des versants au chenal d'un bassin-versant alpin anthropisé: application à l'évaluation des risques d'érosion torrentielle, Torrent de l'Eglise, Tarentaise*. *Géomorphologie: relief, processus, environnement*, Vol. 3, N°2, 167-186.
- Tilling, R. I. 2005. *Volcano Hazards*. In: Martí, J. and Ernst, G. J. E. (eds). *Volcanoes and the Environment*. Cambridge University Press, Cambridge, U.K., p. 55-89.
- Toyos, G.T., 2000, *GIS modelling the risks to debris flow for Arequipa, Southern Peru*, Master PhD, University of Cambridge.
- Trimble Navigation Ltd. 2004. *Why post process GPS Data?* Mapping and GIS White Paper. Trimble Navigation Ltd., Westminster, USA. Pp. 14.
- Vallance J.W. 2000. *Lahars*. In: Sigurdsson H, Houghton B, McNutt SR, Rymer H, Stix J (eds). *Encyclopedia of Volcanoes*. Academic Press: New York. Pp. 601-616.
- Van Gorp, S., 2002, *Systèmes d'Information Géographique et Risques volcaniques: Approche méthodologique et application au cas du volcan Misti et de la zone urbanisée d'Arequipa (sud du Pérou)*, TER, Université Blaise-Pascal, Clermont-Ferrand.
- Van Westen, C.J. Terlien, M.J.T. 1996. *An approach towards deterministic landslide hazard analysis in GIS. A case study from Manizales (Colombia)*. *Earth Surface Processes and Landforms* 21: 853-868.
- Van Westen, C.J., Castellanos, E., Kuriakose, S.K. 2008. *Spatial data for landslide susceptibility, hazard, and vulnerability assessment: an overview*. *Engineering Geology* 102: 112-131.
- Van Westen, C.J., Montoya, L., Boerboom, L. 2003. *Multi-hazard risk assessment using GIS in urban areas: a case study for the city of Turrialba, Costa Rica*. *The Regional Workshop on Best Practices in Disaster Mitigation*. p. 53-72.
- Vargas Franco, R.D., Thouret, J-C., Delaite, G., van Westen, C., Sheridan, M.F., Siebe, C., Mariño, J., Souriot, T., Stinton, A. 2010a. *Mapping and assessing volcanic and flood hazards and risks, with emphasis on lahars, in Arequipa, Peru*: 265-280. In: Groppelli, G, Viereck-Goette, L (eds.) *Stratigraphy and Geology of Volcanic Areas*. Geological Society of America Special Papers 464. pp. 293.

- Vargas Franco, R.D., Thouret, J-C., Martelli, K.M. 2010b. *Physical Vulnerability and Quantitative Risk Assessment of Housing and Infrastructure from The Potential Impacts of Volcanic Mass Flows in Arequipa, Peru*. CoV6/2.1/P/15. Cities on Volcanoes 6 Conference Abstract Volume. Cities on Volcanoes 6 Conference, Tenerife, Spain. May 31 - June 4, 2010.
- Voight, B. 1990. *The 1985 Nevado del Ruiz volcano catastrophe: anatomy and retrospection*. Journal of Volcanology and Geothermal Research 44: 349-386.
- Wechsler, S.P. 2007. *Uncertainties associated with digital elevation models for hydrologic applications: a review*. Hydrologic Earth System Science 11: 1481-1500.
- Westgate, K. and P. O'Keefe. 1976. *Natural Disasters: An Intermediate Text*. Bradford Disaster Research Unit, University of Bradford, Bradford, U.K.,
- Widiwijayanti, C., Voight, B., Hidayat, D., Patra, A., Pitman, E. 2004. *Validation of TITAN2D flow model code for pyroclastic flows and debris avalanches at Soufriere Hills Volcano, Monseratt, BWI*. American Geophysical Union, Fall Meeting 2004, abstract #V43B-1428.
- Widiwijayanti, C., Hidayat, D., Voight, B., Patra, A., Pitman, E.B. 2007. *Modelling dome-collapse pyroclastic flows for crisis assessments on Montserrat with TITAN2D*. Cities on Volcanoes 5 Conference, Shimabara, Japon, 11-P-34.
- Widiwijayanti, C., Voight, B., Hidayat, D., Patra, A., Pitman, E. 2010. *Titan2D simulations of dome-collapse pyroclastic flows for crisis assessments on Montserrat*. American Geophysical Union, Fall Meeting 2010, abstract #V13A-2342.
- Williams, R. 2006. *Modeling lahars using Titan2D for the southern drainage of Volcan Cotopaxi: impact on the city of Latacunga*. Master of Science thesis, Department of Geology, State University of New York at Buffalo. Pp. 75.
- Williams, R., Stinton, A.J., Sheridan, M.F. 2008. *Evaluation of the Titan2D two-phase flow model using an actual event: Case study of the 2005 Vazcún Valley Lahar*. Journal of Volcanology and Geothermal Research, 177: 760-766.
- Wilson, C.J.N., and Stirling, M.W. 2002. *Towards a probabilistic volcano hazard analysis model for New Zealand*. In: Johnston, D.M., Tilyard, D. (eds) Proc 5th Natural Hazards Management Conf. Te Papa, Wellington, 14-15 August 2002. Institute of Geological and Nuclear Sciences, Lower Hutt, New Zealand, Pp 73-81
- Wise, S.M. 2007. *Effect of differing DEM creation methods on the results from a hydrological model*. Computers and Geosciences 33: 1351-1365.
- Wisner, B., Blaikie, P., Cannon, T., Davis, I. 2004. *At risk: Natural hazards, people's vulnerability and disasters*. London: Routledge. (2nd ed.). Pp. 471.
- Witham, C.S. 2005. *Volcanic disasters and incidents: A new database*. Journal of Volcanology and Geothermal Research 148: 191-233.
- Wood, J.D., Fisher, P.F. 1993. *Assessing interpolation accuracy in elevation models*. IEEE Computer Graphics and Applications 13: 48-56.
- Wood, N.J., Soulard, C.E. 2009. *Community exposure to lahar hazards from Mount Rainier, Washington*. U.S. Geological Survey Scientific Investigations Report 2009-5211. Pp.26.

- Yilmaz, H. M. 2007. *The effect of interpolation methods in surface definition: an experimental study*. Earth Surface Processes and Landforms 32: 1346-1361.
- Young, C. 2009. *Personal communication with Cody Young, Bridge Engineer, New Zealand Railways Corporation (NZRC) - KiwiRail, Wellington, New Zealand*. Email correspondence 1 October 2009.
- Zamacolya, J. and Auregui, J.D. 1958. *Apuntes para la historia de Arequipa*. Primer festival del libro arequipeño. -Edición (1958), 15 pp., Arequipa.
- Zanchetta, G., Sulpizio, R., Pareschi, M.T., Leoni, F.M., Santacroce, R. 2004. *Characteristics of May 5 – 6, 1998 volcanoclastic debris-flows in the Sarno area of Campania, Southern Italy: relationships to structural damage and hazard zonation*. Journal of Volcanology and Geothermal Research 133: 377 – 393.
- Zavala, C., Honma, C., Gibu, P., Gallardo, J., Huaco, G. 2004. *Full scale on line test on two story masonry building using handmade bricks*. 13th World Conference on Earthquake Engineering Vancouver, B.C., Canada. Paper No. 2885 - August 1-6, 2004.
- Zuccaro, G., Cacace, F., Spence, R., Baxter, P. 2008. *Impact of explosive eruption scenarios at Vesuvius*. Journal of Volcanological and Geothermal Research, 178: 416-453.

APPENDICES

APPENDIX A: REPORTED FLOODING IN AREQUIPA

APPENDIX B: HOUSING TYPES IN AREQUIPA

APPENDIX C: VULNERABILITY OF BUILDINGS, LAND USE,
AND INFRASTRUCTURE IN AREQUIPA

Appendix A

Reported flooding in Arequipa

Year	Date	Area	Type of event	Damage	Rainfall	Duration	River flow rate	Size
1907	8-Feb	Sabandia	Qda. overflows from heavy rainfall onto street	- Flooded house - No water supply	14.2			Small
	4-Mar	San Lazaro	Qda. overflows from heavy rainfall onto street					
1908	19-Jan	Tiabaya	Rio Chili increases in volume and overflows	- Crops				Small
		Paucarpata Miraflores	The joining of the two Qdas caused damage	- Animals				
1909	Feb	Rio Chili	Chili river flow increases, threatens neighbourhoods Slips	- Crops - 1 person killed	Rains in highlands			Med
1914	4-Feb	Cayma	Cayma floods	- 2 residential areas collapsed	1.33			Small
1915	20-Feb	Rio Chili	Flood urban areas	- Machinery - No power - Fields/crops flooded	7.2			Large
		Chullo and Beaterio	Qda. enter Rio Chili with great force, overflowing and flooding fields	- 40 houses destroyed - Roads destroyed - Dead animals				
		Sabandia	River flow increased	- 1 person killed				
1916	12-Jan	Arequipa	Strong rainfall flooded the city of Arequipa		10.1			Med
	16-Jan	Chullo, San Lazaro, Paucarpata and others	Continuous rain, entering watercourses		4.2			
	10-Feb	Arequipa	Heavy rainfall affecting city		10.5			
	28-Feb	Miraflores and San Lazaro	Flooding in urban area, enter watercourses	- Houses damaged - Destroy water pipes - Damage to Pte. Tingo - Agriculture - Town without water	3			
	23-Mar		Continuous rain, entering watercourses	- Agriculture	6			
1917	22-Jan	San Lazaro Rio Chili	Increase of Rio Chili from San Lazaro		13.2			Small
	22-Mar	Cayma	Torrential rain causing flooding	- Homes	11.8			
1919	11-Mar	Rio Chili Pte Grau	Rio Chili increases in volume and overflows	- Crops - Flooding				Small
1920	16-Jan	Rio Chili	Rio Chili increases in volume and overflows	- Crops - Pte. Tingo damaged				Large
	28-Jan	San Lazaro	Flooding in Qda. San Lazaro					
	7-Feb	Arequipa	Flooding and landslides	- Houses damaged - 2 dead - 42 injured				

Appendix A

Year	Date	Area	Type of event	Damage	Rainfall	Duration	River flow rate	Size
	9 to 10-Feb	Cayma and Yanahuara	Flooding in urban areas	- Collapsing walls and ceiling - 5 injured -				
		San Lazaro and Mariano Melgar	Heavy rainfall	- Roofs collapsing				
1925	2-Feb	Rio Chili, Uchumayo	Rio Chili overflow causing flooding in Uchumayo	- Crops				Med
	14-Mar	Miraflores	Flooding	- Collapsed homes Streets like rivers				
		Sabandia	Flooding and landslides at Pte. Sabandia	- Bridge destroyed				
1926	4 and 15 mar	San Lazaro	Flooding from joining of Quebradas, trees and rocks swept up.			1.5 hours		Small
	17-Mar	Sabandia Paucarpata	Heavy rains flood urban areas	- Farmland - Tramway buried				
1927	3-Feb		Flooding of urban areas, streets like rivers			5 hours		Small
	5-Feb	Socabaya	Heavy rains causing floods	- Walls and roofs				
	24-Feb	Arequipa, Tacna and Arica	Urban area flooded	- Houses flooded				
	March	Rio Chili	Increased river flow					
1929	11-Mar	Rio Chili Sachaca Tiabaya	Increased river flow	- Embankments of Pte. Tingo destroyed - Isolated villages - Tram damaged				Med
	13-Mar	Bolognesi	Urban areas flooded around Pte. Bolognesi. Rio Chili flow increased			3.15 hours		
1930	9 to 27 Jan	Rio Chili, Tiabaya and Tingo	River flow increased with high rainfall. Large stones moved, overflowing of river and flooding.	- Collapse of mud walls - Damage from lightening				Small
1931	March		Heavy rains inundate urban areas					Small
	19-Dec		Heavy rains inundate urban areas		10.1			
1932	29-Jan	City Chiguata	Flooding in city area		10			Med
	10-Feb		Flooding	- Lead water pipes				
	22-Feb	Arequipa, Bolognesi Miraflores, Calle Saenz Peña	Flooding of urban areas	- Homes, fallen walls of houses - Damage to left side of Ptes Bolognesi and Grau	16	2 hours		
	24-Feb			- Homes	16-18			
	3-Mar		Flooding of urban areas	- Crops - Houses - 40 families affected	7			
1933	8-Feb	Rio Chili San Lazaro	Flooding in the city Quebrada increases Rio Chili river flow	- Puente Tiabaya affected	8			Small
	12-Feb	Arequipa	Flooding in urban areas		13			

Appendix A

Year	Date	Area	Type of event	Damage	Rainfall	Duration	River flow rate	Size
1935	17 and 19 Feb	Arequipa, Stadium, Melgar, San de Dois	Flooding in urban areas and streets	- Stadium flooded Tram service interrupted				Small
	29-Mar	Yarabamba	Torrential rain	- Crops - Homes - Homes - School - Crops				
1937	29-Jan	Arequipa and Miraflores	Torrential rain floods urban areas	- Homes		Started at 4pm		Small
	12-Feb	Tiabaya Sachaca and Socabaya	Heavy rains flood urban areas and damage roads linking Tiabaya and Socabaya	- Damage to roads				
1938	11-Feb	Tingo	Heavy rain	- Pte. Tingo embankment at risk				Med
	2-Mar	Paucarpata	Torrential rain floods urban areas, landslides	- Homes - Crops - 1 killed - Road destroyed	7.5			
	8 and 9 Mar	Arequipa Yura	Continuous rain flooding city	- Damage to road	15.7			
1939	18-Jan	San Camilo Market, Pierola and Peru Streets, Pte. Bolognesi	Flooding of urban areas	- Tramlines				Med
	19-Jan	Arequipa, Yarabamba, Quequena, Yanahuara, Paucarpata	Heavy rain, thunderstorms and hail					
	28-Jan	Chullo	Rain and flood damage	- Houses - Crops - Traffic halted				
	10-Feb	Cayma, San Lazaro, Domingo, Tacna, Arica, Miraflores, Paucarpata	Heavy rains causing floods, streets became rivers					
	11-Feb	Sabandia, Rio Chili and Tingo	Torrential rains causing flooding and Rio Chili flooded near Tingo	- Destruction of land near Pte. Tingo Ptes Tingo and Bolognesi damaged				
	March	Beaterio street	Flooding in street					
1941	21-Feb	San Lazaro	Increased rainfall causing flooding	- Crumbling walls				Small
1942	7-Feb	San Lazaro	Flooding of urban areas	- Destroyed bridge				Med
	28-Feb	San Lazaro, Rio Chili and Uchumayo	Heavy rains flood urban areas, increase of Rio Chili river flow, overflows in Uchumayo. Stones moved in flood.	- Walls Municipal theatre - Bridges damaged				
1943	27-Jan	San Lazaro and Rio Chili	Thunderstorm event causes increased flow in Qda. San Lazaro, increases Rio Chili flow. High velocity flow.	- Houses - Animals - Crops - Tram				Large
	8-Feb	San Lazaro and Paucarpata	Flooding in urban areas and roads impassable	- Roads - Houses				
	12-Feb	Carmen Alto, Miraflores and Cercado	Flooding and damage from built-up alluvium					

Appendix A

Year	Date	Area	Type of event	Damage	Rainfall	Duration	River flow rate	Size
	17-Feb	Rio Chili, Miraflores, Cercado, and Tingo San Lazaro and Tingo	Heavy rain causes flooding, Rio Chili increases to a level never seen before flooding of neighbourhoods Qda San Lazaro overflows Jerusalem Street and Pte. Grau., flooding nearby neighbourhoods	- Homes - Crops - Crops - Houses - Canal - Affects Chilina power plant - Potable water supply pipe from Yumina				
1944	12-Feb	Chullo, Cayma, Carmen and Churinsaya	Rain causing flooding	- Houses - Crops - Irrigation ditches Chilpinilla treatment plant				Small
1946	18-Feb	Chullo, Charcani, Tahuaycani, Antiquilla Rio Chili, Arequipa Sachaca Huayco Arequipa, Miraflores, Ptes Grau and Bolognesi	Heavy rains causing flooding Rio Chili increases in volume and overflows, water 2m in neighbouring streets. Rio Chili floods urban areas	- Crops - Houses - Houses - Crops - Textile plant - Homes - Homes leaking Goyeneche Hospital flooded - Protective walls Crops and farms Furniture and household goods Vehicles - Animals		4.5 hours		Large
		Puno, Sepulvera, Cuartel Salaverry, San Geronimo, Maria Isabel, Palomar, Pampilla, Manzanitos and Quiroz Lambramani, Dolores, Apacheta, La Pampilla and Chilpinilla River Sabandia, Charocato and Chiguata San Lazaro International club	Flooding, water height 50 cm in flooded areas. Bank flooded	- Vehicles - 1 killed - Railway - Tram - Houses - Tram - Crops - Houses - 15 houses - Vehicle - Damage to Grounds, tennis court and buildings				
1949	18-Feb 24-Mar	Rio Chili, Pte. Bolognesi, Arancota, Tiabaya San Augustin, Callejon el Solar, Pte. Grau, Maria Isabel, IV Centenario and Manzanitos	Rio Chili river overflows around Pte. Bolognesi and reaches height of 2 m. Flooding of urban areas, streets like rivers	- Crops - Animals - Tram service interrupted - Homes - Collapsed walls and roofs - Tram service interrupted		2 hours		Large

Appendix A

Year	Date	Area	Type of event	Damage	Rainfall	Duration	River flow rate	Size
	25-Mar	Pampas de Polanco, Selva Alegre and Miraflores	Streams flooded areas	- Tourist hotel - Canals and ditches - Park - Water - Sewer - Houses - Public lighting				
		Miraflores, Avenues Pro hogar, Goyeneche, Progreso, Miguel, Grau, Misti, Puno, Paz Soldan, near Santa Catalina cathedrals	Flooding in urban areas, streets resemble rivers	- Houses - Santa Catalina Cathedral affected - Telephone service - Roads				
		Lambrani and Avenue Porongoche	Heavy rain causes flooding	- Crops				
	28-Mar	Characato, Sabandia and Socabaya	Flooding					
1952	11-Jan	Arequipa, Chilina	Flooding	- Chilina central				Small
	16-Jan	Pte Bolivar	Flooding	- Tram service interrupted - Pte. Bolivar affected				
	22-Jan	Rio Chili and Uchumayo	Heavy rain leads to flooding, Rio Chili increases and overflows	- Crops				
1953	2 and 6 Feb	Uchumayo						Small
	3-Mar	Chullo and Zamacola		- Sewage		2 hours		
1955	14-Jan	Lambramani, Dolores, Poprongoche, Sabandia and Paucarpata	Heavy rains cause flooding	- Irrigation canals - Roads				Large
		Tingo and Tiabaya	Rains increase river flow	- Crops - Bridge - Road				
	20-Jan	Cayma, Chullo and Yanahuara	Flooding					
		Rio Chili, Tingo, Manzanito and Pte. Bolognesi	Heavy rain causing flooding	- Houses				
	19-Feb	Arequipa	Heavy rain causing flooding of urban areas					
	15-Mar	Rio Chili, Ptes Bolognesi, Grau, Tiabaya and Tingo, Arancota, and Tingo.	Heavy rain in highlands increases Rio Chili passing under Ptes Grau and Bolognesi at some height causing flooding and danger to Pte. Tingo.	- Crops - Flood defences - Irrigation - Track - Embankments of Pte. Tiabaya - Houses - 80 homeless - Pte. Tingo				
1957	01 and 3 March	Cercado, Miraflores and Mariana Melgar	Heavy rain leads to flooding, floods to ceiling height.	- Walls, ceiling and foundation damage of houses				Small
1961	14, 16, 18 and 22 Jan	Rio Chili	Continuous rainfall leads to flooding of urban areas.					Large
	25-Jan	Rio Chili, Cercado, Vallecito, Maria Isabel, Yanahuara, Miraflores, Mariano Melgar and Paucarpata	Continuous rain, streets become rivers and inundate urban areas. Rio Chili river flow increases.	- Affecting tram service - 112-205 houses		5 hours	80	

Appendix A

Year	Date	Area	Type of event	Damage	Rainfall	Duration	River flow rate	Size
	26-Jan	Rio Chili, Socabaya, Sabandia, Characato, Yanahuara, Paucarpata, Tingo, Cercado and Pampilla	Flooding	- 2 people killed			27.38 for 37 sec?	
	28 and 31 Jan	Miraflores, Alto Selava Alegre, San Lazaro, Uchumayo, Moyebaya and Tiabaya	Heavy rain leads to flooding	- Affects Puente Izcuchaca - Collapsed homes - Affecting tram service.				
	25 to 26 Feb 14-Mar		Heavy rains leading to flooding in urban areas	- Cracked roads - 2 houses				
1962	18-Feb		Increased rainfall intensity Rio Chili flow increases	- Pte. Tingo - Flood defences				Small
1963	13-Jan	Rio Chili	Heavy rain increases Rio Chili flow				33.65	Small
	15-Jan 21-Feb	San Lazaro Misti, Manuel Prado and 13 Enero	Persistent rain flooded urban areas				100	
	17-Mar	Yumina, Sabandia and Characato	Heavy rain and hail flooding areas			5 hours		
1968	11-Jan	Rio Chili	Heavy rain increases Rio Chili flow	- Yura cement plant				Small
	14-Jan 16-Jan	Rio Socabaya Cercado, Miraflores, Mariana Melgar, Uchumayo and Paucarpata	Inundation Rain flooded urban areas	- Animals - Crops				
	7 to 8 Feb 2-Mar	Rio Chili Characato, Sabandia, and Mollebaya	Increased Rio Chili flow Flooding	- Roads - Crops				
1969	21-Jan	Rio Chili	Flooding	- Crops - Animals - Roads				Small
1970	10 to 11 Jan	Rio Chili	Rain overflow Rio Chili	- Crops				Med
	3-Feb 26-Feb	Rio Chili Cercado, Miraflores and Mariana Melgar	Increasing Rio Chili flow Rain flooded urban areas	- 26 homes - Crops			26.5 50	
	27-Feb	Chullo, Cayma, Yanahuara and Umacollo	Flooding					
1971	27-Feb 2-Mar	Arequipa and Yarabamba	Rain flooded urban areas	- Roads	1.4		62	Small
1972	5-Jan	Cercado, Miraflores, Mariana Melgar, Cerro Colorado, Socabaya, Miguel Grau, 15 de Agosto, Sabandia and Paucarpata	Rain flooded urban areas	- Homes constructed rock and brick Crops		4.5 hours		Large
	8-Jan	Cercado, Miraflores, Mariana Melgar, Cayma and Paucarpata	Rain flooded urban areas	- Road				
	15-Jan	San Lazaro, Las Palmeras		- 47 houses - Water main - Lost belongings		3 hours		

Appendix A

Year	Date	Area	Type of event	Damage	Rainfall	Duration	River flow rate	Size
	16-Jan	Alto San Martin, Santo Domingo, Mariano Bustamante, Miraflores, Avenue Venezuela, and Manzanitos	Flooding with mud	- 16 houses - Drinking water pipe				
	19-Jan	Avenue Mcal Castilla, Lambramani, Porongoche, Dolores, Pampilla, and Paul VI	Rain flooded urban areas	- 12 homes - Roads - Cemetery - Vehicles				
	25-Jan	Chullo, Pte. Urb. Primavera, Umnacollo and Av. Victor Andres Belaunde	Flood	- 25 houses				
	4-Feb	J Hunter Socabaya, Selva Alegre, and P.J. Apurimac	Flood	- 26 houses				
	11-Feb	Rio Socabaya	Flooded urban areas	- Crops				
	12-Feb	Cercado, Mariano Melgar, Pampilla and Socabaya	Flooded urban areas	- 8 brick factories				
	13-Feb	P.J. Progresista and San Juan Mostajo	Flooded urban areas					
	14-Feb	Arequipa and avenue Jesus	Flooded urban areas	- 3 killed - Pedestrian bridge collapsed				
	15-Feb	Santa Rosa, Pte. Av. Jesus and Av. Mariscal Castilla	Flooded urban areas					
	16-Feb	Rio Chili, Tingo, Tiabaya Huayco and Uchumayo		- Crops				
	17-Feb	Arequipa, Goyeneche, San Juan de Dois, Independencia, Maria Isabel and Av. Alcides Carrion	Flood urban areas and streets became rivers	- Vehicle - 3 people missing				
	18-Feb	Av. Alcides Carrion, Mariano Melga and Paucarpata	Flooded urban areas	- Roads blocked General hospital Isolated suburbs				
	19-Feb	Cercado, Yanahuara, Rio Chili and Pte. Bolognesi	Flooded urban areas and Rio Chili level increases	- Crops and farms				
	20-Feb	Urban areas	Flooded urban areas	- Roads - People missing				
	21-Feb	Rio Chili	Rio Chili level increases	- 12 homes				
1973	10-Jan	Paul VI, Arequipa, Mariano Melgar and Alto Alegre	Flooded urban areas, streets turned into streams	- Animals - 6 families affected - 10 people injured				Large
	11 to 12 Jan	San Martin, Miraflores, Alcides Carrion, Pampilla and Socabaya	Rains flooded Arequipa	- 12 houses - Textile factory - 15 families affected			200	
		Rio Chili San Lazaro,	Rain increases flow and overwhelms left side. Water exceeded 2.30m above retaining wall of 3.50m Flow increase, influence Rio Chili	- Hydroelectric plant (landslide Charcani IV), no electricity Telephone service Transportation difficulty				

Appendix A

Year	Date	Area	Type of event	Damage	Rainfall	Duration	River flow rate	Size
	13-Jan	Paucarpata, Mariano Melgar, 15 Agosto, Jorge Chavez, Miguel Grau, Santa Rosa, Pampilla, Av. Alcides Carrion, San Lazaro, Miraflores etc.	Torrential rain causing flooding	- Crops - 70 families affected - 30 Houses - Roads - Charcani, no electricity		4.5 hours		
	6-Feb	Rio Chili	Increasing Rio Chili flow				18	
	8-Feb	Arequipa, Mcal Castilla, Goyeneche, Independencia, Pampilla, Alcides Carrion, Maria Isabel etc.	Torrential rain causing flooding	- Roads				
	10-Feb	Rio Chili and San Lazaro	Rio Chili level increases, San Lazaro adding to flow rate.	- Pte Bolognesi foundations affected			180	
	11 to 12 Feb	Rio Chili, Congata and Huayco	Increasing Rio Chili flow	- Crops - Houses - Roads				
1974	14-Jan	Arequipa, Rio Chili San Camilo	Flooding	- 1 house			46.42	Med
	21-Jan	Santa Catalina and IV Centenario	Urban area flooded	- Santa Catalina				
	30-Jan	Paucarpata, Mariano Melgar, Miraflores, Goyenenche, La paz, Independencia and Maria Isabel	Heavy rains flood urban areas		Intensity: 14.10			
	2-Feb	Mariano Melgar, Miraflores, Paucarpata, Progresiva, Miguel, Arequipa, 16 de Enero, 15 de Agosto, Alto San Martin, Misti, Santo Domingo etc.	Increasing Rio Chili flow	- Houses - Vehicles				
	3-Feb		Torrential rain causing flooding	- Houses				
1975	1-Jan		Heavy rains flood urban areas, sediment and debris flow	- Houses - Crop	7.2			Med
	30-Jan	Arequipa	Heavy rains flood urban areas					
	4-Feb		Heavy rains flood urban areas		11.4			
	20-Feb	Rio Chili, Cerro Verde, and Congata	Increasing Rio Chili flow	- Crops - Isolated suburbs				
	4-Mar	Mariano Melgar, Miraflores, A. Selva Alegre, Apurimac, Miguel Grau, Progresiva, 15 Agosto etc.	Flooding					
	8-Mar	Arequipa, San Lazaro	Flooding urban areas	- 13 families affected Destroyed dams				
1976	22-Jan	Paucarpata, Salaverry, Mariscal Castilla, Mariano Melgar	2m of water in the streets	- 20 Families affected	24			Med

Appendix A

Year	Date	Area	Type of event	Damage	Rainfall	Duration	River flow rate	Size
	24-Jan	Arequipa, Paucarpata, Pj. Progresista, 15 de Agosto, Av. Jesus, Miraflores, Melgar, Av. Castilla, Alcides Carrion etc.	Heavy rains flood urban areas Scour of bridge Rio Chili overflowed	- Pathways - Roads blocked - Danger collapse - Pte. Bolognesi - Crops	25	3 hours rainfall, 7 mm	24	
	25 to 26 Jan	Miguel Grau, Progresiva, 15 Agosto, Santa Rosa, Jorge Chavez, Israel etc.	Flooding	- Houses - Villages isolated				
	28-Jan	Rio Socabaya	Flooding	- Isolated Villages - Pte. Sabandia - Utility pipes - Drainage - Water - Roads - Crops				
	3-Feb	Rio Chili, Uchumayo and Tiabaya	Increasing Rio Chili flow and overflowed					
	24-Feb	Lambrani, Avenue Venezuela, Obando etc.	Flooding, 1.5m of water entering streets/homes	- 4 homes - Homes damaged	24			
1977	17-Feb				52.9			Small
	27-Feb	Cayma, Chullo, Yanahuara and Sachaca	Flooding	- Irrigation ditches - Crops - Intake destroyed	7.2	3 hours		
	12-Mar	Miraflores, San Lazaro and Arequipa	Flooding		1.7	3 hours		
	13-Mar	Paucarpata, Pampilla, and Tingo	Heavy rains flood urban areas	- Crops - Houses - Interrupt traffic				
	14-Mar	Mariano Melgar, Miraflores, Av. Venezuela, Palomar and Manzanita	Flooding		5.3			
1979	26-Mar	Maria Isabel	Heavy rains flooded urban areas, streets like rivers	- Homes - Public lighting	5.2	4 hours		Small
1980	22-Feb		Heavy rain		14.4			Small
	13-Mar		Heavy rain		10			
	16-Mar		Heavy rains flood urban areas		14.4			
1981	19-Feb	Rio Chili, Charcani	Stone and mud compound Charcani IV	- Charcani IV - Power outages	8.5			Small
	25 and 26 Feb	Rio Chili	High Rio Chili flow threaten land		25th: 49.6, 26th: 8.5			
1984	10-Feb	Rio Chili	Heavy rain, flow increases for Rio Chili		13.2			Med
	13, 16 and 18 Feb	Rio Chili, Tingo and Uchumayo	Rio Chili overflows	- Farmland			70	
	19-Feb	Rio Chili, Ptes Grau, San Martin, Tingo and Tiabaya	Rio Chili affects pillars of Pte. Grau, and affects Ptes San Martin, Tingo, and Tiabaya - river height of San Martin	- Pillars Pte. Grau - Retaining walls of Pte. Grau damaged - Affects Ptes San Martin, Tingo, and Tiabaya - Textile factory threatened	44			
	20-Feb	Rio Chili, Pte Grau, Rio Socabaya	Continuous river flow increases	- Pte. Grau affected - 27 Kiosks				

Appendix A

Year	Date	Area	Type of event	Damage	Rainfall	Duration	River flow rate	Size
1985	22-Feb	Arequipa, Av. Mcal Castilla, Jesus, Goyeneche, Independencia	Heavy rains flooded urban areas, streets like rivers	- Roads - Homes				Small
	23-Feb	13 de Enero, J. Hunter	Heavy rains flood urban areas		6.6		80	
	24-Feb		Heavy rains flooded urban areas, streets like rivers	- Charcani electric				
	7-Mar		Heavy rains flood urban areas	- Vehicles - Roads	3.7			
1986	23-Jan	Rio Chili, Arancota, Congata, Tiabaya, Paucarpata, Mariano Melgar	Chili river flow increases	- Crops - Zamacola canal	28.8			200
	5-Feb	Arequipa, Socabaya, Paucarpata, Mariano Melgar, Miraflores, Cercado Arequipa, Barrio Obrero)	Heavy rains flood urban areas, water reached 1.0 m	- 12 houses - 50 houses flooded	37.85			
1987	22-Jan	Chullo, San Lazaro, Arequipa	Flooded urban areas					Med
	23-Jan	Socabaya	Rio Socabaya overflowed	- Isolated suburbs				
	24-Jan	Paucarpata, Socabaya, 15 Agosto, Dolores, Santa Clara, Los Olivos, Av Jesus, Alcides Carrion		- Water - Sewage - Damage to Pte. Jesus				
	8-Feb	Paucarpata, Arequipa, California	Heavy rain causes flooding	- Homes				
	22-Feb	San Lazaro, pte. Bolognesi, Mcal Jesus, Melgar and Santa Rosa	Rio Chili river increases, streets like rivers	- Houses - Crops and fields		2 hours		
1989	3 to 4 Feb	Arequipa, Av. Jesus, Mcal Castilla, Lambramani, Alcides Carrion, San Lazaro, Av. Marina	Heavy rains flooded urban areas, streets like rivers, dam with construction of Pte. Bajo Grau, Flooding Av. Marina	- Houses - Water - Drainage	37.85	4 hours		Large
	6 to 7 Feb	Carrion Avenue, Arequipa, Rio Chili	Flooding in urban areas	- Storm network Sewer - Water - Roads	113.5	2 hours (intensity 41 mm?)		
	8 to 9 Feb	Rio Chili, Av Marina, Paucarpata, Uchumayo, Tingo, Socabaya, etc.	Flooding due to Pte. Bajo Grau, 2-3 m floods, rocks and mud	- 330 families affected - Poles - Vehicles - Houses - Roads - Trees - Waterpipes Drainage - Crops - Foundation damage to Pte. Bolognesi - 20 m retaining walls - 5 killed - Electricity				
1994	18 to 19 Jan	Arequipa	Flooding and water flowing in streets	- Sewage				Large

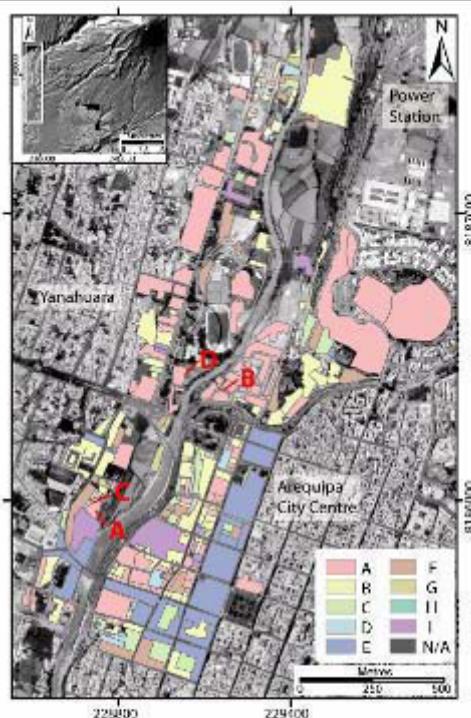
Appendix A

Year	Date	Area	Type of event	Damage	Rainfall	Duration	River flow rate	Size
	17-Feb	Arequipa, Miraflores, Mariano Melgar, Huayco, Paucarpata	Flooding, landslides	- Crops			30	
	21 to 24 Feb	Av Marina, Los Alamos, Los Pinos, Tiabaya, Pte. Grau, San Martin and Tingo	Flood caused damage	- Houses - Farmland - Ptes Tingo, Bolognesi, Grau, St Martin weakened Crops - Isolated suburbs Roads blocked Retaining walls near Pte. Grau - 4 deaths	34.33	8 hours	200	
1995	26 to 27 Jan	Arequipa, Independencia, La Marina, Goyoneche, Jorge Chavez, Venezuela, La Paz, Mariscal Castilla, Alcides, Carrion etc.	Flooding	- Electricity - Water pipe - Sewer	73.5			Med
	15 to 19 Mar	Pampas de Polcano, Chilina, Miraflores, Socobaya, Yarabamba, Arica, Miguel Grau, arequipa etc.	Flooding, erosion in streets, Egasa flooded	- Vehicles buried - 8 houses flooded - 12 Houses Electricity - Homes flooded	45	3 hours		
1996	22-Jan	Paucarpata, Mariano Melgar, Alto Selva Alegre, Miraflores, San Lazaro, Maria Isabel, Jerusalem,	Flooding of urban areas, streets like rivers	- Sewer	19			Small
	28-Feb		Heavy rain causing flooding			1.5 hrs	54	
1997	16-Feb	Pampas de Polcano, Alto Selva Alegre, Tiabaya, Uchumayo		- Crops and farms			32	Large
	26-Feb	Maria Isabel, Pampas de Polcano, Umacollo, Obando, Rio Chili etc.	Flooding of 30 cm	- Telephone service Electricity - Flooded houses Sewers - Isolated suburbs - 5 killed		3 hours	130	
1999	14 Mar	Arequipa, Paucarpata, Mariano Melgar, Alto Selva Alegre, Miraflores, San Lazaro	Flooding of urban areas	- Homes - Foundations and bridge abutments undermined - Bridges - Water pipelines -	29.97			Large
2001	19 Mar	Arequipa, Paucarpata, Mariano Melgar, Miraflores, San Lazaro	Flooding of urban areas	- Homes - Roads - Bridges - Vehicles	34.10			Large
2011	21 Feb	Arequipa, Uchumayo, Mariano Melgar, Huarangal, Alto Selva Alegre, Miraflores, San Lazaro	Flooding of urban areas and farmland	- Homes - Crops - Farmland - Roads - City without water			236	Large

Appendix B

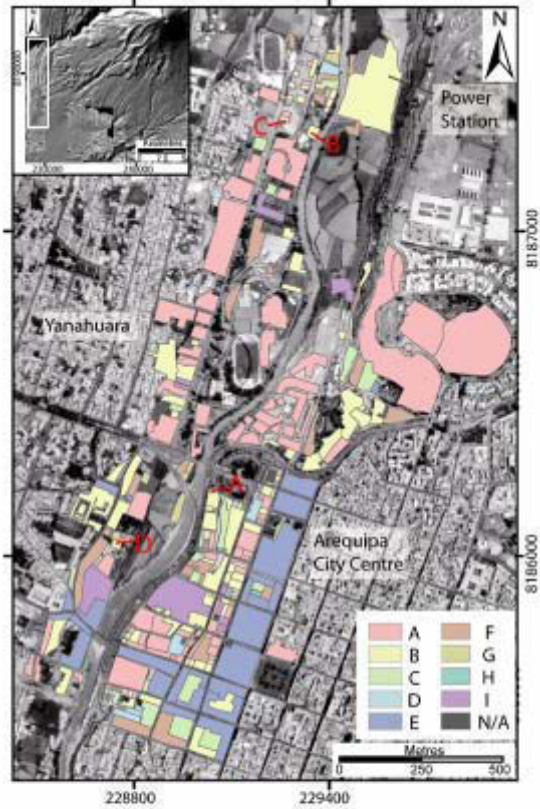
House Type A

- Unconfined masonry panels (unreinforced perforated clay bricks or concrete blocks).
- Cast-in-situ reinforced concrete frames (horizontal and vertical).
- Roof is mostly flat or pitched, reinforced concrete slabs.
- Large glass windows throughout, often aluminium framing secured with steel bars.
- Door generally solid and wooden consisting of steel security screen/bars.
- Building well finished. Painted, fenced, security, well-kept.



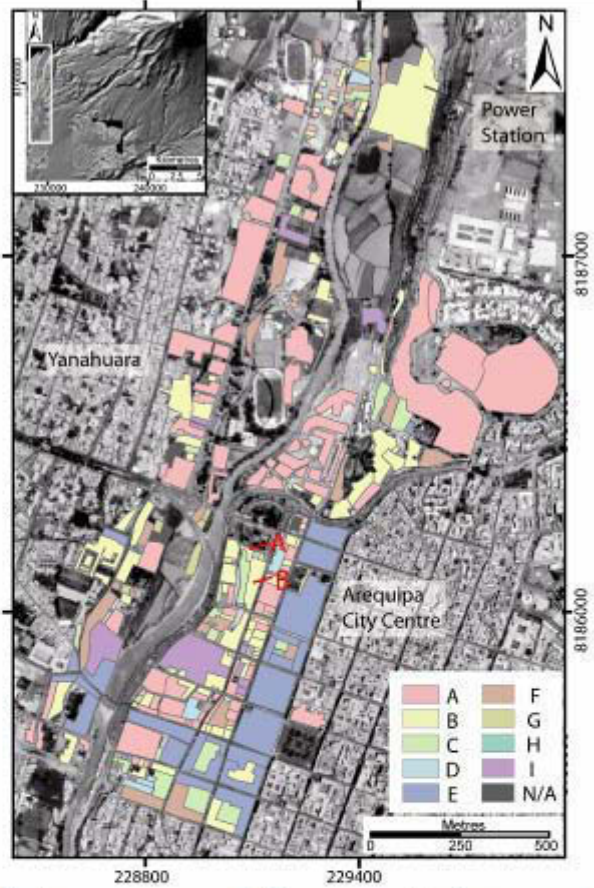
House Type B

- Same structural components as Type A, however structure not complete (even though occupied).
- Often the ground floor is completed.
- Windows, doors and roofs the same as Type A buildings.
- The evolution of the structure is positive.
- House well finished (less so that type A however) with positive evolution.



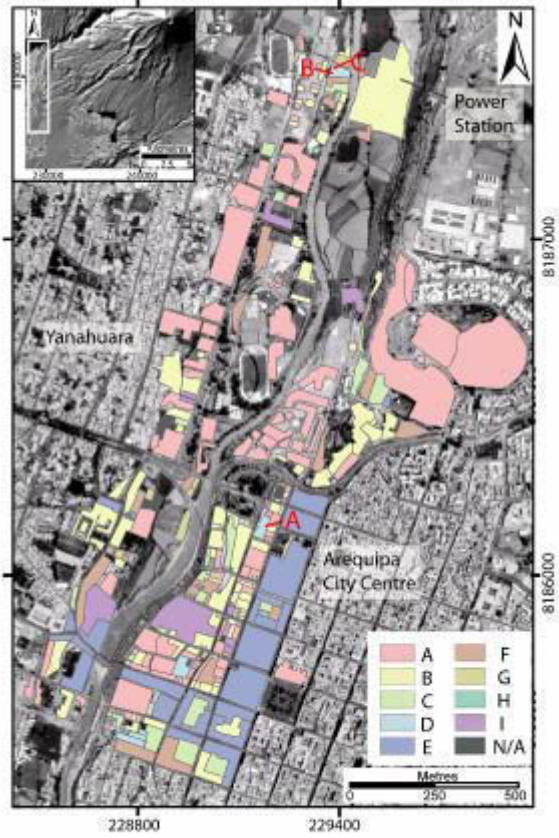
House Type C

- Same structural components as Type A , however vertical extension unfinished, and some material is unstable.
- Windows, doors and roofs often the same as Type A buildings. Roofs maybe be constructed with corrugated iron.
- Overall long-term evolution will be positive, however environment and building not well kept.



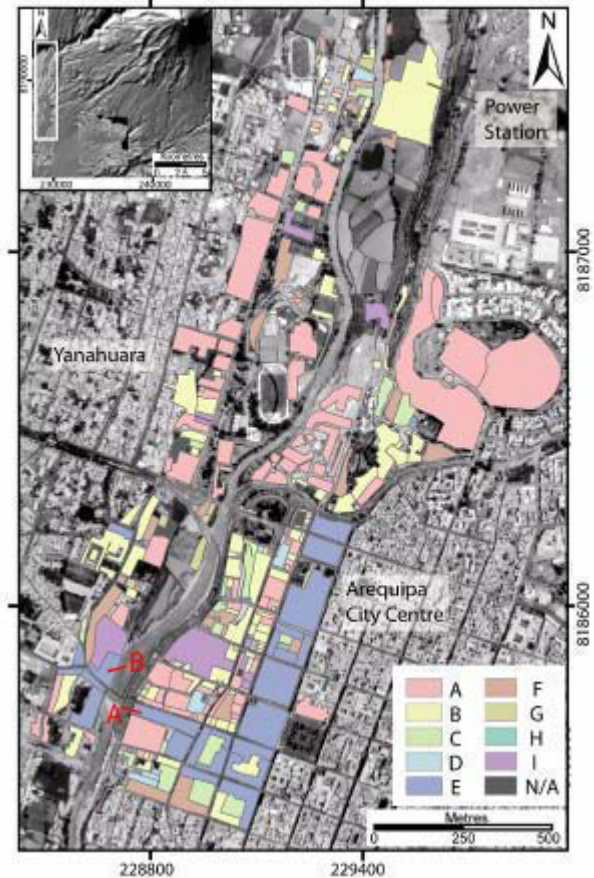
House Type D

- Same structural components as Type A buildings, however building characteristics similar to Type B with incremental and unfinished construction practices.
- 2-4 storeys.
- Vertical extension unfinished and some material that has been used are unstable



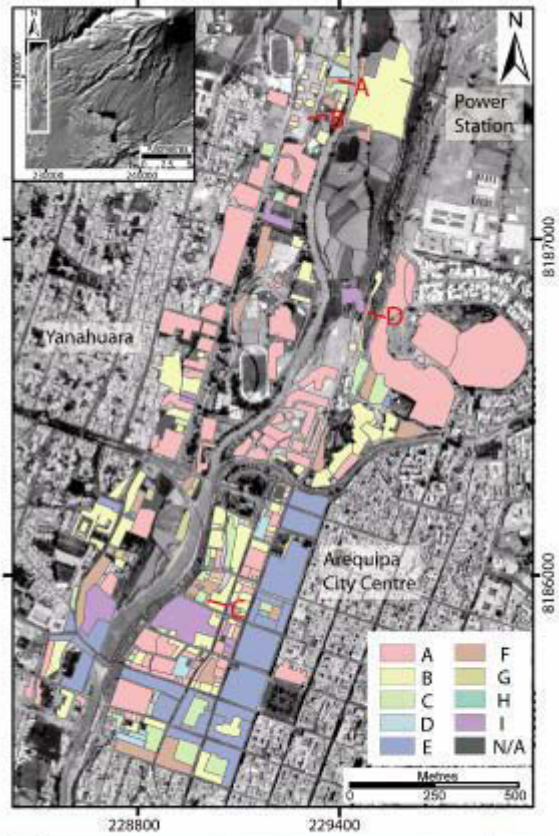
House Type E

- Building is typically colonial style and constructed from ignimbrite brick and/or adobe.
- First storey of building similar to Types B and C.
- The upkeep of the building is poor and can appear 'shabby'. Parts of the building are likely to be unstable.
- Windows tend to be smaller than newer houses constructed in Types A-C.



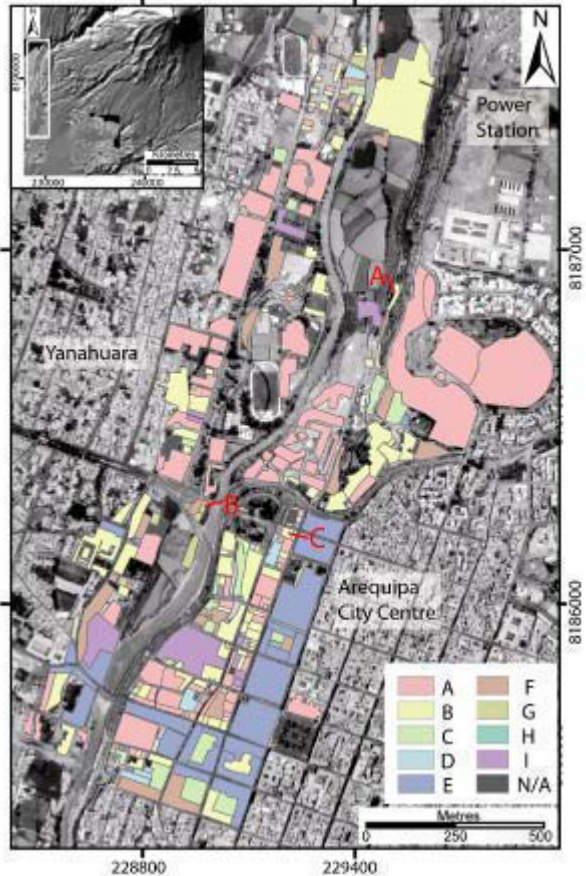
House Type F

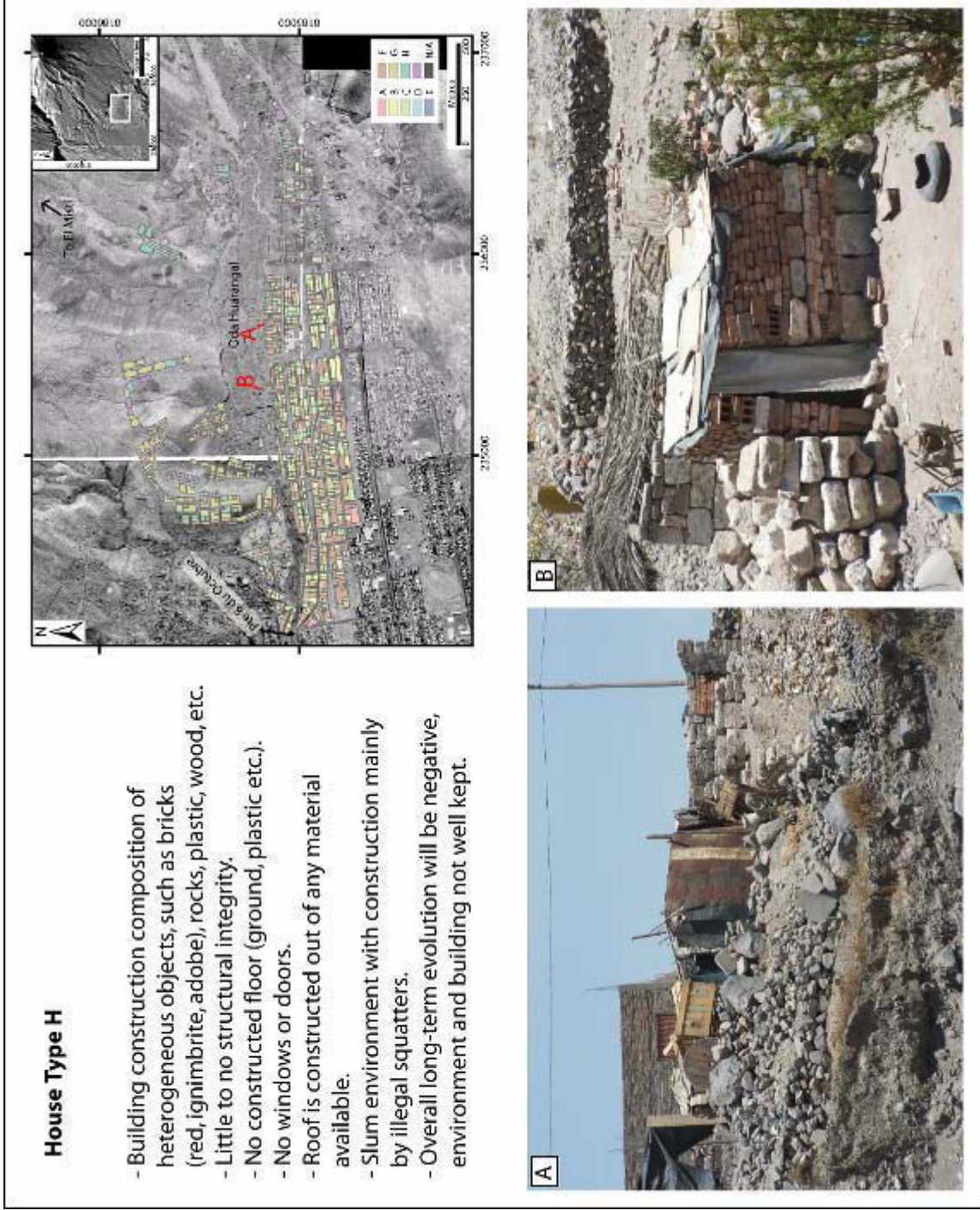
- Same structural components as Type A.
- Structure is degraded and unstable, often unfinished or constructed poorly, or damaged (earthquake) and not remedied.
- Windows often small and few, with aluminium or wood framing.
- Doors are mainly tin/aluminium, somewhat flimsy, with or without security.
- Roofs maybe be the same as type A or constructed of corrugated iron. Corrugated iron often held in place by rocks and wood.
- Environment and building not well kept, overall long-term evolution will be negative.



House Type G

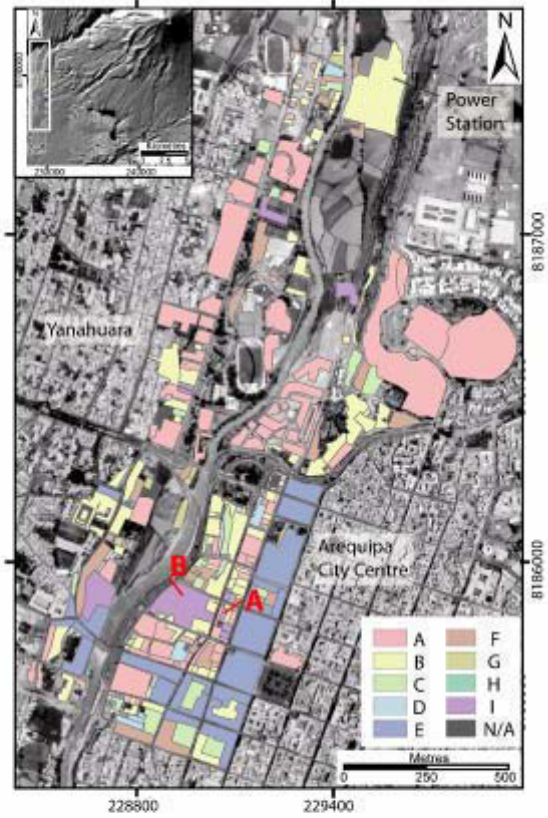
- Building comprises of an old base constructed from stones and ignimbrite.
- Walls are ignimbrite, brick or adobe.
- The building is not confined by either reinforced horizontal or vertical cast-in-situ concrete, and in many cases appear quite unstable.
- Roofs typically constructed with corrugated iron placed on wooden rafters and held in place by rocks, bricks, wood etc. in some cases they are nailed into place.





House Type I

- Abandoned and destroyed housing.
- Some destroyed in the 2001 earthquake and never rebuilt or cleared.
- Unsafe, unstable with squatters.



Appendix C

Land use vulnerability in Arequipa								
Criteria (coefficient (0 - low importance/susceptibility, 1 - high importance/susceptibility))								
Facility used during a crisis		Population exposure		Value		Economic repercussion		
Emergency facilities (administration, accommodation)	Ensuring emergency supplies	People exposed during the day	People exposed during the night	Place of community importance (cultural/social)	Value to the individual	Loss of income	Cost of rebuilding	
1- Dwelling	0.10	0.00	0.30	0.90	0.10	0.60	0.00	0.20
2- Rural dwelling	0.10	0.00	0.50	0.90	0.10	0.60	0.10	0.20
3- Commercial with dwelling	0.10	0.10	0.90	0.80	0.10	0.60	0.70	0.30
4- Accommodation	0.50	0.00	0.50	0.90	0.10	0.20	0.80	0.50
5- Medical centre	1.00	1.00	1.00	0.80	1.00	1.00	0.20	0.80
6- Police	1.00	1.00	1.00	0.70	1.00	1.00	0.10	0.50
7-Religious establishment	0.80	0.10	0.90	0.10	0.90	0.70	0.10	0.90
8- Educational establishment	0.80	0.00	0.90	0.00	0.70	0.50	0.50	0.80
9- Public area	0.70	0.00	0.90	0.10	0.30	0.30	0.10	0.30
10- Restaurant	0.00	0.20	0.80	0.70	0.10	0.10	0.80	0.50
11- Other commercial	0.10	0.10	0.90	0.10	0.10	0.10	0.80	0.50
12- Administration	0.10	0.10	0.90	0.10	0.10	0.10	0.80	0.50
13- Industry	0.10	0.70	0.90	0.50	0.20	0.20	0.90	0.80
14- Service station	0.00	0.80	0.90	0.10	0.10	0.20	0.80	0.50
15- Carpark	0.30	0.00	0.70	0.10	0.00	0.00	0.10	0.30
16- Agriculture	0.10	0.50	0.90	0.10	0.00	0.50	0.90	0.80
17- Monument	0.00	0.00	0.90	0.10	0.90	0.70	0.10	0.80
18- Abandoned	0.00	0.00	0.10	0.10	0.00	0.00	0.00	0.00
19- No construction	0.20	0.00	0.00	0.00	0.00	0.00	0.00	0.00
20- Unknown	0.00	0.00	0.00	0.00	0.00	0.00	0.00	0.00
Rationale:	Medical facilities and police are considered the most essential during a crisis, and the facilities must remain open for the safety of the community. Religious and educational establishments, and public areas can be used as evacuation centres and thus, are regarded as essential land use also. Industries, service stations and agriculture are considered as important land use types during a crisis to ensure the cities economy and to supply residents with essential goods (i.e. Food to residents, petrol to emergency services.		The majority of land-use types expose people during the day to a high degree. E.g. religious establishments are not only used by church goers in Arequipa, but are a popular attraction for many tourists, especially in the city centre. Dwellings, hotels, and medical centres have the most people exposed during the night. Restaurants and public spaces are also popular in the evenings.		Medical centres and police stations hold high regard and are also essential not only to the community but the individual. Religious establishments are held in high regard in Arequipa, as well as monuments which are important for the UNESCO world heritage city status. Dwellings are considered important to the individual because it is their 'home'.		Industry and agriculture are considered the most vulnerable land-use in terms of loss of income. Service stations, restaurants, hotels, and other commercial land use are also vulnerable in terms of lost income. The rebuild cost for religious establishments is considered the highest. This is due to their elaborate nature.	

Building vulnerability in Arequipa

Criteria	Class									Coefficient 0 = very good, 1 = very bad
	Type A	Type B	Type C	Type D	Type E	Type F	Type G	Type H	Type I	
Frame Materials										
1. Steel										0.1
2. Concrete - Reinforced Cement Concrete (RCC)	0.1	0.1	0.1	0.1	0.1	0.1				0.1
3. Wood										0.1
4. No frame										1.0
<p>Rationale: Steel, reinforced concrete and wood are good materials for building frame construction hence the 0.1 coefficient. A building with no frame has no structural support and therefore assigned the 1.0 coefficient which is assigned to building types G and H.</p>										
Wall materials										
1. Concrete (RCC)										0.1
2. Concrete	0.3	0.3	0.3	0.3	0.3					0.3
3. Bricks (red clay)	0.4	0.4	0.4	0.4	0.4		0.4			0.4
4. Ignimbrite (thick walls)										0.5
5. Ignimbrite with no mortar										0.8
6. Adobe										0.7
7. Adobe with no mortar										1.0
8. Wood										0.7
9. Stone with no mortar										1.0
10. Makeshift (plastic, stone, others)										1.0
<p>Rationale: Reinforced concrete is the strongest material for wall construction, followed by concrete. Adobe, stone and makeshift wall materials with no mortar are the most vulnerable possessing little to no structural integrity. Housing types G and H are constructed of these vulnerable materials with a coefficient of 1.0 (very bad).</p>										
Roof Type										
1. Flat	0.2	0.2	0.2	0.2	0.2	0.2	0.2	0.2		0.2
2. Pitched	0.4	0.4	0.4							0.4
<p>Rationale: In terms of debris flows, lahars, floods etc. flat roof types are less vulnerable than pitched. This is because the flow can get up under the eaves forcing the roof off the building. Pitched roofs also possess a greater surface area to be exposed to the force of a flow. However, flat roofs are also vulnerable to collapse from the weight of debris (in the case of debris flows). House types A – C have both pitched and flat roofs in Arequipa with the majority of other house types possessing flat roof types.</p>										
Roof material (weight)										
1. Concrete slab	0.1	0.1	0.1	0.1						0.1
2. Brick and concrete	0.2	0.2	0.2	0.2	0.2					0.2

3. Tile	0.2	0.2	0.2		0.2	0.2	0.2		0.2
4. Wood					0.3		0.4	0.4	0.4
5. Makeshift materials							0.8	0.8	0.8
Rationale: The roof material is important because light roofs are prone to being damaged during a flow event (as discussed in the pitch of the roof). Light materials (makeshift) for roofing feature in house types G and H.									
Storeys									
1. One story	0.7	0.7	0.7		0.7	0.7	0.7	0.7	0.7
2. 2 stories	0.5	0.5	0.5		0.5	0.5			0.5
3. =>3 stories	0.1	0.1	0.1	0.1					0.1
Rationale: Water enters through the lower stories and multi-storey buildings are able to withstand flood waters better than single storey buildings. Single storey buildings are also overcome with flood waters first, and multi-storey buildings allow for residents to move to upper storeys to escape the rising water.									
Proportion of windows (1 -2 t floors)									
1. 0-5%									0.1
2. 5-20%					0.3	0.3	0.3	0.3	0.3
3. 20-50%	0.5	0.5	0.5	0.5					0.5
4. >50%							0.7		0.7
Rationale: Windows are a weak point in a buildings construction – the greater the number of windows the more weak points and also entry points to water/flow ingress. Therefore buildings with a greater proportion of windows are assigned a higher coefficient to reflex these weak points. In the case of Arequipa makeshift buildings are assigned this high coefficient because they possess no windows.									
Type of window									
1. Aluminium frame	0.2	0.2	0.2	0.2	0.2	0.2			0.2
2. Wood frame					0.6	0.6	0.6		0.6
Rationale: Wooden frames are more vulnerable to aluminium frames because water can seep into window frames causing damage by weakening the frames, causing swelling and eventually rotting.									
Foundations and depth									
1. Piled				0.1					0.1
2. Solid wall	0.3	0.3	0.3	0.3	0.3	0.3			0.3
3. Slab	0.4	0.4	0.4						0.4
4. Fill					0.6	0.6			0.6
5. No foundation							1.0	1.0	1.0
Rationale: A good foundation is essential for a buildings resistance to flood and lahar damage. Flows are capable of scouring a foundation causing instability and/or collapse of the structure (as seen in Quebrada Huarangal and Mariano Melgar). With no, or a poor, foundation buildings have little ‘grounding’ or structural support. Piled foundations are the least susceptible with piles driven a good depth into the ground to provide structural stability to the entire building.									

Infrastructure vulnerability in Arequipa

Elements		Criteria: Coefficients from 0 (low importance) to 1 (high importance)									
		Lifeline	Population exposure		Economic repercussion		Construction		Other		
		Critical/essential	Day	Night	Loss of income	Rebuild cost	Age	Materials	Energy output	Distance from river	Height above river
Roadways	Highway	0.9	0.8	0.4	0.7	0.6	-	0.2	-	0.1	-
	Main road	0.7	0.7	0.3	0.5	0.4	-	0.4	-	0.5	-
	Minor road	0.5	0.5	0.2	0.3	0.3	-	0.5	-	0.5	-
	Unsealed road	0.1	0.2	0.1	0.1	0.1	-	0.8	-	0.7	-
<p>Rationale: Highways are regarded as the most critical infrastructure as they provide, in general, the most direct route in and out of the city and also to different suburbs. Highways are better maintained than other roads and provide more reliable transportation networks which are capable of carrying a higher traffic numbers during the day and night. Loss of income is taken into account because a disruption to the transportation network would result in traffic delays. Traffic delays would not only disrupt the employees but stop/delay stock and/or deliveries. The rebuild cost of highways is more than unsealed and minor roads. Carriageways are larger (dual over single) and have higher specifications for the carriageway due to higher traffic volumes. Unsealed roads are closer to the river in general than the other roads.</p>											
Bridges	Chilina walking	0.1	0.2	0.1	0.1	0.1	0.1	0.8	-	0.9	0.8
	Chilina	0.3	0.3	0.1	0.2	0.2	0.4	0.4	-	0.9	0.8
	Grau	0.8	0.8	0.4	0.6	0.8	0.7	0.5	-	0.9	0.3
	Bajo Grau	0.8	0.7	0.3	0.4	0.4	0.2	0.3	-	0.9	0.8
	Bolognesi	0.7	0.6	0.2	0.6	0.8	0.7	0.5	-	0.9	0.3
	Quinones	0.9	0.7	0.3	0.4	0.7	0.2	0.3	-	0.9	0.6
	8 du Octubre	0.5	0.7	0.2	0.2	0.1	0.2	0.4	-	0.9	0.9
<p>Rationale: The most critical bridge is Quinones because it connects main access highways between the east and west, and also provides access to the city centre – a major tourist attraction. Grau and Bajo Grau also connect main roads from the Yanahuara district in the west to the city centre and to suburbs in the east and north east. The Chilina walking bridge is regarded the least critical bridge because there is no vehicular traffic and it is situated on private property, therefore the foot traffic is very low. Population is most exposed on Grau due to the high traffic volume with taxis, buses, cars accessing the city from the west and also the bridge is a very popular tourist attraction. If Grau or Bolognesi is damaged and/or destroyed the loss of income to the region would be high not only from severe traffic disruptions but also from tourism, as both bridges are attractions in the city. The rebuild cost of these old masonry arch bridges would be a lot higher than the other bridges due to both the style of construction, and the cost and amount of material. The oldest bridge is Grau and Bolognesi making these bridges more vulnerable than other bridges, due to innovations in bridge design since their construction, and both bridges have sustained damage from floods and earthquakes in the past. Both Bajo Grau and Quinones are regarded as the least susceptible in terms of construction material as they comprise reinforced concrete and have been designed to streamline water flow underneath with no pillars within the river channel (C. Henry, C. Young, Pers. Comm. 2009). The Chilina walking bridge is considered as the most susceptible constructed of lightweight steel with a wooden deck and it is poorly anchored. All bridges are given the highest coefficient in distance from river, with the 8 du Octubre bridge as the bridge with the lowest deck height.</p>											
Other transport	Railways	0.5	0.6	0.2	0.5	0.6	-	0.2	-	0.3	-
	Airport	0.9	0.8	0.1	0.7	0.7	0.3	0.2	-	0.1	-
<p>Rationale: Railways are not considered critical for transportation, especially passenger, in Arequipa. However, during a volcanic crisis they could be valuable for the transportation of essential of food, water, medical and emergency supplies if other transportation routes are closed. The airport connects Arequipa to other cities in Peru, indispensable for essential supplies and tourism to the region. The airport is very busy during the daytime thus the high coefficient for daytime exposure. The economic repercussion due to the loss of the Arequipa Airport would again be hugely influenced by the tourism industry, and the cost of reconstruction would be relatively high. The airport and railways are of good construction and not relatively old. The airport is very far from the Rio Chili and the Quebrada Huarangal, railways and railway buildings closer to the Rio Chili towards the south of the city centre.</p>											
Hydroelectric power stations	Charcani I	0.8	0.2	0.1	0.5	0.7	0.6	0.3	0.1	0.9	-
	Charcani II	0.8	0.2	0.1	0.5	0.7	0.6	0.3	0.1	0.9	-
	Charcani III	0.8	0.2	0.1	0.5	0.7	0.5	0.3	0.2	0.9	-
	Charcani IV	0.8	0.2	0.1	0.5	0.7	0.3	0.3	0.4	0.9	-
	Charcani V	0.8	0.2	0.1	0.5	0.9	0.2	0.1	0.9	0.9	-

Appendix C

	Charcani VI	0.8	0.2	0.1	0.5	0.7	0.3	0.3	0.6	0.9	-
	Hydroelectric dams	0.8	0	0	0.1	0.5	-	0.2	-	0.9	-
Other power	Power station	0.8	0.7	0.3	0.7	0.7	0.2	0.1	0.6	0.8	-
Power poles and lines	Wood	0.8	0	0	0.7	0.4	-	0.8	-	0.5	-
	Concrete	0.8	0	0	0.7	0.6	-	0.3	-	0.5	-

Rationale:

Power supply to Arequipa, including all aspects from the hydroelectric dams to wood power poles, are regarded as critical infrastructure. The population needs power and a small disruption of can have an affect on the city. The Chilina power station has the highest coefficient for population exposure because it is a large factory with a good number of employees, and also the station deals with customer enquiries. The loss of income from the Chilina power station would be the largest due to the high power output, and the large number of employees. The power poles and lines would also be considered as high in terms of loss of income because without the poles and lines there would be no power. The rebuild cost of Charcani V would be large because it is located high up in the Rio Chili canyon and a tunnel has been built through the side of the volcano. Charcani V and the Chilina power station are the youngest power stations and therefore constructed from using more innovative techniques. The energy output of the Charcani V power station is the highest and the loss or disruption this station would be significant, thus the highest assigned coefficient. All of the hydroelectric stations and dams are located within, or directly adjacent to the river hence the 0.9 coefficient.

Water supply systems	Water canal open	0.8	0.3	0.1	0.7	0.5	-	0.2	-	0.7	-
	Water canal covered	0.8	0	0	0.7	0.6	-	0.1	-	0.7	-
	Irrigation canals	0.7	0.3	0.1	0.7	0.6	-	0.7	-	0.7	-
	Water treatment plant	0.8	0.7	0.1	0.6	0.7	-	0.2	-	0.1	-
	Water pipes	0.8	0	0	0.7	0.6	-	0.3	-	0.5	--

Rationale:

Water supply is essential to any community with Arequipa relying on water from the Rio Chili for the potable supply. Population exposure is low except at the treatment plant. Also the population uses the open water canals for irrigation and cleaning, thus exposed. The flow-on effect from loss of water to the economy would be significant especially to the agricultural industry which relies on irrigation for crop growth. The rebuild cost of the canals and the water treatment plant would be relatively high, with the irrigation canals most poorly constructed. The canals are located on the terraces next to the Rio Chili. The main water treatment plant is located to the south of the airport – high above river level.

Criteria: Coefficients from 0 (low importance) to 1 (high importance)

		Lifeline		Population exposure		Economic repercussion		Construction		Other	
		Critical/essential	Day	Night	Loss of income	Rebuild cost	Age	Materials	Energy output	Distance from river	Height above river
Waste water supply systems	Waste water and sewerage pipes	0.8	0	0	0.6	0.6	-	0.3	-	0.5	-
Telecommunications	Telecommunication lines	0.8	0	0	0.6	0.6	-	0.3	-	0.5	-

Rationale:

Waste water and telecommunications are regarded as essential infrastructure, not just for day-to-day but during times of crisis. The loss of income due to a loss of waste water and telecommunications would be fairly significant. A disrupted waste water system could result in poor health therefore disrupting the population. Telecommunications are vital to business and therefore a loss of income in this respect would be significant. Both systems have varying construction materials and vary in distance to the river, hence the 0.5 coefficient.